



# **PVT AND PHASE BEHAVIOUR OF PETROLEUM RESERVOIR FLUIDS**

**ALI DANESH**

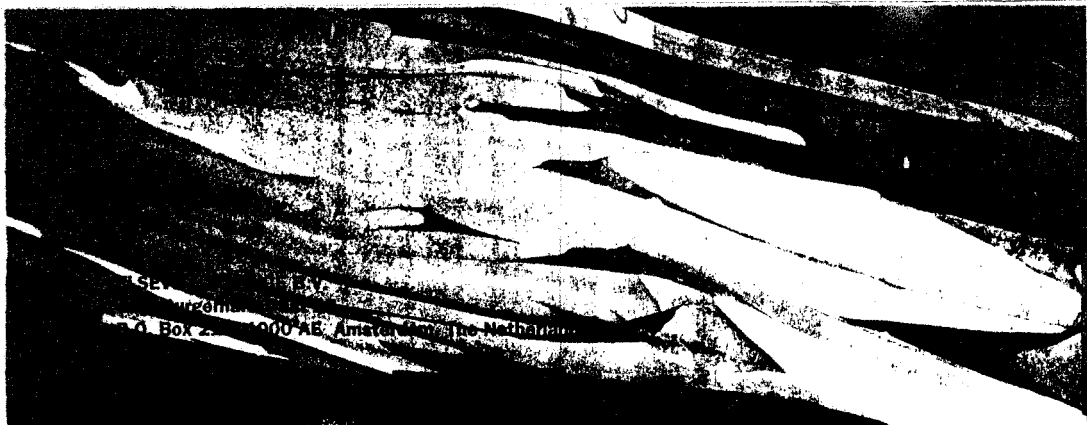
*Department of Petroleum Engineering  
Heriot Watt University  
Edinburgh, Scotland*



1998

ELSEVIER

Amsterdam – Lausanne – New York – Oxford – Shannon – Singapore – Tokyo



Library of Congress Cataloging in Publication Data

A catalog record from the Library of Congress has been applied for.

ISBN: 0 444 82196 1

© 1998 Elsevier Science B.V. All rights reserved.

No part of this publication may be reproduced, stored in a retrieval system or transmitted in any form or by any means, electronic, mechanical, photocopying, recording or otherwise, without the prior written permission of the publisher, Elsevier Science B.V., Copyright & Permissions Department, P.O. Box 521, 1000 AM Amsterdam, The Netherlands.

Special regulations for readers in the U.S.A. – This publication has been registered with the Copyright Clearance Center Inc. (CCC), 222 Rosewood Drive, Danvers, MA, 01923. Information can be obtained from the CCC about conditions under which photocopies of parts of this publication may be made in the U.S.A. All other copyright questions, including photocopying outside of the U.S.A., should be referred to the publisher.

No responsibility is assumed by the publisher for any injury and/or damage to persons or property as a matter of products liability, negligence or otherwise, or from any use or operation of any methods, products, instructions or ideas contained in the material herein.

☺ The paper used in this publication meets the requirements of ANSI/NISO Z39.48-1992 (Permanence of Paper).

Printed in The Netherlands.

# CONTENTS

## PREFACE

## NOMENCLATURE

<b>1.</b>	<b>PHASE BEHAVIOUR FUNDAMENTALS</b>	<b>1</b>
1.1	RESERVOIR FLUID COMPOSITION	1
1.2	PHASE BEHAVIOUR	3
	Pure Compound	4
	Corresponding States	10
	Multicomponent Mixture	15
1.3	CLASSIFICATION OF RESERVOIR FLUIDS	22
	Dry Gas	24
	Wet Gas	25
	Gas Condensate	25
	Volatile Oil	27
	Black Oil	28
1.4	REFERENCES	29
1.5	EXERCISES	30
<b>2.</b>	<b>PVT TESTS AND CORRELATIONS</b>	<b>33</b>
2.1	FLUID SAMPLING	34
	Well Preparation	34
	Sample Collection	36
2.2	PVT TESTS	38
2.2.1	Dry Gas	40
2.2.2	Wet Gas	41
2.2.3	Black Oil	42
2.2.4	Gas Condensate	52
2.2.5	Volatile Oil	65
2.3	EMPIRICAL CORRELATIONS	66
2.3.1	Black Oil	67
	Bubble Point Pressure	68
	Gas in Solution	70
	Oil Formation Volume Factor	70
	Total Formation Volume Factor	71
	Oil Density	73
	Oil Viscosity	77
2.3.2	Natural Gas	79
	Volumetric Data	80
	Gas Viscosity	83
2.3.3	Formation Water	86
	Water Content of Hydrocarbon Phase	87
	Hydrocarbon solubility in Water	90
	Water Formation Volume Factor	92
	Compressibility of Water	92
	Water Density	93
	Water Viscosity	93
2.4	REFERENCES	95
2.5	EXERCISES	99

<b>3.</b>	<b>PHASE EQUILIBRIA</b>	105
3.1	CRITERIA FOR EQUILIBRIUM	105
	Chemical Potential	107
	Fugacity	108
	Activity	111
3.2	EQUILIBRIUM RATIO	111
	Raoult's Law	112
	Henry's Law	114
	Empirical Correlations	116
3.3	REFERENCES	125
3.4	EXERCISES	127
<b>4.</b>	<b>EQUATIONS OF STATE</b>	129
4.1	VIRIAL EOS AND ITS MODIFICATIONS	130
	Starling-Benedict-Webb-Rubin EOS	131
4.2	CUBIC EQUATIONS OF STATE	132
4.2.1	Two-Parameter EOS	138
	<i>Soave-Redlich-Kwong EOS</i>	140
	<i>Peng-Robinson EOS</i>	141
	<i>Volume Shift</i>	141
4.2.2	Three-Parameter EOS	145
	<i>Schmidt-Wenzel EOS</i>	146
	<i>Patel-Teja EOS</i>	147
4.2.3	Attraction Term Temperature Dependency	149
4.3	MIXING RULES	153
4.3.1	Random Mixing Rules	154
4.3.2	Non-Random Mixing Rules	158
4.4	REFERENCES	162
4.5	EXERCISES	165
<b>5.</b>	<b>PHASE BEHAVIOUR CALCULATIONS</b>	167
5.1	VAPOUR-LIQUID EQUILIBRIUM CALCULATIONS	168
	Root Selection	175
	Rapid Flash Calculations	179
5.2	STABILITY ANALYSIS	183
	Stability Limit	189
5.3	CRITICAL POINT CALCULATIONS	192
5.4	COMPOSITIONAL GRADING	195
	Equilibrium Assumption	197
	Non-Equilibrium Fluids	198
	Heat of Transport	200
	Significance	201
5.5	REFERENCES	203
5.6	EXERCISES	206
<b>6.</b>	<b>FLUID CHARACTERISATION</b>	209
6.1	EXPERIMENTAL METHODS	210
	Distillation	210
	Gas Chromatography	215
6.2	CRITICAL PROPERTIES	221
	Lee-Kesler Correlations	221
	Riazi-Daubert Correlations	222
	Perturbation Expansion Correlations	223
6.3	DESCRIPTION OF FLUID HEAVY END	227
	Single Carbon Number Function	228
	Continuous Description	234



	Direct Application	241
6.4	REFERENCES	247
6.5	EXERCISES	249
7.	<b>GAS INJECTION</b>	253
7.1	MISCIBILITY CONCEPTS	254
	Miscibility in Real Reservoir Fluids	258
7.2	EXPERIMENTAL STUDIES	260
	Slim Tube	260
	Rising Bubble Apparatus	265
	Contact Experiments	266
7.3	PREDICTION OF MISCIBILITY CONDITIONS	270
	First Contact Miscibility	270
	Vaporising Gas Drive	270
	Condensing-Vaporising Gas Drive	273
7.4	REFERENCES	277
7.5	EXERCISES	279
8.	<b>INTERFACIAL TENSION</b>	281
8.1	MEASUREMENT METHODS	282
8.2	PREDICTION OF INTERFACIAL TENSION	285
	Parachor Method	285
	Corresponding States Correlation	288
	Comparison of Predictive Methods	289
8.3	WATER-HYDROCARBON INTERFACIAL TENSION	292
8.4	REFERENCES	295
8.5	EXERCISES	297
9.	<b>APPLICATION IN RESERVOIR SIMULATION</b>	301
9.1	GROUPING	302
	Group Selection	302
	Group Properties	308
	Composition Retrieval	310
9.2	COMPARISON OF EOS	314
	Phase Composition	316
	Saturation Pressure	318
	Density	319
	Gas and Liquid Volumes	320
	Robustness	322
9.3	TUNING OF EOS	323
	Fluid Characterisation	324
	Selection of EOS	325
	Experimental Data	325
	Selection of Regression Variables	327
	Limits of Tuned Parameters	330
	Methodology	330
9.4	DYNAMIC VALIDATION OF MODEL	331
	Relative Permeability Function	333
	Viscosity Prediction	334
	Implementation	338
9.5	EVALUATION OF RESERVOIR FLUID SAMPLES	340
9.6	REFERENCES	345
9.7.	EXERCISES	349
	<b>APPENDICES</b>	353
	<b>INDEX</b>	385

## PREFACE

Reliable measurement and prediction of phase behaviour and properties of petroleum reservoir fluids are essential in designing optimum recovery processes and enhancing hydrocarbon production. This book explains relevant fundamentals and presents practical methods of determining required properties for engineering applications by judicious review of established practices and recent advances.

Although the emphasis is on the application of PVT and phase behaviour data to engineering problems, experimental methods are reviewed and their limitations are identified. This should provide the reader with a more thorough understanding of the subject and a realistic evaluation of measured and predicted results.

The book is based on the material developed over many years as lecture notes in courses presented to staff in gas and oil industry, and postgraduate students of petroleum engineering. It covers various aspects of the subject, hence can be tailored for different audience. The first two chapters along with selected sections from chapters 3 and 5 can serve as the subject matter of an introductory course, whereas the rest would be of more interest to practising engineers and postgraduate students. Ample examples are included to illustrate the subject, and further exercises are given in each chapter. Graphical methods and simple correlations amenable to hand calculations are still used in the industry, hence they are included in this book. The emphasis, however, is on the more advanced compositional approaches which are attaining wider application in industry as high computational capabilities are becoming readily available.

I would like to thank Professor DH Tehrani for reviewing the manuscript and valuable suggestions stemming from his vast industrial experience. Also, I am grateful to Professors M. Michelsen and C. Whitson for their helpful comments on sections of the book. Much of the material in this book is based on the author's experience gained through conducting research sponsored by the petroleum industry, at Heriot-Watt University. I am indebted to the sponsors, my students and colleagues for their contributions that made this book possible. In particular, I would acknowledge valuable contributions of Professor AC Todd, Mr F Goozalpour, Dr DH Xu, Mr K Movaghar Nezhad and Dr D Avlonitis. My son Amir cheerfully helped me in preparing the book graphics.

## NOMENCLATURE

$a$	attractive term parameter of equation of state
$A$	dimensionless attractive term parameter of equation of state
$b$	repulsive term(co-volume) parameter of equation of state
$B$	dimensionless repulsive term parameter of equation of state
$B_g$	gas formation volume factor
$B_o$	oil formation volume factor
$B_t$	total formation volume factor
$C_g$	gas isothermal compressibility coefficient
$C_o$	oil isothermal compressibility coefficient
$f$	fugacity
$G$	Gibbs energy
$h$	height
$\bar{h}$	molar enthalpy
$H$	total enthalpy
$H_i$	Henry's constant
$h_i$	partial molar enthalpy
$k$	permeability
$k_{ii}$	binary interaction parameter
$k_{rg}$	gas relative permeability
$k_{ro}$	oil relative permeability
$K$	equilibrium ratio
$K_w$	Watson characterisation factor
$m$	slope in $\alpha$ correlation with temperature
$M$	molecular weight (molar mass)
$n$	mole or carbon number
$N$	number of components
$N_p$	number of pseudo-components
$P$	pressure
$P_b$	bubble point pressure
$P_k$	convergence pressure
$P_\sigma$	parachor
$P^S$	vapour pressure
$R$	universal gas constant
$R_s$	gas in solution
$S$	specific gravity, relative density at 288 K (60 °F)
$T$	temperature
$T_b$	normal boiling point temperature
$\bar{u}$	molar internal energy
$v$	molar volume
$\bar{v}$	velocity
$V$	volume
$x_i$	mole fraction
$y_i$	mole fraction in vapour phase
$z_i$	mole fraction
$Z$	compressibility factor
$Z_{RA}$	Rackett compressibility factor

## GREEK LETTERS

$\alpha$	temperature dependency	coefficient of attractive term
$\beta$	mean value parameter of $\Gamma$ distribution function	
$\epsilon_i$	activity	
$\phi$	fugacity coefficient	
$\gamma$	parameter of $\Gamma$ distribution function	
$\eta$	calculated critical compressibility factor	
$\kappa$	total number of phases	
$\mu$	chemical potential	
$\rho$	mass density	
$\rho_M$	molar density	
$\sigma$	interfacial tension	
$\tau$	lowest molecular weight in $\Gamma$ distribution function	
$\omega$	acentric factor	
$\Omega$	EOS parameter coefficient	
$\Theta$	activity coefficient	
$\lambda$	any phase	

## ACRONYMS

bbl	barrel
BIP	binary interaction parameter
CCE	constant composition expansion
CGR	condensate to gas volumetric ratio
CVD	constant volume depletion
DL	differential liberation
EOS	equation(s) of state
GOR	gas to oil volumetric ratio (sc)
GLR	gas to liquid volumetric ratio (sc)
GPA	Gas Processors Association
GPM	gallon of liquid per thousand cubic feet of gas (sc)
IFT	interfacial tension
MMP	minimum miscibility pressure
MME	minimum miscibility enrichment
PNA	paraffins-naphthenes-aromatics
PR	Peng-Robinson EOS
PT	Patel-Teja EOS
sc	standard conditions
SCF	standard cubic feet
SRK	Soave-Redlich-Kwong EOS
STB	stock tank barrel
SW	Schmidt-Wenzel EOS
TBP	true boiling point temperature
VPT	Valderrama-Patel-Teja EOS
ZJRK	Zudkevitch-Joffe-Redlich-Kwong EOS

## SUPERSCRIPTS

F	feed, mixture
h	hydrocarbon phase
L	liquid phase
o	reference state
s	saturation
V	vapour phase
W	water phase

## SUBSCRIPTS

b	base or bubble point
c	critical point
d	differential liberation process
g	gas
h	hydrocarbon
o	oil
r	reduced property = value/value at critical point
s	salt
w	water



# 1

## PHASE BEHAVIOUR FUNDAMENTALS

Petroleum reservoir fluids are composed mainly of hydrocarbon constituents. Water is also present in gas and oil reservoirs in an interstitial form. The influence of water on the phase behaviour and properties of hydrocarbon fluids in most cases is of a minor consideration. The phase behaviour of oil and gas, therefore, is generally treated independent of the water phase, unless water-hydrocarbon solid structures, known as hydrates, are formed.

The behaviour of a hydrocarbon mixture at reservoir and surface conditions is determined by its chemical composition and the prevailing temperature and pressure. This behaviour is of a prime consideration in the development and management of reservoirs, affecting all aspects of petroleum exploration and production.

Although a reservoir fluid may be composed of many thousands of compounds, the phase behaviour fundamentals can be explained by examining the behaviour of pure and simple multicomponent mixtures. The behaviour of all real reservoir fluids basically follows the same principle, but to facilitate the application of the technology in the industry, reservoir fluids have been classified into various groups such as the dry gas, wet gas, gas condensate, volatile oil and black oil.

### 1.1 RESERVOIR FLUID COMPOSITION

There are various hypotheses regarding the formation of petroleum from organic materials. These views suggest that the composition of a reservoir fluid depends on the depositional environment of the formation, its geological maturity, and the migration path from the source to trap rocks [1]. Reservoir gasses are mainly composed of hydrocarbon molecules of small and medium sizes and some light non-hydrocarbon compounds such as nitrogen and carbon dioxide, whereas oils are predominantly composed of heavier compounds.

Fluids advancing into a trapping reservoir may be of different compositions due to being generated at different times and environments. Hence, lateral and vertical compositional variations within a reservoir will be expected during the early reservoir life. Reservoir fluids

are generally considered to have attained equilibrium at maturity due to molecular diffusion and mixing over geological times. However, there are ample evidences of reservoirs still maintaining significant compositional variations, particularly laterally as the diffusive mixing may require many tens of million years to eliminate compositional heterogeneities [2]. Furthermore, the pressure and the temperature increase with depth for a fluid column in a reservoir. This can also result in compositional grading with depth. For operational purposes, this behaviour is of considerable interest for near critical fluids, and oils containing high concentrations of asphaltic material. The compositional grading and its estimation based on thermodynamic concepts will be discussed in Section 5.3.

The crude oil composition is of major consideration in petroleum refining. A number of comprehensive research projects sponsored by the American Petroleum Institute have investigated crude oil constituents and identified petroleum compounds. API-6 studied the composition of a single crude oil for 40 years. The sulphur, nitrogen and organometallic compounds of crude oil samples were investigated in projects API-48, API 52 and API-56 respectively. API-60 studied petroleum heavy ends. Nelson [3] gives a review of petroleum chemistry and test methods used in the refining industry.

Highly detailed information on the constituents composing a reservoir fluid is not of very much use in exploration and production processes. Reservoir fluids are commonly identified by their constituents individually to pentanes, and heavier compounds are reported as groups composed mostly of components with equal number of carbons such as C<sub>6</sub>'s, C<sub>7</sub>'s, C<sub>8</sub>'s. All the compounds forming each single carbon number group do not necessarily possess the same number of carbons as will be discussed in Section 6.1. The most common method of describing the heavy fraction is to lump all the compounds heavier than C<sub>6</sub> and report it as C<sub>7+</sub>.

Hydrocarbon compounds can be expressed by the general formula of C<sub>n</sub>H<sub>2n+ξ</sub> with some sulphur, nitrogen, oxygen and minor metallic elements mostly present in heavy fractions. Hydrocarbon compounds are classified according to their structures, which determine the value of ξ. The major classes are paraffins (alkanes), olefins (alkenes), naphthenes, and aromatics. The paraffin series are composed of saturated hydrocarbon straight chains with ξ=2. Light paraffins in reservoir fluids are sometimes identified and reported as those with a single hydrocarbon chain, as normal, and others with branched chain hydrocarbons, as iso. The olefin series (ξ=0) have unsaturated straight chains and are not usually found in reservoir fluids due to their unstable nature. The naphthenes are cyclic compounds composed of saturated ring(s) with ξ=0. The aromatics (ξ=-6) are unsaturated cyclic compounds. Naphthenes and aromatics form a major part of C<sub>6</sub>-C<sub>11</sub> groups and some of them such as methyl-cyclo-pentane, benzene, toluene and xylene are often individually identified in the extended analysis of reservoir fluids. For example, the structural formulas of the above groups of hydrocarbons with six carbons are shown in Figure 1.1.

As reservoir hydrocarbon liquids may be composed of many thousand components, they cannot all be identified and measured. However, the concentration of hydrocarbon components belonging to the same structural class are occasionally measured and reported as groups, particularly for gas condensate fluids. The test to measure the concentration of paraffins, naphthenes, and aromatics as groups is commonly referred to as the PNA test [4]. Further information on the structure of reservoir fluid compounds and their labelling according to the IUPAC system can be found in [5]. The compositional analysis of reservoir fluids and their characterisation will be discussed in Chapter 6.

Nitrogen, oxygen and sulphur are found in light and heavy fractions of reservoir fluids. Gas reservoirs containing predominantly N<sub>2</sub>, H<sub>2</sub>S, or CO<sub>2</sub> have also been discovered. Polycyclic hydrocarbons with fused rings which are more abundant in heavier fractions may contain N, S, and O. These compounds such as carboids, carbenes, asphaltenes and resins are identified by their solubility, or lack of it, in different solvents [6]. The polar nature of these compounds



can affect the properties of reservoir fluids, particularly the rock-fluid behaviour, disproportionately higher than their concentrations [7]. These heavy compounds may be present in colloidal suspension in the reservoir oil and precipitate out of solution by changes in the pressure, temperature or compositions occurring during production.

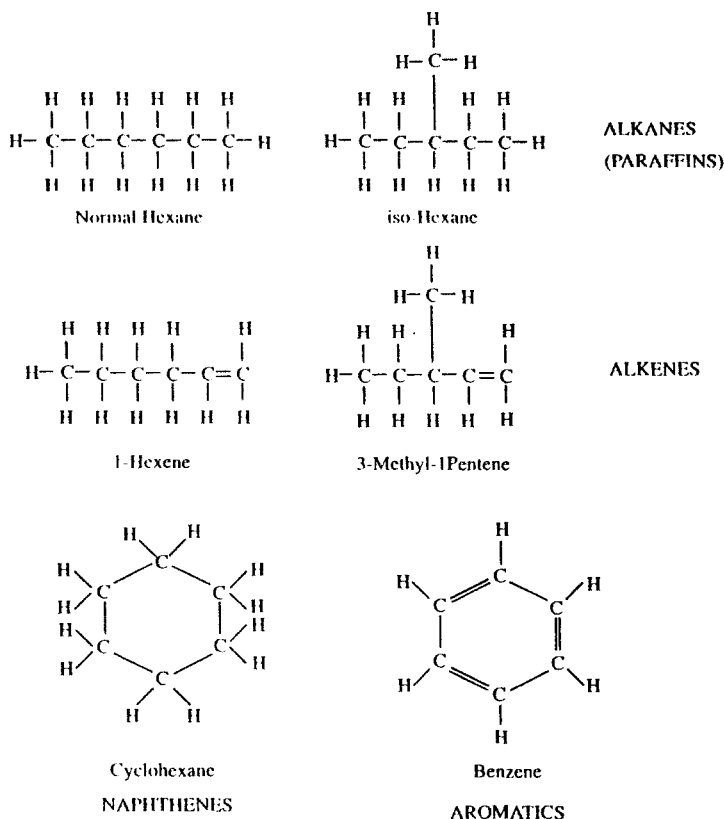


Figure 1.1. Structural formula of various groups of hydrocarbons with six carbons.

## 1.2 PHASE BEHAVIOUR

Reservoir hydrocarbons exist as vapour, liquid or solid phases. A phase is defined as a part of a system which is physically distinct from other parts by definite boundaries. A reservoir oil (liquid phase) may form gas (vapour phase) during depletion. The evolved gas initially remains dispersed in the oil phase before forming large mobile clusters, but the mixture is considered as a two-phase system in both cases. The formation or disappearance of a phase, or variations in properties of a phase in a multi-phase system are rate phenomena. The subject of phase behaviour, however, focuses only on the state of equilibrium, where no changes will occur with time if the system is left at the prevailing constant pressure and temperature. A

system reaches equilibrium when it attains its minimum energy level, as will be discussed in Chapter 3. The assumption of equilibrium between fluid phases in contact in a reservoir, in most cases, is valid in engineering applications. Fluids at equilibrium are also referred to as saturated fluids.

The state of a phase is fully defined when its composition, temperature and pressure are specified. All the intensive properties for such a phase at the prevailing conditions are fixed and identifiable. The intensive properties are those which do not depend on the amount of material (contrary to the extensive properties), such as the density and the specific heat. The term property throughout this book refers to intensive properties.

At equilibrium, a system may form of a number of co-existing phases, with all the fluid constituents present in all the equilibrated phases. The number of independent variables to define such a system is determined by the Gibbs *phase rule* described as follows.

A phase composed of  $N$  components is fully defined by its number of moles plus two thermodynamic functions, commonly temperature and pressure, that is, by  $N+2$  variables. The intensive properties are, however, determined by only  $N+1$  variables as the concentration of components are not all independent, but constrained by,

$$\sum_{i=1}^N x_i = 1 \quad (1.1)$$

where,  $x_i$  is the mole fraction of component  $i$ . Thus, for a system with  $\kappa$  phases, the total number of variables are equal to  $\kappa(N+1)$ . However, the temperature, pressure, and chemical potential of each component throughout all phases should be uniform at equilibrium conditions, as will be described in Chapter 3. This imposes  $(N+2)(\kappa-1)$  constraints. Hence, the number of independent variables, or so-called the degrees of freedom,  $F$ , necessary to define a multiphase system is given by:

$$F = \kappa(N+1) - (N+2)(\kappa-1) = N - \kappa + 2 \quad (1.2)$$

For a single-component (pure) system, the degrees of freedom is equal to three minus the number of phases. The state of the equilibrium of a vapour-liquid mixture of a pure fluid, therefore, can be determined by identifying either its pressure or its temperature.

### Pure Compound

The phase behaviour of a pure compound is shown by the pressure-temperature diagram in Figure 1.2. All the conditions at which the vapour and liquid phases can coexist at equilibrium are shown by the line AC. Any fluid at any other pressure-temperature conditions, is unsaturated single phase as required by the phase rule. The fluid above and to the left of the line is referred to as a compressed or under saturated liquid, whereas that below and to the right of the line is called a superheated vapour or gas.

The line AC is commonly known as the vapour pressure curve, as it shows the pressure exerted by the vapour coexisting with its liquid at any temperature. The temperature corresponding to the atmospheric pressure is called the *normal boiling point* or simply the boiling point of the compound. The boiling point,  $T_b$ , of some compounds found in reservoir fluids are given in Table A.1 in Appendix A. Figure 1.3 shows the logarithm of vapour pressure plotted against an arbitrary temperature scale for some compounds. The scale, which is an adjusted reciprocal of the absolute temperature, has been selected so that the vapour pressures of water and most hydrocarbons can be exhibited by straight lines. This plot is known as the Cox chart. A pure substance cannot exist as liquid at a temperature above its

critical temperature. Hence the vapour pressure values at temperatures above the critical temperatures, shown by  $\otimes$  in Figure 1.3, are not real, but simply extrapolated values.

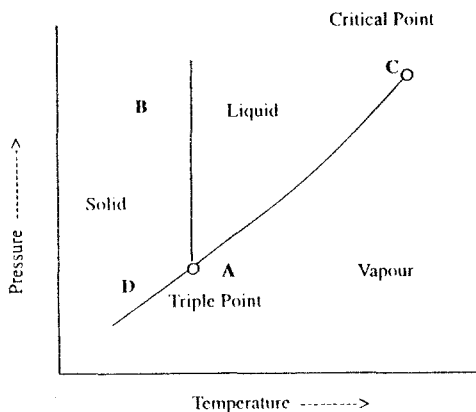


Figure 1.2. Pressure-temperature diagram of pure substance.

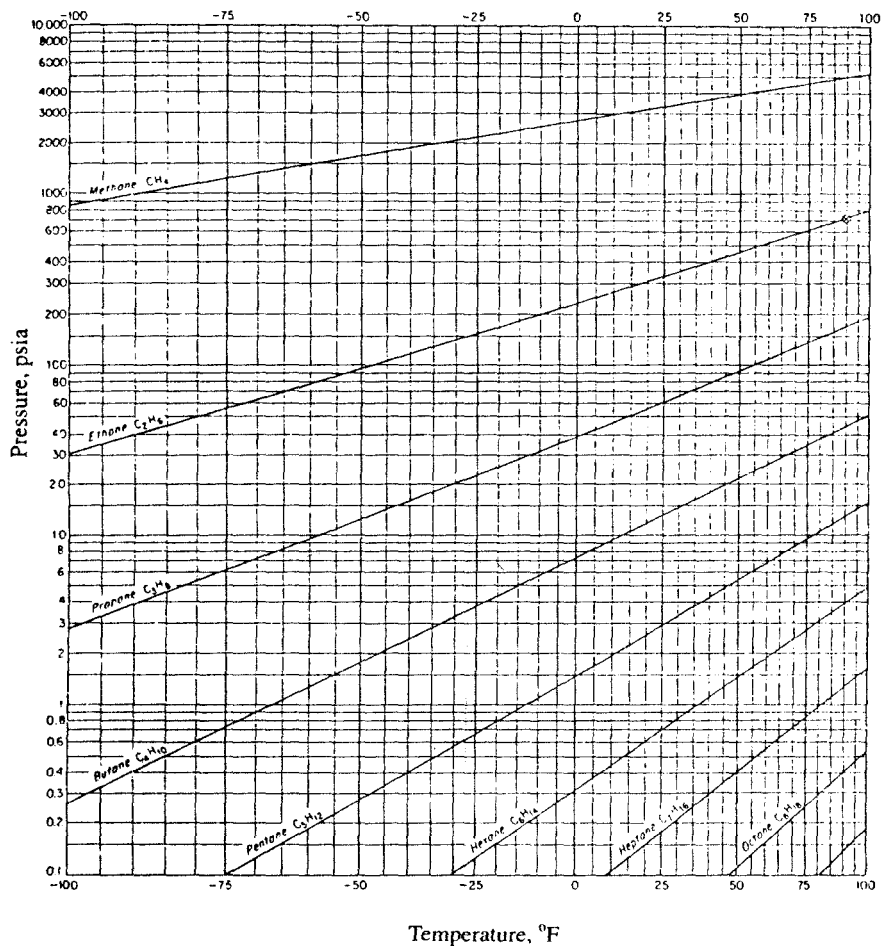
The line AB on Figure 1.2 is the solid-liquid equilibrium line, which is also known as the melting point curve. The intersection of the vapour-liquid and liquid-solid lines is the triple point. It is the only point where the three phases can coexist for a pure system.

The line AD is the solid-vapour equilibrium line or the sublimation curve. The solid carbon dioxide (dry ice) vaporising into its gaseous form is a common example of this region of the phase behaviour diagram.

The variation of saturated fluid density with temperature for a pure compound is shown in Figure 1.5. The densities of vapour and liquid phases approach each other as the temperature increases. They become equal at conditions known as the *critical point*. All the differences between the phases are reduced as the system approaches the critical point. Indeed, *the phases become the same and indistinguishable at the critical point*.

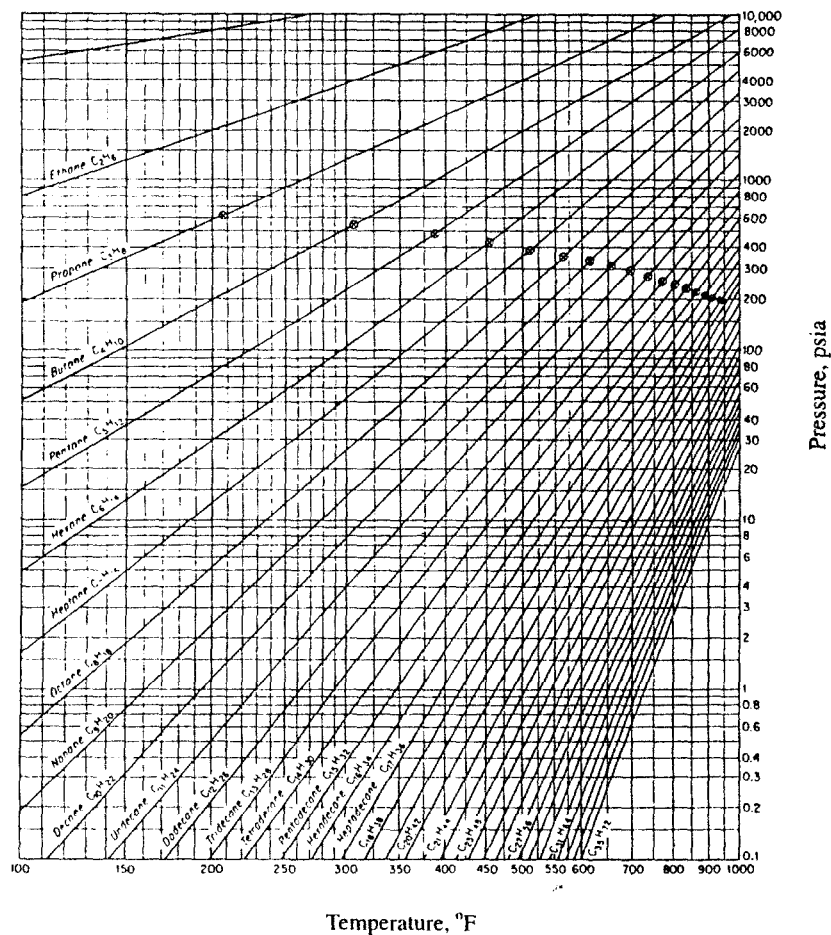
Figure 1.4 shows the variation of saturated fluid density with temperature for a number of pure hydrocarbons. All the compounds show a similar trend, that is, the vapour and liquid densities become equal at the critical point. Other properties also show the same trend. The critical temperature,  $T_c$ , and the critical pressure,  $P_c$ , are the maximum temperature and pressure at which a *pure compound* can form coexisting phases.

The terms vapour and liquid are referred to the less and the more dense phases of a fluid at equilibrium. Hence, a pure compound at a temperature above its critical value cannot be called either liquid or vapour. The continuity of vapour and liquid is schematically shown in Figure 1.6. The density at each point is shown by the shading intensity, where the darker shading corresponds to a higher density. The discontinuity across the vapour-pressure curve becomes less significant as the temperature increases and vanishes above the critical point. The superheated vapour E can be changed gradually to the compressed liquid F, through an arbitrary path EGF, without any abrupt phase change.



$$K = (T + 459.67) / 1.8 \quad \text{MPa} = 0.006895 \text{ psia}$$

Figure 1.3. Vapour pressure of normal paraffins. McGraw-Hill Companies Copyright. Reproduced from [8] with permission.



$$K = (T + 459.67) / 1.8 \quad \text{MPa} = 0.006895 \text{ psia}$$

Figure 1.3 (Cont). Vapour pressure of normal paraffins. McGraw-Hill Companies Copyright. Reproduced from [8] with permission.

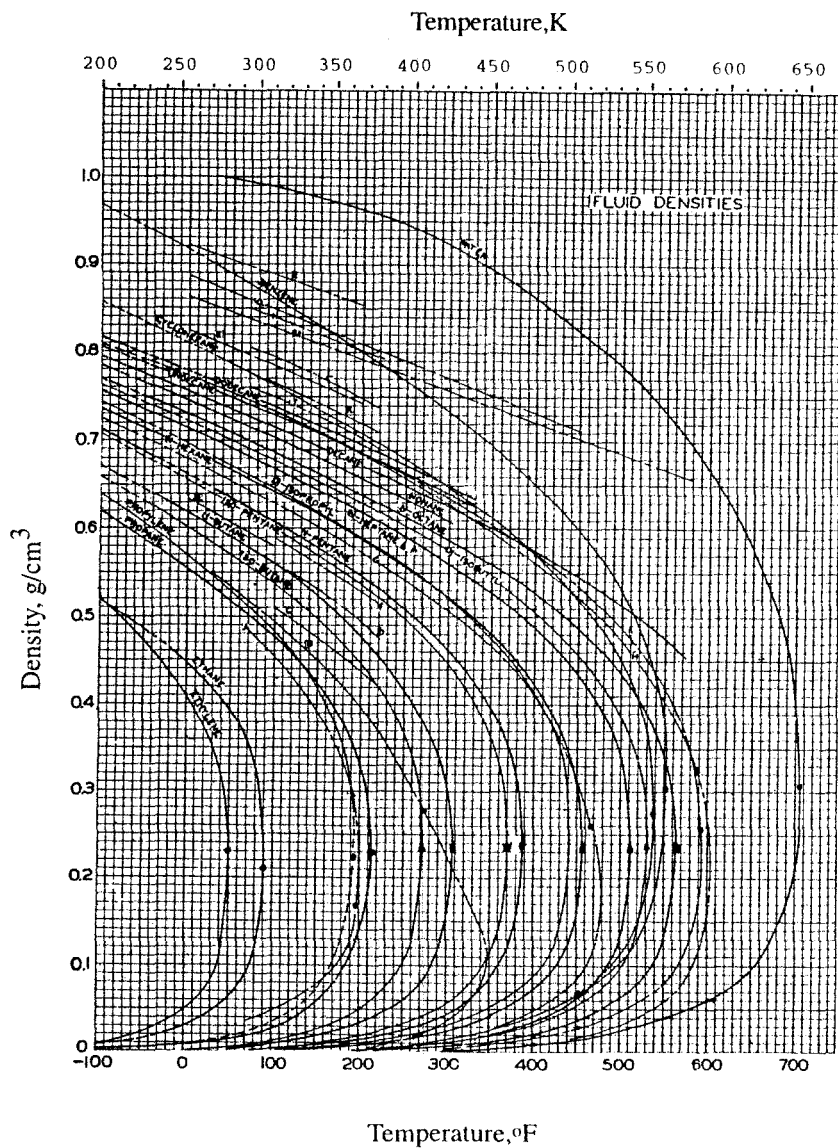


Figure 1.4. Saturated fluid density of pure compounds (curves identified by letters are related to binary and multicomponent fluids described in Reference 8). McGraw-Hill Companies Copyright. Reproduced from [8] with permission.

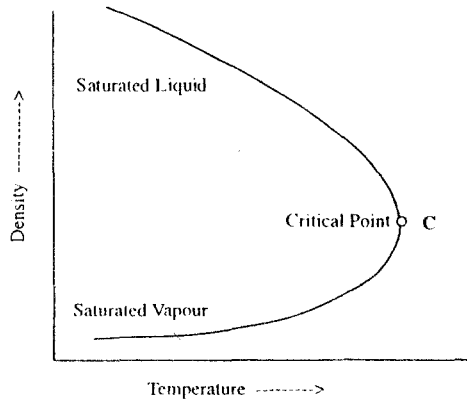


Figure 1.5. Variations of saturated fluid density with temperature.

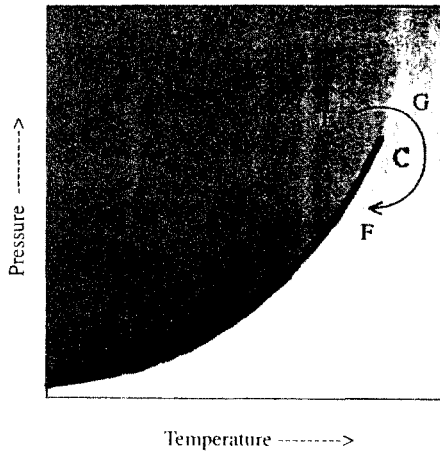


Figure 1.6. Continuity of vapour and liquid. McGraw-Hill Companies Copyright. Reproduced from [8] with permission.

The pressure-volume diagram of a pure substance is shown in Figure 1.7. Consider the compressed liquid, Point A, at a temperature below the critical temperature. The reduction of fluid pressure at constant temperature increases its volume. As the liquid is relatively incompressible the fluid expansion is small until the vapour pressure is reached, at Point B, where the first bubble evolves. Further expansion of the system results in changing the liquid into the vapour phase. For a pure substance the pressure remains constant and equal to the vapour pressure, a consequence of the phase rule, until the last drop of the liquid vaporises, Point D. This point, where the vapour is in equilibrium with an infinitesimal amount of liquid is called the dew point.

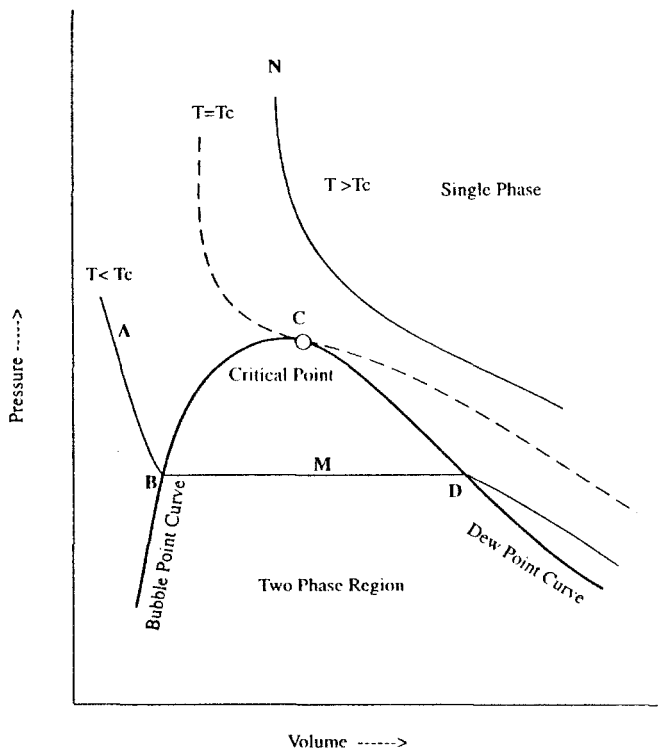


Figure 1.7. Pressure-volume diagram of pure fluid.

The system bubble points at various temperatures form the bubble point curve, whereas the dew points form the dew point curve. The two curves meet at the critical point and together identify the phase envelope. Any fluid within the phase envelope, Point M, forms two equilibrated phases with the vapour/liquid molar ratio equal to  $\overline{BM}/\overline{MD}$ . The bubble point and dew point curves appear as a single vapour pressure curve on a pressure-temperature plot for a pure compound, Figure 1.2.

The change of phase from liquid to vapour is accompanied by a large increase in volume at low temperatures (Figure 1.7). The expansion reduces as the temperature approaches the critical point. Indeed the system changes from all liquid into all vapour, or vice versa, without any change in the mixture volume at the critical point. An isothermal expansion of a fluid at a temperature above the critical temperature does not result in any phase change, Point N. This fluid is called a supercritical fluid.

### Corresponding States

All gases behave ideally when the pressure approaches zero. The pressure volume relation for an ideal gas is,

$$Pv = RT$$

$$(1.3)$$



where  $v$  is the molar volume,  $P$  is (absolute) pressure,  $T$  is (absolute) temperature, and  $R$  is the universal gas constant (Table A.3 in Appendix A). Hence one mole of any ideal gas occupies the same volume at a given pressure and temperature.

In engineering applications, gases at the standard conditions can be treated as ideal. The occupied volume of one mole of gas at various standard conditions, calculated by Eq.(1.3), is given in Table 1.1.

Table 1.1.  
Molar volume of ideal gas at various standard conditions.

Unit	Temperature	Pressure	Volume
Field	60.0 °F	14.69 psia	380 ft <sup>3</sup> /lbmol
Metric	273.15 K	1 atm	22.414 m <sup>3</sup> /kgmol
SI	288 K	100 kPa	23.95 m <sup>3</sup> /kgmol

As one mole of a hydrocarbon gas and one mole of air occupy the same volume at the standard conditions, the specific gravity of gas relative to air (relative density),  $S_g$ , is simply determined by,

$$S_g = M_g / M_{\text{air}} \quad (1.4)$$

where,  $M_{\text{air}}$  is the molecular weight (molar mass) of air, equal to 28.96 kg/kgmol.

Due to intermolecular forces real gases do not behave ideally, particularly at elevated pressures. Eq.(1.3) is extended to real systems by including a compressibility factor,  $Z$ , as,

$$Pv = ZRT \quad (1.5)$$

The compressibility factor can be determined from various theoretical-empirical equations of state (Chapter 4), or determined from a generalised chart for gases as shown in Figure 1.8. Note that the compressibility factor depends only on the ratio of temperature to critical temperature (absolute), the *reduced temperature*,  $T_r$ , and the ratio of pressure to critical pressure, the *reduced pressure*,  $P_r$ .

The above approach is based on a very important concept, known as the *corresponding states principle*, which states that substances behave similarly when they are at the same relative proximity to their critical points. This implies that all substances behave similarly at their critical points, hence, should have equal critical compressibility factor,  $Z_c$ ,

$$Z_c = \frac{P_c v_c}{RT_c} \quad (1.6)$$

The real value of critical compressibility factor, however, is not the same for all compounds (Table A.1 in Appendix A). The compressibility chart, however, provides reliable estimates particularly for supercritical gases and at low pressure conditions. Charts relating the compressibility factor to the reduced pressure and temperature, similar to Figure 1.8, but specific to compounds such as methane, ethane, propane, have been produced to improve the accuracy of predicted values [10].

Application of the corresponding states principle to the vapour pressure of pure compounds, follows a similar trend. The logarithm of vapour pressure of pure compounds approximately varies linearly with the reciprocal of temperature as shown in Figure 1.3. It can be expressed, therefore, as

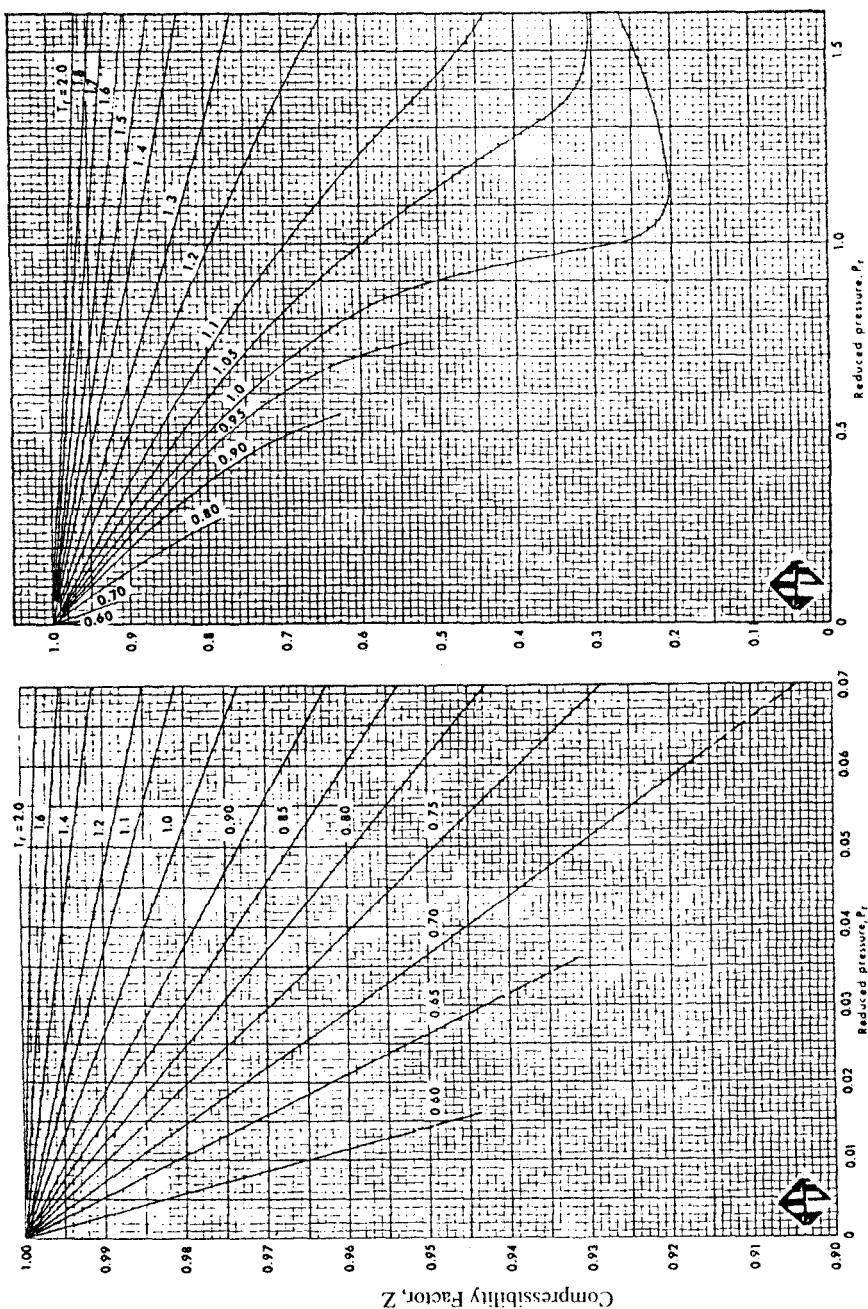


Figure 1.8. Compressibility chart for low pressure gases. GPA Copyright. Reproduced from [9] with permission.

$$\log(P^s/P_c) = \zeta_1 - \frac{\zeta_2}{(T/T_c)} \quad (1.7)$$

where  $P^s$  is the vapour pressure and  $\zeta_1$  and  $\zeta_2$  are constants for each substance.

At the critical point  $P^s/P_c = T/T_c = 1$ , hence  $\zeta_1 = \zeta_2$  and,

$$\log(P_r^s) = \zeta_1 \left(1 - \frac{1}{T_r}\right) \quad (1.8)$$

If the corresponding states principle were exact, the vapour pressure curves of all the compounds, plotted in the reduced form, should have the same slope, that is equal  $\zeta_1$ , falling on the same line. In practice, this does not occur.

The deviation of models based on the two parameter corresponding states principle is due to differences in molecular structures of various compounds, resulting in different intermolecular forces. The inclusion of a third parameter, additional to the reduced temperature and pressure, which concurs to the molecular structure should improve the reliability of the corresponding states principle.

Pitzer [11] noticed that the reduced vapour pressure curves of simple spherical molecules, such as argon, krypton and xenon, indeed lie on the same curve with a reduced vapour pressure of 0.1 at the reduced temperature of 0.7. Hence, for other substances he selected the deviation of the reduced vapour pressure curve from that of spherical molecules at  $T_r=0.7$  as the third parameter of the corresponding states principle, and introduced the acentric factor, as,

$$\omega = -\log(P^s/P_c)_{(at\ T_r=0.7)} - 1.0 \quad (1.9)$$

The above definition gives an acentric factor of zero for simple spherical molecules, and positive values for other compounds except hydrogen and helium. The acentric factor generally increases with increasing size of homologue hydrocarbons. The values of acentric factor for some compounds are given in Table A.1 in Appendix A.

The acentric factor has been widely accepted as the third parameter in generating generalised correlations, based on the corresponding states principle, particularly those related to fluid phase equilibria. For example, the vapour pressure of pure compounds can be reliably estimated using the Lee and Kesler [12] correlation which is based on the three parameter corresponding states,

$$P^s/P_c = \exp(f^{(0)} + \omega f^{(1)}) \quad (1.10)$$

where,  $f^{(0)}$ , and  $f^{(1)}$  are functions of the reduced temperature,

$$f^{(0)} = 5.92714 - 6.09648/(T_r) - 1.28862 \ln(T_r) + 0.16934(T_r)^6$$

$$f^{(1)} = 15.2518 - 15.6875/(T_r) - 13.4721 \ln(T_r) + 0.43577(T_r)^6$$

### Example 1.1.

Calculate the vapour pressure of normal hexane at 355.15 K, using:

(a) the Cox chart, (b) the Lee-Kesler equation.

*Solution:*

(a) From Figure 1.3, at  $T=355.15\text{ K}$  ( $179.6^\circ\text{F}$ ), the vapour pressure is read equal to  $0.15\text{ MPa}$  ( $21\text{ psia}$ ).

(b) The critical properties of normal hexane are read from Table A.1 in Appendix A, and used in Eq.(1.10) to calculate the vapour pressure as follows:

$T_c, \text{K}$	$P_c, \text{MPa}$	$\omega$	$T_r$	$f^{(a)}$	$f^{(b)}$	$P^s, \text{MPa}$
507.6	3.025	0.3013	0.69966	-2.306192	-2.306921	<b>0.1504</b>

The use of critical compressibility factor as the third parameter for developing generalised correlations to predict volumetric data has also proved successful. An example is the Rackett equation [13] for the saturated molar volume of pure compounds,

$$v^s/v_c = Z_c^{(1-T_r)^{2/3}} \quad (1.11)$$

where  $v^s$ , and  $v_c$  are the saturated liquid and critical molar volumes, respectively. A more reliable estimation of the liquid molar volume is expected from the modification of the Rackett equation by Spencer and Danner [14], where the critical compressibility factor has been replaced by the parameter  $Z_{RA}$ , known as the Rackett compressibility factor,

$$v^s = (RT_c/P_c)Z_{RA}^{[1+(1-T_r)^{2/3}]} \quad (1.12)$$

The values of  $Z_{RA}$  for some substances [15] are given in Table A.1 in Appendix A. For other compounds, it can be estimated from the Yamada-Gunn correlation [16]:

$$Z_{RA} = 0.29056 - 0.08775\omega \quad (1.13)$$

The application of acentric factor and critical compressibility factor in developing generalised correlations will be described further, particularly in Chapter 4 dealing with equations of state.

#### Example 1.2.

Calculate the density of saturated normal butane liquid at  $393\text{ K}$ , using the Rackett equation. A cylinder contains  $1\text{ kg}$  of saturated liquid butane at  $393\text{ K}$ . What is the volume of liquid butane remaining in the cylinder after consuming  $0.5\text{ kg}$  of butane?

*Solution:*

Reading the critical properties of normal butane from Table A.1 in Appendix A and substituting them in Eq.(1.12), at  $393\text{ K}$ , we obtain:

$M, \text{kg/kgmol}$	$T_c, \text{K}$	$P_c, \text{MPa}$	$Z_{RA}$	$T_r$	$v^s, \text{m}^3/\text{mol}$	Density, $\text{kg/m}^3$
58.123	425.12	3.796	0.2730	0.92444	0.13665	425.3

where the density,  $\rho^s$ , has been calculated as,

$$\rho^s = M/v^s$$

The volume of cylinder, containing  $1\text{ kg}$  of the saturated liquid butane, is:

$$V = m/\rho = 1/425.3 = 0.002351\text{ m}^3$$

The cylinder pressure remains constant, equal to the normal butane vapour pressure, as long as the mixture remains two phases at 393 K. The vapour pressure can be calculated from the Lee-Kesler equation, Eq.(1.10), similar to that in Example 1.1, which results in:

$$P^*=2.2160 \text{ MPa, at } 393 \text{ K.}$$

The vapour density at the above conditions can be calculated from Eq.(1.7). The compressibility factor,  $Z$ , is read from Figure 1.8, at prevailing reduced values of:  $P_r=P/P_c=2.216/3.796=0.5838$  and  $T_r=0.9244$ , to be  $Z=0.67$ . The universal gas constant is read, from Table A.3 in Appendix A, to be  $0.0083144 \text{ MPa}\cdot\text{m}^3/(\text{K}\cdot\text{kgmol})$ .

Hence,

$$v = ZRT/P = 1.003 \text{ m}^3/\text{kgmol, and the vapour density is ,}$$

$$\rho^v = M/v^v = 58.123/1.003 = 57.95 \text{ kg/m}^3$$

The mass balance results in,

$$m = V^l \rho^l + V^v \rho^v$$

$$0.5 = V^l \times 425.3 + (0.002351 - V^l) \times 57.95$$

$$\text{Liquid butane volume, } V^l = 0.0009902 \text{ m}^3$$

### Multicomponent Mixture

The phase behaviour of a multi-component system is more elaborate than that of a pure compound. The complexity generally compounds as components with widely different structures and molecular sizes comprise the system. Reservoir fluids are mainly composed of hydrocarbons with similar structures. Their phase behaviour, therefore, is not generally highly complex.

The phase behaviour of a binary system, although relatively simple, is very much similar to a real multi-component reservoir fluid. It is, therefore, an appropriate substitute for explaining the qualitative behaviour of reservoir hydrocarbon mixtures.

The phase rule indicates that in a binary vapour-liquid system, both the temperature and the pressure are independent variables. The pressure-temperature diagram of a binary mixture is schematically shown in Figure 1.9. The phase envelope, inside which the two phases coexist, is bounded by the bubble point and dew point curves. The two curves meet at the critical point (C), where all differences between the two phases vanish and the phases become indistinguishable. Note that the two phases can coexist at some conditions above the critical point. The highest pressure (B) and the highest temperature (D) on the phase envelope are called the *cricondenbar* and the *cricondentherm*, respectively.

The pressure-volume diagram of a binary mixture is schematically shown in Figure 1.10. Note that the system pressure decreases during an isothermal expansion between its bubble and dew points, contrary to that for a pure compound.

The phase diagram of a mixture is determined by its composition. Figure 1.11 shows the phase diagram of ethane-heptane system. The critical temperature of different mixtures lies between the critical temperatures of the two pure compounds. The critical pressure, however, exceeds the values of both components as pure, in most cases. The locus of critical points is shown by the dashed line in Figures 1.11. The greater the difference between the critical

points of the two components, the higher the mixture critical pressure can rise as shown in Figure 1.12. No binary mixture can exist as a two-phase system outside the region bounded by the locus of critical points.

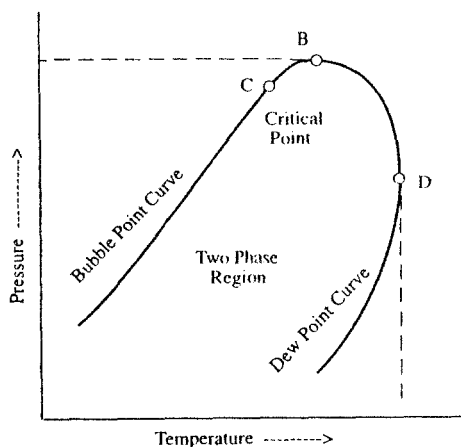


Figure 1.9. Schematic pressure-temperature diagram of a binary mixture.

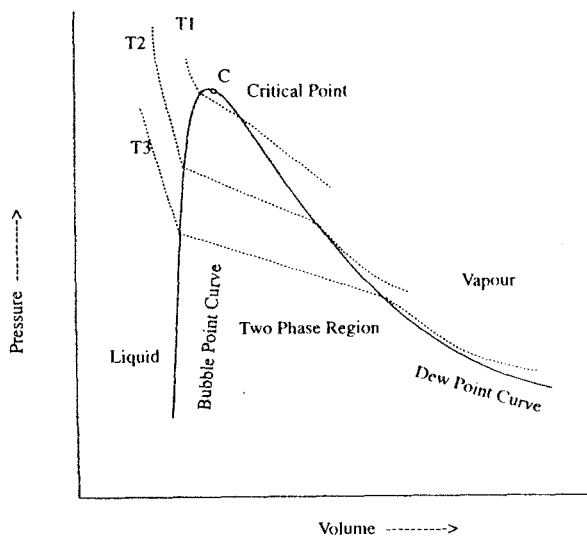


Figure 1.10. Pressure-volume diagram of binary mixtures.

The corresponding states principle, described for pure substances, is also used for multicomponent systems. Pseudo critical values are used, however, instead of true critical properties in applying fluid models developed for pure substances, such as those in Figure 1.8, and Eq.(1.11).

Pseudo critical properties of a mixture are calculated by applying a mixing rule to the critical properties of its constituents. A number of mixing rules have been proposed, but molar averaging, also known as Kay's mixing rule, is the most common rule,

$${}_p\theta_c = \sum_i z_i \theta_{ci} \quad (1.14)$$

where  $z_i$  is the mole fraction,  ${}_p\theta_c$  is any pseudo critical property, such as temperature, pressure, and volume, and  $\theta_{ci}$  is the critical property of component  $i$ . Properties scaled relative to the pseudo critical values are referred to as pseudo reduced properties, such as,

$$\text{pseudo reduced temperature: } {}_pT_r = T/{}_pT_c \quad (1.15)$$

and,

$$\text{pseudo reduced pressure: } {}_pP_r = P/{}_pP_c \quad (1.16)$$

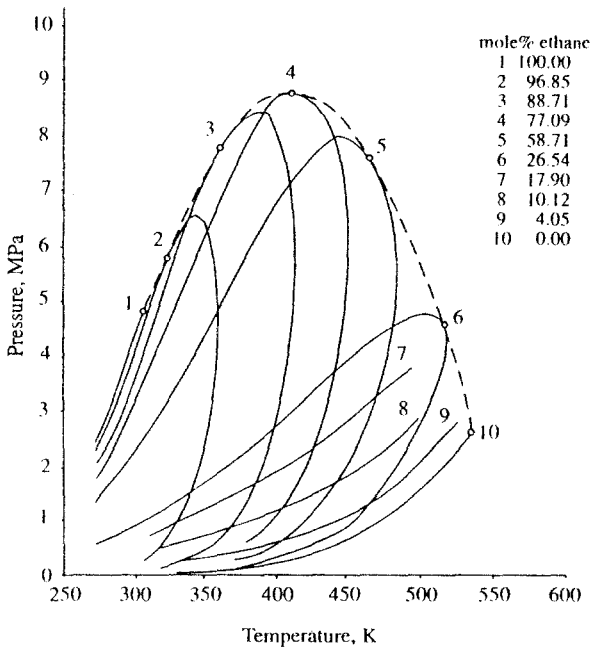


Figure 1.11. Phase diagram of ethane - normal heptane. McGraw-Hill Companies Copyright. Reproduced from [8] with permission.

The true critical properties, however, are different from the pseudo values calculated by averaging. The true critical pressure often shows the highest deviation from the pseudo value, as evidenced in Figure 1.12. The prediction of true critical properties will be described in Section 5.3.

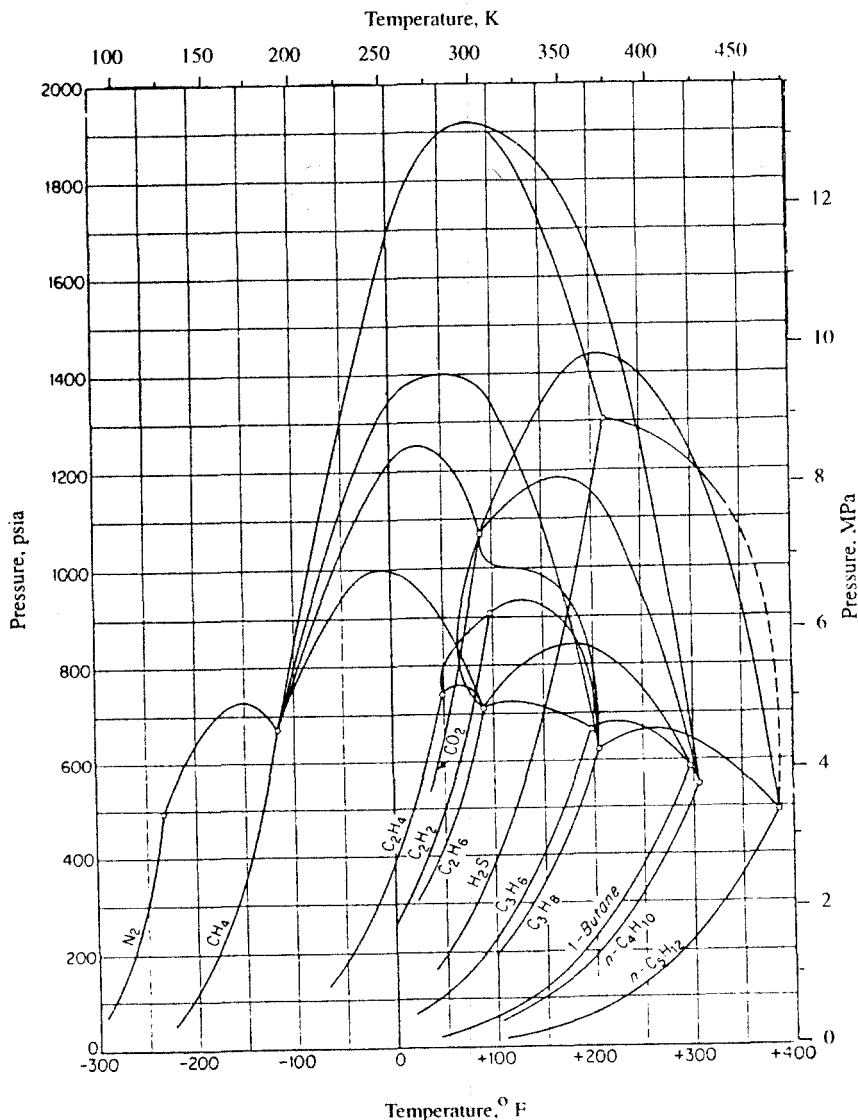


Figure 1.12. Critical loci for binary mixtures. McGraw-Hill Companies Copyright. Reproduced from [8] with permission.



A typical phase diagram of multi-component system at constant composition is shown in Figure 1.13. Vapour and liquid phases coexist at any pressure-temperature conditions within the phase envelope. The liquid/mixture volumetric ratios are shown by the constant quality lines. Note that the distance between iso-volume or quality lines decreases as the critical point is approached. Small pressure or temperature changes at a region near the critical point cause major phase changes.

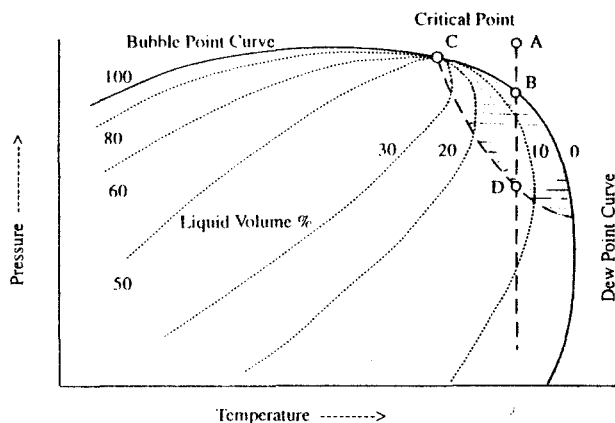


Figure 1.13. Phase diagram of a multicomponent mixture.

An isothermal reduction of pressure for a vapour-like fluid, Point A, forms the first drop of liquid at the dew point, Point B. Further reduction of pressure will result in further condensation, as indicated by the quality lines. This phenomenon is known as the *retrograde condensation*. The condensation will cease at some point, Point D, and the condensed phase will revaporise by further reduction of pressure. The shaded region of the phase diagram, where pressure reduction results in condensation is referred to as the retrograde region. Note that the above behaviour occurs only if the gas temperature lies between the critical temperature and the cricondentherm. Figure 1.13 shows that there are two dew point pressures at any temperature for retrograde gases. The upper dew point is sometimes called the retrograde dew point. The lower dew point is of little practical significance for most gas condensate fluids.

The relative position of the critical point to the cricondentherm and the cricondenbar on the phase envelope can lead to other retrograde phenomena. Figure 1.14 shows that an isobaric increase of temperature from point 1 to point 2 results in condensation. This behaviour, which can also be called retrograde condensation, is of little interest in reservoir operations. It indicates, however, that raising the temperature of a high pressure rich gas may not be a proper procedure to avoid condensation in fluid handling. The vaporisation of liquid by isobaric temperature decrease, shown in Figure 1.15, or by isothermal pressure increase is known as retrograde vaporisation.

The vapour-liquid phase diagram of a typical multi-component system, Figure 1.13, describes the behaviour of reservoir fluids in most cases. There are, however, exceptional cases. Weinaug and Bradley [17] observed an unusual behaviour for a naturally occurring hydrocarbon mixture as shown in Figure 1.16. Note that an isothermal reduction of pressure, e.g. at 160°F,

results in an increase of the liquid volume after an initial normal behaviour. A similar behaviour has also been reported [18] for a multicomponent hydrocarbon oil, as shown in Figure 1.17. Note that the gas/liquid volumetric ratio increases initially below the bubble point, as expected. The trend reverses over a limited pressure range, prior to behaving normally again. The calculated gas to liquid ratio in molar term is shown also in Figure 1.17. The ratio increases very gradually over the whole tested pressure range, without any peculiarity. The reason for the apparent disagreement between the two plots, is the change in molar volumes of the two phases.

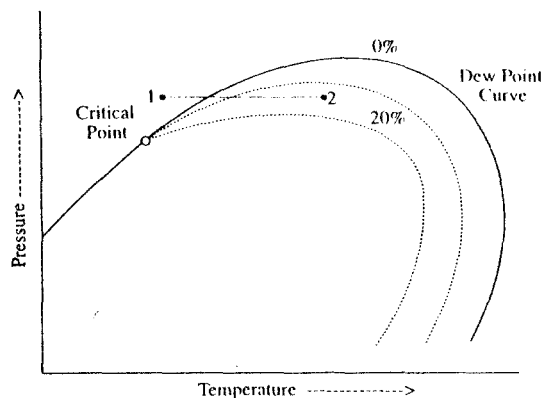


Figure 1.14. Retrograde condensation at constant pressure.

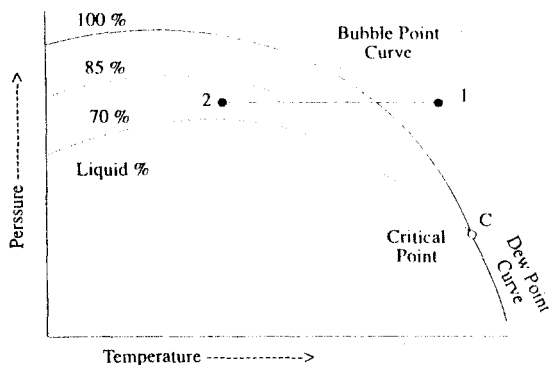


Figure 1.15. Retrograde vaporisation at constant pressure.

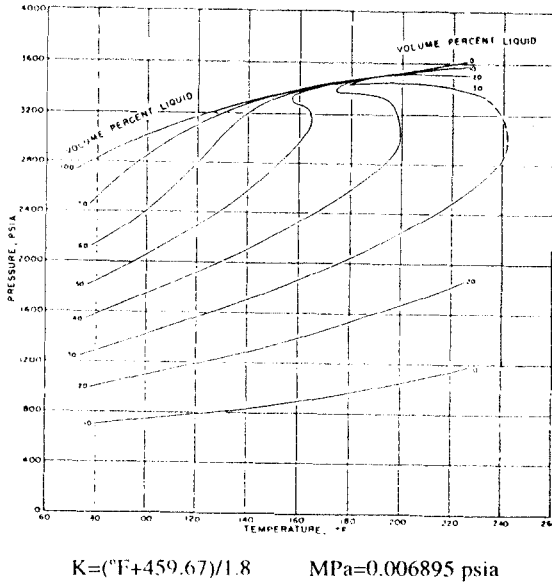


Figure 1.16. Phase diagram of a hydrocarbon mixture. SPE Copyright. Reproduced from [17] with permission.

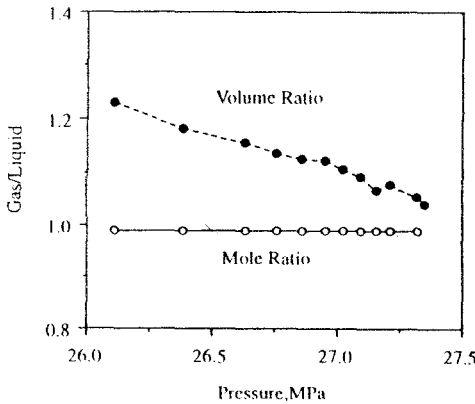


Figure 1.17. Variations of gas to liquid ratio by reducing pressure below bubble point. SPE Copyright. Reproduced from [18] with permission.

A single phase hydrocarbon reservoir fluid may form more than two phases during depletion. Solid, or semi-solid phases, such as asphaltenes can form at some conditions. A high pressure gas, rich in hydrocarbon compounds of different homologous series, may condense two immiscible liquid phases, each rich with one structural type of molecules. Gas mixtures rich in CO<sub>2</sub> or H<sub>2</sub>S at low temperatures can form a rich liquid phase immiscible with the hydrocarbon rich condensate phase.

### 1.3 CLASSIFICATION OF RESERVOIR FLUIDS

The typical phase diagram of a reservoir hydrocarbon system, shown in Figure 1.13, can be used conveniently to describe various types of reservoir fluids. A reservoir contains gas if its temperature is higher than the fluid critical temperature, otherwise it contains oil. The depletion of reservoir will result in retrograde condensation in the reservoir if the reservoir temperature lies between the critical temperature and the cricondentherm, whereas no liquid will form if it is above the cricondentherm. The oil in a reservoir with a temperature close to its critical point is more volatile than that at a lower temperature. A small reduction of pressure below the bubble point, in a reservoir with a temperature just below the fluid critical temperature, may vaporise half the oil volume. It is evident, therefore, that the location of reservoir temperature on the phase diagram can be used to classify reservoir fluids.

The temperature of a reservoir is determined by its depth. The phase behaviour of a reservoir fluid is determined by its composition. Typical compositions of various classes of reservoir hydrocarbon fluids are given in Table 1.2. Critical temperatures of heavy hydrocarbons are higher than those of light compounds. Therefore, the critical temperature of hydrocarbon mixtures predominantly composed of heavy compounds is higher than the normal range of reservoir temperatures, and these fluids behave liquid-like, i.e., oil. Whereas the temperature of a reservoir mainly composed of methane, with a critical temperature of 190.6 K, will be higher than the mixture critical temperature.

Table 1.2.  
Typical compositions of various reservoir fluids.

Component, Mole%	Dry Gas	Gas Condensate	Volatile Oil	Black Oil
N <sub>2</sub>	6.25	0.29	0.12	0.16
CO <sub>2</sub>	2.34	1.72	1.50	0.91
C <sub>1</sub>	81.13	79.14	69.59	36.47
C <sub>2</sub>	7.24	7.48	5.31	9.67
C <sub>3</sub>	2.35	3.29	4.22	6.95
iC <sub>4</sub>	0.22	0.51	0.85	1.44
nC <sub>4</sub>	0.35	1.25	1.76	3.93
iC <sub>5</sub>	0.09	0.36	0.67	1.44
nC <sub>5</sub>	0.03	0.55	1.12	1.41
C <sub>6</sub>		0.61	1.22	4.33
C <sub>7+</sub>		4.80	16.64	33.29

When the reservoir pressure falls below the saturation point, the phase diagram of the original reservoir fluid is no longer valid. Gas and liquid phases are produced at a ratio different to that in the original combined state, resulting in changes of the overall composition. The gravitational segregation of the two phases with different densities will also inhibit the contact between the phases, hence preventing the achievement of equilibrium throughout the reservoir.

In a hydrocarbon reservoir consisting of a gas cap and an oil column two separate phase diagrams, one for each phase can be considered. The two phases are both saturated, with the saturation pressures ideally equal to the reservoir pressure at the gas-oil contact as shown in Figure 1.18. Hence, when a saturated gas reservoir is discovered, an oil column below it is generally expected. Similarly a saturated oil reservoir may strongly indicate the presence of a gas cap.

Petroleum reservoir fluids can be classified according to various criteria. Although identifying a fluid as gas or oil is adequate in most phase behaviour studies, it is more common to classify the fluid in accordance to its volumetric behaviour at the reservoir and surface conditions. This approach yields a few set of formulations, known as material balance equations, which can be appropriately applied to each class of fluid for reservoir studies.

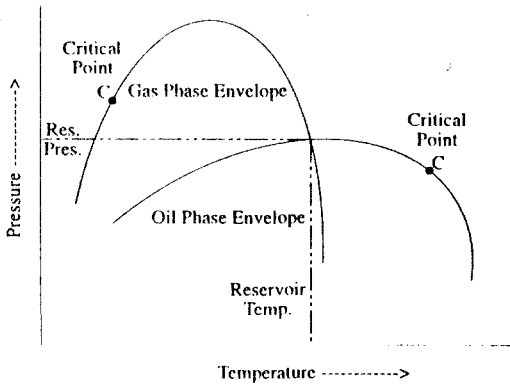


Figure 1.18. Phase diagrams of segregated oil and gas phases in the vicinity of gas/oil contact.

The reservoir fluid is produced and measured at the surface as the stock tank oil and gas at standard conditions, as shown schematically in Figure 1.19. As the material balance equations relate the produced fluids to those in the reservoir, the initial producing gas to liquid volumetric ratio is considered as the most important indicator of the class of a reservoir fluid. The gas to oil ratio, GOR, is most commonly defined as the number of cubic feet of the associated gas produced at standard conditions per barrel of stock tank oil in the Field units. For gas-condensate fluids, where the produced fluid is predominantly gas, the inverse of the above definition, known as the condensate to gas ratio, CGR, is often used.

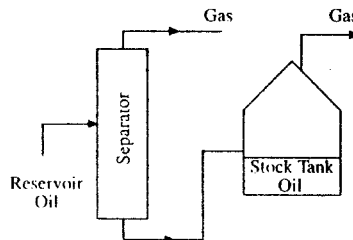


Figure 1.19. Schematic diagram of stabilising produced oil as stock tank oil and gas at standard conditions.

The stock tank oil gravity generally varies significantly for different classes of fluids, hence it can also be used as an indicator. The gravity is expressed as API degrees in field units,

$$^{\circ}\text{API} = (141.5/S_o) - 131.5 \quad (1.17)$$

where  $S_o$  is the stock tank oil specific gravity, or relative density, to water at 60 °F (288 K).

The concentration of heavy fraction,  $C_{7+}$ , in reservoir fluid correlates reasonably well with GOR. As the stock tank oil is mostly comprised of this fraction, it can also be used as an indicator of the reservoir fluid type. Figure 1.20 shows that an initial producing GOR of 570 v/v (3,200 SCF/STB) and 12.5 mole%  $C_{7+}$  are valid boundaries for gas and oil systems [19], as shown in Figure 1.20.

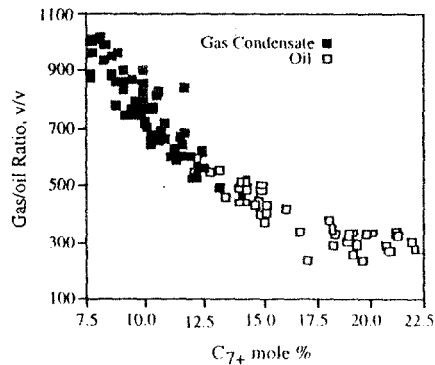


Figure 1.20.  $C_{7+}$ -GOR relation for typical oil and gas condensate fluids. Courtesy of Hart Publication Inc. Reproduced from [19].

The most common method of identifying petroleum reservoir fluids is to classify them as dry gas, wet gas, gas condensate (retrograde gas), volatile oil and black oil.

### Dry Gas

Dry gases are predominantly composed of methane and non-hydrocarbons such as nitrogen and carbon dioxide. Figure 1.21 shows the phase diagram of a dry gas. The phase envelope is relatively tight and mostly located below the ambient temperature. Note that the gas remains single phase from the reservoir to the separator conditions. Water, however, may condense at the surface conditions due to the gas cooling. PVT tests in the laboratory are limited to the gas compressibility measurement.

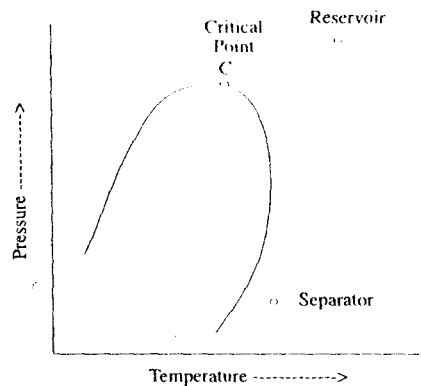


Figure 1.21. Phase diagram of dry gas.

### Wet Gas

A wet gas is mainly composed of methane and other light components with its phase envelope located entirely over a temperature range below that of the reservoir. A wet gas, therefore, will not drop-out condensate in the reservoir during depletion, (1) to (2), as shown in Figure 1.22. The separator conditions lie, however, within the phase envelope, producing some condensate at the surface. Gas fields in the Southern North Sea are good examples of this type of reservoirs.

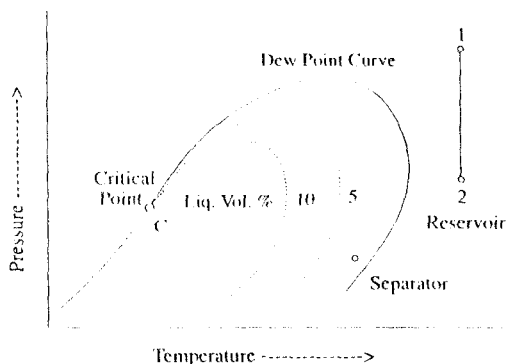


Figure 1.22. Phase diagram of wet gas.

As no condensate is formed in the reservoir, material balance equations for a dry gas are equally suitable for a wet gas. The only PVT test required at the reservoir conditions is the gas compressibility measurement. Separator tests are generally conducted to determine the amount and properties of the condensed phase at the surface conditions.

A wet gas reservoir is commonly produced by simple blow-down, similar to a dry gas, as no condensate is formed in the reservoir. Producing gas to condensate ratios are typically above 10,000 v/v (50,000 SCF/STB) and remain constant during the entire life of the reservoir. The condensate colour is usually water-white with a low specific gravity which remains unchanged during the reservoir production life.

### Gas Condensate

A typical gas condensate phase diagram is shown in Figure 1.23. The presence of heavy hydrocarbons expands the phase envelope relative to a wet gas, hence, the reservoir temperature lies between the critical point and the cricondentherm. The gas will drop-out liquid by retrograde condensation in the reservoir, when the pressure falls below the dew point, from (1) to (2) in Figure 1.23. Further condensation from the produced gas also occurs at separator conditions due to cooling.

The amount of potentially condensable hydrocarbons in the reservoir increases with the richness of the gas, as heavy compounds shift the critical temperature towards the reservoir temperature. Whereas a gas with a cricondentherm near the reservoir temperature will behave very much like a wet gas. Gas to liquid ratios range between 570 to 30,000 v/v (3,200 to 150,000 SCF/STB)[19]. For practical purposes a gas condensate reservoir with a GOR of above 10,000 v/v (50,000 SCF/STB) can be treated as a wet gas. The producing GOR initially remains constant until the reservoir pressure falls below the dew point and increases thereafter. For gases with GOR of above 20,000 v/v (100,000 SCF/STB), the condensation in reservoir

has negligible effect on the properties of produced gas, but it can noticeably reduce the gas recovery rate.

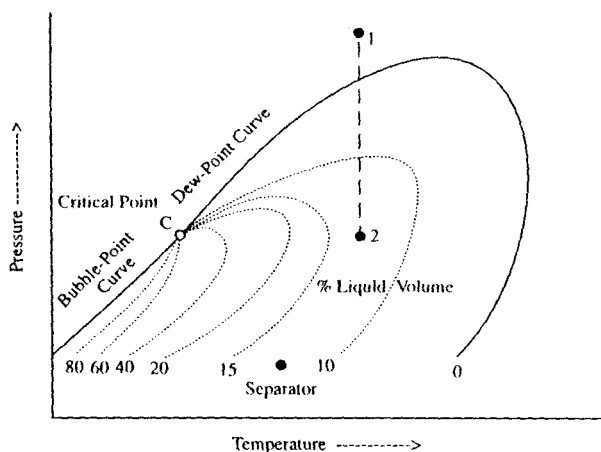


Figure 1.23. Phase diagram of gas condensate.

The concentration of heptanes plus is generally less than 12.5 mole% in gas condensate fluids as fluids containing more than that almost always behave liquid like in the reservoir. Exceptional cases with condensates as high as 15.5 mole% and oils with as low as 10 mole% of heptanes plus have also been reported [20].

The condensate colour can be water-white or dark. Dark condensates usually have relatively high specific gravity and are associated with high dew point gases. Condensate specific gravity ranges between 0.74 and 0.82 (60 to 40 °API), although values as high as 0.88 (as low as 29 °API) have been reported [21].

Material balance equations developed for dry gases can be used for a gas condensate reservoir as long as its pressure remains above the dew point. A compositional material balance method should be used below the dew point. It is commonly assumed that the condensate formed in reservoir remains immobile due to its low saturation, and is mostly non-recoverable. Recent results [22], however, have indicated that the condensate can flow even at very low saturations.

Figure 1.24 shows a common characteristic of gas condensate fluids. The liquid drop-out reaches a maximum and then decreases by vaporisation during pressure depletion. This behaviour may imply that when the reservoir pressure decreases sufficiently, the condensate will be recovered by revaporisation. However, by the time the pressure falls below the dew point, the original phase diagram is no longer valid as the system composition changes during the production period. PVT tests simulating reservoir conditions will be described in Chapter 2.

Condensation and loss of valuable compounds in reservoirs could be avoided by maintaining the reservoir pressure above the fluid dew point by gas recycling. In practice, however, this is



very seldom carried out because of shortage of gas. Partial pressure maintenance is more common to minimise the losses of condensate, where it is economical to do so. In recycling operations intermediate and heavy compounds of the produced fluid are separated and the remaining lean gas is injected back into the reservoir. The recycled gas which is predominantly methane, not only reduces the pressure decline rate, but also makes the system leaner. The removal of a sufficient amount of heavy hydrocarbons from a gas condensate reservoir may ideally shift the entire phase diagram farther away from the reservoir temperature to form a wet gas reservoir. The reservoir can then be produced by blow down without much loss of valuable liquid. But the lack of complete displacement and mixing of the recycled gas with the in-situ fluid limits the success of the above operation. However, the liquid loss by depletion will be lower after recycling.

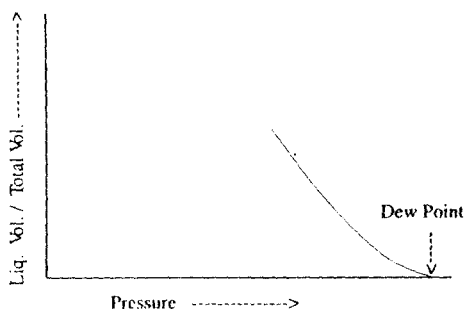


Figure 1.24. Liquid drop-out behaviour of gas condensate.

### Volatile Oil

Volatile oils have many common features with gas condensates, but as they contain more heavy compounds they behave liquid-like at reservoir conditions. The phase envelope of a volatile oil is relatively wider than that of a gas condensate, with a higher critical temperature due to its larger concentration of heavy compounds. A typical volatile oil phase diagram is shown in Figure 1.25. The reservoir temperature is near the critical temperature, hence, volatile oils are referred to as near-critical oils. Note that iso-volume lines are tighter and closer near the bubble point curve. A small reduction of pressure below the bubble point vaporises a significant fraction of the oil, hence the name "volatile oil". Separator conditions typically lie on low quality (iso-volume) lines.

Initial producing gas to liquid ratios (GOR) of volatile oils typically range between about 310 and 570 v/v (1,750-3,200 SCF/STB) [5]. The GOR increases when the reservoir pressure falls below the bubble point during the reservoir life. The stock tank liquid is coloured with a specific gravity usually lower than 0.82 (higher than 40 °API). The specific gravity decreases during production below the bubble point, particularly at high producing GOR, as a significant liquid production is due to condensation of the rich associated gases.

Saturation pressures of volatile oils are high. Gases produced below the bubble point, therefore, are quite rich and behave as retrograde gases. The amount of liquid recovered from the gas constitutes a significant portion of the total oil recovery. Compositional material balance methods should be applied generally to study volatile oil reservoirs.

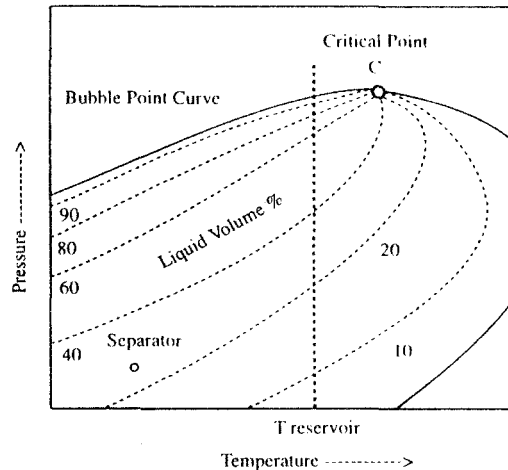


Figure 1.25. Phase diagram of a volatile oil.

### Black Oil

Black oils, or ordinary oils, are the most common type of oil reserves. The name does not reflect the colour, but to distinguish it from the volatile oil. The oil is generally composed of more than about 20 mole% heptanes and heavier compounds. Its phase envelope, therefore, is the widest of all types of reservoir fluids, with its critical temperature well above the reservoir temperature. A typical black oil phase diagram is shown in Figure 1.26. The quality lines are broadly spaced at reservoir conditions with separator conditions lying on relatively high quality lines. The above characteristics lead to a low shrinkage of oil when produced.

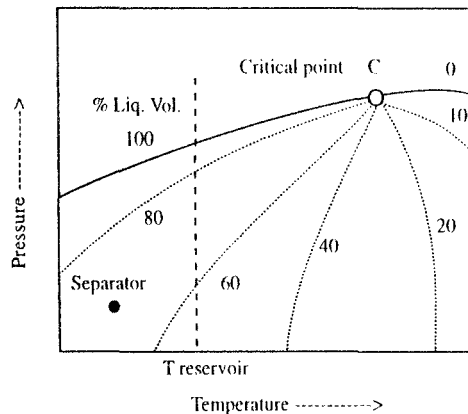


Figure 1.26. Phase diagram of a black oil.

Initial producing GOR's are less than about 310 v/v (1,750 SCF/STB). The GOR may decrease initially when the reservoir pressure falls below the bubble point, as the evolved gas remains immobile at very low saturations. The GOR, then increases sharply as the gas to oil mobility ratio within the reservoir varies inversely with the viscosity ratio, which is typically of two orders of magnitude. In fractured reservoirs, however, where the fractures provide a good conduit for the gas to rise by gravity, the GOR declines throughout the producing life of the field, as long as the pressure keeps declining and no gas coning takes place. The stock tank liquid is dark with a specific gravity higher than 0.80 (lower than 45 °API) [20]. The variation of the specific gravity is relatively small, in comparison with that of volatile oils, during the reservoir production life.

The saturation pressure of black oils is relatively low. Contribution of heavy compounds present in evolved gases in reservoir to the total liquid recovery is not significant. Hence, volumetric material balance equations, which treat the reservoir fluid as a two component system, i.e., oil and gas, may be sufficient for some reservoir studies. Indeed, as there is no definite boundary between black and volatile oils, the acceptability of results obtained by the volumetric method is a practical criterion for distinguishing between the two types.

#### 1.4. REFERENCES

1. Hunt, J.A.M: "Petroleum Geochemistry and Geology", W.H. Freeman and Co., San Francisco (1979).
2. England, W.A. and Mackenzie, A.S: "Geochemistry of Petroleum Reservoirs", *Geologische Rundschau*, 78, 214-237(1989).
3. Nelson, W.L.: "Petroleum Refinery Engineering", 4th Ed., McGraw-Hill, New York (1958).
4. Institute of Petroleum: "Methods for Analysis and Testing ",The Institute of Petroleum, John Wiley and Sons, New York (1984).
5. McCain, W.D: "The Properties of Petroleum Fluids", 2nd Ed., Pennwell Books, Tulsa (1990).
6. Sachanen, A.N: "The Chemical Constituents of Petroleum", Reinhold Pub. Co. (1945).
7. Larter, S.R., and Aplin, A.C: "Reservoir Geochemistry: Methods, Applications and Opportunities" In: England, W.A. and Cubitt, J. (eds) "The Geochemistry of Reservoirs" Geol. Soc. Publication (1994).
8. Katz, D. et al: " Handbook of Natural Gas Engineering ", McGraw-Hill Book Company (1959).
9. Gas Processors Suppliers Association, ed.: "SI Engineering Data Book", Tulsa, Oklahoma (1980).
10. Brown G.G., Katz D.L., Oberfell G.G. and Alden R.C: "Natural Gasoline and the Volatile Hydrocarbons", NGA of America, Tulsa, (1948).
11. Pitzer, K.S., Lippmann D.Z., Curl, R.F. Jr., Huggins C.M. and Petersen, D.E: "The Volumetric and Thermodynamic Properties of Fluids. II. Compressibility Factors, Vapor Pressure and Entropy of Vaporisation." *J. of the American Chemical Society*, 77, 3433-3440, (July 5, 1955).

12. Lee, B.I. and Kesler, M.G.: "A Generalised Thermodynamics Correlation Based on Three-Parameter Corresponding States", *AIChE J.*, 21 No.4, 510-527 (May, 1975).
13. Rackett, H.G.: "Equation of State for Saturated Liquids", *J. Chem. Eng. Data*, 15 No.4, 514-517, (1973).
14. Spencer, C.F. and Danner, R.P.: "Prediction of Bubble Point Pressure of Mixtures", *J. Chem. Eng. Data*, 18, No.2, 230-234, (1973).
15. Spencer, C.F. and Adler, S.B.: "A Critical Review of Equations for Predicting Saturated Liquid Density", *J. Chem. Eng. Data*, Vol. 23, No. 1, 82-89 (1978).
16. Yamada, T. and Gunn, R.: "Saturated Liquid Molar Volumes: the Rackett Equation", *J. Chem. Eng. Data*, 18 No.2, 234-236 (1973).
17. Weinaug, C.F. and Bradley, H.B.: "Phase Behaviour of a Natural Hydrocarbon System", *Trans. AIME*, 192, 233 (1951).
18. Danesh, A., Xu, D., and Todd A.C.: "An Evaluation of Cubic Equation of State for Phase Behaviour Calculations Near Miscibility Conditions", SPE/DOE 20267, Paper Presented at the Seventh Symposium on Enhanced Oil Recovery, Tulsa, Oklahoma, April 22-25 (1990).
19. McCain Jr, W.D., and Bridges B: "Volatile Oils and Retrograde Gases-What's the Difference?", *Petroleum Engineer International*, 35-36 (Jan., 1994).
20. Moses, P.L.: "Engineering Applications of Phase Behaviour of Crude Oil and Condensate Systems", *JPT*, 715-723 (July, 1986).
21. Kilgren, K.H.: "Phase Behaviour of a High-Pressure Condensate Reservoir Fluid", *JPT*, 1001-1005 (Aug., 1966).
22. Danesh, A., Henderson, G.D. and Peden, J.M.: "Experimental Investigation of Critical Condensate Saturation and its Dependence on Connate Water Saturation", *SPE Res. Eng. Journal*, 336-342 (Aug., 1991).

## 1.5 EXERCISES

1.1. Calculate the vapour pressure of normal decane at 355 K, using:

(a) the Cox chart, (b) the Lee-Kesler equation, (c) a linear relation between the logarithm of vapour pressure and inverse of temperature connecting the normal boiling point and the critical point.

1.2. Plot the vapour pressure vs. temperature for the following compounds on the reduced scales of  $(P/P_c)$  and  $(T/T_c)$ : methane, normal hexane, benzene, normal decane, and eicosane. Suggest a physical property, such as the acentric factor, or critical compressibility factor, as the third parameter in a three-parameter corresponding state model for the vapour pressure

1.3. A cylinder contains 1 kg of saturated liquid butane at 385 K. What will be the cylinder pressure after consuming 950 g of butane.

1.4. A 5 litre cylinder contains 1.5 kg of propane at 393 K. Estimate its pressure. How much propane will be left in the cylinder when the pressure falls by half.

1.5. Estimate the critical temperature and pressure of a mixture composed of 55 mole% ethane and 45 mole% normal heptane.



## 2 PVT TESTS AND CORRELATIONS

Accurate and reliable phase behaviour and volumetric data are essential elements for proper management of petroleum reservoirs. The information is required to evaluate reserves, to develop the optimum recovery plan, and to determine the quantity and quality of produced fluids. Most reservoirs are produced by depletion in which the reservoir pressure declines as fluids are recovered. The reservoir temperature stays practically constant in most recovery methods. The main variable that determines the behaviour of fluids, under reservoir conditions, during depletion is, therefore, the reservoir pressure. Hence, relatively simple tests which simulate recovery processes are conducted by varying the fluid pressure. The main emphasis is on the volumetric data at the reservoir and surface temperatures, hence the name (pressure-volume-temperature) PVT data.

In the simplest approach of predicting the PVT data, the reservoir oil is considered to be composed of two pseudo components, i.e., gas and oil. These pseudo components, are identified by flashing the reservoir fluid at the standard conditions, and characterising the separated gas and oil phases by their specific gravity and molecular weight values. Compositional data on the produced fluids are mainly determined for their applications in hydrocarbon processing.

The prime information from PVT tests are the ratio of phase volume at reservoir conditions to that at surface conditions, and the solubility of gas in oil. The information is generally sufficient in studies of black oil reservoirs, and the approach is referred to as the black oil method. Compositional studies, where detailed information on the fluid constituents are used to estimate fluid properties, are often conducted for gas condensate and volatile oil reservoirs. Only in special cases such as gas injection or miscible displacement the compositional approach is used for black oil reservoirs.

A compositional phase behaviour model, in principle, is capable of predicting all the PVT data, using only the composition of the original reservoir fluid. The models, however, are required to be evaluated and tuned against the measured PVT data prior to being used in reservoir studies with confidence, as will be discussed in Section 9.3. The compositional method, which can provide reliable information rapidly using advanced computers, is becoming more popular. Empirical correlations and charts, mainly reminiscence of days when hand calculations were the norm to predict PVT data, however, are still used.

In this chapter phase behaviour considerations related to the sampling of reservoir fluids are described. The most commonly conducted PVT tests are detailed next. Selected empirical correlations, to estimate PVT properties from limited field data, are also given. These correlations have been generated over years, using laboratory data. They were mostly developed originally in graphical forms. In this book the mathematical expressions of the correlations are presented in preference to their original graphical forms. The correlations use field units, and are reported as such in this chapter. A conversion table is given in Table A.5 in Appendix A.

## 2.1 FLUID SAMPLING

Reservoir fluids should be sampled as early as possible during the production life of a reservoir. When the reservoir pressure falls below the initial saturation pressure the hydrocarbon phase forms two phases of gas and liquid. The mole ratio of the two phases flowing into the well is not generally equal to that formed in the reservoir. Hence, the collection of a representative sample becomes a highly demanding, and in many cases an impossible task.

The sample can be collected either as a single phase at the bottom hole, when the pressure is still above the saturation value, or at the surface. The bottom hole samples are usually collected during formation testing, prior to production. Surface sampling is conducted on producing wells either at the well head, as a sample representing the producing mixture stream, or as separated gas and liquid samples out of the separator(s).

As long as the reservoir pressure has never been below its saturation pressure, and a single phase sample flows into the sampling bottle, the chance of collecting a representative sample is high. Producing fluids, however, are generally at two-phase conditions. Hence, the sampling procedure should aim at collecting both phases at such conditions where the subsequent recombination provides the original reservoir fluid. Sampling procedures have been discussed in details [1-5]. First, it should be ensured that representative fluids are flowing out of the formation, by properly conditioning the well before sampling. Next, fluid samples should be collected from all co-existing phases, and recombined at the producing ratio. Sampling from an oil reservoir, particularly an undersaturated one, is relatively a much simpler task than that from a gas condensate reservoir.

### Well Preparation

In oil sampling, if the well bottom hole pressure has fallen below the oil bubble point, the well is generally conditioned by a period of reduced flow, followed by a shut-in period of about 1-3 days. This lowers the pressure draw-down and raises the oil pressure, possibly above its original bubble point. The method is not suitable for a gas condensate reservoir. The pressure build-up may vaporise the condensed liquid in the reservoir into the gas phase to form a gas condensate even richer than the original fluid. Unless, the condensation was limited only within a small zone around the wellbore, allowing the disposal of the richer gas over a reasonable period of conditioning, the collected sample will not be representative.

The formation of condensate initiates around the wellbore, where the pressure is at its lowest value in the reservoir, Figure 2.1. The two-phase region gradually grows into the reservoir



bulk as the pressure declines during production. As the depletion rate is low, the advancement of the two-phase region is slow. Hence, it is reasonable to assume a quasi-steady-state condition around the producer, with minimal changes over a short period. At such conditions, the overall composition of the gas-condensate mixture flowing into the wellbore is the same as that flowing into the two-phase region, as no condensate accumulation occurs in that region. Hence the reservoir outflow, if collected properly, should represent the original single phase reservoir fluid.

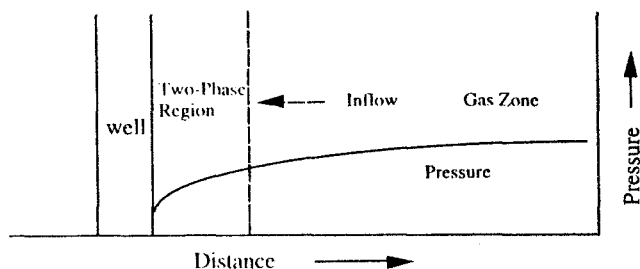


Figure 2.1. Schematic diagram of two-phase flow around wellbore.

The validity of the above assumption, can be evaluated by numerical simulation of the flow near the wellbore using a compositional model [6], as will be described in Section 9.5. Sudden changes of rate will disturb the steady state conditions and the outflow composition. It is advisable, therefore, to maintain the rate prior to sampling.

Producing the gas at a low rate to maintain the bottom hole pressure above the dew point can ensure the flow of single phase gas into the wellbore. It is imperative, however, that the well flow rate remains above a minimum value for the continual up-lifting of the condensate formed within the wellbore.

The liquid phase is transferred up the well partly as entrained drops in the gas core, and partly as a film on the wall by the gas shearing effect (annular-mist flow). The transfer of liquid between the film and droplets is a continuous process along the liquid path up the well. When the gas flow rate is reduced below a minimum value, the energy transferred to the liquid by the flowing gas may not be sufficient to carry the liquid. Then, the direction of liquid flow in the film is reversed and the entrained drops fall back, both resulting in well flooding. The minimum flow rate for continual removal of liquids (condensate or water) by the flowing gas can be determined by analysing the film flow and the entrained drop movement. Turner et al. [7] developed a mechanistic two-phase flow model and applied it to the removal of liquid in a gas well. The authors compared the minimum gas velocity required to lift the entrained liquid with that for transferring the film upward, and concluded that the former was the controlling limit.

The major forces which determine the velocity of a liquid drop are the downward gravity, and the upward gas drag. The gravity force is determined by the size of the drop and the liquid-gas density difference, whereas the drag force is dominated by the gas velocity and the physical properties of the two phases. An increase in the gas velocity increases the ratio of the drag force to the gravity force. Turner et al. balanced the two forces and derived the following relation for the minimum gas velocity to unload the well,

$$\bar{v}_{gm} = 2.67 \sigma^{1/4} (\rho_o - \rho_g)^{1/4} / \rho_g^{1/2} \quad (2.1)$$

where  $\bar{v}_{gm}$  is the minimum gas velocity, m/s,  $\sigma$  is the gas-condensate interfacial tension, mN/m, and  $\rho_o$  and  $\rho_g$  are the oil and gas density, kg/m<sup>3</sup>, respectively, all at the well head conditions. Turner et al.[7] used the following average values in the above equation ,

Condensate density :	721 kg/m <sup>3</sup> (45 lb/ft <sup>3</sup> )
Gas-condensate interfacial tension:	20 mN/m
Gas specific gravity:	0.6
Gas temperature:	322 K (120°F)

and proposed the following equation,

$$\bar{v}_{gm} = 1.49 \left( \frac{100 - P}{P^2} \right)^{1/4} \quad (2.2)$$

where P is the wellhead pressure in MPa. The minimum gas velocity can be converted to the gas production rate, knowing the tubing inside diameter and estimating the gas compressibility factor, Section 2.3.2

### Sample Collection

Surface samples are commonly collected from test separators. The oil (condensate) and gas samples must be collected as single phase fluids. The production rate of each phase should be monitored over an extended period to ensure a steady and stable flow. The separator temperature and pressure, along with the producing gas/liquid volumetric ratio are reported to the PVT laboratory. The information is used to evaluate the integrity of collected samples received in the laboratory, and to use in the recombination process.

The condensate carry over by gas in a separator can significantly distort the measured condensate to gas ratio. The effect can be serious for lean gas condensate systems. An alternative surface sampling method is the collection of flowing phases in the tubing at the well head. A narrow tube, with the inlet facing the flow direction, is inserted in the centre of the tubing. A two phase sample, consisting of the gas and entrained droplets, is collected through the narrow tubing into the sampling bottle. The sample flowing is collected with a fluid velocity in the tube equal to the average fluid velocity in the tubing. This is to avoid preferential collection of gas or condensate because of their different densities and momentum changes due to changes in the fluid velocity. The method, known as the iso-kinetic sampling [8], relies on the assumption that the condensate is homogeneously distributed in the tubing flow. The homogeneity can be improved by inserting a mixing section ahead of the sampling tube.

Samples received in the laboratory are evaluated for their integrity, primarily by measuring the opening pressure and comparing it with the reported sampling conditions. As the collected samples are saturated fluids, they often form two phases in the sampling bottle due to cooling. The pressure of collected liquid samples are often lowered purposely below the saturation pressure to form two phases for safety reasons, to avoid excessive pressure during transportation in case they are exposed to high temperature. Any leakage from a sampling bottle containing a gas-liquid mixture will change the sample composition. A lower opening pressure does not necessarily indicate a fluid loss, as it could be due to the thermal contraction. This may be examined by heating the bottle to the sampling temperature. A phase behaviour model can also be used afterwards, when the fluid composition and PVT data are known, to estimate the expected opening pressure, and to adjust the fluid composition if a fluid loss was indicated [9]. Further information on the use of phase behaviour models to evaluate and improve collected samples are given in Section 9.5.

Separator samples are recombined in the laboratory according to the reported gas/liquid ratio recorded in the field during sampling. When flow meters with coefficients depending on the

fluid properties are used to measure the production rates, the reported ratio should be adjusted using the values measured in the laboratory, instead of the approximate data used in the field.

When the reservoir fluid is saturated and the compositional grading within the reservoir is minimal, see section 5.4., the pressure-temperature at the gas oil contact identifies the saturation point. Hence, the measured saturation pressure of the recombined fluid should be compared with the field data. For a recombined oil sample, a match between the two values indicates a representative sample. When the oil bubble point is known with confidence, it is advisable to adjust the recombination ratio to achieve it, instead of relying on the reported gas/liquid ratio. The recombined sample is expected to reasonably represent the reservoir oil, as the bubble point is sensitive to the gas/liquid ratio and increases with it.

A match between the measured dew point in the laboratory and the field reported value is desirable, but does not necessarily indicate a representative gas sample. The dew point may increase or decrease by increasing the condensate/gas ratio, depending on the sample. Figure 2.2 shows the liquid drop-out behaviour of a North Sea gas condensate at the reservoir temperature prepared at different recombination ratios. Note the marked difference between the condensate drop-out behaviour of different fluids, whilst their dew points are almost the same. It is quite evident that matching the dew point is not a reliable method for recombining a gas condensate sample. The use of phase behaviour models to evaluate and improve the fluid recombination ratio is described in Section 9.5.

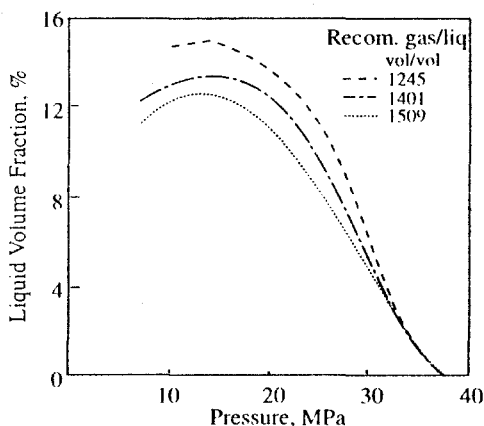


Figure 2.2. Variations of condensate drop-out with adjusting recombination ratio.

Samples tested in PVT laboratories are fluids collected at the bottom hole or at the surface, and are not necessarily the same as those present within pores of a reservoir. Significant differences in composition between produced fluids and core extracts have been reported [10,11]. Core extracts often indicate a richer fluid in heavy fractions particularly surface active materials. This can be mostly due to the adsorption of polar compounds onto the core surface, which make them immobile during conventional sampling. The effect of adsorbed material on the multi-phase flow behaviour of oil-water in pores is probably more significant than on the PVT properties in most cases. The samples collected from a flowing stream, however, may not be suitable for special phase behaviour studies such as asphaltene deposition. A small amount of unrecovered adsorbed material is not expected to significantly change the saturation pressure and the gas-liquid volumetric fraction of an oil sample, but the effect on the gas

condensate dew point may be very marked as its phase behaviour is dominated by the concentration and properties of the heavy end.

When different samples are properly collected from the same reservoir, the samples are generally expected to be similar. In saturated reservoirs containing an oil column and a gas cap, the samples collected from each zone are expected to be reasonably in equilibrium with each other at the reservoir pressure and temperature. Compositional grading due to gravity and temperature gradient may however exist in a reservoir, with samples collected from different depths being vastly different. The compositional grading can be very severe, resulting in a column of fluid changing from a gas at the top to oil at the bottom, without any phase boundary. Phase behaviour models can be used to evaluate the extent of compositional changes due to grading in order to evaluate the samples. The compositional grading is described in Section 5.4.

## 2.2 PVT TESTS

PVT tests are designed to study and quantify the phase behaviour and properties of a reservoir fluid at simulated recovery conditions. The effect of interstitial water on the phase behaviour of hydrocarbon fluids are ignored in most tests, and the PVT tests are conducted in the absence of water. The majority of tests are depletion experiments, where the pressure of the single phase test fluid is lowered in successive steps either by increasing the fluid volume or removing part of it. The reduction of pressure results in formation of a second phase, except in dry and wet gas mixtures.

The formation of a new phase is generally accompanied by some degree of supersaturation. The pressure of an oil sample can be lowered below its bubble point gradually whilst maintaining it as a single phase fluid. Such a fluid, however, is in metastable conditions, as further described in Section 5.2.

Tests conducted in laboratories on liquid samples contained in a porous medium, have resulted in some degree of supersaturation, with values as high as 5 MPa [12,13]. High supersaturation has been observed in tests where the pressure has been lowered rapidly. In a reservoir where the pressure decline is slow, significant supersaturation is not expected [14].

Surface forces can be significant in tight pores, affecting the phase behaviour of fluids. Capillary condensation, where gas condenses in pores due to fluid-solid interaction, is a well known phenomenon [15,16]. The effect would be of significance in pores typically less than  $10^{-8}$ m. Gas condensate reservoirs are generally assumed to be water wet, with tight cavities filled with water. Hence, the capillary condensation effect may be ignored. Tests in a cell packed with 30-40 mesh bead have resulted in the same dew point as that measured conventionally in an equilibrium cell [17].

The above review suggests that the assumption of equilibrium between the phases in reservoirs, and neglecting the surface effect on fluid equilibria, is a reasonable engineering approach. This has greatly simplified experimental and theoretical studies of the phase behaviour of reservoir fluids. In conventional PVT tests, the fluids are given ample time and agitation in equilibrium cells, to approach equilibrium. At certain conditions, such as in rapid pressure build-up near the wellbore or in high pressure gradient flow, the deviation from equilibrium may become significant. Should non-equilibrium information become important to field operation, such as bubble nucleation in water invaded reservoirs during depletion [18,19], especial tests could be designed to generate the required data.

An important test on all reservoir fluid samples is the determination of the fluid composition. The most common method of *compositional analysis* of high pressure fluids is to flash a relatively large volume of the fluid sample at the atmospheric pressure to form generally two stabilised phases of gas and liquid. The two phases are individually analysed and then

numerically recombined, using the ratio of the separated phases. The gas and liquid phases are commonly analysed by gas chromatography and distillation, respectively. Details on compositional analysis and various techniques applied to characterise reservoir fluids are described in Section 6.1.

The above analysis approach, known as the "blow-down" method, can give reliable results for large samples of high pressure liquids, where the error involved in measurement of the two phase ratio is relatively small. For small samples or high pressure gases, where the condensate volume formed by blow down is low, the technique is unreliable.

*Full stream sampling*, where a small amount of high pressure fluid is directly injected into a gas chromatograph, has received some attention as an alternative to the blow down method in the past decade. The basic principle is to flow the high pressure test fluid through a special valve to trap a small quantity of the sample in the valve for injection. The trapped high pressure fluid is then exposed to hot flow of a carrier gas, which vaporises the sample into a gas chromatograph column for analysis. The valve itself is generally heated up to help eluting heavy constituents. The sampling valve with the fluid trapped inside may be physically removed from the sampling port and transferred to a gas chromatograph [20,21], or just isolated from the equilibrium cell, and then heated up. The vaporised sample is directed to a gas chromatograph through a heated transfer line [22].

The idea of full stream (*direct*) sampling is quite interesting, particularly for the compositional analysis of equilibrated phases in PVT tests, where the removal of a large quantity of a phase will disturb the overall composition. Certain operational problems, however, have prevented its wide application. Although the sample volume actually injected into the gas chromatograph is very small, of the order of microlitres, a large amount of the fluid is required to fill up the sampling loop system, which includes a number of isolating valves, and most of it is lost when the sampling valve is removed or heated. All the lines have to be cleaned and evacuated after each injection to repeat the analysis. The introduction of a high pressure fluid into an evacuated line generally results in phase changes, hence, a large volume of the fluid has to be passed through the loop to ensure a representative sample for injection.

The large loss of the test fluid during the sampling and the problems associated with the transfer lines and isolating valves have been avoided by designing special vapour-liquid cells in which the sampling valve can be installed directly onto the equilibrium cell [23]. A small volume of the test fluid enters the valve, locked in, and the valve is detached from the cell for the fluid to be transferred to a gas chromatograph. The test fluid does not flow through the above valves and, as the exposure of a high pressure fluid to an empty cavity is generally accompanied by some phase changes, removal of a representative sample cannot be ensured. Repeated sampling is not an easy or a safe operation in the above arrangement, as the sampling valve has to be assembled to a high pressure cell kept in a constant temperature environment.

The heavy constituents of the sample in all the above methods may be partially retained between the sampling valve and the gas chromatograph column and, as the injection volume is very small, the concentration of these constituents could be highly under-estimated. Therefore, the methods have been more successful in the analysis of gases than liquids that have very heavy constituents.

A direct sampling technique in which a small sample of a high pressure fluid in a narrow tube is pinched by an auxiliary fluid (solvent) at the test pressure has been proposed [24] to avoid the above problems. The flow of the solvent directs the slim slug of the sample into a high pressure valve which has replaced the injector of a gas chromatograph. When the uncontaminated sample reaches the valve, it is then exposed to flow of a hot carrier gas which injects the sample into the gas chromatograph. The preference of the direct compositional analysis, as conducted by the above method, to the conventional blow-down technique, will be further discussed in Section 2.2.4.

### 2.2.1 Dry Gas

As no phase change occurs for a dry gas, its composition remains unchanged during production. The only PVT test required for a dry gas is the pressure-volume relation at the reservoir temperature.

A volume of the gas is loaded into a cell maintained at the reservoir temperature. The gas volume is measured at the reservoir pressure and a number of pressure intervals below it. The specific gravity of the gas, relative to air at 60 °F (288 K)<sup>8</sup> is determined by measuring the weight of a known volume of the gas, or by using the gas molecular weight knowing its composition.

The gas specific gravity,  $S_g$ , and the molecular weight,  $M_g$ , are related by the following relation, as gases almost obey the ideal gas law at the atmospheric pressure .

$$S_g = M_g / M_{air} = M_g / 28.96 \quad (1.4)$$

The volume of gas at reservoir conditions required to produce one unit volume of gas at the standard conditions is defined as the gas formation volume factor,  $B_g$ ,

$$B_g = \frac{V_R}{V_{sc}} = Z \left( \frac{T}{T_{sc}} \right) \left( \frac{P_{sc}}{P} \right) \quad (2.3)$$

where  $V_R$  is the gas volume at reservoir conditions of pressure  $P$  and temperature  $T$  with the gas compressibility factor of  $Z$ , and  $V_{sc}$  is the gas volume at the standard conditions of pressure  $P_{sc}$  and temperature  $T_{sc}$  equal to 0.1 MPa (1 bar) or 14.7 psia, and 288 K or (-159.67+60) °R, respectively. Substituting the values at the above standard conditions in Eq.(2.3),

$$B_g = 3.47 \times 10^{-4} Z (T/P) \quad (2.4)$$

where  $T$  and  $P$  are in K and MPa, respectively.

$$(B_g = 0.0283 Z (T/P) \quad T : ^\circ R, P: \text{psia})$$

The measured pressure-volume data are employed to calculate the compressibility factor,  $Z$ , and the gas formation volume factor  $B_g$ , using Eqs.(2.4-2.6)

$$Z = \frac{PV}{nRT} \quad (2.5)$$

where  $n$  is the total number of moles, calculated by dividing the total mass,  $m$ , loaded in the cell by the gas molecular weight,

$$Z = PM(V/m)/(RT) \quad (2.6)$$

$(V/m)$  is the specific volume, and is equal to the inverse of the density,  $\rho$ . The value of  $R$  for different units are given in Table A.3 in Appendix A.

The isothermal compressibility coefficient of the gas,  $C_g$ , can be calculated also using the variation of  $Z$  with pressure,

<sup>8</sup> Various standards for temperature, including 60 °F, 0 °C, 15 °C and 288 K, have been adopted. The most common values are 60 °F, in Field Units, and 288 K, in SI absolute scale, which are used in this book interchangeably.

$$C_g = -\frac{1}{V} \left( \frac{\partial V}{\partial P} \right)_T = \frac{1}{P} - \frac{1}{Z} \left( \frac{\partial Z}{\partial P} \right)_T \quad (2.7)$$

A typical gas formation volume factor plot is shown in Figure 2.3.

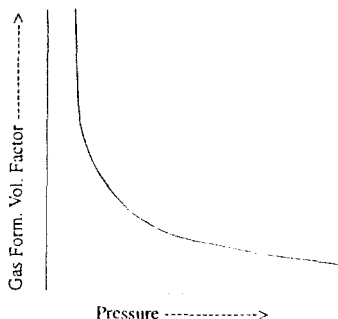


Figure 2.3. Schematic variations of gas formation volume factor with pressure.

#### Example 2.1.

100 cm<sup>3</sup> of a gas at the reservoir conditions of 380.3 K (225 °F) and 20.79 MPa (3000 psig) was brought to the standard conditions, where the gas occupied a volume of 18,533 cm<sup>3</sup>. The produced gas specific gravity is 0.650. Calculate B<sub>g</sub>, Z, and the gas density at the reservoir conditions.

*Solution:*

Writing Eq.(2.3), we obtain,

$$B_g = V_R/V_s = (100/18533) = Z(380.3/288.15) \times (0.1/20.79) = 0.005396$$

$$Z = 0.8500$$

The gas molecular weight is calculated from Eq.(1.4),

$$M_g = S_g M_{sm} = 0.650 \times 28.96 = 18.82$$

Using Eq.(2.6), the density is calculated, as,

$$\rho = (PM)/(ZRT) = (20.79 \times 18.82) / (0.8500 \times 0.0083144 \times 380.3) = 146 \text{ kg/m}^3$$

where the universal gas constant is taken from Table A.3 in Appendix A.

### 2.2.2 Wet Gas

PVT tests for a wet gas at reservoir conditions are similar to those for a dry gas. Separate tests are, however, needed to determine the amount and properties of produced fluids at the surface conditions. The formation volume factor of a wet gas, B<sub>wg</sub>, is defined as the volume of the gas at reservoir conditions required to produce one unit volume of the stock-tank liquid. In the field units, the gas volume is usually expressed in terms of barrel in the above definition.

A more practical definition of the gas formation volume factor, currently used in reservoir simulators, is the number of barrels of reservoir gas (including the liquids dissolved in it) at reservoir pressure and temperature, per cubic foot of the dry gas produced from it at standard conditions. This is analogous to oil formation volume factor, described in Section 2.2.3.

The molecular weight and specific gravity of produced condensate are measured in the laboratory. The molecular weight is commonly determined by dissolving the liquid in benzene and measuring the depression of its freezing point. The liquid density, hence, its specific gravity relative to water, is determined by a pycnometer or an oscillating tube densitometer.

The apparent specific gravity (or relative density to air) of the reservoir gas is determined by calculating the reservoir gas molecular weight, and using Eq.(1.4). Having measured the mass and molecular weight of produced gas and oil (condensate) phases, the mixture molecular weight can be determined by material balance calculations,

$$M_m = (m_g + m_o) / \left( \frac{m_g}{M_g} + \frac{m_o}{M_o} \right) \quad (2.8)$$

Empirical correlations, Section 2.3.2, are also available to estimate the reservoir gas specific gravity from production data when some of the separators data, particularly in multi-stage separation, are missing.

### 2.2.3 Black Oil

The phase transition of an undersaturated oil during depletion is depicted in Figure 2.4. Away from the wellbore, zone A, where the pressure is still above the bubble point, the oil expands as a single phase liquid. The pressure in zone B is just below the bubble point and the volume of the evolved gas is too small to allow its mobilisation. In zone C, the evolved gas flows towards the producer, but segregates from the oil due to gravity and surface forces. In the wellbore, the two phases are considered to flow together due to the dominant mixing. It is assumed that the phases are at the equilibrium throughout as the pressure depletion rate is quite low. The above reservoir processes are simulated in the laboratory by the equilibrium flash vaporisation test, for zones A, and B, and the differential vaporisation test, for zone C. All the reservoir tests are conducted at the reservoir temperature. A series of flash tests at selected temperatures are also conducted to simulate the surface conditions.

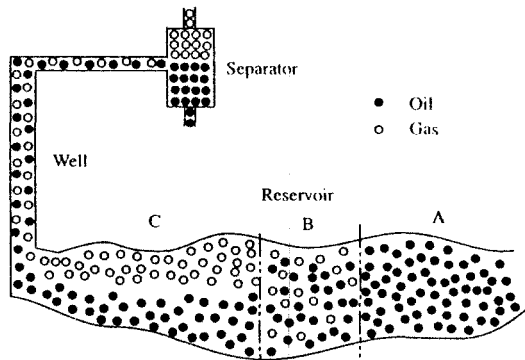


Figure 2.4. Phase transition in an under saturated oil reservoir.



In the flash vaporisation test a sample of oil is placed in an equilibrium cell at a pressure equal or greater than the initial reservoir pressure. The pressure is reduced incrementally by expanding the fluid volume. The total volume,  $V_t$ , is measured at each pressure stage. The test is also known as flash liberation, flash expansion, constant composition expansion, and pressure volume relation.

Typical PVT test data as reported by a laboratory is given in Table 2.1. The pressure-volume data of the black oil, with composition as in Table 2.1A, is shown in Table 2.1B. The data is also plotted in Figure 2.5. The pressure at which the slope of pressure-volume line changes is the bubble-point pressure. The slope of the curve above the bubble point, Table 2.1C, is a measure of the isothermal compressibility of oil,

$$C_o = -\frac{1}{V} \left( \frac{\partial V}{\partial P} \right)_T \quad (2.9)$$

where  $C_o$  is the oil isothermal compressibility coefficient. The system volume is commonly reported by the *relative volume*, defined as the ratio of the total volume to the initial bubble point volume.

Table 2.1.

Selected tables from a typical PVT report on black oil. Reproduced from Core Laboratories Inc. report with permission.

Fluid : Good Oil
Reservoir Temperature: 378 K (220 °F)
Original Reservoir Pressure: 283.7 bar, (4100 psig)

Table 2.1A.

Composition of reservoir oil.

Component	Mol %	Weight %
Hydrogen Sulfide	Nil	Nil
Carbon Dioxide	0.91	0.43
Nitrogen	0.16	0.05
Methane	36.47	6.24
Ethane	9.67	3.10
Propane	6.95	3.27
i Butane	1.44	0.89
n-Butane	3.93	2.44
i Pentane	1.44	1.11
n-Pentane	1.41	1.09
Hexanes	4.33	3.97
Heptanes plus	33.29	77.41

Heptanes plus properties at sc. Density=851.5 kg/m<sup>3</sup> (34.5 °API), Molecular Weight=218

The laboratory data is often evaluated, smoothed, and extrapolated by a dimensionless function  $Y$ , defined as,

$$Y = [(P_b - P)/P] / [(V_t - V_b)/V_b] \quad (2.10)$$

where the subscript b, refers to the hubble point conditions. A plot of  $Y$  function versus pressure should yield a line either straight or very slightly curved.

Table 2.1B

Pressure volume relation at reservoir temperature, 220 °F (378 K).

Pressure		Relative Volume	Y Function	Density
psig	bar	(1)		g/cm <sup>3</sup>
5000	345.7	0.9639		0.6808
4500	311.3	0.9702		0.6763
4100	283.7	0.9756		0.6726
4000	276.8	0.9770		0.6716
3500	242.3	0.9845		0.6665
3000	207.8	0.9928		0.6609
2900	200.9	0.9946		0.6597
2800	194.1	0.9964		0.6585
2700	187.2	0.9984		0.6572
2620	181.6	1.0000		0.6562
2605	180.6	1.0021		
2591	179.6	1.0042		
2516	174.5	1.0157		
2401	166.5	1.0353		
2253	156.3	1.0648	2.497	
2090	145.1	1.1041	2.418	
1897	131.8	1.1627	2.325	
1698	118.1	1.2415	2.229	
1477	102.8	1.3611	2.122	
1292	90.1	1.5000	2.033	
1040	72.7	1.7839	1.911	
830	58.2	2.1709	1.810	
640	45.1	2.7603	1.718	
472	33.5	3.6961	1.637	

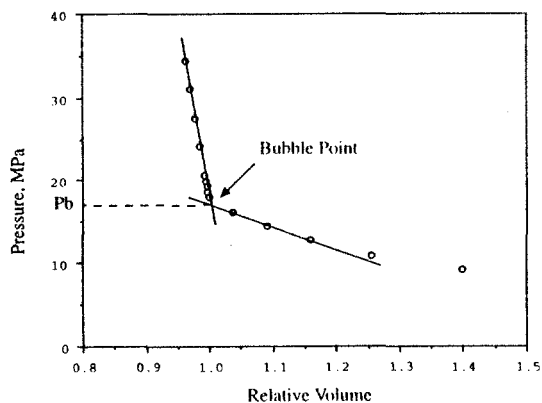
(1) Relative Volume:  $V/V_{sat}$  is barrels at indicated pressure per barrel at saturation pressure.

Figure 2.5. Pressure-volume plot of Good Oil at 220 °F (378 K) to determine its bubble point pressure.

Table 2.1C  
Volumetric data of oil.

1.	Saturation pressure (bubble-point pressure):	2620 psig @ 220°F (181.6 bar @ 378 K)
2.	Density at saturation pressure:	40.97 lb/ft <sup>3</sup> (656.2 kg/m <sup>3</sup> )
3.	Thermal expansion of reservoir oil @ 5000 psig (345.7 bar) =	$\frac{V @ 220^{\circ}\text{F} (378\text{K})}{V @ 60^{\circ}\text{F} (288\text{K})} = 1.08795$
4.	Compressibility of saturated oil @ reservoir temperature: (Vol/Vol)/psi ((Vol/Vol)/bar):	
	From 5000 psig (345.7 bar) to 4000 psig (276.8 bar)=	$13.5 \times 10^{-6}$ ( $1.96 \times 10^{-4}$ )
	From 4000 psig (276.8 bar) to 3000 psig (207.8 bar)=	$15.9 \times 10^{-6}$ ( $2.30 \times 10^{-4}$ )
	From 3000 psig (207.8 bar) to 2620 psig (181.6 bar)=	$18.7 \times 10^{-6}$ ( $2.72 \times 10^{-4}$ )

In the *differential vaporisation* or liberation test, the oil pressure is reduced below its bubble point at the reservoir temperature by expanding the system volume. All the evolved gas is then expelled at constant pressure by reducing the equilibrium cell volume, Figure 2.6. This procedure is repeated in 10-15 pressure stages down to the atmospheric pressure. At each stage the remaining oil volume, the expelled gas volume at the cell and standard conditions, and the gas specific gravity are measured. The gas formation volume factor is calculated from Eq.(2.3), but often divided by 5.61 converting it to barrel per standard cubic foot (bbl/SCF) when using the Field units as the gas volume at reservoir conditions is to be added to the oil volume in barrel to determine the total hydrocarbon volume.

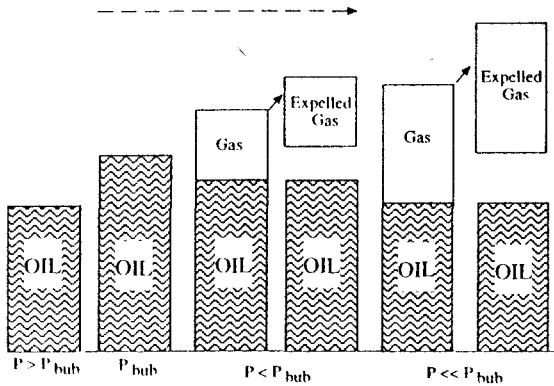


Figure 2.6. Schematic diagram of differential vaporisation (liberation) test.

The compressibility factor of produced gas is determined from,

$$Z = (V P T_{sc}) / (V_{sc} P_{sc} T) \quad (2.11)$$

where  $V$  is the expelled gas volume at the test pressure  $P$ , and temperature  $T$ , both in absolute scales.

The remaining oil volume, at the atmospheric pressure, at the end of the test is converted to the volume at 60°F (288 K), commonly using an average thermal contraction coefficient of 0.00046 (v/v)/°F, and referred to as the residual oil. The volume of oil at each stage is reported by the relative oil volume,  $B_{od}$ , defined as the ratio of oil volume/residual volume, Table 2.1D.

The total volume of gas evolved at each pressure and all previous pressure stages, at the standard conditions (sc), is calculated and converted to the volume at the test pressure, using the prevailing  $B_g$ , and is added to the oil volume to obtain the total (two-phase) volume. The total volume is reported by the relative total volume,  $B_{td}$ , defined as the ratio of total volume/residual volume. The evolved gas is reported by the solution gas to oil ratio,  $R_{sd}$ , defined as the difference between the total gas evolved at the atmospheric pressure (the final stage), and each pressure stage in SCF, divided by the residual oil volume, in barrels, as shown in Table 2.1D.

The differential relative volume data can be evaluated and smoothed by plotting  $\log(1-B_{td}/B_{tdh})$  versus  $\log(P_b-P)$ . The relation is expected to be linear.

Table 2.1D  
Differential vaporisation (liberation) test results.

Pressure		Solution Gas/Oil Ratio (1)		Relative Oil Volume (2)	Relative Total Volume (3)	Oil Density	Compress. Factor	Gas Format. Volume Factor (4)	Incremental Gas Gravity
psig	bar	SCF/bbl	vol/vol			g/cm <sup>3</sup>			
2620	181.6	854	152	1.600	1.600	0.6562			
2350	163.0	763	136	1.554	1.665	0.6655	0.846	0.00685	0.825
2100	145.8	684	122	1.515	1.748	0.6731	0.851	0.00771	0.818
1850	128.6	612	109	1.479	1.859	0.6808	0.859	0.00882	0.797
1600	111.3	544	97	1.445	2.016	0.6889	0.872	0.01031	0.791
1350	94.1	479	85	1.412	2.244	0.6969	0.887	0.01245	0.794
1100	76.8	416	74	1.382	2.593	0.7044	0.903	0.01552	0.809
850	59.6	354	63	1.351	3.169	0.7121	0.922	0.02042	0.831
600	42.4	292	52	1.320	4.254	0.7198	0.941	0.02931	0.881
350	25.1	223	40	1.283	6.975	0.7291	0.965	0.05065	0.988
159	12.0	157	28	1.244	14.693	0.7382	0.984	0.10834	1.213
0	1.0	0	0	1.075		0.7892			2.039

Gravity of residual oil = 35.1°API @ 60°F

- (1) Volume of gas at the standard conditions per volume of residual oil.
- (2) Volume of oil at indicated pressure and temperature per volume of residual oil at the standard conditions.
- (3) Volume of oil plus liberated gas at indicated pressure and temperature per volume of residual oil at the standard conditions.
- (4) Volume of gas at indicated pressure and temperature per volume at the standard conditions.

In the *separator test*, a known volume of the reservoir oil at its bubble point is flashed generally in two stages, where the last stage represents the stock tank as shown in Figure 2.7. For oils with high gas in solution, more than one intermediate separator is often used. A field average temperature is selected for the separator tests. The test is usually conducted at a number of separator pressures to determine the optimum field separation conditions, Table 2.1E. The stock tank pressure is always atmospheric.

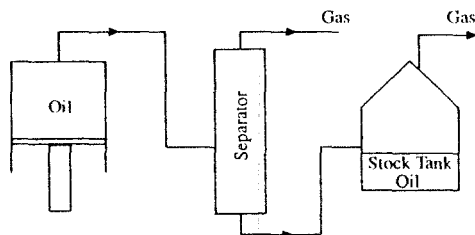


Figure 2.7. Schematic diagram of separator test.

The composition and specific gravity of flashed gases are measured, Table 2.1F. The volume and the specific gravity of the stock tank oil at 60°F (288 K) are also determined. All the volumetric results are reported relative to the stock tank oil volume. The ratio of reservoir oil volume to stock tank oil volume is given by the oil formation volume factor,  $B_o$ , defined as the number of reservoir oil barrels to produce one stock tank barrel of oil in Field units. The evolved gas is reported by the solution gas to oil ratio,  $R_{sb}$  defined as the volumetric ratio of the total gas evolved (sc) to the stock tank oil (SCF/STB in Field units).

The distribution of components between the produced gas and stock tank oil depends on the number of separation stages, and the pressure and temperature of separators. The optimum arrangement is the one which produces more of the stock tank oil, considering also other economic criteria. The stock tank oil generally contains only a trace of methane and an insignificant amount of ethane, regardless of the separation conditions. The concentration of  $C_{7+}$  in the gas phase is very small in most cases. It is the relative distribution of the intermediate fractions between the phases that determines the optimum separation conditions. The effect of separator arrangement becomes more significant for volatile oils.

Table 2.1E.  
Separator test results at 75 °F (297 K).

Separator Pressure		Gas/Oil Ratio (1)	Gas Oil Ratio (2)	Stock Tank Gravity °API @ 60°F	Formation Volume Factor (3)	Separator Volume Factor (4)	Specific Gravity of Flashed Gas
psig	bar	SCF/bbl	SCF/STB		vol/vol	vol/vol	
50 to 0	4.45 0	715 41	737 41	40.5	1.481	1.031 1.007	0.840 1.338
100 to 0	7.9 0	637 91	676 92	40.7	1.474	1.062 1.007	0.786 1.363
200 to 0	14.8 0	542 177	602 178	40.4	1.483	1.112 1.007	0.732 1.329
300 to 0	21.7 0	478 245	549 246	40.1	1.495	1.148 1.007	0.704 1.286

- (1) Gas/Oil Ratio in cubic feet of gas @ 60°F and 14.65 psia per barrel of oil @ indicated pressure and temperature.
- (2) Gas/Oil Ratio in cubic feet of gas @ 60°F and 14.65 psia per barrel of stock tank oil @ 60°F.
- (3) Formation Volume Factor is barrels of saturated oil @ 2620 psig and 220°F per barrel of stock tank oil @ 60°F.
- (4) Separator Oil Volume Factor is barrels of oil @ indicated pressure and temperature per barrel of stock tank oil @ 60°F.

The results of separator tests for the oil given in Table 2.1E are shown in Figure 2.8 [25]. The optimum separator pressure is about 100 psig where the formation volume factor (FVF) is minimum and the maximum stock tank oil is produced. The crude oil gravity, °API, also attains its maximum value at the optimum pressure whereas the gas to oil volumetric ratio (GOR) is at its minimum. All these indicators point to a higher accumulation of intermediate components in the oil phase with a separator pressure of about 100 psig. Operational limitations may, however, dictate other pressure conditions in the field.

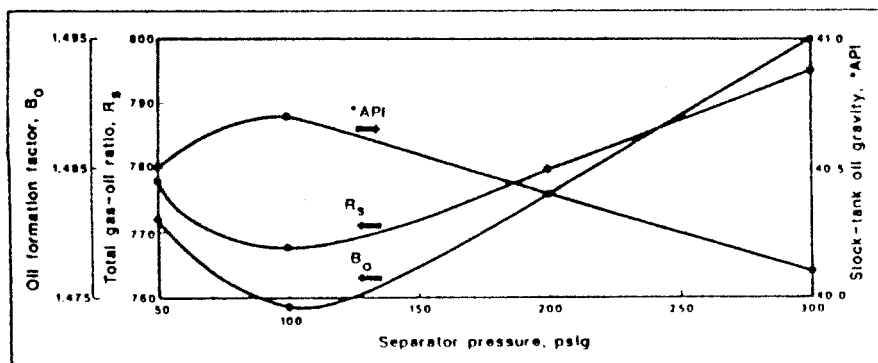


Figure 2.8. variations of oil properties with separator pressure. Reprinted from [25], courtesy of PennWell Publishing Company.

Table 2.1F.

Compositional analysis of separator gas at 100 psig and 75°F (7.9 bar and 297 K).

Component	Mol %	GPM	Mol. W.	Liq. Dens., g/cm <sup>3</sup>
Hydrogen Sulfide	0.00			
Carbon Dioxide	1.67		44.010	.8172
Nitrogen	0.32		28.013	.8086
Methane	71.08		16.043	.2997
Ethane	15.52	4.128	30.070	.3558
Propane	7.36	2.017	44.097	.5065
i-Butane	0.92	.299	58.123	.5623
n-Butane	1.98	.621	58.123	.5834
i-Pentane	0.33	.120	72.150	.6241
n-Pentane	0.26	.094	72.150	.6305
Hexanes	0.27	.104	84	.6850
Heptanes plus	0.29	.128	103	.7370

Calculated gas gravity (air = 1.000) = 0.786

Processing of separator gases to liquefy intermediate hydrocarbons may be economically feasible. The amount of these compounds is expressed in terms of gallons per thousand standard cubic feet of gas or GPM in field units. The GPM of a component is calculated from:

$$(\text{GPM})_i = (1000/380)y_i M_i (7.481/p_i) = 0.315y_i M_i / S_i \quad (2.12)$$

where,  $y_i$  and  $M_i$  are the mole fraction and the molecular weight of the component  $i$  in the produced gas phase, respectively;  $p_i$  and  $S_i$  are the density, lb/ft<sup>3</sup>, and the specific gravity of the component  $i$ , as liquid, at standard conditions (Table A.1 in Appendix A).

#### Example 2.2.

Calculate the liquid n-butane content of the gas produced from the separator of the Good Oil at 100 psig and 75 °F.

#### Solution:

The specific gravity and Molecular weight of normal butane are read from Table A.1 equal to 0.5840 and 58.12, respectively. Hence,

$$\text{GPM} = 0.315 \times 0.0198 \times 58.12 / 0.5840 = 0.621 \text{ gallon of liquid per thousand ft}^3 \text{ (sc) of gas}$$

The oil viscosity is commonly measured by a rolling ball viscometer at the reservoir temperature and a number of pressure steps above and below the bubble point. The pressure below the bubble point is achieved by depleting the viscometer fluid chamber and expelling the gas. The produced gas viscosity is often calculated using a prediction method, Section 2.3.2. The results for the Good Oil are shown in Table 2.1G.

Table 2.1G.  
Viscosity of oil at reservoir temperature.

Pressure		Oil Viscosity	Calculated Gas Viscosity [69]	Oil/Gas Viscosity Ratio
psig	bar	centipoise	centipoise	
5000	345.7	0.450		
4500	311.3	0.434		
4000	276.8	0.418		
3500	242.3	0.401		
3000	207.8	0.385		
2800	194.1	0.379		
2620	181.6	0.373		
2350	163.0	0.394	0.0196	20.1
2100	145.8	0.416	0.0183	22.7
1850	128.6	0.440	0.0173	25.5
1600	111.3	0.469	0.0164	28.7
1350	94.1	0.502	0.0156	32.2
1100	76.8	0.542	0.0149	36.4
850	59.6	0.590	0.0142	41.6
600	42.4	0.653	0.0134	48.6
350	25.1	0.742	0.0125	59.1
159	12.0	0.854	0.0116	73.9
0	1.0	1.29		

1 centipoise = 1 mPa.s

The behaviour of a reservoir oil during depletion is simulated by a combination of all three types of tests discussed above. The reservoir oil remains single phase as long as the pressure is above its bubble point, and its behaviour is simulated by the simple isothermal expansion in the pressure-volume test. The gas evolved just below the bubble point initially remains immobile in pores. Hence, the pressure-volume test (flash vaporisation) almost describes the process, although part of the liquid phase is recovered whilst the gas is immobile. The evolved gas begins to move away from the oil as the gas saturation exceeds a critical value. The process then becomes more similar to the differential vaporisation. A part of the gas, however, remains in contact with the oil contrary to the differential vaporisation test. The flash separation simulates the flow of gas and oil in the well bore and their subsequent separation in the separator.

The values of  $B_{ob}$  and  $R_{sb}$  determined by the separator test represent the original reservoir fluid behaviour at the initial bubble point. Both variables, that is, the oil formation volume factor, and the solution gas to oil ratio, decrease as the pressure falls below the bubble point. The differential liberation test is considered to simulate the evolution of gas and the associated shrinkage of oil in the reservoir below the bubble point. In material balance calculations, the properties of fluid produced at the surface are related to those at reservoir conditions by the results of separator tests, and not those of differential liberation. As  $B_{od}$  and  $R_{sd}$ , determined by differential liberation, at pressures below the initial bubble point are available in PVT reports, these values are often mistaken as the formation volume factor and the solution gas in material balance calculations. The differential liberation test data are based on the residual oil in the reservoir, whereas the volume factor and solution gas data based on the stock tank oil must be used in material balance calculations. The corresponding values by the differential test are almost always higher and can lead to errors of 10 to 20% in the calculated oil in place and

recoverable oil [26]. These confusions could have been avoided mostly if the residual oil had been reported at the reservoir temperature, and separator tests had been conducted on liberated oil samples as well as the original reservoir oil.

The reported data by conventional PVT tests can be combined, however, to determine the required data for reservoir studies [27]. The main assumptions are:

- (1) The gas in solution at reservoir conditions below the bubble point that will be liberated at the surface by flash vaporisation is equal to the difference between the original gas in solution and the liberated gas by differential liberation at the reservoir pressure.
- (2) The relation between the FVF of flashed and differentially liberated samples remains constant over the entire operating pressure.

The oil formation volume factor  $B_o$  at any pressure below the bubble point is then calculated by,

$$B_o = B_{od} \frac{B_{ob}}{B_{odb}} \quad (2.13)$$

where the subscripts b, and d refer to the initial bubble point, and the differential test conditions, respectively.

The adjusted formation factor for the oil in Table 2.1, below the bubble point, is shown in Figure 2.9.

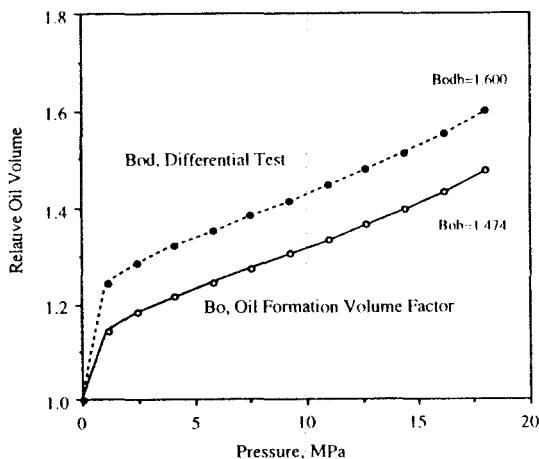


Figure 2.9. Adjustment of oil relative volume factor.

The gas in solution below the bubble point by flash test can also be calculated by combining the differential liberation data and flash test results of the original oil. The gas evolved below the



bubble point is equal to the original gas  $R_{sdlb}$  minus the remaining gas  $R_{sd}$  by the differential process. The unit of this gas is in SCF per barrel of the residual oil. The evolved gas per STB is then equal to,

$$(R_{sdlb} - R_{sd}) \frac{B_{ob}}{B_{oalb}} \quad (2.14)$$

Hence, the gas in solution  $R_s$  is equal to,

$$R_s = R_{sh} - (R_{sdlb} - R_{sd}) \frac{B_{ob}}{B_{oalb}} \quad (2.15)$$

The calculated  $R_s$  for the oil in Table 2.1 is shown in Figure 2.10. The above two assumptions in converting the differential liberation data to the separator data become less reliable as more gas is liberated from the oil. The calculated data are unacceptable near the residual oil conditions. However, as there is very little engineering application for the near residual data, the method is used widely for black oil systems due to its simplicity and acceptable accuracy.

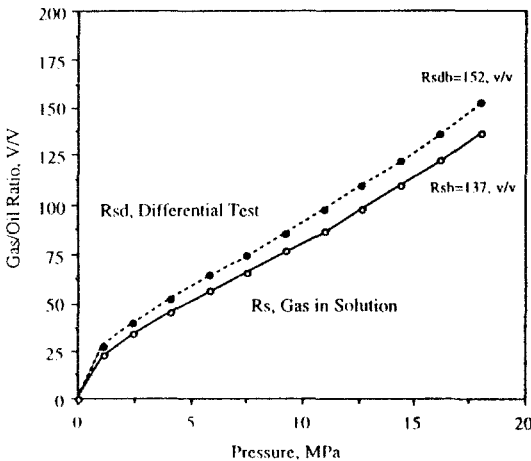


Figure 2.10 Adjustment of gas in solution.

The ratio of total gas and oil volume at the reservoir conditions to the stock tank oil volume is expressed by the total volume factor,  $B_t$ . It may be defined as the reservoir volume occupied by one unit volume of the stock tank oil and its associated gas. Hence,

$$B_t = B_o + B_g (R_{sh} - R_s) \quad (2.16)$$

If the solution gas in Field units is described by  $\text{ft}^3/\text{bbl}$ , the gas volume must be divided by 5.61,

$$B_t = B_o + B_g (R_{sb} - R_s) / 5.61 \quad (2.16a)$$

Using the differential liberation data, we can write,

$$B_t = B_{ob} \frac{B_{od}}{B_{odb}} + B_g (R_{sdb} - R_{sd}) \frac{B_{ob}}{B_{odb}} \quad (2.17)$$

and in Field units,

$$B_t = B_{ob} \frac{B_{od}}{B_{odb}} + B_g \frac{(R_{sdb} - R_{sd})}{5.61} \frac{B_{ob}}{B_{odb}} \quad (2.17a)$$

The variation of  $B_t$  with pressure and its comparison with  $B_o$  are shown in Figure 2.11.

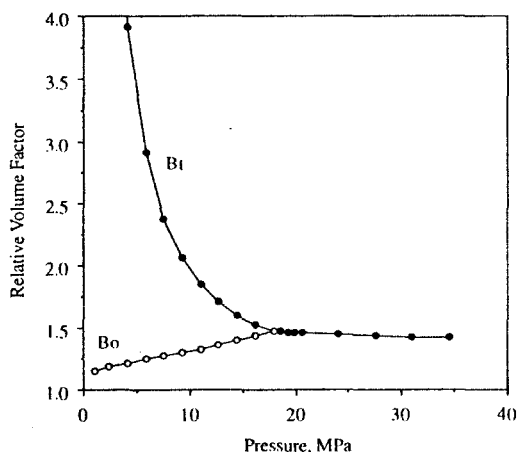


Figure 2.11. Variations of oil and total formation volume factors with pressure.

### 2.2.4 Gas Condensate

The compositional analysis of gas condensate fluids is conducted generally in more details than that of oil. The compositional data are used often in phase behaviour models, particularly in reservoir simulation. The fluid is commonly analysed by flashing it at the atmospheric pressure and measuring the composition of the stabilised gas and liquid phases, as described in the blow down method. The fluid heavy fraction is analysed to identify major components, and also to characterise it by extended carbon groups, as the results of phase behaviour models are very sensitive to the heavy end description of gas condensate systems. Selected tables from a PVT laboratory report on a North Sea gas condensate sample are presented as Tables 2.2, whereas Table 2.2A shows typical measured compositional data. Table 2.2B describes the distribution and properties of heavy components as single carbon number groups determined by distillation. The properties of single carbon number groups measured in the liquid phase are considered to be the same as those in the well stream. Details on testing the liquid fraction to characterise the fluid are given in Section 6.1.

Table 2.2.  
Selected tables from a typical PVT report on gas condensate.

Fluid: A North Sea Gas Condensate
Reservoir Temperature: 394 K (250 °F)
Reservoir Pressure: 49.64 MPa (7198 psia)

Table 2.2A.  
Detailed compositional analysis of the well stream.

Components	Mol %
Nitrogen	0.298
Carbon dioxide	1.720
Methane	79.139
Ethane	7.483
Propane	3.293
i-Butane	0.515
n-Butane	1.255
i-Pentanes	0.359
n-Pentane	0.551
i-Hexanes	0.282
n-Hexane	0.334
i-Heptanes	0.111
Benzene	0.271
Cyclanes C <sub>7</sub>	0.389
n-Heptane	0.235
i-Octanes	0.145
Toluene	0.150
Cyclanes C <sub>8</sub>	0.253
n-Octane	0.168
i-Nonanes	0.158
Aromatics C <sub>8</sub>	0.143
Cyclanes C <sub>9</sub>	0.061
n-Nonane	0.113
i-Decanes	0.176
Aromatics C <sub>9</sub>	0.054
n-Decane	0.084
Undecanes	0.318
Dodecanes	0.273
Tridecanes	0.253
Tetradecanes	0.225
Pentadecanes	0.178
Hexadecanes	0.144
Heptadecanes	0.126
Octadecanes	0.127
Nonadecanes	0.063
Eicosanes-plus	0.553

Molecular Weight 27.3

"Eicosanes-plus" characteristics: Molecular Weight = 353

Density at 288 K = 852.1 kg/m<sup>3</sup>

The two most common tests at the reservoir temperature are the constant composition expansion, CCE, and the constant volume depletion, CVD. In CCE, or the pressure-volume test, a known amount of gas condensate is loaded into a visual cell above the initial reservoir pressure. The system pressure is lowered stepwise by incrementally expanding the cell volume. Gas and condensate volumes are recorded at each pressure step as well as the observed dew point, Table 2.2C. A typical pressure-volume curve, with the data reported in Table 2.2C, is shown in Figure 2.12. An abrupt change of slope at the dew point does not generally occur. Hence, the dew point cannot be measured accurately by monitoring pressure-

volume changes. In rich gas condensate samples, i.e., close to their critical temperatures, the dew point is manifested by formation of a large amount of condensate. The measured dew point is, therefore, quite accurate. These fluids may also show a gradual reversible colour change, getting darker, as the dew point is approached. In most cases the initial liquid build-up is gradual, which makes the measured dew point quite subjective. The volume of condensed liquid in the above test for the North Sea gas, Table 2.2, is shown in Figure 2.13. Note that the condensate fraction is defined relative to the total volume.

Table 2.2B.  
Distillation results of the liquid fraction.

Component	Weight %	Range of distillation temperature, °C		Density at 288 K kg/m <sup>3</sup>	Molecular weight
Carbon Dioxide	0.00				
Methane	0.00				
Ethane	0.05				
Propane	0.41				
Butanes	1.39				
Pentanes	2.44				
Hexanes	3.56	36.0	– 70.0	714.5	86
Heptanes	7.70	70.0	– 100.0	739.0	89
Octanes	8.11	100.0	– 127.0	749.4	105
Nonanes	7.04	127.0	– 152.0	764.1	121
Decanes	5.31	152.0	– 175.5	776.6	138
Undecanes	5.89	175.5	– 197.0	785.7	151
Dodecanes	5.48	197.0	– 219.0	796.9	164
Tridecanes	5.51	219.0	– 236.5	810.5	178
Tetradecanes	5.29	236.5	– 254.5	814.4	192
Pentadecanes	4.50	254.5	– 271.5	822.5	206
Hexadecanes	3.88	271.5	– 288.0	829.5	220
Heptadecanes	3.60	288.0	– 303.0	832.2	234
Octadecanes	3.88	303.0	– 318.0	835.7	249
Nonadecanes	2.03	318.0	– 332.0	838.1	263
Eicosanes-plus	23.93	332.0	–	852.1	353

"Undecanes-plus" characteristics: Molecular Weight=231 Density at 288 K=834.6 kg/m<sup>3</sup>

Table 2.2C.  
Pressure-volume relation of the reservoir fluid at 394 K.

Pressure		Relative volume (V/V <sub>sc</sub> ), (3)	Specific volume 10 <sup>-3</sup> (m <sup>3</sup> /kg)	Compressibility factor, Z, (4)	Volume of retrograde liquid, (5) %
bar	psig				
551.0	7975	0.9395	2.8012	1.2866	0.00
521.0	7540	0.9599	2.8620	1.2429	0.00
501.0	7250	0.9765	2.9113	1.2158	0.00
(2) 496.4	7183	0.9787	2.9181	1.2074	0.00
491.0	7105	0.9826	2.9297	1.1991	0.00
481.0	6960	0.9935	2.9620	1.1876	0.00
(1) 471.5	6822	1.0000	2.9815	1.1718	0.00
466.0	6743	1.0068	3.0017	1.1660	0.30
456.0	6598	1.0174	3.0333	1.1530	0.82
441.0	6380	1.0312	3.0747	1.1302	1.73
421.0	6090	1.0550	3.1456	1.1039	2.92
391.0	5655	1.0971	3.2710	1.0661	4.79
351.0	5075	1.1687	3.4844	1.0195	7.18
311.0	4495	1.2632	3.7664	0.9764	9.40
271.0	3915	1.3959	4.1619	0.9401	11.02
231.0	3335	1.5841	4.7229	0.9094	12.40
181.0	2610	1.9773	5.8953	0.8894	13.15

- (1) Saturation pressure at indicated temperature.
- (2) Initial reservoir pressure.
- (3)  $V_{sat}$  = volume of fluid at saturation pressure and indicated temperature.
- (4)  $Z = PV/nRT$  ( $n$  total number of moles)
- (5) (Volume of retrograde liquid at indicated pressure)/(total volume at saturation pressure)  $\times 100$

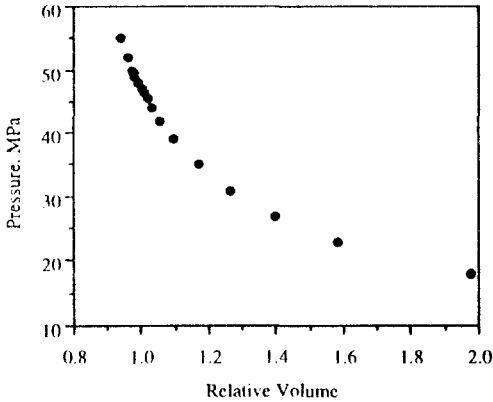


Figure 2.12 Pressure-volume curve for gas condensate at 394 K.

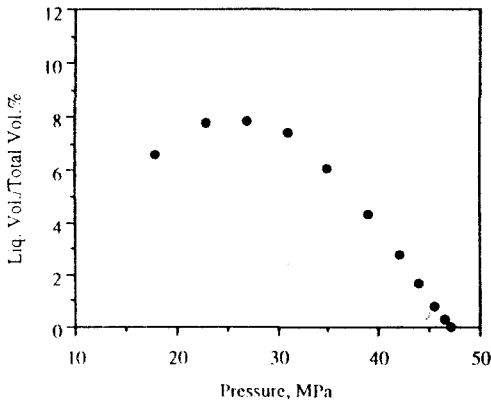


Figure 2.13 Liquid build-up curve for gas condensate at 394 K.

It is commonly assumed that the condensate dropped out in pores remains immobile. The depletion process is, therefore, simulated by CVD. The test consists of a series of expansion followed by expelling the excess gas at constant pressure in such a way that the cell volume remains constant at the end of each stage, as shown in Figure 2.14. The expelled gas at each pressure stage is collected and its composition, volume and compressibility (deviation) factor

are determined. The condensate volume is also measured. As the gas composition remains unchanged above the dew point during depletion, the test can be simplified by just expanding the cell volume without removing any fluid from it (pressure-volume test). The compressibility factor is then calculated, using Eq.(2.5). The volume at the dew point is considered as the reference (constant) volume in this procedure. The results of CVD test on a North Sea gas condensate are given in Table 2.2D.

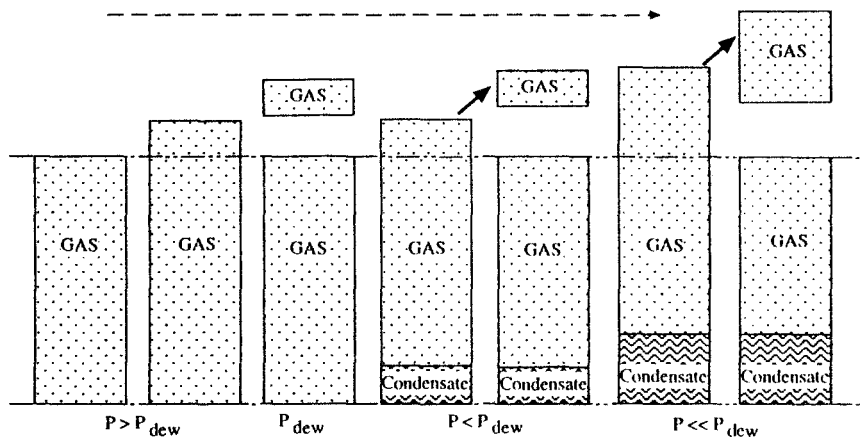


Figure 2.14. Schematic diagram of constant volume depletion.

Figure 2.15 shows the liquid drop-out volume in CVD test, as the fraction of cell volume at the dew point, which is taken as the reference volume. The liquid volume produced in CCE test is also shown in Figure 2.15 for comparison. The liquid drop-out in both tests has been defined as the ratio of the liquid volume to the volume at the dew point. Note that the accumulated condensate volumes are very much the same during the condensing region. The dropped out liquid vaporises back into the gas phase at lower pressure conditions. It should be remembered that the transfer of components between the phases always occurs in both directions, and it is the overall result which exhibits itself by the condensing and vaporising regions.

The liquid volume, as shown in Figure 2.15, increases with the pressure reduction below the dew point at a significant rate. PVT test data often show a liquid build-up tail, where the condensate build-up below the dew point is insignificant over a considerable pressure range. Exceptional cases, with a liquid build-up tail extending over 10 MPa [28], have been reported.

The tailing behaviour in the liquid build-up curve has been the subject of considerable interest with diverse views on its cause. The initial gradual and small build-up of the condensate phase has been attributed to the contamination of collected samples with hydraulic fluids from various sources during drilling, production and sampling. The test procedure can also affect the observed dew point and the liquid build-up behaviour. A 2 MPa tail was successfully eliminated when the dew point was approached over weeks instead of the common practice of over hours or minutes[29]. There is no firm evidence, however, that the tailing cannot be the true characteristic of a real reservoir fluid. Indeed, the presence of immobile interstitial water and marked differences between the solubilities of different compounds in it, and the adsorption of surface active and heavy compounds on reservoir rock surface may contribute to the above behaviour.

Table 2.2D.  
Constant volume depletion test results at 394 K.

Pressure		Cumulated Production, (3)	Specific gravity (relative to air) of produced gas	Compressibility factor of produced gas, Z	Volume of retrograde liquid, (4)
bar	psig	(%)			%
551.0	7975	0.00	0.943	1.2866	0.00
521.0	7540	0.00	0.943	1.2429	0.00
501.0	7250	0.00	0.943	1.2158	0.00
(2) 496.4	7183	0.00	0.943	1.2074	0.00
491.0	7105	0.40	0.943	1.1991	0.00
481.0	6960	1.51	0.943	1.1876	0.00
(1) 471.5	6822	2.17	0.943	1.1718	0.00
401.0	5800	9.67	0.889	1.0767	4.31
341.0	4930	17.66	0.845	1.0056	7.53
271.0	3915	29.89	0.797	0.9479	10.18
211.0	3045	42.90	0.760	0.9176	11.28
141.0	2030	60.29	0.737	0.9171	11.32
81.0	1160	76.17	0.728	0.9476	10.49

(1) Saturation pressure at indicated temperature.

(2) Initial reservoir pressure.

(3) (Moles of wet gas produced/moles of fluid at initial reservoir pressure)×100

(4) (Volume of retrograde liquid at indicated pressure/total volume at saturation pressure)×100

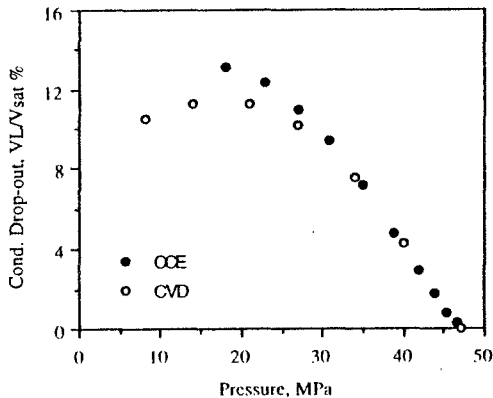


Figure 2.15. Liquid drop-out behaviour of the North Sea gas condensate at 394 K in CCE and CVD tests.

The produced gas density and composition, Table 2.2E, are commonly measured by flashing the gas at the laboratory conditions, and analysing the collected fluid phases. Properties of the condensate accumulated in the equilibrium cell during depletion are not measured, except in the last pressure stage when the condensate is also expelled from the cell, Table 2.2F. The condensate properties at other pressure stages are calculated by the material balance [30].

The condensate density,  $\rho_0$  at the  $j$ th depletion stage is calculated by,

$$\rho_{oj} = \left[ m_{in} - \sum_j m_{gj} - \rho_{gj} (V - V_{oj}) \right] / V_{oj} \quad (2.18)$$

where,

- $m_{in}$  = initial mass of gas condensate
- $\sum m_g$  = total mass of gas produced
- $\rho_g$  = density of gas at equilibrium with condensate
- $V$  = total cell volume
- $V_o$  = condensate volume

The condensate composition can be calculated by the component material balance as,

$$x_{ij} = \left[ n_{in} y_{i,in} - \sum_j n_{gj} y_{ij} - (V - V_{oj}) \rho_{gj} y_i / M_{gj} \right] / \left[ n_{in} - \sum_j n_{gj} - (V - V_{oj}) \rho_{gj} / M_{gj} \right] \quad (2.19)$$

where:

- $n_{in}$  = initial number of moles
- $n_g$  = number of moles of gas removed
- $M_g$  = molecular weight of gas at equilibrium with condensate
- $x_i$  = mole fraction of component  $i$  in condensate
- $y_i$  = mole fraction of component  $i$  in gas at equilibrium with condensate
- $y_{i,in}$  = initial number of moles of component  $i$

The equilibrium ratios at each pressure step can then be determined using the calculated condensate composition and the measured gas composition.

Table 2.2E.

Compositional analysis of produced gas in constant volume depletion test at 394 K.

bar	471.5	401.0	341.0	271.0	211.0	141.0
Pressure						
psig	6822	5800	4930	3915	3045	2030
Hydrogen Sulfide	0.00	0.00	0.00	0.00	0.00	0.00
Nitrogen	0.30	0.30	0.31	0.32	0.32	0.33
Carbon Dioxide	1.72	1.71	1.71	1.72	1.73	1.75
Methane	79.17	79.93	80.77	81.61	82.33	82.71
Ethane	7.48	7.44	7.41	7.46	7.54	7.64
Propane	3.29	3.22	3.21	3.20	3.19	3.22
i-Butane	0.52	0.51	0.50	0.50	0.49	0.49
n-Butane	1.25	1.23	1.21	1.18	1.15	1.15
i-Pentanes	0.36	0.35	0.34	0.33	0.32	0.32
n-Pentane	0.55	0.54	0.52	0.50	0.48	0.48
Hexanes	0.62	0.58	0.55	0.52	0.49	0.46
Heptanes	1.00	0.90	0.84	0.76	0.70	0.64
Octanes	0.71	0.68	0.61	0.53	0.43	0.37
Nonanes	0.47	0.46	0.40	0.32	0.24	0.17
Decanes	0.31	0.28	0.25	0.20	0.14	0.09
Undecanes-plus	2.25	1.87	1.37	0.85	0.45	0.18
Molecular weight	27.3	25.8	24.5	23.1	22.0	21.4
Gas specific gravity (relative to air)	0.943	0.889	0.845	0.797	0.760	0.737
Molecular weight of "Undecanes-plus":	231	207	202	190	180	174



Reliable results for the condensate phase by material balance calculations can only be obtained by an accurate analysis of produced gases. The loss of heavy compounds in the produced gas results in an unrealistically high condensate density, and higher concentrations of light components in the condensate phase. It may even lead to negative mass of light components in the condensate, such as nitrogen, with low concentrations in the mixture. Drohm et al. [31] studied CVD data of 80 experiments and found negative component fractions in 71 cases and condensate densities heavier than water in 45 cases. The above problem can be alleviated by direct sampling of the gas and condensate phases at equilibrium. Additional to the compositional analysis of the high pressure sample, the density can be measured in-situ by oscillating tube densitometer [32]. Material balance calculations can be used then to evaluate the reliability of data instead of calculating the properties of the condensate phase and the associated equilibrium ratios.

Table 2.2F.

Compositional analysis of remaining fluids at 81 bar in constant volume depletion test.

Components or fractions	Remaining gas (mol. %)	Remaining oil (mol. %)
Hydrogen Sulfide	0.00	0.00
Nitrogen	0.32	0.03
Carbon Dioxide	1.77	1.29
Methane	82.58	28.06
Ethane	7.79	4.94
Propane	3.32	4.03
i-Butane	0.51	0.80
n-Butane	1.22	2.36
i-Pentanes	0.33	0.85
n-Pentane	0.50	1.42
Hexanes	0.46	2.85
Heptanes	0.64	6.28
Octanes	0.34	5.66
Nonanes	0.13	4.75
Decanes	0.07	3.50
Undecanes-plus	0.02	33.18
Molecular weight	21.1	116.0
Gas specific gravity (relative to air)	0.728	-
Molecular weight of "Undecanes-plus"	166	240

The internal consistency of the measured compositional data can also be evaluated by plotting the equilibrium ratio vs. a parameter which indicates the volatility of the components. Figure 2.16 shows the most commonly used plot, known as the Hoffmann [33] plot for a North Sea gas condensate. The composition of both phases has been measured directly in a CVD test at 373 K. Each data point refers to a component identified by a function which depends on its critical pressure,  $P_c$ , critical temperature,  $T_c$ , and the boiling point temperature,  $T_b$  at the atmospheric pressure of  $P_a$ . The equilibrium ratio data are expected to fall on a straight line. A reasonable deviation from the straight line for non-hydrocarbon compounds, such as nitrogen and carbon dioxide, and component groups containing unusually high fractions of aromatics or naphthenes is expected.

The composition of produced gas as measured during CVD test by the conventional method is generally far inferior to the required accuracy for describing a phase which is after all the product. The reported compositional information is seldom used in evaluation and tuning of phase behaviour models due to the lack of reliability.

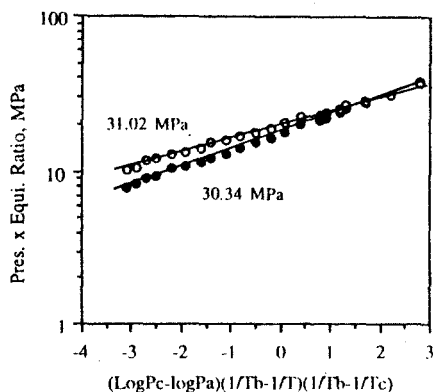


Figure 2.16. Internal consistency check of measured composition in CVD test by Hoffmann plot.

*Example 2.3.*

Calculate the two-phase compressibility factor,  $Z$ , of the cell content in the constant volume depletion test reported in Table 2.2D. Plot  $P/Z$  vs. the total production and comment on the observed trend.

*Solution:*

The two-phase  $Z$  is calculated as,

$$Z = (PV)/(nRT)$$

where  $V$  is the reservoir volume and remains constant during depletion. The volume of one kgmole of gas, molar volume, at the initial reservoir pressure can be calculated, using the measured  $Z$  for single phase gas,

$$V = 1.2074 \times 1 \times 0.0083144 \times 394.3 / 49.64 = 0.079740 \text{ m}^3$$

Substituting the volume in the above equation produces the two-phase  $Z$  as shown in the following table.

P, MPa	47.15	40.1	34.1	27.1	21.1	14.1	8.1
Number of Moles	97.83	90.33	82.34	70.11	57.1	39.71	23.83
$Z_{1\text{-phase}}$	1.17227	1.07977	1.00731	0.94017	0.89880	0.86365	0.82676
$P/Z$	40.22	37.14	33.85	28.82	23.48	16.33	9.80

The linear variation of  $P/Z$  and total production is expected as,

$$\frac{P}{Z} = \left( \frac{RT}{V} \right) (n_{in} - n_p),$$

and  $(RT/V)$  is constant.

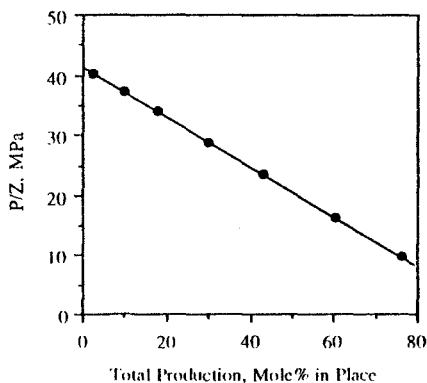


Figure E2.3. Variations of  $P/Z$  with total number of moles of produced fluid.

In a real reservoir in the absence of water advancement, the volume can be treated as constant, neglecting compaction. When the produced fluid is only gas, the produced number of moles,  $n_p$ , is proportional to the gas volume at standard conditions ( $1 \text{ kgmol} = 23.95 \text{ m}^3$ , Table 1.1). Hence the above trend can be shown in terms of gas volume produced.

#### Example 2.4.

The constant volume depletion test results of a gas condensate fluid are given in Tables 2.2D-E. (a) Determine the density of condensate phase by material balance calculations results. (b) Calculate the composition of condensate at 81 bar by material balance, and compare the results with the measured values.

#### Solution:

(a)

Basis: 100 kgmoles of gas at the initial reservoir pressure of 49.64 MPa, with  $m_m = 100 \times 27.3 = 2730 \text{ kg}$ .

The (constant) reservoir volume is calculated, using the measured compressibility factor, equal to  $7.974 \text{ m}^3$  (Example 2.3). Using the reported number of moles and the compressibility factor at the dew point results in,

$$V = nZRT/P = 97.83 \times 1.1718 \times 0.0083144 \times 394 / 47.15 = 7.971 \text{ m}^3$$

The difference in calculated reservoir volume by the two methods is due to the accuracy of reported data. An average value of  $7.972 \text{ m}^3$  will be used in the material balance calculations as follows.

Table 2.2D	$P_i$ , MPa	47.15	40.1	34.1	27.1	21.1	14.1	8.1
Table 2.2E-F	$M_g$	27.3	25.8	24.5	23.1	22.0	21.4	21.1
Table 2.2D	$Z_g$	1.1718	1.0767	1.0056	0.9479	0.9176	0.9171	0.9476
Table 2.2D	$100 \times (V_o/V)$	0	4.31	7.53	10.18	11.28	11.32	10.49

Table 2.2D	cum. prod. mole, $n_p$	2.17	9.67	17.66	29.89	42.9	60.29	76.17
100- $n_p$	mole in cell, $n$	97.83	90.33	82.34	70.11	57.10	39.71	23.83
$n_i - n_{i+1}$	mole gas rem., $n_i$	2.17	7.50	7.99	12.23	13.01	17.39	15.88
$\rho_g = M_g P / (Z_g RT)$	gas density, $\text{kg/m}^3$	335.07	293.10	253.42	201.45	154.31	100.36	55.02
$n_{gi} M_{gi}$	mass gas rem., $m_{gi}$ , kg	59.2	193.5	195.8	282.5	286.2	372.1	335.1
$m_{in} - \Sigma m_{gi}$	total mass in cell, $m$ , kg	2670.8	2477.3	2281.5	1999.0	1712.8	1340.6	1005.6
$V(1 - V_{oi}/V)$	gas vol in cell, $V_g$ , $\text{m}^3$	7971	7627	7371	7159	7072	7068	7135
$V - V_{oi}$	con. vol, $V_{oi}$ , $\text{m}^3$	0.0	343.5	600.2	811.4	899.1	902.3	836.1
$\rho_n V_{oi}$	mass gas in cell, $m_g$ , kg	2670.8	2235.5	1867.8	1442.2	1091.2	709.4	392.5
$m - m_{gi}$	mass cond. in cell, $m_c$ , kg	0.0	241.7	413.7	556.8	621.5	631.2	613.0
$m_{oi}/V_{oi}$	Cond. den., $\rho_{oi}$ , $\text{kg/m}^3$		703.7	689.2	686.1	691.3	699.6	733.2

(b)

The number of moles of gas phase in the cell at any stage is determined as  $n_{gi} = m_{gi}/M_{gi}$ , with the number of moles of condensate calculated as,  $n_{ci} = n_i - n_{gi}$ . The number of moles of each component is then calculated as:

$$n_{ij} = n_{in} y_{i,in} - \sum_j n_{gj} y_{ij}$$

The results are as follows:

Pressure, MPa	49.64	47.15	40.1	34.1	27.1	21.1	14.1	8.1
mole gas in cell	100	97.830	86.648	76.238	62.434	49.601	33.149	18.603
mole cond in cell	0	0.000	3.682	6.102	7.676	7.499	6.561	5.227
Component	kgmol							
Nitrogen	0.300	0.293	0.271	0.246	0.207	0.165	0.108	0.057
Carbon Dioxide	1.720	1.683	1.554	1.418	1.207	0.982	0.678	0.397
Methane	79.170	77.452	71.457	65.004	55.023	44.312	29.928	16.815
Ethane	7.480	7.318	6.760	6.168	5.255	4.274	2.946	1.709
Propane	3.290	3.219	2.977	2.721	2.329	1.914	1.354	0.827
i-Butane	0.520	0.509	0.470	0.431	0.369	0.306	0.220	0.139
n-Butane	1.250	1.223	1.131	1.034	0.890	0.740	0.540	0.346
i-Pentanes	0.360	0.352	0.326	0.299	0.258	0.217	0.161	0.109
n-Pentane	0.550	0.538	0.498	0.456	0.395	0.332	0.249	0.170
Hexanes	0.620	0.607	0.563	0.519	0.456	0.392	0.312	0.239
Heptanes	1.000	0.978	0.911	0.844	0.751	0.660	0.548	0.447
Octanes	0.710	0.695	0.644	0.595	0.530	0.474	0.410	0.356
Nonanes	0.470	0.460	0.425	0.393	0.354	0.323	0.293	0.273
Decanes	0.310	0.303	0.282	0.262	0.238	0.220	0.204	0.193
Undecanes-plus	2.250	2.201	2.061	1.951	1.848	1.789	1.758	1.754
Total	100.000	97.830	90.330	82.340	70.110	57.100	39.710	23.830

At each stage the number of moles of each component in the gas phase can be determined as,  $n_{gi} = n_i y_i$ . The number of moles of each component in the condensate phase is then determined as,  $n_{ci} = n_i - n_{gi}$ . The calculated results at the last stage are given in the following table, and compared with the measured values. The percentage deviation of calculated equilibrium ratios from the measured values indicates the reliability of experimental data, except for nitrogen.

Component	mole in	mole in	cal. $x_{ci}$	meas. $x_{ci}$	calculated	measured	$K_i$ deviation
-----------	---------	---------	---------------	----------------	------------	----------	-----------------

	gas	cond.	mole %	mole %	$K_i$	$K_i$	%
Nitrogen	0.060	-0.002	-0.04	0.03	-7.34125	10.66667	168.8
Carbon Dioxide	0.329	0.068	1.30	1.29	1.36668	1.37209	0.4
Methane	15.362	1.453	27.79	28.06	2.97164	2.94298	-1.0
Ethane	1.449	0.260	4.96	4.94	1.56910	1.57692	0.5
Propane	0.618	0.209	4.01	4.03	0.82852	0.82382	-0.6
i-Butane	0.095	0.045	0.85	0.80	0.59849	0.63750	6.1
n-Butane	0.227	0.119	2.28	2.36	0.53437	0.51695	-3.4
i-Pentanes	0.061	0.047	0.91	0.85	0.36439	0.38824	6.1
n-Pentane	0.093	0.077	1.46	1.42	0.34151	0.35211	3.0
Hexanes	0.086	0.153	2.93	2.85	0.15702	0.16140	2.7
Heptanes	0.119	0.328	6.27	6.28	0.10210	0.10191	-0.2
Octanes	0.063	0.293	5.60	5.66	0.06076	0.06007	-1.1
Nonanes	0.024	0.249	4.76	4.75	0.02734	0.02737	0.1
Decanes	0.013	0.180	3.44	3.50	0.02035	0.02000	-1.7
Undecanes plus	0.004	1.751	33.49	33.18	0.00060	0.00060	0.9
Total	18.603	5.227	100	100			

The CVD test can be considered to simulate the fluid behaviour in the reservoir bulk, where the condensate can be reasonably assumed immobile. At conditions near the producer within the condensate ring, where quasi-steady state conditions may be assumed, the CCE test simulates the behaviour more closely as the condensate flows with the gas, and the mixture composition remains almost constant.

The deposited condensate in a reservoir can partially be recovered by injecting a lean gas into the reservoir, and producing the gas enriched by the vaporised condensate. The produced gas is stripped from its intermediate and heavy components at the surface prior to being recycled back into the reservoir. The recycling process below the dew point can be simulated in the laboratory by initially conducting a CVD down to the recycling pressure prior to introducing the recycled gas into the equilibrium cell. The recycled gas is introduced at constant pressure by allowing the cell volume to expand. The cell is returned back to its initial volume by expelling the equilibrated gas at constant pressure. The produced gas volume and composition, and the shrinkage of condensate are measured. Figure 2.17 shows the results of methane cycling of a North Sea gas condensate. Note that the liquid volume fraction decreases by 20% after contacting two pore volumes of injected methane.

The flow of fluids towards the wellbore will establish a pressure gradient within the reservoir. As the gas volume increases at lower pressures, and the flow area is reduced near the wellbore, the pressure gradient will increase sharply as the well bore is approached. This will result in a rapid flow of rich gas into the near well region and a liquid build-up in pores at a fraction much higher than that measured in CVD test, as the rich gas keeps flowing towards the low pressure region depositing more condensate. When the well will be shut-in or the rate reduced, the pressure will build-up again. The behaviour of the mixture composed of a high liquid fraction could be liquid-like, instead of gas-like. Clearly the CVD data cannot provide adequate information to evaluate and tune the phase behaviour model for simulation of such a build-up test.

A laboratory test similar to that of gas cycling, but using the original gas instead of the lean gas, followed by stepwise pressure increase can simulate the above process and provide phase behaviour data for its modelling. Figure 2.18 shows the variation of fluid saturation pressure near the wellbore for a North Sea gas condensate fluid in such a test. The fraction of pore occupied by condensate increased from 28 % to 63% due to the inflow of 1.1 pore volume of gas. Note that the accumulation of condensate did not significantly change the mixture

saturation point for this tested rich gas condensate system. The system, however, changed from a gas-like to liquid-like fluid, showing a bubble point at the last tested stage, instead of a dew point.

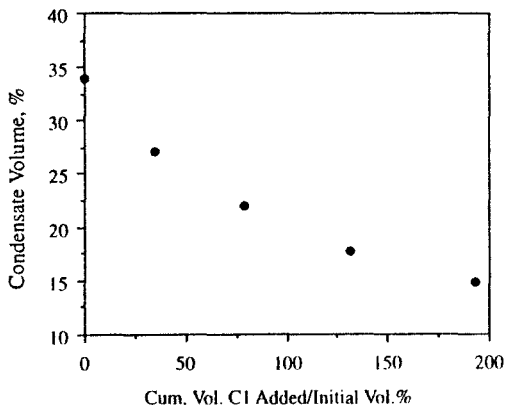


Figure 2.17. Reduction of condensate volume in methane cycling at 373 K and 27.58 MPa.

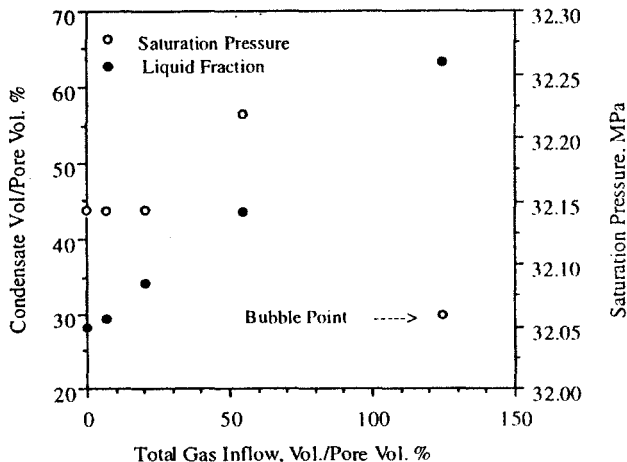


Figure 2.18. Variations of the fluid saturation pressure due to gas inflow near the wellbore.

It is a common practice to inject some lean gas into a gas condensate reservoir to capture as much as possible of the pressure decline and possibly maintain its pressure above the dew point to avoid the liquid loss by deposition in reservoir during pressure depletion. Figure 2.19 shows the results of a laboratory test, simulating pressure maintenance of a rich gas condensate reservoir by methane injection. Note that the addition of methane to the rich gas has resulted in

increasing the dew point. Hence, it can promote condensation, if the reservoir pressure is not far above the initial dew point, instead of preventing it. However, it will be limited only to the zone near the injector, where methane is mixed with the original fluid. The overall mixture will become progressively leaner, resulting in a lower liquid drop-out during late stages of production, when the injection will be stopped and the remaining gas produced by depletion.

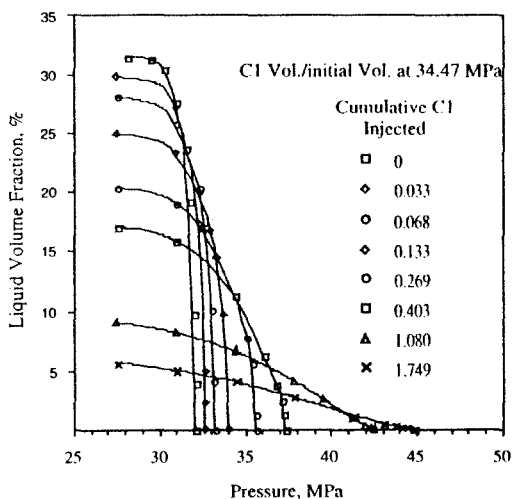


Figure 2.19. Variations of dew point and liquid fraction in CCE test with methane injection.

Although laboratory data generated on gas condensate fluids can be used directly in reservoir studies, they are often used to tune a phase behaviour model, Section 9.3. The model is then used conveniently in simulation of the recovery process.

### 2.2.5 Volatile Oil

PVT tests on volatile oil samples are not well defined and documented. Tests similar to those described for black oils are commonly conducted on volatile oils. As the evolved gas phase below the bubble point almost immediately becomes mobile, the differential test seems to simulate the process. However, the mobile gas which is produced with the oil behaves as a rich retrograde gas and contributes significantly to the collected liquid at the surface conditions.

The production of volatile oil by depletion is not an effective method for optimum oil recovery. As the pressure falls below the bubble point, a large volume of the gas is produced which may attain a mobility exceeding that of the oil, resulting in a large gas production and leaving the oil behind in the reservoir. Therefore a constant volume depletion test, similar to that for gas condensate is sometimes conducted.

None of the pressure depletion tests commonly conducted in laboratories can simulate the fluid behaviour as occurs in the field. The tests should, however, provide sufficient compositional and volumetric data for tuning of a phase behaviour model. The constant composition expansion test at the reservoir temperature provides most of the required data on the oil behaviour at reservoir conditions. The amount of condensate collected from produced gases in separator and differential liberation tests should also be measured and reported.

An on site simple pressure-volume test of the collected oil sample is a useful guide to identify the oil type and decide on the required tests. The change of slope at bubble point is less pronounced for volatile oils in comparison with that for black oil samples. The slope changes so gradually for very near critical oils that the bubble point may not be detected. For such a fluid, a visual method, similar to that for gas condensate, is preferred. Figure 2.20 compares the pressure-volume behaviour of a North Sea volatile oil with that of the black oil, described in Table 2.1.

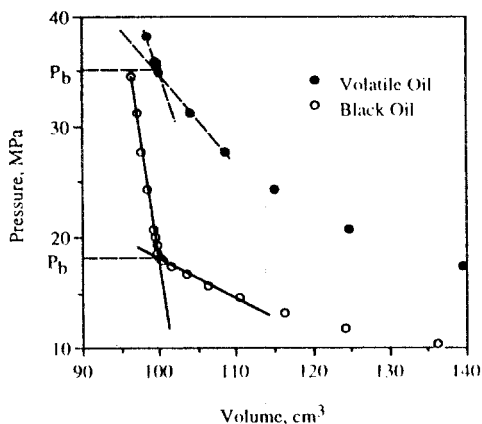


Figure 2.20. Comparison of pressure-volume behaviour of volatile oil and black oil.

### 2.3 EMPIRICAL CORRELATIONS

Many investigators have used PVT laboratory test results, and field data, to develop generalised correlations for estimating properties of reservoir fluids. The main properties which are determined from empirical correlations are the bubble point, gas solubility, volume factors, density, compressibility, and viscosity. The correlations typically match the employed experimental data with an average deviation of less than a few percent. It is not unusual, however, to observe deviations with an order of magnitude higher when applied to other fluids.

The correlations can be classified broadly into two groups. First, those which consider oil, gas, and water as three pseudo components, and treat a reservoir fluid as composed of these pseudo components. The second group consists of those correlations which use the fluid composition, typically identified to  $C_6$  by discrete compounds and the rest as  $C_{7+}$ , to estimate the fluid properties. The first approach, is the common one. The reliability of these correlations significantly depends on the reservoir fluid characteristics. If the fluid is "typical", and falls within the range of tested fluids used in that particular correlation, an acceptable accuracy can be expected.

There are many fluid property correlations. A number of these correlations have used data of certain localities, hence, their application is limited. Some correlations have received higher attention and wider acceptability than others. The correlations have been reviewed and compared by several investigators, resulting in no clear superiority order amongst the correlations. Some of them, however, have shown their reliability in various comparative



studies [34-38]. A few of the more widely used correlations are given in this chapter. Table 2.3 provides information on the range of data used in the correlations to help selecting a correlation for a specific case.

Table 2.3.

Ranges of data used in black oil correlations.

Correlation	Standing	Lasater	Vasquez-Beggs	Glaso	Marhoun
Ref. No:	39	40	41	42	43
Bubble Point Pressure, psia	130-7000	48-5780	15-6055	165-7142	130-3573
Temperature, °F	100-258	82-272	162-180	80-280	74-240
Form.Vol.Fac., bbl/STB	1.024-2.15		1.028-2.226	1.025-2.588	1.032-1.997
Gas/Oil Ratio, SCF/STB	20-1425	3-2905	0-2199	90-2637	26-1602
Tank Oil Gravity, °API	16.5-63.8	17.9-51.1	15.3-59.5	22.3-48.1	19.4-44.6
Gas Specific Gravity	0.59-0.95	0.574-1.22	0.511-1.351	0.650-1.276	0.752-1.367
Separator Pressure, psia	265-465	15-605	60-565	415	
Separator Temp., °F	100	36-106	76-150	125	

The selected correlations are presented in this section using field units as follows:

P : Pressure, psia

T : Temperature, degrees Fahrenheit, °F (=1.8K-459.67), in oil and water correlations, degrees Rankine, °R (=1.8K), in gas correlations: Eqs.(2.58-76).

v : Molar volume, ft<sup>3</sup>/lbmol (=0.062428 m<sup>3</sup>/kgmol)

ρ : Density, lbm/ft<sup>3</sup> (=16.018 kg/m<sup>3</sup>)

R<sub>g</sub>: Dissolved or liberated gas, SCF/bbl (=5.6146 m<sup>3</sup>/m<sup>3</sup>)

### 2.3.1 Black Oil

Black oil correlations treat the oil as composed of two components, i.e., the stock tank oil and the collected dry gas at standard conditions. Each component is characterised by its specific gravity. An accurate prediction of the phase behaviour of complex multi-component systems with only a few variables should not, however, be expected. Black oil correlations should cautiously be used for volatile oils.

There are a large number of correlations to determine properties of a typical black oil. All the correlations use the reservoir temperature, gas and oil specific gravity, and the solution gas to oil ratio to determine the properties of saturated oil. Several authors have provided correction factors to include the effects of non-hydrocarbon compounds and separator conditions. All the authors have used a large number of experimental data to regress the parameters of their proposed correlations to minimise the differences between the predicted and measured values.

Standing [39] used a total of 105 data points on 22 different crude oils from California to develop his correlations. Lasater [40] presented a bubble point correlation using 158 measured bubble point data on 137 crude oils from Canada, Western and Mid-Continental United States and South America. Vasquez and Beggs [41] developed correlations for the solution gas to oil ratio and formation volume factor using 6004 data points. Glaso [42] used data from 45 oil samples mostly from the North Sea region to develop his correlations. Marhoun [43] used 160 bubble point data on 69 Middle Eastern crude samples to develop a bubble point pressure correlation. Ahmed [44] used the combined reported data of Glaso and Marhoun to develop a correlation for determining the oil formation volume factor. Asgarpour et al.[45], Labedi [46], and Petrosky-Farshad [47], used data on fluids from reservoirs in Western Canada, Africa, and Texas-Louisiana, respectively to develop various correlations. De Ghetto et al.[38] used about 3700 measured data points on 195 crude oil samples from the Mediterranean Basin, Africa, Persian Gulf, and North Sea, to evaluate published correlations, and modified some of them to improve predicted results.

The main application of these correlations is the estimation of reservoir fluid properties using field data. The gas evolved at the stock tank is often vented and not measured. As the amount of vented gas could exceed 10% of the total dissolved gas in the reservoir oil, its value should be estimated and added to the gas volume evolved in the separators. The solution gas vented at the stock tank can be estimated [48] from the information on the last separator before the stock tank,

$$\log(R_{st}) = 0.3818 - 5.506 \log(S_o) + 2.902 \log(S_{gs}) + 1.327 \log(P_s) - 0.7355 \log(T_s) \quad (2.20)$$

$$T_s < 140^\circ \text{F}$$

where,  $R_{st}$  is the stock tank vented gas in SCF/STB,  $S_o$  is the stock tank oil specific gravity,  $S_{gs}$ ,  $P_s$  and  $T_s$ , are the separator gas specific gravity, pressure, and temperature ( $^\circ\text{F}$ ).

The gas gravity used in the correlations is the average value of all collected gases from the separators,

$$S_g = \sum R_j S_{gj} / \sum R_j \quad (2.21)$$

where  $j$  refers to the separation stages, including the stock tank oil if information is available.

#### Example 2.5.

Estimate the evolved gas from Good Oil at the stock tank conditions with separator pressures equal to those reported in Table 2.1E. Compare the results with measured values.

#### Solution:

The evolved gas is estimated using the separator pressure and temperature ( $75^\circ\text{F}$ ), and gas specific gravity data, and the stock tank oil specific gravity as follows:

$P_s$	$^\circ\text{API}$	$S_o$	$S_g$	$R_s$ calc.	$R_s$ meas.	% dev.
65	40.5	0.823	0.840	45	41	10
115	40.7	0.822	0.786	80	92	-12
215	40.4	0.823	0.732	148	178	-16
315	40.1	0.825	0.704	217	246	-11

#### Bubble Point Pressure

Standing initially produced a graphical correlation [39] for determining the bubble point pressure, and later [49] expressed the graph by the following correlation,

$$P_b = 18.2 \left[ \left( R_s / S_g \right)^{0.83} (10)^a - 1.4 \right] \quad (2.22)$$

where

- $a$  =  $0.00091T - 0.0125(\text{API})$
- $P_b$  = bubble point pressure, psia
- $R_s$  = solution gas to oil ratio SCF/STB
- $T$  = Temperature,  $^\circ\text{F}$

A deviation of about 15% is expected from the above correlation [37,38].

Vasquez and Beggs [41] point out that the gas gravity depends on the separator conditions. Hence, the authors used the gas gravity normalised to a separator pressure of 100 psig.

$$P_b = \left[ (C_1 R_s / S_{gn}) (10)^a \right]^{C_2} \quad (2.23)$$

where,

$$a = -C_3 (\text{API}) / (T + 460)$$

and the values of the coefficients are:

Coefficient	API ≤ 30	API > 30
C <sub>1</sub>	27.62	56.18
C <sub>2</sub>	0.914328	0.84246
C <sub>3</sub>	11.172	10.393

$S_{gn}$  is the gas normalised specific gravity related to the separator gas gravity,  $S_g$ , by,

$$S_{gn} = S_g \left[ 1 + 5.912 (10^{-5}) (\text{API}) T_s \log (P_s / 114.7) \right] \quad (2.24)$$

where  $P_s$  and  $T_s$  are the actual separator pressure, psia, and temperature, °F, respectively.

#### Example 2.6.

Estimate the bubble point of Good Oil at 220 °F, using the measured separator test data at 100 psig, Table 2.1E.

*Solution:*

The total gas in solution, and gas specific gravity, using Eq.(2.21), are calculated

$$R_s = \Sigma R_i = 676 + 92 = 768 \text{ SCF/STB}$$

$$S_g = \Sigma R_i S_{gi} / \Sigma R_i = (676 \times 0.786 + 92 \times 1.363) / 768 = 0.855$$

The bubble point is estimated using the Standing correlation, Eq.(2.22),

$$a = 0.00091 \times 220 - 0.0125 \times 40.7 = -0.30855$$

$$P_b = 2503 \text{ psia}$$

Alternatively, the Vasquez-Beggs correlation, Eq.(2.23), can be used to estimate the bubble point. As the separator pressure is 100 psig,

$$S_{gn} = S_g = 0.855$$

$$\text{Hence, } a = -10.393 \times 40.7 / 680 = -0.6220516$$

$$P_b = 2741 \text{ psia}$$

The measured value is 2635 psia.

An on site simple pressure-volume test of the collected oil sample is a useful guide to identify the oil type and decide on the required tests. The change of slope at bubble point is less pronounced for volatile oils in comparison with that for black oil samples. The slope changes so gradually for very near critical oils that the bubble point may not be detected. For such a fluid, a visual method, similar to that for gas condensate, is preferred. Figure 2.20 compares the pressure-volume behaviour of a North Sea volatile oil with that of the black oil, described in Table 2.1.

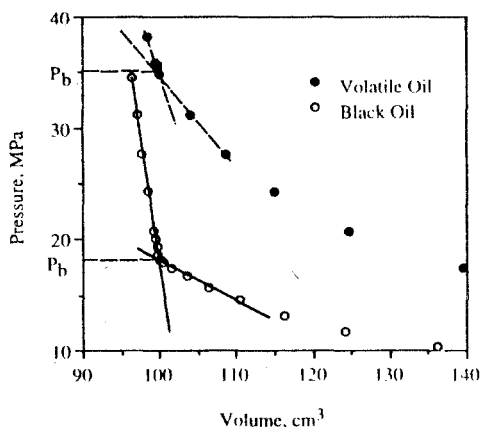


Figure 2.20. Comparison of pressure-volume behaviour of volatile oil and black oil.

### 2.3 EMPIRICAL CORRELATIONS

Many investigators have used PVT laboratory test results, and field data, to develop generalised correlations for estimating properties of reservoir fluids. The main properties which are determined from empirical correlations are the bubble point, gas solubility, volume factors, density, compressibility, and viscosity. The correlations typically match the employed experimental data with an average deviation of less than a few percent. It is not unusual, however, to observe deviations with an order of magnitude higher when applied to other fluids.

The correlations can be classified broadly into two groups. First, those which consider oil, gas, and water as three pseudo components, and treat a reservoir fluid as composed of these pseudo components. The second group consists of those correlations which use the fluid composition, typically identified to  $C_6$  by discrete compounds and the rest as  $C_{7+}$ , to estimate the fluid properties. The first approach, is the common one. The reliability of these correlations significantly depends on the reservoir fluid characteristics. If the fluid is "typical", and falls within the range of tested fluids used in that particular correlation, an acceptable accuracy can be expected.

There are many fluid property correlations. A number of these correlations have used data of certain localities, hence, their application is limited. Some correlations have received higher attention and wider acceptability than others. The correlations have been reviewed and compared by several investigators, resulting in no clear superiority order amongst the correlations. Some of them, however, have shown their reliability in various comparative

studies [34-38]. A few of the more widely used correlations are given in this chapter. Table 2.3 provides information on the range of data used in the correlations to help selecting a correlation for a specific case.

Table 2.3.

Ranges of data used in black oil correlations.

Correlation	Standing	Lasater	Vasquez-Beggs	Glaso	Marhoun
Ref. No:	39	40	41	42	43
Bubble Point Pressure, psia	130-7000	48-5780	15-6055	165-7142	130-3573
Temperature, °F	100-258	82-272	162-180	80-280	74-240
Form. Vol Fac., bbl/STB	1.024-2.15		1.028-2.226	1.025-2.588	1.032-1.997
Gas/Oil Ratio, SCF/STB	20-1425	3-2905	0-2199	90-2637	26-1602
Tank Oil Gravity, °API	16.5-63.8	17.9-51.1	15.3-59.5	22.3-48.1	19.4-44.6
Gas Specific Gravity	0.59-0.95	0.574-1.22	0.511-1.351	0.650-1.276	0.752-1.367
Separator Pressure, psia	265-465	15-605	60-565	415	
Separator Temp., °F	100	36-106	76-150	125	

The selected correlations are presented in this section using field units as follows:

P : Pressure, psia

T : Temperature, degrees Fahrenheit, °F (=1.8K-459.67), in oil and water correlations, degrees Rankine, °R (=1.8K), in gas correlations: Eqs.(2.58-76).

v : Molar volume, ft<sup>3</sup>/lbmol (=0.062428 m<sup>3</sup>/kgmol)

ρ : Density, lbm/ft<sup>3</sup> (=16.018 kg/m<sup>3</sup>)

R<sub>g</sub>: Dissolved or liberated gas, SCF/bbl (=5.6146 m<sup>3</sup>/m<sup>3</sup>)

### 2.3.1 Black Oil

Black oil correlations treat the oil as composed of two components, i.e., the stock tank oil and the collected dry gas at standard conditions. Each component is characterised by its specific gravity. An accurate prediction of the phase behaviour of complex multi-component systems with only a few variables should not, however, be expected. Black oil correlations should cautiously be used for volatile oils.

There are a large number of correlations to determine properties of a typical black oil. All the correlations use the reservoir temperature, gas and oil specific gravity, and the solution gas to oil ratio to determine the properties of saturated oil. Several authors have provided correction factors to include the effects of non-hydrocarbon compounds and separator conditions. All the authors have used a large number of experimental data to regress the parameters of their proposed correlations to minimise the differences between the predicted and measured values.

Standing [39] used a total of 105 data points on 22 different crude oils from California to develop his correlations. Lasater [40] presented a bubble point correlation using 158 measured bubble point data on 137 crude oils from Canada, Western and Mid-Continental United States and South America. Vasquez and Beggs [41] developed correlations for the solution gas to oil ratio and formation volume factor using 6004 data points. Glaso [42] used data from 45 oil samples mostly from the North Sea region to develop his correlations. Marhoun [43] used 160 bubble point data on 69 Middle Eastern crude samples to develop a bubble point pressure correlation. Ahmed [44] used the combined reported data of Glaso and Marhoun to develop a correlation for determining the oil formation volume factor. Asgarpour et al.[45], Labedi [46], and Petrosky-Farshad [47], used data on fluids from reservoirs in Western Canada, Africa, and Texas-Louisiana, respectively to develop various correlations. De Ghetto et al.[38] used about 3700 measured data points on 195 crude oil samples from the Mediterranean Basin, Africa, Persian Gulf, and North Sea, to evaluate published correlations, and modified some of them to improve predicted results.

The main application of these correlations is the estimation of reservoir fluid properties using field data. The gas evolved at the stock tank is often vented and not measured. As the amount of vented gas could exceed 10% of the total dissolved gas in the reservoir oil, its value should be estimated and added to the gas volume evolved in the separators. The solution gas vented at the stock tank can be estimated [48] from the information on the last separator before the stock tank,

$$\log(R_{st}) = 0.3818 - 5.506 \log(S_o) + 2.902 \log(S_{gs}) + 1.327 \log(P_s) - 0.7355 \log(T_s) \quad (2.20)$$

$$T_s < 140^\circ\text{F}$$

where,  $R_{st}$  is the stock tank vented gas in SCF/STB,  $S_o$  is the stock tank oil specific gravity,  $S_{gs}$ ,  $P_s$  and  $T_s$ , are the separator gas specific gravity, pressure, and temperature ( $^\circ\text{F}$ ).

The gas gravity used in the correlations is the average value of all collected gases from the separators,

$$S_g = \sum R_j S_{gj} / \sum R_j \quad (2.21)$$

where  $j$  refers to the separation stages, including the stock tank oil if information is available.

### Example 2.5.

Estimate the evolved gas from Good Oil at the stock tank conditions with separator pressures equal to those reported in Table 2.1E. Compare the results with measured values.

### Solution:

The evolved gas is estimated using the separator pressure and temperature ( $75^\circ\text{F}$ ), and gas specific gravity data, and the stock tank oil specific gravity as follows:

$P_s$	$^\circ\text{API}$	$S_o$	$S_g$	$R_s$ calc.	$R_s$ meas.	% dev.
65	40.5	0.823	0.840	45	41	10
115	40.7	0.822	0.786	80	92	-12
215	40.4	0.823	0.732	148	178	-16
315	40.1	0.825	0.704	217	246	-11

### Bubble Point Pressure

Standing initially produced a graphical correlation [39] for determining the bubble point pressure, and later [49] expressed the graph by the following correlation,

$$P_b = 18.2 \left[ \left( R_s / S_g \right)^{0.83} (10)^a - 1.4 \right] \quad (2.22)$$

where

- $a$  =  $0.00091T - 0.0125(\text{API})$
- $P_b$  = bubble point pressure, psia
- $R_s$  = solution gas to oil ratio SCF/STB
- $T$  = Temperature,  $^\circ\text{F}$

A deviation of about 15% is expected from the above correlation [37,38].

Vasquez and Beggs [41] point out that the gas gravity depends on the separator conditions. Hence, the authors used the gas gravity normalised to a separator pressure of 100 psig.

$$P_b = \left[ (C_1 R_s / S_{gn}) (10)^a \right]^{C_2} \quad (2.23)$$

where,

$$a = -C_3 (API)/(T+460)$$

and the values of the coefficients are:

Coefficient	API ≤ 30	API > 30
C <sub>1</sub>	27.62	56.18
C <sub>2</sub>	0.914328	0.84246
C <sub>3</sub>	11.172	10.393

$S_{gn}$  is the gas normalised specific gravity related to the separator gas gravity,  $S_g$ , by,

$$S_{gn} = S_g \left[ 1 + 5.912 (10^{-5}) (API) T_s \log (P_s / 114.7) \right] \quad (2.24)$$

where  $P_s$  and  $T_s$  are the actual separator pressure, psia, and temperature, °F, respectively.

#### Example 2.6.

Estimate the bubble point of Good Oil at 220 °F, using the measured separator test data at 100 psig, Table 2.1E.

*Solution:*

The total gas in solution, and gas specific gravity, using Eq.(2.21), are calculated

$$R_s = \Sigma R_s = 676 + 92 = 768 \text{ SCF/STB}$$

$$S_g = \Sigma R_s S_g / \Sigma R_s = (676 \times 0.786 + 92 \times 1.363) / 768 = 0.855$$

The bubble point is estimated using the Standing correlation, Eq.(2.22),

$$a = 0.00091 \times 220 - 0.0125 \times 40.7 = -0.30855$$

$$P_s = 2503 \text{ psia}$$

Alternatively, the Vasquez-Beggs correlation, Eq.(2.23), can be used to estimate the bubble point. As the separator pressure is 100 psig,

$$S_{gn} = S_g = 0.855$$

$$\text{Hence, } a = -10.393 \times 40.7 / 680 = -0.6220516$$

$$P_b = 2741 \text{ psia}$$

The measured value is 2635 psia.

### Gas in Solution

All the bubble point graphs and correlations can be used to estimate the amount of gas in solution at a given saturation pressure. de Ghetto et al. [38] compared the correlations for predicting the solution gas, and found the correlation of Vasquez-Beggs, Eq.(2.23), more reliable than others with a standard deviation of 29.5%. The liberated gas is calculated as the difference between the gas in solution at the original bubble point minus that at the operating pressure.

### Oil Formation Volume Factor

The oil formation volume factor of saturated oils has been correlated by a number of investigators using the gas in solution  $R_s$ , (gas to oil ratio), gas gravity, oil gravity and reservoir temperature as the correlating parameters.

Standing initially produced a graphical correlation [39] for estimating the oil formation volume factor, and later [49] expressed the graph by the following correlation,

$$B_o = 0.9759 + 0.000120 \left[ R_s (S_g / S_o)^{0.5} + 1.25T \right]^{1.2} \quad (2.25)$$

The Vasquez and Beggs [41] correlation, which accounts for the separator pressure is as follows,

$$B_o = 1.0 + C_1 R_s + (T - 60) (API / S_{gn}) (C_2 + C_3 R_s) \quad (2.26)$$

where  $S_{gn}$  is the normalised gas gravity, Eq.(2. 24), and the values of the coefficients are:

Coefficient	API ≤ 30	API > 30
C1	$4.677 \times 10^{-4}$	$4.670 \times 10^{-4}$
C2	$1.751 \times 10^{-5}$	$1.100 \times 10^{-5}$
C3	$-1.811 \times 10^{-8}$	$1.337 \times 10^{-9}$

The oil formation volume factor can be estimated with a deviation less than 5% from the above correlations [37,38].

The Arps correlation [50] can be used to roughly estimate the oil formation volume factor when the properties of gas and oil are not known.

$$B_o = 1.05 + 0.0005 R_s \quad (2.27)$$

The oil formation volume factor of an *undersaturated oil* is calculated by correcting the estimated formation factor at the saturation pressure for its compressibility at the reservoir temperature. The oil isothermal compressibility coefficient,  $C_o$ , is related to the oil formation volume factor as,

$$C_o = -(\partial B_o / \partial p)_T / B_o \quad (2.28)$$

or

$$B_{op} = B_o \exp[-C_o (P - P_h)] \quad (2.29)$$

where,



$B_{op}$  is the oil formation volume factor at the pressure  $p$ , and  $C_o$  is the average oil isothermal compressibility coefficient over the pressure range of  $P_b$  to  $P$ .

The value of the isothermal compressibility coefficient,  $C_o$ , can be estimated from [41],

$$C_o = (-1433.0 + 5.0 R_s + 17.2 T - 1180.0 S_g + 12.61 API) / (10^5 P) \quad (2.30)$$

The above correlation is believed to generally underpredict the compressibility, particularly at high pressures [37], with an average absolute deviation of about 25%.

When the pressure gradient of a static oil column within the reservoir is known, the oil density is conveniently calculated from,

$$\rho_o = 144 (dp/dh) \quad (2.31)$$

where the pressure gradient,  $dp/dh$ , is in psi/ft, and  $\rho_o$  is the oil density at the prevailing pressure and temperature in  $lbm/ft^3$ .

The oil formation volume factor, then, can be determined by the material balance equation for one stock tank barrel of oil, resulting in,

$$B_o = (62.4 S_o + 0.0136 R_s S_g) / \rho_o \quad (2.32)$$

#### Example 2.7.

Estimate the isothermal compressibility coefficient of Good Oil at 220 °F and 4500 psig. Compare the result with the measured value.

*Solution:*

The isothermal compressibility coefficient is estimated using Eq.(2.30) with the data calculated in Example 2.6.

$$R_s = 768 \text{ SCF/STB} \quad S_g = 0.855 \quad \text{"API}=40.7 \quad T=220 \text{ °F} \quad P=4515 \text{ psia}$$

$$C_o = 1.26 \times 10^{-5} \text{ psi}^{-1}$$

The result of pressure-volume test at the reservoir conditions, Table 2.1B, can be used to calculate the oil compressibility,

$$C_o = \left[ -(\partial V / \partial P) / V \right]_T \approx (-\Delta V / V) / \Delta P$$

Using the pressure-volume data at 4000-5000 psig, we obtain,

$$\text{at } 4000\text{-}4500 \text{ psig : } C_o = 1.28 \times 10^{-5} \text{ psi}^{-1}$$

$$\text{at } 4500\text{-}5000 \text{ psig : } C_o = 1.36 \times 10^{-5} \text{ psi}^{-1}$$

The average value at 4515 psia is equal to  $1.32 \times 10^{-5} \text{ psi}^{-1}$ .

#### Total (Two-Phase) Formation Volume Factor

The total formation volume factor of oil at a pressure below the original bubble point pressure can be estimated from a number of correlations. Glaso [42] proposed the following correlation,

$$\log B_t = 0.080135 + 0.47257 \log B_t^* + 0.17351 (\log B_t^*)^2 \quad (2.33)$$

where  $B_t^*$  is a correlating number defined by:

$$B_t^* = R_s T^{0.5} S_o^C / (S_g^{0.3} P^{1.1089}) \quad (2.34)$$

and

$$C = 2.9 / 10^{0.00027R_s}$$

The Marhoun [43] correlation is,

$$B_t = 0.314693 + 0.106253 \times 10^{-4} A + 0.18883 \times 10^{-10} A^2 \quad (2.35)$$

where,

$$A = R_s^{0.644516} S_o^{0.724874} (T + 460)^{2.00621} / (S_g^{1.079340} P^{0.761910})$$

Note that  $R_s$  in the above correlations is the original oil gas in solution, with partly still dissolved in oil at the prevailing pressure and the rest evolved as the gas phase.

### Example 2.8.

Estimate: (a) the gas in solution, (b) oil formation volume factor, and (c) total formation volume factor of Good Oil at 1600 psig and 220 °F. Assume a 100 psig and 75 °F separator. Compare the estimated values with the measured data, Table 2.1E-D.

*Solution:*

(a)

Using the Standing correlation, Eq.(2.22), at a saturation pressure of 1615 psia, we estimate the gas in solution,

$$R_s = 456 \text{ SCF/STB}$$

The estimated value by the Vasquez-Beggs correlation, Eq.(2.23), is equal to 410 SCF/STB.

The measured value is determined by combining the reported differential liberation and separator test data, as described by Eq.(2.15),

$$R_s = R_{sb} - (R_{sdb} - R_{sd}) \frac{B_{ob}}{B_{odb}}$$

$$R_s = 768 - (854 - 544) \times 1.474 / 1.600 = 482 \text{ SCF/STB}$$

(b)

Using the Standing correlation, Eq.(2.25), with  $R_s = 456$  SCF/STB, we estimate the oil formation volume factor,

$$B_o = 1.309$$

The estimated value by the Vasquez-Beggs correlation, Eq.(2.26), with  $R_s=410$  SCF/STB is equal to 1.279.

The measured value is determined from Eq.(2.13),

$$B_o = B_{odl} \frac{B_{ob}}{B_{odb}} = 1.445 \times 1.474 / 1.600 = 1.331$$

(c)

The total formation volume factor can be estimated from the Glaso correlation, Eq.(2.33), with  $R_s=768$  SCF/STB.

$$C=1.79902831 \quad B_1=2.32277288 \quad B_2=1.889$$

The predicted value by the Marhoun correlation, Eq.(2.35), is as follows:

$$A=128671.275$$

$$B_1=1.994$$

The measured value is determined from Eq.(2.16),

$$B_t = B_o + B_g (R_{sh} - R_s) / 5.61 = 1.331 + 0.01034 \times (768 - 482) / 5.61 = 1.858$$

### *Oil Density*

The density of saturated oil can be estimated from Eq.(2.32) using the calculated oil formation volume factor from any of the generalised correlations. The isothermal compressibility coefficient can be used to adjust the calculated saturated oil density due to compression for an under saturated oil,

$$\rho_{op} = \rho_o \exp[C_o(P - P_b)] \quad (2.36)$$

where  $\rho_{op}$  is the oil density at pressure  $P$ .

The oil density can be estimated also by calculating the mass and volume of the oil at reservoir conditions. In this approach the effective volume of the evolved gas, as a hypothetical liquid, is estimated and added to the stock tank oil volume at the standard conditions. Katz [51] developed a chart for estimating the apparent liquid density of natural gas, which was later described by the following correlation [49],

$$\rho_{al} = 38.52 \times 10^{-0.00326 \text{ } ^\circ\text{API}} + (94.75 - 33.93 \log \text{ } ^\circ\text{API}) \log S_g \quad (2.37)$$

where  $\rho_{al}$  is the apparent density of gas in the liquid state, lbm/ft<sup>3</sup>.

The apparent density of the oil,  $\rho_{ao}$ , including the dissolved gas, at the standard conditions is determined by dividing the total mass by the apparent volume for one STB of oil, as,

$$\rho_{ao} = [(R_s / 380)(28.96 S_g) + 5.61 \times 62.4 S_o] / [5.61 + [(R_s / 380)(28.96 S_g) / \rho_{al}]]$$

which reduces to,

$$\rho_{ao} = [0.07621 R_s S_g + 350 S_o] / [5.61 + (0.07621 R_s S_g / \rho_{al})] \quad (2.38)$$

where  $\rho_{ao}$  is in  $\text{lbm/ft}^3$ .

The apparent oil density is corrected for pressure, and then temperature as follows,

$$\rho_o = \rho_{ao} + \Delta\rho_P - \Delta\rho_T \quad (2.39)$$

where the correction due to pressure is,

$$\Delta\rho_P = (0.167 + 16.181 \times 10^{-0.0425\rho_{ao}})(P/1000) - 0.01(0.299 + 26.3 \times 10^{-0.0603\rho_{ao}})(P/1000)^2 \quad (2.40)$$

and that due to temperature is,

$$\Delta\rho_T = \left[ 0.0133 + 152.4(\rho_{ao} + \Delta\rho_P)^{-2.45} \right] (T - 60) - \left[ 8.1 \times 10^{-6} - 0.0622 \times 10^{-0.0764(\rho_{ao} + \Delta\rho_P)} \right] (T - 60)^2 \quad (2.41)$$

Eqs.(2.40-41) were proposed initially by Standing and Katz [52] as working charts, and later numerically by Standing [49].

When the oil composition is known, Standing and Katz [52] proposed to calculate the apparent oil density by the following method.

It is assumed that hydrocarbon compounds heavier than ethane (including  $\text{H}_2\text{S}$ ) retain their individual volumes as pure in the mixture. Therefore, the density of a  $C_{7+}$  mixture is determined from,

$$\rho_{C_7+} = \left( \sum_{C_1}^{C_7+} x_i M_i \right) / \left( \sum_{C_1}^{C_7+} x_i M_i / \rho_i \right) \quad (2.42)$$

where  $x_i$  is the mole fraction of component  $i$ , and  $\rho_i$  is the density at the standard conditions (Table A.1 in Appendix A). The measured density of  $C_{7+}$  fraction is used in this method.

The contribution of ethane and methane to the apparent oil density is then calculated in turn by considering their effective volume as dissolved in the liquid,

$$\rho_{C_2+} = \rho_{C_3+} (1 - 0.01386w_{C_2} - 0.000082w_{C_2}^2) + 0.379w_{C_2} + 0.0042w_{C_2}^2 \quad (2.43)$$

and

$$\rho_{ao} = \rho_{C_1+} = \rho_{C_2+} (1 - 0.012w_{C_1} - 0.000158w_{C_1}^2) + 0.0133w_{C_1} + 0.00058w_{C_1}^2 \quad (2.44)$$

$$40 < \rho_{C_3+} < 60 \text{ lbm/ft}^3$$

$$w_{C_1} < 16$$

$$w_{C_2} < 10$$

where  $w_{C_2}$ , and  $w_{C_1}$  are the weight percent of  $C_2$  in  $C_{2+}$ , and  $C_1$  in  $C_{1+}$  (total mixture), respectively. The apparent density is then adjusted for pressure and temperature as in Eqs.(2.39-41).

If  $\text{CO}_2$  is present at a low concentration, it can be treated on the additive volume basis, using an effective specific gravity of 0.420. The mass of nitrogen, if present at low concentration, is added to  $w_{C_1}$ .

The method predicts highly accurate density data for the stock tank oil and low bubble point pressure oils. The reasons for its success are the direct use of measured  $C_{7+}$  density, which often comprises bulk of the mass, and the validity of the additive volume assumption in hydrocarbon liquid mixtures. The method also provides a reliable estimate for oil samples with high bubble point pressure.

Pedersen et al. [53] also presented a set of correlations representing the Standing-Katz graphical method. A similar method, based on the volume addition at the standard conditions and corrections for pressure and temperature has been proposed by API [54].

#### Example 2.9.

Estimate the Good Oil (Table 2.1) density at its bubble point, using the Katz equivalent liquid volume method.

*Solution:*

The apparent density of the dissolved gas in liquid state is calculated from Eq.(2.37),  $\rho_g=25.65 \text{ lbm/ft}^3$

The apparent density of the oil, including the dissolved gas, at the standard conditions is calculated from Eq.(2.38),  $\rho_{so}=44.66 \text{ lbm/ft}^3$

The density corrections due to pressure and temperature are calculated from Eq.(2.40), and Eq.(2.41), respectively, as follows:

$$\Delta\rho_p=0.92 \text{ lbm/ft}^3 \quad \Delta\rho_T=4.55 \text{ lbm/ft}^3$$

which results in,  $\rho_o=41.03 \text{ lbm/ft}^3$

The estimated value matches the measured value of  $40.97 \text{ lbm/ft}^3$  ( $0.6562 \text{ g/cm}^3$ ) within the experimental accuracy (Table 2.1D).

When the oil composition is known, the method of *Alani and Kennedy* [55] can be used with confidence to predict density even for highly volatile oils. The authors used experimental density data to develop a cubic equation for the oil molar volume,

$$v^3 - \left( \frac{R(T + 460)}{P} + b \right) v^2 + av/P - ab/P = 0 \quad (2.45)$$

where,

$$\begin{aligned} v &= \text{molar volume, ft}^3/\text{lbmol} \\ T &= \text{temperature, } ^\circ\text{F} \\ P &= \text{pressure, psia} \\ R &= 10.7335, (\text{psia})(\text{ft}^3/\text{lbmol})/^{\circ}\text{R} \end{aligned}$$

a and b depend on the component and temperature, and for pure compounds are given by,

$$a = \lambda \cdot e^{n/(T+460)} \quad (2.46)$$

$$b = m(T + 460) + C \quad (2.47)$$

where the constants in Eqs.(2.46-47) are given in Table 2.4.

Table 2.4.  
Constants of Alani and Kennedy equation

Component	$\lambda$	n	$m \times 10^4$	C
C <sub>1</sub> (70-300 °F)	9160.6413	61.893223	3.3162472	0.50874303
C <sub>1</sub> (301-460 °F)	147.47333	3247.4533	- 14.072637	1.8326695
C <sub>2</sub> (100-249 °F)	46709.573	- 404.48844	5.1520981	0.52239654
C <sub>2</sub> (250-460 °F)	17495.343	34.163551	2.8201736	0.62309877
C <sub>3</sub>	20247.757	190.24420	2.1586448	0.90832519
i-C <sub>4</sub>	32204.420	131.63171	3.3862284	1.1013834
n-C <sub>4</sub>	33016.212	146.15445	2.9021257	1.1168144
C <sub>5</sub>	37046.234	299.62630	2.1954785	1.4364289
C <sub>6</sub>	52093.006	254.56097	3.6961858	1.5929406
H <sub>2</sub> S*	13200.0	0	17.900	0.3945
N <sub>2</sub> *	4300.0	2.293	4.490	0.3853
CO <sub>2</sub> *	8166.0	126.00	1.8180	0.3872

\* The constants for these compounds were calculated later by Lohrenz et al. [56].

For the C<sub>7+</sub> fraction:

$$a_{C_{7+}} = \exp \left[ 3.8405985 \times 10^{-3} M_{C_{7+}} - 9.5638281 \times 10^{-4} M_{C_{7+}} / S_{C_{7+}} + 2.6180818 \times 10^2 / (T + 460) + 7.3104464 \times 10^{-6} M_{C_{7+}}^2 + 10.753517 \right] \quad (2.48)$$

$$b_{C_{7+}} = 3.4992740 \times 10^{-2} M_{C_{7+}} - 7.2725403 S_{C_{7+}} + 2.2323950 \times 10^{-4} (T + 460) - 1.6322572 \times 10^{-2} M_{C_{7+}} / S_{C_{7+}} + 6.2256545 \quad (2.49)$$

The values of a and b for mixtures are determined by molar averaging,

$$a = \sum a_i x_i \quad (2.50)$$

$$b = \sum b_i x_i \quad (2.51)$$

When Eq.(2.45) has more than one real root, the lowest value is taken as the liquid density.

It should be noted that the Alani-Kennedy equation of state can be used only to determine the hydrocarbon liquid density, and no other thermodynamic properties, as its parameters have been optimised to match only the density data. Chapter 4 provides a detailed coverage of cubic equations of state. All those equations can be used to predict the oil and gas density when the fluid composition is known.

#### Example 2.10.

Calculate the Good Oil density at its bubble point, using the Alani-Kennedy method.

*Solution:*

The two parameters for C<sub>1</sub>-C<sub>6</sub> are calculated from Eqs.(2.46-47), with iC<sub>4</sub> and nC<sub>4</sub> added together. The parameters for C<sub>7+</sub> are calculated from Eqs.(2.48-49). The results are as given in the following table, with the mixture parameters and molecular weight calculated by molar averaging.

Component	100x	a	b	ax	bx	M	Mx
C1	36.47	10033.56	0.7342478	3659.240	0.2677802	16.043	585.1
C2	9.67	25767.48	0.8727392	2491.715	0.0843939	30.07	290.8
C3	6.95	26784.27	1.0551130	1861.507	0.0733304	44.096	306.5
i-C4	1.44	39082.69	1.3316469	562.791	0.0191757	58.123	83.7
n-C4	3.93	40932.80	1.3141589	1608.659	0.0516464	58.123	228.4
C5	2.85	57558.03	1.5857214	1640.404	0.0451931	72.15	205.6
C6	4.33	75745.96	1.8442812	3279.800	0.0798574	86.177	373.1
N2	0.16	4314.52	0.6906200	6.903	0.0011050	44.01	7.0
CO2	0.91	9828.37	0.5108240	89.438	0.0046485	28.01	25.5
C7+	33.29	176019.35	3.6344215	58596.840	1.2098989	218	7257.2
Total	100.00			73797.297	1.8370294		93.6

Substituting the mixture parameters in Eq.(2.45), with the pressure and temperature equal to those at the bubble point, results in the following cubic equation:

$$v^3 - 4.60696491v^2 + 28.0065645v - 51.448883 = 0$$

The above cubic equation has one real root (Appendix C),

$$v = 2.266 \text{ ft}^3/\text{lbmol}$$

The density is calculated as,

$$\rho = M/v = 93.6/2.266 = 41.32 \text{ lbm/ft}^3 \text{ (690 kg/m}^3\text{)}$$

The estimated value deviates about 0.8 % from the measured value of 40.97 lbm/ft<sup>3</sup> (0.6562 g/cm<sup>3</sup>, Table 2.1D).

### Oil Viscosity

The live oil viscosity is often estimated from correlations which account for the effect of dissolved gas and pressure on the viscosity of dead (stabilised) oil.

The viscosity of gas-free crude oil can be estimated from correlations of Beal [57], Beggs-Robinson [58], Egbogah-Ng [59], or Labedi [60], to name a few.

Beggs and Robinson [58] correlated viscosity data of 600 oil samples within a wide range of pressure and temperature as follows,

$$\mu_{od} = 10^A - 1 \quad (2.52)$$

where,

$$\log A = 3.0324 - 0.02023^\circ \text{API} - 1.163 \log T \quad (2.53)$$

and  $\mu_{od}$  is the dead oil viscosity in cp at temperature T in °F.

Egbogah and Ng [59] modified the expression for A, as

$$\log A = 1.8653 - 0.025086 (\text{API}) - 0.56441 \log T \quad (2.54)$$

The correlations which estimate the dead oil viscosity from the oil gravity and temperature only are not very reliable and errors over 25% are expected from the above correlations [38].

Beggs and Robinson [58] proposed the following correlation to estimate the effect of dissolved gas,

$$\mu_{oh} = C \mu_{od}^B \quad (2.55)$$

where,

$$C = 10.715 (R_s + 100)^{-0.515}$$

$$B = 5.44 (R_s + 150)^{0.138}$$

and  $\mu_{oh}$  is the saturated oil viscosity at its bubble point pressure.

An average deviation of about 20% [38] is expected from the above correlation using the measured dead oil viscosity. The deviation will be much higher due to compounding of errors when estimated dead oil viscosity is used.

Vasquez-Beggs [41] proposed the following correlation to account for the effect of pressure on the oil viscosity above its bubble point pressure  $p_b$ .

$$\mu_o = \mu_{oh} (P/P_b)^D \quad (2.56)$$

where,

$$D = 2.6 P^{1.187} \exp(-11.513 - 8.98 \times 10^{-5} P)$$

In the comparative study of De Ghetto [38], the correlation of Labedi [60], performed more reliably than others with a standard deviation of 13%. The Labedi correlation, which is based on linear changes of viscosity with pressure above the bubble point as reported often experimentally, is as follows,

$$\mu_o = \mu_{oh} + (P/P_b - 1) \left( 10^{-2.488} \mu_{od}^{0.9036} P_b^{0.6151} / 10^{0.0197 \text{ } ^\circ \text{API}} \right) \quad (2.57)$$

#### Example 2.11.

Calculate the Good Oil viscosity at 5000 psig and 220 °F.

#### Solution:

Using the Beggs-Robinson correlation, the dead oil viscosity, Eq.(2.52), is calculated as 1.020 cp. The Egbogah-Ng correlation, Eq.(2.54), results in a dead oil viscosity of 1.152 cp. The measured value is 1.29 cp.

The viscosity at the bubble point is calculated using Eq.(2.55), with  $R_s=768$  SCF/STB,

$$C=0.32859013 \quad B=0.5421982 \quad \mu_{oh}=0.355 \text{ cp}$$

The reported measured viscosity at the bubble point pressure of 2635 psia is 0.373 cp.

The effect of pressure,  $P=5015$  psia, on the oil viscosity can be estimated using the Vasquez-Beggs correlation, Eq.(2.56),



$$D=0.40886446$$

$$\mu_a=0.461 \text{ cp}$$

The Labedi correlation, Eq.(2.57), estimates the viscosity at 5015 psia equal to 0.422 cp. The reported measured value is 0.450 cp.

### 2.3.2 Natural Gas

Whereas the phase behaviour of black oil is controlled mainly by its content of light components (gas), the behaviour of rich gas depends strongly on the concentration and distribution of its heavy components. Hence, reliable estimation of phase change and the associated properties, using the same approach as that for black oil, cannot be expected. Single phase gas properties, however, can be estimated reasonably using empirical correlations.

Gas is generally characterised, in the empirical correlations, by its specific gravity relative to air at one atmosphere and 520 °R (60 °F). Its molecular weight can be calculated simply from Eq.(1.4). *In all the gas correlations in this section, the temperature is in the absolute scale of Rankine.*

Rich gases form condensate at the standard (laboratory) conditions. Hence, their measured specific gravity should be adjusted by including the condensed phase. In laboratory tests, when the separated gas and condensate are analysed and the overall composition is known, the mixture molecular weight can be calculated by molar averaging, and its specific gravity is determined from Eq.(1.4). When the composition is not known, but the mass and molecular weight of gas and condensate are known, Eq.(2.8) provides the mixture molecular weight value.

In the absence of measured condensate molecular weight, Eq.(2.58) may be used to estimate it [61],

$$M_a = 5954 / (\text{API} - 8.811) = 42.43 S_o / (1.008 - S_o) \quad (2.58)$$

Substituting Eq.(2.58) in Eq.(2.8), and writing it for one STB of condensate similar to Eq.(2.38), we obtain,

$$M_m = \left[ (R_s / 380)(28.96 S_g) + 5.61 \times 62.4 S_o \right] / \left[ \frac{(R_s / 380)(28.96 S_g)}{28.96 S_g} + \frac{5.61 \times 62.4 S_o}{42.43 S_o / (1.008 - S_o)} \right]$$

which will reduce to,

$$M_m = \left[ 0.07621 R_s S_g + 350 S_o \right] / \left[ (R_s / 380) + 8.25(1.008 - S_o) \right] \quad (2.59)$$

The reservoir gas specific gravity can be calculated simply by dividing its molecular weight by that of air (28.96). When using field production data, the gas evolved in the stock tank is often not measured. Gold et al. [61] examined experimental data on 234 gas samples, and proposed the following correlation to estimate gas specific gravity, when only the first stage separator gas data is available in a three stage separation process, including the stock tank,

$$S_g = (R_{s1} S_{g1} + G_a + 4600 S_o) / (R_{s1} + V_e) \quad (2.60)$$

where  $R_1$  and  $S_{g1}$  are the first stage separator gas to oil ratio (relative to the stock tank oil) and specific gravity, respectively,  $G_a$  is related to the mass of gas produced from the stock tank, and the second stage separator if present.  $V_c$  is the volume of gas produced from the stock tank, the second stage separator if present, and the volume of the stock tank oil if it were gas. The values of  $G_a$  and  $V_c$  are estimated as,

$$G_a = A_1(P_1 - 14.65)^{A_2} S_{g1}^{A_3} (^{\circ}\text{API})^{A_4} (T_1 - 460)^{A_5} (T_2 - 460)^{A_6} \quad (2.61)$$

$$V_c = B_0 + B_1 P_1^{B_2} S_{g1}^{B_3} (^{\circ}\text{API})^{B_4} (T_1 - 460)^{B_5} (T_2 - 460)^{B_6} \quad (2.62)$$

where  $P_1$  and  $T_1$  are the first stage separator pressure, psia, and temperature,  $^{\circ}\text{F}$ , respectively, and  $T_2$  is the second stage separator temperature, if present. The values of constants are as follows:

Three-stage separation,

$A_1 = 2.99222$	$A_2 = 0.970497$	$A_3 = 6.80491$	$A_4 = 1.07916$
$A_5 = -1.19605$	$A_6 = 0.553669$		
$B_0 = 535.916$	$B_1 = 2.62310$	$B_2 = 0.793183$	$B_3 = 4.66120$
$B_4 = 1.20940$	$B_5 = -0.849115$	$B_6 = 0.269869$	

Two-stage separation,

$A_1 = 1.45993$	$A_2 = 1.33940$	$A_3 = 7.09434$	$A_4 = 1.14356$
$A_5 = -0.934460$			
$B_0 = 635.530$	$B_1 = 0.361821$	$B_2 = 1.05435$	$B_3 = 5.08305$
$B_4 = 1.58124$	$B_5 = -0.791301$		

The estimated specific gravity by the above method is expected to be within 2% of laboratory determined value, increasing to a deviation of 6% when non-hydrocarbon content of the gas is between 2 and 25 mole %. It is not recommended for gases containing more than 25 mole % non-hydrocarbons.

### *Volumetric Data*

The equation of state, Eq.(1.5), relating the pressure, volume, and temperature, is adequate to provide all the required volumetric information, such as the gas formation volume factor, density and isothermal compressibility coefficient. The key parameter is the compressibility factor,  $Z$ , which can be estimated using a generalised chart. Figure 2.21 shows the chart for sweet natural gases as prepared by Standing and Katz [62]. The chart was developed by using data on methane binary mixtures with ethane, propane, and butane and other natural gases over a wide range of composition with a maximum molecular weight of 40.

The success of the chart has motivated many investigators to reproduce it by numerical correlations. Takacs [63], compared eight correlations amenable for computer calculations, both for accuracy and computational effort. The correlation of Dranchuk and Abou-Kassem [64] was found to reliably reproduce the data with an average absolute deviation of 0.3%. The correlation is basically the eleven parameter Benedict-Webb-Rubin equation, modified by Starling [65] as will be described in Section 4.1, with the parameters determined by fitting the equation to the chart.

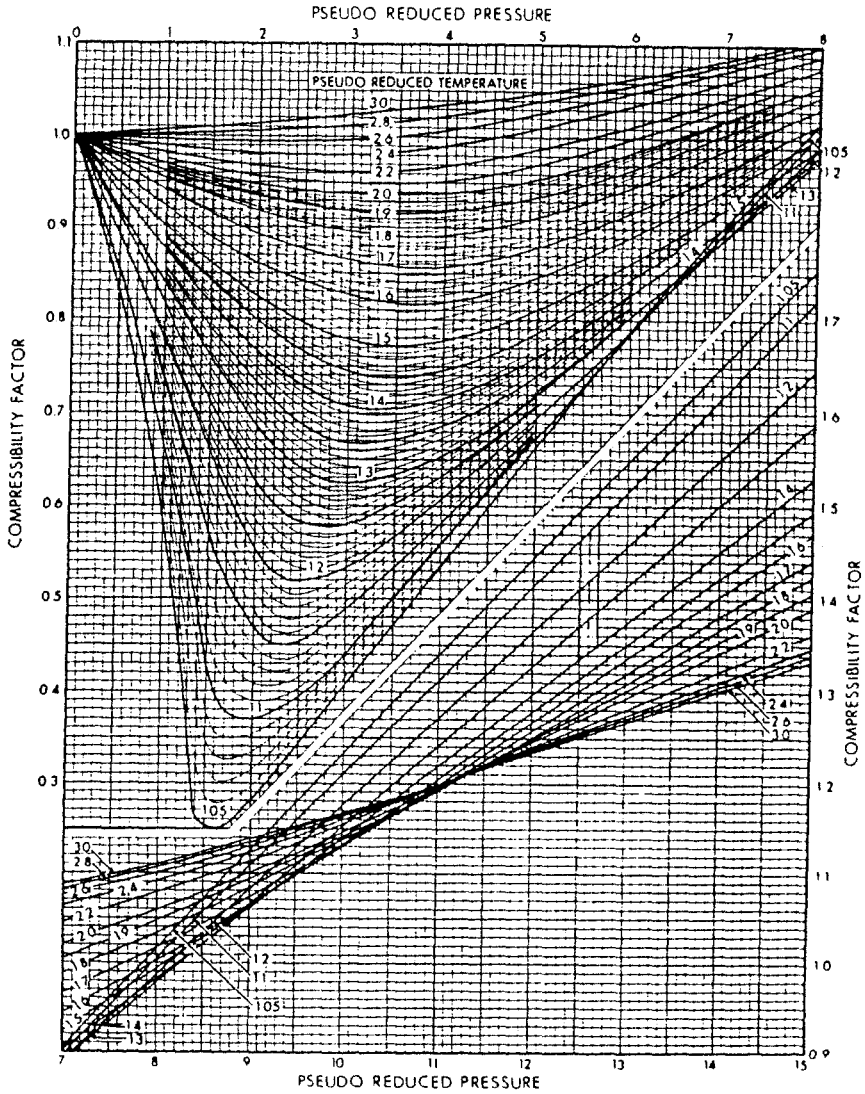


Figure 2.21. Compressibility factor of natural gases. SPE Copyright. Reproduced from [62] with permission.

$$Z = 1 + (A_1 + A_2/p_r T_r + A_3/p_r T_r^3 + A_4/p_r T_r^4 + A_5/p_r T_r^5) p_r + (A_6 + A_7/p_r T_r + A_8/p_r T_r^2) p_r^2 - A_9(A_7/p_r T_r + A_8/p_r T_r^2) p_r^5 + A_{10}(1 + A_{11} p_r^2)(p_r^2/p_r T_r^3) \exp(-A_{11} p_r^2) \quad (2.63)$$

where  $p_r$ , the pseudo reduced density, is defined as,

$$p_r = 0.27 [p_r / (Z p_r T_r)] \quad (2.64)$$

and the constants are,

$$\begin{aligned} A_1 &= 0.3265 & A_2 &= -1.0700 & A_3 &= -0.5339 & A_4 &= 0.01569 & A_5 &= -0.05165 \\ A_6 &= 0.5475 & A_7 &= -0.7361 & A_8 &= 0.1844 & A_9 &= 0.1056 & A_{10} &= 0.6134 & A_{11} &= 0.7210 \end{aligned}$$

Eq.(2.63) is valid over the following ranges:

$$1 < p_r T_r \leq 3 \quad \text{and} \quad 0.2 \leq p_r < 30 \quad \quad 0.7 < p_r T_r \leq 1 \quad \text{and} \quad p_r P_r < 1$$

The pseudo critical temperature and pressure are often calculated by molar averaging of the critical properties of the gas components, Kay's mixing rule Eq.(1.4). Other mixing rules to calculate the pseudo properties for estimating the compressibility factor are also available. Sutton [66] used data on 264 fluids to back calculate their pseudo critical properties for improving predicted Z using the above equation, and proposed to use the following correlations,

$$p_r P_c = 756.8 - 131.0 S_g - 3.6 S_g^2 \quad (2.65)$$

$$p_r T_c = 169.2 + 349.5 S_g - 74.0 S_g^2 \quad (2.66)$$

The above correlations in SI units are,

$$p_r P_c = 5.218 - 0.9032 S_g - 0.0248 S_g^2 \quad (2.65a)$$

$$p_r T_c = 94.00 + 194.2 S_g - 41.1 S_g^2 \quad (2.66a)$$

where the pressure and temperature are in MPa and K, respectively.

Even when the gas composition is known, the use of above correlations to estimate the pseudo critical properties is recommended in preference to using any mixing rule. It should be emphasised that the calculated pseudo critical properties from the above correlations should be used only in calculating the reduced values for estimating Z from Eq.(2.63), or Figure 2.22. The above approach results in estimation of the compressibility factor with a deviation less than 2% [37,66].

Natural gases which contain significant quantities of sour gases, behave differently than that shown in Figure 2.22. Wichert and Aziz [67] defined a critical temperature adjustment factor, E, which is a function of CO<sub>2</sub> and H<sub>2</sub>S concentrations in the mixture,

$$E = 120 \left[ (y_{H_2S} + y_{CO_2})^{0.9} - (y_{H_2S} + y_{CO_2})^{1.6} \right] + 15 (y_{H_2S}^{0.5} - y_{H_2S}^{4.0}) \quad (2.67)$$

where y is the component mole fraction in the mixture. The correction factor is used to adjust the pseudo-critical properties, as,

$${}_pT_c^{cor} = {}_pT_c - E \quad (2.68)$$

$${}_pP_c^{cor} = ({}_pP_c - {}_pP_c^{cor}) / [{}_pT_c + y_{H2S}(1 - y_{H2S}) E] \quad (2.69)$$

The natural gas compressibility factor, as calculated from Figure 2.22, may be increased by 1% for each 5 mole % nitrogen in the gas [25].

#### Example 2.12.

Estimate the compressibility factor of the gas condensate, reported in Table 2.2, at the reservoir temperature and  $P=550$  barg, using the generalised chart.

#### Solution:

The gas specific gravity is initially calculated to estimate its critical temperature and pressure, using Eq.(2.65) and Eq.(2.66), respectively.

$$S_g = 27.3/28.96 = 0.9427 \quad T_c = 432.91 \text{ } ^\circ\text{R} \quad P_c = 630.1 \text{ psia}$$

$$T_r = (250 + 459.6)/432.91 = 1.639 \quad P_r = 7990/630.1 = 12.68$$

The above reduced values result in  $Z=1.31$ , using Figure 2.21. Substitution of the reduced values in Eq.(2.63) results in  $Z=1.2996$ . The estimated value deviates only by 1% from the measured value of 1.2866. The correction of gas critical properties due to  $N_2$  and  $CO_2$  content was ignored in the above example.

#### Gas Viscosity

The gas viscosity generally increases with pressure. The increase of temperature decreases the liquid viscosity, whereas it increases the gas viscosity at low and moderate pressures. At high pressure, the gas viscosity behaviour approaches that of liquid as shown in Figure 2.22 [68].

Lee et al. [69] measured the viscosity of four natural gases over a temperature range of 560-800  $^\circ\text{R}$ , up to 8000 psia, and proposed the following correlation,

$$\mu_g = 10^{-4} a \exp [b (\rho_g / 62.43)^c] \quad (2.70)$$

where

$$a = (9.379 + 0.0160M) T^{-1.5} / (209.2 + 19.26M + T)$$

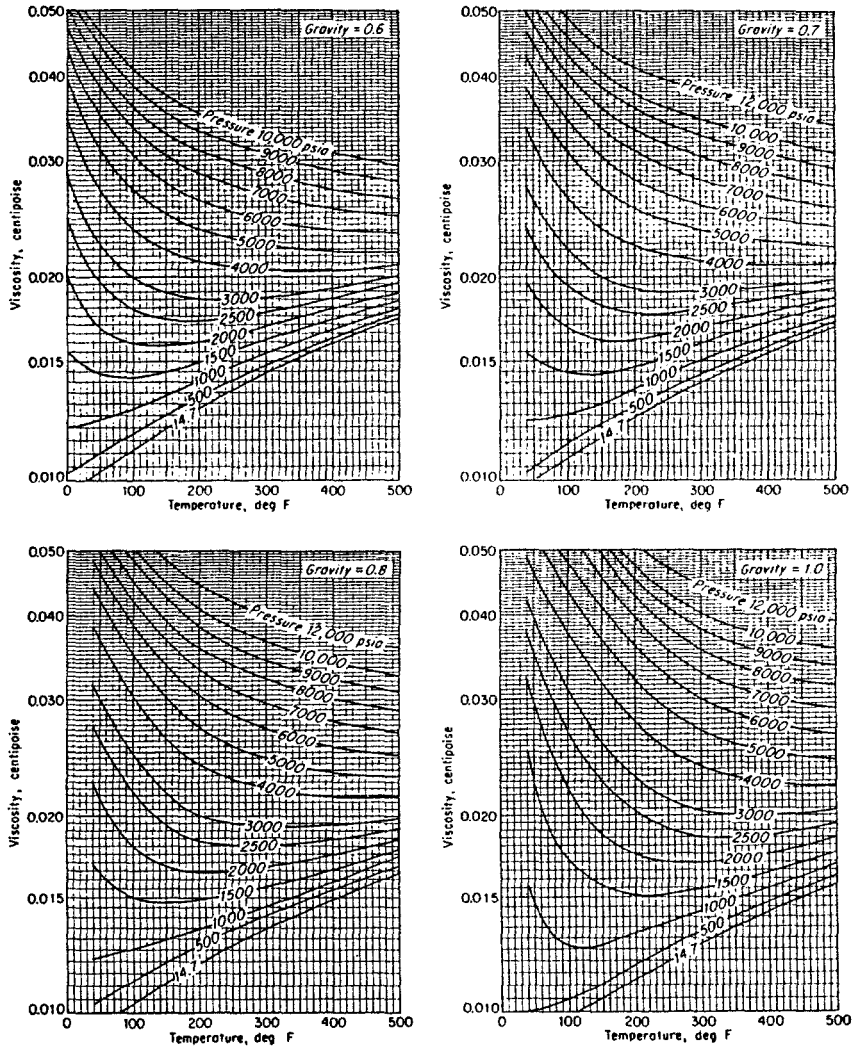
$$b = 3.448 + 0.01009M + (986.4/T)$$

$$c = 2.4 - 0.2b$$

$\mu_g$  is the gas viscosity (cp) at the absolute temperature of  $T$  ( $^\circ\text{R}$ ),  $M$  is the gas molecular weight, and  $\rho_g$  is the gas density at prevailing pressure and temperature, in  $\text{lbm/ft}^3$ .

The correlation of Carr et al. [70] is often used to estimate the natural gas viscosity, particularly for gases containing significant amounts of non-hydrocarbon components. It initially estimates the gas viscosity at the atmospheric pressure and the prevailing temperature,

$$\mu_h = [1.709 \times 10^{-5} - 2.062 \times 10^{-6} S_g] (T - 460) + 8.188 \times 10^{-3} - 6.15 \times 10^{-3} \log S_g \quad (2.71)$$



$$K = (^\circ\text{F} + 459.67) / 1.8$$

$$\text{MPa} = 0.006895 \times \text{psia}$$

$$\text{mPa.s} = \text{cp}$$

Figure 2.22. Viscosity of natural gases. McGraw-Hill Companies Copyright. Reproduced from [68] with permission.

For gases containing non-hydrocarbon compounds, the following corrections to the calculated atmospheric viscosity must be included,

$$\mu_1 = \mu_h + \lambda_{N_2} + \lambda_{CO_2} + \lambda_{H_2S} \quad (2.72)$$

where,

$$\lambda_{N_2} = y_{N_2} \times 10^{-3} [9.59 + 8.48 \log S_g] \quad (2.73)$$

$$\lambda_{CO_2} = y_{CO_2} \times 10^{-3} [6.24 + 9.08 \log S_g] \quad (2.74)$$

$$\lambda_{H_2S} = y_{H_2S} \times 10^{-3} [3.73 + 8.49 \log S_g] \quad (2.75)$$

and  $y$  is the mole fraction of non-hydrocarbon component in the gas.

The calculated viscosity at the atmospheric pressure,  $\mu_1$ , is then adjusted for pressure, using the gas pseudo reduced temperature and pressure, over ranges of 1-3, and 1-20, respectively, as,

$$\ln \left( \mu_r T_r \frac{\mu_g}{\mu_1} \right) = a_0 + a_{1p} P_r + a_{2p} P_r^2 + a_{3p} P_r^3 + T_r (a_4 + a_{5p} P_r + a_{6p} P_r^2 + a_{7p} P_r^3) \\ + T_r^2 (a_8 + a_{9p} P_r + a_{10p} P_r^2 + a_{11p} P_r^3) + T_r^3 (a_{12} + a_{13p} P_r + a_{14p} P_r^2 + a_{15p} P_r^3) \quad (2.76)$$

where  $\mu_r T_r$  and  $P_r$  are the pseudo reduced temperature and pressure, respectively, and the values of the coefficients are :

$$\begin{aligned} a_0 &= -2.46211820E-00 & a_1 &= 2.97054714E-00 & a_2 &= -2.86264054E-01 & a_3 &= 8.05420522E-03 \\ a_4 &= 2.80860949E-00 & a_5 &= -3.49803305E-00 & a_6 &= 3.60373020E-01 & a_7 &= -1.04432413E-02 \\ a_8 &= -7.93385684E-01 & a_9 &= 1.39643306E-00 & a_{10} &= -1.49144925E-01 & a_{11} &= 4.41015512E-03 \\ a_{12} &= 8.39387178E-02 & a_{13} &= -1.86408848E-01 & a_{14} &= 2.03367881E-02 & a_{15} &= -6.09579263E-04 \end{aligned}$$

The correlation was originally given in graphical forms by Carr et al. [70], and was converted to Eqs. (2.71-75) by Standing [49], and to Eq.(2.76) by Dempsey [71].

### Example 2.13.

Estimate the viscosity of the gas condensate described in Example 2.12.

### Solution:

The gas viscosity can be estimated using Figure 2.22 at 250 °F and 7990 psia. Interpolating between the charts at  $S_g=0.8$  and  $S_g=1.0$  for the gas with  $S_g=0.9427$ , we obtain a gas viscosity of 0.0372 cp.

An alternative method is the Lee et al. correlation, Eq.(2.70). The three parameters are calculated at  $T=(250+459.6)$  °R and  $M=27.3$ , as follows:

$$a=128.464652 \quad b=5.11353592 \quad c=1.37729282$$

The gas density is calculated using  $Z=1.2866$ ,

$$\rho = MP/(ZRT) = 27.3 \times 7990 / (1.2866 \times 10.732 \times 709.6) = 22.262 \text{ lbm/ft}^3. \text{ Hence, } \mu_g = 0.04347 \text{ cp}$$

### 2.3.3 Formation Water

The mutual solubilities of water and hydrocarbons are small, and in most cases the hydrocarbon phase behaviour can be studied independently of the water phase. As the temperature increases the volatility of water increases, and its contribution to the gas phase in the reservoir becomes significant. A thermodynamically consistent approach is to treat water as just another component, along with hydrocarbon and other non-hydrocarbon components, and to determine the system behaviour. This approach will be discussed in Section 4.3, using equations of state.

Connate water in a petroleum reservoir can be assumed to be in equilibrium with hydrocarbon phases. When water, which is not in equilibrium with the reservoir hydrocarbon phase encroaches into a reservoir, such as in a water injection process, the dissolution of light hydrocarbons from the oil into the water will, given enough time for diffusion, reduce the oil bubble point. Figure 2.23 shows the reduction of the bubble point pressure of a North Sea black oil at 293 K, when contacted with water.

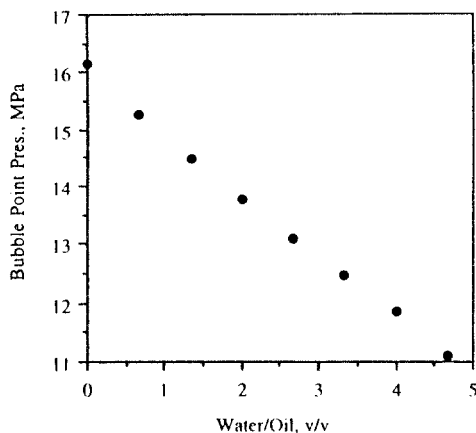


Figure 2.23. Variations of oil bubble point pressure contacted with fresh water.

Under certain conditions of pressure and temperature, water and some gases may form solid crystalline compounds known as clathrate gas hydrates, or simply hydrates. Figure 2.24 shows the hydrate formation conditions for natural gas-water systems. The pressure required to form solid hydrates increases with temperature. Hydrates are not reviewed in this book. Sloan [72] covers the subject comprehensively.

In conventional applications, where the hydrocarbon-water mutual solubility is small, simple empirical correlations can be used to estimate the water phase properties, and the water content of hydrocarbon phases. Water formed by condensation from the gas phase is salt free. The reservoir formation water may contain salt, from less than that of the normal sea water, to almost being saturated with salt. Although various units are employed to describe the salt content [25], the weight percent of salt/brine is often used in the correlations. The presence of salt reduces the mutual solubility of hydrocarbon-water. As the solubility of hydrocarbon compounds in water decreases with increase of water salinity, some investigators ignore the dissolved gas, and propose to use brine physical property correlations for the formation water.



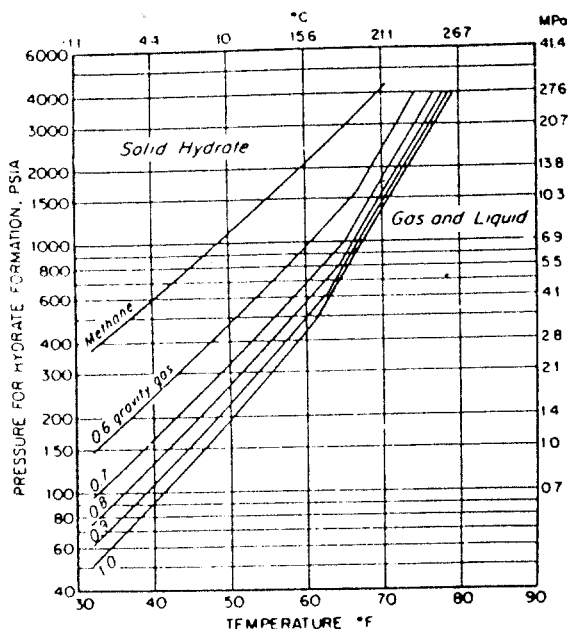


Figure 2.24. Hydrate phase boundary with natural gas. McGraw-Hill Companies Copyright. Reproduced from [68] with permission.

### Water Content of Hydrocarbon Phase

The solubility of water in liquid hydrocarbons at their vapour pressures is shown in Figure 2.25 [73]. The solubility increases with temperature. The effect of pressure on liquid-liquid equilibria is generally small.

The water vapour content of natural gases in equilibrium with water is commonly evaluated from Figure 2.26, including corrections for the molecular weight of gas and salinity of water [73].

The mole fraction of water in the gas phase can be estimated by dividing water vapour pressure, at the prevailing temperature, by the prevailing pressure at low pressure conditions (Raoult's law, see Section 3.2). The vapour pressure of pure water, from its freezing point to critical point, can be calculated by the following relation [74],

$$P_w^s = \exp \left[ A + B/(T + 459.6) + C \ln(T + 459.6) + D(T + 459.6)^E \right] \quad (2.77)$$

where  $T$  is in °F,  $P$  in psia and the constants are,

$$A = 69.103501$$

$$B = -13064.76$$

$$C = -7.3037$$

$$D = 1.2856E-06$$

$$E = 2$$

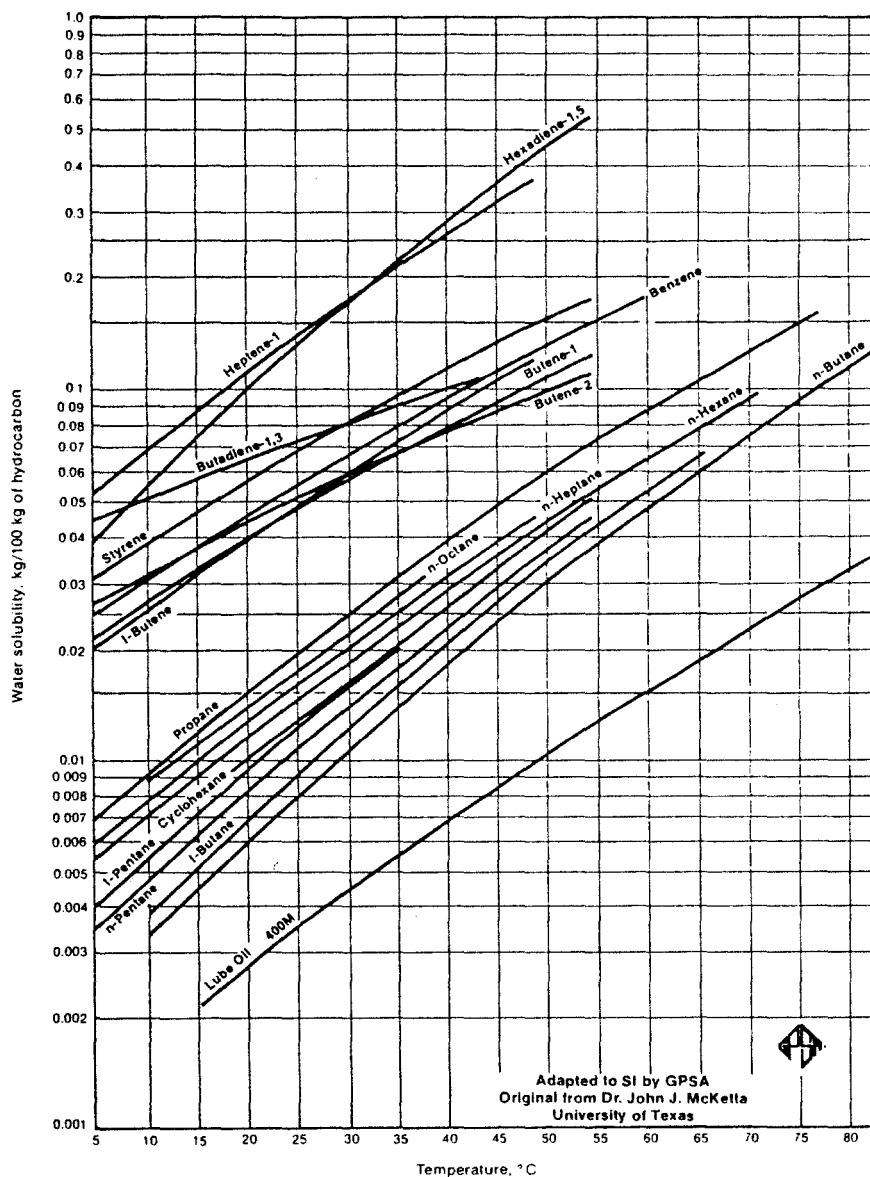


Figure 2.25. Water content of liquid hydrocarbons. GPA Copyright. Reproduced from [73] with permission.

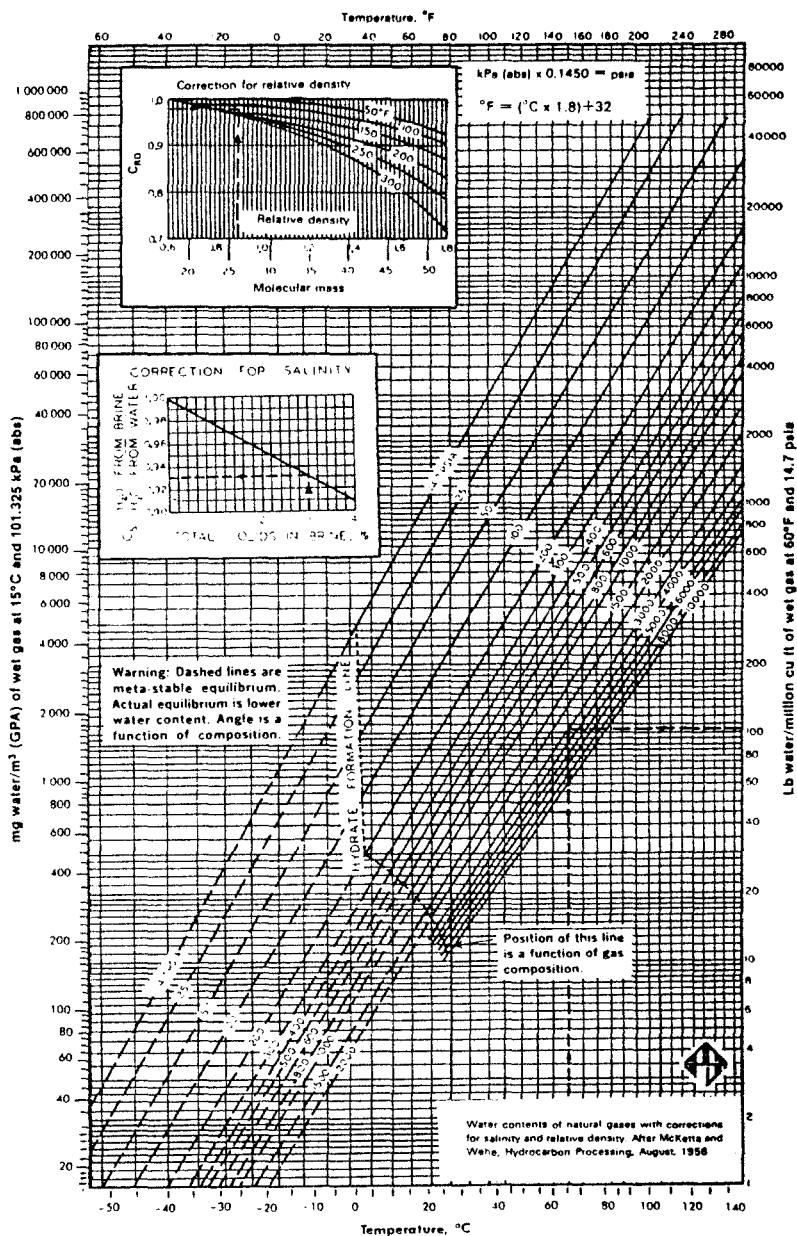


Figure 2.26. Water vapour content of natural gas in equilibrium with water. GPA Copyright Reproduced from [73] with permission.

As one lbmole of gas occupies a volume of 380 SCF, Table 1.1, the amount of water in gas is determined as,

$$m_w = (18/380) P_w^s / P \quad \text{lbm/SCF}$$

The above correlation in SI units, P in MPa and T in K is as follows,

$$P_w^s = 10^{-6} \exp(A + B/T + C \ln T + DT^E) \quad (2.77a)$$

$$A=73.649 \quad B=-7258.2 \quad C=-7.3037 \quad D=4.1653 \times 10^{-6} \quad E=2$$

$$m_w = (18/23.95) P_w^s / P \quad \text{kg/m}^3(\text{sc})$$

The extrapolation of the salinity correction factor in Figure 2.27 to high salt concentrations is believed to underpredict the water vapour content of a gas in equilibrium with brine. The graphical correlation of Katz [68] for the salinity correction factor is recommended instead. The graphical correlation, developed from water vapour pressure depression due to salt, can be expressed as [25],

$$\phi_s = 1 - 4.920 \times 10^{-3} w_s - 1.7672 \times 10^{-4} w_s^2 \quad (2.78)$$

where  $w_s$  is the weight percent of salt in brine.

#### Example 2.14.

Estimate the water content of the above gas condensate at its dew point in equilibrium with water containing 10%, by weight, salt.

#### Solution:

The water vapour content is read from Figure 2.26 at 250 °F (121 °C) and 6837 psia, (47.14 MPa) to be 430 lb water per million ft<sup>3</sup> of wet gas at the standard conditions (6.89 g/m<sup>3</sup>) prior to any adjustment for the gas molecular weight and the water salinity. Figure 2.26 shows a correction factor of 0.96 for the gas with molecular weight of 27.3. A correction factor of 0.93 is obtained from Eq.(2.78) for the salt content of 10%. Hence,

$$W_w = 430 \times 0.96 \times 0.93 = 384 \text{ lb water/ million ft}^3 \text{ of wet gas at the standard conditions (6.15 g/m}^3\text{)}.$$

#### Hydrocarbon Solubility in Water

The solubility of hydrocarbon gases in water increases with pressure and decreases with temperature to a minimum value before increasing, as shown in Figure 2.28 for methane [74]. The gas solubility decreases with increasing carbon number. The solubility of hydrocarbons in water can be estimated by applying Henry's law for dilute solutions, as described in Section 3.2.

Figure 2.27 is often used to estimate the solubility of natural gas in water. The chart can be represented within 5% accuracy [25] by,

$$R_w = A_0 + A_1 P + A_2 P^2 \quad (2.79)$$

where  $R_w$  is the ft<sup>3</sup> gas (sc) dissolved in a barrel of water at pressure P in psia. The coefficients depend on the temperature, as,

$$A_0 = 8.15839 - 6.12265 \times 10^{-2}T + 1.91663 \times 10^{-4}T^2 - 2.1654 \times 10^{-7}T^3$$

$$A_1 = 1.01021 \times 10^{-2} - 7.44241 \times 10^{-5}T + 3.05553 \times 10^{-7}T^2 - 2.94883 \times 10^{-10}T^3$$

$$A_2 = -10^{-7}(9.02505 - 0.130237T + 8.53425 \times 10^{-4}T^2 - 2.34122 \times 10^{-6}T^3 + 2.37049 \times 10^{-9}T^4)$$

$$1000 < P < 10,000 \quad \text{and} \quad 100^\circ\text{F} < T < 340^\circ\text{F}$$

where  $T$  is in  $^\circ\text{F}$ .

The presence of salt in water reduces the gas solubility. The correlation of McKetta-Wehe, as presented by McCain [25], is as follows.

$$\log(R_{ws}/R_w) = 0.0840655w_s T^{-0.185854} \quad (2.80)$$

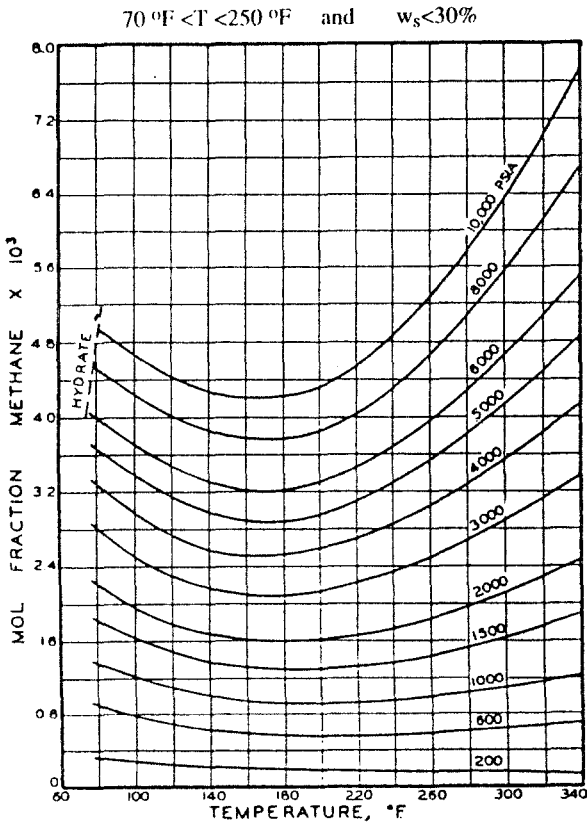


Figure 2.28. Solubility of methane in water. SPE Copyright. Reproduced from [75] with permission.

### Water Formation Volume Factor

The volume of water at reservoir conditions when brought to the surface generally decreases, unless from highly undersaturated reservoirs, due to the combined effect of liberated gas, thermal compaction, and pressure expansion. McCain [25] proposed the following correlation.

$$B_w = (1 + \Delta V_{wP})(1 + \Delta V_{wT}) \quad (2.81)$$

where  $\Delta V_{wP}$  and  $\Delta V_{wT}$  are the volume changes due to pressure and temperature, respectively, as follows:

$$\Delta V_{wP} = -(3.58922 \times 10^{-7} + 1.95301 \times 10^{-9} T)P - (2.25341 \times 10^{-10} + 1.72834 \times 10^{-13} T)P^2 \quad (2.82)$$

$$\Delta V_{wT} = -1.0001 \times 10^{-2} + 1.33391 \times 10^{-4} T + 5.50654 \times 10^{-7} T^2 \quad (2.83)$$

The correlation is valid at  $T < 260^\circ\text{F}$  and  $P < 5000$  psia, over a wide range of salt concentration, as presumably, the effect of salt on thermal expansion of water is cancelled by its effect on the gas solubility in water [37].

### Compressibility of Water

The isothermal compressibility coefficient of gas free water ( $C_{wf}$ ) can be calculated from [76],

$$C_{wf} = 10^{-6} (C_0 + C_1 T + C_2 T^2) \quad (2.84)$$

where  $C_{wf}$  is in  $\text{psi}^{-1}$ , at temperature  $T$ ,  $^\circ\text{F}$ , and the coefficients depend on the pressure, as,

$$C_0 = 3.8546 - 0.000134P$$

$$C_1 = -0.01052 + 4.77 \times 10^{-7} P$$

$$C_2 = 3.9267 \times 10^{-5} - 8.8 \times 10^{-10} P$$

where  $P$  is in psia.

The dissolution of gas in water increases its compressibility, as,

$$C_w = C_{wf} (1 + 8.9 \times 10^{-3} R_w) \quad (2.85)$$

where  $R_w$  is gas water ratio in SCF/bbl.

The following multiplying factor to correct the isothermal compressibility coefficient due to salt has been proposed [77],

$$\psi_s = 1 + (-0.052 + 2.7 \times 10^{-4} T - 1.14 \times 10^{-6} T^2 + 1.121 \times 10^{-9} T^3) w_s \quad (2.86)$$

where  $T$  is in  $^\circ\text{F}$ , and  $w_s$  is the weight percent of salt in brine.

*Water Density*

The formation water density at the standard conditions can be estimated from [25],

$$\rho_{w(sc)} = 62.368 + 0.438603w_s + 1.60074 \times 10^{-3}w_s^2 \quad (2.87)$$

Neglecting the mass of dissolved gas in water at reservoir conditions, the water density can be calculated, as,

$$\rho_w = \rho_{w(sc)} / B_w \quad (2.88)$$

where  $B_w$  is the formation volume factor at the prevailing conditions.

*Water Viscosity*

The viscosity of brine (cp) at the atmospheric pressure can be estimated from [25],

$$\mu_{wT} = (109.574 - 8.40564w_s + 0.313314w_s^2 + 8.72213 \times 10^{-3}w_s^3)T^{-D} \quad (2.89)$$

$$100^\circ\text{F} < T < 400^\circ\text{F} \quad \text{and} \quad w_s < 26\%$$

where,

$$D = 1.12166 - 2.63951 \times 10^{-2}w_s + 6.79461 \times 10^{-4}w_s^2 + 5.47119 \times 10^{-5}w_s^3 - 1.55586 \times 10^{-6}w_s^4$$

The effect of pressure on the brine viscosity is estimated, as,

$$\mu_w / \mu_{wT} = 0.9994 + 4.0295 \times 10^{-5}P + 3.1062 \times 10^{-9}P^2 \quad (2.90)$$

$$86^\circ\text{F} < T < 167^\circ\text{F} \quad \text{and} \quad 14,000 \text{ psia} < P$$

*Example 2.15.*

The gas condensate, reported in Table 2.2, is at equilibrium with the reservoir water. The water salinity,  $w_s$ , is 10%. Estimate: (a) the amount of dissolved gas in water, and (b) the isothermal compressibility coefficient, (c) density, and (d) viscosity of water at the gas hydrocarbon dew point conditions.

*Solution:*

(a)

Assuming the natural gas solubility in water is approximately the same as that of methane, Figure 2.27 shows the mole fraction of gas in water equal to  $4.1 \times 10^{-3}$ . The dissolved gas can be converted in terms of SCF/barrel as

$$(\text{mole gas})/(\text{mole water}) = 0.0041/(1 - 0.0041) = 0.00412$$

$$R_w = (380 \text{ SCF gas/mole gas}) \times (\text{mole water}/18 \text{ lb water}) \times (62.4 \text{ lb water/ft}^3 \text{ water}) \times (5.61 \text{ ft}^3/\text{bbl}) \times (0.00412 \text{ mole gas / mole water}) = 30.4 \text{ SCF/bbl } (5.41 \text{ m}^3/\text{m}^3)$$

The dissolved gas can alternatively be calculated from Eq.(2.79). At 250 °F the values of the coefficients are as follows:

$$A_0 = 1.447265 \quad A_1 = 0.00598559 \quad A_2 = -2.483\text{E-}07$$

resulting in  $R_w=30.76$  SCF/bbl at 6837 psia.

The reduction of solubility due to the salt content is estimated using Eq.(2.80).

$$R_{iw}/R_w=0.6707$$

Hence,

$$R_{iw}=20.6 \text{ SCF/bbl } (3.67 \text{ m}^3/\text{m}^3)$$

(b)

The isothermal compressibility coefficient of the gas free water is estimated from Eq.(2.84). At 6837 psia, the coefficients are calculated as follows:

$$C_a=2.9384 \quad C_1=-0.007259 \quad C_2=3.325 \times 10^{-4}$$

resulting in  $C_w=3.20 \times 10^{-6} \text{ psi}^{-1}$  at 250 °F. Applying Eq.(2.85), the calculated compressibility coefficient is adjusted for  $R_{iw}=20.6$  SCF/bbl, resulting in  $C_w=3.79 \times 10^{-6} \text{ psi}^{-1}$ .

The reduction of compressibility due to salt is estimated from Eq.(2.86),

$$\psi_s=0.6176$$

Hence,

$$C_{ws}=2.34 \times 10^{-6} \text{ psi}^{-1} (3.39 \times 10^{-4} \text{ MPa})$$

(c)

The water density at the standard conditions, including 10% salt, is calculated using Eq.(2.87) equal to 66.91 lbm/ft<sup>3</sup>.

The water formation volume factor, at 250 °F and 6837 psia, is calculated using Eq.(2.81), with the volume changes due to pressure and temperature as follows,

$$\Delta V_{wp}=-0.0183454 \quad \Delta V_{wT}=0.05776263 \quad B_w=1.0383$$

Hence,

$$\rho=66.91/1.0383=64.44 \text{ lbm/ft}^3 (1032 \text{ kg/m}^3)$$

(d)

The viscosity of formation water at the atmospheric pressure, temperature of 250 °F, and 10% salt is calculated using Eq.(2.89),

$$D=0.9648084 \quad \mu_{wT}=0.31854 \text{ cp}$$

The effect of pressure on viscosity 6837 psia is estimated, using Eq.(2.90)

$$\mu_w/\mu_{wT}=1.42$$

Hence,

$$\mu_w=0.4523 \text{ cp (mPa.s)}$$



## 2.4 REFERENCES

1. Reudelhuber, F.O: "Separator Sampling of Gas Condensate Reservoirs", *Oil and Gas J.*, 138-140 (June, 1954).
2. Reudelhuber, F.O: "Better Separator Sampling of Crude Oil Reservoirs", *Oil and Gas J.*, 181-183 (Nov., 1954).
3. Reudelhuber, F.O: "Sampling Procedures for Oil Reservoir Fluids", *JPT*, 15-18 (Dec., 1957).
4. American Petroleum Institute: "API Recommended Practice for Sampling Petroleum Reservoir Fluids", API 44 (1966).
5. Hearn, R.S. (compiled by): "Sampling and Analysing Gas/Condensate Reservoir Fluids", UKOOA Report (March, 1986).
6. McCain Jr., W.D. and Alexander, R.A: "Sampling Gas Condensate Wells", *SPE Res. Eng.*, 358-362 (Aug., 1992).
7. Turner, R.G., Hubbard, M.G. and Dukler, A.E: "Analysis and Prediction of Minimum Flow Rate for the Continuous Removal of Liquids from Gas Wells", *JPT*, 1475-1482 (Nov., 1969).
8. Flaitz, J.M. and Parks, A.S: "Sampling Gas Condensate Wells", *Trans. AIME Proc.*, 146, 232-245 (1941).
9. Kikani, J. and Ratulowski, J: "Consistency Check and Reconciliation of PVT Data from Samples Obtained with Formation Testers Using EOS Models", *SPE 36743, Proc. of SPE Ann. Conf.*, 615-622 (Oct., 1996).
10. Leythaeuser, D. and Ruckheim, J: "Heterogeneity of Oil Composition within a Reservoir as a Reflectance of Accumulation History", *Geochimica et Cosmochimica Acta*, 53, 2119-2123 (1989).
11. Horstad, I., Larter, S.R., Dypvik, H., Aagaard, P., Bjornvik, A.M., Johansen, P.E. and Eriksen, S: "Degradation and Maturity Controls on Oil Field Petroleum Column Heterogeneity in the Gulfaks Field, Norwegian North Sea", *Organic Geochemistry*, 16, 1-3, 497-510 (1990).
12. Kennedy, H.T. and Olson, R: "Bubble Formation in Supersaturated Hydrocarbon Mixtures", *Trans. AIME*, 195, 271-278 (1952).
13. Wieland, D.R. and Kennedy, H.T: "Measurement of Bubble Frequency in Cores", *Trans. AIME*, 210, 122-125 (1957).
14. Firoozabadi, A., Ottesen, B. and Mikkelsen, M: "Measurement of Supersaturation and Critical Gas Saturation", *SPE Formation Evaluation*, 337-344, (Dec., 1992).
15. Yeh, G.C., Shah, M.S. and Yeh, B.V: "Vapour-Liquid Equilibria of Non Electrolyte Solutions in Small Capillaries. 1. Experimental Determination of Equilibrium Compositions", *ACS*, 2, 90 (1986).
16. Yeh, G.C. and Yeh, B.V: "Vapour-Liquid Equilibria of Non Electrolyte Solutions in Small Capillaries. 2. Theoretical Calculations of Equilibrium Compositions", 60th Colloid and Surface Science Symposium, ACS, (June, 1986).

17. Sigmund, P.M., Dranchuk, P.M., Morrow, N.R. and Purvis, R.A: "Retrograde Condensation in Porous Media", SPEJ, 93-104 (April, 1973).
18. Kortekaas, T.F.M. and van Poelgeest, F: "Liberation of Solution Gas During Pressure Depletion of Virgin and Watered-out Oil Reservoirs", SPE Trans. 291, 329-335 (Aug., 1991).
19. Moulu, J.C. and Longeron, D: "Solution Gas Drive, Experiments and Simulation", Proc. of 5th Europ. IOR Symp., Budapest, 145-154 (April, 1989).
20. Jacoby, R.H. and Tracht, J.H: "Fluid sampling: a better technique", Hydrocarbon Processing, 101-102 (Feb., 1970).
21. Jacoby, R.H. and Tracht, J.H: "Collection of Samples under Pressure for Chromatographic Analysis and a System for Handling Gas Condensate Type Fluids", J. of Chromatog. Science, 13 (1), 44 (1975).
22. Varotsis, N., Stewart, G., Todd, A.C. and Clancy, M: "Phase Behaviour of Systems Comprising North Sea Reservoir Fluids and Injection Gases", JPT, 38 (11), 1221-1233 (1986).
23. Legret, D., Richon, D. and Renon, H: "Vapour Liquid Equilibria up to 100 MPa: A New Apparatus", AIChE, 27 (2), 203-207 (1981).
24. Danesh, A. and Todd, A.C: "A Novel Sampling Method for Compositional Analysis of High Pressure Fluids", J. Fluid Phase Equilibria, 57, 161-171 (1990).
25. McCain Jr., W.D: "The Properties of Petroleum Fluids", 2nd Ed., Pennwell Books, Tulsa (1990).
26. Moses, P.L: "Engineering Applications of Phase Behaviour of Crude Oil and Condensate Systems", JPT, 715-723 (July, 1986).
27. Dodson, C.R., Goodwill, D. and Mayer, E.H: "Application of Laboratory PVT Data to Reservoir Engineering Problems", JPT, 287-298 (Dec., 1953).
28. Robinson, D.B: "The Interface Between Theory and Experiment", J. Fluid Phase Equilibria, 52, 1-14 (1989).
29. "Reservoir Fluid Studies, 1993-1996 Final Report", Report No: PVT/97/1, Dept. of Pet. Engng., Heriot-Watt University (Jan., 1997).
30. Bashbush, J.L: "A Method to Determine K Values from Laboratory Data and Its Applications", SPE 10127, Proc. of 56th Ann. Conf. (Oct., 1981).
31. Drohm, J.K., Trengove, R.D. and Goldthorpe, W.H: "On the Quality of Data from Standard Gas-Condensate PVT Experiments". SPE 17768, SPE Gas Technology Symposium, Dallas, Texas (1988).
32. Danesh, A., Todd, A.C., Somerville, J. and Dandekar, A: "Direct Measurement of Interfacial Tension, Density, Volume and Compositions of Gas-Condensate System", Trans. AIChE, 68, 325-330 (1990).
33. Hoffmann A.E., Crump J.S. and Hocott C.R: "Equilibrium Constants for Gas-Condensate Systems", Trans. AIME, 198, 1-10 (1953).

34. Chierici, G.L., Giucci, G.M. and Sclocchi, M: "Two-Phase Vertical Flow in Oil Well-Prediction of Pressure Drop", JPT, 927-938 (Aug., 1974).
35. Ostermann, R.D., Ehlig-Economides, C.A. and Owolabi, O.O: "Correlations for the Reservoir Fluid Properties of Alaskan Crudes", SPE 11703 presented at the 1983 California Regional Meeting (March, 1983).
36. Sutton, R.P. and Farshad, F.F: "Evaluation of Empirically Derived PVT Properties for Gulf of Mexico Crude Oils", SPE 13172, Proc. of 59th Ann. Tech. Conf. (1984).
37. McCain Jr., W.D: "Reservoir Fluid Property Correlations", SPE Res. Eng., 266-272 (May, 1991).
38. De Ghetto, G., Paone, F. and Villa, M: "Reliability Analysis on PVT Correlations", SPE 28904, Proc. of Euro. Pet. Conf., London, 375-393 (Oct., 1994).
39. Standing, M.B: "A Pressure-Volume-Temperature Correlation for Mixtures of Californian Oils and Gases", Drill. and Prod. Proc., 275-287 (1947).
40. Lasater, J.A: "Bubble Point Pressure Correlation", Trans. AIME, 213, 379-381 (1958).
41. Vasquez, M. and Beggs, H.D: "Correlations for Fluid Physical Property Prediction", JPT, 968-970 (June, 1980).
42. Glaso, O: "Generalised Pressure-Volume-Temperature Correlations", JPT, 785-795 (May, 1980).
43. Marhoun, M.A: "PVT Correlation for Middle East Crude Oils", JPT, 650-665 (May, 1988).
44. Ahmed, T: "Hydrocarbon Phase Behaviour", Gulf Publishing Co., 1st Ed. (1990).
45. Asgharpour, S., McLauchlin, L., Wong, D. and Cheung, V: "Pressure-Volume-Temperature Correlations for Western Canadian Gases and Oils", Pet. Soc. of CIM, Paper No: 88-39-62 (1988).
46. Labedi, R: "Use of Production Data to Estimate Volume Factor, Density and Compressibility of Reservoir Fluids", J. of Pet. Sci. and Eng., 4, 375-90 (1990).
47. Petrosky, G.E. and Farshad, F.F: "Pressure-Volume-Temperature Correlations for Gulf of Mexico Crude Oils", SPE 26644, Proc. of 68th Ann. Conf., 395-406 (1993).
48. Rollins, J.B., McCain Jr, W.D. and Creeger, J.T: "Estimation of Solution Gas-Oil Ratio of Black Oils", JPT, 42, 92-94 (Jan., 1990).
49. Standing, M.B: "Volumetric and Phase Behaviour of Oil Field Hydrocarbon Systems, 9th Printing, SPE, Dallas, Texas (1981).
50. Frick, T.C: "Petroleum Production Handbook", Volume II, SPE, Dallas (1962).
51. Katz, D.L: "Prediction of the Shrinkage of Crude Oils", Drill. and Prod. Prac., API, 137-147 (1942).
52. Standing, M.B. and Katz, D.L: "Density of Crude Oils Saturated with Natural Gas", AIME Trans., 159-165 (1941).

53. Pedersen, K.S., Thomassen, P. and Fredenslund, A.A: "Thermodynamics of Petroleum Mixtures Containing Hydrocarbons. 2. Flash and PVT Calculations with the SRK Equation of State", *Ind. Eng. Chem. Proc. Des. and Dev.*, 23, 566-573 (1984).
54. American Petroleum Institute, Technical Data Book, Petroleum Refining, API, New York (1982).
55. Alani, H.G. and Kennedy, H.T: "Volumes of Liquid Hydrocarbons at High Temperatures and Pressures", *JPT*, 272-273 (Nov., 1960).
56. Lohrenz, J., Bary, B.G. and Clark, C.R: "Calculating Viscosities of Reservoir Fluids from their Compositions", *JPT*, 1171-1176 (Oct., 1964).
57. Beal, C: "The Viscosity of Air, Water, Natural Gas, Crude Oil and its Associated Gases at Oil Field Temperatures and Pressures", *Trans. AIME*, 94, 115 (1946).
58. Beggs, H.D. and Robinson, J.R: "Estimating the Viscosity of Crude Oil Systems", *JPT*, 27, 1140-1141 (1975).
59. Egboghah, E.O. and Ng, J.T: "An Improved Temperature Viscosity Correlation for Crude Oil Systems", *J. Pet. Sci. and Eng.*, 5, 197-200 (1990).
60. Labedi, R: "Improved Correlations for Predicting the Viscosity of Light Crudes", *J. Petr. Sci. and Engng.*, 8, 221-234 (1992).
61. Gold, D.K., McCain Jr., W.D. and Jennings, J.W: "An Improved Method for the Determination of the Reservoir Gas Specific Gravity for Retrograde Gases", *JPT*, 41, 747-752 (July, 1989).
62. Standing, M.B. and Katz, D.L: "Density of Natural Gases", *AIME Trans.*, 146, 140-49 (1942).
63. Takacs, G: "Comparisons Made for Computer Z-Factor Calculations", *Oil and Gas J.*, 64-66 (Dec., 1976).
64. Dranchuk, P.M. and Abou-Kassem, J.H: "Calculation of Z-Factors for Natural Gases using Equation of State", *JCPT*, 34-36 (July-Sep., 1975).
65. Starling, K.E: "Fluid Thermodynamic Properties for Light Petroleum Systems", *Gulf Pub.* (1973).
66. Sutton, R.P: "Compressibility Factors for High Molecular Weight Reservoir Gases", *SPE 14265, Proc. of 60th Ann. Tech. Conf.* (Sept., 1985).
67. Wichert, E. and Aziz, K: "Calculate Zs for Sour Gases", *Hydrocarbon Processing*, 119-122 (May, 1972).
68. Katz, D., et al: "Handbook of Natural Gas Engineering", McGraw Hill (1959).
69. Lee, A. and Gonzalez, M.H. and Eakin, B.E: "The Viscosity of Natural Gases", *JPT*, 997-1000 (Aug., 1966).
70. Carr, N.L., Kobayashi, R. and Burrows, D.B: "Viscosity of Hydrocarbon Gases Under Pressure", *Trans. AIME*, 201 (1954).

71. Dempsey, J.R: "Computer Routine Treats Gas Viscosity as a Variable", Oil and Gas J., 141 (Aug., 1965).
72. Sloan, E.D: "Clathrate Hydrates of Natural Gases", Marcel Dekker Inc (1990).
73. Gas Processors Suppliers Association: "SI Engineering Data Book", (1980).
74. Daubert, T.E. and Danner, R.P: "DIPPR Data Compilation Tables of Properties of Pure Compounds", AIChE, New York, (1985).
75. Culberson, O.L. and McKetta Jr., J.J: "Phase Equilibria in Hydrocarbon-Water Systems III - Solubility of Methane in Water at Pressures to 10,000 psia", Trans. AIME, 192, 223-226 (1951).
76. Meehan, D.N: "A Correlation for Water Compressibility", Petroleum Engineer, 125-126 (Nov., 1980).
77. Numbere, D., Brigham, W. and Standing, M.B: "Correlations for Physical Properties of Petroleum Reservoir Brines", PRI Report, Stanford University (Nov., 1977).

## 2.5 EXERCISES

2.1. The PVT test results of a reservoir oil are given in the following tables. Calculate the gas in solution, oil formation volume factor, and total formation volume factor at 2277 psig, with the intermediate separator operating at the optimum pressure.

Reservoir Temperature = 195 °F.

Initial Reservoir Pressure = 5712 psig

### Reservoir fluid composition.

Components	Mol%
Nitrogen	0.90
Carbon dioxide	1.49
Methane	51.54
Ethane	6.57
Propane	4.83
i Butane	0.68
n Butane	2.39
i Pentane	0.91
n Pentane	1.47
Hexanes	2.17
Heptanes	4.30
Octanes	3.96
Nonanes	1.93
Decanes	1.66
Undecanes	1.38
Dodecanes +	13.82

C<sub>12</sub>, Characteristics:

M=265 S=0.883

### Pressure-volume test at 195 °F.

Pressure psig	Relative volume	Density kg/m <sup>3</sup>
5712	0.9804	645

5427	0.9849	642
5137	0.9897	639
4850	0.9947	635
4566	1.0000	632
4544	1.0011	
4492	1.0038	
4382	1.0099	
4281	1.0159	
4100	1.0278	
3869	1.0456	
3618	1.0694	
3314	1.1055	
2940	1.1660	
2641	1.2328	
2331	1.3242	
1924	1.5077	

## Differential vaporisation at 195 °F.

Pressure psig	Oil Vol. factor	Sol. Gas SCF/bbl	Compres. Factor
5712	1.798		
5427	1.807		
5137	1.815		
4850	1.825		
4566	1.834	1541	Pb
3983	1.695	1261	0.889
3556	1.614	1092	0.865
3136	1.542	939	0.845
2707	1.480	806	0.839
2277	1.422	680	0.843
1849	1.370	564	0.852
1415	1.320	451	0.873
986	1.271	344	0.897
566	1.222	238	0.931
214	1.166	135	0.960
0	1.059	0	1.000

Residual Oil SG = 0.844 (36.0 °API)

## Composition of liberated gas (mole%) in differential liberation test.

Pres. psig	3983	3556	3136	2707	2277	1849	1415	986	566	214	0
N2	2.00	1.97	1.89	1.75	1.59	1.32	1.02	0.75	0.44	0.17	0.00
CO2	1.99	2.00	2.05	2.10	2.18	2.25	2.39	2.59	2.97	2.97	1.84
Methane	77.72	79.37	80.46	81.29	81.58	81.58	80.72	78.31	72.58	55.72	16.68
Ethane	6.95	6.90	6.93	6.97	7.20	7.48	8.17	9.38	12.14	18.15	19.36
Propane	4.25	4.10	4.00	3.89	3.82	3.94	4.20	4.99	6.74	12.73	28.40
i-Butane	0.60	0.52	0.46	0.42	0.40	0.40	0.42	0.49	0.67	1.29	4.21
n-Butane	2.03	1.70	1.48	1.32	1.25	1.21	1.27	1.48	1.94	3.98	14.57
i-Pentane	0.67	0.54	0.44	0.38	0.34	0.32	0.32	0.37	0.47	0.95	3.88
n-Pentane	0.93	0.76	0.64	0.55	0.50	0.47	0.48	0.53	0.66	1.33	5.14
Hexanes	0.97	0.78	0.64	0.54	0.49	0.46	0.46	0.51	0.63	1.23	3.51
Heptanes +	1.89	1.36	1.01	0.79	0.65	0.57	0.55	0.60	0.76	1.23	2.41
MW	23.39	22.38	21.71	21.24	21.01	20.93	21.13	21.79	23.36	28.52	44.77
SG	0.807	0.773	0.749	0.733	0.725	0.723	0.729	0.752	0.806	0.984	1.545

Two stage separator test at 84 °F.

Pressure psig	1st Sep. SCF/STB	GOR SCF/STB	Total GOR Vol. Factor	Formation Oil SG
600	1076	1358	1.678	0.835
400	1147	1342	1.645	0.831
200	1245	1360	1.659	0.833
0*	1474	1474	1.759	0.840

\* One stage separation (stock tank only).

Composition of separator gas (mole%).

Pressure, psig	600	400	200	0
Nitrogen	1.66	1.58	1.42	1.24
Carbon dioxide	2.27	2.30	2.36	2.24
Methane	84.19	82.50	80.44	72.28
Ethane	7.27	8.07	8.82	9.28
Propane	3.13	3.79	4.63	6.90
i-Butane	0.26	0.31	0.39	0.86
n-Butane	0.67	0.83	1.11	2.93
i-Pentane	0.13	0.15	0.22	0.83
n-Pentane	0.18	0.20	0.26	1.21
Hexanes	0.13	0.17	0.21	1.06
Heptanes +	0.11	0.10	0.14	1.17
MW	19.52	19.95	20.39	24.57
SG	0.674	0.689	0.704	0.848

Reservoir oil viscosity at 195 °F.

Pressure, psig	Viscosity, cp
6400	0.605
6045	0.580
5689	0.560
5334	0.540
4978	0.520
4566*	0.500
4267	0.505
3556	0.520
2845	0.565
2133	0.630
1422	0.725
711	0.895
284	1.085
0	1.412

\* Bubble point

2.2. Calculate the liquid propane content of the produced gas in Exercise 2.1, with the optimum separator pressure.

2.3. The laboratory data is often evaluated and smoothed by the dimensionless function  $Y$ , defined in Eq.(2.10). A plot of  $Y$  function versus pressure is expected to yield either a straight line or very slightly curved. What is the implicit assumption in the above approach?

2.4. The results of constant volume depletion test on a gas condensate sample, as reported by a laboratory, are as follows:

## Composition of reservoir gas.

Component	Mole%	Density, kg/m <sup>3</sup>	Mol. Weight
Nitrogen	0.386		
Carbon dioxide	2.524		
Methane	78.585		
Ethane	7.029		
Propane	3.360		
i-Butane	0.440		
n-Butane	1.114		
i-Pentanes	0.396		
n-Pentane	0.502		
Hexanes	0.661	686.4	86
Heptanes	1.277	744.5	89
Octanes	0.902	761.6	102
Nonanes	0.588	775.9	118
Decanes	0.337	783.6	136
Undecanes	0.345	789.4	147
Dodecanes	0.256	798.0	162
Tridecanes	0.245	814.2	176
Tetradecanes	0.186	830.1	190
Pentadecanes	0.163	831.6	204
Hexadecanes	0.120	834.8	218
Heptadecanes	0.098	835.2	232
Octadecanes	0.091	836.0	246
Nonadecanes	0.065	846.1	260
Eicosanes plus	0.330	870.4	335

C<sub>11+</sub> Properties: Molecular Weight=335 Density = 870.4 kg/m<sup>3</sup>

## Constant volume depletion test results at 373.1 K (212 °F).

Pressure		Cumulative Gas Production	Specific Gravity of Produced Gas	Compressibility Factor of Produced gas	Volume of Retrograde Liquid
bar	psig	(mol %)			%
(1) 389.4	5632	0.00	0.923	1.037	0.00
(2) 373.0	5394	2.33	0.923	1.017	0.00
321.0	4640	9.91	0.879	0.956	3.58
271.0	3915	19.49	0.831	0.912	6.52
221.0	3190	31.58	0.787	0.875	8.61
171.0	2465	45.63	0.758	0.873	9.31
121.0	1740	61.23	0.737	0.880	9.09
71.0	1015	76.88	0.732	0.914	8.40

(1) Initial reservoir pressure.

(2) Saturation pressure at indicated temperature (dew point).

## Composition of produced gas.

Pressure	bar	321.0	271.0	221.0	171.0	121.0
	psig	4640	3915	3190	2465	1740
Hydrogen Sulfide		0.00	0.00	0.00	0.00	0.00
Nitrogen		0.39	0.39	0.40	0.40	0.40
Carbon Dioxide		2.44	2.48	2.49	2.50	2.50
Methane		79.58	80.57	81.53	82.34	82.78
Ethane		7.05	7.02	7.04	7.12	7.23
Propane		3.35	3.30	3.28	3.21	3.23



i-Butane	0.43	0.42	0.41	0.40	0.40
n-Butane	1.11	1.07	1.04	1.00	0.96
i-Pentanes	0.37	0.34	0.33	0.31	0.31
n-Pentane	0.49	0.47	0.45	0.38	0.39
Hexanes	0.62	0.59	0.54	0.46	0.42
Heptanes	1.20	1.11	0.96	0.80	0.66
Octanes	0.83	0.74	0.62	0.48	0.38
Nonanes	0.50	0.40	0.30	0.20	0.12
Decanes	0.29	0.20	0.14	0.10	0.06
Undecanes plus	1.35	0.90	0.47	0.30	0.16
Molecular weight	25.5	24.1	22.8	22.0	21.4
$C_{11+}$ Molecular weight	197	186	178	176	169

## Composition of remaining fluids at 71 bar.

Components or fractions	Remaining gas (mol. %)	Remaining oil (mol. %)
Hydrogen Sulfide	0.00	0.00
Nitrogen	0.40	0.05
Carbon Dioxide	2.51	0.90
Methane	82.56	15.31
Ethane	7.42	3.79
Propane	3.38	4.39
i-Butane	0.42	0.82
n-Butane	1.04	2.90
i-Pentanes	0.32	1.57
n-Pentane	0.39	2.20
Hexanes	0.41	4.04
Heptanes	0.59	10.39
Octanes	0.28	9.23
Nonanes	0.11	7.90
Decanes	0.05	4.84
Undecanes-plus	0.12	31.67
Molecular weight	21.2	116.9
$C_{11+}$ Molecular weight	167	204

(a) Calculate the two-phase compressibility factor of the cell content, and plot  $P/Z$  vs. the total volume of produced gas.

(b) Determine the density and composition of condensate phase at  $P = 71$  bar by material balance calculations.

2.5. The results of a constant volume depletion test have been used to calculate the equilibrium ratios by material balance equations. The  $K$  vs.  $P$  plot shows that the equilibrium ratio curves of  $C_3$  and  $iC_4$  cross at a pressure value. Is this physically possible?

2.6. An undersaturated oil is produced through one intermediate stage separator at 200 psia and 120 °F, with a  $GOR = 600$  SCF/STB. The stock tank oil  $API = 40^\circ$ , and  $S_g = 0.7$ . The reservoir pressure and temperature are 6500 psia and 210 °F, respectively.

(a) Estimate the oil bubble point pressure at reservoir temperature.

(b) Calculate the static oil pressure gradient in the reservoir.

(c) What will be the oil and total formation volume factor when the reservoir pressure falls 400 psi below the bubble point.

2.7. Estimate the density of oil reported in Exercise 2.1 at its bubble point, using the Katz-Standing and Alani-Kennedy methods. Compare the results with the measured value.

2.8. Estimate the viscosity of the above oil, and compare it with the measured value.

2.9. A rich gas is produced and stabilised in three separation stages. The first stage separator is at 1500 psia and 140 °F with a producing gas to oil ratio of 8000 SCF/STB, and the gas specific gravity of 0.73. The second stage separator temperature is 100 °F. The produced condensate specific gravity is 0.760. Estimate the reservoir gas molecular weight.

2.10. Estimate the compressibility factor of the gas condensate, reported in Exercise 2.4, at the initial reservoir condition, using the generalised chart.

2.11. What is the minimum flow rate of a gas with a specific gravity of 0.6 to continuously remove condensate in a well with a wellhead pressure of 2000 psia at 120 °F? The tube nominal diameter is 4 in.

2.12. The viscosity of a North Sea gas condensate at 100 °F, and 5500 psia has been measured equal to 0.0588 cp. The gas molecular weight is 28.7. Estimate the gas viscosity at the above conditions, using the Lee et al. correlation.

2.13. A gas reservoir is at 300 °F and 6000 psia. The gas specific gravity is 0.6 and the connate water salinity is 200,000 ppm. The first stage separator temperature and pressure are 50 °F and 1500 psia, respectively.

(a) How much liquid water is produced by condensation in the separator.

(b) Is there a possibility of hydrate formation at the above conditions?

2.14. A lean gas is at equilibrium with water at reservoir pressure of 6527 psia and 279 °F. The water salinity,  $w_s$ , is 10%. Estimate: (a) the amount of dissolved gas in water, and (b) the isothermal compressibility coefficient, (c) density, and (d) viscosity of the water at the above conditions.

2.15. A sample of the reservoir oil described in Exercise 2.6. is brought into equilibrium with equal volume of fresh water at the reservoir conditions to simulate a water drive process. Estimate the reduction of the oil bubble point pressure at the above temperature due to its contact with water.

### 3

## PHASE EQUILIBRIA

Production of reservoir fluids often is accompanied with variations in composition, pressure and temperature. This leads not only to changes in fluid properties, but also to formation of new phases, or elimination of some of the existing phases. As changes within the reservoir are often quite slow, it is reasonable to assume that all the co-existing phases, at any point in the reservoir, are in equilibrium. Hence, the problem basically reduces to determination of the equilibrium conditions for a multicomponent system.

Fluid equilibria, and the associated engineering applications, are of interest in many fields, with well established principles. Thermodynamics have long been used to investigate fluid equilibria, and to reduce general criteria and laws to practical tools. This subject has been extensively covered in numerous text books and paper collections. References [1-2] provide basic thermodynamic concepts of fluid phase equilibria. In this chapter, certain concepts, definitions, and thermodynamic relations which are fundamental to fluid equilibria are reviewed. These will form the foundation for all the methods used to determine fluid behaviour in the remaining chapters of this book.

### 3.1 CRITERIA FOR EQUILIBRIUM

For a closed system, i.e. not exchanging mass with its surroundings, the change of system total energy  $E$ , stored as the internal energy  $U$ , potential energy  $E_p$ , and kinetic energy  $E_k$ , is only due to transfer of heat  $Q$ , and work  $W$ , across its boundary as stated by the first law of thermodynamics,

$$\Delta E = \Delta U + \Delta E_p + \Delta E_k = Q - W \quad (3.1)$$

where the heat given to the system and work done by the system have been assigned positive signs in the above equation. When such a system undergoes an ideal but unreal reversible

process, with no changes in the kinetic and potential energy at uniform pressure  $P$  and temperature  $T$ , the combined first and second laws of thermodynamics states [2],

$$dU = TdS - PdV \quad (3.2)$$

where  $S$  and  $V$  are the system entropy, and volume respectively.

If the process is irreversible, the change of entropy is higher than that in the above equation, leading to,

$$dU < TdS - PdV \quad (3.3)$$

Since all real processes are irreversible, the above inequality states that for a process at constant  $S$  and  $V$ ,  $U$  tends to decrease as the state of equilibrium is approached.

Thermodynamic relations can be employed to develop similar statements amongst other state properties.

The Gibbs energy  $G$ , is defined as,

$$G \equiv H - TS \quad (3.4)$$

where  $H$  is the system enthalpy,

$$H \equiv U + PV \quad (3.5)$$

Substituting Eqs.(3.4-5) in (3.2-3), we obtain,

$$dG \leq -SdT + VdP \quad (3.6)$$

which states that, at constant  $T$  and  $P$  the Gibbs energy tends to decrease in real processes, and remains constant in a reversible process,

$$(\partial G)_{P,T} \leq 0 \quad (3.7)$$

That is, in the equilibrium state, which is the ultimate condition of any real process, the system Gibbs energy is minimum, i.e.,

$$(\partial G)_{P,T} = 0 \quad (3.8)$$

and

$$(\partial^2 G)_{P,T} > 0 \quad (3.9)$$

Similar expressions using another energy term, that is, the Helmholtz energy, can also be derived as the requirement for equilibrium,

$$(\partial A)_{T,V} = 0 \quad (3.10)$$

and

$$(\partial^2 A)_{T,V} > 0 \quad (3.11)$$

where,  $A$  is the Helmholtz energy defined as,

$$\Lambda = U - TS \quad (3.12)$$

The minimum Gibbs energy, as the general criterion of equilibrium, is often used to derive working expressions. The Helmholtz energy may, however, lead to simpler expressions in some applications, as described in Section 5.3.

It should be noted that Eqs.(3.8-9) are necessary, but not sufficient conditions. At equilibrium, the system energy is at its lowest value amongst all possible conditions, including all possible minima occurring in the calculated Gibbs function. Hence, the equilibrium should be determined by searching for the global minimum value of Gibbs energy. Further information on the Gibbs energy minimisation to identify equilibrium conditions is given in Section 5.2

### Chemical Potential

A closed system consisting of a number of phases in contact, called a heterogeneous closed system, can be treated as a collection of open systems, where each phase is considered to be a homogeneous one, exchanging mass with other open systems.

In an open system the change of Gibbs energy cannot be expressed by Eq.(3.6) as the energy can vary by components of the system crossing the phase boundary. Hence,

$$dG = -SdT + VdP + \sum_i^N (\partial G / \partial n_i)_{T,P,n_{j \neq i}} dn_i \quad (3.13)$$

where  $n_i$  is the number of moles of each component, with the subscript  $n_j$  referring to all mole numbers except  $n_i$ , and  $N$  is the total number of components in the system.

The derivative of an extensive property relative to the number of moles of any component at constant pressure, temperature and other mole numbers, is defined as the partial molar property of that component. The partial molar Gibbs energy is called *chemical potential*,  $\mu_i$

$$\mu_i = (\partial G / \partial n_i)_{T,P,n_{j \neq i}} \quad (3.14)$$

It can be shown [1], that,

$$\mu_i = (\partial G / \partial n_i)_{T,P,n_{j \neq i}} = (\partial \Lambda / \partial n_i)_{T,V,n_{j \neq i}} = (\partial H / \partial n_i)_{S,P,n_{j \neq i}} = (\partial U / \partial n_i)_{S,V,n_{j \neq i}} \quad (3.15)$$

Substituting Eq.(3.14) in Eq.(3.13), we obtain,

$$dG = -SdT + VdP + \sum_i \mu_i dn_i \quad (3.16)$$

For a closed system consisting of  $\theta$  phases, the above equation can be written for each phase. The change of total Gibbs energy of the closed system is, therefore,

$$dG = \sum_{h=1}^{\theta} (-S)_h dT + \sum_{h=1}^{\theta} (V)_h dP + \sum_{h=1}^{\theta} (\sum_i \mu_i dn_i)_h \quad (3.17)$$

where  $h$  denotes each phase.

At uniform and constant temperature and pressure conditions, the general requirement of equilibrium, given by Eq.(3.8), leads to,

$$(dG)_{T,P} = \sum_{h=1}^{\theta} (\sum_i \mu_i dn_i)_h = 0 \quad (3.18)$$

As the total system is closed with no chemical reaction, the total number of moles of each component remains constant within the system,

$$\sum_{h=1}^{\theta} (dn_i)_h = 0 \quad i=1,2,\dots,N \quad (3.19)$$

Considering Eqs.(3.18) and (3.19), and since changes in mole numbers of each component are arbitrary, we obtain,

$$\mu_i^{(1)} = \mu_i^{(2)} = \mu_i^{(3)} = \dots = \mu_i^{(\theta)} \quad i=1,2,\dots,N \quad (3.20)$$

The above general requirement, that is, the equality of chemical potential of each component throughout all the co-existing phases at equilibrium, becomes a practical engineering tool if the chemical potential can be related to measurable quantities. This is achieved by expressing the chemical potential in terms of auxiliary thermodynamic functions, such as fugacity or activity.

### Fugacity

As relations amongst state properties are independent of the process path [2]. Eq.(3.6) for a reversible process can be used to express the Gibbs energy change, hence, the chemical potential,

$$dG = -SdT + VdP \quad (3.21)$$

For a pure substance partial molar properties are the same as molar properties. Hence, the change of chemical potential of the pure substance  $i$ , is given by,

$$d\mu_i = dg_i = -s_i dT + v_i dP \quad (3.22)$$

where  $g$ ,  $s$  and  $v$  are the molar Gibbs energy, molar entropy and molar volume respectively.

At constant temperature the above equation reduces to,

$$(\partial\mu_i / \partial P)_T = v_i \quad (3.23)$$

which leads to a simple expression for the chemical potential of an ideal gas, with the pressure-volume relation as,

$$Pv_i = RT \quad (3.24)$$

that is,

$$(\partial\mu_i / \partial P)_T = RT / P \quad (3.25)$$

where  $R$  is the universal gas constant.

Integrating Eq.(3.25) at constant temperature, we obtain,

$$\mu_i - \mu_i^0 = RT \ln(P/P^0) \quad (3.26)$$

The above equation provides a simple relation for the change of chemical potential of a pure ideal gas when its pressure changes from  $P^0$  to  $P$  isothermally.

Lewis [1] generalised Eq.(3.26) for application to real systems, by defining a "corrected pressure" function ' $f$ ', called *fugacity* (escaping tendency) as follows,

$$\mu_i - \mu_i^0 = RT \ln(f_i/f_i^0) \quad (3.27)$$

where  $\mu_i^0$  and  $f_i^0$  are the chemical potential and fugacity of the component  $i$ , respectively, at a reference state.

For an ideal gas, therefore, the fugacity is equal to its pressure, and the fugacity of each component is equal to its partial pressure.

The ratio of fugacity to pressure is defined as the fugacity coefficient  $\phi$ . For a multicomponent system,

$$\phi_i = f_i / (Pz_i) \quad (3.28)$$

where  $z_i$  is the mole fraction of the component  $i$ . Since all systems behave as ideal gases at very low pressures,

$$\phi_i \rightarrow 1 \quad \text{when} \quad P \rightarrow 0 \quad (3.29)$$

The departure of fugacity coefficients from unity is, therefore, a measure of non-ideality of the system.

Writing Eq.(3.27) for the component  $i$ , in each phase of a heterogeneous system, with all reference states at the same temperature, the equality of the chemical potential at equilibrium given by Eq.(3.20), leads to,

$$f_i^{(1)} = f_i^{(2)} = f_i^{(3)} = \dots = f_i^{(N)} \quad i=1,2,\dots,N \quad (3.30)$$

That is, the fugacity of each component should be equal throughout all the phases in a heterogeneous system at equilibrium.

Eq.(3.30) is as general as Eq.(3.20) for relating the properties of equilibrated phases. It, however, has the advantage of employing a function which can be more easily understood and evaluated as a "corrected pressure". Fugacity can be imagined as a measure of the escaping tendency of molecules from one phase to an adjacent phase. Hence, in a multicomponent system, if the fugacity of a component in the two adjacent phases is the same, the two phases will be in equilibrium with no net transfer of molecules from one phase to another.

The fugacity can be related rigorously to measurable properties using thermodynamic relations[1],

$$\ln \phi_i = \frac{1}{RT} \int_V^{\infty} \left[ \left( \frac{\partial P}{\partial n_i} \right)_{T,V,n_{j \neq i}} - \frac{RT}{V} \right] dV - \ln Z \quad i=1,2,\dots,N \quad (3.31)$$

where  $V$  is the total volume,  $n_i$  is the number of moles of component  $i$ , and  $Z$ , is the mixture compressibility factor given by,

$$Z = PV / nRT \quad (3.32)$$

where,  $n$ , is the total number of moles in the mixture with  $N$  components,

$$n = \sum_i^N n_i \quad (3.33)$$

Eq.(3.31) simply yields the fugacity coefficient, provided that the value of  $(\partial P / \partial n_i)_{T, V, n_{j \neq i}}$  over the whole range of the integrate, i.e.  $V$  at  $P$ , to  $V = \infty$  at  $P = 0$ , can be evaluated. This is an achievable task, with an acceptable engineering accuracy, using semi-empirical equations of state as described in Chapter 4.

The order of integration and differentiation in Eq.(3.31) may be interchanged, resulting in,

$$\ln \phi_i = \frac{\partial}{\partial n_i} \left[ \int_V^\infty \left( \frac{P}{RT} - \frac{n}{V} \right) dV \right]_{T, V, n_{j \neq i}} - \ln Z \quad i=1, 2, \dots, N \quad (3.34)$$

The integral is the residual, defined as the actual property minus that calculated by assuming the ideal gas behaviour, Helmholtz energy divided by  $(RT)$ . The advantage of the above form is that the integration has to be done only once, and all properties can be calculated as derivatives of the residual Helmholtz function [3]. The use of describing the behaviour of a system by evaluating its Helmholtz energy, in preference to the Gibbs energy, will be discussed in Section 5.3.

The fugacity coefficient of a pure compound can be determined by incorporating Eq.(3.32) into the general expression for the fugacity coefficient, Eq.(3.31),

$$\ln \phi = \int_0^P \left( \frac{Z-1}{P} \right) dP = (Z-1) - \ln Z + \frac{1}{RT} \int_v^\infty \left( \frac{RT}{v} - P \right) dv \quad (3.35)$$

where  $v$  is the molar volume. Depending on the form of the equation of state, one of the above two expressions for the fugacity can be simpler to use.

#### Example 3.1.

The compressibility factor of a pure gas at 290 K can be related to its pressure as,

$$Z = 1 - 6.5 \times 10^{-2} P - 7.5 \times 10^{-4} P^2 \quad P < 15 \text{ MPa}$$

where  $P$  is in MPa. Calculate the gas fugacity at 10 MPa.

*Solution:*

Substituting the above expression of  $Z$  in Eq.(3.35), we obtain,

$$\ln \phi = \int_0^P \left( \frac{Z-1}{P} \right) dP = \int_0^P \left( \frac{-6.5 \times 10^{-2} P - 7.5 \times 10^{-4} P^2}{P} \right) dP$$



$$\ln \phi = \left[ -6.5 \times 10^{-2} P - 7.5 \times 10^{-4} P^2 / 2 \right]_{P_0}^{P_0} = -0.6875$$

$$\phi = 0.5028$$

$$f = \phi \times P = 5.028 \text{ MPa}$$

### Activity

Either of  $\mu_i^0$  or  $f_i^0$  may be selected arbitrarily as the reference state property in Eq.(3.27). The fugacity is most often the chosen reference property. The substance  $i$ , as pure or in a mixture, at any pressure can be selected as the reference state. The only limitation for selecting the reference state is that its temperature must be equal to the equilibrium temperature. It is often selected as the pure substance at the system total pressure, or at its vapour pressure, at the prevailing temperature. A proper choice of the reference state facilitates the application of thermodynamic relations to engineering problems.

The ratio of the fugacity at the state of interest to that at the reference state is called the activity,  $\epsilon_i$ ,

$$f_i / f_i^0 \equiv \epsilon_i \quad (3.36)$$

The activity can, therefore, be considered as a measure of fugacity contribution or activeness of a component in a mixture,

$$f_i = \epsilon_i f_i^0 \quad (3.37)$$

It is intuitive that the fugacity of each component should depend on its concentration in the mixture. Hence, the above equation suggests that the activity should be closely related to the concentration. The ratio of activity to concentration, often in mole fractions, is called the activity coefficient  $\Theta_i$ ,

$$\Theta_i = \epsilon_i / x_i \quad (3.38)$$

Hence,

$$f_i = \Theta_i x_i f_i^0 \quad (3.39)$$

The activity coefficient is a very useful auxiliary function to describe liquid phases in phase equilibrium calculations. Extensive studies have been conducted to relate the activity coefficient to other thermodynamic functions, and numerous models have been reported to determine its value for liquid components [1].

### 3.2 EQUILIBRIUM RATIO

Let us consider two phases of liquid, L, and vapour, V, at equilibrium. Eq.(3.30) for such a system is,

$$f_i^L = f_i^V \quad i=1,2,\dots,N \quad (3.40)$$

Applying Eq.(3.28) to both phases, we obtain:

$$f_i^L = x_i P \phi_i^L \quad i=1,2,\dots,N \quad (3.41)$$

$$f_i^V = y_i P \phi_i^V \quad i=1,2,\dots,N \quad (3.42)$$

Hence,

$$K_i \equiv y_i / x_i = \phi_i^L / \phi_i^V \quad i=1,2,\dots,N \quad (3.43)$$

where  $K_i$  is called the equilibrium ratio and is defined as the ratio of mole fraction of component  $i$  in the vapour phase  $y_i$ , to that in the liquid phase  $x_i$ . A general and rigorous approach to determine the fugacity coefficient of a component in both phases from volumetric information, using an equation of state, is given in Chapter 4.

The lack of success of some equations of state in describing the volumetric behaviour of complex liquid mixtures has lead to the use of the activity concept to determine fugacities in the liquid phase. Using Eq.(3.37), instead of Eq.(3.28), to obtain the fugacity of each component in the liquid phase, we obtain,

$$K_i = \Theta_i f_i^o / P \phi_i^V \quad (3.44)$$

The above approach, known as the "split" method, can give reliable results for systems with vapour and liquid phase properties far apart. The split method proposed by Chao-Seader [4] has been extensively used in the oil industry to predict the phase behaviour of gas-oil systems, particularly at transfer line conditions. At high pressures, especially close to critical conditions, where the liquid and vapour phases behave similarly, the above approach is not recommended. Phase behaviour models which use an equation of state for the gas and an activity model for the liquid phase may also miss the retrograde behaviour of gas condensate systems. In general, the use of a single equation of state to describe all fluid phases should be adequate in almost all petroleum engineering problems, as described in Chapter 4.

The fugacity can also be evaluated by simple methods, employing limiting assumptions, but still useful for engineering purposes at a variety of conditions. An attractive assumption is that the fugacity of each component in mixture is linearly proportional to its concentration. This assumption, known as the ideal solution, is generally valid for mixtures composed of similar components, or for dilute solutions,

$$f_i = \lambda_i C_i \quad (3.45)$$

where  $\lambda_i$  and  $C_i$  are the proportionality constant and the concentration of the component  $i$  in the mixture, respectively. Depending on the definition of the proportionality constant, two widely used methods, Raoult's law and Henry's law, will result.

### Raoult's Law

First, consider the case that Eq.(3.45) is valid over the whole range of concentration, including  $C_i=1$ , i.e. pure component, the proportionality constant should, therefore, be equal to the fugacity of component  $i$ , as a pure substance,

$$f_i = z_i f_{i,pure} \quad (3.46)$$

where the concentration is expressed by the mole fraction  $z_i$ .

The above equation is known as the Lewis fugacity rule. Comparing Eq.(3.46) with Eq.(3.39), it can be concluded that the Lewis rule is valid for mixtures with all activity coefficients equal to unity.

For vapour and liquid phases at equilibrium Eqs.(3.40) and (3.46) lead to,

$$y_i f_{i,\text{pure}}^V = x_i f_{i,\text{pure}}^L \quad (3.47)$$

Assuming that the vapour is an ideal gas, we obtain,

$$f_{i,\text{pure}}^V = P \quad (3.48)$$

The effect of pressure on fugacity of a condensed phase at low pressure is small [1] and can be neglected. The fugacity of a pure liquid at low pressure can, therefore, be assumed equal to its fugacity at the saturation pressure. The fugacities of saturated vapour and liquid are equal, as the two phases are at equilibrium. Furthermore, the vapour fugacity at low pressure can be assumed equal to its pressure. Hence, the liquid fugacity can be taken equal to the vapour pressure of the substance at the prevailing temperature,

$$f_{i,\text{pure}}^L = P_i^S \quad (3.49)$$

where  $P_i^S$  is the saturation (vapour) pressure of the pure compound,  $i$ .

Substituting Eqs.(3.48) and (3.49) into Eq.(3.47), we obtain,

$$y_i P = x_i P_i^S \quad (3.50)$$

or

$$K_i = P_i^S / P \quad (3.51)$$

Eq.(3.51) is known as Raoult's law. Considering the above assumptions, it is only valid at low pressure for simple mixtures.

#### Example 3.2:

Calculate equilibrium ratios of  $C_1$ , and  $nC_{10}$  in a vapour-liquid mixture at 344.3 K, and 6.895MPa, using Raoult's law.

#### Solution:

The equilibrium ratios are calculated from Eq.(3.51), where the vapour pressure at 344.3 K is estimated using the Lee-Kesler equation, Eq.(1.10), similar to Example 1.1:

Component	$f^{(0)}$	$f^{(1)}$	$P^s$ , MPa
$C_1$	7.68167	13.75706	11681.07
$nC_{10}$	-4.25215	-5.00538	0.0025552

The estimated value of methane vapour pressure, 11681 MPa, by the Lee-Kesler equation is not acceptable. The prevailing temperature of 344.3 K is well above the methane critical temperature of 190.56 K, and pure methane cannot exist as liquid at this temperature. Hence, the calculated vapour pressure by the Lee-Kesler equation, or any other vapour pressure correlation, is an unreal value and just an extrapolation of the vapour pressure curve above the critical temperature. Simple correlations, such as the Cox chart, Figure 1.3, generally provide more reasonable values comparing with complex

functions that include parameters adjusted by matching experimental vapour pressure data.

Figure 1.3 shows an extrapolated vapour pressure of 48.26 MPa (7000 psia) for methane at 344.3 K (160 °F).

Substituting the estimated vapour pressure values in Eq.(3.51), the calculated equilibrium ratios are as follows:

$$K_{ci}=7.000, \quad K_{ac10}=0.0003706$$

Experimental values  $K_{ci}=3.998$ , and  $K_{ac10}=0.0027$  [27].

### Henry's Law

The proportionality of component fugacity to its concentration, as assumed in Eq.(3.45) is valid for components at low concentrations in most liquid mixtures,

$$f_i = H_i x_i \quad (3.52)$$

where  $H_i$  is called *Henry's constant*, which is experimentally determined.

The concentration of component,  $i$ , is generally expected to be less than 3 mole % for the above equation to be valid [1]. It is, therefore, a useful equation to determine the solubility of hydrocarbons in water where the solubility is generally low.

At low pressure, where the assumption of ideal gas is valid, Eq.(3.48) can be used to describe fugacities in the gas phase,

$$Py_i = H_i x_i \quad (3.53)$$

which is known as Henry's law. Hence,

$$K_i = H_i/P \quad (3.54)$$

Figure 3.1 compares Henry's law with the Lewis rule, Eq.(3.46). Note that whilst the fugacity of a component is proportional to its concentration across the whole range of concentration for the Lewis rule, the proportionality is only limited to the low concentration range for Henry's law. The proportionality constants are generally different.

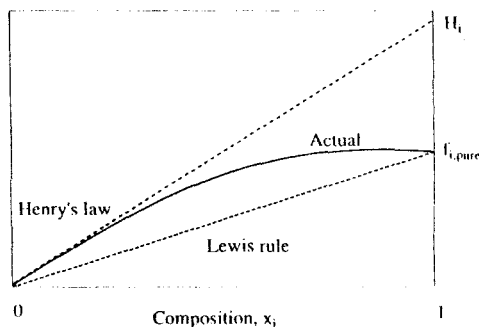


Figure 3.1. Comparison of Henry's law with Lewis rule.

Henry's constant of a component in a solvent is considered to be independent of its concentration, but a function of temperature, and to a lesser extent pressure. Henry's constants for gaseous components of reservoir fluids in water, at low pressure, are given in Figure 3.2

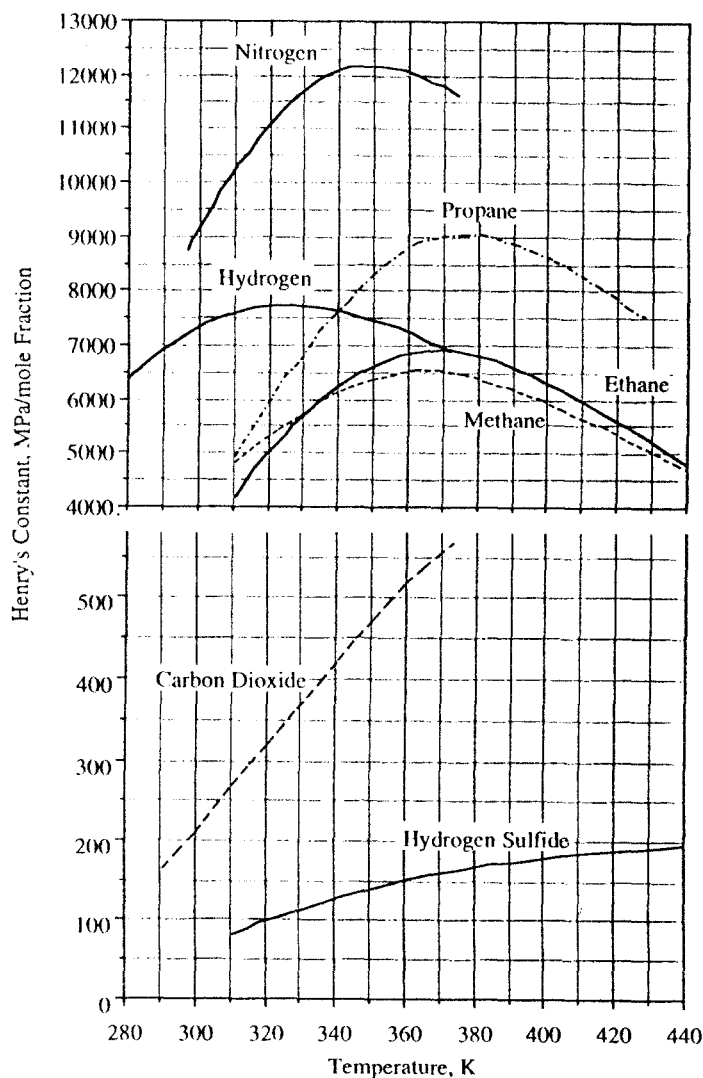


Figure 3.2 Henry's constants for solubility of hydrocarbons in water. Reprinted with permission [6], Copyright (1953) American Chemical Society.

The dependency of Henry's constant on pressure can be determined rigorously by thermodynamic relations as,

$$H_i = H_i^0 \exp[v_i^\infty (P - P^0)/RT] \quad (3.55)$$

where  $H_i^0$  is Henry's constant at  $P^0$ , and  $v_i^\infty$  is the partial molar volume of component  $i$  in the solvent at infinite dilution, assumed constant over the prevailing pressure and composition ranges. Eq.(3.55) is known as the Krichevsky-Kasarnovsky equation [5].

Limited information on  $v_i^\infty$  of compounds in water are available in the literature [6]. The partial molar volume varies with temperature, and becomes pressure dependent near the critical point. An average value of 35, 40, 55, and 80 cm<sup>3</sup>/gmol, can be used for nitrogen, methane, ethane, and propane respectively.

### Example 3.3.

Estimate the solubility of methane in water at 373 K, and 65 MPa using Henry's law. Compare the result with the value shown in Figure 2.28.

Solution:

The Henry's constant for methane at 65 MPa is calculated from Eq.(3.55):

At  $T=373$  K,  $H^0=6.5 \times 10^3$  MPa/mol fraction (Figure 3.2), and  $P^0=0.10$  MPa.

$$H_{C1} = (6.5 \times 10^3 \text{ MPa/mol fraction}) \exp[(40 \times 10^{-3} \text{ m}^3/\text{kgmol}) \times (65.00 - 0.10) \text{ MPa} / (0.0083144 \times 373 \text{ MPa} \cdot \text{m}^3/\text{kgmol})] = 1.4378 \times 10^4 \text{ MPa/mol fraction.}$$

The solubility of methane is calculated using Eq.(3.52),

$$f_{C1}^V = P y_{C1} \phi_{C1}^V = H_{C1} x_{C1}$$

The gas can be assumed as pure methane due to low volatility of water relative to methane:  $y_{C1}=1$ . The fugacity coefficient of methane vapour at the prevailing conditions can be calculated by an equation of state as applied in Example 4.1. Assuming  $\phi_{C1}^V=1$ , we obtain,

$$f_{C1}^V = P = 65 \text{ MPa} = (1.4378 \times 10^4 \text{ MPa/mol fraction}) \times x_{C1}$$

$$x_{C1} = 4.52 \times 10^{-3} \quad \text{mole fraction of methane in water.}$$

The solubility value is read from Figure 2.28 equal to  $4.3 \times 10^{-3}$ .

### Empirical Correlations

In spite of recent developments in theoretically based phase behaviour models, empirical K-value correlations are still used in vapour-liquid equilibrium calculations, particularly at low and intermediate pressure conditions, where the K-value can be assumed independent of the mixture composition for reservoir hydrocarbon fluids.

It is well established that, for a multicomponent mixture, graphs of experimentally determined K-values versus pressure at constant temperature tend to converge to  $K_i = 1$  for all the

components at a certain pressure known as the convergence pressure, Figure 3.3. This appears to suggest that, the composition of both phases should be the same at the convergence pressure. As similarity of both phases only occurs at the critical point, it implies that for any petroleum fluid, the critical temperature may be selected arbitrarily, which cannot be correct. The fact is that the convergence pressure does not physically exist, unless the prevailing temperature is the mixture critical temperature. At other temperatures, the mixture will be an under saturated single phase at that pressure. It is however, a very useful parameter to correlate experimentally determined K-values with pressure at any given temperature as an end point.

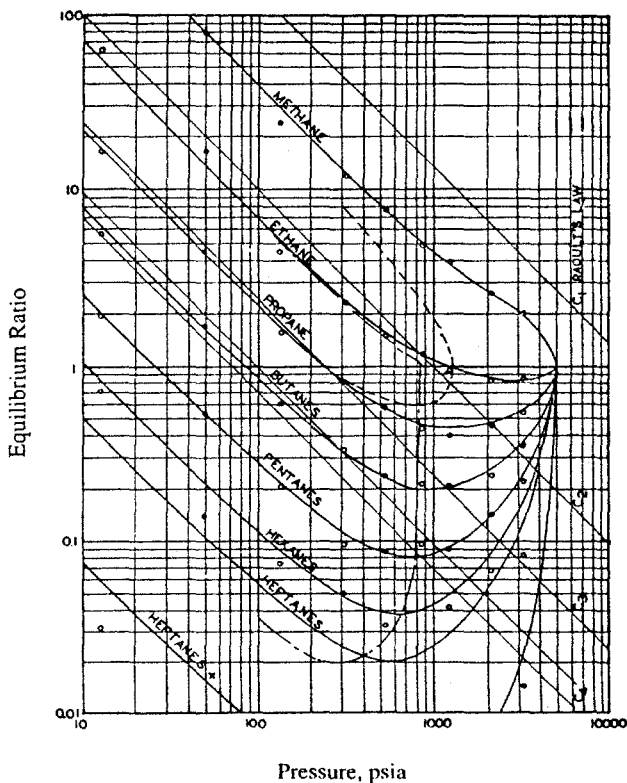


Figure 3.3. Equilibrium ratios of a hydrocarbon mixture at 322 K (120°F). SPE-AIME Copyright. Reproduced from [7] with permission.

The predicted equilibrium ratios, using Raoult's law, Eq.(3.51), are also shown in Figure 3.3. As the system temperature is constant, hence, the vapour pressure of all the components, the logarithmic plots of the K-values with pressure are all parallel straight lines with a slope of -1, as determined by Eq.(3.51). The deviation of predicted values by Raoult's law grossly increases at high pressure conditions, particularly where K-values tend to increase with pressure as opposed to Raoult's law.

For a binary system, the convergence pressure is the critical pressure of a mixture which has a critical temperature equal to the system temperature. The composition of such a mixture is different from that of the system under consideration, unless it is at its critical temperature. Figure 3.4 shows the pressure-temperature diagram of ethane-normal heptane mixtures at different compositions, with the locus of the critical points identified by the dotted curve. At 450 K, for example, the convergence pressure is determined to be equal to 8.23 MPa for all C<sub>2</sub>-nC<sub>7</sub> mixtures regardless of the composition. The composition of equilibrated phases, hence, the equilibrium ratio, at a pressure-temperature condition do not depend on the mixture compositions for binary systems due to the phase rule, Eq.(1.2). The generated K-values on any binary mixture are, therefore, valid for all compositions.

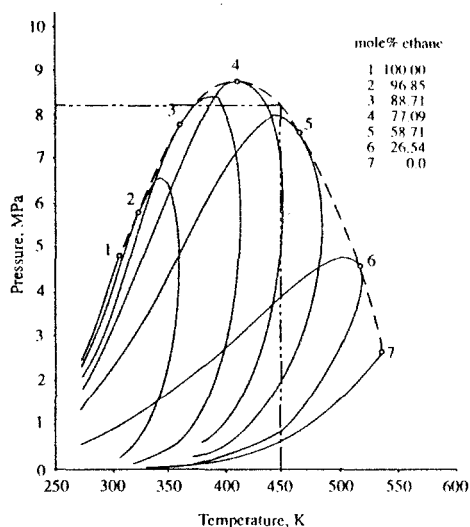


Figure 3.4. Determination of the convergence pressure for a binary mixture. McGraw-Hill Companies Copyright. Reproduced from [7] with permission.

K-values in multicomponent hydrocarbon systems at high pressure depend on composition. A common assumption is, that the convergence pressure alone can reasonably describe the above dependency. Hence, equilibrium ratios are often correlated as functions of the pressure, temperature and convergence pressure. There are a number of correlations to estimate the equilibrium ratio [8], and different methods to calculate the convergence pressure of multicomponent systems in the literature. Care should be taken to use the same method of convergence pressure calculation as used in the development of the K-value correlation.

The Gas Processors Association in 1957 presented K-value graphical correlations for paraffins from methane to decane, ethylene, propylene, nitrogen and carbon dioxide, using the convergence pressure calculated by the Hadden method [9]. The K-charts have been revised since frequently. The 1976 revised charts for convergence pressures of 5000 psia (34.47 MPa) [10] are given in Appendix D. The equilibrium ratios of CO<sub>2</sub> at low concentrations can be estimated, within an accuracy of  $\pm 10\%$ , as,

$$K_{CO_2} = (K_C K_{C_2})^{0.5} \quad (3.56)$$



where  $K_{C1}$  and  $K_{C2}$  are the equilibrium ratios of methane and ethane in the mixture respectively.

The Hadden method of calculating the convergence pressure treats the mixture as a pseudo binary system composed of the lightest component, and all other components grouped as a single heavy pseudo component. The pseudo component formed by grouping will be, therefore, different for vapour and liquid phases. In the GPA method the convergence pressure is the one calculated for the liquid phase. Hence, the calculation of convergence pressure is iterative, except for bubble point calculation, because the liquid composition is not known in advance.

The calculation procedure, as suggested by GPA [10], is as follows:

- (1) Assume the liquid phase composition, or use the feed composition in the first trial.
- (2) Select the lightest hydrocarbon component, methane almost in all cases, which is present at least 0.1 mole % in the liquid phase.
- (3) Calculate the weighted average critical temperature and critical pressure for the remaining heavier components to form a heavy pseudo component.
- (4) Trace the critical locus of the binary consisting of the light and pseudo heavy component on Figure D.1 (Appendix D), by interpolating between the neighbouring critical loci.
- (5) Read the convergence pressure at the prevailing temperature.
- (6) Obtain K-values for the system components from the K-charts corresponding to the estimated convergence pressure.
- (7) Calculate the equilibrium conditions and determine the liquid composition.
- (8) Repeat steps 2 through 7 until the assumed and calculated convergence pressures check within an acceptable tolerance.

When the calculated convergence pressure is between the values for which charts are provided, interpolation between charts may be necessary. Clearly, a reasonable interpolation can only be expected when the operating pressure is lower than the convergence pressure of the two charts used for interpolation. Phase equilibrium calculations using K-values will be described in Section 5.1.

GPA K-values have been fitted to functions of various forms for computer calculations [11]. The K-value of the  $C_{7+}$  fraction of an oil mixture can be estimated by various methods. A rule of thumb [7] suggests a value equal to 15% of the  $C_7$ . It can also be estimated as equal to the K-value of a hydrocarbon compound, or that of a single carbon group as described in Chapter 6, with the same specific gravity or molecular weight as that of the  $C_{7+}$ .

In Chapter 6 on fluid characterisation, various methods to describe the  $C_{7+}$  fraction, and to estimate its properties are proposed. It is more appropriate to describe the  $C_{7+}$  fraction by a number of pseudo components. However, the following correlations may be used to estimate the critical properties of the  $C_{7+}$  fraction.

Standing [12], represented the graphical correlation of Mathews, Roland, and Katz [13] as,

$$T_{c,C_n} = 338 + 202 \times \log(M_{C_n} - 71.2) + (1361 \times \log M_{C_n} - 2111) \log S_{C_n} \quad (3.57)$$

$$P_{c,C_{7+}} = 8.191 - 2.97 \times \log(M_{C_{7+}} - 61.1) + (S_{C_{7+}} - 0.8)[15.99 - 5.87 \times \log(M_{C_{7+}} - 53.7)] \quad (3.58)$$

where  $T_c$  and  $P_c$  are in K and MPa, respectively.

Other correlations to estimate the critical properties of the  $C_{7+}$  fraction are also available [14,15].

#### Example 3.4.

The composition of an oil sample and its equilibrated gas, at 10.45 MPa and 325.0 K, are given in the following table.

Component	mole %	
	Gas	Liquid
$C_1$	82.14	27.36
$C_2$	11.22	10.93
$C_3$	4.06	8.56
$iC_4$	0.42	1.46
$nC_4$	1.07	4.73
$iC_5$	0.24	1.77
$nC_5$	0.30	2.77
$C_6$	0.21	3.87
$C_{7+}$	0.33	38.56

$C_{7+}$  Characteristics  $M=210$   $S=0.8399$

Calculate the convergence pressure of the liquid phase at the above conditions.

#### Solution:

The critical properties of  $C_1$ - $C_6$  are read from Table A.1 in Appendix A, and those of  $C_{7+}$  are calculated using Eqs.(3.57-58). It should be noted that  $C_{7+}$  is not normal hexane, but a group of compounds with boiling points between those of normal pentane and normal hexane. This subject is described in Chapter 6, where more appropriate critical properties for the hexane group are introduced. Methane is selected as the light component, with the rest grouped as a pseudo heavy component based on mass weighting, as follows:

Component	M	$T_c$ , K	$P_c$ , MPa	$x_i$	$w_i$	$p_c T_c$ , K	$p_c P_c$ , MPa
Equation				$x_i M_i / \sum x_i M_i$	$x_i M_i$	$T_c w_i$	$P_c w_i$
$C_1$	16.043	190.56	4.599	0.2736			
$C_2$	30.07	305.32	4.872	0.1093	0.03344	10.211	0.16293
$C_3$	44.096	369.83	4.248	0.0856	0.03842	14.209	0.16321
$iC_4$	58.123	408.14	3.648	0.0146	0.00864	3.526	0.03151
$nC_4$	58.123	425.12	3.796	0.0473	0.02800	11.904	0.10629
$iC_5$	72.15	460.43	3.381	0.0177	0.01302	5.993	0.04401
$nC_5$	72.15	469.7	3.37	0.0277	0.02034	9.553	0.06854
$C_6$	86.177	507.6	3.025	0.0387	0.03392	17.218	0.10261
$C_{7+}$	210.0	691.2	1.812	0.3856	0.82422	569.732	1.49363
Total				1.0000	1.00000	642.35	2.173

The heavy pseudo component with  $T_c=642.35$  K (696.56 °F) and  $P_c=2.173$  MPa (315.2 psia) is slightly heavier than  $nC_{11}$ , as located in Figure C.1. The locus of critical points of methane and pseudo component is drawn parallel to that of  $C_1$ - $nC_{10}$ , interpolating between

it and that of  $C_1$ - $nC_{17}$  (kerosol), which results in a convergence pressure of about 41.37 MPa (6000 psia) at 325 K (125.3 °F).

### K-Values at Intermediate Pressures

At pressures below 7 MPa (1000 psia), the effect of mixture composition on equilibrium ratios of hydrocarbons is not significant, therefore, K-values can be correlated in terms of pressure and temperature only.

Standing [16] correlated the experimental K-values of Oklahoma City crude oil/natural gas samples generated by Katz and Hachmuth [17], using Eq.(3.59) proposed by Hoffmann et al. [18].

$$\log KP = \eta' + \beta' [\alpha' (1/T_b - 1/T)] \quad (3.59)$$

$$\eta' = -0.96 + 6.53 \times 10^{-2} P + 3.16 \times 10^{-4} P^2 \quad (3.60)$$

$$\beta' = 0.890 - 2.46 \times 10^{-2} P - 7.36 \times 10^{-4} P^2 \quad (3.61)$$

where P is pressure in MPa, and  $T_b$  (normal boiling point) and T are in K.  $\alpha'$  is the slope of the straight line connecting the critical point and the boiling point at atmospheric pressure,  $P_a$ , on a log vapour pressure vs.  $(T)^{-1}$  plot.

$$\alpha' = \left[ \log(P_c / P_a) \right] / \left[ 1/T_b - 1/T_c \right] \quad (3.62)$$

The plot of  $\log KP$  vs.  $\alpha' (1/T_b - 1/T)$  for components of a system at a given pressure often forms a straight line for intermediate and heavy fractions, as shown in Figure 3.5. Standing modified values of  $\alpha'$  and  $T_b$  for methane and ethane and non-hydrocarbon compounds to fit the same straight line as other components. The values of  $\alpha'$  and  $T_b$  are given in Table 3.1.

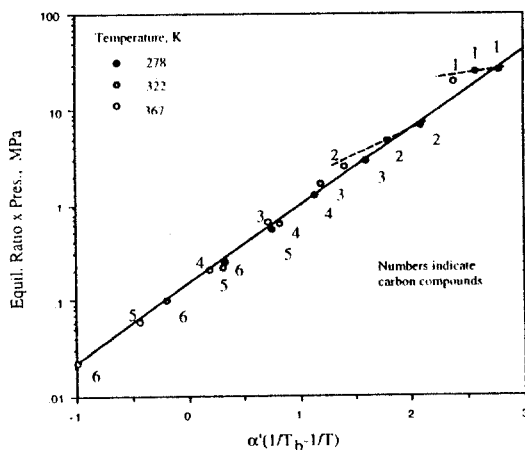


Figure 3.5. Equilibrium ratios at 5.52 MPa and various temperatures. SPE Copyright. Reproduced from [16] with permission.

The values of  $\alpha'$  and  $T_b$  for  $C_{7+}$  fractions can be obtained from:

$$\alpha' = 563 + 180n - 2.364n^2 \quad (3.63)$$

$$T_{bn} = 167 + 33.25n - 0.539n^2 \quad (3.64)$$

where  $n$  is the number of carbons of the normal paraffin that has the same  $K$ -value as that of the  $C_{7+}$  fraction. It can be estimated by comparing the molecular weight of the  $C_{7+}$  fraction with those of normal paraffins, Table A.1 in Appendix A. Standing correlated  $n$  for the Oklahoma City crude oil samples by,

$$n = 3.85 + 0.0135T + 0.2321P \quad (3.65)$$

where  $T$  is in K and  $P$  is in MPa.

Table 3.1.  
Values of  $\alpha'$  and  $T_b$  for use in Standing's equilibrium ratio correlation.

Compound	$\alpha'$ , K	$T_b$ , K
Nitrogen	261	61
Carbon Dioxide	362	108
Hydrogen Sulphide	631	184
Methane	167	52
Ethane	636	168
Propane	999	231
iso-Butane	1132	262
n-Butane	1196	273
iso-Pentane	1316	301
n-Pentane	1378	309
iso-Hexanes	1498	335
n-Hexane	1544	342
Hexanes (lumped)	1521	339
n-Heptane	1704	372
n-Octane	1853	399
n-Nonane	1994	424
n-Decane	2127	447

Although the equilibrium ratio correlation was based on a limited number of data, it has been shown to be reliable for crude oils from various regions of the world, some containing substantial amounts of non-hydrocarbons [19].

Other generalised  $K$ -value correlations, either neglecting the effect of mixture composition [20, 21] or using a single parameter such as the convergence pressure to characterise the mixture [22,23] have also been developed by various investigators. These correlations would be mainly valuable in generating initial guess values for using in an equation of state to calculate fugacities, as described in Chapter 5.

Wilson [20] proposed the following equation to estimate the equilibrium ratio below 3.5 MPa (500 psia):

$$K_i = (P_c / P) \exp[5.37(1 + \omega_i)(1 - T_{ci} / T)] \quad (3.66)$$

where  $\omega$  is the acentric factor and  $T_c$  and  $P_c$  are the absolute critical temperature and pressure respectively. The Wilson equation basically uses Raoult's law, with the vapour pressure related to the critical properties using the definition of the acentric factor, Eq.(1.9).

The Mollerup equation [21] to estimate K-values, as initial guesses in flash calculations, is equivalent to the above, but for a constant acentric factor of 0.01.

The Wilson equation generally provides reliable estimation of K-values for sub-critical components, but overestimates those of the supercritical components [24]. The equation has been extended to higher pressures [22] as,

$$K_i = (P_{ci} / P_k)^{\Lambda-1} (P_{ci} / P) \exp[5.37\Lambda(1 + \omega_i)(1 - T_{ci} / T)] \quad (3.67)$$

where

$$\Lambda \equiv 1 - [(P - P_s) / (P_k - P_s)]^n$$

and  $P_k$  is the convergence pressure, as correlated by Standing [12],

$$P_k = 0.414 M_{C_{7+}} - 29.0 \quad (3.68)$$

where  $P_k$  is in MPa. The exponent  $n$  varies between 0.5 and 0.8, depending on the fluid, with a default value of 0.6.

The above modification to the Wilson equation may lead to unrealistic values resulting to non-convergence in phase behaviour calculations.

#### Example 3.5.

Estimate equilibrium ratios of the gas-oil system described in Example 3.4, using the Standing method and the Wilson equation. Compare the results with the experimental values.

#### Solution:

The critical properties of  $C_1$ - $C_6$  are read from Table A.1 in Appendix A. The properties of  $C_{7+}$  are calculated as follows.

#### Standing Correlation

Substituting the pressure and temperature in Eq.(3.65), the equivalent carbon number of  $C_{7+}$  is determined equal to 10.66, which results in  $\alpha'=2213$  K and  $T_b=460.2$  K, using Eq.(3.63) and Eq.(3.64), respectively.

The coefficients of Eq.(3.59) at 10.45 MPa are calculated as,

$$\eta' = 0.067465, \text{ using Eq.(3.60)}$$

$$\beta = 0.5526, \text{ using Eq.(3.62)}$$

The results are given in the following table.

#### Wilson Equation

The estimation of critical properties of a pseudo component, using its specific gravity and molecular weight, is described in Section 6.2. A simple approach is to represent  $C_{7+}$  with a normal alkane with the same molecular weight. In this case,  $C_{18}$ , with a molecular weight of 212 is considered to represent  $C_{7+}$ . The critical properties of  $C_{7+}$  are, therefore, estimated equal to  $T_c=736$  K,  $P_c=1.340$  MPa, and  $\omega=0.7697$ .

The convergence pressure for the modified Wilson equation is calculated from Eq.(3.68), equal to 57.94 MPa, with the value of  $A=0.644$ .

The calculated equilibrium ratios using the Standing method,  $K_s$ , the Wilson equation,  $K_w$ , and the modified Wilson equation,  $K_{mw}$ , are compared with the experimental values,  $K_e$ , in the following table.

Component	$\alpha$ , K	$T_h$ , K	$K_s$	$K_w$	$K_{mw}$	$K_e$
Equation			3.59	3.66	3.67	
$C_1$	167	52	3.4601	4.1626	4.6099	3.0022
$C_2$	636	168	1.1454	0.6666	1.4170	1.0274
$C_3$	999	231	0.5490	0.1731	0.5947	0.4749
$iC_4$	1132	262	0.3245	0.0693	0.3298	0.2855
$nC_4$	1196	273	0.2727	0.0499	0.2669	0.2268
$iC_5$	1316	301	0.1686	0.0207	0.1517	0.1353
$nC_5$	1378	309	0.1478	0.0162	0.1292	0.1091
$C_6$	1521	339	0.0874	0.0057	0.0661	0.0539
$C_7+$	2214	460	0.0088	0.0000	0.0005	0.0086

Note that although the pressure is above the working range of the Standing correlation, it predicts the results more reliably than others. The modification has improved the Wilson equation in general, except for predicting the equilibrium ratio of methane.

All the above K-value correlations can be used to check the internal consistency of measured equilibrium ratios. Figure 3.6 compares the Hoffmann plot with that of modified Wilson plot, where  $\log K_i$  has been plotted vs.  $(1+\omega_i)(1-T_{ci}/T)$  at constant pressure for intermediate compounds of an oil sample. A straight line can clearly fit the data, including non-paraffins, by the Wilson method, which uses the acentric factor, more closely than that of the Hoffmann method.

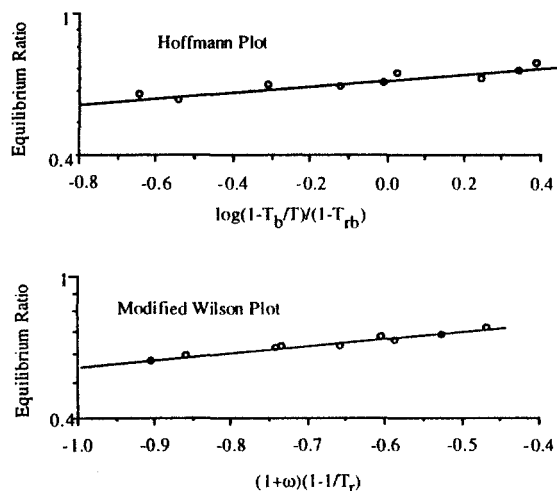


Figure 3.6. Equilibrium ratios of intermediate compounds of a gas-oil mixture at 20.79 MPa and 373 K.

The equilibrium ratios of components of an oil measured in a test, simulating oil vaporisation in reservoir by methane injection in three contact stages at constant pressure and temperature, are shown in Figure 3.7. The variation of  $K_i$  for each component is solely due to changes in the mixture composition by gas contacting oil. The results clearly indicate that the correlations ignoring the compositional effect cannot provide reliable estimates of the equilibrium ratio at high pressure conditions. The measured data at any overall composition can, however, be represented reasonably by a straight line.

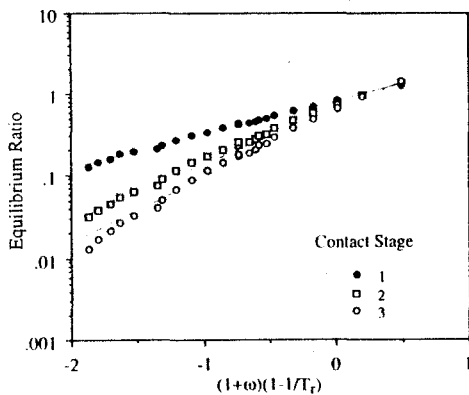


Figure 3.7. Measured equilibrium ratios in a test simulating oil vaporisation by methane at 34.58 MPa and 373K.

Although the data at high pressure may not fall on a straight line, one would expect them to follow a monotonous trend. Therefore, any measured point that is completely outside the general trend could be suspect. The Hoffmann or Wilson plot is thus a good tool for checking the integrity of the measurements. Other linear plots between  $\log K_i$  and component properties such as  $T_{ci}^2$ ,  $T_{bi}^{-1}$  [25] and the molecular weight [26] have also been proposed which can be used to evaluate measured data and estimate equilibrium ratios.

### 3.3 REFERENCES

1. Prausnitz, J.M., Lichtenthaler, R.N. and de Azevedo, E.G: "Molecular Thermodynamics of Fluid-Phase Equilibria", 2nd Edition, Prentice-Hall Inc., NJ (1986).
2. Smith, J.M. and Van Ness, H.C: "Introduction to Chemical Engineering Thermodynamics", Third Edition, McGraw-Hill (1975).
3. Michelsen, M.L: Private Communications.
4. Chao, K.C. and Seader, J.D: "A General Correlation of Vapour-Liquid Equilibria in Hydrocarbon Mixtures", AIChE J., Vol. 7, No. 4, 598-605 (Dec., 1961).
5. Krichevsky, IR and Kasarnovsky, JS: "Thermodynamical Calculations of Solubilities of Nitrogen and Hydrogen in Water at High Pressures", J. Am. Chem. Soc., 57, 2168(1935).

6. Kobayashi, R. and Katz, D.L.: "Vapour-Liquid Equilibria for Binary Hydrocarbon-Water Systems", *Ind. Eng. Chem.*, 45, 440 (1953).
7. Katz, D., et al: "Handbook of Natural Gas Engineering", MacGraw Hill (1959).
8. Lawal, A.S. and Silberberg, I.H.: "A New Correlation of Vapour-Liquid Equilibrium Ratios Internally Consistent with Critical Behaviour", SPE 10287, *Proc. of 56th Ann. Conf.*, (Oct., 1981).
9. Hadden, S.T.: "Convergence Pressure in Hydrocarbon Vapour-Liquid Equilibria", *Chem. Eng. Symp. Series* 49, No. 7, 53-66 (1953).
10. Gas Processors Suppliers Association, ed.: "SI Engineering Data Book", Tulsa, Oklahoma (1980).
11. MacDonald, R.C.: "Reservoir Simulation with Interphase Mass Transfer", Report No. UT 71-2, The University of Texas at Austin (1971).
12. Standing, M.B.: "Volumetric and Phase Behaviour of Oil Field Hydrocarbon Systems", 9th Printing, SPE, Dallas, Texas (1981).
13. Mathews, T.A., Roland, C.H., and Katz, D.L.: "High Pressure Gas Measurement", *Proc. NGAA*, 41 (1942).
14. Rowe, AM: "Internally Consistent Correlations for Predicting Phase compositions for Use in Reservoir Compositional Simulators", SPE Paper 7475, *Pres. at the 53rd Ann. Fall Tech. Conf and Exh. of the Society of Petroleum Engineers*, Houston, Texas, Oct. 1-3 (1978).
15. Ahmed, T.: "Hydrocarbon Phase Behaviour", Gulf Publishing Company, Houston (1989).
16. Standing M.B.: "A Set of Equations for Computing Equilibrium Ratios of a Crude Oil/Natural Gas System at Pressures Below 1000 Psia", *JPT*, 1193-1195 (Sept., 1979).
17. Katz, D.L. and Hachmuth, D.H.: "Vaporisation Equilibrium Constants in a Crude Oil-Natural Gas System", *I & EC*, 29, 1072-1077 (1937).
18. Hoffmann, A.E., Crump, J.S. and Hocott, C.R.: "Equilibrium Constants for Gas-Condensate Systems", *Trans. AIChE*, 198, 1-10 (1953).
19. Glaso, O.S. and Whitson, C.H.: "The Accuracy of PVT Parameters Calculated from Computer Flash Separation at Pressures Less Than 1000 Psia", *JPT*, 1811-1813 (Aug., 1982).
20. Wilson, G.: "A Modified Redlich-Kwong EOS, Application to General Physical Data Calculations", Paper No 15C, presented at the AIChE 65th National Meeting (May, 1968).
21. Michelsen, M.L.: "Calculation of Phase Envelopes and Critical Points for Multicomponent Mixtures", *J. Fluid Phase Equilibria*, 4, 1-10 (1980).
22. Whitson, C.H. and Torp, S.B.: "Evaluating Constant Volume Depletion Data", SPE 10067, *Proc. of 56th Ann. Conf.* (Oct., 1981).
23. Voratsis, N.: "A Robust Prediction Method for Rapid Phase Behaviour Calculations", SPE 16943, *Proc. of 62nd Ann. Conf.* (Sept., 1987).



24. Michelsen, M.L.: "Phase Equilibrium Calculations, What is Easy and What is Difficult?", Computers Chem.Eng'ng., 17 No. 5/6, 431-439 (1993).
25. Campbell, J.M.: "Gas Conditioning and Processing", Vol. 1, Campbell Petroleum, Oklahoma (1976).
26. Danesh, A., Xu, D.-H. and Todd, A.C.: "A Grouping Method to Optimise Oil Description for Compositional Simulation of Gas-Injection Processes", SPE Res. Eng., 343-348 (1992).
27. Sage, B.H. and Lacey, W.N.: "Phase-Equilibria in Hydrocarbon Systems", Ind. Eng. Chem., Vol. 34, No. 12, 1526-1531 (Dec. 1942).

### 3.4 EXERCISES

3.1. Prove Eq.(3.35)

3.2. The vapour and liquid phases of a binary mixture are at equilibrium at  $T=300\text{ K}$  and  $12\text{ MPa}$ . The mole fraction of component 1 in the equilibrated gas and liquid phases is  $0.9990$  and  $0.2500$ , respectively. The compressibility factor of component 1 as a pure gas at  $300\text{ K}$  can be related to its pressure as,

$$Z = 1 - 5.45 \times 10^{-2} P - 6.35 \times 10^{-4} P^2$$

where  $P$  is in MPa.

Calculate the fugacity coefficient of component 1 in the liquid phase.

3.3. A mixture of  $C_1$  and  $nC_8$  is flashed at  $423.1\text{ K}$  and  $7.093\text{ MPa}$ . Use Raoult's law, the Standing method, the Wilson equation and the GPA chart to predict the equilibrium ratio of methane and normal decane at the above conditions. The measured mole fraction of methane in the equilibrated gas and liquid phases is  $0.949$  and  $0.229$ , respectively. [Kohn, J.P., Bradish, W.F., J. Chem. Eng. Data, 9, 5, (1964)].

3.4. The measured composition of equilibrated vapour and liquid phases at  $10.45\text{ MPa}$  and  $324.8\text{ K}$  are given in the following table.

Component, mole%	Gas	Liquid
CO <sub>2</sub>	70.98	50.15
N <sub>2</sub>	0.59	0.13
C <sub>1</sub>	18.18	7.26
C <sub>2</sub>	5.16	3.99
C <sub>3</sub>	2.45	3.78
iC <sub>4</sub>	0.31	0.72
nC <sub>4</sub>	0.88	2.41
iC <sub>5</sub>	0.23	0.59
nC <sub>5</sub>	0.32	1.51
C <sub>6</sub>	0.31	2.77
C <sub>7+</sub>	0.59	26.69
Gas comp. factor	0.578	
Liq. density, kg/m <sup>3</sup>		765.9

C<sub>7+</sub> Characteristics,  $M=208$ ,  $S=0.8382$

Predict the equilibrium ratios at the above conditions using GPA charts, the Standing method and the Wilson equation. Compare the results with measured values.

3.5. An equi-molar binary gas mixture composed of ethane and  $\text{CO}_2$  is in equilibrium with water at 350 K and 30 MPa. Assume the gas fugacity coefficients equal to one, and use Henry's law to estimate the gas solubility in water.

## 4 EQUATIONS OF STATE

The equality of fugacity of each component throughout all phases was proved, in Chapter 3, to be the requirement for chemical equilibrium in multicomponent systems. The fugacity coefficient,  $\phi_i$ , defined as the ratio of fugacity to pressure, of each component in any phase is related to pressure, temperature and volume by Eq.(3.31),

$$\ln \phi_i = \frac{1}{RT} \int_v^\infty \left[ \left( \frac{\partial P}{\partial n_i} \right)_{T,v,n_{j \neq i}} - \frac{RT}{v} \right] dv - \ln Z \quad i=1,2,\dots,N \quad (3.31)$$

The fugacity coefficient can, therefore, be determined from the above with the aid of an equation relating pressure, temperature, volume and compositions, that is, an equation of state (EOS).

In general, any equation of state which provides reliable volumetric data over the full range of the integral in Eq.(3.31) can be used to describe the fluid phase behaviour. Several types of EOS have been successfully applied to hydrocarbon reservoir fluids.

The simplest, and highly successful equation, is the semi-empirical van der Waals type EOS with two or three parameters. Since 1873, when van der Waals improved the ideal gas equation by including parameters that represented the attractive and repulsive intermolecular forces, the equation has been revised and modified by numerous investigators. Other equations with many parameters have also been used to describe the phase behaviour, some with reasonable success. Amongst these equations, the Benedict-Webb-Rubin (BWR) type [1], which is an empirical extension to the virial EOS, can be applied to both liquid and vapour phases of reservoir fluids. These equations provide no additional reliability in phase behaviour studies, in spite of their complexity, in comparison with the van der Waals type EOS. They are, however, valuable tools to describe volumetric behaviour, particularly of pure compounds, due to their large number of parameters, hence, high flexibility.

Equations of state are basically developed for pure components, but applied to multicomponent systems by employing some mixing rules to determine their parameters for mixtures. The mixing rules are considered to describe the prevailing forces between molecules of different substances forming the mixture. Simple mixing rules, such as those that assume compounds are randomly distributed within the mixture, are quite adequate to describe hydrocarbon mixtures of reservoir fluids. More complex mixing rules, however, are required to represent the interaction between hydrocarbons and asymmetric compounds such as water, which is present in reservoirs, or methanol which is sometimes added to reservoir fluids as a hydrate inhibitor.

Although thermodynamics rigorously describe the equilibrium conditions and relate them to volumetric data, as given by Eq.(3.31), it is the capability of EOS and the associated mixing rules that determines the success of phase equilibrium prediction, as will be described in this chapter.

#### 4.1 VIRIAL EOS AND ITS MODIFICATIONS

The virial equation is based on theories of statistical mechanics [2], and can be expressed as an infinite series of either molar volume (molar density), or pressure,

$$Z = 1 + B/v + C/v^2 + D/v^3 + \dots \quad (4.1)$$

$$(Z = 1 + B\rho_M + C\rho_M^2 + D\rho_M^3 + \dots)$$

or,

$$Z = 1 + B'P + C'P^2 + D'P^3 + \dots \quad (4.2)$$

where  $Z$  is the compressibility factor,  $v$  and  $p$  are the molar volume and the molar density, respectively, and  $P$  is the pressure.  $B$ ,  $C$ ,  $D$ , etc., are called the second, third, fourth, and so on, virial coefficients, and depend only on temperature for each compound.

The coefficient  $B$  accounts for the interaction between two molecules, whereas  $C$  is that for three molecules and so on. For example, if the effect of a third molecule on the prevailing forces between two molecules can be ignored, the third and higher terms can be neglected. As the fluid becomes more dense, the higher terms become more significant and cannot be ignored. The equation reduces to  $Z=1$ , that is the ideal gas equation, when pressure approaches zero.

Numerous theoretical and experimental studies on determination of virial coefficients, mostly the second virial coefficient, have been reported. As high order coefficients are hard to determine, the equation can be applied to the vapour phase only. It is, therefore, of little

value to reservoir fluid studies, where a single equation of state is to describe the behaviour of both vapour and liquid phases. It is, however, very useful in showing guidelines for applying semi-empirical EOS to mixtures, as the virial coefficients can be described rigorously for mixtures using statistical mechanics. This subject is described in Section 4.3.

### Starling Modification of Benedict-Webb-Rubin EOS (BWRS)

The Benedict-Webb-Rubin EOS (BWR) [1] is an empirical extension of the virial EOS. A modification of the Benedict-Webb-Rubin EOS as proposed by Starling [3] with 11 parameters has been applied successfully to petroleum reservoir fluids,

$$P = \rho_M RT + \left( B_o RT - \Lambda_o - \frac{C_o}{T} + \frac{D_o}{T^2} - \frac{E_o}{T^3} \right) \rho_M^2 + \left( bRT - a - \frac{d}{T} \right) \rho_M^3 + \alpha \left( a + \frac{d}{T} \right) \rho_M^6 + \frac{c \rho_M^3}{T^2} (1 + \gamma \rho_M^2) \exp(-\gamma \rho_M^2) \quad (4.3)$$

where  $\rho_M$  is the molar density and the 11 coefficients can be evaluated from the following generalised equations:

$$\rho_{Mc} B_o = 0.443690 + 0.115449\omega$$

$$\frac{\rho_{Mc} \Lambda_o}{RT_c} = 1.28438 - 0.920731\omega$$

$$\frac{\rho_{Mc} C_o}{RT_c^2} = 0.356306 + 1.70871\omega$$

$$\frac{\rho_{Mc} D_o}{RT_c^4} = 0.0307452 + 0.179433\omega$$

$$\frac{\rho_{Mc} E_o}{RT_c^5} = 0.006450 - 0.022143\omega \exp(-3.8\omega)$$

$$\rho_{Mc}^2 b = 0.528629 + 0.349261\omega$$

$$\frac{\rho_{Mc}^2 a}{RT_c} = 0.484011 + 0.754130\omega$$

$$\frac{\rho_{Mc}^2 d}{RT_c^3} = 0.0732828 + 0.463492\omega$$

$$\rho_{Mc}^3 \alpha = 0.0705233 - 0.044448\omega$$

$$\frac{\rho_{Mc}^3 c}{RT_c^3} = 0.504087 + 1.32245\omega$$

$$\rho_{Mc}^2 \gamma = 0.544979 - 0.270896\omega$$

where  $T_c$ ,  $\rho_{Mc}$  and  $\omega$  are the critical temperature, critical molar density and acentric factor, respectively. The above critical properties, including  $v_c = (1/\rho_{Mc})$ , for pure compounds are given in Table A.1 in Appendix A.

The application of BWR type equations demands a high computational time and effort, due to their high powers in volume and large number of parameters, hence, unsuitable for reservoir fluid studies where many sequential equilibrium calculations are required. More importantly, for multicomponent systems each parameter must be determined using a mixing rule, which at best is quite arbitrary. The choice of mixing rules often has a more pronounced effect on the predicted results, than EOS itself. Although acceptable phase behaviour results can be obtained by BWRS [4], it has been surpassed by the simpler, yet more reliable van der Waals type cubic equation of state.

## 4.2 CUBIC EQUATIONS OF STATE

van der Waals improved the ideal gas equation by considering the intermolecular attractive and repulsive forces, and introduced his well-known equation of state in 1873,

$$\left(P + \frac{a}{v^2}\right)(v - b) = RT \quad (4.4)$$

where  $a/v^2$  and  $b$  represent the attractive and repulsive terms respectively, and  $v$  is the molar volume.

As the pressure approaches infinity, the molar volume becomes equal to  $b$ . Hence,  $b$  is also considered as an apparent volume of the molecules and called co-volume. It should be always less than the molar volume  $v$ .

The above equation in terms of volume or compressibility factor takes a cubic form as follows:

$$v^3 - \left(b + \frac{RT}{P}\right)v^2 + \left(\frac{a}{P}\right)v - \frac{ab}{P} = 0 \quad (4.5)$$

or

$$Z^3 - (1 + B)Z^2 + AZ - AB = 0 \quad (4.6)$$

where the dimensionless parameters  $A$  and  $B$  are defined as,

$$A \equiv \frac{aP}{(RT)^2} \quad (4.7)$$

$$B \equiv \frac{bP}{RT} \quad (4.8)$$

Hence, van der Waals type EOS are often referred to as cubic EOS. A typical volumetric behaviour of EOS of van der Waals type is shown in Figure 4.1.

For a pure compound at temperatures below the critical temperature, e.g.  $T_1$ , the equation may give three real roots for volume (or  $Z$ ) at pressure  $P_1$ , as shown in Figure 4.1. The highest value,  $v_1$  (or  $Z_1$ ) corresponds to that of vapour, whereas the lowest value,  $v_3$  (or  $Z_3$ )

corresponds to that of liquid. The predicted volume within the two phase conditions,  $v_2$  (or  $Z_2$ ), is of no physical significance.

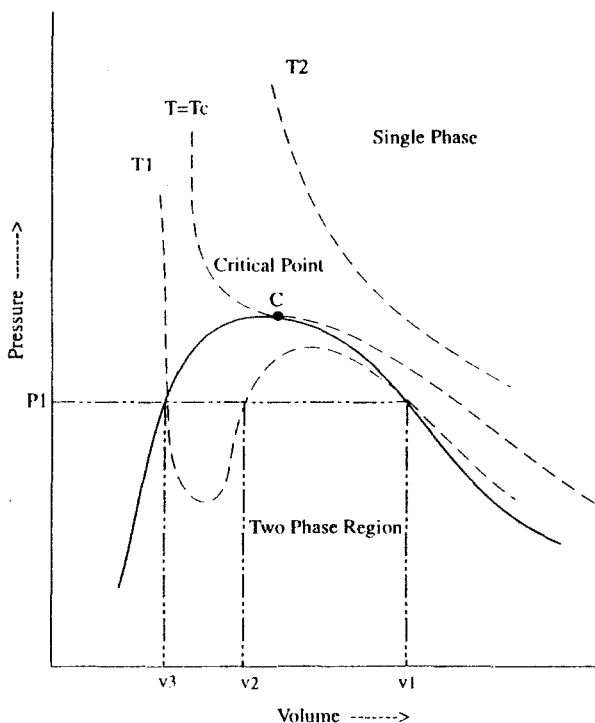


Figure 4.1. Volumetric behaviour of pure compound as predicted by cubic EOS of van der Waals type.

The predicted maximum and minimum volumes within the two-phase region, however, indicate the pressure limits within which the fluid can be compressed or expanded whilst it remains a metastable single phase fluid. This behaviour will be described further in Section 5.2. The difference between the limits reduces as the temperature increases and vanishes at the critical point. At a temperature above the critical point, e.g., at  $T_2$  on the Figure, the equation provides only one physically acceptable root. For the critical isotherm, a horizontal inflection point should, therefore, exist at the critical point,

$$\left(\frac{\partial P}{\partial v}\right)_{T=T_c} = \left(\frac{\partial^2 P}{\partial v^2}\right)_{T=T_c} = 0 \quad (4.9)$$

Applying the above requirements to the van der Waals equation, the values of  $a$  and  $b$  are determined as:

$$a = \frac{9}{8} RT_c v_c = \frac{27}{64} \left( \frac{R^2 T_c^2}{P_c} \right) \quad (4.10)$$

$$b = \frac{1}{3} v_c = \frac{1}{8} \left( \frac{RT_c}{P_c} \right) \quad (4.11)$$

where the subscript c, refers to the values at the critical point.

The van der Waals equation of state (vdW) gives a critical compressibility factor of 0.375 for all compounds, whereas very few compounds, such as quantum gases, have  $Z_c$  greater than 0.3.

*Example 4.1.*

In Example 3.3, the solubility of methane in water was calculated by assuming the methane fugacity coefficient equal to one. Use vdW to estimate the fugacity coefficient and improve the accuracy of predicted gas solubility.

*Solution:*

Substituting the pressure in the fugacity expression for pure compounds, Eq.(3.35), using vdW, we obtain,

$$\begin{aligned} \ln \phi &= (Z - 1) - \ln Z + \frac{1}{RT} \int_{\infty}^v \left( \frac{RT}{v} - P \right) dv = \\ &= (Z - 1) - \ln Z + \frac{1}{RT} \int_{\infty}^v \left( \frac{RT}{v} - \frac{RT}{v-b} + \frac{a}{v^2} \right) dv \end{aligned}$$

Integration of the above equation results in,

$$\ln \phi = (Z - 1) - \ln Z + \frac{1}{RT} \left[ RT \ln \frac{v}{v-b} - \frac{a}{v} \right]_{\infty}^v$$

Implementing the limits, and making the equation dimensionless, using Eqs.(4.7-8), we obtain:

$$\ln \phi = (Z - 1) - \ln(Z - B) - A/Z$$

The parameters of vdW are calculated, using Eqs.(4.9-10) and methane critical properties given in Table A.1 in Appendix A, as,

$$a = \frac{27}{64} \left( \frac{R^2 T_c^2}{P_c} \right) = (27/64) \times (0.0083144 \times 190.56^2 / 4.599) = 0.230274 \text{ MPa} \cdot (\text{m}^3/\text{kgmol})^2$$

$$b = \frac{1}{8} \left( \frac{RT_c}{P_c} \right) = (1/8) \times 0.0083144 \times 190.56 / 4.599 = 0.304254 \text{ m}^3/\text{kgmol}$$

with the dimensionless values, defined in Eq.(4.7-8), as follows,

$$A = 1.556251$$

$$B = 0.902574$$



Substituting the above values in Eq (4.6), results in the following cubic equation for Z,

$$Z^3 - 1.90257 Z^2 + 1.55625 Z - 1.40463 = 0$$

with only one real root,

$$Z = 1.49069$$

Substituting the above value of the compressibility factor in the fugacity expression results in,

$$\phi = 0.97779$$

Hence the concentration of dissolved methane in water, corrected for the fugacity coefficient, is,

$$f_{C1}^V = P \times \phi = 6.5 \times 0.97779 \text{ MPa} = (1.4378 \times 10^1 \text{ MPa/mol fraction}) \times x_{C1}$$

$$x_{C1} = 4.42 \times 10^{-1} \quad \text{mole fraction of methane in water.}$$

A simple equation, such as vdW, cannot accurately model the behaviour of dense fluids particularly that of complex fluid mixtures. Numerous modifications have been made to improve its capability by modifying the attractive and repulsive terms. The two parameters of *a* and *b* in the original vdW can be determined simply from the boundary conditions at the critical point, whereas in modified versions, additional to the above, experimental data on pure fluids have also been used generally to determine the parameters. These equations are, therefore, semi-empirical.

Hard sphere fluid models have been selected [5] to describe repulsive forces. The equation proposed by Carnahan and Starling [6] has been used extensively to develop new forms such as perturbed hard chain [7], and chain of rotators [8]. In spite of recent efforts [9] to simplify the earlier modifications in order to make them more practical, they have not received much attention as engineering tools.

Although van der Waals considered that his representation of repulsive forces, expressed by a constant *b*, required more improvement than that of the attractive term, in practice the modification of the latter has been more rewarding. Almost all popular van der Waals type EOS have improved their capabilities by modifying the attractive term. They can be expressed by the following general form,

$$P = \frac{RT}{v-b} - \frac{a}{v^2 + uv + w^2} \quad (4.12)$$

In a two-parameter form of the equation *u* and *w* are related to *b* whereas in a three-parameter form *u*, and *w* are related to *b*, and/or a third parameter *c*. In a four-parameter modification *u* and *w* are related to *b* and/or *c* and a fourth parameter *d*.

The above general equation in terms of the compressibility factor is,

$$Z^3 - (1+B-U)Z^2 + (A-BU-U-W^2)Z - (AB-BW^2-W^2) = 0 \quad (4.13)$$

where the dimensionless parameters *A* and *B* are the same as those defined in Eqs.(4.7) and (4.8), respectively, and

$$U \equiv \frac{uP}{RT} \quad (4.14)$$

$$W \equiv \frac{wP}{RT} \quad (4.15)$$

The two-parameter EOS are the most popular equations, where the parameters are expressed by,

$$a = \Omega_a \frac{R^2 T_c^2}{P_c} \quad (4.16)$$

$$b = \Omega_b \frac{RT_c}{P_c} \quad (4.17)$$

Note that the expressions for the parameters in the modified equations are similar to those of the original vdW, but the coefficients have been generalised as  $\Omega_a$  and  $\Omega_b$ . The other parameters, in EOS which use more than two, are generally of co-volume nature, hence, expressed by an equation similar to Eq.(4.17), but with different coefficients.

The substitution of Eq.(4.12) into the expression for fugacity of a pure substance, Eq.(3.35), results in the following generalised expression, using the same approach as in Example 4.1,

$$\ln \phi = (Z - 1) - \ln(Z - B) + \frac{A}{\sqrt{U^2 + 4W^2}} \ln \frac{2Z + U - \sqrt{U^2 + 4W^2}}{2Z + U + \sqrt{U^2 + 4W^2}} \quad (4.18)$$

There is hardly any theoretical foundation, or strongly convincing arguments, for selecting a particular form of EOS amongst many described by the general form of Eq.(4.12). The success and popularity of certain equations are more due to features other than the selected form in most cases. For example, the method used to determine the EOS parameters could have a higher impact on the predicted results, than the mathematical form of the equation.

Although EOS primarily provides volumetric (density) data, its major contribution as an engineering tool is through its coupling with thermodynamic relations in predicting phase behaviour and physical properties of fluids. As the parameters of a semi-empirical EOS are determined by matching its prediction to experimental data, the inclusion of more parameters in EOS makes it more flexible. Whereas a two-parameter EOS would suffice to predict the vapour pressure, hence, phase equilibria, the inclusion of a third parameter will generally improve the prediction of density along with reliable vapour pressure. Two or three parameter EOS are considered adequate for all applications in the petroleum industry.

The main departure from the original vdW, which has resulted in the success of modified equations, is not the revision of the attractive term functional form, but treating it as a temperature dependent parameter,

$$a = a_c \alpha \quad (4.19)$$

where  $\alpha$  expresses the dependency of the parameter,  $a$ , on temperature and  $a_c$  depends only on the critical properties of the compound as given by,

$$a_c = \Omega_a \frac{R^2 T_c^2}{P_c} \quad (4.20)$$

With the exception of Redlich and Kwong [10] who originally proposed the temperature dependency of  $a$  in 1948 as  $\alpha = T_r^{-0.5}$ ; recent investigators have used vapour pressure data to determine  $\alpha$ .

The above discussion highlights the similarity between all the commonly used equations of state and suggests that there is very little fundamental difference between them. All the two-parameter equations have selected a form of Eq.(4.12), assumed,  $a$ , to be temperature dependent, and have determined the temperature dependency by matching the vapour pressure data. The addition of the third parameter has increased the flexibility, where the investigators have determined it generally by matching saturated liquid data. The van der Waals type EOS have been comprehensively reviewed in literature [11-16].

#### Example 4.2.

Prove that the areas between the saturation pressure line and the predicted volume isotherm by a cubic equation of state are equal for a pure substance. The above equality, known as the Maxwell equal area rule, is considered equivalent to equality of fugacities of saturated vapour and liquid phases, hence, applicable in determining the parameters of an empirical EOS.

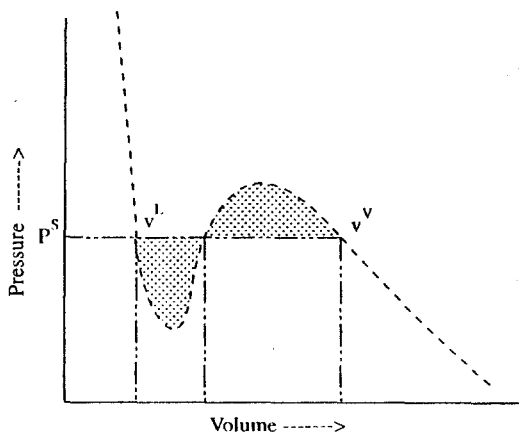


Figure E4.2. Pressure-volume isotherm of a pure fluid as predicted by cubic EOS.

#### Solution:

Integrating Eq.(3.22) from the saturated liquid to the saturated vapour, we obtain,

$$\int_L^V d\mu = \int_L^V s dT + \int_L^V v dP = \mu^V - \mu^L = 0$$

because the vapour and liquid are at equilibrium.

The integral over  $dT$  is equal to zero at the isotherm. Hence,

$$\int_{L}^V v dP = \int_{L}^V d(Pv) - \int_{L}^V P dv = 0$$

or,

$$P(V^V - V^L) - \int_{L}^V P dv = 0$$

Which is only satisfied when the two shaded areas are equal.

#### 4.2.1 Two-Parameter EOS

*Redlich and Kwong* [10] modified the attractive term of vdW as,

$$P = RT/(v - b) - a/[T_r^{0.5} v(v + b)] \quad (4.21)$$

The values of  $\Omega_a$  and  $\Omega_b$  were considered to be constant, hence, determined to be 0.42747 and 0.08664 respectively, using Eq.(4.9).

*Zudkevitch and Joffe* [17], and *Joffe et al.* [18] assumed that  $\Omega_a$  and  $\Omega_b$  in the Redlich-Kwong equation of state (RK) were temperature-dependent. The values of  $\Omega_a$  and  $\Omega_b$  for each pure substance at any temperature were obtained by matching the predicted liquid density data to the measured value, and equalisation of saturated liquid and vapour phase fugacities. Above the critical temperature, the parameters were taken as constants and equal to their values at  $T_r = 1$ . The above approach was necessary as two equilibrated phases cannot exist for a pure compound above the critical point. Figure 4. 2 shows the variation of  $\Omega_a$  and  $\Omega_b$  with  $T_r$  as derived and correlated with the acentric factor by *Yarborough* [19]. The sharp change of both parameters near the critical point clearly ruled out the extrapolation of the relation above the critical point, an approach which is generally used in other EOS.

Matching of the predicted data to measured values at saturation to determine EOS parameters has been used almost by all recent investigators. Whereas *Zudkevitch-Joffe* suggested determining the parameters when required at the prevailing conditions, others have generated generalised correlations for parameters by applying the method. The use of correlations to determine the parameters definitely simplifies the calculation task, but reduces the accuracy as any generalised correlation is bound to have some deviations from the correlated data. The method suggested by *Zudkevitch and Joffe* does not significantly increase the calculational effort when applied to a petroleum reservoir where the temperature is treated mostly constant, and the parameters are calculated only once. Any reliable correlation in literature [20], such as those of *Lee-Kestler*, Eq.(1.10), and modified *Rackett*, Eq.(1.12), can be used instead of experimental data to calculate vapour pressure and saturated liquid density respectively.

The approaches of Redlich-Kwong, and *Zudkevitch-Joffe* to improve vdW, that is making the parameters of EOS temperature dependent and using the saturated data to determine the parameters, have been adopted in all the successful modifications of vdW. A few of the currently prevalent EOS will be presented here.

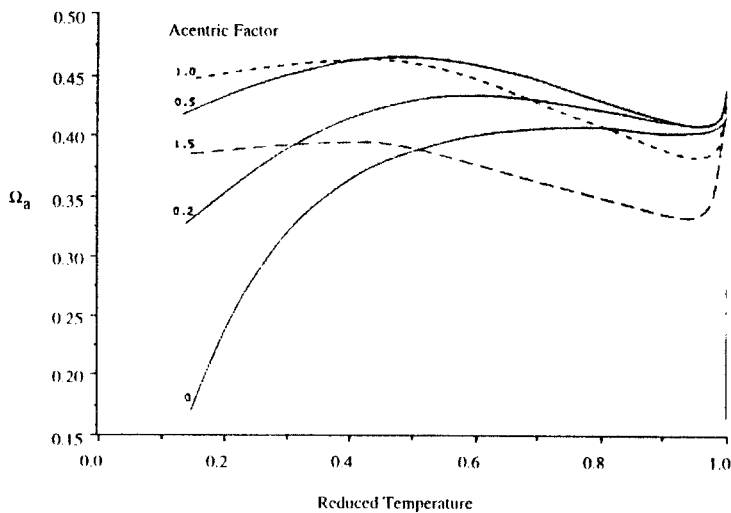


Figure 4.2a. Generalised values of  $\Omega_a$  in ZRK. Reprinted with permission [19], Copyright (1979) American Chemical Society.

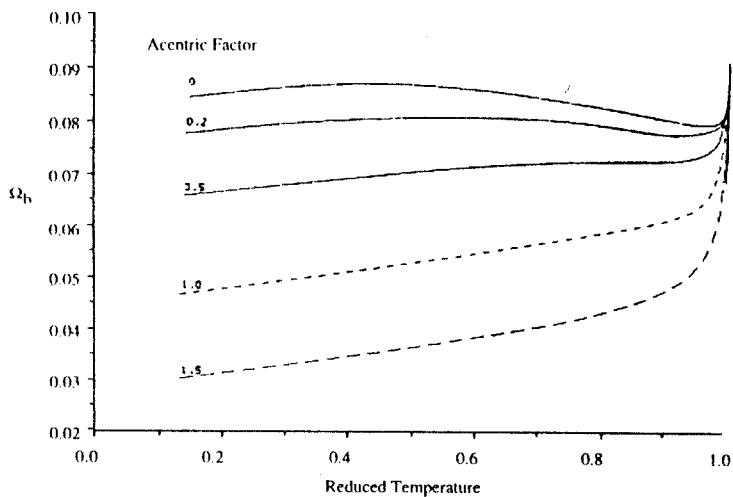


Figure 4.2b. Generalised values of  $\Omega_h$  in ZRK. Reprinted with permission [19], Copyright (1979) American Chemical Society.

*Example 4.3.*

A class of equations relating volumetric properties to temperature and pressure, is that based on the corresponding states principle, which considers that fluids behave identically at conditions of equal reduced properties. Reduce the Redlich-Kwong EOS to a corresponding states form of  $Z=Z(T_r, P_r)$ . Compare the result for  $T=1.5$ , over a  $P_r$  range of 0.5-3, with that of the generalised compressibility chart shown in Figure 2.22.

*Solution:*

The Redlich-Kwong EOS in terms of the compressibility factor is the same as Eq.(4.26), with the following expressions for A and B according to Eqs.(4.7) and (4.8), respectively,

$$A = aP/(RT)^2 = (0.42747T_r^{-0.5}R^2T_c^2/P_c)P/R^2T^2 = 0.42747T_r^{-0.5}P_r$$

$$B = bP/RT = (0.08664RT_c/P_c)P/RT = 0.08664T_r^{-1}P_r$$

Substituting the above two expressions in Eq.(4.24), results in,

$$Z^3 - Z^2 + [(0.42747P_r/T_r^{2.5} - 0.08664P_r/T_r - (0.08664P_r/T_r)^2]Z - 0.037036P_r^2/T_r^{3.5} = 0$$

Substituting  $T_r=1.5$  and various  $P_r$  values in the above equation results in a cubic equations, with the results as follows. The comparison with the values of Z read from Figure 2.22 is also shown.

$P_r$	0.5	1.0	2.0	3.0
Z, RK	0.952	0.907	0.834	0.798
Z, Fig. 2.22	0.950	0.903	0.823	0.778

*Soave-Redlich-Kwong EOS (SRK)*

Soave [21] replaced the temperature dependency of the attractive term in RK,  $T_r^{-0.5}$ , by a more general function  $\alpha$ :

$$P = RT/(v - b) - a_c \alpha / [v(v + b)] \quad (4.22)$$

where

$$a_c = 0.42747 R^2 T_c^2 / P_c$$

$$b = 0.08664 R T_c / P_c$$

and

$$\alpha = [1 + m(1 - T_r^{0.5})]^2 \quad (4.23)$$

The function  $\alpha$  was selected, and m was correlated with the acentric factor by equating fugacities of saturated liquid and vapour phases at  $T_r=0.7$ .

$$m = 0.480 + 1.574\omega - 0.176\omega^2 \quad (4.24)$$

Soave et al. [22], later suggested to divide the value of m determined from the above equation by 1.18 to improve the results.

Graboski and Daubert [23] used the API vapour pressure data and modified Eq.(4.24) to improve pure-component vapour pressure predictions,

$$m = 0.48508 + 1.55171 \omega - 0.15613 \omega^2 \quad (4.25)$$

SRK in terms of the compressibility factor  $Z$  takes the following form,

$$Z^3 - Z^2 + (A - B - B^2) Z - AB = 0 \quad (4.26)$$

where the definitions of  $A$  and  $B$  are given in Eqs.(4.7) and (4.8) respectively.

Comparing SRK with the general EOS, Eq.(4.12), the values of  $u=b$  and  $w=0$ .

SRK is quite capable of predicting vapour-liquid equilibria, but it does not provide reliable liquid density.

#### *Peng-Robinson EOS (PR)*

Peng and Robinson [24] modified the attractive term mainly to improve the prediction of liquid density in comparison with SRK,

$$P = RT/(v - b) - a_c \alpha / [v(v + b) + b(v - b)] \quad (4.27)$$

where,

$$a_c = 0.457235 R^2 T_c^2 / P_c$$

and

$$b = 0.077796 R T_c / P_c$$

They used a similar form of  $\alpha$  as proposed by Soave, Eq.(4.23), but used vapour-pressure data from the normal boiling point to the critical point, and correlated  $m$  as,

$$m = 0.37464 + 1.5422\omega - 0.26992\omega^2 \quad (4.28)$$

The correlation was later modified to improve predictions for heavier components [25],

$$m = 0.3796 + 1.485\omega - 0.1644\omega^2 + 0.01667\omega^3 \quad (4.29)$$

PR in terms of the compressibility factor  $Z$  takes the following form,

$$Z^3 - (1-B)Z^2 + (A - 2B - 3B^2) Z - (AB - B^2 - B^3) = 0 \quad (4.30)$$

PR is obtained by substituting  $u$  and  $w$  in Eq.(4.12) by  $2b$  and  $b$ , respectively.

#### *Volume Shift*

A comparison of the predicted liquid molar volume by leading two parameter EOS with experimental data of pure compounds generally shows a systematic deviation. The deviation is almost constant over a wide pressure range away from the critical point. Hence, subtracting the predicted molar volume by a constant correction term can improve the

predicted liquid density. The effect on the predicted vapour volume is generally insignificant due to its large value relative to that of liquid away from the critical point.

Peneloux et al. [26] were the first who introduced the volume shift concept, i.e. shifting the volume axis, and applied it to SRK,

$$v^{\text{cor}} = v - c \quad (4.31)$$

where  $v^{\text{cor}}$  is the corrected molar volume, and  $c$  is the correction term determined by matching the measured and predicted saturated liquid volumes at  $T_f = 0.7$ .

EOS are applied to multicomponent mixtures by introducing mixing rules to determine mixture parameters, as will be described in Section 4.5. The following mixing rule is used to determine  $c$  for mixtures:

$$c = \sum_{i=1}^N x_i c_i \quad (4.32)$$

where,  $x_i$  is the mole fraction of component,  $i$ , in the mixture.

The inclusion of the third parameter in EOS changes the calculated fugacity coefficient using Eq.(3.31), as,

$$\phi_i^{\text{cor}} = \phi_i \exp(-c_i P / RT) \quad (4.33)$$

where  $\phi_i^{\text{cor}}$  and  $\phi_i$  are the modified and original fugacity coefficients of component  $i$ , respectively.

When the fugacity of each component is calculated by the same EOS in both vapour and liquid phases, the above modification will not affect the predicted equilibrium conditions. It only multiplies the fugacity of each component in both phases by an equal amount, resulting in the same value of equilibrium ratio, Eq.(3.43). Hence, the third parameter can be employed merely to adjust the predicted volume, and need not be included in EOS for calculating the vapour-liquid equilibrium ratio.

The volume shift generally improves the predicted liquid density, and has a minimal effect on the vapour density at low and moderate pressures as its molar volume is relatively large compared to the value of  $c$ . At high pressure condition, the inclusion of  $c$  parameter may not necessarily improve the predicted gas density as it is just a correction term for the liquid density. However, it is advisable to adjust the gas phase volume by the third parameter to maintain consistency, particularly near the critical point where properties of the two phases approach each other.

Peneloux et al. correlated the volume translation parameter  $c$  as,

$$c = 0.40768(0.29441 - Z_{RA}) \frac{RT_c}{P_c} \quad (4.34)$$

where  $Z_{RA}$  is the Rackett compressibility factor as developed by Spencer and Danner in the modified Rackett equation, Eq.(1.12).

$$v^s = (RT_c / P_c) Z_{RA}^{(1+\tau_r)/2} \quad (1.12)$$



Jhaveri and Youngren [27], similarly to Peneloux et al., applied the volume shift concept to PR, and related  $c$  to the parameter  $b$ , by defining a dimensionless shift parameter,  $S_E$ ,

$$S_E = c / b \quad (4.35)$$

$S_E$  was determined by matching the predicted and measured molar volumes for various hydrocarbons. The shift parameters for light compounds are given in Table 4.1.

Table 4.1.  
Values of shift parameter in Peng-Robinson equation of state.

component	C <sub>1</sub>	C <sub>2</sub>	C <sub>3</sub>	iC <sub>4</sub>	nC <sub>4</sub>	iC <sub>5</sub>	nC <sub>5</sub>	C <sub>6</sub>
$S_E$	-0.1540	-0.1002	-0.08501	-0.07935	-0.06413	-0.04350	-0.04183	-0.01478

The authors correlated the shift parameter to the molecular weight as,

$$S_E = 1 - \psi / M^\chi \quad (4.36)$$

where  $\psi$  and  $\chi$  are positive coefficients. Suggested values for the coefficients are given in Table 4.2.

Table 4.2.  
Coefficients of shift parameter correlation, Eq.(4.36).

Component Type	$\psi$	$\chi$
Paraffins	2.258	0.1823
Naphthenes	3.004	0.2324
Aromatics	2.516	0.2008

The value of  $\chi$  for heavy fractions of a reservoir fluid can be used as a tuning parameter to match the predicted to measured saturated liquid densities, as will be described in Section 9.3.

Mathias et al. [28] pointed out that application of the above method to PR raises the calculated liquid volume above the experimental value for almost all tested pure compounds above a reduced temperature of around 0.85, and the deviation reaches its maximum at the critical point. Therefore, an additional volume correction term scaled according to proximity of the prevailing conditions to the critical point, was proposed,

$$v^{cor} = v - c + \delta_c \left( \frac{\xi}{\xi + \lambda} \right) \quad (4.37)$$

where  $\delta_c$  is the volume correction, additional to  $c$ , to match the critical volume by EOS, determined using experimental data, and  $\lambda$  is a dimensionless distance to the critical point.  $\xi$  is a constant, determined by regression of saturated vapour and liquid volumes, and found to be 0.41 for PR. The dimensionless distance,  $\lambda$ , was related to the slope of the pressure-density isotherm as,

$$\lambda = (1/RT_c) \left( \partial P / \partial \rho \right)_T \quad (4.38)$$

A similar approach, to improve the predicted density near the critical point by EOS, was also suggested independently by Chou and Prausnitz [29], who applied it to SRK and found a value of 0.35 for  $\xi$ . The proposed method was extended to binary mixtures, with an additional term related to derivatives of the molar Helmholtz energy. It was, however,

concluded that the near critical contribution did not appreciably affect the results for mixtures in most cases.

*Example 4.4.*

Calculate the vapour pressure of normal hexane at 477.6 K using PR. What are the predicted values of the saturated vapour, and liquid density?

*Solution:*

At the saturation point, the fugacities of hexane as vapour and liquid should be equal. Hence, a pressure is assumed and the fugacities are calculated, using PR. The pressure is iterated until the two calculated fugacities become equal.

Substituting  $u=2b$  and  $w=b$  in the generalised fugacity expression for pure compounds, Eq.(4.18), results in,

$$\ln \phi = (Z - 1) - \ln(Z - B) + \frac{A}{2B\sqrt{2}} \ln \frac{Z + (1 - \sqrt{2})B}{Z + (1 + \sqrt{2})B}$$

The parameters of PR are calculated, using Eq.(4.27), and normal hexane critical properties, Table A.1 in Appendix A, as,

$$a_c = 0.457235R^2T_c^2/P_c = 0.457235 \times (0.0083144 \times 507.6)^2 / 3.025 = 2.692273 \text{ MPa} \cdot (\text{m}^3/\text{kgmol})^2$$

$$b = 0.077796 RT_c/P_c = 0.077796 \times 0.0083144 \times 507.6 / 3.025 = 0.108539 \text{ m}^3/\text{kgmol}$$

The temperature dependency factor of the attractive term,  $\alpha$ , is calculated from Eq.(4.29), and Eq.(4.23), for  $\omega=0.3013$  at  $T_r=477.6/507.6=0.94089$ ,

$$m = 0.3796 + 1.485\omega - 0.1644\omega^2 + 0.01667\omega^3 = 0.812562$$

$$\alpha = [1 + m(1 - T_r^{0.5})]^2 = 1.049349$$

Hence,

$$a = \alpha a_c = 2.825135 \text{ MPa} \cdot (\text{m}^3/\text{kgmol})^2$$

Assuming a saturation pressure of 1.86 MPa, using Figure 1.3 or Eq.(1.10), the two dimensionless parameters, defined by Eqs.(4.7-8), are calculated as,

$$A = 0.33324353$$

$$B = 0.0508396$$

which results in the following cubic equation for  $Z$ , Eq.(4.6),

$$Z^3 - 0.9491604 Z^2 + 0.22381034 Z - 0.0142259 = 0$$

The above equation has three real roots, Appendix B,

$$Z_1 = 0.62954$$

$$Z_2 = 0.10557$$

$$Z_3 = 0.21405$$

The intermediate root is rejected, and  $Z_1$  and  $Z_2$  are assigned to the vapour and liquid phase, respectively.

Substituting the above two values of the compressibility factor in the fugacity expression results in,

$$\phi_1 = \phi^V = 0.729704$$

$$\phi_2 = \phi^L = 0.746610$$

For a pure compound the equality of fugacity reduces to the equality of fugacity coefficient. The comparison of the calculated fugacity coefficients indicates that the assumed pressure is close to the saturation pressure, but requires improvement. The next pressure may be estimated as,

$$P_{(r+1)} = \left[ P(\phi^L / \phi^V) \right]_{(r)}$$

where  $r$  is the iteration number.

The above approach results in a pressure equal to 1.9031 MPa, for the next step. The iteration converges to,

$$P^s = 1.9458 \text{ MPa}$$

$$\phi^L = \phi^V = 0.71716$$

The estimated value by the Lee-Kesler equation, Eq.(1.10), is 1.936 MPa.

The cubic equation at the above pressure is as follows,

$$Z^3 - 0.9468152 Z^2 + 0.23376031 Z - 0.015562 = 0$$

with the following roots:

$$Z_1 = 0.60089$$

$$Z_2 = 0.10958$$

$$Z_3 = 0.23634$$

Rejecting the intermediate root, and calculating the molar volume, Eq.(1.5), we obtain,

$$v = ZRT/P \quad v^L = 0.22362 \text{ m}^3/\text{kgmol} \quad v^V = 1.22623 \text{ m}^3/\text{kgmol}$$

The volume shift for normal hexane is calculated, Eq.(4.35), as,

$$c = S_1 b = -0.01478 \times 0.108539 = -0.001604 \text{ m}^3/\text{kgmol}$$

which results in the following corrected molar volumes, Eq.(4.31),

$$v^{cor} = v - c \quad v^{L,cor} = 0.22523 \text{ m}^3/\text{kgmol} \quad v^{V,cor} = 1.2279 \text{ m}^3/\text{kgmol}$$

The densities of the saturated phases are:

$$\rho = M/v \quad \rho^L = 382.6 \text{ kg/m}^3 \quad \rho^V = 70.18 \text{ kg/m}^3$$

The measured values, Figure 1.5, are  $\rho^L = 423$ , and  $\rho^V = 72 \text{ kg/m}^3$ . The modified Rackett equation, Eq.(1.12), predicts a saturated liquid density of  $424.3 \text{ kg/m}^3$ .

#### 4.2.2 Three-Parameter EOS

A two-parameter EOS predicts the same critical compressibility factor,  $Z_C$ , for all substances, i.e. 0.307 and 0.333 by PR and SRK respectively, whereas  $Z_C$  varies within a range of 0.2 to

0.3 for hydrocarbons. Although the inaccuracy of predicted volume at the critical point, not necessarily leads to unreliable volumetric data at all conditions, it demonstrates the inflexibility of two-parameter EOS for matching both the vapour pressure and volume. The inclusion of a third parameter relaxes the above limitation. The third parameter is generally determined by employing volumetric data.

#### Schmidt-Wenzel EOS (SW)

Figure 4.3 shows the deviation of liquid density at  $T_r=0.7$  predicted by SRK and PR for a number of pure substances. Note that SRK is more reliable for substances with small acentric factors, whereas PR gives reliable data for compounds with acentric factors around  $(1/3)$ . Based on the above observation, and an error analysis of the general EOS, Eq.(4.9), Schmidt and Wenzel [30] incorporated the acentric factor as the third parameter in the attractive term as,

$$P = RT / (v - b) - a_c \alpha / [v^2 + (1 + 3\omega)bv - 3\omega b^2] \quad (4.39)$$

Substituting acentric factor values of zero and  $1/3$  in the Schmidt-Wenzel EOS (SW) will reduce it to SRK and PR respectively, where these equations predict the liquid density reliably. SW can, therefore, be considered a general form of SRK and PR.

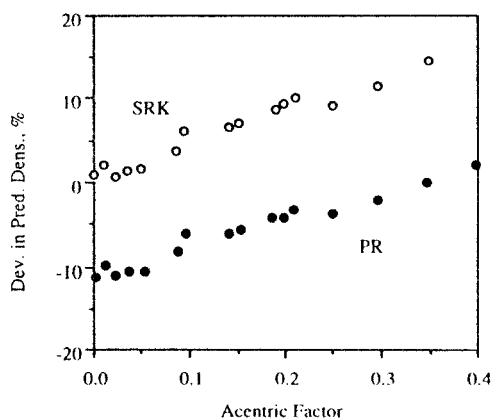


Figure 4.3 The deviation of predicted from measured liquid density by SRK and PR [30].

The authors used the boundary conditions at the critical point, Eq.(4.9) to determine  $a_c$ , and  $b$ , as,

$$a_c = \Omega_{ac} \frac{R^2 T_c^2}{P_c}, \quad \Omega_{ac} = [1 - \eta(1 - q)]^3 \quad (4.40)$$

$$b = \Omega_b \frac{RT_c}{P_c}, \quad \Omega_b = \eta q \quad (4.41)$$

where  $\eta$  is the critical compressibility factor, as predicted by Eq.(4.39), and is related to the correlating parameter  $q$ , by

$$\eta = 1 / \{3 (1 + q\omega)\} \quad (4.42)$$

and  $q$ , defined as  $b/v_c$ , is the smallest positive root of the following equation,

$$(6\omega + 1) q^3 + 3q^2 + 3q - 1 = 0 \quad (4.43)$$

with an approximate value of,

$$q = 0.25989 - 0.0217\omega + 0.00375\omega^2$$

Schmidt and Wenzel selected the same form of  $\alpha$  as proposed by Soave, Eq.(4.23), but correlated,  $m$ , with the acentric factor and reduced temperature by matching vapour pressure data of pure compounds,

$$m \equiv m_1 = m_0 + 0.01429 (5T_r - 3m_0 - 1)^2 \quad \text{for } \omega \leq 0.4 \quad (4.44)$$

$$m \equiv m_2 = m_0 + 0.71 (T_r - 0.779)^2 \quad \text{for } \omega \geq 0.55 \quad (4.45)$$

where,

$$m_0 = 0.465 + 1.347\omega - 0.528\omega^2 \quad \text{for } \omega \leq 0.3671$$

$$m_0 = 0.5361 + 0.9593\omega \quad \text{for } \omega > 0.3671$$

and for intermediate values of  $0.4 < \omega < 0.55$

$$m = [(0.55 - \omega) / 0.15] m_1 + [(\omega - 0.4) / 0.5] m_2 \quad (4.46)$$

For supercritical compounds,

$$\alpha = 1 - (0.4774 + 1.328\omega) \ln T_r \quad (4.47)$$

The inclusion of  $\omega$  in EOS as the third parameter by Schmidt and Wenzel resulted in a variable calculated critical compressibility, according to the value of acentric factor. The predicted values are, however, about 15% higher than the true values. This was known to the authors, but was accepted as the price for an overall optimum accuracy in predicted volumes. Substituting  $u=(1+3\omega)b$ , and  $w^2=3\omega b^2$  in the generalised EOS, Eq.(4.12), will reduce it to SW.

#### *Patel-Teja EOS (PT)*

Patel and Teja [31] modified the attractive term by including a more flexible third parameter,  $c$ , as,

$$P = RT / (v - b) + a_c \alpha / [v(v + b) + c (v - b)] \quad (4.48)$$

where the parameter  $c$  is defined by,

$$c = \Omega_c \frac{RT_c}{P_c} \quad (4.49)$$

and

$$\Omega_c = 1 - 3\eta \quad (4.50)$$

$\eta$  is an adjusted critical compressibility factor, determined by matching the predicted and measured saturated liquid densities. It was correlated with the acentric factor as,

$$\eta = 0.329032 - 0.076799\omega + 0.0211947\omega^2 \quad (4.51)$$

The authors found that the use of true critical compressibility factor will result in the overall loss of accuracy in predicted density, a conclusion also reached by Schmidt and Wenzel.

Applying the condition at the critical point, Eq.(4.9), the other coefficients were derived as,

$$\Omega_b^3 + (2 - 3\eta)\Omega_b^2 + 3\eta^2\Omega_b - \eta^3 = 0 \quad (4.52)$$

$\Omega_b$  is taken as the smallest positive root of the above equation with an approximate value of

$$\Omega_b = 0.32429\eta - 0.022005 \quad (4.53)$$

and

$$\Omega_{ac} = 3\eta^2 + 3(1 - 2\eta)\Omega_b + \Omega_b^2 + (1 - 3\eta) \quad (4.54)$$

The Patel-Teja EOS (PT) reduces to PR or SRK by substituting the value of 0.307, or 0.333 for  $\eta$ , respectively. Note that these values are predicted by the two equations as the critical compressibility factors for all substances. Hence, PT can also be considered a general form of SRK and PR which will reduce to either of them at their prevailing constant critical compressibility factors.

The temperature dependency function of the attractive term in PT is similar to that proposed by Soave, Eq.(4.23). The authors determined  $m$ , using the vapour pressure data of pure compounds, and correlated it with the acentric factor, as,

$$m = 0.452413 + 1.30982\omega - 0.295937\omega^2 \quad (4.55)$$

Substituting  $u=b+c$  and  $w^2=cb$  in the generalised EOS, Eq.(4.12), will reduce it to PT.

Valderrama and Cisternas [32] and later Valderrama [33] modified PT by using the critical compressibility factor,  $Z_c$ , to correlate its parameters,

$$\Omega_{ac} = 0.66121 - 0.76105Z_c \quad (4.56)$$

$$\Omega_b = 0.02207 + 0.20868Z_c \quad (4.57)$$

$$\Omega_c = 0.57765 - 1.87080Z_c \quad (4.58)$$

$$m = 0.46283 + 3.58230\omega Z_c + 8.19417(\omega Z_c)^2 \quad \text{for } T_r < 1 \quad (4.59)$$

$$m = 0$$

$$\text{for } T_r > 1$$

The above correlations were developed by matching predicted and experimental data without being restricted by the conditions at the critical point, Eq.(4.9). This appears to be a major step in ignoring the actual behaviour of pure fluids in favour of an overall improvement in predicted values by EOS. It has, however, achieved its objective as demonstrated in Section 9.2 where the performance of various equations are compared.

The volume shift concept can also be applied to three-parameter EOS. The improvement, if any, will be expected to be minimal, as the saturated density data have been generally used to determine the third parameter. It was pointed out, however, that the prediction of these equations deteriorates near the critical point. This deficiency can be corrected using the approach described by Eq.(4.37), but without including the conventional shift, c.

$$v^{cor} = v + \delta_c \left( \frac{\xi}{\xi + \lambda} \right) \quad (4.60)$$

The above correction can be applied to VPT, but the distance parameter  $\lambda$  is not zero at the critical point, as VPT does not satisfy the boundary condition of Eq.(4.9). Hence a correction term for the distance parameter needs to be included [34].

The dimensionless distance given by Eq.(4.38) represents the approach to the critical point for pure fluids. Its extension to multi-component systems, however, is questionable. Furthermore in most reservoir engineering problems, the critical point is approached by compositional variations, and not by changes of pressure and temperature. Hence, all the state points along the path have different compositions and different critical points.

An alternative dimensionless distance to the critical point, which is as valid for variable composition cases, is the relative value of the equilibrium ratios of the mixture components [34]. At the critical point, all K-values are equal to one, hence the proximity to the critical state can be expressed by,

$$\lambda = (K_l/K_h) - 1 \quad (4.61)$$

where  $K_l$  and  $K_h$  are the equilibrium ratios of the lightest and the heaviest components of the mixture at any state point.

Figure 4.4 shows the improvement in predicted density of a binary mixture by including the near critical correction [34] in VPT. Both definitions of the distance parameter, i.e., the pressure derivatives (PC), and the equilibrium ratio (KC) have been used.

It should be noted that the inclusion of variable density correction term in EOS changes the predicted equilibrium conditions, contrary to the constant volume shift, and increases the complexity of the mathematical expressions of the fugacity coefficient. Hence it is advisable to use it only for adjusting the predicted density by the original EOS, instead of including it in EOS.

### 4.2.3 Attractive Term Temperature Dependency

As indicated by Wilson [35], a reliable prediction of vapour pressure of pure compounds by any EOS is a prerequisite for its reliability in estimating vapour-liquid equilibria of multicomponent systems. This has been achieved, almost with no exception in all recent modifications of vdW, by adjusting the relationship between  $\alpha$  and the reduced temperature to match the vapour pressure data.

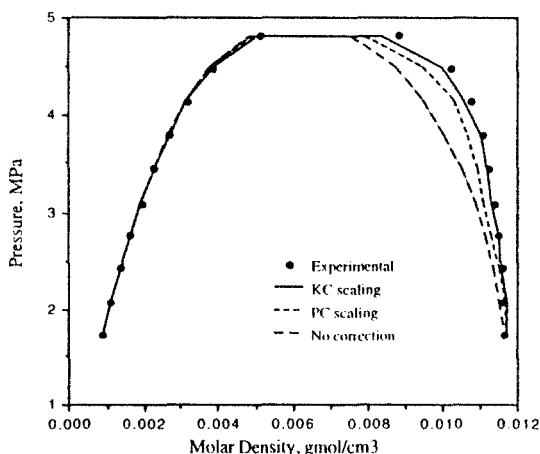


Figure 4.4. Effect of near critical volume correction on predicted density of ethane-propene mixture at 311 K.

The most direct approach is that of Zudkevitch-Joffe, as explained in Section 4.2.1. The common approach has been, however, to introduce a generalised correlation for  $\alpha$  in conjunction with the proposed equation of state. The most common functional form is that proposed originally by Soave, Eq.(4.23). Although the same form has been used by most of the leading EOS, it is not uncommon to find different functional forms, or correlations for their coefficients, for the same equation of state. The popularity of an EOS may be judged even by the number of modifications to its temperature dependency factor!

The  $\alpha$  function attains generality by relating its coefficients to some properties of compounds. The acentric factor is the popular choice. It is reasonable, however, to expect that a generalised equation in terms of the acentric factor, such as Eqs.(4.25, 29, 52), may not be adequate to describe all compounds of vastly different characteristics. The  $\alpha$  parameter for asymmetric compounds can be related individually to the reduced temperature, e.g., Eq.(4.88), to improve the predicted results for complex systems. However, a single generalised correlation should be adequate generally to correlate hydrocarbon components of reservoir fluids.

Correlations as those given by Soave are in general quite reliable to predict the vapour pressure of relatively light compounds, particularly at high values of reduced temperatures. To improve their capabilities over wider ranges, higher order polynomials of acentric factor, and reduced temperature have been used. Examples are:

$$m = 0.378893 + 1.4897153\omega - 0.17131848\omega^2 + 0.0196554\omega^3 \quad (4.62)$$

as proposed by Stryjek and Vera [36] for PR or Eq.(4.29) proposed by Peng-Robinson later, in preference to their original correlation, to improve the model for heavier compounds.

The following three-coefficient functional form was proposed by Mathias and Copeman [37], in preference to that of Soave,



$$\alpha = \left[ 1 + C_1(1 - \sqrt{T_r}) + C_2(1 - \sqrt{T_r})^2 + C_3(1 - \sqrt{T_r})^3 \right]^2 \quad (4.63)$$

where the coefficients  $C_1$ ,  $C_2$ , and  $C_3$ , are to be determined for each compound by matching its vapour pressure.

Soave [22] reviewed ten different functions for  $\alpha$ , proposed by various investigators, and preferred the original form, as given by Eq.(4.23).

Twu et al. [38] pointed out that the use of the conventional  $\alpha$  function, Eq.(4.23), with the slope,  $m$ , correlated by power three of the acentric factor, makes  $\alpha$  a sixth order function of the acentric factor. Hence, the extrapolation of function to heavy compounds with high values of the acentric factor can lead to large deviations, particularly at low reduced temperatures. The authors evaluated  $\alpha$  in PR and showed that it varied linearly with the acentric factor at constant reduced temperature. Figure 4.5 shows variations of  $\alpha$  at several reduced temperatures as determined for PR by matching the measured and predicted vapour pressure of pure compounds.

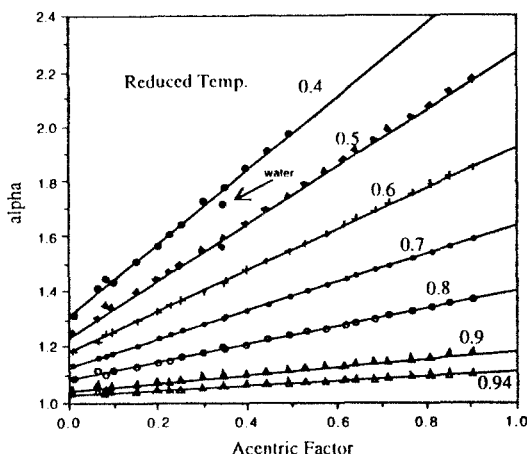


Figure 4.5. Variations of  $\alpha$  with acentric factor in PR at constant reduced temperature [38].

Based on the above observation, the authors suggested the following function,

$$\alpha = \alpha^{(0)} + \omega(\alpha^{(1)} - \alpha^{(0)}) \quad (4.64)$$

where  $\alpha^{(0)}$ , and  $\alpha^{(1)}$  are related only to the reduced temperature.

The above approach clearly reduces the risk of extrapolating the  $\alpha$  function to compounds with high acentric factors.

Twu et al. [38] correlated  $\alpha$  of sub-critical components for PR as,

$$\alpha^{(0)} = T_r^{-0.171813} \exp[0.125283(1 - T_r^{1.77634})] \quad (4.65)$$

$$\alpha^{(1)} = T_r^{-0.607352} \exp[0.511614(1 - T_r^{2.20517})]$$

and for SRK [39],

$$\alpha^{(0)} = T_r^{-0.201158} \exp[0.141599(1 - T_r^{2.29528})] \quad (4.66)$$

$$\alpha^{(1)} = T_r^{-0.660145} \exp[0.500315(1 - T_r^{2.63165})]$$

The average absolute deviation of predicted vapour pressure for pure hydrocarbons by PR from the triple point to the critical point was found to be 3.28%, 8.21%, and 12.08% using the Twu et al.'s proposed correlation, the Stryjek-Vera correlation, Eq.(4.62), and the original correlation of PR, respectively. The average absolute deviation by SRK using the proposed correlation, Eq.(4.66), was found to be 3.37%, comparable with that of Twu et al. for PR, in spite of apparent difference between the two equations. The results clearly demonstrate the importance of the selected functional form of  $\alpha$ , and the vapour pressure data used in correlating it.

The success of EOS in predicting phase behaviour using various functional forms for the temperature dependency of the attractive term, all correlated by matching vapour pressure data, raises an important question. How reliable their extrapolations are for supercritical compounds? Light components of reservoir fluids, particularly methane which constitutes a large fraction of reservoir fluids, are generally at temperatures well above their critical points, where no vapour pressure data exist to be used in correlating the parameters. The prevailing approach is to assume, almost in all the leading EOS, that the correlation is also valid for super critical conditions. Whereas Zudkevitch and Joffe assumed values of  $\Omega_a$ , and  $\Omega_b$  for supercritical compounds to be the same as those at the critical point in the Redlich-Kwong EOS. A few investigators have suggested different correlations for supercritical compounds [30, 38, 40].

There is no limitation in evaluating the reliability of any  $\alpha$  correlation at super critical conditions if volumetric data is to be predicted. There are abundant density data on super critical compounds. The  $\alpha$  function, however, is the tool to improve the vapour pressure prediction.

An alternative to using vapour pressure data of pure compounds to correlate  $\alpha$ , is employing phase behaviour data of binary systems comprising of one super critical component. This approach extends the temperature range of relevant data, and it is only logical to expect higher reliability when employing any correlation within its correlated domain.

The approach has an additional practical advantage. As binary data are used in correlating the parameters of EOS, the interaction between pairs of non-similar molecules and/or the deficiencies of EOS for binary systems, are taken into account to some extent. Hence, the need for the use of binary interaction parameters (BIP) in mixing rules, described in Section 4.3, will be reduced. This will allow for a significant simplification in phase behaviour calculations, see Section 5.1, resulting in reduction of the computational requirement for mixtures described by a large number of components. The reduction of computing time spent in flash calculations is highly desirable in compositional reservoir simulations, where many millions of flashes may be performed in a study.

The above approach was applied [41,42] to PR, as the most widely used equation in the industry. Over 5,000 vapour-liquid equilibrium experimental data of binary systems containing a super critical component, with hydrocarbons ranging from  $C_1$  to  $nC_{12}$ , were used to develop a correlation for supercritical components. The bubble point pressure of the liquid phase and the composition of the equilibrated vapour phase, as predicted by PR, were matched to experimental data by adjusting the parameter  $\alpha$  of the super critical components. The optimum value of  $\alpha$  for super critical hydrocarbon components was found to be reasonably expressed by Eq.(4.29) replacing  $m$ , with,  $m'$ , where

$$m' = 1.21m \quad (4.67)$$

The predicted dew points by the modified PR, using the above correlation without any BIP, as well as those by the original PR, with and without BIPs, are compared for a 5-component mixture in Figure 4.6. Note that the predictions by the modified  $\alpha$  function (shown by mPR) are superior to those of the original with and without the use of BIP.

The above example clearly indicates the impact of the temperature dependent term of EOS on predicted results, and the success of using binary data to determine its correlation for supercritical compounds. The approach may be implemented in any EOS, resulting in modified correlations for super critical components [39].

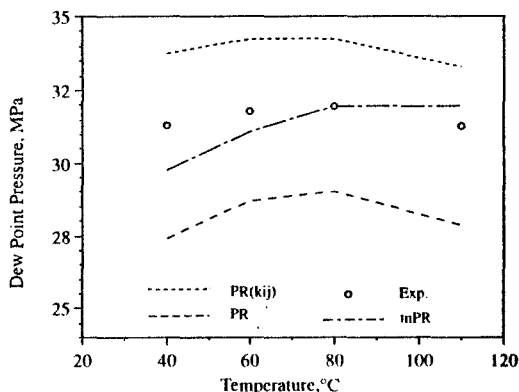


Figure 4.6. Predicted dew point of a mixture with composition:  $C_1=82.05$ ,  $C_3=8.95$ ,  $nC_5=5.00$ ,  $nC_{10}=1.99$ , and  $nC_{16}=2.01$  mole %.

### 4.3 MIXING RULES

Equations of state are applied to multicomponent systems by employing mixing rules to determine their parameters for mixtures. The parameters of EOS are considered to represent the attractive and repulsive forces between the molecules. Hence the mixing rule should describe the prevailing forces between molecules of different substances forming the mixture.

### 4.3.1 Random Mixing Rules

As pointed out in Section 4.1, the coefficients of virial equation (Eq. 4.1) describe the non-ideal behaviour of a real fluid due to interaction amongst various combinations of molecules. Statistical mechanics can be employed to derive mixing rules for the coefficients of virial equation. It can be argued that the mixing rule used in any EOS should attain the same form as that of the virial equation at conditions where both equations are valid.

For gases at low pressures, the third and higher virial coefficients can be neglected. The second coefficient, which represents the interaction between two neighbouring molecules, is sufficient to describe the volumetric behaviour. The mixing rule for the second coefficient,  $B$ , is of the quadratic form,

$$B = \sum_i \sum_j x_i x_j B_{ij} \quad (4.68)$$

where  $B_{ij}$  is the coefficient due to interaction between molecules  $i$  and  $j$ .

Employing Eq.(4.1), the second coefficient is determined as,

$$B = \lim_{\rho \rightarrow 0} (\partial Z / \partial \rho)$$

Using a van der Waals type equation to describe  $Z$  at low pressures, the above equation results in,

$$B = \lim_{\rho \rightarrow 0} (\partial Z / \partial \rho) = b - (a / RT) \quad (4.69)$$

Hence, the mixing rules for  $a$  and  $b$ , at least at low pressures, should be compatible with that in Eq.(4.68), i.e., it should be of quadratic form.

The attractive force between molecules  $i$  and  $j$ , represented in EOS by parameter,  $a_{ij}$ , which is of an energy nature, can be expressed in a simple geometric average form [43] as,

$$a_{ij} = (a_i a_j)^{1/2} \quad (4.70)$$

The repulsive force between molecules  $i$  and  $j$ , represented in EOS by parameter  $b_{ij}$ , which has the characteristic of volume, can be determined by arithmetic average,

$$b_{ij} = (b_i + b_j) / 2 \quad (4.71)$$

Eqs.(4.70) and (4.71) describing the interaction between a pair of different molecules are more intuitive than rigorous. Other forms, perhaps with equally valid arguments, can also be considered. For example, considering the distance between the two molecules, instead of averaging their volumes results in,

$$b = \left( \frac{b_i^{1/3} + b_j^{1/3}}{2} \right)^3 \quad (4.72)$$

Applying the quadratic mixing rule for the parameters of EOS, we obtain,

$$a = \sum_i \sum_j x_i x_j (a_i + a_j)^{0.5} \quad (4.73)$$

$$b = \sum_i \sum_j x_i x_j b_{ij} = \sum_i \sum_j x_i x_j (b_i + b_j)/2 = \sum_i x_i b_i \quad (4.74)$$

A mixing rule similar to that of  $b$  is also used for other parameters in EOS that contain more than two parameters, when the additional parameters are of the co-volume characteristic,

$$c = \sum_i x_i c_i \quad (4.75)$$

Similarly, the above molar mixing rule is also used for auxiliary parameters such as the volume correction,  $\delta_c$ , defined in Eqs.(4.37). The suggested mixing rule for the acentric factor, used as the third parameter in the Schmidt-Wenzel EOS, by the authors is,

$$\omega = \left( \sum_i x_i \omega_i b_i^{0.7} \right) / \left( \sum_i x_i b_i^{0.7} \right) \quad (4.76)$$

The above mixing rules, known as the van der Waals mixing rules, treat all the components similarly, hence, referred to as the random mixing rules. For reservoir hydrocarbon fluids the random mixing rules (which only consider the interaction between pairs of neighbouring molecules and neglect interaction between three or more molecules) are adequate.

It is common to incorporate an additional parameter in Eq.(4.71) to express the attractive term between pairs of non-similar molecules,

$$a_{ij} = (a_i a_j)^{1/2} (1 - k_{ij}) \quad (4.77)$$

where  $k_{ij}$  is known as the binary interaction parameter.

Using the above description, the random mixing rule of the attractive term becomes,

$$a = \sum_i \sum_j x_i x_j (a_i + a_j)^{0.5} (1 - k_{ij}) \quad (4.78)$$

The use of binary interaction parameter for the repulsive term, particularly in mixtures with high concentration of CO<sub>2</sub> [44], has also been suggested, but has not gained popularity,

$$b_{ij} = [(b_i + b_j)/2](1 - k'_{ij}) \quad (4.79)$$

where  $k'_{ij}$  are the repulsive BIP.

The binary interaction parameter (BIP) is generally determined by minimising the difference between predicted and experimental data, mainly the saturation pressure, of binary systems. A BIP should, therefore, be considered as a fitting parameter and not a rigorous physical term. Hence, the interaction parameters developed for any EOS should generally be used only for that EOS.

As the effect of third and higher molecules on the interaction between two molecules is assumed to be insignificant, the binary interaction parameter so determined is considered to be valid for multicomponent systems too. The interaction parameters between hydrocarbons with little difference in size are generally considered to be zero, but the values of  $k_{ij}$  for non-hydrocarbon-hydrocarbon components and also light-heavy hydrocarbons are non-zero. Values of BIP for the EOS described in Section 4.2 are given in Tables A.4 in Appendix A, where  $k_{ij} = k_{ji}$ , and  $k_{ii} = 0$ .

Correlations to estimate BIP for specific EOS, such as SRK[45] and PR[46], as well as general ones [47,48, 49] have been suggested. The most commonly used correlation [47] is,

$$k_{ij} = \vartheta_i \left[ 1 - \left( \frac{2 \left( v_i^{1/3} v_j^{1/3} \right)^{1/2}}{v_i^{1/3} + v_j^{1/3}} \right)^\theta \right] \quad (4.80)$$

where the constants  $\vartheta_i$ , and  $\theta$ , are determined for each EOS using the available binary data, or adjusted in tuning of EOS for a particular fluid system, as will be described in Section 9.3. A default value of  $\theta=6$  may be used [50].

There is no doubt that the inclusion of binary interaction parameters in EOS mixing rules will provides more flexibility, and in most cases reliability at least within a limited working range. It is particularly a powerful tool to tune (calibrate) EOS for a reservoir fluid against the available experimental data. Additional flexibility can also be obtained by making BIP temperature [46], pressure [51], and composition dependent [52]. It should be noted that making BIP dependent on pressure or composition causes additional complexity in the expression for fugacity of each component as the pressure derivatives in Eq.(3.31) are only at constant temperature and total volume, and not at constant pressure or composition.

The flexibility achieved by inclusion of BIP, particularly variable ones, can be quite misleading, as excellent results can be obtained for binary systems. That, however, only demonstrates a successful curve fitting. The results for multicomponent systems particularly within wide ranges of temperature and composition may be quite disappointing. A comparative study of ten EOS [53] indicated that the Patel and Teja equation as modified by Valderrama, without any BIP was more successful in modelling of the phase behaviour of reservoir hydrocarbon fluids than others with BIP. An improvement in EOS or a more thorough fluid characterisation should reduce the need to use BIP for hydrocarbon fluids which do not contain compounds of vastly different characteristics. An example on improving EOS instead of using BIP was shown in Figure 4.6. The reduction of computational time for flash calculations in the absence of BIP will be described in Section 5.1.

The application of mixing rules in EOS, will allow the calculation of component fugacity coefficients, as given by Eq.(3.31). The expression for fugacity coefficient, using the generalised EOS, Eq.(4.12), and the random mixing rules is given in the Appendix C.

#### Example 4.5.

The Soave-Redlich-Kwong, and the Peng-Robinson EOS are the most widely used equations in the petroleum industry. It is common to express these equations by the following general form,

$$P = \frac{RT}{v-b} - \frac{a}{(v+\delta_1 b)(v+\delta_2 b)}$$

where,  $\delta_1$ , and,  $\delta_2$ , are constants equal to 1 and 0 in SRK, and  $1 + \sqrt{2}$ , and  $1 - \sqrt{2}$  in PR, respectively.

Prove that the fugacity of each component in a mixture, using the above EOS and the random mixing rules is given by,

$$\ln \phi_i = \frac{b_i}{b} (Z - 1) - \ln(Z - B) - \frac{A}{B(\delta_2 - \delta_1)} \left( \left( 2 \sum_{j=1}^N x_j a_{ij} \right) / a - b_i / b \right) \ln \left( \frac{Z + \delta_2 B}{Z + \delta_1 B} \right) \quad (\text{E4.5})$$

*Solution:*

The fugacity coefficient is calculated from Eq.(3.31),

$$\ln \phi_i = \frac{1}{RT} \int_V \left[ \left( \frac{\partial P}{\partial n_i} \right)_{T,V,n_{j \neq i}} - RT/V \right] dV - \ln Z \quad (3.31)$$

where  $V$  is the total volume. Hence, the equation of state is written in terms of total volume by substituting  $v=V/n$ , where  $n$  is the total number of moles,

$$n = \sum_{i=1}^N n_i$$

We obtain,

$$P = \frac{nRT}{V - nb} - \frac{n^2 a}{(V + \delta_1 nb)(V + \delta_2 nb)}$$

The derivative of pressure at constant total volume, pressure and all mole numbers except  $n_i$  is calculated as,

$$\left( \frac{\partial P}{\partial n_i} \right)_{T,V,n_{j \neq i}} = \frac{RT}{V - nb} + \frac{nRT [\partial(nb)/\partial n_i]}{(V - nb)^2} - \frac{\partial(n^2 a)/\partial n_i (n^2 a)}{(V + \delta_1 nb)(V + \delta_2 nb)} + \frac{\left\{ \delta_1 \delta_2 [\partial(nb)^2/\partial n_i (nb)^2] + (\delta_1 + \delta_2) V [\partial(nb)/\partial n_i] \right\} (n^2 a)}{[(V + \delta_1 nb)(V + \delta_2 nb)]^2}$$

Applying the random mixing rules to calculate  $a$  and  $b$ , Eq.(4.78) and Eq.(4.74) respectively,

$$n^2 a = \sum_{i=1}^N \sum_{j=1}^N n^2 x_i x_j a_{ij} = \sum_{i=1}^N \sum_{j=1}^N n_i n_j a_{ij}$$

$$nb = \sum_{i=1}^N n x_i b_i = \sum_{i=1}^N n_i b_i$$

the derivatives of the two parameters are obtained as,

$$\left[ \partial(nb) / \partial n_i \right]_{T, V, n_{j \neq i}} = b_i$$

$$\left[ \partial(n^2 a) / \partial n_i \right]_{T, V, n_{j \neq i}} = 2 \sum_{j=1}^N n_j a_{ij} = 2n \sum_{j=1}^N x_j a_{ij}$$

Substituting the above calculated terms in Eq.(3.31) and integrating it between the two limits will result in,

$$\ln \phi_i = -\ln Z(1 - nb/V) + \frac{nb_i}{V - nb} + \frac{a}{RT(\delta_1 - \delta_2)b} \left( \left( 2 \sum_{j=1}^N n_j a_{ij} \right) / na - b_i / b \right) \times \\ \ln \frac{V + n\delta_2 b}{V + \delta_1 nb} - \frac{naVb_i}{RTb(V + \delta_1 nb)(V + \delta_2 nb)}$$

Substituting

$$\frac{-an^2}{(V + \delta_1 nb)(V + \delta_2 nb)} = P - \frac{nRT}{V - nb}, \text{ i.e., the equation of state, and } V = nv = nbZ/B$$

in the above will result in Eq.(E4.5).

### Non-Random Mixing Rules

The van der Waals mixing rules are quite adequate to describe hydrocarbon mixtures of reservoir fluids. They cannot, however, represent the interaction between hydrocarbons and asymmetric compounds such as water, or methanol which is often added to reservoir fluids as a hydrates inhibitor. Although additional flexibility that is achieved by increasing the number of coefficients in binary interaction parameters, may provide acceptable results for binary mixtures containing these compounds, the model can fail completely for multicomponent systems [54].

The assumption of random mixing in systems containing highly polar and asymmetric compounds is not justified as the existence of particular forces between some molecules, such as those due to permanent dipoles, may result in non-uniform distribution at the molecular level. Local composition mixing rules address this behaviour by relating the attractive term in EOS to composition with a higher order polynomials than quadratic.

The majority of mixing rules for the above term can be represented by the following form,

$$a = a^C + a^A \quad (4.81)$$

where the attractive term is separated into two parts,  $a^C$ , which is the conventional random mixing term given by Eq.(4.78), and  $a^A$ , which is the asymmetric term due to polarity.

Various expressions have been proposed and successfully tested to binary systems for the asymmetric term. Schwartzentruber and Renon [55] have shown that most of them can be expressed by the following general form,



$$a^{\Lambda} = \sum_i \sum_j -l_{ij}(x_i - x_j)x_i x_j (a_i a_j)^{1/2} \quad (4.82)$$

where  $l_{ij} = l_{ji}$  is the binary interaction coefficient for the asymmetric term.

The above mixing rule is quite flexible, particularly with temperature dependent interaction coefficients, and capable of describing the behaviour of multicomponent mixtures containing highly asymmetric components when used in a cubic EOS.

The mixing rule, however, is not consistent with the quadratic form of the second virial coefficient. Schwartzentruber and Renon [55] have shown that the above inconsistency can be avoided by introducing an additional parameter,  $\chi$ , in the general EOS, Eq.(4.12), as,

$$p = \frac{RT}{v-b} - \frac{a + \chi/(v-b)}{v^2 + uv - w^2} \quad (4.83)$$

with the following mixing rule for the additional parameter of EOS,

$$\chi = \sum_i \sum_j \sum_k x_i x_j x_k \chi_{ijk} \quad (4.84)$$

and the conventional random mixing rules for the remaining parameters.

The above modification satisfies the mixing rules of the virial coefficients, as  $a_{ij}$  expresses the interaction between two molecules by a quadratic form, and  $\chi_{ijk}$  represents the interaction between three molecules by a cubic form, similar to parameters of B and C of the virial equation, respectively. It also appears to have maintained the dependency of the attractive term to power three of concentration required by the local composition mixing rule,

$$a^{\Lambda} = \chi/(v-b) = \left( \sum_i \sum_j \sum_k x_i x_j x_k \chi_{ijk} \right) / (v-b) \quad (4.85)$$

The above equation basically belongs to a class of mixing rules, known as the density dependent mixing rules. The asymmetric term becomes negligibly small as the pressure approaches zero, with the volume attaining a large value, reducing the mixing rule to the conventional random mixing rule and consistent with that of the virial equation. The cubic form of concentration is, however, deceiving, as the volume of a mixture depends on the concentration of its components, unless their partial molar volumes are very similar, which effectively reduces the asymmetric term to a quadratic form [55]. This has been observed in practice by various investigators [56,57]. It is perhaps a sounder engineering practice to use mixing rules of the type of Eq.(4.82), and not be quite consistent with the virial mixing rules, than lose reliability of results by adhering to them.

The mixing rule, Eq.(4.82), with the cubic dependency on composition suffers also from the invariance condition [58], that is, if one of the components is divided in two or more components identical to it, different expressions for the attractive term are obtained. This defect is of practical interest for mixtures containing significant amounts of very similar components. Mathias et al. [59] tested the mixing rule of Panagiotopoulos and Reid [60], which is of a form similar to Eq.(4.82), and demonstrated that this deficiency causes erroneous predictions of water solubility in benzene-cyclohexane mixture. Modifications of the cubic mixing rules to avoid this deficiency for multicomponent systems, whilst reducing them to the same form as Eq.(4.82) for binary systems, have been proposed [55, 59].

Avlonitis et al. [57], proposed a mixing rule similar to Eq.(4.82) as follows:

$$a^A = \sum_p x_p^2 \sum_i l_{pi} x_i (a_p a_i)^{1/2} \quad (4.86)$$

Here the subscript  $p$  refers to the index of polar components, and  $l_{pi}$  is the binary interaction coefficient. The binary interaction coefficient should be a decreasing function of temperature as the asymmetric non-ideality reduces with temperature [43].

The above mixing rule, generally, should not be affected adversely by the invariance condition when applied to reservoir fluids. The authors, however, eliminated the problem

completely by substituting  $x_p^2$  with  $S_p x_p$  in Eq.(4.86), where  $S_p = \sum_p x_p$ . Hence,

$$a^A = \sum_p x_p S_p \sum_i l_{pi} x_i (a_p a_i)^{1/2} \quad (4.87)$$

For a binary polar-non-polar system the modified form is identical to Eq.(4.86), hence, the same binary interaction coefficients can be used for both forms. For mixtures consisting of polar components only,  $S_p = 1$ , and the term  $a^A$  becomes identical to  $a^C$  with polar-polar interaction coefficients equal to zero.

The authors [57] applied the mixing rule to the Valderrama modification of Patel-Teja EOS to model the phase behaviour of reservoir fluids including water, and methanol which is commonly used as hydrates inhibitor. To further improve the accuracy of predictions of both the vapour pressure and the saturated volumes of pure polar components of water and methanol, the constants in the correlation of  $\alpha(T_r)$ , Eq.(23) were determined by regressing pure compounds data, instead of using the generalised correlation, as

$$\alpha(T_r) = \{ 1 + m[1 - (T_r)^\Psi] \}^2 \quad (4.88)$$

where for methanol  $m=0.76757$ ,  $\Psi=0.67933$ , and for water  $m=0.72318$ ,  $\Psi=0.52084$ .

The binary interaction coefficients were expressed by,

$$l_{pi} = l_{pi}^0 - l_{pi}^0 (T - 273) \quad (4.89)$$

where  $l_{pi}^0$  and  $l_{pi}^1$  are dimensionless constants, and  $T$  is in K. The above function will change sign at some high temperature values where it can be set equal to zero. The binary interaction parameters and coefficients were obtained by forcing agreement of the model to binary data, with the results given in Table A.4.6 in Appendix A.

The detrimental effects of the invariance condition can be demonstrated clearly for a mixture shown in Table 4.3, by subdividing water in two identical components, denoted as "water 1" and "water 2". The three-phase equilibrium of the four component mixture has been predicted by VPT using two expressions for the asymmetric contribution, Eq.(4.86), and the invariant version Eq.(4.87).

Note that if only one polar component is present in the mixture, the mixing rule and its corresponding invariant version lead to identical results, since  $S_p = x_p$ . In all other cases the predicted composition of the water-rich liquid depends very strongly on the ratio of the identical water components. A maximum effect is observed at equimolar amounts of "water

1" and "water 2". The predicted composition of the non-polar-rich phases are only very slightly affected by the invariance condition, since in this case the terms in Eq.(4.86) containing polar component mole fraction products contribute negligibly.

The mixing rule of Eq.(4.86) has a number of important advantages for application to reservoir fluids. Computation time is short and is comparable to that of the random mixing rules, as additional summations of mole fraction products are only for polar components, typically just a few. This also avoids the dilution problem occurring with the mixing rule in Eq.(4.82), that is, vanishing of the cubic term when the number of components increases. Furthermore, no particular computational memory and space requirements are imposed for application of the proposed model, since the number of binary parameters is limited to only three.

Knudsen et al. [54] evaluated the capability of different leading mixing rules to describe the phase behaviour of mixtures containing asymmetric compounds by comparing prediction with experimental data. The Huron-Vidal model [61], based on the principle of minimisation of excess Gibbs energy, overall performed more reliably than others, whereas the random mixing rule with four binary parameters failed.

Table 4.3.

Effect of invariance condition on predicted phase equilibria of  $C_1$ - $H_2S$ - $CO_2$ - $H_2O$  at  $T=311.1$  K, and  $P=6.26$  MPa [57].

Component	"water 2" / "water 1"	Methane	Hydr. sulfi.	Carb. diox.	Water*
Feed		0.0504	0.3986	0.0503	0.5008
Water-rich liquid					
Expt.	-	0.000490	0.0284	0.00350	0.9677
Calcd. Inv.	-	0.000402	0.0269	0.00326	0.9696
Calcd.	0	0.000402	0.0269	0.00326	0.9696
	1/9	0.000104	0.0162	0.00151	0.9823
	3/7	0.000016	0.0082	0.00052	0.9915
	1/1	0.000008	0.0065	0.00036	0.9933
Hydrogen sulfide-rich liquid					
Expt.	-	0.0653	0.8197	0.1049	0.0101
Calcd. Inv.	-	0.0602	0.8391	0.0894	0.0113
Calcd.	0	0.0602	0.8391	0.0894	0.0113
	1/9	0.0601	0.8385	0.0901	0.0114
	3/7	0.0601	0.8383	0.0903	0.0114
	1/1	0.0601	0.8382	0.0903	0.0114
Vapour					
Expt.	-	0.3213	0.5028	0.1739	0.00214
Calcd. Inv.	-	0.3216	0.5248	0.1517	0.00194
Calcd.	0	0.3216	0.5248	0.1517	0.00194
	1/9	0.3209	0.5244	0.1527	0.00197
	3/7	0.3207	0.5243	0.1530	0.00198
	1/1	0.3207	0.5243	0.1531	0.00199

\*Calculated water is the sum of the amounts of "water 1" and "water 2"

The local composition mixing rules relying on description of non-random forces by increasing the order of concentration polynomials are more successful in modelling the vapour-liquid equilibria than the liquid-liquid equilibria. The prediction deteriorates particularly for systems near the plait point, equivalent to the vapour-liquid critical point [59].

#### 4.4 REFERENCES

1. Benedict, M., Webb, G.B. and Rubin, L.C.: "An Empirical Equation for Thermodynamic Properties of Light Hydrocarbons and Their Mixtures, Methane, Ethane, Propane and n-Butane", *J. Chem. Phys.*, 8, 334-345 (April, 1940).
2. Mason, E.A. and Spurling, T.H.: "The Virial Equation of State", in *The International Encyclopedia of Physical Chemistry and Chemical Physics*, Pergamon Press Inc (1969).
3. Starling, K.E.: "Fluid Thermodynamic Properties for Light Petroleum Systems", Gulf Pub. (1973).
4. Starling, K.E.: "A New Approach for Determining Equation-of-State Parameters Using Phase Equilibria Data", *SPEJ*, 363-371, *Trans. AIME*, 237 (Dec., 1966).
5. Thiele, E.: "Equation of State for Hard Spheres", *J. Chem. Phys.*, 39, 474-479 (1963).
6. Carnahan, N.F. and Starling, K.E.: "Intermolecular Repulsions and the Equation of State for Fluids", *AIChE*, 18, 1184-1189 (1972).
7. Donohue, M.D. and Prausnitz, J.M.: "Perturbed Hard-Chain Theory for Fluid Mixtures, Thermodynamic Properties for Mixtures in Natural Gas and Petroleum Technology", *AIChE*, 24, 849-860 (1978).
8. Chien, C.H., Greenkorn, R.H. and Chao, K.C.: "A Chain of Rotators Equation of State", *AIChE*, 29, 560-571 (1983).
9. Lin, H.M., Kim, H., Guo, T.M. and Chao, K.C.: "Cubic Chain of Rotators Equation of State and VLE Calculations", *J. Fluid Phase Equilibria*, 13, 143-152 (1985).
10. Redlich, O. and Kwong, J.N.S.: "On the Thermodynamics of Solutions", *Chemical Review*, 44, 233-244 (1948).
11. Abbott, M.M.: "Equations of State in Engineering and Research", *Advan. Chem. Ser.*, 182 (1979).
12. Ahmed, Y., Sugie, H. and Lu, B.C.Y.: "Comparative Study of Eight Equations of State for Predicting Hydrocarbon Volumetric Phase Behaviour", *SPE* 15673 (1986).
13. Firoozabadi, A.: "Reservoir-Fluid Phase Behaviour and Volumetric Prediction with Equations of State", *JPT*, 40(4), 397-406 (1988).
14. Martin, J.J.: "Cubic Equations of State - Which?", *Ind. Eng. Chem. Fundam.*, 18(2), 81-97 (1979).
15. Anderko, A.: "Equation of State Methods for the Modelling of Phase Equilibria", *J. Fluid Phase Equilibria*, 61, 145-225 (1990).
16. Tsionopoulos, C. and Heidman, J.L.: "From Redlich-Kwong to the Present", *J. Fluid Phase Equilibria*, 24, 1-23 (1985).
17. Zudkevitch, D. and Joffe, E.: "Correlation and Prediction of Vapour-Liquid Equilibria with the Redlich-Kwong Equation of State", *AIChE*, 16(1), 112 (1970).
18. Joffe, J., Schroeder, G.M. and Zudkevitch, D.: "Vapour-Liquid Equilibrium with the Redlich-Kwong Equation of State", *AIChE*, 496-498, (1970).

19. Yarbrough, L.: "Application of a Generalised Equation of State to Petroleum Reservoir Fluid", Equations of State in Engineering, Advances in Chemistry Series, Chao, K.C. and Robinson, R.L. (eds), American Chemical Soc., No. 182, 385-435 (1979).
20. Reid, R.C., Prausnitz, J.M. and Sherwood, T.K.: "The Properties of Gases and Liquids", 4th ed, McGraw Hill (1986).
21. Soave, G.: "Equilibrium Constants from a Modified Redlich-Kwong Equation of State", Chem. Eng. Sci., 27, 1197-1203, (1972).
22. Soave, G., Barolo, M. and Bertucco, A.: "Estimation of High Pressure Fugacity Coefficients of Pure Gaseous Fluids by a Modified SRK Equation of State", J. Fluid Phase Equilibria, 91, 87-100 (1993).
23. Graboski, M.S. and Daubert, T.E.: "A Modified Soave Equation of State For Phase Equilibrium Calculations. 1. Hydrocarbon Systems", Ind. Eng. Chem. Process Des. Dev., 17(4), 443-448 (1978).
24. Peng, D.Y. and Robinson, D.B.: "A New Two-Constant Equation of State", Ind. Eng. Chem. Fundam., 15(1), 59-64 (1976).
25. Robinson, D.B. and Peng, D.Y.: "The Characterisation of the Heptanes and Heavier Fractions for the GPA Peng-Robinson Programs", GPA Research Report 28, Tulsa (1978).
26. Pencloux, A., Rauzy, E. and Freze, R.: "A Consistent Correction for Redlich-Kwong-Soave Volumes", J. Fluid Phase Equilibria, 8, 7-23 (1982).
27. Jhaveri, B.S. and Youngren, G.K.: "Three-Parameter Modification of the Peng-Robinson Equation of State to Improve Volumetric Predictions", SPE 13118 (1984).
28. Mathias, P.M., Naheiri, T. and Oh, E.M.: "A Density Correction for the Peng-Robinson Equation of State", J. Fluid Phase Equilibria, 47, 77-87 (1989).
29. Chou, G.R. and Prausnitz, J.M.: "A Phenomenological Correction to an Equation of State for the Critical Region", AIChE, 35(9), 1487-1496 (1989).
30. Schmidt, G. and Wenzel, H.: "A Modified van der Waals Type Equation of State", Chem. Eng. Sci., 135, 1503-1512 (1980).
31. Patel, N.C. and Teja, A.S.: "A New Cubic Equation of State for Fluids and Fluids Mixtures", Chem. Eng. Sci., 77(3), 463-473 (1982).
32. Valderrama, J.O. and Cisternas, L.A.: "A Cubic Equation of State for Polar and Other Complex Mixtures", J. Fluid Phase Equilibria, 29, 431-438 (1986).
33. Valderrama, J.O.: "A Generalised Patel-Teja Equation of State for Polar and Non-Polar Fluids and Their Mixtures", J. Chem. Eng. Japan, 23(1), 87-91 (1990).
34. Danesh, A., Xu, D. and Todd, A.C.: "An Evaluation of Cubic Equations of State for Phase Behaviour Calculations Near Miscibility Conditions", SPE/DOE 20267, Proc. of 7th Symp. on EOR (April, 1990).
35. Wilson, G. M.: "Vapour-liquid Equilibrium, Correlation by Means of a Modified Redlich-Kwong Equation of State", Advan. Cryog. Eng., 9, 168-176 (1964).

36. Stryjek, R. and Vera, J.H: "An Improved Equation of State", ACS Symp. Ser. 300, Washington DC (1986).
37. Mathias, P.M. and Copeman, T.W: "Extension of the Peng-Robinson Equation of State to Complex Mixtures: Evaluation of the Various Forms of the Local Composition Concept", *J. Fluid Phase Equilibria*, 13, 91-108 (1983).
38. Twu, C.H., Coon, J.E. and Cunningham, J.R: "A New Generalised Alpha Function for a Cubic Equation of State, Part 1. Peng-Robinson Equation", *J. Fluid Phase Equilibria*, 105, 49-59 (1995).
39. Twu, C.H., Coon, J.E. and Cunningham, J.R: "A New Generalised Alpha Function for a Cubic Equation of State, Part 2. Redlich-Kwong Equation", *J. Fluid Phase Equilibria*, 105, 61-69 (1995).
40. Kubic, W.L: "A Modification of Martin Equation of State for Calculating Vapour Liquid Equilibria", *J. Fluid Phase Equilibria*, 9, 79-97 (1982).
41. "Reservoir Fluid Studies, Final Research Report", Vol. I, Department of Petroleum Engineering, Heriot-Watt University, UK, Report No: PVT/93/2 (July, 1993).
42. Danesh, A., Xu, D.H., Tehrani, D. and Todd, A.C: "Improving Predictions of Equation of State by Modifying its Parameters for Super Critical Components of Hydrocarbon Reservoir Fluids", *J. Fluid Phase Equilibria*, 112, 45-61 (1995).
43. Prausnitz, J.M., Lichtenthaler, R.N. and de Azevedo, E.G: "Molecular Thermodynamics of Fluid-Phase Equilibria", 2nd ed., Prentice-Hall Inc (1986).
44. Turek, E.A., Metcalf, R.S., Yarbrough, L. and Robinson, R.L: "Phase Equilibria in Carbon Dioxide-Multicomponent Systems, Experimental Data and Improved Prediction Techniques", SPE 9231, Proc. of 55th Ann. Conf. (Sept., 1980).
45. Elliot, J. and Daubert, T: "Revised Procedure for Phase Equilibrium Calculations with Soave Equation of State", *Ind. Eng. Chem. Proc. Des. Dev.*, 23, 743-748 (1985).
46. Varotsis, N., Stewart, G., Todd, A.C. and Clancy, M.: "Phase Behaviour of Systems Comprising North Sea Reservoir Fluids and Injection Gases", *JPT*, 38(11), 1221-1233 (Nov., 1986).
47. Chueh, P.L. and Prausnitz, J.M: "Vapour-Liquid Equilibria at High Pressures, Calculation of Partial Molar Volume in Non-Polar Liquid Mixtures", *AIChE*, 13, 6, 1099-1113 (1967).
48. Katz, D.L. and Firoozabadi, A: "Predicting Phase Behaviour of Condensate/ Crude Oil Systems Using Methane Interaction Coefficients", *JPT*, 1649-55 (Nov., 1978).
49. Teja, A.S: "Binary Interaction Coefficients for Mixtures Containing the n-Alkanes", *Chem. Eng. Sci.*, 33, 609-610 (1978).
50. Whitson, C.H., Anderson, T.F. and Soreide, I: "C<sub>7+</sub> Characterisation of Related Equilibrium Fluids Using Gamma Distribution", in "C<sub>7+</sub> Characterisation", Chorn, L.G. and Mansoori, G.A., Eds, Taylor & Francis, 35-56 (1989).
51. Voros, N.G. and Tassios, D.P: "Vapour-Liquid Equilibria in Nonpolar/Weakly Polar Systems with Different Types of Mixing Rules", *J. Fluid Phase Equilibria*, 91, 1-29 (1985).

52. Bjorlykke, O.P. and Firoozabadi, A: "Measurement and Computation of Near-Critical Phase Behaviour of a C1/nC24 Binary Mixture", SPE Res.Eng., 271 (1992).
53. Danesh, A., Xu, D. and Todd, A.C: "Comparative Study of Cubic Equations of State for Predicting Phase Behaviour and Volumetric Properties of Injection Gas-Reservoir Oil Systems", J. Fluid Phase Equilibria, 63, 259-278 (1991).
54. Knudsen, K., Stenby, E.H. and Fredenslund, A.A: "A Comprehensive Comparison of Mixing Rules for Calculation of Phase Equilibria in Complex Systems", J. Fluid Phase Equilibria, 82, 361-368 (1993).
55. Schwartzentruber, J. and Renon, H: "Equation of State: How to Reconcile Flexible Mixing Rules, the Virial Coefficient Constraint, and the "Michelsen-Kistenmacher Syndrome" for Multicomponent Systems", J. Fluid Phase Equilibria, 67, 99-110 (1991).
56. Melhem, G.A., Saini, R. and Goodwin, B.M: "A Modified Peng-Robinson Equation of State", J. Fluid Phase Equilibria, 47, 189-237 (1989).
57. Avlonitis, D., Danesh, A., Todd, A.C: "Prediction of VL and VLL Equilibria of Mixtures Containing Petroleum Reservoir Fluids and Methanol with a Cubic EOS", J. Fluid Phase Equilibria, Vol. 94, 181-216 (1994).
58. Michelsen, M.L. and Kistenmacher, H: "On Composition-Dependent Interaction Coefficients", J. Fluid Phase Equilibria, 58, 229-230 (1990).
59. Mathias, P.M., Klotz, H.C. and Prausnitz, J.M: "Equation of State Mixing Rules for Multicomponent Mixtures: the Problem of Invariance", J. Fluid Phase Equilibria, 67, 31-44 (1991).
60. Panagiotopoulos, A.Z. and Reid, R.C: "New Mixing Rules for Cubic Equations of State for Highly Polar, Asymmetric Mixtures", ACS Symp. Ser. 300, 571-582 (1986).
61. Huron, M.J. and Vidal, J: "New Mixing Rules in Simple Equations of State for Vapour-Liquid Equilibria of Strongly Non-Ideal Mixtures", J. Fluid Phase Equilibria, 3, 255-271 (1979).

#### 4.5 EXERCISES

- 4.1. A one litre cylinder contains 160.43 g of methane at 373 K. Calculate its pressure using BWSR.
- 4.2. Prove Eq.(4.13).
- 4.3. Show that the values of  $\Omega_a$  and  $\Omega_b$  in RK are equal to 0.42747 and 0.08664, respectively.
- 4.4. Prove Eq.(4.18).
- 4.5. Calculate the vapour pressure of normal hexane at 477.6 K using SRK. What are the predicted values of the saturated vapour and liquid density?
- 4.6. Calculate the value of critical compressibility factor as predicted by PR.
- 4.7. Reduce the PR to a three parameter corresponding state form of  $Z=Z(T_r, P_r, \omega)$ . Compare the calculated values of  $Z$  at  $T_r=1.5$ ,  $P_r=2$  and  $\omega=0$  and, also  $\omega=0.6$ , with those of the generalised compressibility chart shown in Figure 2.22.

- 4.8. Derive an expression for the critical compressibility factor as predicted by SW in terms of the acentric factor.
- 4.9. Compare the value of attractive term temperature coefficient,  $\alpha$ , in PR for  $nC_{20}$  at  $T_r=0.8$  as calculated by the original and modified correlations by the authors, and also by the Twu correlation.
- 4.10. Prove Eq.(4.69).
- 4.11. Prove Eq.(4.33).
- 4.12. PR predicts the density of a mixture of  $C_1$ - $nC_{10}$  (50-50 mol %) equal to  $520 \text{ kg/m}^3$ . Improve the predicted result by including the volume shift correction.
- 4.13. Predict the density of a single phase mixture composed of  $C_1=59.30\%$ ,  $C_4=37.46\%$  and  $nC_8=3.24\%$  (molar) at  $311.0 \text{ K}$  and  $12.07 \text{ MPa}$ , using PR, SRK and VPT. (Measured value= $297 \text{ kg/m}^3$ ).
- 4.14. Derive the expression for fugacity coefficient of a component in a mixture using the random mixing rules and the generalised EOS. (Answer in Appendix B).
- 4.15. In Exercise 3.5, the solubility of ethane and  $CO_2$  in water was calculated by assuming the gas fugacity coefficients equal to one. Use PR to estimate the fugacity coefficients, in order to improve the accuracy of predicted gas solubility.



## 5 PHASE BEHAVIOUR CALCULATIONS

Phase equilibrium calculations for petroleum reservoir fluids may in general involve the treatment of a number of fluid and solid phases. When displacing oil in a reservoir with  $\text{CO}_2$  at low temperature two liquid phases, one hydrocarbon rich and one  $\text{CO}_2$  rich, can be in equilibrium with the vapour phase. The appearance of two distinct liquid hydrocarbon phases formed by retrograde condensation has also been reported. The formation and deposition of solid-like material of asphaltic nature resulting from compositional changes in miscible displacement or variations in pressure and temperature are well documented. Water in general is always present in reservoirs as a separate phase, and it can also form solid phases of hydrates at certain conditions of pressure and temperature. All co-existing fluids and solids in general should ultimately attain equilibrium, given sufficient time.

Typical calculations of equilibrium conditions can be classified in two categories. In the first category, the composition and properties of the co-existing phases at a given set of temperature and pressure are required. In the second case, the saturation condition, either temperature or pressure is searched for a given composition and pressure, or temperature. The main interest in dealing with solid-like phases, such as asphaltenes, waxes and hydrates, is the determination of their formation conditions. In such cases the overall composition of fluid phases remains unchanged and the phase equilibrium calculations for fluid phases can be performed generally independent of the solid phase. Also, because the effect of water on the hydrocarbon phase behaviour can be neglected in most cases, the majority of phase equilibrium calculations are limited only to two phases, that is, vapour-liquid equilibria. The uniformity of fugacity of each component throughout all phases, solids and fluids, as the requirement for chemical equilibrium can be employed, however, to determine equilibrium conditions regardless of the number of phases. Mathematical methods for calculating vapour-liquid equilibria can also be extended to any number of phases. The number and state of the phases at equilibrium may not be known, however, in advance. This can be determined by minimising the Gibbs energy, as will be described.

Fluid samples collected from various locations and depths within a reservoir often show some discrepancies. In some cases, the observed differences are due to improper sampling. The reservoir could also be compartmental, with limited communications between different sections. The lack of reservoir fluid maturity can also cause compositional variations within a reservoir as mentioned in Section 1.1. Moreover, as the temperature and pressure change with depth in reservoir, a degree of compositional grading should always be expected. The compositional gradient with depth is often negligible, and the variations are within the experimental accuracy in collecting samples. It can, however, become quite significant for near critical fluids, and reservoir oils containing high concentrations of asphaltic materials. The variation of fluid composition with depth may be estimated by applying thermodynamic concepts introduced in Chapter 3. The fluid column can be assumed at equilibrium, ignoring the heat flux due to the temperature gradient, or be treated at steady state conditions with compositional grading controlled by the balance of chemical and thermal forces, using non-equilibrium thermodynamics. Both approaches will be described in this chapter.

### 5.1 VAPOUR-LIQUID EQUILIBRIUM CALCULATIONS

Let one mole of mixture be flashed at pressure  $P$  and temperature  $T$  into  $n^L$  moles of liquid and  $n^V$  moles of vapour. The total material balance for the system is,

$$n^L + n^V = 1 \quad (5.1)$$

with material balance for each component,  $i$ , as,

$$z_i = x_i n^L + y_i n^V \quad i=1, 2, \dots, N \quad (5.2)$$

where  $z_i$ ,  $x_i$  and  $y_i$  are mole fractions of the component  $i$ , in the mixture, liquid and vapour, respectively.

$$\sum_{i=1}^N x_i = \sum_{i=1}^N y_i = 1 \quad (5.3)$$

where  $N$  is the total number of components in the system.

At equilibrium, the fugacity of any component,  $i$ , in the vapour is equal to that in the liquid. The equality of fugacity can be expressed by the equilibrium ratio,  $K_i$ , as given by Eq.(3.43),

$$K_i = y_i / x_i \quad i=1, 2, \dots, N \quad (3.43)$$

The material balance equations, Eqs.(5.1-3), and the equilibrium requirement, Eq.(3.43) provide the required  $2N+2$  independent equations to determine the  $2N+2$  unknowns of  $x_i$ ,  $y_i$ ,  $n^L$  and  $n^V$ . The number of variables can be reduced, however, by combining the above equations.

Substituting the equilibrium ratio  $K_i = y_i/x_i$  into Eq.(5.2), and solving for  $x_i$  and  $y_i$  using Eq.(5.1) results in,

$$x_i = \frac{z_i}{1 + (K_i - 1)n^V} \quad (5.4)$$

and

$$y_i = \frac{K_i z_i}{1 + (K_i - 1)n^v} \quad (5.5)$$

Similar equations can also be derived in terms of  $n^l$  instead of  $n^v$ .

For known values of  $K_i$ , any of the above two equations can be substituted in Eq.(5.3) to determine the value of  $n^v$  (or  $n^l$ ). An iterative method is required to solve the resulting equation. The following equation, known as the Rachford-Rice [1] equation, is generally the preferred form, as its value monotonically decreases with increasing  $n^v$ ,

$$f(n^v) = \sum_{i=1}^N (y_i - x_i) = \sum_{i=1}^N \frac{z_i (K_i - 1)}{1 + (K_i - 1)n^v} = 0 \quad (5.6)$$

The above equation yields a physically correct root for  $n^v$  between 0 and 1, provided that,

$$\sum_{i=1}^N K_i z_i > 1 \quad (5.7)$$

and

$$\sum_{i=1}^N z_i / K_i > 1 \quad (5.8)$$

The mixture is at its bubble point when  $n^v$  approaches zero. Hence Eq.(5.6) reduces to,

$$\sum_{i=1}^N z_i K_i = 1 \quad (5.9)$$

and

$$y_i = K_i x_i = K_i z_i \quad (5.10)$$

At any temperature the bubble point pressure can be determined as the pressure at which  $K$ -values satisfy Eq.(5.9). The bubble point is most sensitive to the mixture light components, which exhibit large  $K$  values.

At the dew point,  $n^v$  approaches 1. Hence Eq.(5.6) reduces to,

$$\sum_{i=1}^N z_i / K_i = 1 \quad (5.11)$$

and

$$x_i = y_i / K_i = z_i / K_i \quad (5.12)$$

The dew point pressure is that at which  $K$ -values satisfy Eq.(5.11). The dew point is most sensitive to the mixture heavy components, which exhibit small  $K$ -values.

Eq.(5.6) can be used to identify the state of a fluid mixture at a given pressure and temperature. If a physically unacceptable root of either  $n^v > 1$  or  $n^v < 0$ , was found the mixture may be considered to be either all vapour, or all liquid, respectively. The above identification is valid if reasonably accurate K-values are used. A more rigorous approach to identify the state of a mixture is given in Section 5.2 using the Gibbs energy minimisation method.

### Example 5.1.

It is often a convenient practice, yet reliable in most applications, to replace a reservoir fluid by a binary mixture in simulating certain reservoir processes in the laboratory. A reservoir hydrocarbon fluid has been modelled by a mixture of  $C_1$  and  $nC_{10}$  (60-40 mole%). The reservoir temperature and pressure are 377.6 K and 27.58 MPa, respectively. The oil is produced through a one stage intermediate separator at 344.3 K and 6.895 MPa.

(a) What is the state of the fluid at reservoir conditions? Use the GPA K-charts given in Appendix D.

(b) Calculate the bubble point pressure.

(c) Equilibrium flash equations for a binary system can be solved analytically, when using K-charts. Derive the appropriate expression, and calculate the gas and liquid mole fractions, and the phase composition, at the separator conditions.

### Solution:

Component 1:  $C_1$

Component 2:  $nC_{10}$

(a)

The convergence pressure at 377.6 K (220 °F) is estimated from Figure D.1 (Appendix D):  $P_k = 5000$  psia (34.47 MPa).

The equilibrium ratios of  $C_1$  and  $nC_{10}$  are then read from Figures D.2 and D.13 (Appendix D), respectively, at 377.6 K and 27.58 MPa (4000 psia):

$$K_1 = 1.4$$

$$K_2 = 0.13$$

$$\text{Checking } \sum_{i=1}^N z_i K_i,$$

$$\sum_{i=1}^2 z_i K_i = 0.6 \times 1.4 + 0.4 \times 0.13 = 0.89 < 1.$$

Hence, the fluid is a compressed (undersaturated) liquid.

For an undersaturated vapour,  $\sum_{i=1}^N z_i / K_i < 1$ , whereas for a two phase system both Eq.(5.7) and Eq.(5.8) should be satisfied.

(b)

At the bubble point Eq.(5.9) must be satisfied. The K-values are read from the charts at 377.6 K by iterating on pressure:

P, psia, (MPa)	$K_1$	$K_2$	$z_1 K_1$	$z_2 K_2$	$\sum_{i=1}^2 z_i K_i$
3500, (24.13)	1.60	0.06	0.96	0.02	0.98
3000, (20.68)	1.80	0.03	1.08	0.01	1.09
3400, (23.44)	1.64	0.05	0.98	0.02	1.00

The experimental value is 23.50 MPa (3408 psia) [2]. Note that  $\sum_{i=1}^N z_i K_i$  strongly depends on the  $K$ -value of methane, due to its high volatility and concentration. A reasonable initial guess for a reservoir oil in most cases could be the pressure at which  $(Kz)_C=1$ .

(c)

For a binary system Eq.(5.6) reduces to:

$$n^V = [z_1(K_1 - K_2)/(1 - K_2) - 1]/(K_1 - 1) \quad (\text{E5.1})$$

The degrees of freedom for a binary vapour-liquid system at equilibrium conditions are only two, according to the Gibbs phase rule, Eq.(1.2). Hence at a given temperature and pressure, the  $K$ -values are constant and independent of the overall composition.

Using Figures D.2 and D.13, at 344.3 K and 6.895 MPa (1000 psia),

$K_1=3.8$ ,  $K_2=0.0029$ , (experimental values  $K_1=4.005$ , and  $K_2=0.0027$  [49]).

Eq.(E5.1) results in, vapour mole fraction:  $n^V=0.457$ , liquid mole fraction:  $n^L=0.543$ .

Eqs.(5.4-5) give the composition of equilibrated phases as follows,

$$x_1=0.263, \quad x_2=0.737, \quad y_1=0.999, \quad y_2=0.001$$

$$(x_1=0.2496, \quad x_2=0.7504, \quad y_1=0.9980, \quad y_2=0.0020, \text{ experimental values}).$$

At low and moderate pressures, where the dependency of equilibrium ratio on phase composition can be neglected, flash calculations are relatively simple, as  $K$ -values are known. In general,  $K$ -values vary with composition, hence, the solution is reached by iteration.

The calculation can begin by initialising  $K$ -values in Eq.(5.6) estimated from Raoult's law, with an appropriate correlation for the vapour pressure, e.g., Eq.(1.10), or the more widely used Wilson equation, Eq.(3.66). The solution of Eq.(5.6) yields the compositions of the two phases using Eqs.(5.4) and (5.5). The calculated compositions are then used to re-evaluate  $K_i$ 's, using an equation of state (EOS) or  $K$ -value correlations, to be substituted in Eq.(5.6) for the next round of iteration. The iterative calculations are complete when values of check functions are all smaller than certain pre-set tolerances. The above procedure, using EOS, is schematically shown in Figure 5.1. A simple successive substitution iteration method has been used in the flow chart. Successive substitution methods may prove to be very slow in converging to a solution, particularly in the critical region. Various methods to improve the convergence rate, such as promotion in equilibrium ratio updating, and the use of Newton type methods, which have a faster convergence rate than successive substitution methods, have been reported in the literature [3-8].

It should be noted that the solution of  $x_i=y_i=z_i$  always satisfies the set of equilibrium flash equations, Eqs.(5.1-5). The above trivial solution is a major problem in phase equilibrium calculations when equations of state are used in determining the fugacity coefficients. This occurs often in the critical region, where the compositions of equilibrated phases are very close. The trivial solution should not be mistaken as the critical point predicted by the equation of state. The use of equations of state to estimate the critical point is described in Section 5.3. The trivial solution, however, may be the only mathematical solution at conditions such as the equilibrium flash in single phase region.

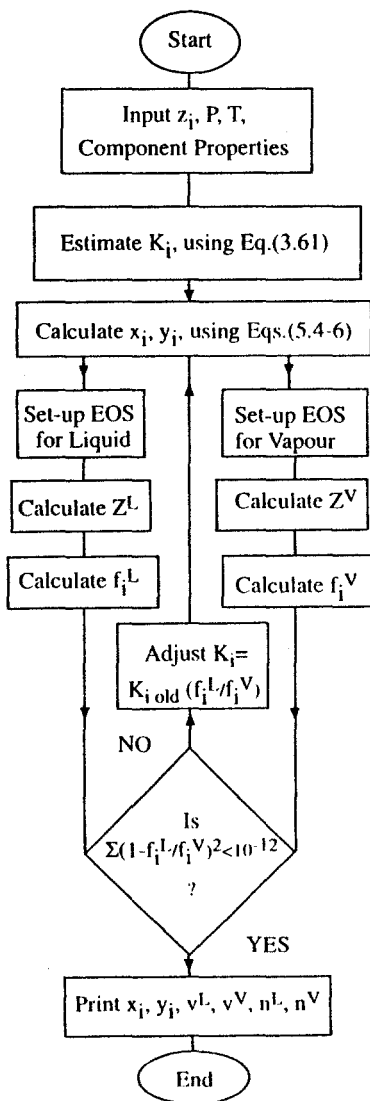


Figure 5.1. Flow chart of flash calculations using equation of state.

*Example 5.2.*

Calculate the bubble point of the fluid in Example 5.1, using the Peng-Robinson equation of state.

**Solution:**

The approach is similar to that for flash calculations as shown in Figure 5.1. The liquid composition remains unchanged in bubble point calculations, therefore, the vapour composition can be calculated from Eq.(3.43) instead of solving material balance equations, Eqs.(5.4-6), as in flash calculations. However, the pressure is not known in bubble point calculations and must be estimated and iterated in converging to the solution.

(1) The properties of Component 1, C1, and Component 2, nC10, are read from Table A.1 in Appendix A.

Number	Component	MW kg/kgmol	Tc K	Pc MPa	acentric factor
1	Methane	16.043	190.56	4.599	0.0115
2	n-Decane	142.285	617.7	2.110	0.4923

The Peng-Robinson EOS parameters for fluid components at T=377.6 K are calculated as follows,

Comp.	$x_i$	$a_i$ MPa.(m <sup>3</sup> /kgmol) <sup>2</sup>	$m$	$\alpha$	$a$ MPa.(m <sup>3</sup> /kgmol) <sup>2</sup>	$b$ m <sup>3</sup> /kgmol
Equation		4.27	4.29	4.23	$a_i \alpha$	4.27
1	0.6	0.24957517	0.39665578	0.70275305	0.17538971	0.02680134
2	0.4	5.71576076	1.07281059	1.52284853	8.70423787	0.18935786

The liquid mixture parameters,  $b$  and  $a$ , are calculated using the mixing rules, Eqs.(4.74) and (4.78), respectively. The binary interaction parameter between methane and n-decane is read from Table A.4.3 in Appendix A:  $k_{12}=k_{21}=0.0500$ , and  $k_{11}=k_{22}=0$ .

$$b = \sum_i x_i b_i = 0.6 \times 0.02680134 + 0.4 \times 0.18935786 = 0.09182395 \text{ m}^3/\text{kgmol}$$

$$a = \sum_i \sum_j x_i x_j (a_i \cdot a_j)^{0.5} (1 - k_{ij}) =$$

$$0.6 \times 0.6 \times 0.17538971 \times 1 + 0.6 \times 0.4 \times (0.17538971 \times 8.70423787)^{0.5} \times (1 - 0.050) + 0.4 \times 0.6 \times (8.70423787 \times 0.17538971)^{0.5} \times (1 - 0.050) + 0.4 \times 0.4 \times 8.70423787 \times 1 = 2.01923838 \text{ MPa.(m}^3/\text{kgmol)}^2$$

(2) A bubble point pressure of 27.58 MPa (4000 psia) is assumed as the initial guess. The final result should not depend on the initially selected value.

(3) The Wilson equation, Eq.(3.66), is used to estimate the equilibrium ratios at 27.58 MPa, and 377.6 K:  $K_1=2.457$ , and  $K_2=0.0004684$ .

(4) The vapour composition is calculated using Eq.(3.43),  $y_i = K_i x_i$ , resulting in  $y_1=1.474$ , and  $y_2=0.0001874$ . Note that  $\sum y_i$  is not equal to 1 which only occurs at the correct bubble point pressure.

(5) The Peng-Robinson EOS, Eq.(4.25), is set-up for both phases. The dimensionless values of EOS parameters are calculated from Eqs.(4.7-8).

**Liquid Phase:**

A=5.6501, and B=0.8067, which results in the following cubic equation for the liquid compressibility factor, Eq.(4.30):

$$Z^3 - 0.19332Z^2 - 2.08487Z - 3.38239 = 0$$

The above equation has only one real root (Appendix C),  $Z^L = 1.0985$

Vapour Phase:

A procedure similar to that of liquid results in  $A = 1.0661$  and  $B = 0.3468$  for the vapour phase, with only one real root for its compressibility factor cubic equation,

$$Z^V = 0.89802.$$

(6) The fugacity of each component is calculated in both phases, using Eq.(E.4.5),

$$\ln \phi_i = \frac{b_i}{b} (Z - 1) - \ln(Z - B) - \frac{A}{B(-2\sqrt{2})} \left( \frac{2 \sum_{j=1}^N x_j a_{ij}}{a} - \frac{b_i}{b} \right) \ln \left( \frac{Z + (1 - \sqrt{2})B}{Z + (1 + \sqrt{2})B} \right) \quad (\text{E.5.2})$$

where  $a_{ij} = (a_i a_j)^{0.5} (1 - k_{ij})$ .

The calculated values of fugacity coefficients, fugacities, and equilibrium ratios are as follows:

Comp.	P, MPa	$x_i$	$y_i$	$\phi_i^L$	$\phi_i^V$	$f_i^L$ , MPa	$f_i^V$ , MPa	$K_i$
Equation				E5.2	E5.2	$\phi_i^L x_i P$	$\phi_i^V y_i P$	$\phi_i^L / \phi_i^V$
1	27.58	0.60000	1.474	1.3643	0.9157	22.56	37.22	1.4899
2	27.58	0.40000	0.0001874	0.003345	0.02295	0.03690	0.0001186	0.14575

Clearly the fugacity of components are not equal in the two phases at the above selected pressure. The resulting error value of  $\sum_i (1 - f_i^L / f_i^V)^2 = 10^{-5}$  is far remote from the objective value of  $< 10^{-12}$ .

(7) The pressure is adjusted for the next iteration as follows:

At equilibrium,  $f_i^L = f_i^V = \phi_i^V y_i P$ . Hence,

$$\sum_i y_i = \sum_i f_i^L / \phi_i^V P = (1/P) \sum_i f_i^L / \phi_i^V = 1$$

That is, the pressure can be adjusted as,

$$P_{(r+1)} = \left( \sum_i f_i^L / \phi_i^V \right)_{(r)} = P_{(r)} \left( \sum_i x_i \phi_i^L / \phi_i^V \right)_{(r)} = P_{(r)} \left( \sum_i x_i K_i \right)_{(r)} \quad (\text{E.5.2}')$$

where  $r$  is the iteration number. Other methods to iterate the pressure with faster convergence rates have also been suggested [9].

Applying the pressure updating method given by Eq.(E.5.2'), the next pressure is,

$$P = 22.56 / 0.9157 + 0.03690 / 0.02295 = 26.24 \text{ MPa}$$



(8) Now with the new pressure and equilibrium ratios, steps (4) to (7) are repeated. The results of a few initial, intermediate and final iterations are given in the following tables.

Iter. No.	Pres., MPa	$y_1$	$y_2$	$Z^L$	$Z^V$
2	26.24	0.8932	0.05829	1.0513	0.91638
3	25.59	0.9329	0.04261	1.0285	0.92134
14	24.31	0.9774	0.02225	0.9828	0.9289
29	24.294	0.97777	0.022228	0.98213	0.92877

Iter. No.	$f_1^L$ MPa	$f_1^V$ MPa	$f_2^L$ MPa	$f_2^V$ MPa	$K_1$	$K_2$	Error
2	21.86	20.92	0.03383	0.04628	1.5548	0.10653	7.43E-02
3	21.52	21.13	0.03246	0.04182	1.5841	0.082677	5.05E-02
14	20.87	20.87	0.02989	0.2991	1.6292	0.055615	4.97E-07
29	20.861	20.861	0.029834	0.029834	1.6296	0.055569	3.58E-12

During the iteration of Eq.(5.6), values of  $n^V > 1$  or  $n^V < 0$  may be obtained at conditions where both phases physically exist, due to unreliable  $K$ -values. The common method is to reject these values and continue the iteration with new physically acceptable values. However, this can disturb the convergence trend towards the solution increasing the number of iterations required. It is advisable to continue the iteration with the obtained values as realistic data will generally follow after a few iterations, if the system is in the two-phase region. The values of  $n^V > (1-K_{\min})^{-1}$  and  $n^V < (1-K_{\max})^{-1}$  should, however, be rejected as these will yield negative phase compositions. This approach known as "negative flash" has been addressed by a number of authors [10] and investigated by Whitson and Michelsen [11].

The negative flash approach is most effective for high pressure conditions, or complex mixtures, where equilibrium ratios,  $K_i$ 's, depend on phase composition and the iteration process can become quite extensive.

Conventional flash calculation procedures, such as the one described above, are for known temperature and pressure conditions. When the phase change is due to a sudden or a steep pressure reduction, such is vaporisation of oil or condensation of gas through wellbore or pipe restrictions, the system enthalpy may be assumed constant due to low heat loss. In such conditions, flash calculations at a given pressure enthalpy, instead of pressure-temperature, by invoking energy balance equations are required. Alternatively a series of conventional isothermal flash calculations at various temperatures can be conducted, followed by calculation of the system enthalpy, to find the temperature at which the system enthalpy is unchanged. Agrawal et al. [12] compared the above approach with the method which solves material balance and energy equations simultaneously, and concluded that the former approach was more robust, albeit slower.

### Root Selection

Cubic equations of state (EOS) can be conveniently solved by analytical or numerical methods. The analytical solution of the generalised EOS, Eq.(4.12), is given in Appendix C. Both approaches are almost equally effective when optimally implemented [13].

The mathematical behaviour of EOS for multicomponent systems is the same as that for a pure compound. At a temperature above the pseudo critical temperature, it will provide only one root for the molar volume, or the compressibility factor, at a given pressure. At temperatures below the pseudo critical temperature, three real roots for the molar volume at any pressure

may be obtained. The pseudo critical condition can be determined using the same criterion as that for the pure compound. That is,

$$\left(\frac{\partial P}{\partial v}\right)_{T=T_c} = \left(\frac{\partial^2 P}{\partial v^2}\right)_{T=T_c} = 0 \quad (4.9)$$

The above set of equations provide the same relation between the pseudo critical pressure, temperature, volume, and the equation of state parameters, as described in Chapter 4 for pure compounds, i.e. Eqs.(4.10-11). It should be noted that, the calculated horizontal inflection point by Eq.(4.9) does not occur at the true critical point of the mixture.

At pressures corresponding to the maximum and the minimum molar volumes predicted by EOS, Figure 4.1, two of the roots will be equal. With some EOS, such as the Peng-Robinson EOS, it is possible to obtain a molar volume smaller than the co-volume. This should be rejected as the co-volume,  $b$ , is regarded as the molar volume when the pressure approaches infinity. The general behaviour of typical EOS has been detailed in [14].

When EOS, written in terms of compressibility factor (or molar volume), has three real roots, the intermediate root is ignored, and the lower and the higher values of compressibility factor (or molar volume) are assigned to the liquid and vapour phases, respectively. It is obvious that for multicomponent systems, where compositions of vapour and liquid phases at equilibrium are different, only the root assigned to the phase whose composition has been used in determining EOS parameters, will be of interest.

In some cases it may not be straight forward to identify a fluid as vapour or liquid. When three roots are found for such systems, the intermediate root is ignored, and the one which gives the lower Gibbs energy from the other two is selected. The selection of the smaller root identifies the fluid as the liquid-like, whereas that of the larger root indicates a vapour-like fluid.

The change of Gibbs energy can be calculated using Eqs.(3.14) and (3.27), with fugacities determined by EOS. For example, using the Peng-Robinson or Soave-Redlich-Kwong EOS with component fugacity coefficients as,

$$\ln \phi_i = \frac{b_i}{b} (Z - 1) - \ln(Z - B) - \frac{A}{B(\delta_2 - \delta_1)} \left( \left( 2 \sum_{j=1}^N x_j a_{ij} \right) / a - b_i / b \right) \ln \left( \frac{Z + \delta_2 B}{Z + \delta_1 B} \right) \quad (E4.5)$$

or using the total fugacity coefficient given by Eq.(4.18), the system molar Gibbs energy difference at the two roots  $Z_h$  and  $Z_l$  is determined as,

$$(G_h - G_l) / RT = (Z_h - Z_l) + \ln \left( \frac{Z_l - B}{Z_h - B} \right) - \frac{A}{B(\delta_2 - \delta_1)} \ln \left[ \left( \frac{Z_l + \delta_1 B}{Z_l + \delta_2 B} \right) \left( \frac{Z_h + \delta_2 B}{Z_h + \delta_1 B} \right) \right] \quad (5.13)$$

If the above is positive,  $Z_l$  is selected, otherwise,  $Z_h$  is the correct root.

### Example 5.3.

The Peng-Robinson EOS is used to predict the density of a single phase equimolar mixture of  $C_3$  and  $nC_4$  at 396 K and 3.86 MPa. Apply the minimum Gibbs energy concept to select the proper root.

*Solution:*

The parameters of EOS are determined for the equi-molar mixture of  $C_3$  (Component 1) and  $nC_4$  (Component 2), at 396 K,

Comp.	$x_i$	$a_i$	$m$	$\alpha$	$a$	$b$
Equation		4.27	4.29	4.23	$a_c \alpha$	4.27
1	0.5000	1.01770302	0.60201108	0.95856673	0.97553625	0.05631263
2	0.5000	1.50486716	0.6704416	1.04728482	1.57602453	0.07243918

Mixture parameters,  $b$  and  $a$ , are calculated using the random mixing rules, Eqs.(4.74) and (4.78), respectively, with  $k_{12}=0.0033$  from Table A.4.3 in Appendix A.

$$b = \sum_i x_i b_i = 0.0643759 \quad \text{m}^3/\text{kgmol}$$

$$a_{12}=a_{21} = (1-k_{12})(a_1 a_2)^{0.5} = 1.23585538 \quad \text{MPa} \cdot (\text{m}^3/\text{kgmol})^2$$

$$a = \sum_i \sum_j x_i x_j a_{ij} = 1.25581788 \quad \text{MPa} \cdot (\text{m}^3/\text{kgmol})^2$$

The above values result in the following dimensionless parameters at 3.86 MPa:

$$A=0.44715879 \quad \text{and} \quad B=0.07547177$$

Substituting the parameters in Eq.(4.30) results in the following cubic equation,

$$Z^3 - 0.92452827Z^2 + 0.27912728Z - 0.027622 = 0$$

The above equation has three real roots:

$$Z_h = 0.394179 \quad Z_l = 0.280758 \quad Z_g = 0.249591$$

Rejecting the intermediate root,  $Z_l$ , and substituting  $\delta_1 = 1 + \sqrt{2}$ , and  $\delta_2 = 1 - \sqrt{2}$  in Eq.(5.13) to obtain the expression for the Peng-Robinson EOS, we obtain,

$$(G_h - G_l)/RT = -0.00046$$

Hence,  $Z_h$  represents the stable phase with a lower energy level, and the fluid is vapour-like.

The density is calculated as,

$$\rho_M = P/(ZRT) = 3.86/(0.394179 \times 0.0083144 \times 396) = 2.9742 \quad \text{kgmol/m}^3$$

$$M = \sum x_i M_i = 51.109 \quad \text{kgmol/mol}$$

$$\rho = \rho_M M = 152.01 \quad \text{kg/m}^3$$

When at a selected temperature-pressure, EOS gives one real root, that root will be expected to be the correct root for the phase under consideration. Phase behaviour calculations using EOS is an iterative process as compositions of all or some of the phases, hence the parameters of EOS, are not known in advance. The initially estimated composition for a phase may provide a wrong single root, as shown schematically in Figure 5.2.

The pressure-volume relation, at a constant temperature, for the correct composition of a vapour phase, as predicted by EOS, is shown by the solid line in Figure 5.2. Clearly the correct root for the vapour phase is  $Z_3$ , which is the highest of all. The pressure-volume relation for the vapour with an initially estimated composition is shown by the dashed line. As only one root is obtained,  $Z_4$ , it will be assigned to the vapour phase. The root is, however, far away from the correct value.

The problems associated with improper roots during iterative phase behaviour calculations, due to poorly assigned distribution of components between the phases, have been addressed by several investigators [e.g., 15, 16]. At temperatures below the pseudo critical temperature, where three real roots may exist, the correct root can be identified by comparing them with the pseudo critical volume [16]. If the predicted root is less than the pseudo critical volume, it is that of the liquid phase, otherwise that of the vapour phase. Poling et al. [15] have also studied the above problem, including the spurious derivatives near the predicted two-phase zone boundary, and have suggested empirical criterion to avoid selecting wrong root.

If comparison of the predicted volume with that of pseudo critical value indicated the presence of a wrong root for the phase under consideration, the estimated values used in equilibrium calculations should be adjusted. For flash calculations at a given temperature-pressure, increasing or decreasing the concentration of light components should promote the identification of that phase by EOS as vapour or liquid.

In the near critical region, often only a single root is found for each phase. Both roots may well be liquid-like or vapour-like which may correct themselves during further iterations. Interfering in the iterative process by adjusting roots, may have an adverse effect on the convergence [13].

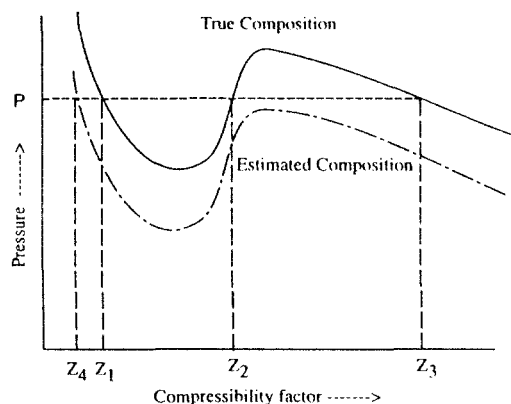


Figure 5.2. Improper root selection due to inaccurate phase composition.

#### Example 5.4.

What is the maximum temperature at which the Peng-Robinson EOS provides three real roots for a single phase equimolar mixture of  $C_1$  and  $nC_4$ .

*Solution:*

The mathematical behaviour of a cubic EOS for a single phase multicomponent mixture, where its composition remains unchanged, is the same as that for a pure compound. Hence, the temperature at which the cubic EOS shows the inflection point is the maximum temperature for three real roots. This can be obtained from Eq.(4.9), similar to that for a pure compound. The calculated value, however, is not the critical temperature of the mixture, but it can be regarded as the EOS derived pseudo critical temperature.

$$\left(\frac{\partial P}{\partial v}\right)_{T,P_c} = \left(\frac{\partial^2 P}{\partial v^2}\right)_{T,P_c} = 0$$

Setting the above two derivatives equal to zero for the Peng-Robinson EOS results in two equations similar to Eq.(4.27), as,

$$a_m = 0.457235R^2 \left( T_c^2 / P_c \right)$$

$$b_m = 0.077796R \left( T_c / P_c \right)$$

Combining the two equations, and eliminating the pseudo critical pressure results in,

$$P_c T_c = 0.17014446(a_m / Rb_m) \quad (\text{E5.4})$$

Note that  $a_m$  is also a function of temperature:

$$a_m = \sum_i \sum_j x_i x_j (\alpha_i a_{ci} + \alpha_j a_{cj})^{0.5} (1 - k_{ij})$$

where,

$$\alpha_i = [1 + m_i (1 - (P_c T_c / T_{ci})^{0.5})]^2$$

and,  $m$  is determined from Eq.(4.29).

Using the information determined in Example 5.3 on  $a_{ci}$ ,  $m_i$ ,  $b_m = 0.0643759 \text{ m}^3/\text{kgmol}$ ,  $R = 0.0083144 \text{ MPa.m}^3/\text{kgmol.K}$ , and substituting them in Eq.(E5.4), results in an equation with the pseudo reduced temperature as the only unknown, which gives:

$$P_c T_c = 397.95 \text{ K}$$

The corresponding pseudo critical pressure is,

$$P_c = 3.9985 \text{ MPa}$$

### Rapid Flash Calculations

Mathematical methods and associated problems in solving equilibrium flash equations have been extensively studied [17, 3-8]. Particular considerations have been given to development of robust and efficient algorithms for application in compositional reservoir simulation.

In the numerical simulation of reservoir processes, finite difference methods are commonly employed where the reservoir is described by many equilibrium cells. The fluid conditions in each cell at each time step is determined by equilibrium flash calculations, using compositional

models and complex iteration procedures. For a large reservoir, the total number of equilibrium flashes may exceed many hundred thousands, resulting in expensive computation. Hence, the reduction of computational time of flash calculations is an important consideration in compositional reservoir simulation.

The number of equations describing the equilibrium between the phases increases with the number of components. Reservoir fluids are composed of many compounds. The common method of reducing the computational time is to group fluid components (Section 9.1), describing the fluid by a few pseudo components. The main draw back of this method is the loss of detailed compositional information on produced reservoir fluids, which is often required in the design and operation of fluid processing plants at the surface.

Michelsen [18] has shown that the number of equations to be solved in flash calculations, using a cubic equation of state, can be reduced to three for two parameter EOS, with little additional complexity, regardless of the number of components when no binary interaction parameter is used in the mixing rules (Section 4.3). For example, the implementation of the method using the Peng-Robinson EOS is as follows:

With no binary interaction parameter, the random mixing rule for the attractive term  $a$ , Eq.(4.78), reduces to,

$$a = \sum_{i=1}^N \sum_{j=1}^N z_i z_j (a_i a_j)^{\frac{1}{2}} = \left( \sum_{i=1}^N z_i a_i^{\frac{1}{2}} \right)^2 = (a')^2 \quad (5.14)$$

$$\text{where: } a' = \sum_{i=1}^N z_i a_i^{\frac{1}{2}}, \text{ and } a_i' = a_i^{\frac{1}{2}}$$

Substituting the above in Eq.(E4.2), the fugacity coefficient can be expressed as,

$$\ln \phi_i = q_0 + q_1 a_i' + q_2 b_i \quad (5.15)$$

where  $q_0, q_1, q_2$  depend only on the mixture properties,  $a', b, T$  and  $P$  as,

$$q_0 = -\ln \left[ \frac{P(v-b)}{RT} \right]$$

$$q_1 = -\frac{a'}{\sqrt{2}(bRT)} \ln \left[ \frac{v + (\sqrt{2} + 1)b}{v + (1 - \sqrt{2})b} \right]$$

$$q_2 = \frac{1}{b} \left( \frac{Pv}{RT} - 1 \right) + \frac{a'}{2b} q_1$$

The molar volume,  $v$ , is determined conveniently using EOS at given values of  $a', b, T$  and  $P$ .

Multiplying Eq.(5.2) by  $a_i'$ , and summing up for all the components, we get,

$$\sum z_i a_i' = n^v \sum y_i a_i' + (1 - n^v) \sum x_i a_i' \quad (5.16)$$

or,

$$a^F = n^V a^{V'} + (1 - n^V) a^{L'} \quad (5.17)$$

where indices F, V and L refer to the feed, vapour and liquid phases respectively.

Similarly for parameter, b, we obtain,

$$b^F = n^V b^{V'} + (1 - n^V) b^{L'} \quad (5.18)$$

Hence, for a set of  $a^{V'}$  and  $b^{V'}$ , the EOS parameters of the liquid phase can be determined from,

$$a^{L'} = \frac{a^F - n^V a^{V'}}{1 - n^V} \quad (5.19)$$

and

$$b^{L'} = \frac{b^F - n^V b^{V'}}{1 - n^V} \quad (5.20)$$

The computational procedure, as suggested by Michelsen, which involves only the three independent variables  $a^{V'}$ ,  $b^{V'}$  and  $n^V$ , is as follows:

- (1) At the given T and P, evaluate  $a_i^L$  and  $b_i^L$  for each component and calculate  $a^F$  and  $b^F$ . Estimate the values of  $a^{V'}$ ,  $b^{V'}$  and  $n^V$ .
- (2) Calculate  $a^{L'}$  and  $b^{L'}$  from Eqs.(5.19-20) and evaluate  $\phi_i^{L'}$  and  $\phi_i^{V'}$  from Eq.(5.15). Calculate  $K_i = \phi_i^{L'} / \phi_i^{V'}$ , and  $x_i$  and  $y_i$  from Eqs.(5.4) and (5.5).
- (3) Evaluate check functions,

$$e_1 = \sum (y_i - x_i)$$

$$e_2 = \frac{\sum y_i a_i^{V'}}{a^{V'}} - 1$$

$$e_3 = \frac{\sum y_i b_i^{V'}}{b^{V'}} - 1$$

If any of the above values is more than its selected tolerance, perform an **iterative correction** of  $a^{V'}$ ,  $b^{V'}$  and  $n^V$ , then return to step (2), otherwise the solution has reached.

Figure 5.3 shows the variation of the computer CPU time vs. the number of components for predicting equilibrium conditions of a black oil when contacted with a rich gas at 373 K and 20.79 MPa in four consecutive stages, simulating the advancement of injected gas in a reservoir [19]. The number of components describing the 25 component mixture has been reduced by grouping them. The figure demonstrates that the CPU time required by the conventional formulation, using a quasi-Newton method, is about two orders of magnitude higher than the Michelsen method with no BIP when the mixture is described by 25 components. Note that the computational time decreases sharply for the conventional method when the number of components describing the fluid decreases, whereas the reduction for the Michelsen method is insignificant. The reduction in computational time by employing the

Michelsen method depends also on the mathematical methods used to solve the set of equations. The improvement could be less striking with methods more efficient than the one used in the above example.

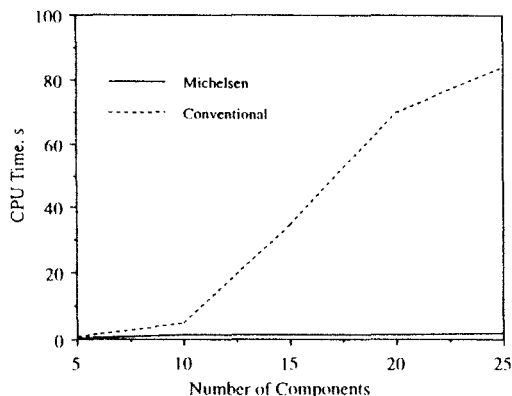


Figure 5.3. Comparison of computational time between the conventional and Michelsen methods.

The proposed method of estimating the parameters of the vapour phase to initialise calculations, described in Step (1) above, may lead to lack of convergence for gas condensate systems. In flash calculation of vapour-like fluids, it is advisable to estimate  $a^L$ ,  $b^L$  instead of those for vapour. Then the values for the vapour will be calculated from equations equivalent to Eqs.(5.19-20) as follows,

$$a^{v} = \frac{a^F - (1 - n^v)a^L}{n^v} \quad (5.21)$$

and

$$b^v = \frac{b^F - (1 - n^v)b^L}{n^v} \quad (5.22)$$

The check functions in Step (3) should also be changed accordingly, and evaluated for the liquid parameters. The above modification improves the robustness of the Michelsen method for gas condensate fluids [20].

The implementation of zero binary interaction parameter for hydrocarbon-hydrocarbon compounds of reservoir fluids is quite reasonable, as pointed out in Section 4.3. However, for fluids with significant concentrations of non-hydrocarbon components, such as  $\text{CO}_2$ , the use of binary interaction between non hydrocarbon-hydrocarbon is required. In such cases, for any non-hydrocarbon component two additional equations will be included which must be solved simultaneously with the three equations. The advantage of the simplified method is expected, therefore, to be minimal in such cases.



## 5.2 STABILITY ANALYSIS

The requirement of minimum Gibbs energy, at equilibrium conditions leads to the uniformity of the chemical potential, hence, uniformity of the fugacity, of each component throughout all co-existing phases, as described in Chapter 3. A set of material balance equations and equality of fugacity, similar to those given in the above section for vapour-liquid equilibria, are in general adequate to determine equilibrium conditions in most petroleum engineering problems. The number of phases at equilibrium, however, must be known.

It is not generally difficult to identify a reservoir fluid as a liquid-like or a vapour-like mixture from its composition, with the exception of near critical fluids. Hence, the saturation pressure can be calculated at a given temperature, as shown in the above section. The fluid is considered to form two phases, except for lean gas mixtures, below its saturation pressure. This approach should suffice for most flash calculations. However, one can consider many cases where more than two phases are present at equilibrium. The occurrence of three phase systems in rich CO<sub>2</sub> fluids, and precipitation of asphaltenes and waxes are common examples. Water is almost always present in reservoirs as a liquid phase separate from the hydrocarbon rich liquid phase. The presence of water at low temperature conditions can lead to formation of a number of solid phases of hydrates and ice. Hence, at a given temperature and pressure, the number of phases may not always be known in advance. The Gibbs phase rule, discussed in Section 1.2, does not impose any practical limitation on the number of possible phases, in real reservoir fluids, as they are composed of many components.

The rigorous method of determining the equilibrium at a given pressure and temperature is to find the conditions at which the Gibbs energy of the system is at its global minimum *for all possible combination of phases and component distribution*. This was expressed mathematically in Chapter 3, as

$$(\partial G)_{P,T} = 0, \quad (3.8)$$

and

$$(\partial^2 G)_{P,T} > 0 \quad (3.9)$$

The minimisation of Gibbs energy to determine the equilibrium conditions, and to avoid false solutions, can be illustrated geometrically by examining the Gibbs energy surface for binary systems [21].

Consider a binary system with the composition-pressure diagram, at constant temperature, as shown in Figure 5.4. Note that depending on the mixture composition,  $x^F$ , and pressure,  $P$ , the system can form one, two, or three phases of vapour V, Liquid L1, and Liquid L2, at equilibrium.

The chemical potential of each component within a phase is defined as,

$$\mu_i = (\partial G / \partial n_i)_{T,P,n_{j \neq i}} \quad (3.15)$$

Hence, the molar Gibbs energy,  $g$ , of each phase can be calculated from the above definition as,

$$g = x_1 \mu_1 + x_2 \mu_2 \quad (5.23)$$

where,  $x_i$ , is the mole fraction,

$$x_i = n_i / n \quad (5.24)$$

where  $n$  is the total number of moles in each phase, and  $g = G/n$

The chemical potential of each component, relative to a reference value, can be calculated by thermodynamic relations, Eqs.(3.27) and (3.31), using an appropriate EOS.

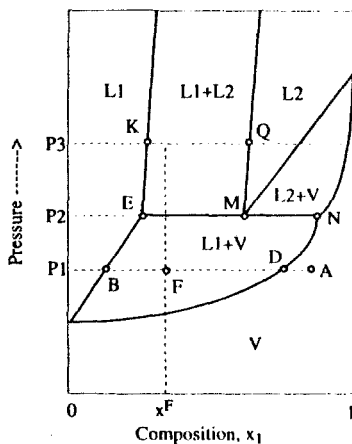


Figure 5.4. Schematic pressure-composition diagram of a binary mixture at constant temperature.

The molar Gibbs energy of the binary system, as a hypothetical single phase fluid, at pressure  $P_1$ , calculated by EOS, is conceptually shown in Figure 5.5.

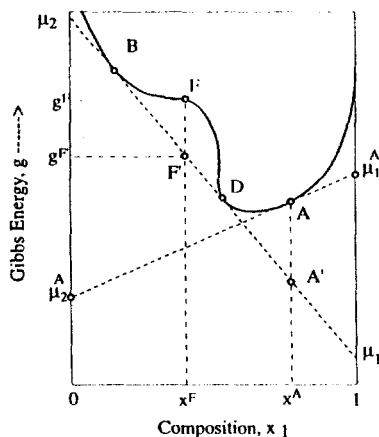


Figure 5.5. Variations of calculated Gibbs free energy with composition at pressure  $P_1$ .

Substituting the chemical potential by its equivalent, that is the derivative of Gibbs energy, in Eq.(5.23), we obtain,

$$\mu_1 = g - x_2(\partial g / \partial x_2) \quad (5.25)$$

and

$$\mu_2 = g - x_1(\partial g / \partial x_1) \quad (5.26)$$

That is, a line tangent to the Gibbs energy curve, for example at point A, intersects the Gibbs energy axis (erected at  $x_i=1$ ) at a value equal to the chemical potential of component  $i$  at the point of tangency, as illustrated in Figure 5.5 by  $\mu_1^A$  and  $\mu_2^A$ .

Hence, for the line tangent to the Gibbs energy surface at two points, B and D, we get,

$$\mu_1^B = \mu_1^D = \mu_1 \quad (5.27)$$

and

$$\mu_2^B = \mu_2^D = \mu_2 \quad (5.28)$$

That is, the liquid phase L1 at point B, and the vapour phase V at point D, Figure 5.4, are at equilibrium.

Now, consider a mixture at point F in Figure 5.4. If the mixture remains a homogeneous single phase, its Gibbs energy is equal to  $g^F$  as shown in Figure 5.5. If it splits into two equilibrated phases of B and D, the mixture Gibbs energy will be reduced to the value at  $F'$ , that is  $g^{F'}$ .

$$G = n g^{F'} = n^B g^B + n^D g^D \quad (5.29)$$

Since the mixture F can attain a lower level of energy by splitting into two phases of B and D, it must be unstable as a single phase. The number of moles of each phase at equilibrium can be determined by material balance (lever rule),

$$n^B + n^D = n \quad (5.30)$$

$$n^B(x_1^D - x_1^F) = n^D(x_1^F - x_1^B) \quad (5.31)$$

The mixture A, however, is a stable single phase because it cannot split into the two phases of B and D, lowering its energy level to that at  $A'$ , due to the material balance restriction,

$$n^B(x_1^D - x_1^A) = n^D(x_1^A - x_1^B) \quad (5.32)$$

which can only be satisfied if the mole number of one of the phases is negative, a physical impossibility.

The above observation can be used to eliminate non-existing phases in flash calculations. It was indicated in Section 5.1 that during vapour-liquid equilibrium calculations, phases with negative mole numbers may appear temporarily during iterations prior to converging to the final solution with all of them positive. However, an ultimate convergence to a solution with a negative phase mole indicates that the system is an under saturated single phase at the given

temperature and pressure. When iterating on the vapour mole fraction,  $n^V$ , a negative value indicates an under saturated gas, a value higher than one indicates an under saturated liquid.

The calculated molar Gibbs energy of the binary mixture, assumed single phase, at pressure  $P_2$  (Figure 5.4) is shown in Figure 5.6. A single line can be drawn tangent to the energy curve at points E, M and N indicating the three equilibrated phases of L1, L2, and V respectively. Any mixture with a composition between those of E and N will split into the three equilibrated phases with the amount of each phase determined by material balance. For example, the mixture F will lower its Gibbs energy from  $g^F$  to  $g^{F'}$ , by forming three co-existing phases. Note that a **wrong** assumption of two-phase equilibrium for the F mixture, such as E-M, or E-N, will also lead to the same overall Gibbs energy level of  $g^{F'}$ . Hence the Gibbs energy minimisation **cannot** identify the number of phases in this case. For a binary system with three equilibrated phases, the degree of freedom is one. Hence, the three phase equilibrium will occur only at  $P_1$ , fixed by the selected temperature, as a unique solution.

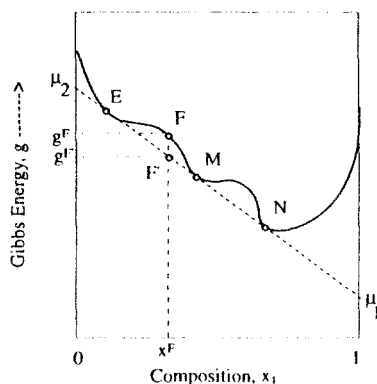


Figure 5.6. Variations of calculated Gibbs free energy with composition at pressure  $P_2$ .

Figure 5.7 shows the mixture molar energy as a hypothetical single phase at pressure  $P_3$  (Figure 5.4) for different compositions. A feed with composition F can split into two different two-phase systems at equilibrium, as shown by the two tangent lines drawn to the Gibbs energy curve. Both identified two-phase systems, satisfy material balance and equality of chemical potential requirements. Although in both cases the mixture energy is reduced relative to the hypothetical single phase condition, only the phases at K and Q, indicating L1 and L2 liquid phases, represent the true solution, with the mixture energy at its lowest possible value of  $g^{F'}$ .

All the above examples lead to this conclusion that a mixture remains a stable single phase when the Gibbs energy surface is concave upward at all concentrations. Otherwise, the mixture may split into equilibrated phases indicated by the points on the Gibbs energy curve with a common tangent. Amongst all the tangent points which satisfy material balance equations, only those by the tangent which identifies the lowest energy level at the mixture composition correspond to the true solution.

The above conclusion, reached by examining a binary mixture, is equally valid for multicomponent systems. The geometrical illustration, however, would be impractical, as the Gibbs energy curve becomes a hyper surface with tangent hyper planes. Nevertheless, the analysis indicates that the tangent plane criterion is a necessary and sufficient condition for equilibrium.

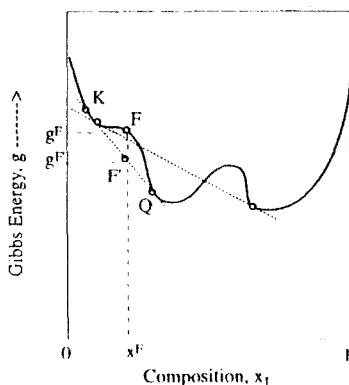


Figure 5.7. Variations of calculated Gibbs free energy with composition at P3.

The determination of the Gibbs energy surface and all the associated tangent points is relatively a simple task for binary mixtures, but not a practical proposition for multicomponent systems. The tangent plane criterion has, however, been used by many investigators to develop numerical implementation of stability analysis[22-24].

The method developed by Michelsen [22] can be successfully applied to various multiphase equilibria problems. The method is schematically as follows:

1. A plane is drawn tangent to the Gibbs energy surface at the feed composition.
2. A second phase is assumed to be present. Its composition is so determined that the tangent plane at that point on the Gibbs surface becomes parallel to the first plane.
3. If the second plane, for all possible compositions, was found to be above the first one, the original mixture is stable, otherwise it is considered to split into two phases, and flash calculations are subsequently performed.
4. For one of the phases obtained by equilibrium flash calculations, the above steps are repeated until all the phases are found to be stable. As the previously determined phases share the same tangent plane, the stability analysis should yield identical results irrespective of the selected phase.

The crucial element in the above procedure is the second step, that is determination of the second tangent plane. It was demonstrated in Figure 5.5 that the tangent line intersects the Gibbs energy axis at a value equal to the chemical potential of that component at the point of tangency. The distance between the two parallel tangent lines, therefore, is equal to the difference between the chemical potentials of each component at the points of tangency. Note that the difference is the same for both components as the lines are parallel. The same conclusion is valid for multicomponent mixtures, that is,

$$\mu_i^y - \mu_i^x = \lambda \quad i=1,2,\dots,N \quad (5.33)$$

where,  $\lambda$ , is the distance between the two parallel planes tangent to the Gibbs surface at the two phases of y, and x. If the mixture x, is to be stable, the value of  $\lambda$ , must be non-negative for all possible compositions of mixture y.

Substituting for chemical potential, Eqs.(3.27) and (3.28), in the above,

$$RT[\ln(Py_i\phi_i^y) - \ln(Px_i\phi_i^x)] = \lambda \quad i=1,2,\dots,N \quad (5.34)$$

where  $y_i$ , and  $x_i$ , are the compositions of the searched mixture,  $y$ , and the feed,  $x$ , with fugacity coefficients  $\phi_i^y$ , and  $\phi_i^x$ , respectively.

Expanding the above equation, and defining a new variable,  $Y_i$ , as,

$$Y_i = y_i \exp(-\lambda / RT) \quad (5.35)$$

where,

$$y_i = Y_i / \sum_1^N Y_i \quad (5.36)$$

we get,

$$\ln Y_i + \ln \phi_i^y - \ln x_i - \ln \phi_i^x = 0 \quad i=1,2,\dots,N \quad (5.37)$$

The mixture  $x$  is stable provided that  $\sum Y_i \leq 1$  at all solutions of the above equation, as it indicates a non-negative  $\lambda$ . At  $\sum Y_i = 1$ ,  $\lambda=0$ , and the two tangent planes are identical, that is, the mixture,  $x$ , is at its saturation conditions in equilibrium with an infinitely small amount of phase,  $y$ .

The method of solution of Eq.(5.37) is similar to the conventional two-phase equilibrium flash, as it can be presented by,

$$Y_i / x_i = \phi_i^x / \phi_i^y = K_i \quad (5.38)$$

It is not, however, restricted by material balance equations. Note that  $Y_i$  is not the mole fraction, but can be interpreted as a measure of the mole number in phase,  $y$ , as described by Eq.(5.36). Locating all the solutions to Eq.(5.37) requires a global search.

For a two-phase vapour-liquid analysis, the composition of the new phase may be estimated from,

$$Y_i = K_i x_i \quad (5.39)$$

or

$$Y_i = x_i / K_i \quad (5.40)$$

for liquid-like and vapour-like mixtures, respectively. For near critical fluids where the nature of fluid cannot be clearly identified, both estimates should be considered, as one could converge to the trivial solution of  $y=x$ .

The Wilson equation, Eq.(3.66) can be used to estimate  $K$  values for vapour-liquid equilibrium, but for liquid-liquid, or solid phases other estimates are required. Michelsen [25] suggests that the initial estimate of the new phase composition is not crucial, and pure phases only composed of the lightest or the heaviest components can be selected for hydrocarbon

mixtures. Examples can be found where such initial guesses may miss a possible solution. Further information on the selection of initial estimates and associated numerical methods of solving Eq.(5.37) are given by Michelsen [25].

An additional benefit of applying the above procedure is that when the lack of stability is verified by converging to a solution with  $\sum Y_i > 1$ , the converged  $K_i$  values may provide appropriate initial estimates for subsequent flash calculations. This provision could help equilibrium calculations near the critical point where close estimation of initial equilibrium ratios becomes essential.

The above approach of stability analysis which starts with a single phase may become quite time consuming when more than two phases are expected to exist at a given pressure and temperature. For example, in transportation of unprocessed well stream fluids through a pipeline, at least three phases of vapour, hydrocarbon liquid, and water are generally present. At low temperature conditions, such as at the sea bed temperature in offshore production, the formation of hydrate, wax and asphaltene phases are a strong possibility. An equilibrium study of this problem necessitates the existence of at least four phases in typical pipeline conditions. An alternative approach [26], based on the tangent plane criterion, is to assume a reasonable maximum number of phases at equilibrium, and then search for the non-existing phases using material balance restrictions, as discussed in the negative flash approach.

### Stability Limit

The formation of a new phase is generally preceded by some degree of supersaturation. The bubble nucleation in a liquid at a pressure below its bubble point value can be inhibited to a large extent by expanding the liquid gradually, avoiding fluid agitation, and ensuring the lack of minute gas pockets in the liquid prior to the expansion. Such systems are metastable with an energy level which will be reduced by forming a new phase.

Figure 5.8 shows the variation of total volume with pressure for a pure fluid at temperatures below its critical point. At temperature  $T_1$ , the reduction of pressure results in a stable expansion of the undersaturated fluid down to A, i.e., saturated liquid. Further expansion should result in generation of an additional phase B, a saturated vapour, forming a stable two-phase system at equilibrium with liquid. The formation of the vapour phase at point A may, however, be inhibited or delayed, resulting to further expansion of the liquid as a metastable phase, shown by the dotted line in Figure 5.8. A similar behaviour can be envisaged by starting with a single phase vapour and compressing it to a volume lower than that at B.

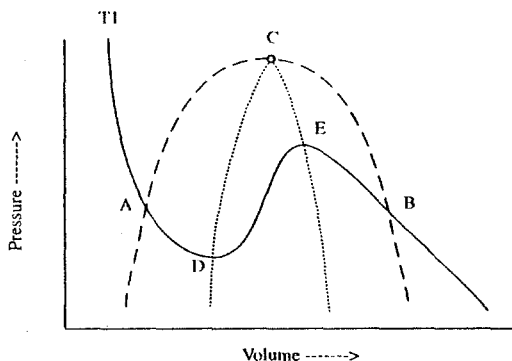


Figure 5.8. Stability limit for a pure fluid.

Assuming a continuous transition from one phase to another, which will not physically occur except at the critical point, a minimum and a maximum pressure, at points D and E respectively, will be expected. This behaviour is also predicted by a cubic equation of state, when the phase change is neglected, as shown in Figure 4.1. The expansion of the liquid phase passed D should result in increase of pressure which is not mechanically feasible. A similar argument is valid for compression of the vapour passed E. These points are referred to as the limits of *intrinsic stability* as they indicate the boundary for a metastable single phase fluid. The curves formed by the two limits at various temperatures below the critical temperature, as shown in Figure 5.8, are called the *spinodal curves*. Note that the gap between the upper and lower intrinsic stability limits decreases with temperature and vanishes at the critical point. Indeed, the stability limit and the phase boundary coincide at the critical point.

The above description of mechanical stability for a pure substance is a special case of the general criterion for stability as given by Eq.(3.9). The intrinsic stability limit, is the condition at which the reduction of Gibbs energy is just to be violated, that is,

$$d^2G = 0 \quad (5.41)$$

Figure 5.9 shows the stability limit for a binary system on the Gibbs energy plot at constant pressure and temperature. Note that while the mixture F must form two phases of B and A at equilibrium to be stable, it can remain as a metastable single phase. An increase of  $x_1$  will force the mixture further into the metastable region till it reaches point N, where an inflection point on the  $g$  curve exists. That will be the limit of intrinsic stability, and the mixture must split into two phases of B and A.

The above criterion can be expressed in terms of other energy parameters, such as the Helmholtz or the internal energy. They are all equivalent to describing the thermodynamic stability limit as the bound outside which entropy will decrease in real processes, a violation of the second law of thermodynamics, see Section 3.1.

The determination of intrinsic stability limit provides information on the limit of supersaturation of a reservoir fluid in a depletion process. The condition of intrinsic stability is a subcase of the tangent plane condition. Whereas in the latter, a global search is required, the former can be identified simply by evaluating the 'g' surface at the feed conditions.

A main application of determining the intrinsic stability limit is in determination of the critical point by an equation of state. It was noted in Figure 5.8, that the binodal curve and the phase envelope meet at the critical point. This feature has been used successfully to determine the critical point of multi component systems, as both the binodal curve and the phase envelope can be expressed by energy terms, similar to those in Eqs.(3.8), and (5.41), and rigorously calculated using thermodynamic relations.

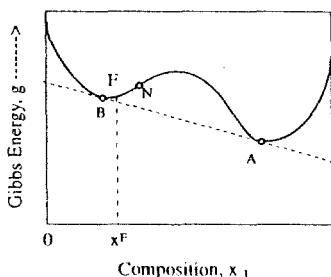


Figure 5.9. Intrinsic stability limit of a binary mixture at constant pressure and temperature.



*Example 5.6.*

Prove that the mechanical stability limit for a pure compound, as described in Figure 5.8, can be derived by the general energy concept. Find the stability limit of normal hexane at 473.0 K, using the Soave-Redlich-Kwong EOS (SRK).

*Solution:*

Describing the stability limit criterion, Eq.(5.41), in terms of the Helmholtz energy, Eq.(3.12), with variables of temperature and volume, we obtain,

$$d^2\Lambda=0$$

where,

$$d\Lambda = -SdT - PdV + \sum_i \mu_i dn_i$$

For a pure compound at constant temperature the above reduces to,

$$d\Lambda = -PdV$$

Hence,

$$(\partial^2 \Lambda / \partial V^2)_T = -\frac{1}{n} (\partial P / \partial v)_T = 0$$

That is, the stability limits for the vapour and liquid phases of a pure compound lie at the maximum and minimum pressure values, respectively, on the isotherm as described by EOS.

Calculating the derivative of pressure with respect to volume at constant temperature, using SRK, we obtain,

$$v^4 + (2b - 2a/RT)v^3 + (b^2 + 3ab/RT)v^2 - ab^3/RT = 0$$

The EOS parameters for normal hexane are calculated at 473.0 K as follows:

Tc K	Pc MPa	$\omega$	$a_c$ MPa.(m <sup>3</sup> /kgmol) <sup>2</sup>	m	$\alpha$	a MPa.(m <sup>3</sup> /kgmol) <sup>2</sup>	b m <sup>3</sup> /kgmol
Equation			4.22	4.25	4.23	$a_c \alpha$	4.22
507.6	3.025	0.2659	2.517012	0.938436	1.066155	2.683527	0.120877

Substituting the values of a and b in the above equation results in,

$$v^4 - 1.1229661v^3 + 0.26205757v^2 - 0.00120518 = 0$$

with the roots as:

$$\begin{aligned} v_1 &= -0.06014 \text{ m}^3/\text{kgmol} \\ v_2 &= 0.08275 \text{ m}^3/\text{kgmol} \\ v_3 &= 0.30412 \text{ m}^3/\text{kgmol} \\ v_4 &= 0.79623 \text{ m}^3/\text{kgmol} \end{aligned}$$

The first two roots are not acceptable, i.e., one negative and the other smaller than  $b=0.120877 \text{ m}^3/\text{kgmol}$ , whereas the third and fourth roots represent the volume limits

for liquid and vapour phases, respectively. The associated pressures at the stability limits can simply be determined from SRK by substituting the values of volume and temperature,

$$P^L = 0.6995 \text{ MPa}$$

$$P^V = 2.148 \text{ MPa}$$

### 5.3 CRITICAL POINT CALCULATIONS

Variations of fluid compositions in a reservoir may result in the critical state. Practical examples are miscible gas displacement fluids (Chapter 7), and fluid columns in reservoirs exhibiting severe compositional grading with depth, which will be discussed in Section 5.4. There exist numerous combinations of mixture constituents which produce critical fluids at any given set of pressure-temperature in multicomponent systems. The critical pressure and temperature of a mixture with fixed composition, however, are unique and can be identified relatively reliably both experimentally and also by various prediction methods.

Determination of the true critical point of a reservoir fluid may not be of much interest to a practising engineer, but it can be quite useful in studying the behaviour of near critical volatile oil and gas condensate systems. Calculations of vapour-liquid equilibria for these fluids near the saturation pressure is difficult, particularly if the equation of state describing both phases is to be calibrated, or so-called *tuned* (see Section 9.3), against experimental data. A knowledge of the critical point can be used to identify problem areas and avoid unnecessary numerical complications.

The pseudo critical properties of a mixture are conveniently calculated by mixing the critical properties of its constituents. The most common approach is molar mixing (Kay's rule),

$${}_p\theta_c = \sum_i z_i \theta_{ci} \quad (1.14)$$

where  $z_i$  is the mole fraction,  ${}_p\theta_c$  is any pseudo critical property, such as temperature, pressure, or volume, and  $\theta_{ci}$  is the critical property of component  $i$ . The true critical properties are, however, different from the pseudo values.

The concept of excess critical property, defined as the difference between the actual value and the calculated value by the ideal mixing rule of Eq.(1.14), has been used to predict critical properties. Teja et al. [27] used a modified Wilson equation successfully to describe the excess properties. Mixing rules, incorporating experimentally determined interaction coefficients, have also been suggested [28] to predict critical properties. The main disadvantage of all the empirical methods is that the predicted critical properties may not be consistent with the fluid phase envelope as predicted by EOS. Therefore, they fail the whole purpose of the exercise.

Rigorous thermodynamic methods, using EOS, can be applied to predict the critical point. The approach is not only more reliable than using empirical correlations [29], but also provides consistent data with the phase envelope predicted by the same EOS.

The Gibbs criteria for the critical point lead to the search for a stable point which lies on the stability limit as schematically shown in Figure 5.8, and expressed by Eq.(5.41). Peng and Robinson [30] applied the method by calculating the Gibbs energy derivatives using the Peng-Robinson EOS. The method was evaluated by predicting the critical pressure and temperature of 32 multicomponent mixtures, which resulted to the average absolute deviations of 2.33% and 1.31%, respectively, in comparison with the experimental data. The method requires the evaluation of third derivatives of the Gibbs energy with respect to concentrations of components, which form elements of a number of high order determinants, hence, computationally quite demanding.

Heidemann and Khalil [31] proposed applying the critical point criteria as stated by variations of Helmholtz energy, instead of the Gibbs energy, because it leads to less complex equations when pressure explicit cubic EOS are used:

$$L = \begin{vmatrix} A_{11} & A_{12} & \dots & A_{1N} \\ A_{21} & \dots & \dots & \dots \\ \dots & \dots & \dots & \dots \\ A_{N1} & A_{N2} & \dots & A_{NN} \end{vmatrix} = 0 \quad (5.42)$$

$$M = \begin{vmatrix} \Lambda_{11} & \Lambda_{12} & \dots & \Lambda_{1N} \\ \dots & \dots & \dots & \dots \\ \Lambda_{N-1,1} & \Lambda_{N-1,2} & \dots & \Lambda_{N-1,N} \\ \partial L / \partial n_1 & \partial L / \partial n_2 & \dots & \partial L / \partial n_N \end{vmatrix} = 0 \quad (5.43)$$

where,

$$A_{ij} = \left( \frac{\partial^2 A}{\partial n_i \partial n_j} \right)_{T,V} \quad (5.44)$$

That is,  $A_{ij}$  are the second derivatives of the total Helmholtz energy with respect to moles at constant temperature and total volume. The definition of the Helmholtz energy is given in Eq.(3.12), and it can be calculated, similar to the Gibbs energy, using EOS.

Later Michelsen and Heidemann [32] proposed a more computationally efficient procedure to solve the above equations particularly when all binary interaction coefficients are set equal to zero. The computational effort in determining the critical point by EOS is comparable to that of an equilibrium flash [13].

Model fluids, often binary systems, are frequently tested in laboratories to investigate fluid behaviour. Estimated critical properties of these simple mixtures are useful in designing mixture compositions and test conditions. The critical temperature is particularly valuable in designing tests to simulate liquid-like, or vapour-like behaviour. Simple empirical correlations are adequate in most cases.

A simple method to estimate the true critical temperature is to use the Li's mixing rule [33]:

$$T_c = \sum_i \lambda_i T_{ci} \quad (5.45)$$

The effective concentration,  $\lambda_i$ , is defined as,

$$\lambda_i = \frac{z_i v_{ci}}{\sum_i z_i v_{ci}} \quad (5.46)$$

where  $z_i$  and  $v_{ci}$  are the mole fraction and critical molar volume of component  $i$ , respectively. The method was tested for 135 binary hydrocarbon mixtures, with an average deviation of less than 4 K, increasing to 11 K for multicomponent systems [34]

Empirical correlations generally fail to predict the critical pressure of multicomponent systems as its relation with the concentration of fluid components is highly non-linear. Figure 1.12 clearly demonstrates such complexity as the mixture critical pressure is mostly higher than those of the comprising compounds.

A simplified correlation of Kreglewski and Kay [35] can be used to estimate the critical pressure as follows:

$$P_c = p P_c \left[ 1 + (5.808 + 4.93\omega) \left( \frac{T_c}{p T_c} - 1 \right) \right] \quad (5.47)$$

where  $p P_c$  and  $p T_c$  are the mixture pseudo critical pressure and temperature calculated by Eq.(1.14), respectively, and  $\omega$  is the molar average acentric factor.

The correlation estimated the critical pressure of 967 mixtures with an average error of 1.3 bar [29]. Mixtures containing methane were not included in the evaluation, because of the lack of reliability of the correlation, similar to other available correlations, for such systems. The locus of critical points of binary mixtures as shown in Figure 1.12 or Figure D1, Appendix D, can be used for rough estimation of the critical pressure of mixtures containing methane.

The simple molar averaging of critical compressibility factors of fluid components generally provides reasonable estimates for hydrocarbon mixtures. The estimated critical compressibility factor, temperature and pressure can be used to predict the mixture critical volume,

$$v_c = Z_c R T_c / P_c \quad (5.48)$$

#### Example 5.7.

Estimate the critical properties of a mixture of ethane-normal heptane (60:40 mole%), using the critical properties of pure constituents and reasonable mixing rules.

#### Solution:

The properties of pure components are read from Table A.1 in Appendix A, and average values are calculated as follows:

component	$T_c$ , K	$P_c$ , MPa	$v_c$ , m <sup>3</sup> /kgmol	$Z_c$	$\omega$	$x_i$	$\lambda_i$
ethane	305.32	4.872	0.1455	0.2793	0.0995	0.6000	0.3377
n-heptane	540.2	2.74	0.428	0.2611	0.3495	0.4000	0.6622

component	$\lambda_i T_c$	$x_i T_c$	$x_i P_{ci}$	$x_i \omega_i$	$x_i Z_i$	$x_i v_{ci}$
ethane	103.11	183.19	2.923	0.0597	0.16758	0.0873
n-heptane	357.76	216.08	1.096	0.1398	0.10444	0.1712
Sum	460.87	399.27	4.019	0.1995	0.27202	0.2585

The calculated critical temperature of 461 K agrees with the reported value of 460 K [36], whereas the pseudo value of 399 K does not.

Substituting the above values in Eq.(5.47), we get  $P_c=8.22$  MPa which is in reasonable agreement with the reported value of about 7.80 MPa [36]. The pseudo critical pressure of 4.02 MPa is markedly deviated. Applying  $P_c=Z_cRT_c/v_c$  and using the molar average compressibility factor of 0.2720, and the critical volume of 0.2585 m<sup>3</sup>/kgmol result in an unacceptable value of  $P_c=4.03$  MPa.

## 5.4 COMPOSITIONAL GRADING

It was pointed out that lateral and vertical compositional variations within a reservoir are expected during the early reservoir life. One might expect the reservoir fluids to have attained equilibrium at maturity due to molecular diffusion and mixing over geological times. However, the diffusive mixing may require many tens of million years to eliminate compositional heterogeneities. When the reservoir is considered mature, it is often assumed that fluids are at equilibrium. At uniform temperature and pressure, that is, when the thermal and mechanical equilibrium are established, the above assumption leads to the uniformity of fugacity of each component throughout all co-existing phases as the requirement for the chemical equilibrium (Section 3.1). For a single phase fluid, the uniformity of fugacity is equivalent to the uniformity of concentration.

The pressure and temperature, however, are not uniform throughout a reservoir. The temperature increases with depth with a gradient of about 0.02-0.03 K/meter, and even much higher in extreme cases. The pressure also changes according to the hydrostatic head for fluids at rest. Therefore, compositional variations within a reservoir, particularly those with a tall column of fluid should be expected.

Table 5.1 shows the fluid composition of a North Sea reservoir at different depths [37]. Note that the methane concentration has decreased from 72.30 mole% to 54.92 mole% over a depth interval of only 81 meters. Such a major change of composition cannot be ignored as it strongly affects the estimation of reserve, and production planning.

In general, the mixture is expected to get richer in heavier compounds, containing less of light components, such as methane, with depth. The variations of composition and temperature of fluid with depth result in changes of saturation pressure with depth. The oil saturation pressure generally decreases with decreasing methane concentration, whereas the gas condensate dew point increases with increasing heavy fractions.

Table 5.1. Variations of fluid composition with depth in a reservoir.

Fluid	D, Well 1	C, Well 2	B, Well 2	A, Well 2
Depth (meter subsea)	3136	3156	3181	3217
Nitrogen	0.65	0.59	0.60	0.53
Carbon Dioxide	2.56	2.48	2.46	2.44
Methane	72.30	64.18	59.12	54.92
Ethane	8.79	8.85	8.18	9.02
Propane	4.83	5.60	5.50	6.04
i-Butane	0.61	0.68	0.66	0.74
n-Butane	1.79	2.07	2.09	2.47
n-Pentane	0.75	0.94	1.09	1.33
Hexanes	0.86	1.24	1.49	1.71
Heptanes	1.13	2.14	3.18	3.15
Octanes	0.92	2.18	2.75	2.96
Nonanes	0.54	1.51	1.88	2.03
Decanes	0.28	0.91	1.08	1.22
Undecanes Plus	3.49	6.00	9.25	10.62
Molecular Weight	33.1	43.6	55.4	61.0
Undecanes plus characteristics				
Molecular Weight	260	267	285	290
Specific gravity	0.8480	0.8625	0.8722	0.8768

The pressure in reservoirs increases with depth. If the saturation pressure remains below the reservoir pressure at all depths, no gas-oil contact exists in the reservoir. The fluid can, however, behave oil-like and gas-like at the low and high sections of the reservoir, respectively, by going through a local critical point. If the saturation pressure at any point becomes equal to the reservoir pressure, the gas oil contact is expected to appear at that point, with compositional grading in both phases, as shown in Figure 5.10.

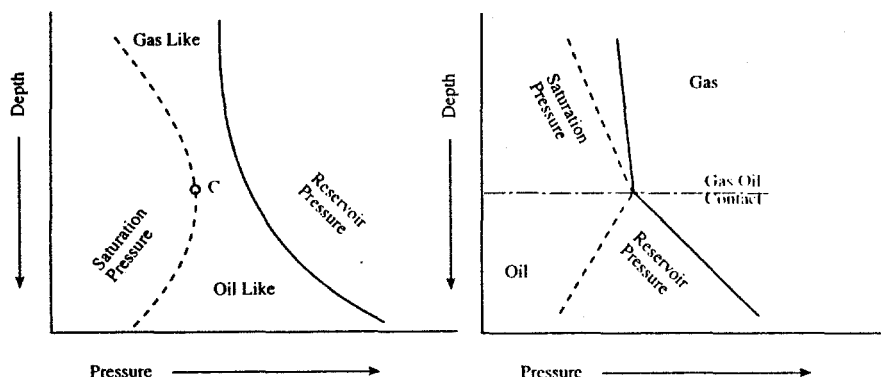


Figure 5.10. Phase variations in reservoirs with compositional grading.

The variations of properties of the reservoir fluid, described in Table 5.1, with depth are given Table 5.2. Note that the hydrocarbon mixture has a bubble point of 37.3 MPa at a depth of 3181 meter subsea, whereas it shows a dew point of 37.8 MPa at 25 meter above that point. The reservoir pressure was above the saturation pressure at all depths, and no gas-oil contact was observed in that reservoir.

The estimation of compositional grading might help evaluating the reliability of fluid samples taken at different depths. Furthermore, the fluid composition and properties at different depths can be predicted when this information is available only within a limited depth interval. The possibility of existence of an oil column under a gas reservoir, or the presence of a number of isolated reservoirs mistaken as a single reservoir can also be investigated.

Table 5.2. Properties of fluids at different depths in the North Sea reservoir.

Fluid	D, Well 1	C, Well 2	B, Well 2	A, Well 2
Depth (meter subsea)	3136	3156	3181	3217
Measured Reservoir Pressure, MPa	44.93	44.89	44.41	45.35
Measured Reservoir Temperature, K	384.2	379.8	380.9	382.0
Density at Res. Pressure, kg/m <sup>3</sup>	400.4	530.8	557.7	573.4
Saturation Pressure, MPa	39.0	37.8	37.3	33.0
Saturation Point	Dew Point	Dew Point	Bub. Point	Bub. Point
Density at Sat. Pressure, kg/m <sup>3</sup>	397.4	503.0	540.0	546.2
Separator Pressure, MPa	6.5	1.6	1.7	1.2
Separator Temperature, °C	285.4	308.1	310.9	290.9
Separator GOR, m <sup>3</sup> /m <sup>3</sup>	1005.0	611.0	390.0	304.0
Tank Oil Specific Gravity	0.7877	0.8170	0.8254	0.8185

The variation of composition with depth in a reservoir can be predicted by assuming equilibrium within the reservoir. In this approach the coupling of thermal and compositional gradient is ignored, and reversible thermodynamic relations are used to account for the effect of

pressure change, due to the hydrostatic head, on the equality of chemical potential as the criterion of chemical equilibrium. A more rigorous approach, however, is to relax the assumption of equilibrium and apply irreversible thermodynamic concepts by considering the coupling of heat and mass diffusion. Both approaches are addressed in this book.

It should be emphasised that the methods are applicable to static and non-depleted reservoirs. In producing reservoirs, the pressure and temperature gradients depend on fluid flow characteristics and cannot be expressed by static gradients. Furthermore dispersion can strongly affect the transfer processes in these reservoirs. In reservoirs depleted below the saturation pressure, the forced and natural convection, due to the developed density variations within each fluid column, can become the dominant factors in controlling the compositional variations in comparison with those imposing thermodynamic equilibrium.

### Equilibrium Assumption

Assigning an average temperature to the fluid column under consideration, the energy equation, Eq.(3.1), for a fluid at rest reduces to,

$$dE = dU + d(mgh) \quad (5.49)$$

where  $m$ , is the mass of the fluid element at the height  $h$ , and  $g$ , is the gravitational acceleration.

Applying thermodynamic relations, similar to the approach used in Section 3.1, will result in equivalent equations, but with an additional energy term due to the gravity. The uniformity of chemical potential of each component throughout the system, Eq.(3.15), will be replaced by,

$$\mu_i^{(1)} + M_i g h^{(1)} = \mu_i^{(2)} + M_i g h^{(2)} = \dots = \mu_i^{(\tau)} + M_i g h^{(\tau)} \quad (5.50)$$

where,  $M$  is the molecular weight, and the superscripts refer to various heights with a total number of selected points designated by  $\tau$ .

Hence for two points along the fluid column, we obtain,

$$\mu_i^{(1)} - \mu_i^{(2)} = -(M_i g h^{(1)} - M_i g h^{(2)}) \quad (5.51)$$

Expressing the difference in chemical potential with that in terms of fugacity as given by Eq.(3.22), we get,

$$RT \ln[f_i^{(1)} / f_i^{(2)}] = -M_i g [h^{(1)} - h^{(2)}] \quad (5.52)$$

or,

$$f_i^{(1)} = f_i^{(2)} \exp \left[ \frac{M_i g (h^{(2)} - h^{(1)})}{RT} \right] \quad i=1,2,\dots,N \quad (5.53)$$

which reduces to Eq.(3.24), that is, equality of fugacity, when the two points are at the same level.

When the composition of a fluid, hence, the fugacities of all its components are known at a point within the reservoir, the composition at any depth could be determined by using the above equation. The fugacities can be calculated by Eq.(3.25) using EOS. When using a two-parameter EOS with the volume shift, Section 4.2.1, the shift parameter should be

included in calculating the fugacities. This is required, as the fugacity coefficient multiplier due to the shift, Eq.(4.33), is different at the two levels.

Montel and Gouel [38] used the Peng-Robinson EOS to estimate the compositional grading in the fluid column reported in Table 5.1. The estimated change in methane concentration due to the gravity over the above depth was only 6 mole%, compared to the reported value of 17 mole%. They attributed part of the deviation to the deficiency of EOS to model the phase behaviour.

Eq.(5.53) suggests that compositional grading becomes more significant when the mixture is composed of molecules with widely different molecular weights. This is of particular significance in oil systems with large concentrations of heavy components such as asphaltenes. The main problem with applying the above method to these fluids is the lack of adequate fluid characterisation. The heavy ends are generally reported as pseudo-components or groups, each composed of many compounds, with an average molecular weight assigned to each group. When compositional grading occurs, the concentration of compounds within each pseudo-component changes, and the use of a fixed value of molecular weight reduces the reliability of the predicted results.

In tall columns, where assigning a uniform average temperature to the whole fluid column will not be justifiable, the reservoir can be divided into segments, each at an average temperature increasing downward. The compositional grading can then be evaluated for each section with calculated composition at the bottom of each section used as that of the top in the adjacent lower section.

### Non-Equilibrium Fluids

The equilibrium criteria, Section 3.1, prohibit the existence of any gradient or flux within a fluid system at equilibrium. As the reservoir temperature increases with depth, producing heat flux, the assumption of equilibrium for a fluid column is not valid. However, if deviations from equilibrium locally are not very large, which is the case in petroleum reservoirs, irreversible thermodynamic concepts may be applied to analyse compositional variations. For such systems, it can be assumed that the equilibrium exists locally, hence, the same thermodynamic functions relating state properties of equilibrium systems will be valid.

Onsager has presented a theory for the systematic investigation of irreversible processes[39]. According to his theory, all driving forces within a system, such as temperature and concentration gradients, can cause fluxes of different natures, such as those of heat and mass. Any force can give rise to any flux. The above statement can be expressed by the general phenomenological relation as,

$$J_j = \sum_{k=1}^{\xi} L_{jk} X_k \quad j=1,2,\dots,\xi \quad (5.54)$$

where  $J_j$  is the flux  $j$ ,  $X_k$  is the driving force  $k$ ,  $\xi$  is the total number of driving forces, and  $L_{jk}$  is called the phenomenological coefficient.

For example, the coefficients  $L_{jj}$  can be the heat conductivity and the diffusion coefficient for the heat flux and the mass flux, respectively. The coefficients  $L_{jk}$  with  $j \neq k$  express the cross or interference phenomena, such as that of mass flux due to thermal gradient (Soret effect), and that of heat flux due to concentration gradient (Dufour effect).

Making proper choices of fluxes and forces, as suggested by Onsager, the matrix of phenomenological coefficients becomes symmetrical.



$$L_{jk} = L_{kj} \quad (5.55)$$

which is referred to as the Onsager reciprocal relations.

For a mixture with  $N$  components, the flux of component  $i$ , and heat  $q$ , are given by the phenomenological equations as,

$$J_i = \sum_{k=1}^N L_{ik} X_k + L_{iq} X_q \quad (5.56)$$

and

$$J_q = \sum_{k=1}^N L_{qk} X_k + L_{qq} X_q \quad (5.57)$$

Defining,

$$L_{qi} = \sum_{k=1}^N L_{ik} Q_k \quad (5.58)$$

we obtain,

$$J_i = \sum_{k=1}^N L_{ik} (X_k + Q_k X_q) \quad (5.59)$$

where  $Q$  is called the *heat of transport*.

Combining the above equations for the fluxes of heat and mass, it can be shown that at the isothermal condition,

$$J_q = \sum_{i=1}^N Q_i J_i \quad (5.60)$$

That is,  $Q_i$  is the heat transported by one unit quantity (mass or mole) of component  $i$ , hence the name *heat of transport*.

As the fluid composition remains unchanged with time, the net flux of each component,  $J_i$ , must be zero. Hence

$$\sum_{k=1}^N L_{ik} (X_k + Q_k X_q) = 0 \quad (5.61)$$

The driving forces for mass,  $X_k$ , and heat,  $X_q$ , can be determined by combining continuity equations for mass, energy, and momentum, and employing thermodynamic relations to determine the rate of entropy production describing irreversible processes [39],

$$X_k = F_k - T \text{grad}(\mu_k / T) \quad (5.62)$$

and

$$X_q = -(\text{grad } T) / T \quad (5.63)$$

where  $F$  is the body force acting on unit mass, and  $\mu$  is the chemical potential.

The chemical potential is a function of fluid pressure, temperature, and composition. Hence,

$$\text{grad} \mu_k = (\partial \mu_k / \partial T)_{p, x_i} \text{grad} T + (\partial \mu_k / \partial P)_{T, x_i} \text{grad} P + \sum_{i=1}^N (\partial \mu_k / \partial x_i)_{p, T, x_{j \neq i}} \text{grad} x_i \quad (5.64)$$

Applying thermodynamic relations to evaluate variations of chemical potential with temperature and pressure, and taking gravity as the only body force acting on the fluid, the following equation is derived by combining Eqs.(5.62-64),

$$\sum_{i=1}^N (\partial \mu_k / \partial x_i)_{p, T, x_{j \neq i}} \text{grad} x_i = (M_k - \rho v_k)g - Q_k^* (\text{grad} T / T) \quad (5.65)$$

where  $v_k$  is the partial molar volume of the component  $k$ ,  $\rho$  is the mixture density, and  $Q^*$  is defined as,

$$Q_k^* = Q_k - h_k \quad (5.66)$$

where,  $h_k$  is the partial molar enthalpy.  $Q^*$  is called the pure heat of transport, as it does not include the energy transferred by the mass, expressed by the enthalpy term.

Neglecting the thermal gradient, Eq.(5.65) reduces to the conventional equation expressing the compositional gradient due to gravity effect,

$$\sum_{i=1}^N (\partial \mu_k / \partial x_i)_{p, T, x_{j \neq i}} \text{grad} x_i = (M_k - \rho v_k)g \quad (5.67)$$

which will reduce to Eq.(5.52) when applied to two points along the fluid column.

Eq.(5.65) relates the compositional gradient to the temperature gradient at any direction, where the vertical variations are only of significance and interest. The density, partial molar volumes, and the variation of chemical potential with composition, can all be determined using an equation of state, Appendix C. The information on the heat of transport, however, is sparse.

### Heat of Transport

Transfer parameters can generally be estimated by methods using concepts of statistical mechanics. Bearman et al. [40] proposed a method to estimate the heat of transport for binary liquid systems. Broadly, the pure heat of transport was presented as the sum of an equilibrium term and a non-equilibrium contribution, where appropriate expressions were developed for each term. Neglecting the non-equilibrium term and assuming the liquid as a regular solution, the expression for  $Q^*$  is as follows,

$$Q_1^* / x_2 = \frac{v_1 v_2}{2v} \left( \frac{L_2}{v_2} - \frac{L_1}{v_1} \right) \quad (5.68)$$

where  $v_1$ , and  $v_2$ , are the partial molar volumes of components 1 and 2, respectively, and  $v$  is the mixture molar volume.  $L$  is the heat of vaporisation,

$$L_i = h_i - h_i^o \quad (5.69)$$

where  $h_i$ , and,  $h_i^0$  are the partial enthalpies of the component  $i$ , in the mixture and in the ideal gas state, respectively.

Oost et al. [41] applied the above expression, which was developed for liquids, to dense gases with reliable results. Therefore, it may be applied to describe the heat of transport in oil and gas condensate systems.

There is very little information on the heat of transport in multi-component systems. A simple approach is to reduce multi-component mixtures to pseudo-binary systems, as

$$x_m = 1 - x_k \quad (5.70)$$

$$L_m = \sum_{j=1, j \neq k}^N L_j x_j / x_m \quad (5.71)$$

$$v_m = \sum_{j=1, j \neq k}^N v_j x_j / x_m \quad (5.72)$$

where the subscript  $m$ , refers to the pseudo component composed of all components except  $k$ .

Hence, Eq.(5.68) will be as,

$$Q'_k / x_m = \frac{v_k v_m}{2v} \left( \frac{L_m}{v_m} - \frac{L_k}{v_k} \right) \quad (5.73)$$

The partial heat of vaporisation and molar volumes can be calculated by any reliable equation of state, Appendix C.

### Significance

Although some degree of compositional grading due to non-equilibrium is expected in all reservoirs, Eq.(5.65) shows that the effect of gravity and temperature gradient is more significant when  $(\partial \mu_k / \partial x_i)_{p,T, x_{j \neq i}}$  is small. At the critical point, indeed at all the points on the stability limit curve, Eq.(5.41), the determinant of the above derivatives is equal to zero, and profound compositional grading should occur [42].

The measured and predicted, using EOS, critical point of the fluid reported in Table 5.1 at the depth of 3156 meter subsea, were 293 K & 40 MPa, and 363 K & 40 MPa, respectively [38]. Figure 5.11 compares the predicted variation of  $C_{11+}$  of the above fluid with depth at various temperatures when only the grading due to gravity has been considered. Note that as the mixture temperature increases, approaching the critical value, the compositional grading with depth becomes more significant.

The compositional grading, particularly for near critical fluids, have been studied by a number of investigators[38,43,44]. Although the coupling of compositional and thermal gradients have been acknowledged by most of the authors, the lack of adequate information to evaluate the heat of transport has resulted in ignoring the thermal effect in most studies.

Chaback [45] compared the effect of thermal gradient to that of the gravity for an equi-molar mixture of methane and normal butane at a typical reservoir condition of 378 K and 10.34 MPa. Using a value of 333 kJ/kg for the heat of transport of methane [46] and a thermal

gradient of 0.02 K/m, the thermal compositional gradient was estimated to be about half of that due to the gravity, and operating at the opposite direction.

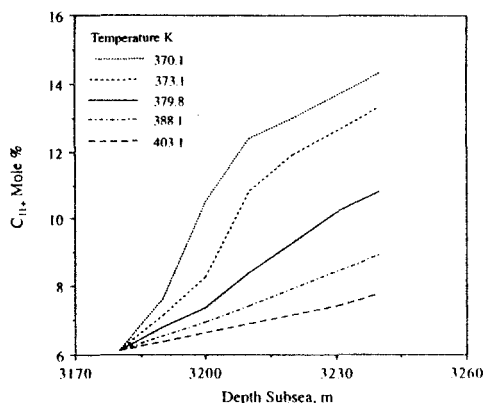


Figure 5.11. Variations of  $C_{11+}$  of Fluid C, reported in Table 5.1, with depth at various temperatures.

Eq.(5.67) shows that the compositional grading due to gravity is more pronounced for mixtures with components of vastly different sizes. The lightest and the heaviest components of a homologue group tend to grade more significantly than intermediate ones, with the heavies more concentrated with depth. Shulte [47] conducted a sensitivity analysis of compositional grading due to gravity, using equations of state, and concluded that aromatics play a major role. Comparing two reservoir fluid mixtures which were only different in the amount of aromatic contents, he showed the tendency of these compounds to concentrate with depth, increasing the concentration of light components at the top. As aromatic compounds are relatively much denser than paraffins and naphthenes with similar molecular weights and volatility, such a conclusion should be expected.

Holt et al. [48] studied the compositional grading by considering both the gravitational and thermal effects and reported similar behaviour for aromatic and paraffin oil systems contrary to the Shulte's conclusion. The reason appears to be due to neglecting the thermal effect by Shulte.

The heat of transport, hence, the thermal effect, depends on the latent heat of vaporisation. Aromatics, due to strong bonding, have higher values of latent heat than paraffins with similar molecular weights. Hence, neglecting the thermal effect for aromatics is a much more severe assumption than that for paraffins. As the thermal and gravitational effects generally operate at opposite directions, such an assumption will exaggerate the compositional grading for aromatics, particularly due to their high density as discussed above.

Table 5.3 shows the composition of two oil samples with different aromatic contents, very similar to those studied by Shulte[47]. The predicted compositional grading of methane, at 361 K and 34.5 MPa, with and without the thermal effect, at 0.02 K/m, for the two fluids is shown in Figure 5.12 [49]. The three parameter Peng-Robinson equation of state, and the heat of transport given by Eq.(5.73) have been used to evaluate the compositional grading. Note a significant increase of methane grading with depth by gravity due to the additional aromatic content, as observed by Shulte. However, when the opposing thermal effect is included, the grading decreases and the difference between the two fluid becomes insignificant.

Table 5.3. Composition of high and low aromatic oil samples.

Component mole%	High Arom.	Low Arom.
N <sub>2</sub>	5	5
CO <sub>2</sub>	5	5
C <sub>1</sub>	52	52
C <sub>2</sub>	8	8
C <sub>3</sub>	5	5
iC <sub>4</sub>	10	10
nC <sub>4</sub>	4	4
iC <sub>5</sub>	1	1
nC <sub>5</sub>	1	1
nC <sub>6</sub>	1	5
benzene	5	2
nC <sub>7</sub>	5	5
toluene	5	2
cyt.cyc.hexane	7	3
nC <sub>10</sub>	2	5
nC <sub>14</sub>	2	5

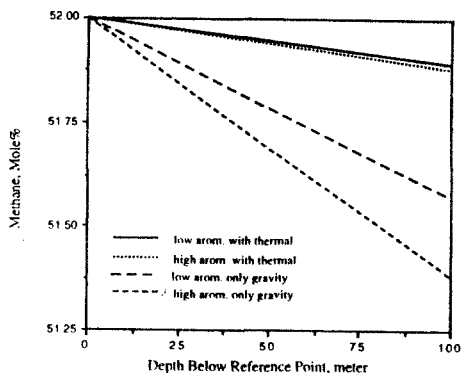


Figure 5.12. Variations of methane concentration with depth, due to combined gravity and thermal effects, and only gravity effect for low and high aromatic fluid samples.

As the thermal and gravitational effects generally oppose each other, it is conceivable that a fluid may maintain the same composition with depth. Figure 5.13 shows the predicted concentration of methane with depth at various temperature gradients. Note that at a thermal gradient of around 0.025 K/m, the compositional grading in the above high aromatic oil is insignificant. At higher thermal gradients, methane concentration may even increase with depth.

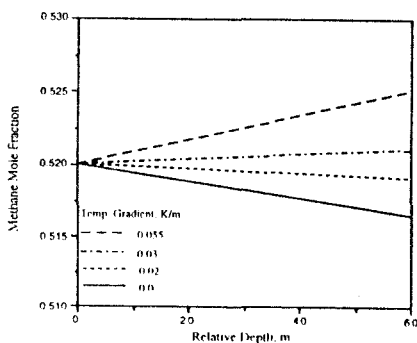


Figure 5.13. Variations of methane concentration with depth due to combined gravity and thermal effects, at various temperature gradients.

## 5.5 REFERENCES

1. Rachford, H.H. and Rice, J.D: "Procedure for Use of Electronic Digital Computers in Calculating Flash Vaporisation Hydrocarbon Equilibrium", *Petrol. Technol.*, Sec. 1, 19, Sec. 2, 3 (Oct., 1952).

2. Sage, B.H., Lacey, W.N: "Volumetric and Phase Behaviour of Hydrocarbons", Gulf Publishing Co. (1949).
3. Fussell, D.D. and Yanosik, J.L: "An Iterative Sequence for Phase Equilibria Calculations Incorporating the Redlich-Kwong Equation of State", SPE J., 173-182 (June, 1978).
4. Nghiem, L.X., Aziz, K. and Li, Y.K: "A Robust Iterative Method for Flash Calculations Using the Soave-Redlich-Kwong or the Peng-Robinson Equation of State", SPE J., 521-530 (June, 1983).
5. Mehra, R.K., Heidemann, R.A. and Aziz, K: "An Accelerated Successive Substitution Algorithm", Canadian J. Chem. Eng., 16, 590-596 (Aug., 1983).
6. Pedersen, K.S., Thomassen, P. and Fredenslund, A: "Thermodynamics of Petroleum Mixtures Containing Heavy Hydrocarbons: 3 Efficient Flash Calculation Procedures Using the SRK-Equation of State", I & EC Proc. Des. Dev., 24, 948-954 (1985).
7. Gosset, R., Heyen, G. and Kalitventeff, B: "An Efficient Algorithm to Solve Cubic EOS", J. Fluid Phase Equilibria, 25, 51-64 (1986).
8. Abhvani, A.S. and Beaumont, D.N: "Development of an Efficient Algorithm for 2-Phase Flash Calculations", SPE RES.ENG., 695-702 (Nov., 1987).
9. Xu, D., Danesh, A. and Todd, A.C: "An Accelerated Successive Substitution Method for Calculation of Saturation Pressure of Multicomponent Fluids" Fluid Phase Equilibria, 72, 15-24, (1992).
10. Li, Y.K. and Nghiem, L.X: "The Development of a General Phase Envelope Construction Algorithm for Reservoir Fluid Studies", SPE 11198, Proc. of 57th Ann. Conf. (Sept., 1982).
11. Whitson, C.H. and Michelsen, M.L: "The Negative Flash", J. Fluid Phase Equilibria, 53, 51-71 (1989).
12. Agrawal, R.K., Li, Y.K., Nghiem, L.X. and Coombe, D.A: "Multi-Phase Multi-Component Isenthalpic Flash Calculations with a Cubic Equation of State", JCPT, 30-3, 69-75 (1991).
13. Michelsen, M.L: Private Communications.
14. Edmister, W.C: "Applied Hydrocarbon Thermodynamics", Gulf Pub. (1984).
15. Poling, B.E., Grens II, E.A. and Prausnitz, J.M: "Thermodynamic Properties from a Cubic Equation of State, Avoiding Trivial Roots and Spurious Derivatives", Ind. Eng. Chem. Proc. Des. Dev., 20, 127-130 (1981).
16. Asselineau, L., Bogdanic, G. and Vidal, J: "A Versatile Algorithm for Calculating Vapour-Liquid Equilibria", J. Fluid Phase Equilibria, 3, 273- (1979).
17. Rijkers, M.P.W. and Heidemann, R.A: "Convergence Behaviour of Single-Stage Flash Calculations", Equations of State Theories and Applications, ACS Symposium Series 300, 476-493 (1985).
18. Michelsen, M.L: "Simplified Flash Calculations for Cubic Equations of State", Ind. Eng. Chem. Process Des. Dev., 25(1), 184-188 (1986).

19. Danesh, A., Xu, D.H., Tehrani, D.H. and Todd, A.C: "Improving Predictions of Equation of State by Modifying its Parameters for Super Critical Components of Hydrocarbon Reservoir Fluids", *J. Fluid Phase Equilibria*, 112, 45-61 (1995).
20. Gozalpour, F., Danesh, A., Todd, A.C. and Tehrani, D.H: "Integrated Phase Behaviour Modelling of Fluids in Reservoir-Surface Processes Using Equation of State" SPE 39630, Proc. of the SPE/DOE Improved Oil Recovery Symposium, Tulsa, Oklahoma, 19-22 April (1998).
21. Baker, L.E., Pierce, A.C. and Luks, K.D: "Gibbs Energy Analysis of Phase Equilibria", *SPE J.*, 731-742 (1982).
22. Michelsen M.L: "The Isothermal Flash Problem, Part I, Stability", *J. Fluid Phase Equilibria*, 9, 1-19 (1982).
23. Michelsen M.L: "The Isothermal Flash Problem, Part II, Phase Split Calculation", *J. Fluid Phase Equilibria*, 9, 21-40 (1982).
24. Nghiem, L.X., Li, Y.K. and Heidemann, R.A: "Application of the Tangent Plane Criterion to Saturation Pressure and Temperature Computations", *J. Fluid Phase Equilibria*, 21, 39-60 (1985).
25. Michelsen, M.L: "Phase Equilibrium Calculations, What is Easy and What is Difficult?", *Computers Chem. Eng'ng.*, 17, No. 5/6, 431-439 (1993).
26. Avlonitis, D: "Thermodynamics of Hydrate Equilibria", PhD Thesis, Department of Petroleum Engineering, Heriot-Watt University, Edinburgh (1992).
27. Teja, A.S., Garg, K.B. and Smith, R.L: "A Method for the Calculation of Gas-Liquid Critical Temperatures and Pressures of Multicomponent Mixtures", *Ind. Eng. Chem. Process Des. Dev.*, 22, 672-676 (1983).
28. Chueh, P.L. and Prausnitz, J.M: "Vapour-Liquid Equilibria at High Pressures: Calculation of Critical Temperatures, Volumes and Pressures of Nonpolar Mixtures", *AIChE*, 13(6), 1107-1113 (1967).
29. Reid, R.C., Prausnitz, J.M. and Poling, B.E: "The properties of Gases and Liquids", 4th Ed., McGraw-Hill Book Company, 121-136 (1987).
30. Peng, D.Y. and Robinson, D.B: "A Rigorous Method for Predicting the Critical Properties of Multicomponent Systems from an Equation of State", *AIChE*, 23(2), 137-144 (1977).
31. Heidemann, R.A. and Khalil, A.M: "The Calculation of Critical Points", *AIChE*, 26(5), 769-778 (1980).
32. Michelsen, M.L. and Heidemann, R.A: "Calculation of Critical Points from Cubic Two-Constant Equation of State", *AIChE*, 27(3), 521-523 (1981).
33. Li, C.C: "Critical Temperature Estimation for Simple Mixtures", *Can. J. Chem. Eng.*, 49 (5), 709-710, (1971).
34. Spencer, C.F., Daubert, T.E. and Danner, P.D: "A Critical Review of Correlations for the Critical Properties of Defined Mixtures", *AIChE*, 19, 522 (1973).

35. Kreglewski, A. and Kay, W.B: "The Critical Constants of Conformal Mixtures", J. Phys. Chem., 73, No. 10, 3359-3366 (Oct., 1969).
36. Katz, D., et al: "Handbook of Natural Gas Engineering", McGraw-Hill Book Company (1959).
37. Neveux, A.R. and Sakthikumar, S: "Delineation and Evaluation of a North Sea Reservoir Containing Near Critical Fluids", SPE 15856, Proc. of SPE European Petroleum Conference, London, (Oct., 1986).
38. Montel, F and Gouel, P.L: "Prediction of Compositional Grading in a Reservoir Fluid Column", SPE 14410, Proc. of 60th Ann. Conf. (Sept., 1985).
39. De Groot, S.R: "Thermodynamics of Irreversible Processes", North-Holland Publishing Co., Amsterdam (1959).
40. Bearman R.J., Kirkwood, J.G. and Fixman, M: "Statistical-Mechanical Theory of Transport Processes, the Heat of Transport in Binary Liquid Solutions", Advances in Chemical Physics, 1, 1-13 (1958).
41. Oost, W.A., Los, J., Cauwenbergh, H. and van Dale, W: "Thermal Diffusion in Moderately Dense Gas Mixtures and the Pair-Correlation Function", Physica, 62, 409-426 (1972).
42. Lira-Galeana, C: "Discussion of Treatment of Variations of Composition with Depth in Gas-Condensate Reservoirs", SPE RES.ENG., 158 (1992).
43. Wheaton, R.J: "Treatment of Variations of Composition with Depth in Gas-Condensate Reservoirs", SPE RES.ENG., 239-244 (1991).
44. Hirschberg, A: "Role of Asphaltenes in Compositional Grading of a Reservoir's Fluid Column", JPT, 8-94 (Jan., 1988).
45. Chaback, J.J: "Discussion of Treatment of Variations of Composition with Depth in Gas-Condensate Reservoirs", SPE RES.ENG., 157 (Feb., 1992).
46. Rutherford, W.M. and Roof, J.G: "Calculation of Thermal Diffusion Factors for the Methane-n-Butane systems in the Critical and Liquid Regions", AIChE, 841 (1963).
47. Shulte, A.M: "Compositional Variations within a Hydrocarbon Column Due to Gravity", SPE 9235, Proc. of 55th Ann. Conf. (Sept., 1980).
48. Holt, T., Lindeberg, E. and Ratkje, S.K: "The Effect of Gravity and Temperature Gradients on Methane Distribution on Oil Reservoirs", SPE unsolic. paper 11761, (March, 1983).
49. Danesh, A. and Movaghar Nezhad, K: "An Investigation on Compositional Gradient with Depth in Petroleum Reservoirs", Journal of Faculty of Engng., Tehran University, 30-1, 59-68 (1997).

## 5.6 EXERCISES

- 5.1. A fluid mixture consists of methane (30 % mol) and normal heptane (70 % mol) at 338 K and 6.5 MPa. What is the state of the fluid ?



5.2. The composition of an oil sample is given in the following table.

Component	mole%
C <sub>1</sub>	27.36
C <sub>2</sub>	10.93
C <sub>3</sub>	8.56
iC <sub>4</sub>	1.46
nC <sub>4</sub>	4.73
iC <sub>5</sub>	1.77
nC <sub>5</sub>	2.77
C <sub>6</sub>	3.87
C <sub>7+</sub>	38.56

C<sub>7+</sub> Characteristics:  $M=210.0$   $S=0.8399$

The oil is flashed at 3 MPa and 325.0 K. Use the Standing method to estimate the equilibrium ratios and calculate the composition and mole fraction of equilibrated gas and liquid phases.

5.3. Most reservoir, wellbore, and surface processes can be simulated by a series of equilibrium flash calculations. Write an algorithm to simulate a constant volume depletion test using EOS.

5.4. What is the maximum pressure at which the Peng-Robinson EOS provides three real roots for an equimolar fluid composed of C<sub>1</sub>-nC<sub>4</sub> at 380 K.

5.5. Calculate the dew point of a gas mixture composed of 90 mol% methane and 10% normal decane at 377.5 K, using SRK (measured value  $P_d=33.72$  MPa).

5.6. Derive an expression to select the proper root of generalised EOS for a fluid, based on the minimum Gibbs energy.

5.7. The oil in Exercise 2 is to be stabilised by one intermediate separator at 325 K. Find the optimum separator pressure to obtain the maximum oil volume at the stock tank conditions (0.1 MPa and 288 K).

5.8. Estimate the critical properties of a mixture of methane and n-decane, 40-60 mole %, using the critical properties of pure constituents and reasonable mixing rules.

5.9. The compressibility factor,  $Z$ , is commonly plotted as a function of the reduced temperature,  $T_r$ , and reduced pressure,  $P_r$ , as shown in figure 2.22. Prove that the extension of any tangent line to constant reduced temperature curves should not cross the  $Z$  axis at a negative value.

5.10. Calculate the reservoir composition at 500 meter below that given in Example 5.1, assuming an average temperature of 377.6 K for the fluid column.



## 6 FLUID CHARACTERISATION

Semi-empirical cubic equations of state (EOS), though developed using experimental data of pure compounds, are successfully applied to predict phase behaviour and volumetric properties of multicomponent systems by employing mixing rules, as described in Chapter 4. Real reservoir fluids, however, could be composed of thousands of components which pose two major restrictions:

- (1) A full description of the fluid by identifying all its constituents may not be possible.
- (2) Phase behaviour calculations for systems defined by a large number of components are time consuming and particularly impractical in compositional reservoir simulation.

A reservoir oil or condensate is commonly described by discrete hydrocarbon components up to  $C_6$  and the non hydrocarbon gases, such as  $N_2$ ,  $CO_2$ ,  $H_2S$  and hydrocarbon groups for heavier fractions. The concentration of certain major non-paraffin constituents, within the  $C_6$  to  $C_9$  groups, such as, benzene, toluene, cyclohexanes and xylene, may also be identified. The hydrocarbon groups are generally determined according to their boiling points by distillation and, or, gas chromatography.

The distilled hydrocarbon groups are characterised by measuring some of their properties such as the average boiling point temperature, molecular weight and density. These properties are used in generalised correlations to estimate other properties, such as the critical properties and the acentric factor, which are required for EOS application. In some cases an extended distillation of heavy fractions may have not been conducted, hence, the required data need to be estimated by other methods.

## 6.1 EXPERIMENTAL METHODS

Samples of reservoir hydrocarbon mixtures, collected at bottom hole or separator conditions, are generally flashed at laboratory conditions and the compositions and properties of the separated gas and liquid phases are measured. The compositional analysis data of the separated phases are then numerically recombined in the surface proportions of gas and liquid to determine the composition of the original reservoir fluid. The errors in compositional analysis of high pressure reservoir fluids associated with the flashing technique, particularly for gas condensate fluids, are discussed in Section 2.2.

The gas composition is determined by gas chromatography (GC) [1], in form of discrete components. The mixture average molecular weight,  $M$ , can be calculated by the molar mixing rule,

$$M = \sum_i y_i M_i \quad (6.1)$$

where  $y_i$  is the mole fraction of component  $i$  in the gas mixture.

The gas density at laboratory conditions can be measured, by weighing a known gas volume, or calculated, approximately from the ideal gas law (by assuming  $Z=1$ ),

$$\rho_g = (P_a M_g) / (RT_o) \quad (1.3)$$

where  $\rho_g$  is the gas density at the atmospheric pressure  $P_a$  and the standard temperature  $T_o$ . The value of universal gas constant,  $R$ , for different sets of units is given in Table A.3 in Appendix A.

The oil composition can be determined by gas chromatography, or more commonly by distillation [2] and reported as liquid fractions. The heaviest fraction, which forms the residue in distillation, can be analysed by liquid chromatography techniques [3].

### Distillation

The liquid phase is generally characterised by fractional distillation and measuring the properties of the collected fractions. The distillation is commonly conducted using a column with 15 theoretical equilibrium stages at a reflux ratio of 5 and is known as the *true boiling point* (TBP) distillation. The standard method is fully described in ASTM 2892-84 [2].

A pot is loaded with the liquid and heated up, vaporising its components according to their boiling points. As light compounds vaporise, increasing the concentration of heavier fractions in the liquid, the temperature is gradually increased. The boiled-off fractions are collected as distillates, each within a temperature band at the column top.

The distillation begins at the atmospheric pressure, but the column pressure is lowered stage-wise to vaporise heavier compounds to avoid high temperatures which can cause hydrocarbon cracking, hence, compositional changes. The distillate temperature is converted to the normal boiling point, that is, at the atmospheric pressure, and the results are given as the percentage volume distilled versus the normal boiling point, as shown in Figure 6.1. As reservoir hydrocarbon liquids generally contain very heavy compounds, such as asphaltenes, a certain amount of the loaded sample will not boil-off, and will be left in the pot as the residue. Methods, such as using empirical correlations [4], have been suggested to extrapolate the TBP curve to 100% distillate. There are, however, more reliable methods to describe the residue by a number of fractions for phase behaviour modelling, as will be described in Section 6.3.

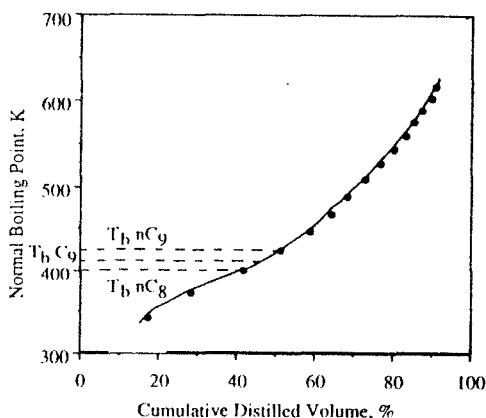


Figure 6.1. True boiling point (TBP) distillation curve of a North Sea condensate sample.

The liquid phase contains many components with properties varying in small increments. Hence, the fractionation of liquid into pure compounds is unfeasible. Each collected fraction comprises a large number of components with close boiling points. Fractions are commonly collected within the temperature range of two consecutive normal alkanes, where each cut begins and ends at the boiling point of normal  $C_{n-1}$  and normal  $C_n$ , respectively, and is referred to by the carbon number  $n$ . For example, the reported  $C_9$  fraction, nonanes, comprises all the compounds collected as distillate, within the temperature range of normal octane and normal nonane boiling points, as shown in Figure 6.1. The fractions are called, hence, single carbon number (SCN) groups. In practice the boundaries are selected about 0.3–0.7 °C, depending on the distillation unit and the fraction, above the normal alkane boiling points, mainly to counteract the liquid hold-up in the apparatus for improved purity.

The purity of SCN groups can further be improved by using a more efficient distillation apparatus. The use of a 90 theoretical equilibrium plate unit, instead of the standard ASTM 15 plate unit, is gaining popularity. Even then, 5–30% of the  $C_n$  fraction could be lighter than the normal  $C_{n-1}$  [5].

Each cut is characterised by its molecular weight, density and normal boiling point. The boiling point is taken at its mid-volume, Figure 6.1. As the boiling points of the neighbouring normal alkanes are close and the distillate recovery is almost linear over a SCN range, the mid-volume temperature is about the same as the arithmetic average of the boiling points of the two normal paraffins at the boundaries. The measured properties are used in some generalised correlations, Section 6.2, to determine the critical properties and the acentric factors. The residue is reported as  $C_{n+}$  e.g.,  $C_{30+}$  when the last drop of distillate is collected at the boiling point of  $nC_{29}$ . The average boiling point of the residue, if required, may be estimated from the correlations given in Section 6.2.

The density of each cut is measured by either weighing a known volume of the liquid, pycnometry, or by the more rapid, yet reliable, oscillating tube densitometer. The latter measures the period of oscillation of a tube filled with the fluid, which depends on its mass, hence, its density. A calibrated unit should provide density data with an accuracy of better than  $\pm 0.001 \text{ g/cm}^3$ .

The average molecular weight of each cut is often determined by measuring the depression of freezing point of a solvent, e.g., benzene, by dissolving oil at a concentration of about 0.15 mole per kg of solvent. A deviation of about 2 units of molecular weight can typically be expected in a carefully conducted test.

If the distillate is accumulated in a receiver, instead of collected as isolated fractions, the properties of each SCN group cannot directly be determined. In such cases, material balance methods, using the density and molecular weight of the whole distillate and the TBP distillation curve, may be used to estimate the concentration and properties of SCN groups [6].

Katz and Firoozabadi [7] extended the data of Bergman et al. [8] on the average boiling point, molecular weight and density of SCN groups of a large number of reservoir fluids. Their data, revised by Whitson [9], to improve consistency in the reported molecular weight, are given in Table 6.1. The properties, known as the generalised single carbon number data, are used when the measured data on a specific fluid is not available. The calculated critical properties of generalised SCN groups, using correlations described in Section 6.2, are given in Table A.2 in Appendix A. Haaland [10], Osjord et al. [11] and Ronningsen et al. [12] have also reported average SCN group properties for North Sea oil and condensate samples, which differ somewhat from those given in Table 6.1.

The properties of paraffins, naphthenes and aromatics, present in each SCN group are different. Hence, the properties of each SCN varies according to the relative concentration of the comprising homologues. Table 6.2 shows the paraffins, naphthenes and aromatics (PNA) content of a North Sea stabilised crude oil and their properties over the C<sub>6</sub>-C<sub>9</sub> range. Note that, for example, the density of naphthene group in C<sub>6</sub> is higher than that of the paraffin group in C<sub>9</sub>. All the hydrocarbon compounds within each SCN group do not have the same number of carbons. Indeed aromatics with the same carbon number as paraffins will appear in the next higher SCN group due to their lower boiling points. For example benzene, toluene and xylenes are counted as C<sub>7</sub>, C<sub>8</sub> and C<sub>9</sub> groups, respectively.

Due to an uneven distribution of hydrocarbon homologues in SCN groups, all the properties of SCN groups should not necessarily follow the same trend. Figure 6.2 shows the variation of SCN group density in different samples. The plot clearly demonstrates that the density of a SCN group can be lower than its preceding neighbour. The molecular weight, however, is expected to increase with increasing carbon number.

The PNA analysis of SCN groups is not generally required for modelling of vapour-liquid equilibria using equations of state. However, detailed information on the content of each SCN group may be required in special cases, e.g., when two hydrocarbon liquid phases or liquid-solid hydrocarbons are formed. Methods, relying on material balance and empirical correlations, have been proposed [4, 13] to estimate the PNA content, using the specific gravity and molecular weight of each fraction. A measured detailed analysis would be more appropriate in such cases instead of estimating them from the correlations.

The overall characteristic of hydrocarbon fractions, is commonly described by the Watson or UOP (Universal Oil Products) characterisation factor,  $K_w$ , as follows:

$$K_w = (1.8T_b)^{1/3} / S \quad (6.2)$$

where  $T_b$  is the boiling point in K and  $S$  is the specific gravity.

For pure hydrocarbons the above definition of characterisation factor results in:

$$12.5 < K_w \leq 13.5$$

Paraffins

$$11.0 < K_w \leq 12.5$$

$$8.5 < K_w \leq 11.0$$

Naphthenes

Aromatics

The characterisation factors of generalised SCN groups are given in Table 6.1.

Table 6.1.

Average normal boiling point, specific gravity, molecular weight and Watson characterisation factor of single carbon number groups [9].

SCN	Boiling Point	Specific Gravity	Molecular Weight	Watson Char. Fact.
	K	rel. dens. at 288K	kg/kgmol	
C6	337	0.690	84	12.27
C7	366	0.727	96	11.97
C8	390	0.749	107	11.87
C9	416	0.768	121	11.82
C10	439	0.782	134	11.82
C11	461	0.793	147	11.85
C12	482	0.804	161	11.86
C13	501	0.815	175	11.85
C14	520	0.826	190	11.84
C15	539	0.836	206	11.84
C16	557	0.843	222	11.87
C17	573	0.851	237	11.87
C18	586	0.856	251	11.89
C19	598	0.861	263	11.90
C20	612	0.866	275	11.93
C21	624	0.871	291	11.93
C22	637	0.876	300	11.95
C23	648	0.881	312	11.95
C24	659	0.885	324	11.96
C25	671	0.888	337	11.99
C26	681	0.892	349	12.00
C27	691	0.896	360	12.00
C28	701	0.899	372	12.02
C29	709	0.902	382	12.03
C30	719	0.905	394	12.04
C31	728	0.909	404	12.04
C32	737	0.912	415	12.05
C33	745	0.915	426	12.05
C34	753	0.917	437	12.07
C35	760	0.920	445	12.07
C36	768	0.922	456	12.08
C37	774	0.925	464	12.07
C38	782	0.927	475	12.09
C39	788	0.929	484	12.09
C40	796	0.931	495	12.11
C41	801	0.933	502	12.11
C42	807	0.934	512	12.13
C43	813	0.936	521	12.13
C44	821	0.938	531	12.14
C45	826	0.940	539	12.14

Table 6.2.

Paraffins, naphthenes and aromatics content of single carbon number groups of C<sub>6</sub> to C<sub>9</sub> of a typical North Sea oil [11].

Component	Weight %	Mole %	Volume %	Mol W.	Dens. g/cm <sup>3</sup>
Hexane Group Paraffins	0.647	1.886	0.836	86.2	0.663
Hexane Group Naphthenes	0.052	0.185	0.059	70.1	0.750
Heptane Group Paraffins	0.713	1.787	0.889	100.2	0.686
Heptane Group Naphthenes	0.930	2.682	1.034	87.1	0.769
Heptane Group Aromatics	0.355	1.140	0.343	78.1	0.884
Octane Group Paraffins	0.870	1.912	1.054	114.2	0.707
Octane Group Naphthenes	1.404	3.435	1.556	102.6	0.772
Octane Group Aromatics	0.958	2.610	0.941	92.1	0.871
Nonane Group Paraffins	0.739	1.446	0.877	128.3	0.721
Nonane Group Naphthenes	0.646	1.331	0.699	122.0	0.792
Nonane Group Aromatics	1.042	2.464	1.022	106.2	0.872

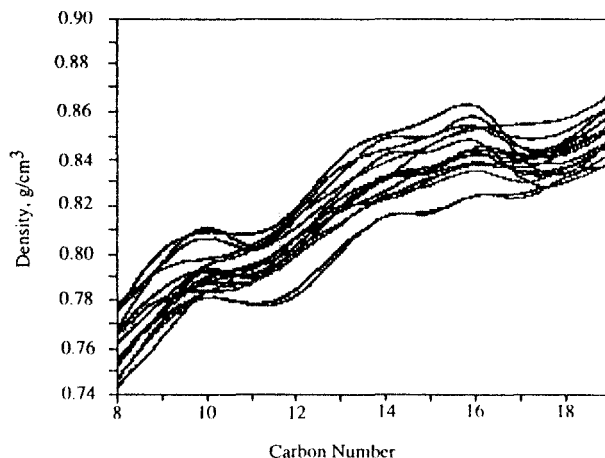


Figure 6.2. Densities of SCN groups of fluid samples from various North Sea reservoirs. Huthig-Fachverlage Copyright. Reproduced from [11] with permission.

The characterisation factor for a mixture can be estimated by the weighted average mixing rule,

$$K_w = \frac{\sum_{i=1}^N w_i K_{wi}}{\sum_{i=1}^N w_i} \quad (6.3)$$

where  $w_i$  is the weight fraction.

A mixture of aromatics and paraffins, therefore, may appear as naphthene evaluated by its  $K_w$ . However, it is a useful single factor describing the characteristics of petroleum fractions. A more reliable characterisation factor, especially for complex fluids, may be obtained by including a third physical property, such as the viscosity or the refractive index. These data are



not, however, commonly available for petroleum fractions. Other characterisation factors, not widely used, have also been proposed [14].

The Watson characterisation factor can be related to properties other than the boiling point and specific gravity, using correlations given in Section 6.2. For example, it can be related to the molecular weight ( $M$ ) and specific gravity ( $S$ ) [9], using the Riazi-Daubert correlation, Eq.(6.4),

$$K_w = 4.5579 M^{0.15178} S^{-0.84573} \quad (6.4)$$

The above relation is particularly useful for the last fraction, referred to as the plus fraction, where its boiling point is not known. The above equation becomes less reliable at  $M > 300$ .

The variation of  $K_w$  is relatively small for different fractions, particularly for heavy fractions in most cases. It can be assumed, therefore, as constant for heavy fractions to evaluate the internal consistency of measured data, or to estimate missing information, as will be described in Section 6.3.

### Gas Chromatography

The gas composition is determined, invariably, by gas chromatography (GC). Recent advances in gas chromatography have enabled laboratories to extend the method to oil analysis with a comparable accuracy. Whilst an extended oil analysis by distillation takes many days and requires relatively a large volume of sample, gas chromatography can identify components as heavy as  $C_{80}$  [15] in a matter of hours using only a small fluid sample.

The sample is injected into a heated zone, vaporised, and transported by a carrier gas, usually helium, into a column packed or internally coated with a stationary liquid or solid phase, resulting in partitioning of the injected sample constituents. General purpose columns partition components mostly according to their boiling points, hence compounds are eluted in a similar order as in distillation. The eluted compounds are carried, by the carrier gas, into a detector where the component concentration is related to the area under the detector response-time curve as shown in Figure 6.3. Individual peaks may be identified by comparing their retention times inside the column with those of known compounds previously analysed at the same GC conditions.

The two most commonly used detectors are the flame ionisation detector (FID) and the thermal conductivity detector (TCD). The FID response is almost proportional to the mass concentration of the ionised compound. It, however, cannot detect non-hydrocarbons such as  $N_2$  and  $CO_2$ . Hence, TCD is often used for analysis of gaseous mixtures that contain non-hydrocarbon components.

Packed columns, with an efficiency ranging from tens to hundreds of equilibrium stages, are the most versatile and frequently used devices. These columns are capable of base line separation of gaseous compounds, hence, determining their concentrations as discrete compounds. The intermediate and heavy fractions are eluted, however, as a continuous stream of overlapping compounds, Figure 6.4. This is very similar to the fractionation behaviour in a distillation unit and treated similarly. That is, all the components detected by GC between the two neighbouring normal paraffins are commonly grouped together, measured and reported as a SCN equal to that of the higher normal paraffin. The GC operating conditions may be adjusted [16], that is, its efficiency lowered, to simulate the 15 tray TBP distillation. The results, known as the simulated distillation, are quite comparable to those generated by the TBP method [2], as shown in Figure 6.5. The percentage area under the FID response curve has been taken to be equivalent to the percentage volume distilled [17].

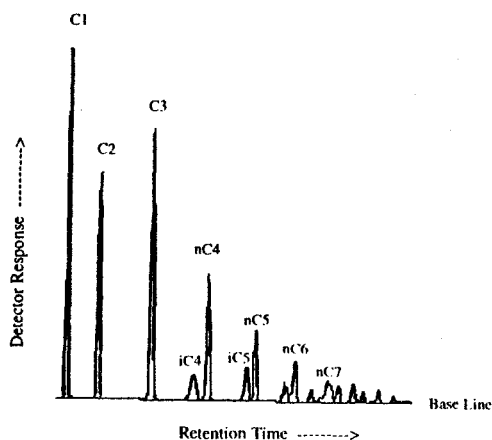


Figure 6.3. Gas chromatogram of a gas sample, using a packed column.

The accuracy in compositional analysis can be improved by calibrating GC, that is, determining the detector response relative to the concentration of each component at the operating conditions, known as the response factor. The common method is to analyse a gravimetrically prepared mixture of components with known concentrations, as the standard. Normal alkanes are often used to represent SCN groups. It is known that the response of detectors to paraffins and aromatics are different. Hence, the use of typical SCN groups, instead of normal alkanes, in preparing standards appears to be more appropriate. The effect, however, is minimal [5] in most cases.

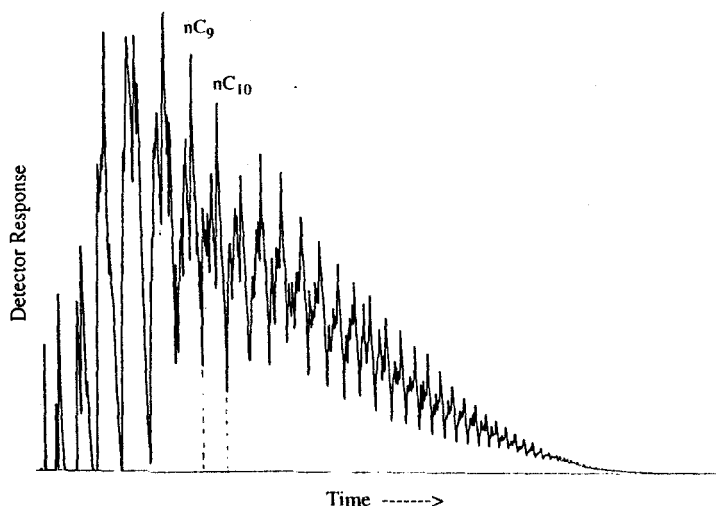


Figure 6.4. Gas chromatogram of a North Sea oil sample, using a packed column.

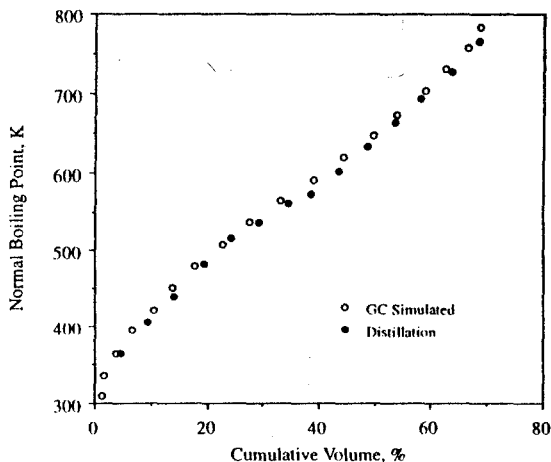


Figure 6.5. Comparison of TBP distillation curve and simulated distillation result, using gas chromatography, of an oil sample.

A major drawback of GC analysis is the lack of information, such as the molecular weight and density, on the identified SCN groups. The lack of molecular weight data is quite limiting as the response of FID, used for oil analysis, is proportional to the mass concentration. Molecular weight data are needed, therefore, to convert the mass fraction to molar basis required for compositional studies.

The very high boiling constituents of a reservoir oil sample cannot be eluted, hence, they cannot be detected by GC. The common method of estimating the non-eluted fraction is to use an internal standard, where one or a few fully detectable compounds, preferably not present in the oil, are added to the oil at a known mass ratio [16]. The comparison of mass ratio as detected by GC with that of gravimetrically prepared mixture, gives an indication of the amount of non-eluted fractions. The method, known as spiking, relies on certain limiting assumptions which may lead to large deviations in measured concentration of non-eluted fractions [5].

Application of a continuous function to describe the component distribution (see Section 6.3) and extending the measured concentration of eluted fractions to determine the non-eluted part is also an option [5]. High temperature columns [15] are capable of almost complete elution of light condensate fluids. However, the concentration of the plus fraction (last reported group) determined by GC, should always be treated with caution.

Capillary columns, equivalent to many thousands of theoretical equilibrium stages, can be used in preference to packed columns, to improve separation and peak recognition, as shown in Figure 6.6 for a North Sea condensate. Table 6.3 presents the components as identified by the peak numbers in Figure 6.6, and their concentration, molecular weight and density.

The molecular weight and density of components identified in each single carbon group can be used to estimate the properties of that group, by the following material balance equations:

$$M = (\sum w_i) / \sum (w_i / M_i) \quad (6.5)$$

$$\rho = (\sum w_i) / \sum (w_i / \rho_i) \quad (6.6)$$

where  $w_i$  is the weight fraction of component  $i$ .

Table 6.3.

Individual components identified by peak numbers in Figure 6.6 [11].

Peak No.	Component	Weight %	Mole %	Volume %	Mol. W	Dens., g/cm <sup>3</sup>
1	C2	0.007	0.058	0.017	30.070	0.3580
2	C3	0.072	0.412	0.122	44.097	0.5076
3	iC4	0.051	0.222	0.078	58.124	0.5633
4	nC4	0.189	0.816	0.276	58.124	0.5847
5	2,2-DM-C3	0.000	0.000	0.000	72.151	0.5967
6	iC5	0.188	0.653	0.257	72.151	0.6246
7	nC5	0.285	0.991	0.386	72.151	0.6309
	Light end total	0.792	3.152	1.137	63.092	0.5964
8	2,2-DM-C4	0.012	0.034	0.015	86.178	0.6539
9	Cy-C5	0.052	0.185	0.059	70.135	0.7502
10	2,3-DM-C4	0.028	0.081	0.036	86.178	0.6662
11	2-M-C5	0.165	0.480	0.214	86.178	0.6577
12	3-M-C5	0.102	0.298	0.131	86.178	0.6688
13	nC6	0.341	0.993	0.440	86.178	0.6638
	Hexanes total	0.699	2.071	0.895	84.745	0.6687
14	M-Cy-C5	0.231	0.689	0.262	84.162	0.7534
15	2,4-DM-C5	0.015	0.038	0.019	100.205	0.6771
16	Benzene	0.355	1.140	0.343	78.114	0.8842
17	Cy-C6	0.483	1.440	0.528	84.162	0.7831
18	2-M-C6	0.000	0.000	0.000	100.205	0.6829
66	1,1-DM-Cy-C5	0.116	0.298	0.131	98.189	0.7590
19	3-M-C6	0.122	0.307	0.152	100.205	0.6915
20	1,cis-3-DM-Cy-C5	0.000	0.000	0.000	98.189	0.7493
21	1,trans-3-DM-Cy-C5	0.052	0.133	0.059	98.189	0.7532
22	1,trans-2-DM-Cy-C5	0.048	0.122	0.054	98.189	0.7559
25	nC7	0.405	1.014	0.504	100.205	0.6880
	Unspecified C7	0.171	0.427	0.215	100.205	0.6800
	Heptanes total	1.997	5.609	2.267	89.426	0.7542
26	M-Cy-C6	0.918	2.348	1.016	98.189	0.7737
27	1,1,3-TM-Cy-C5	0.027	0.061	0.031	112.216	0.7526
28	E-Cy-C5	0.000	0.000	0.000	98.189	0.7708
29	2,2,3-TM-Cy-C5	0.042	0.093	0.050	114.232	0.7200
30	2,5-DM-C6	0.018	0.039	0.022	114.232	0.6977
31	2,4-DM-C6	0.000	0.000	0.000	114.232	0.7045
32	3,3-DM-C6	0.026	0.057	0.031	114.232	0.7141
33	1,trans-2,cis-3-TM-Cy-C5	0.025	0.056	0.028	112.216	0.7579
34	Toluene	0.958	2.610	0.941	92.143	0.8714
35	1,1,2-YM-Cy-C5	0.000	0.000	0.000	112.216	0.7769
36	2,3-DM-C6	0.033	0.073	0.040	114.232	0.7163
37	2-M-C7	0.137	0.300	0.167	114.232	0.7019
38	3-M-C7	0.094	0.206	0.113	114.232	0.7099
39	1,cis-3-DM-Cy-C6	0.190	0.425	0.211	112.216	0.7701
40	1,trans-4-DM-Cy-C6	0.072	0.162	0.081	112.216	0.7668
42	Unspecified naphthene	0.028	0.062	0.031	112.216	0.7700
42	Unspecified naphthene	0.013	0.028	0.014	112.216	0.7700
42	Unspecified naphthene	0.011	0.025	0.012	112.216	0.7700

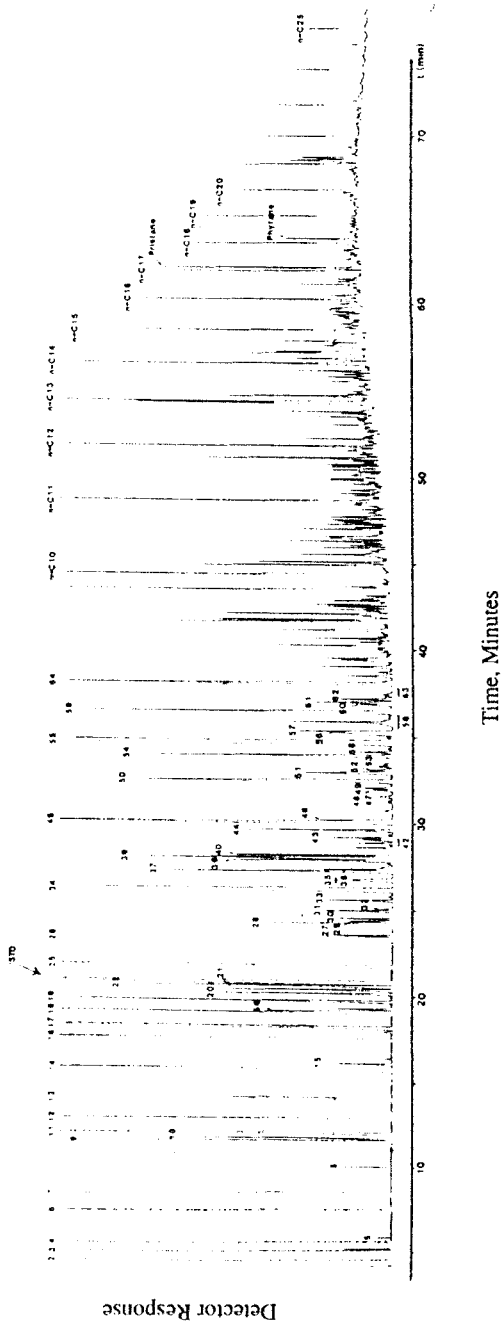


Figure 6.6. Gas chromatogram of a condensate sample using a capillary column. Peak numbers correspond to components in Table 6.3. Huthig-Fachverlage Copyright. Reproduced from [11] with permission.

Table 6.3 (Cont.).

Individual components identified by peak numbers in Figure 6.6.

Peak No.	Component	Weight %	Mole %	Volume %	Mol. W.	Dens., g/cm <sup>3</sup>
43	DM-Cy-C6	0.031	0.069	0.034	112.216	0.7700
44	1,trans-2-DM-Cy-C6	0.089	0.199	0.098	112.216	0.7799
45	nC8	0.434	0.954	0.526	114.232	0.7065
	Unspecified C8	0.086	0.190	0.105	114.232	0.7000
	Octanes total	3.231	7.957	3.551	101.978	0.7791
46	Unspecified naphthene	0.047	0.094	0.051	126.243	0.7900
47	2,2-DM-C7	0.009	0.018	0.011	128.259	0.7144
48	2,4-DM-C7	0.017	0.033	0.020	128.259	0.7192
49	1,cis-2-DM-Cy-C6	0.024	0.054	0.026	112.216	0.8003
50	E-Cy-C6+1,1,3-TM-Cy-C6	0.281	0.599	0.305	118.000	0.7900
51	Unspecified naphthene	0.047	0.093	0.051	126.243	0.7900
52	3,5-DM-C7	0.017	0.034	0.020	128.259	0.7262
53	2,5-DM-C7	0.003	0.006	0.004	128.259	0.7208
54	Ethylbenzene	0.114	0.270	0.112	106.168	0.8714
68	Unspecified naphthene	0.027	0.054	0.029	126.243	0.7900
55	m-+p-xylene	0.697	1.649	0.687	106.168	0.8683
56	4-M-C8	0.020	0.039	0.024	128.259	0.7242
57	2-M-C8	0.054	0.106	0.064	128.259	0.7173
58	Unspecified naphthene	0.009	0.018	0.010	126.243	0.7900
58	Unspecified naphthene	0.082	0.163	0.089	126.243	0.7900
58	Unspecified naphthene	0.007	0.014	0.008	126.243	0.7900
59	Ortho-xylene	0.230	0.545	0.223	106.168	0.8844
60	3-M-C8	0.023	0.045	0.027	128.259	0.7242
61	1-M,3-E-Cy-C6	0.078	0.155	0.083	126.243	0.8000
62	1-M,4-E-Cy-C6	0.034	0.068	0.037	126.243	0.7900
63	Unspecified naphthene	0.006	0.013	0.007	126.243	0.7900
63	Unspecified naphthene	0.004	0.007	0.004	126.243	0.7900
64	nC9	0.471	0.923	0.559	128.259	0.7214
	Unspecified C9	0.124	0.243	0.148	128.259	0.7200
	Nonanes total	2.427	5.241	2.598	116.277	0.7995

A comparison of the calculated properties of single carbon groups using GC data and the above method, with those determined by 90 equilibrium tray distillation on a condensate is shown in Table 6.4. The differences are of the same magnitude as typical deviations in measuring the properties.

A highly useful column for hydrocarbon reservoir fluid analysis is the wide bore capillary column, also known as the megabore column. The column which provides the versatility of packed columns, whilst maintaining a high resolution capability, can be used successfully in compositional analysis of live fluids, without any need for flashing the fluid into gas and liquid samples for GC application [18]. The preference of direct sampling and analysis of high pressure live samples relative to the conventional blow down method is discussed in Section 2.2.

The aromatic content of an oil may also be determined by gas chromatography using a column containing a strongly polar stationary phase column which elutes the components according to their boiling points. The combination of results from polar and conventional columns are then used to determine PNA [8].

Table 6.4.

Comparison of single carbon number group properties measured by distillation and capillary GC analysis.

SCN	Weight %	Distillation		GC		
		Mol. W.	Dens., kg/m <sup>3</sup>	Weight %	Mol. W.	Dens., kg/m <sup>3</sup>
5	0.886	65	621	0.792	63	597
6	0.737	82	695	0.699	85	669
7	2.371	91	751	2.000	89	754
8	2.825	103	778	3.237	102	779
9	2.539	116	793	2.429	116	799
10+	90.642	306	869	90.846	300	868
10	2.479	132	798	2.437	134	801
11	1.916	147	803	2.191	148	803
12	2.352	163	817	2.523	162	812
13	2.091	175	836	3.106	175	827
14	3.667	190	843	3.124	190	840
15	3.722	205	849	3.984	205	845
16	2.034	215	863	3.383	218	851
17	4.135	237	844	4.244	235	842
18	3.772	251	846	3.201	250	845
19	3.407	262	857	3.523	261	854
20+	61.057	426	885	59.130	422	888

## 6.2 CRITICAL PROPERTIES

The critical temperature,  $T_c$ , pressure,  $P_c$ , volume,  $v_c$ , compressibility factor,  $Z_c$ , and the acentric factor,  $\omega$ , of single carbon number groups and the last (plus) fraction of reservoir fluids, similar to those of discrete components, are required for phase behaviour modelling using EOS. These properties are determined from generalised correlations in terms of the specific gravity,  $S$ , boiling point,  $T_b$ , or the molecular weight,  $M$ , of single carbon groups.

Several methods to calculate the critical properties of petroleum fractions are available. The methods have mostly used measured critical properties of pure compounds to develop correlations, either in graphical forms or as equations. The majority of these correlations are reported in [19]. The most widely used, or promising methods, are reviewed in this section. The correlations in their original forms use Field Units, and are given as such in Appendix B. In this section, the correlations are presented with SI units. The units of  $P$ ,  $T$  and  $v$  are MPa, K and m<sup>3</sup>/kmol, respectively.

### Lee-Kesler Correlations [20,21]

$$T_c = 189.8 + 450.6S + (0.4244 + 0.1174S)T_b + (0.1441 - 1.0069S) \times 10^5 / T_b \quad (6.7)$$

$$\ln P_c = 3.3864 - 0.0566/S - (0.43639 + 4.1216/S + 0.21343/S^2) \times 10^{-3} T_b \\ + (0.47579 + 1.182/S + 0.15302/S^2) \times 10^{-6} T_b^2 - (2.4505 + 9.9099/S^2) \times 10^{-10} T_b^4 \quad (6.8)$$

$$\omega = \left( \ln P_{br} - 5.92714 + 6.09648/T_{br} + 1.28862 \ln T_{br} - 0.169347 T_{br}^6 \right) / \quad (6.9)$$

$$\left( 15.2518 - 15.6875/T_{br} - 13.4721 \ln T_{br} + 0.43577 T_{br}^6 \right) \text{ for } T_{br} \leq 0.8$$

$$\omega = -7.904 + 0.1352 K_w - 0.007465 K_w^2 + 8.359 T_{br} \quad (6.10)$$

$$+ (1.408 - 0.01063 K_w) / T_{br} \quad \text{for } T_{br} > 0.8$$

where  $P_{br}=P_b/P_c$ ,  $T_{br}=T_b/T_c$ ,  $P_b$  is the pressure at which  $T_b$  is measured, e.g. the normal boiling point at 0.1013 MPa (1 atmosphere) and  $K_w$  is the Watson characterisation factor, Eq.(6.2). The estimated acentric factors by the above two correlations at  $T_{br}=0.8$  differ about 2%.

The acentric factor correlation, Eq.(6.9) is simply a re-arrangement of the Lee-Kesler vapour pressure correlation, Eq.(1.10).

The correlations of Cavett [22], given in Appendix B, for  $T_c$  and  $P_c$  are also often used in phase behaviour modelling of hydrocarbon systems. The Edmister correlation [23] for the acentric factor is commonly used with the Cavett correlation,

$$\omega = \left\{ \frac{3}{7} \left[ \log(P_c/P_a) \right] / \left[ (T_c/T_b) - 1 \right] \right\} - 1 \quad (6.11)$$

where  $P_a$  is the atmospheric pressure, 0.1013 MPa, at which the normal boiling point,  $T_b$ , is measured. The correlation is derived by combining the vapour pressure relation, Eq.(1.8), and the definition of acentric factor, Eq.(1.9).

The above methods do not provide information on the critical volume or compressibility factor. The critical volume can be calculated from,

$$P_c v_c = Z_c R T_c \quad (6.12)$$

with the critical compressibility factor estimated from the Pitzer correlation,

$$Z_c = 0.2901 - 0.0879\omega \quad (6.13)$$

### Riazi-Daubert Correlations

Riazi and Daubert [24] developed a simple two parameter equation for predicting physical properties of hydrocarbon mixtures.

$$\theta = a \theta_1^b \theta_2^c \quad (6.14)$$

where  $\theta$  is the property to be determined, and  $\theta_1$  and  $\theta_2$  can be any two parameters characterising molecular forces and molecular sizes of a component. Any pair such as ( $T_b$ ,  $M$ ) or ( $T_b$ ,  $S$ ) may be used for  $\theta_1$  and  $\theta_2$ . Properties such as the molecular weight, refractive index, critical properties, density, heat of vaporisation and thermal conductivity were successfully correlated by the above equation [24].

The authors later [25] improved the correlation as,



$$\theta = a [\exp(b\theta_1 + c\theta_2 + d\theta_1\theta_2)]\theta_1^e\theta_2^f \quad (6.15)$$

where, a to f, are constants for each property as given in Table 6.5.

Table 6.5

Constants in Eq.(6.15) for  $T_c$ ,  $P_c$ ,  $v_c$ ,  $M$  and  $T_b$ .

$\theta$	$\theta_1$	$\theta_2$	a	b	c	d	e	f
$T_c$	$T_b$	S	9.5233E+00	-9.3140E-04	-0.54444	6.4791E-04	0.81067	0.53691
$T_c$	M	S	3.0800E+02	-1.3478E-04	-0.61641	0.0000E+00	0.2998	1.0555
$P_c$	$T_b$	S	3.1958E+04	-8.5050E-03	-4.8014	5.7490E-03	-0.4844	4.0846
$P_c$	M	S	3.1166E+02	-1.8078E-03	-0.3084	0.0000E+00	-0.8063	1.6015
$(v_c/M)$	$T_b$	S	6.0490E-05	-2.6422E-03	-0.26404	1.9710E-03	0.7506	-1.2028
$(v_c/M)$	M	S	7.5288E-04	-2.6570E-03	0.5287	2.6012E-03	0.20378	-1.3036
M	$T_b$	S	1.0321E+03	9.7754E-04	-9.53384	1.9990E-03	0.97476	6.51274
$T_b$	M	S	3.7659E+00	3.7741E-03	2.984036	-4.2529E-03	0.401673	-1.58262
$(70 < M < 300)$			$300 < T_b < 610 \text{ K}$					

### Perturbation Expansion Correlations

These methods initially correlate the properties of normal paraffins as the reference, and then extend these correlations to petroleum fractions. The correlations developed by Twu [26], who used the difference between the specific gravity of the hydrocarbon fraction and that of the normal paraffin with the same boiling point as the correlating parameter are as follows.

#### Normal Paraffins

The properties of normal paraffins are correlated with the normal boiling point temperature,

$$T_{cp} = T_b \left[ 0.533272 + 0.343831(10^{-1})T_b + 2.526167(10^{-7})T_b^2 - 1.65848(10^{-10})T_b^3 + 0.0460774/(T_b/100)^{13} \right]^{-1} \quad (6.16)$$

$$P_{cp} = (0.318317 + 0.099334\psi^1 + 2.89698\psi + 3.00546\psi^2 + 8.65163\psi^4)^2 \quad (6.17)$$

$$v_{cp} = [0.82055 + 0.715468\psi + 2.21266\psi^1 + 13411.1\psi^{14}]^{-8} \quad (6.18)$$

$$S_p = 0.843593 - 0.128624\psi - 3.36159\psi^1 - 13749.5\psi^{12} \quad (6.19)$$

where the subscript p refers to properties of normal paraffins and,

$$\psi \equiv 1 - T_b/T_{cp} \quad (6.20)$$

The molecular weight of paraffins is given by the following implicit relation,

$$T_b = \exp \left[ (5.12640 + 2.71579 \ln M_p - 0.286590(\ln M_p)^2 - 39.8544/(\ln M_p) - 0.122488/(\ln M_p)^2) \right. \\ \left. - 13.7512 \ln M_p + 19.6197(\ln M_p)^2 \right] \quad (6.21)$$

which can be solved iteratively using the following initial guess,

$$M_p = T_b / (5.800 - 0.0052T_b) \quad (6.22)$$

### Petroleum Fractions

The properties of any petroleum fraction are estimated by adjusting the calculated properties of the normal paraffin with the same boiling point as follows:

Critical Temperature:

$$T_c = T_{cp} [(1 + 2f_T) / (1 - 2f_T)]^2 \quad (6.23)$$

$$f_T = \Delta S_T \left[ -0.270159 / T_b^{1/2} + \left( 0.0398285 - 0.706691 / T_b^{1/2} \right) \Delta S_T \right]$$

$$\Delta S_T = \exp [5 (S_p - S)] - 1$$

Critical Volume:

$$v_c = v_{cp} [(1 + 2f_v) / (1 - 2f_v)]^2 \quad (6.24)$$

$$f_v = \Delta S_v \left[ 0.347776 / T_b^{1/4} + (-0.182421 + 2.24890 / T_b^{1/4}) \Delta S_v \right]$$

$$\Delta S_v = \exp [4 (S_p^2 - S^2)] - 1$$

Critical Pressure:

$$P_c = P_{cp} (T_c / T_{cp}) (v_{cp} / v_c) [(1 + 2f_p) / (1 - 2f_p)]^2 \quad (6.25)$$

$$f_p = \Delta S_p \left[ \left( 2.53262 - 34.4321 / T_b^{1/2} - 0.00230193 T_b \right) + \left( -11.4277 + 187.934 / T_b^{1/2} + 0.00414963 T_b \right) \Delta S_p \right]$$

$$\Delta S_p = \exp [0.5 (S_p - S)] - 1$$

Molecular Weight:

$$\ln M = (\ln M_p) [(1 + 2f_M) / (1 - 2f_M)]^2 \quad (6.26)$$

$$f_M = \Delta S_M [\Psi + (-0.0175691 + 0.143979 / T_b^{1/2}) \Delta S_M]$$

$$\Psi = 0.0123420 - 0.244541 / T_b^{1/2}$$

$$\Delta S_M = \exp [5 (S_p - S)] - 1$$

The above method, because of its reliability, has been used to calculate the critical properties of generalised SCN groups, using the reported boiling point and specific gravity in Table 6.1, with the results given in Table A.2 in Appendix A.

Riazi and Daubert [25] compared predictions of their correlation, Eq.(6.15) using  $T_b$  and  $S$ , with others for 138 pure compounds, with the results given in Table 6.6.

Table 6.6.

Comparison of several methods for prediction of critical properties.

Method	% Dev. Critical Temperature		% Dev. Critical Pressure	
	Abs. Average	Maximum	Abs. Average	Maximum
Riazi-Daubert	0.5	2.2	2.7	13.2
Twu	0.6	2.4	3.9	16.5
Kesler-Lee	0.7	3.2	4.0	12.4
Cavett	3.0	5.9	5.5	31.2

The saturation pressure and density, predicted by the Soave-Redlich-Kwong EOS [27] for a process where methane was incrementally added to an oil, are shown in Figures 6.7 and 6.8, respectively. The properties of the oil heavy fractions were determined by various methods for phase behaviour calculations. The results clearly demonstrate the major impact of the correlation used to calculate the critical properties on predicted results by EOS.

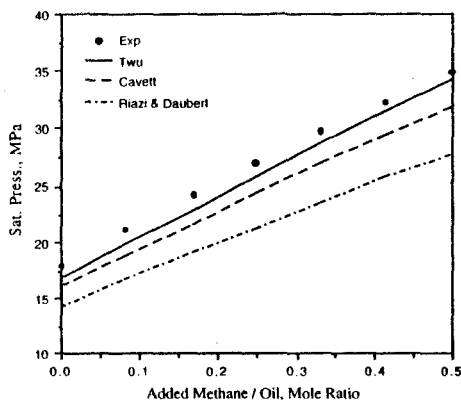


Figure 6.7. Variations of bubble point pressure predicted by Soave-Redlich-Kwong EOS using different correlations to estimate SCN group properties.

The correlations are for single carbon number group properties, and their application to very wide boiling range fractions, such as  $C_{7+}$ , is not recommended. These fractions should be characterised initially as SCN groups, or by a continuous function as described in the next section.

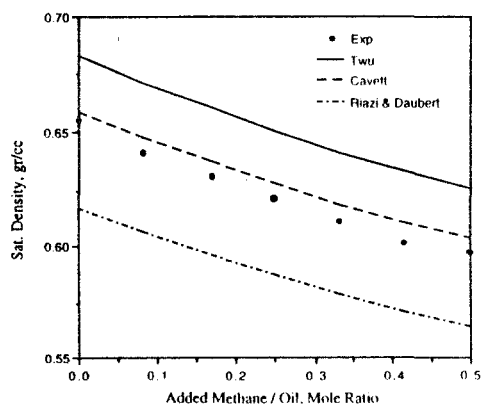


Figure 6.8. Variations of saturated liquid density predicted by Soave-Redlich-Kwong EOS using different correlations to estimate SCN group properties.

#### Example 6.1.

Calculate the critical temperature, pressure, volume and the acentric factor for  $C_{14}$  with properties as reported in the generalised property table, Table 6.1, using the methods of Twu (Lee-Kesler for the acentric factor) and Riazi-Daubert (Edmister for the acentric factor).

#### Solution:

The specific gravity, boiling point and molecular weight of  $C_{14}$  are read as 0.826, 520 K and 190 kg/kgmol, respectively, from Table 6.1.

#### Twu Correlations

The properties of the normal alkane with the same boiling point as that of  $C_{14}$ , that is 520 K, are initially calculated as follows:

	$T_b$ , K	$T_{cp}$ , K	$1-T_b/T_{cp}$	$P_{cp}$ , MPa	$v_{cp}$	$S_p$
Equation	Table A.2	6.16	6.20	6.17	6.18	6.19
	520	686.8	0.2429	1.6348	0.8135	0.7635

Next, the above calculated normal alkane properties are adjusted, based on the difference between the  $C_{14}$  specific gravity, 0.826, and that of the normal alkane calculated above, 0.7635.

	$\Delta S_T$	$f_T$	$T_c$ , K	$\Delta S_v$	$f_v$	$v_c$ , m <sup>3</sup> /kgmol	$\Delta S_p$	$f_p$	$P_c$ , MPa
Equation			6.23			6.24			6.25
	-0.2681	0.003812	708	-0.3276	-0.01399	0.727	-0.03073	0.004386	1.953

As the reduced boiling point temperature is equal to  $520/708=0.734$ , Eq.(6.9) of the Lee-Kesler method is used to calculate the acentric factor, which results in,

$$\omega=0.536$$

The calculated values for single carbon number groups,  $C_6$ - $C_{14}$ , using the above method, are given in Table A.2 in Appendix A.

#### Riazi-Daubert Correlations

The critical properties can be estimated by either using measured  $T_b$ - $S_c$  or M-S data of  $C_{14}$ . The results of both approaches, using Eq.(6.15), are given in the following table.

Data used	$T_c$ , K		$v_c$ , m <sup>3</sup> /kgmol		$P_c$ , MPa	
	$T_b$ , S	M, S	$T_b$ , S	M, S	$T_b$ , S	M, S
	710	711	0.750	0.751	1.902	1.835

The measured values of specific gravity and boiling point, as the most readily available data, are commonly used to estimate the critical properties.

Using the Edmister correlation, Eq.(6.11), along with the above calculated  $T_c$  and  $P_c$ , results in,

$$\omega=0.486$$

### 6.3 DESCRIPTION OF FLUID HEAVY END

Although naturally occurring reservoir hydrocarbons are commonly described by a number of discrete components and component groups, they can be more thoroughly expressed by continuous description. The TBP curve, Figure 6.1, and the gas chromatogram, Figure 6.4, are examples of such continuity.

The continuous description of a fluid mixture has two major applications:

- It can be used to improve and extend fluid characterisation through describing the plus fraction by a number of single and multiple carbon number groups, particularly in the absence of experimental data.
- The continuous distribution function may be used directly in phase behaviour models, instead of discrete component data.

The concentration of SCN groups in a North Sea oil sample is shown in Figures 6.9. Although complex functions may be found to describe the concentration distribution in the whole mixture, it is more advantageous to limit the continuous description to the heavy fractions, where relatively simple functions would suffice. This approach, which describes light components by discrete compounds and heavy fractions by a mathematical function, is sometimes referred to as semi-continuous description.

The continuous description of a fluid is commonly used for compounds heavier than  $nC_6$ , that is for  $C_{7+}$ . The  $C_{8+}$  could be a more appropriate choice in most cases, as the concentration of  $C_8$  fraction is generally the highest amongst the SCN groups, hence, simple decay functions can adequately describe the fluid. A compound may be represented by its carbon number,

molecular weight, boiling point, or other properties. The concentration can be expressed in terms of mole, weight or volume fractions.

The distribution of SCN groups shown in Figure 6.9 is typical of most reservoir hydrocarbon liquids. There are, however, mixtures with component distribution vastly different from the normal trend. Figure 6.10 compares different types of North Sea oil samples. Fluids containing high concentration of aromatics and naphthenes often point to bacterial activity in the reservoir. Biodegradation generally reduces the alkanes and, to a lesser extent, the aromatics. Clearly the distribution of SCN groups in non-conventional samples cannot be represented by simple distribution functions.

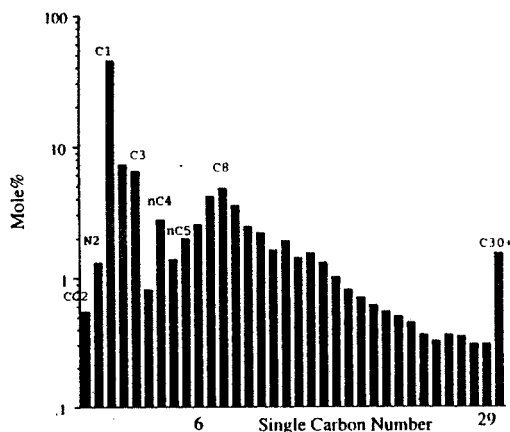


Figure 6.9. Distribution of SCN groups in a North Sea oil.

### Single Carbon Number Function

A simple, but very useful, approach is to use a function to describe the concentration of SCN groups. Various functional forms have been suggested and applied [28-30], with reasonable success. The simplest of all is, that of Katz [28] for the  $C_{7+}$  fraction of condensate systems, as expressed mathematically [19] by,

$$z_{C_n} = 1.38205 z_{C_7} \exp(-0.25903n) \quad (6.27)$$

where  $z_{C_n}$  is the mole fraction of single carbon number group  $C_n$ .

A linear relation between the SCN and logarithm of concentration is generally adequate to describe heavy fractions of most reservoir fluids,

$$\ln z_{C_n} = A + Bn \quad (6.28)$$

where A and B are constants for each fluid. Pedersen et al. [31] proposed the above equation, and evaluated it for a large number of North Sea reservoir fluids with measured compositional analysis to  $C_{80+}$ . The above simple expression was capable of representing the measured data so well that the authors did not see any advantage in having measured compositional analysis beyond  $C_{20+}$  in preference to calculated data from Eq.(6.28).

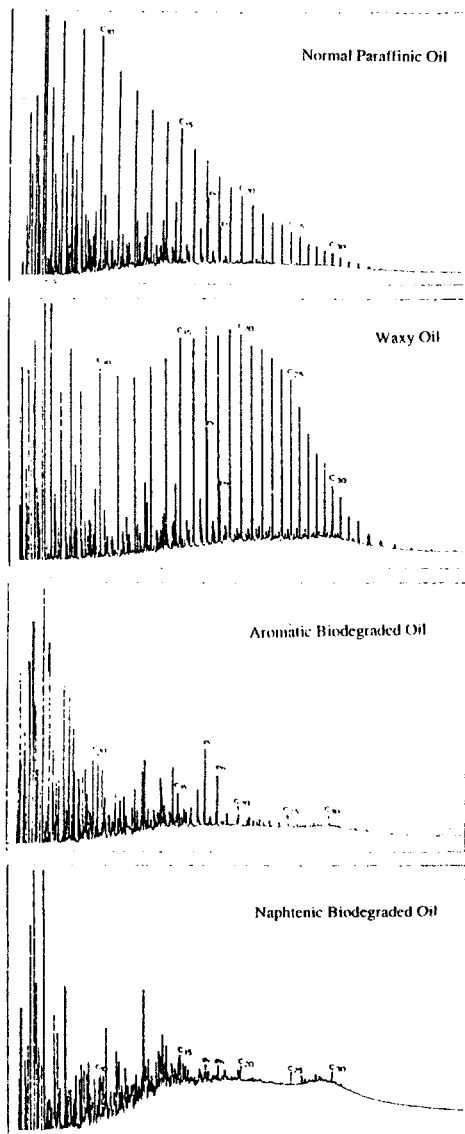


Figure 6.10. Gas chromatograms of four different types of oil samples showing the distribution of various components. Reprinted with permission [12]. Copyright (1989) American Chemical Society.

In phase behaviour calculations the carbon number is not directly used, hence, it must be replaced by some physical properties. The molecular weight is often related to the carbon number by,

$$M_{C_n} = 14n - \delta \quad (6.29)$$

where  $\delta$  depends on the chemical nature of the SCN group. A value of  $\delta=4$  is a reasonable approximation in most cases [30],

$$M_{C_n} = 14n - 4 \quad (6.30)$$

The above correlation, suggests that Eq.(6.28), can equally be written in terms of the molecular weight instead of the carbon number,

$$\ln z_{C_n} = A + BM_{C_n} \quad (6.31)$$

Obviously, the constants in the two equations have different values.

The above exponential function is also as valid when the concentration is expressed in terms of weight fraction instead of mole fraction. The expression in weight basis may even be more appropriate for some fluids. The advantage of weight basis is the lack of need for the molecular weight data of SCN groups, which are not available for very heavy fractions.

When partial analysis of the  $C_{7+}$  is available, the constants can be determined by regression, minimising the sum of squared differences between the calculated and measured concentration of known SCN groups.

### Example 6.2.

The total concentration of  $C_{7+}$  fraction of a gas condensate is 3.92 mole% with the analysis as follows. Extend the analysis to  $C_{30+}$  by SCN groups.

Table E6.2.  
Composition and properties of  $C_{7+}$  fraction.

Component	Mole %	M	S
$C_7$	20.20	94	0.730
$C_8$	21.41	117	0.754
$C_9$	12.11	126	0.769
$C_{10}$	9.23	140	0.785
$C_{11}$	7.17	153	0.799
$C_{12}$	5.68	165	0.806
$C_{13}$	4.27	180	0.820
$C_{14}$	3.05	197	0.843
$C_{15}$	2.43	209	0.844
$C_{16+}$	14.45	374	0.909

### Solution:

Figure E6.2 shows the relation between the molar concentration and molecular weight of SCN groups in this example. Note that the assumption of a linear relation between the logarithm of mole fraction and the molecular weight, Eq.(6.31), is reasonable for this fluid. The two parameters of A and B of Eq.(6.31) can be determined by the least square fit (excluding  $C_{16+}$ ), resulting in,



$$\ln x_{C_n} = 0.4665 - 0.020056M_{C_n}$$

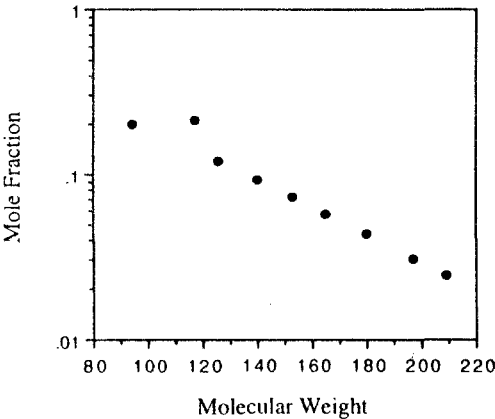


Figure E6.2. Relation of molar concentration with molecular weight for SCN groups.

The molecular weight and specific gravity of SCN from C<sub>16</sub> to C<sub>29</sub>, are assumed to be the same as those in the generalised table properties, Table 6.1. Substituting the molecular weights in the above relation returns the results as given in the following table.

SCN	M	S	$x_i$	$x_i M_i$	$x_i M_i / S_i$
C7	94	0.730	0.2020	18.9880	26.01
C8	117	0.754	0.2141	25.0497	33.22
C9	126	0.769	0.1211	15.2586	19.84
C10	140	0.785	0.0923	12.9220	16.46
C11	153	0.799	0.0717	10.9701	13.73
C12	165	0.806	0.0568	9.3720	11.63
C13	180	0.820	0.0427	7.6860	9.37
C14	197	0.843	0.0305	6.0085	7.13
C15	209	0.844	0.0243	5.0787	6.02
C16	222	0.843	0.0186	4.1237	4.89
C17	237	0.851	0.0137	3.2586	3.83
C18	251	0.856	0.0104	2.6062	3.04
C19	263	0.861	0.0082	2.1467	2.49
C20	275	0.866	0.0064	1.7645	2.04
C21	291	0.871	0.0047	1.3546	1.56
C22	300	0.876	0.0039	1.1659	1.33
C23	312	0.881	0.0031	0.9532	1.08
C24	324	0.885	0.0024	0.7781	0.88
C25	337	0.888	0.0019	0.6236	0.70
C26	349	0.892	0.0015	0.5076	0.57
C27	360	0.896	0.0012	0.4200	0.47
C28	372	0.899	0.0009	0.3411	0.38
C29	382	0.902	0.0008	0.2867	0.32
Total			0.933	131.7	166.99

(a) The  $C_{30+}$  mole fraction is calculated as,

$$x_{C_{30+}} = 1 - \sum_{C_7}^{C_{29}} x_{C_n} = 1 - 0.933 = 0.067$$

(b) The  $C_{7+}$  fraction molecular weight and specific gravity should remain the same when the fluid is described to  $C_{30+}$ . Hence the molecular weight of  $C_{30+}$  is determined as,

$$M_{C_{7+}} = \sum_{C_7}^{C_{16+}} x_{C_n} M_{C_n} = 165.4 = \sum_{C_7}^{C_{29}} x_{C_n} M_{C_n} + x_{C_{30+}} M_{C_{30+}} = 131.7 + 0.067 \times M_{C_{30+}}$$

$$M_{C_{30+}} = 503$$

(c) The volume of  $C_{7+}$  fraction can be considered equal to the sum of volumes of all its components. Hence a similar approach to that of molecular weight can be used to calculate the  $C_{30+}$  specific gravity.

$$M_{C_{7+}} / S_{C_{7+}} = \sum_{C_7}^{C_{16+}} x_{C_n} M_{C_n} / S_{C_n} = 202.86 = 165.4 / S_{C_{7+}}$$

$$S_{C_{7+}} = 0.815$$

The volume balance for  $C_{7+}$  results in,

$$M_{C_{7+}} / S_{C_{7+}} = \sum_{C_7}^{C_{29}} x_{C_n} M_{C_n} / S_{C_n} + x_{C_{30+}} M_{C_{30+}} / S_{C_{30+}} = 166.99 + 0.0671 \times 503 \times M_{C_{30+}} / S_{C_{30+}} = 202.87$$

$$S_{C_{30+}} = 0.940$$

The molecular weight and specific gravity of  $C_{30+}$  could have been calculated in this example by the mass and volume balance for the  $C_{16+}$  fraction only, instead of the  $C_{7+}$  fraction.

When little or no compositional analysis of the  $C_{7+}$  is available, the two constants can be determined by solving the following two material balance equations:

$$\sum_{C_7}^{C_N} z_{C_n} = \sum_{C_7}^{C_N} \exp(A + BM_{C_n}) = z_{C_{7+}} \quad (6.32)$$

$$z_{C_n} M_{C_n} = \sum_{C_7}^{C_N} \exp(A + BM_{C_n}) M_{C_n} = z_{C_{7+}} M_{C_{7+}} \quad (6.33)$$

$C_N$  is the heaviest carbon number assumed to be present in the mixture. Values of 50 [32] to 80 [31], have been suggested as the cut-off carbon number, whereas larger molecules with higher carbon numbers are generally present in oil and gas condensate systems. The choice of the cut-off carbon number, however, has very little effect on predicted results by EOS in most cases, as the contribution of very heavy fractions, due to their low concentrations, is minimal for practical purposes.

*Example 6.3.*

The mole fraction, molecular weight and specific gravity of the C<sub>7+</sub> fraction of a gas condensate sample are 0.0392, 165 and 0.815, respectively. Describe the C<sub>7+</sub> fraction by SCN groups extended to C<sub>20+</sub>.

*Solution:*

Rewriting Eq.(6.31), we obtain,

$$z_{C_n} = e^{(A + BM_{C_n})}$$

$$z_{C_{7+}} = \sum_{C_7}^{C_N} z_{C_n} = e^A \sum_{C_7}^{C_N} e^{BM_{C_n}}$$

Similarly for Eq.(6.33), we obtain,

$$z_{C_{7+}} M_{C_{7+}} = \sum_{C_7}^{C_N} z_{C_n} M_{C_n} = e^A \sum_{C_7}^{C_N} M_{C_n} e^{BM_{C_n}}$$

Hence,

$$M_{C_{7+}} = \left( \sum_{C_7}^{C_N} M_{C_n} e^{BM_{C_n}} \right) / \left( \sum_{C_7}^{C_N} e^{BM_{C_n}} \right)$$

that is,

$$\sum_{C_7}^{C_N} (M_{C_n} - M_{C_{7+}}) e^{BM_{C_n}} = 0 \quad (E6.3)$$

Eq.(E6.3) demonstrates that the slope of the SCN group distribution line, B, depends only on the molecular weight of C<sub>7+</sub>. The parameter A affects only the mole fraction of C<sub>7+</sub> in the mixture, by shifting the line up or down in Figure E6.2.

$$A = \ln z_{C_{7+}} - \ln \left( \sum_{C_7}^{C_N} e^{BM_{C_n}} \right) \quad (E6.3')$$

Normalising the distribution of SCN groups in the C<sub>7+</sub> fraction, by making  $z_{C_{7+}}=1$ , results in,

$$A = \ln z_{C_{7+}} - \ln \left( \sum_{C_7}^{C_N} e^{BM_{C_n}} \right)$$

That is, just the molecular weight of C<sub>7+</sub> fraction is sufficient to describe the distribution of its comprising SCN groups.

Assuming SCN groups with molecular weights equal to those in the generalised table, Table 6.1, and C<sub>45</sub> as the heaviest fraction present in the mixture, Eq.(E6.3) results in,

$$B = -0.0131418.$$

Substituting the B value in Eq.(E6.3'), the value of A is determined equal to -3.8098671. Eq.(6.31) is then used to calculate the mole fraction of SCN groups as given in the following table.

SCN Group	C7	C8	C9	C10	C11	C12	C13	C14	C15	C16
Mole %	0.6273	0.5429	0.4516	0.3807	0.3209	0.2670	0.2221	0.1824	0.1478	0.1198
SCN Group	C17	C18	C19	C20	C21	C22	C23	C24	C25	C26
Mole %	0.0983	0.0818	0.0699	0.0597	0.0484	0.0430	0.0367	0.0313	0.0264	0.0226
SCN Group	C27	C28	C29	C30	C31	C32	C33	C34	C35	C36
Mole %	0.0195	0.0167	0.0146	0.0125	0.0110	0.0095	0.0082	0.0071	0.0064	0.0055
SCN Group	C37	C38	C39	C40	C41	C42	C43	C44	C45	
Mole %	0.0050	0.0043	0.0038	0.0033	0.0030	0.0026	0.0024	0.0021	0.0019	

The  $C_{20+}$  fraction is determined by summing up  $C_{20}$ - $C_{45}$  mole fractions,  $z_{C_{20+}}=0.4074\%$ , with the molecular weight determined as:

$$M_{C_{20+}} = \sum_{C_{20}}^{C_{45}} x_{C_n} M_{C_n} = 343$$

Assuming that SCN groups have the same specific gravity as those in the generalised table, the specific gravity of  $C_{20+}$  is determined similar to that in Example 6.2.

$$z_{C_{20+}} M_{C_{20+}} / S_{C_{20+}} = \sum_{C_{20}}^{C_{45}} z_{C_n} M_{C_n} / S_{C_n}$$

$$S_{C_{20+}}=0.892$$

The normalised mole fractions of SCN groups in the  $C_{20+}$  fraction calculated in this example are given in the following table for comparison with those calculated in Example 6.2, that is, for a fluid with the same  $C_{20+}$  fraction properties.

SCN	E.6.3	E.6.2
C7	0.1600	0.2020
C8	0.1385	0.2141
C9	0.1152	0.1211
C10	0.0971	0.0923
C11	0.0819	0.0717
C12	0.0681	0.0568
C13	0.0567	0.0427
C14	0.0465	0.0305
C15	0.0377	0.0243
C16	0.0306	0.0186
C17	0.0251	0.0137
C18	0.0209	0.0104
C19	0.0178	0.0082
C20+	0.1039	0.0936

### Continuous Description

The above approach of describing the concentration of SCN groups by a function, may appear as a continuous description of the fluid, but it is basically a discrete representation. The function describes the heavy part by a number of SCN groups, and is only valid at the discrete

carbon numbers. In mathematical terms, the function provides the value of concentration integral between  $C_{n-1}$  and  $C_n$ ,

$$z_{C_n} = \int_{C_{n-1}}^{C_n} dz_i \quad (6.34)$$

where  $i$  refers to all the components comprising the SCN group  $n$ .

A more appropriate approach is the continuous description of the fluid, where the distribution of all its constituents, instead of carbon groups, is aimed. Indeed the carbon groups reported by laboratories are determined by integration of compounds comprising the groups. For example, the area under the curve in Figure 6.4 between  $nC_9$  and  $nC_{10}$  is taken as the concentration of  $C_{10}$  group.

The continuous description reflects the true nature of reservoir fluids that are composed of many compounds, with properties varying so gradually that do not allow distinctive identification.

The continuous distribution of components can be expressed by a function,  $F(I)$ , such that,

$$\int F(I) dI = z \quad (6.35)$$

where  $z$  is the total concentration of all the components, represented by  $I$ , within the integral boundaries. If all the components of a fluid is described by the continuous description, then,

$$\int_0^1 F(I) dI = 1 \quad (6.36)$$

In the more practical semi-continuous description, only the heavy part (say  $> C_7$ ) is described by the continuous function,

$$\int_0^1 F(I) dI = z_D \quad (6.37)$$

where  $z_D$  is the concentration of the heavy fraction of the fluid described by the continuous description. The distribution function is generally selected such that the value of integral in Eq.(6.37) becomes equal to 1, that is, it describes the relative concentration within the continuous part. Hence, in the semi-continuous approach the calculated concentration of the continuous constituents should be multiplied by  $z_D$  to normalise it in the total mixture.

The intensity distribution,  $F(I)$ , or the probability of occurrence in statistical terms, is often expressed by molar distribution, and so used in this book. The mass or volume distribution, as obtained in gas chromatography or distillation, respectively, can also be used to describe the concentration. The variable  $I$ , can be the carbon number or any property, such as the molecular weight or the boiling point, characterising the compounds comprising the fluid.

It should be noted that the continuous distribution is valid at all the values of  $I$ , within the identified range of components, contrary to the SCN group function which is valid only at the discrete carbon numbers. The mole fraction of SCN group  $n$ , can be determined simply by integrating the distribution function between  $(n-1)$  and  $n$ ,

$$\int_{I_{n-1}}^{I_n} F(I) dI = z_{C_n} \quad (6.38)$$

Similarly, the mole fraction of any carbon group, or pseudo component, can be determined by incorporating the appropriate boundaries in the above integral.

When the molecular weight of each component,  $M$ , is used to represent it in the distribution function, that is  $I \equiv M$ , the above equation becomes,

$$\int_{M_{n-1}}^{M_n} F(M) dM = z_{C_n} \quad (6.39)$$

which is the area under the curve of  $F(M)$  between  $M_{n-1}$  and  $M_n$ .

The molecular weight of SCN group  $n$ , is determined by,

$$\int_{M_{n-1}}^{M_n} F(M) M dM = M_{C_n} z_{C_n} \quad (6.40)$$

The most widely used distribution function is the gamma probability function, as proposed by Whitson [9], using the molecular weight as the characterisation variable,

$$F(M) = \frac{(M - \tau)^{\gamma-1} \exp[-(M - \tau)/\beta]}{\beta^\gamma \Gamma(\gamma)} \quad (6.41)$$

where  $\Gamma(\gamma)$ , is the gamma function,  $\tau$  is the minimum molecular weight included in the distribution, and  $\gamma$  and  $\beta$  determine the shape of the distribution function with the mean and the variance equal to  $(\gamma\beta + \tau)$  and  $\gamma\beta^2$ , respectively. Hence,

$$\beta = (M_D - \tau) / \gamma \quad (6.42)$$

where  $M_D$  is the average molecular weight of the continuous part, comprised of compounds with molecular weights beginning from  $\tau$  and extending to infinity.

The gamma function is,

$$\Gamma(\gamma) = \int_0^\infty \xi^{\gamma-1} e^{-\xi} d\xi \quad (6.43)$$

which can be estimated from the following expressions [33],

$$\Gamma(\gamma) = 1 + \sum_{i=1}^8 A_i (\gamma - 1)^i \quad 1 \leq \gamma \leq 2 \quad (6.44)$$

where  $A_i$  represents the parameters in the approximate polynomial,

$A_1 = -0.577191652$	$A_5 = -0.756704078$
$A_2 = 0.988205891$	$A_6 = 0.482199394$
$A_3 = -0.897056937$	$A_7 = -0.193527818$
$A_4 = 0.918206857$	$A_8 = 0.035868343$

For  $\gamma$  values outside the range in Eq.(6.44), the recurrence formula may be used to evaluate the gamma function,

$$\Gamma(\gamma - 1) = \frac{\Gamma(\gamma)}{\gamma - 1} \quad (6.45)$$

The distribution function is generally used to describe the  $C_{7+}$  fraction, with its parameters determined by regression to match the available SCN group experimental data, using Eqs.(6.39) and (6.40). The value of  $\tau$  should be between 86 and 100, the molecular weights of  $nC_6$  and  $nC_7$ , respectively, based on the definition of  $C_{7+}$ . It can be treated, however, as a tuning parameter in the regression, or assumed equal to the mid-value of 90 in the absence of measured SCN group data. The function so developed can then be used to extend the fluid description to heavier compounds.

The value of  $\gamma$ , ranging approximately between 0.5 to 2.5 for typical reservoir fluids, controls the distribution skewness. Figure 6.11 shows typical distributions with different values of  $\gamma$  for a  $C_{7+}$  fraction with  $M_{C_{7+}}=200$  and  $\tau=92$ . Values of  $\gamma$  equal to, or less than, one represent mixtures with continuous decline in concentration, whereas values more than one demonstrate a maximum in concentration. The peak will shift towards heavier fractions by increasing the  $\gamma$  value.

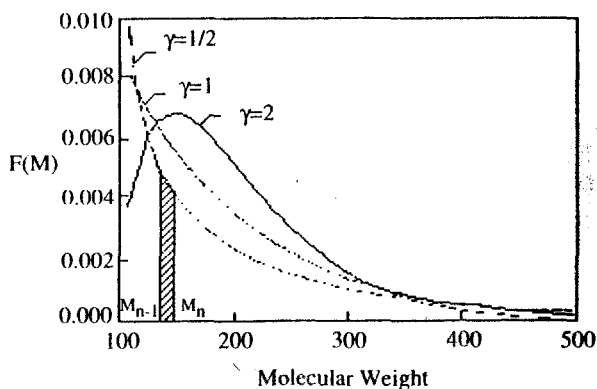


Figure 6.11. Distribution of components represented by the gamma probability function with different values of  $\gamma$ . SPE Copyright. Reproduced from [9] with permission.

As described by Eq.(6.39), the fraction of area under the curve between two molecular weights, identified by the shaded area in Figure 6.11, demonstrates the mole fraction of a pseudo component comprised of all compounds with molecular weights between  $M_{n-1}$  and  $M_n$ .

The value of  $\gamma=1$ , reduces the gamma distribution function to,

$$F(M) = \{\exp[-(M - \tau)/\beta]\} / \beta \quad (6.46)$$

which is a simple exponential distribution,

$$F(M) = \frac{\exp(\tau/\beta)}{\beta} \exp(-M/\beta) \quad (6.47)$$

Substituting the above distribution function in Eq.(6.38), and integrating it, we obtain,

$$z_{C_n} = -\exp(\tau/\beta) \left[ \exp(-M_n/\beta) - \exp(-M_{n-1}/\beta) \right] \quad (6.48)$$

where  $M_n$  and  $M_{n-1}$  are the upper and lower molecular weights of the components present in the SCN group  $n$ .

The molecular weight of SCN groups is determined by substituting the distribution function in Eq.(6.40),

$$M_{C_n} = -\beta \exp(\tau/\beta) \left[ \left( \frac{M_n}{\beta} + 1 \right) \exp(-M_n/\beta) - \left( \frac{M_{n-1}}{\beta} + 1 \right) \exp(-M_{n-1}/\beta) \right] / z_{C_n} \quad (6.49)$$

Eq.(6.48) can be written in the simple logarithmic form of Eq.(6.31) by relating  $M_n$  and  $M_{n-1}$  together. Assuming that  $M_n - M_{n-1} = 14$ , we obtain,

$$\ln z_{C_n} = \ln \left[ \exp \left( \frac{14}{M_D - \tau} \right) - 1 \right] - \frac{M_n - \tau}{M_D - \tau} \quad (6.50)$$

which is similar to Eq.(6.31), with the values of A and B as follows:

$$A = \left\{ \ln \left[ \exp \left( \frac{14}{M_D - \tau} \right) - 1 \right] + \frac{\tau}{M_D - \tau} \right\} \quad (6.51)$$

$$B = -\frac{1}{M_D - \tau} \quad (6.52)$$

Eq.(6.52) can be used to calculate an initial guess for B to solve Eq.(E6.3). Note that  $M_n$  in Eq.(6.50) is the highest molecular weight present in the SCN group and  $M_{C_n}$  in Eq.(6.31) is the molecular weight of SCN group.

#### Example 6.4.

Describe the  $C_{7+}$  fraction of the fluid in Example 6.3 by a continuous function in terms of the molecular weight, and use it to estimate the mole fraction of SCN groups comprising the  $C_{7+}$  fraction.

#### Solution:

The value of  $\gamma$  is assumed equal to one, due to lack of partial analysis of the  $C_{7+}$  fraction. The value of  $\beta$  can be calculated from Eq.(6.42) after selecting the lowest molecular weight present in  $C_{7+}$ , that is,  $\tau$ .

The simplest approach is to select the normal alkane molecular weights as the SCN group boundaries. Hence, normal hexane will be the component with the lowest molecular weight compound present,  $\tau=86$ , which results in  $\beta=79$ . Therefore, the distribution function of the  $C_{7+}$  fraction in terms of the molecular weight, Eq.(6.47), becomes,

$$F(M) = 0.0376 \exp(-M/79)$$



The mole fractions of SCN groups can be determined from Eq.(6.49), with  $M_n=14n+2$  for normal alkane boundaries,

$$\ln z_{C_n} = \ln \left[ \exp \left( \frac{14}{M_b - \tau} \right) - 1 \right] - \frac{(14n + 2) - \tau}{M_b - \tau}$$

which results in,

$$z_{C_n} = z_{C_{71}} \exp(-0.5518671 - M_n/79) = 0.0392 \times \exp(-0.57718 - 0.177215n)$$

Note that the normalised mole fractions, calculated by Eq.(6.50), have been multiplied by the  $C_{71}$  mole fraction.

The mole fraction of each SCN group can be determined from the above equation. The sum of mole fractions becomes equal to  $z_{C_{71}}$ , only when carbon numbers up to infinity are included. The contribution of very heavy compounds to the total mole fraction, however, becomes insignificant, as shown in the following table for various cut-off carbon numbers.

Last carbon number	Last molecular weight	Total normalised mole fractions
30	422	0.9858
40	562	0.9976
50	702	0.9996
60	842	0.9999

In phase behaviour calculations, the properties of identified SCN groups must be known. Although the selection of molecular weights of normal alkanes as the boundaries agrees with the conventional definition of SCN groups, that is the fraction collected between two consecutive normal alkane boiling points, it results to carbon groups with average molecular weights significantly different from those of generalised values. For example, the  $C_{44}$  group of this example has, by the above approach, a molecular weight of 625, whereas that of the generalised SCN group has a molecular weight of 539, Table A.2. This is due to presence of aromatics and naphthenes in the sample under consideration. Hence, the use of SCN group properties for the above characterisation is not justified.

In order to characterise the  $C_n$  fraction with SCN groups similar to those in the generalised table, their molecular weights should be used to identify the group boundaries. The molecular weight boundaries can be determined by solving Eq.(6.49) for the generalised SCN groups. The dependency of calculated boundaries on the  $C_{71}$  molecular weight and selected value of  $\tau$ , is insignificant. The calculated results will not typically deviate more than one unit from the values determined by simple linear averaging,

$$M_n = (M_{C_{n+1}} - M_{C_n})/2 + M_{C_n}$$

The SCN group molecular weight boundaries, and the values of group molecular weight calculated by Eq.(6.49) are given in Table E6.4, and compared with the generalised values. Note that the values are equal within the accuracy of measurement. The given molecular weight boundaries are general and can be used for other fluids in the absence of measured molecular weight.

Table E6.4.  
Generalised SCN group molecular weight boundaries.

SCN	Upper Molecular Weight Boundary	SCN Group Molecular Weight, Eq.(6.49)	Generalised SCN Group Molecular Weight, Table 6.1
	kg/kgmol	kg/kgmol	kg/kgmol
C7	102	96	96
C8	113	107	107
C9	128	120	121
C10	141	134	134
C11	154	147	147
C12	168	161	161
C13	182	175	175
C14	198	190	190
C15	214	206	206
C16	230	222	222
C17	244	237	237
C18	257	250	251
C19	269	263	263
C20	283	276	275
C21	295	289	291
C22	306	300	300
C23	318	312	312
C24	331	324	324
C25	343	337	337
C26	355	349	349
C27	366	360	360
C28	377	371	372
C29	388	382	382
C30	399	393	394
C31	409	404	404
C32	420	414	415
C33	432	426	426
C34	442	437	437
C35	450	446	445
C36	460	455	456
C37	470	465	464
C38	479	474	475
C39	490	484	484
C40	499	494	495
C41	507	503	502
C42	517	512	512
C43	526	521	521
C44	535	530	531
C45	544	539	539

Selecting  $\tau=90$ , the value of  $\beta$  is calculated from Eq.(6.42) equal to 75, with the distribution function as,

$$F(M)= 0.04427 \exp(-M/75)$$

The mole fractions of SCN groups can be determined from Eq.(6.48), with the molecular weight boundaries given in the above table. The results are as follows:

SCN Group	C7	C8	C9	C10	C11	C12	C13	C14	C15	C16
Mole %	0.5573	0.5162	0.4689	0.3784	0.3293	0.2843	0.2436	0.2132	0.1784	0.1401
SCN Group	C17	C18	C19	C20	C21	C22	C23	C24	C25	C26
Mole %	0.1073	0.0800	0.0625	0.0614	0.0459	0.0331	0.0325	0.0288	0.0244	0.0191
SCN Group	C27	C28	C29	C30	C31	C32	C33	C34	C35	C36
Mole %	0.0164	0.0135	0.0116	0.0101	0.0083	0.0076	0.0065	0.0049	0.0043	0.0038
SCN Group	C37	C38	C39	C40	C41	C42	C43	C44	C45+	
Mole %	0.0034	0.0031	0.0027	0.0022	0.0018	0.0018	0.0016	0.0013	0.0104	

The mole fraction of C<sub>45</sub> has been adjusted to make the total mole equal to 3.92%, i.e., the mole fraction of C<sub>7</sub>, in the original fluid.

When sufficient information on the distribution of SCN groups in C<sub>7+</sub> fraction and their molecular weight is available, the parameters of the distribution function can be optimised by matching the measured group data, instead of assuming  $\gamma=1$  and using generalised molecular weight data as in the above example.

Whitson et al. [34] proposed a procedure where the measured mass fraction of each SCN group is used to regress the three parameters of the gamma function while adjusting the molecular weight boundaries of SCN groups. They applied the method to 44 gas condensate and oil samples, and determined the parameters of the gamma probability distribution function for them. The authors concluded that  $\tau$  and  $\gamma$  could be reasonably correlated by,

$$\tau = 110 \left[ 1 - 1 / \left( 1 + \frac{4.043}{\gamma^{0.721}} \right) \right] \quad (6.53)$$

Hence the optimisation can only be conducted for  $\gamma$  and  $\beta$ , with  $\tau$  related to  $\gamma$  by the above equation.

In their proposed method a value for  $\gamma$  is initially assumed, ca.  $\gamma=1$ , and values of  $\tau$  and  $\beta$  are calculated from Eqs.(6.53) and (6.42), respectively. Then the upper boundary of the first group is assumed and its mass fraction is calculated by,

$$w_{C_n} = z_{C_n} M_{C_n} / (\tau + \gamma \beta) \quad (6.54)$$

where  $z_n$  and  $M_n$  are the mole fraction and molecular weight of the selected group using Eqs.(6.39) and (6.40), respectively. If the above calculated mass fraction does not match the experimental value, within a tolerance of  $10^{-7}$ , the upper boundary of the molecular weight is adjusted. The assumption and adjustment of the upper molecular weight boundaries are continued for other carbon groups sequentially, up to the plus fraction. The sum square deviations of calculated molecular weights of the groups, using Eq.(6.40), from the measured values are then evaluated. The parameters of  $\gamma$  and  $\beta$  are optimised by minimising the above sum. After the optimised values are determined the reliability of the model is checked by comparing the calculated molecular weights and mole fractions with the experimental data.

The use of SCN group data to determine the parameters of any continuous description is only reliable when the concentration and molecular weight of sufficient number of SCN groups are known. Whitson et al. [34], evaluated their proposed method using different numbers of SCN group data. In general the method was found reliable when information on more than 15 groups were used in optimisation of the parameters.

### Direct Application

The continuous distribution function can be used in phase behaviour calculations similar to discrete components. The distribution function, as expressed by the integral in Eq.(6.35),

replaces the concentration of individual discrete components. The properties of the components, such as the critical properties required in equations of state, are also expressed by continuous functions of the variable  $I$ , which represent comprising compounds.

For example, the two parameters of a van der Waals type equation of state, using the random mixing rules of Eqs.(4.73-74), for a mixture described by the semi-continuous method, are calculated as,

$$a = \sum_i^N \sum_j^N x_i x_j (a_i \cdot a_j)^{0.5} + \left[ \int_0^1 F(I) (a(I))^{0.5} dI \right]^2 + 2 \sum_i^N x_i a_i^{0.5} \int_0^1 F(I) (a(I))^{0.5} dI \quad (6.55)$$

where the first term accounts the attraction between the discrete compounds, the second is that of the continuous fraction, and the third is due to interaction between the discrete and the continuous parts.

Similarly for the repulsive term, or co-volume, we get,

$$b = \sum_i^N x_i b_i + \int_0^1 F(I) b(I) dI \quad (6.56)$$

The terms  $a(I)$  and  $b(I)$  are some continuous functions of  $I$  with values equal to parameters  $a$  and  $b$ , respectively, for compounds described by the continuous description. Examples of such functions are those given by Cotterman [35], for the Soave-Redlich-Kwong EOS, where he uses the molecular weight as the parameter representing compounds.

The equality of fugacity of each component in co-existing phases at equilibrium is expressed for the discrete and the continuous parts, as follows,

$$f_i^V = f_i^L \quad (3.30)$$

$$f^V(I) = f^L(I) \quad (6.57)$$

The material balance equations required for phase behaviour calculations, Section 5.1, need to be modified also by including the continuous description. For a mixture described by the semi-continuous method, the material balance equations for the total mixture and the discrete components remain the same as Eqs.(5.1-2), with an additional equation for the continuous fraction,

$$n^F F^F(I) = n^L F^L(I) + n^V F^V(I) \quad (6.58)$$

where  $F^F(I)$ ,  $F^L(I)$  and  $F^V(I)$  are the distribution functions for the continuous fractions of feed, liquid and vapour respectively. It has been shown that when a distribution function, such as Eq.(6.41), describes the continuous fraction of a phase, the same type of function also describes the other equilibrated phase [36]. The range of compounds described by all three functions is the same, that is  $\tau$  in Eq.(6.41), but other parameters,  $\gamma$  and  $\beta$ , are generally different.

The use of the distribution function, and the resulting derivatives from Eq.(3.31), to determine the fugacity coefficients leads to complex integral equations which can only be solved

numerically even for simple distribution functions. Amongst the numerical methods applied successfully [36], the method of Gaussian quadrature has proved to be reliable and practical.

The method approximates the value of integral numerically by adding the weighted values of a function at a number of specified values of the variable, called the quadrature points,

$$\int_1 f(I) \exp(-I) d(I) = \sum_k w_k f(I_k) \quad (6.59)$$

where  $w_k$  is the weight and  $f(I_k)$  is the value of the function  $f(I)$  at the quadrature point, or root,  $k$ .

Selecting the gamma probability function, Eq.(6.41), to describe the continuous fraction, the integral in Eq.(6.37) becomes,

$$\int_1 \frac{(M - \tau)^{\gamma-1} \exp[-(M - \tau)/\beta]}{\beta^\gamma \Gamma(\gamma)} dM = 1 \quad (6.60)$$

It should be noted that the function provides the distribution of the constituents within the continuous part, hence, with a total value of 1.

Defining a new variable,

$$\chi \equiv (M - \tau)/\beta \quad (6.61)$$

reduces Eq.(6.60) to,

$$\frac{\chi^{\gamma-1} \exp(-\chi)}{\Gamma(\gamma)} d\chi = 1 \quad (6.62)$$

which can be shown as,

$$\int_0^\infty f(\chi) \exp(-\chi) d\chi = 1 \quad (6.63)$$

where

$$f(\chi) \equiv \frac{\chi^{\gamma-1}}{\Gamma(\gamma)} \quad (6.64)$$

Substitution of the compositional distribution of Eq.(6.63) for  $\int_1 F(I) dI$ , in Eqs.(6.55-56), reduces the integrals in the expressions for  $a$  and  $b$ , to the following general form,

$$\int_0^\infty f(\chi) \exp(-\chi) d\chi \quad (6.65)$$

Obviously the function  $f(\chi)$  is different to that in Eq.(6.63) and depends on the expressions for  $a(M)$  and  $b(M)$ . The roots and weights, however, are the same for the integrals as they all belong to the same class (Gauss-Laguerre) of functions.

Applying the quadrature integration method to Eq.(6.63), we obtain,

$$z_k = w_k f(l_k) = w_k f(\chi_k) = w_k \frac{\chi_k^{\gamma-1}}{\Gamma(\gamma)} \quad (6.66)$$

where,

$$\sum z_k = 1 \quad (6.67)$$

and

$$M_k = \chi_k \beta + \tau \quad (6.68)$$

That is, the values of root and weight at each quadrature point can identify a pseudo component, or a carbon group,  $k$ , with the molecular weight and mole fraction given by Eqs.(6.68) and (6.66), respectively. The calculated mole fractions are relative to the continuous part and should be normalised by multiplying them with  $z_D$ .

Therefore, replacing the continuous part with a number of pseudo components equal to the number of quadrature points, with the molecular weights and mole fractions as given above, should lead to the same values of  $a$  and  $b$ , as those by the continuous approach, Eqs. (6.55-56).

Behrens and Sandler [32] were the first who suggested to use the pseudo components determined at the quadrature points of the feed distribution function in vapour-liquid equilibrium calculations. They assumed a linear logarithmic distribution function,  $\gamma=1$  in Eq.(6.41), with  $C_{50}$  as the last carbon number to describe a number of oil and gas condensate samples. They used two point quadrature integration procedure and demonstrated the capability of the proposed method.

The accuracy of calculations increases with increasing the number of quadrature points. Any large molecular weight can be selected as the cut-off point of the distribution function with little effect on the results. For mathematical simplicity, the distribution can be assumed to extend to infinity. The roots and weights for 2, 3 and 4 point integration, with the continuous function extending to infinity, are given in the following Table.

Table 6.7.  
Roots and weights for the quadrature method.

Two Quadrature Points				
Root, $\chi$	0.5858	3.4142		
Weight, $w_k$	0.8536	0.1464		
Three Quadrature Points				
Root, $\chi$	0.4158	2.2943	6.2900	
Weight, $w_k$	0.7111	0.2785	0.0104	
Four Quadrature Points				
Root, $\chi$	0.3226	1.7458	4.5366	9.3951
Weight, $w_k$	0.6032	0.3574	0.0389	0.0005

Note that even with only four quadrature point integration the weight of the last point, representing the concentration of the last pseudo component, is quite small. Higher numbers of the quadrature points hardly improve the results, particularly as the molecular weight of the last pseudo component will become excessively high for which physical properties cannot be estimated reasonably.

The above approach identifies each pseudo-component by its carbon number, or molecular weight only. Approximate expressions relating critical properties to carbon number, such as

those developed by Ahmed [19] using the generalised SCN group data, can be used to estimate these properties, Table A.2 in Appendix A. A more specific approach for each fluid is to assume that the characterisation factor of all the pseudo components are the same, and use Eq.(6.4) which relates the molecular weight to specific gravity.

$$K_w = 4.5579 M^{0.15178} S^{-0.84573} \quad (6.4)$$

In this approach, the Watson characterisation factor is calculated first for the total continuous part, e.g. the  $C_{7+}$  fraction, using the measured values. The same  $K_w$  is then used for all the pseudo components to determine their specific gravity.

Whitson et al. [37] observed that using a constant Watson characterisation factor for all pseudo components leads to specific gravity values which do not correspond to the specific gravity of the mixture, calculated by,

$$S_D = \left[ \sum_{k=1}^N z_k M_k / \left( \sum_{k=1}^N z_k M_k / S_k \right) \right] \quad (6.69)$$

Hence they solved the above equation simultaneously with Eq.(6.4), and introduced a different characterisation factor,  $C$ ,

$$C = \left[ 0.16637 S_D \sum_{k=1}^N z_k M_k^{0.86459} / (z_D M_D) \right]^{-0.84573} \quad (6.70)$$

and proposed the following relation between the molecular weight and specific gravity,

$$S_k = 6.0108 M_k^{0.13541} C^{-1.18241} \quad (6.71)$$

The calculated specific gravity and the molecular weight of each pseudo component are used in generalised property correlations, such as those proposed by Twu in Section 6.2, to estimate properties required in equations of state.

When the same type of function is used to describe the feed, vapour and liquid phases, the roots and weights at the quadrature points are the same for all the phases. The associated molecular weights of the pseudo components in each phase, however, are bound to be different. They will become the same only when  $\beta$  is the same for all phases, as required by Eq.(6.61). As  $\gamma\beta$  represents the mean of the distribution function, that is the average molecular weight which is different for the two equilibrated phases, the value of  $\beta$ , is generally different for the vapour, liquid and the feed. Figure 6.12 shows the distribution of SCN groups in the co-existing gas and condensate phases of a North Sea reservoir fluid at 11 MPa below its dew point. Clearly, a single distribution function cannot reliably describe both phases. Hence depending on the distribution used, that of feed, liquid, or vapour, the selected pseudo components will be different. Furthermore, the selected values will be only at the quadrature points for the phase whose  $\beta$  value has been used to calculate the group molecular weights.

The above treatment, however, does not significantly impair the results in most cases. The use of pseudo components at correctly selected quadrature points is as effective as describing the fluid by twice as many pseudo components randomly [36]. It is a valuable approach to reduce the number of components describing the fluid to speed up calculations, as described further in Section 9.1.

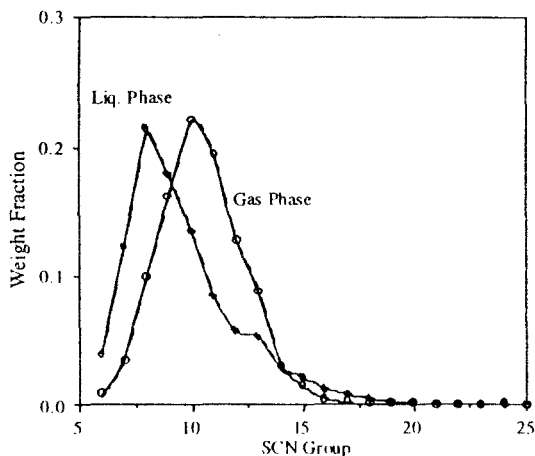


Figure 6.12. Distribution of SCN groups in equilibrated gas and condensate phases of a North Sea reservoir fluid.

#### Example 6.5.

Describe the C7+ fraction of the fluid in Example 6.4 with 4 pseudo components using the quadrature method.

*Solution:*

As  $\gamma=1$ , we obtain,  $\Gamma(\gamma)=1$  from Eq.(6.43) and,  $z_i=w_i$  from Eq.(6.66).

The molecular weight of pseudo-components are calculated from Eq.6.68, as,  
 $M_i = \chi_i \times 75 + 90$

with the results as given in the following table.

Pseudo-comp.	Root, $\chi$	Weight, $w=z$	M	$zM$	$zM^{0.86459}$	S	$z_i M_i / S_i$
1	0.3226	0.6032	114.20	68.88	36.26	0.7675	89.75
2	1.7458	0.3574	220.94	78.96	38.02	0.8393	94.08
3	4.5366	0.0389	430.25	16.74	7.36	0.9185	18.22
4	9.3951	0.0005	794.63	0.40	0.16	0.9981	0.40
Total		1		164.98	81.81	0.8149	202.45

Note that the calculated molecular weight of the mixture is almost equal to that of the measured value, and the contribution of the last pseudo component to it is quite small.

The specific gravity of each component is determined by initially calculating the characterisation factor defined in Eq.(6.70),

$$C = \left[ 0.16637 \times 0.815 \sum_{k=1}^N z_k M_k^{0.86459} / (165) \right]^{-0.84573} = 9.80826772$$



Substituting the above value in Eq.(6.71) provides the specific gravity of pseudo components as given in the above table.

Evaluating the calculated values of specific gravity, by

$$M_{C_7+}/S_{C_7+} = \sum_{k=1}^{k_4} z_k M_k / S_k$$

we obtain,  $S_{7+}=0.8149$ , which is the same as the mixture value.

The normalised mole fractions of the pseudo components calculated above should be multiplied by  $z_{7+}=0.0392$ , to obtain the mole fractions in the total mixture. The critical properties of the identified pseudo components can be calculated from Eq.(6.15), using their molecular weight and specific gravity values.

## 6.4 REFERENCES

1. Perry, A.J: "Introduction to Analytical Gas Chromatography", Dekker (1981).
2. ASTM: "Distillation of Crude Petroleum, Designation D2892-84", Annual Book of ASTM Standards, 821-860 (1984).
3. Varotsis, N. and Guieze, P: "Microdistillation, a Method Combining Gas and Liquid Chromatography to Characterise Petroleum Liquids", J. of Chromatography, 403, 159-170 (1987).
4. Pedersen, K.S., Thomasen, P. and Fredenslund, A: "Thermodynamics of Petroleum Mixtures Containing Heavy Hydrocarbons. I: Phase Envelope Calculations by use of the Soave-Redlich-Kwong Equation of State", Ind. Eng. Chem. Process Des. Dev., 23, 163-170 (1984).
5. Reid, A.L: "Characterisation of North Sea Reservoir Fluids", MPhil Thesis, Heriot-Watt University, Edinburgh, UK (1992).
6. Miquel, J., Hernandez, J. and Castells, F: "A New Method for Petroleum Fractions and Crude Oil Characterisation", SPE Res.Eng., 265-270 (1992).
7. Katz, D.L. and Firoozabadi, A: "Predicting Phase Behaviour of Condensate/ Crude Oil Systems Using Methane Interaction Coefficients", JPT, 1649-55 (Nov., 1978).
8. Bergman, D.F., Tek, M.R. and Katz, D.L: "Retrograde Condensation in Natural Gas Pipelines", Monograph Series, AGA, NY (1975).
9. Whitson C.H: "Characterising Hydrocarbon Plus Fractions", SPE J., 683-694 (Aug., 1983).
10. Haaland, S: "Characterisation of North Sea Crude Oils and Petroleum Fractions", Thesis, NIT, University of Trondheim (May, 1981).
11. Osjord, E.H., Ronningsen, H.P. and Tau, L: "Distribution of Weight, Density and Molecular Weight in Crude Oil Derived from Computerised Capillary GC Analysis", J. High Res. Chromatography, 8, 683-690 (1985).
12. Ronningsen, H.P., Skjevraak, I. and Osjord, E: "Characterisation of North Sea Petroleum Fractions: Hydrocarbon Group Types, Density and Molecular Weight", Energy and Fuels, 3, 744-755 (1989).

13. Robinson, D.B. and Peng, D.Y: "The Characterisation of the Heptanes and Heavier Fractions for the GPA Peng-Robinson Programs", GPA Research Report 28, Tulsa (1978).
14. Yarbrough, L: "Application of a Generalised Equation of State to Petroleum Reservoir Fluid", Equations of State in Engineering, Advances in Chemistry Series, Chao, K.C. and Robinson, R.L. (eds), American Chemical Soc., No. 182, 385-435 (1979).
15. Curvers, J. and van den Engel, P: "Gas Chromatographic Method for Simulated Distillation up to a Boiling Point of 750°C Using Temperature-Programmed Injection and High Temperature Fused Silica Wide-Bore Columns", J. High Resolution Chromatography, 12, 16-22 (1989).
16. McTaggart, N.G, Glaysher, P. and Harding, A.F: "Correlation of Simulated True Boiling Point Curves by Gas Liquid Chromatography and 15 Plate Distillation Data", Calculation of Properties of Petroleum Products, ASTM, STP, 577, 81-94 (1975).
17. Chorn, L.G: "Simulated Distillation of Petroleum Crude Oil by Gas Chromatography, Characterising the Heptanes-Plus Fraction", J. Chro. Sci, 22, 17-20 (1984).
18. Danesh, A. and Todd, A.C: "A Novel Sampling Method for Compositional Analysis of High Pressure Fluids", J. Fluid Phase Equilibria, 57, 161-171 (1990).
19. Ahmed, T: "Hydrocarbon Phase Behaviour", Gulf Publishing Company, Houston (1989).
20. Kesler, M.G. and Lee, B.I: "Improve Predictions of Enthalpy of Fractions", Hydro Proc., 153-158 (March, 1976).
21. Lee, B.I. and Kesler, M.G: "Improve Vapour Pressure Prediction", Hydro Proc., 163-167 (July, 1980).
22. Cavett, R.H: "Physical Data for Distillation Calculations, Vapour-Liquid Equilibria", Proc. of 27th API Meeting, San Francisco, 351-366 (1962).
23. Edmister, W.C: "Applied Hydrocarbon Thermodynamics, Part 4, Compressibility Factors and Equations of State", Pet. Ref., 37, 173-179 (1958).
24. Riazi, M.R. and Daubert, T.E: "Simplify Property Predictions", Hydrocarbon Proc., 59(3), 115-116 (1980).
25. Riazi, M.R. and Daubert, T.E: "Characterisation Parameters for Petroleum Fractions", I & EC Res., 26, 755-759 (1987).
26. Twu, C.H: "An Internally Consistent Correlation for Predicting the Critical Properties and Molecular Weights of Petroleum and Coal Tar Liquids", J. Fluid Phase Equilibria, 16, 137-150 (1984).
27. Graboski, M.S. and Daubert, T.E: "A Modified Soave Equation of State For Phase Equilibrium Calculations I Hydrocarbon Systems", Ind. Eng. Chem. Process Des. Dev., 17(4), 443-448 (1978).
28. Katz, D: "An Overview of Phase Behaviour of Oil and Gas Production", JPT, 1205-1214 (June, 1983).

29. Lohrenz, J., Bray, B.G. and Clark, C.B: "Calculating Viscosities of Reservoir Fluids from their Compositions", JPT, 1171-76 (Oct., 1964).
30. Ahmed, T., Cady, G. and Story, A: "A Generalised Correlation for Characterising the Hydrocarbon Heavy Fractions", SPE 14266, Proc. of 60th Ann. Conf. (Sept., 1985).
31. Pedersen, K.S., Blilie, A.L. and Meisingset, K.K: "PVT Calculations on Petroleum Reservoir Fluids Using Measured and Estimated Compositional Data of the Plus Fraction", Ind. Eng. Chem. Proc. Res., 31, 1378-1384, (1992).
32. Behrens, R.A. and Sandler, S.I: "The Use of Semicontinuous Description to Model the  $C_7$  Fraction in Equation of State Calculations", SPE/DOE 14925, Proc. of 5th Symposium on EOR, Tulsa (April., 1986).
33. Abramowitz, M. and Stegun, I.A. (Eds.): "Handbook of Mathematical Functions", Dover Publications Inc., New York, 256-257 (1972).
34. Whitson, C.H., Anderson, T.F. and Soreide, I: "Application of the Gamma Distribution Model to Molecular Weight and Boiling Point Data for Petroleum Fractions", Chem. Eng. Comm., 96, 259-278 (1990).
35. Cotterman, R.L: "Phase Equilibria for Systems Containing Very Many Components, Development and Application of Continuous Thermodynamics", PhD Dissertation, Univ. of Calif. at Berkeley (1985).
36. Cotterman, R.L. and Prausnitz, J.M: "Flash Calculations for Continuous or Semicontinuous Mixtures Using an Equation of State", I & EC Proc. Des. Dev., 24, 434-443 (1985).
37. Whitson, C.H., Anderson, T.F. and Soreide, I: " $C_7$ , Characterisation of Related Equilibrium Fluids Using Gamma Distribution", in " $C_7$ , Characterisation", Ed: Chorn, L.G. and Mansoori, G.A., Taylor & Francis, 35-56 (1989).

## 6.5 EXERCISES

6.1. The composition of a live sample has been determined by flashing the fluid at the laboratory conditions, and analysing the collected gas and liquid phases by gas chromatography. The composition of gas, in mole basis measured by a TCD detector, and liquid, in mass basis measured by a FID detector, are given in the following table. Calculate the mixture composition in mole basis.

Component	Gas Mole%	Liquid Weight%
N <sub>2</sub>	0.19	0.00
C <sub>1</sub>	68.51	0.02
C <sub>2</sub>	14.08	0.05
C <sub>3</sub>	8.35	0.19
i-C <sub>4</sub>	1.68	0.14
C <sub>4</sub>	2.81	0.33
i-C <sub>5</sub>	1.19	0.53
C <sub>5</sub>	1.84	1.10
C <sub>6</sub>	0.75	2.17
C <sub>7</sub>	0.37	3.41
C <sub>8</sub>	0.17	5.28

C9	0.05	4.63
C10	0.01	4.37
C11	0.00	4.20
C12	0.00	3.17
C13	0.00	4.46
C14	0.00	3.38
C15+	0.00	62.57

Liquid Phase Molecular Weight= 206

6.2. One method of estimating properties of SCN groups, or evaluating the measured values, is to relate the molecular weight and specific gravity by assuming a constant (UOP) characterisation factor. Is this a reasonable assumption?

6.3. Calculate the critical temperature, pressure, volume and acentric factor for a pseudo-component with  $T_b=612$  K,  $S=0.866$  and  $M=275$  kg/kgmol, using the methods of Cavett (Edmister for the acentric factor), and Riazi-Daubert (Lee-Kesler for the acentric factor). Compare the calculated results with those of  $C_{20}$  reported in Table A.2.

6.4. The concentration of  $C_{7+}$  fraction of a gas condensate is 4.771 mole % with the analysis as follows. Extend the analysis to  $C_{30+}$  by SCN groups.

Composition and properties of  $C_{7+}$  fraction.

Component	Mole%	Density, kg/m <sup>3</sup>	Mol. Weight
Heptanes	21.09	739.0	89
Octanes	15.01	749.4	105
Nonanes	9.96	764.1	121
Decanes	6.58	776.6	138
Undecanes	6.67	785.7	151
Dodecanes	5.71	796.9	164
Tridecanes	5.30	810.5	178
Tetradecanes	4.72	814.4	192
Pentadecanes	3.73	822.5	206
Hexadecanes	3.02	829.5	220
Heptadecanes	2.64	832.2	234
Octadecanes	2.66	835.7	249
Nonadecanes	1.32	838.1	263
Eicosanes plus	11.59	852.1	353

6.5. The mole fraction, molecular weight and specific gravity of  $C_{7+}$  fraction of a gas condensate are 0.04771, 165 and 0.8012, respectively. Describe the  $C_{7+}$  fraction by a continuous function in terms of the molecular weight, and use it to estimate the mole fraction of SCN groups comprising the  $C_{7+}$  fraction.

6.6. The composition of a gas condensate sample is as follows.

Components	Mol %
Nitrogen	0.298
Carbon dioxide	1.72
Methane	79.139
Ethane	7.483
Propane	3.293

## 6.5. Exercises

i-Butane	0.515
n-Butane	1.255
i-Pentanes	0.359
n-Pentane	0.551
Hexanes	0.616
Heptanes+	4.771

The  $C_7$  description of the fluid is the same as that given in Exercise 6.4.

Describe the  $C_7$  fraction by two and also four pseudo components, using the quadrature method. Predict the dew point and saturated density of the gas condensate at  $T=394$  K using a phase behaviour model and describing the  $C_7$  fraction by a single, two and four groups (Measured values in Table 2.2C).

6.7. The composition of an oil sample is as follows [31]:

Component	mole fraction	MW	SG
N2	0.0069		
CO2	0.0012		
C1	0.4709		
C2	0.0569		
C3	0.0439		
i-C4	0.0095		
C4	0.0242		
i-C5	0.0111		
C5	0.0146		
C6	0.0226		
C7	0.0393	91.9	0.735
C8	0.0452	105.2	0.745
C9	0.0323	121.0	0.784
C10	0.0230	133.0	0.789
C11	0.0203	148.0	0.794
C12	0.0188	163.0	0.806
C13	0.0162	177.0	0.819
C14	0.0176	190.0	0.832
C15	0.0139	204.0	0.834
C16	0.0103	217.0	0.844
C17	0.0122	235.0	0.841
C18	0.0085	248.0	0.847
C19	0.0097	260.0	0.860
C20	0.0032	269.4	0.874
C21	0.0080	282.5	0.870
C22	0.0053	297.7	0.872
C23	0.0044	310.1	0.875
C24	0.0034	321.8	0.877
C25	0.0048	332.4	0.881
C26	0.0039	351.1	0.886
C27	0.0031	370.8	0.888
C28	0.0030	381.6	0.895
C29	0.0024	393.7	0.898
C30+	0.0294	612.0	0.935

Describe the  $C_{7+}$  fraction by the gamma probability function. Use the quadrature method to represent the  $C_{7+}$  fraction by two, and also four groups. Predict the oil bubble point at  $T=345.8$ , using a phase behaviour model and describing  $C_{7+}$  by a single, two and four groups. Compare the results (Measured value  $P_b=23.7$  MPa).

## 7

**GAS INJECTION**

Injecting gas into an oil reservoir to increase the oil recovery, has long been applied. It can improve the recovery through maintaining the reservoir pressure, displacing oil, or vaporising the intermediate and heavy fractions of the oil. As the injected gas is not initially at equilibrium with the reservoir oil, the contact between the phases results in mass transfer, hence, changes in properties of the two phases. The displacement of oil by gas becomes highly efficient when the properties of the advancing gas and displaced oil become similar. That is, the two phases achieve complete miscibility and the vapour-liquid interface vanishes. At the pore level, the miscible displacement is practically 100% efficient, as the lack of interface eliminates the retainment of the oil in pores.

It is reasonable to assume that the equilibrium is reached at the gas-liquid interface. Hence, phase behaviour concepts and modelling methods previously described can be applied to investigate gas injection processes. The concept of miscibility in gas injection, and the experimental and theoretical methods to evaluate and design miscible displacement, however, merit particular considerations. In this chapter, miscibility concepts are initially described for simple mixtures, and then applied to real reservoir fluids by presenting methods to estimate miscibility conditions.

## 7.1 MISCIBILITY CONCEPTS

Miscibility concepts can be expressed conveniently by examining the phase behaviour of a ternary system, simulating the injection gas-reservoir oil mixture, using a triangular diagram.

The phase behaviour of a three component mixture (L: Light, I: Intermediate, H: Heavy) at a constant temperature and pressure is shown in Figure 7.1 by a ternary diagram. Each corner of the triangular diagram represents a component as pure, 100%, whilst all binary mixtures are on the lines connecting the two corners, e.g., Point D. Any point within the diagram represents a three component mixture, e.g., Point M and its composition is determined by its position relative to the corners. When two fluids of different compositions are mixed, the overall mixture lies on the line connecting the two fluids, which is called the *dilution or operating line*, and its position can be determined by the lever rule.

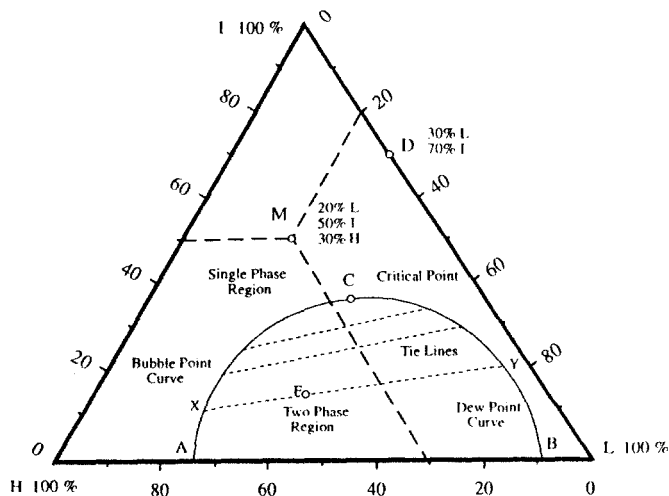


Figure 7.1. Ternary diagram presentation of fluid phase equilibria at constant pressure and temperature.

The phase envelope is shown by the curve ACB in Figure 7.1. Any mixture, F, inside the two phase envelope forms a vapour phase, Y, and a liquid phase, X, at equilibrium, lying on the phase boundary curve. The line XY, connecting the two phases at equilibrium is known as the *tie line*. Hence, the left hand side of the curve, AC, represents saturated liquids, i.e. the bubble point curve, whereas the right hand side, CB, represents saturated gases, i.e. the dew point curve. The two parts of the curve converge at the critical point C, also known as the plait point. Any mixture outside the phase envelope is a single phase under-saturated fluid. Phase envelopes, and the associated tie lines, at different pressures can be shown on the same diagram, where increasing the pressure generally results in the shrinkage of the phase envelope. A ternary system may form more than two phases, or have a number of isolated



two-phase regions, but the diagram shown in Figure 7.1 resembles most of the practical cases, and is quite adequate for describing the miscibility concepts.

Figure 7.1 shows that the binaries made of I and I, and similarly of I and H, form single phase mixtures when mixed at any proportion, whereas, L and H form a single phase fluid when mixed only within a limited ratio. Two fluids are considered to be miscible, when they form a single phase at all proportions, at constant pressure and temperature. It is evident that any two fluids with the operating line not crossing the two phase region within the phase envelope are miscible.

Figure 7.2 shows that an injection gas comprised only of I is miscible when contacted with Oil B, whereas Gas A is not. It can become, however, miscible either by enrichment with I to A' or by raising the system pressure to shrink the phase envelope as shown by the dashed phase envelope. When the injection gas and reservoir oil, mixed at any ratio, form a single phase, they are called *first contact miscible*. First contact miscibility can be achieved only for highly rich gases, or at very high pressures for lean systems.

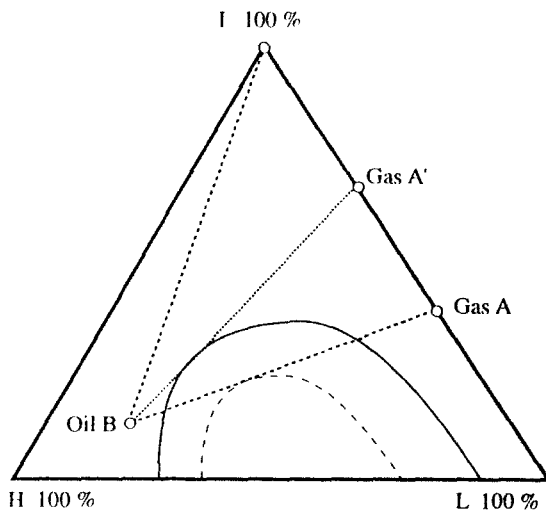


Figure 7.2. First contact miscibility.

An injection gas which is not miscible with an oil at first contact, may achieve miscibility during multiple contacts by getting enriched through vaporising the intermediate fractions of oil. The process, known as the *vaporising gas drive* (VGD) is conceptually shown in Figure 7.3.

The injection gas, L, comprised of the light fluid only, after contacting Oil A, forms two equilibrated phases of liquid  $X_1$ , and gas  $Y_1$ , with an overall mixture  $F_1$ . Note that the gas phase,  $Y_1$ , is the original gas L after it has picked up some intermediate and heavy fractions from the oil phase. The gas phase,  $Y_1$ , moves forward and makes further contacts with the

fresh oil and progressively becomes richer particularly in the intermediates, as shown by  $Y_2$ ,  $Y_3$ ... The gas ultimately becomes miscible with oil at C, that is, where the tangent line at the critical point, which is the critical tie line with zero length, goes through the oil composition. It is quite evident, that the compositional path must go through the critical point, as it is the only condition that equilibrated phases lose distinctions, and a continuous transition from gas to oil can be achieved without any phase boundary.

The above injection gas, pure L, however, does not achieve multiple contact miscibility with Oil B, as the enrichment of the advancing gas is limited by the tie line  $X'_2Y'_2$  (limiting tie line) which, if extended, goes through Oil B. It is evident that the miscibility cannot be achieved when the oil composition and the phase envelope are at the same side of the critical point tangent line (critical tie line extension). The vaporising gas drive miscibility for oil B can be achieved, however, by raising the pressure sufficiently to shrink the phase envelope, as shown by the dotted boundary. The pressure at which the critical tie line extension goes through the oil is the minimum required pressure to achieve miscibility, hence, called the *minimum miscibility pressure* (MMP). At MMP, the limiting tie line becomes the critical tie line as the gas phase enriches through multiple contacts with the original oil attaining the critical composition.

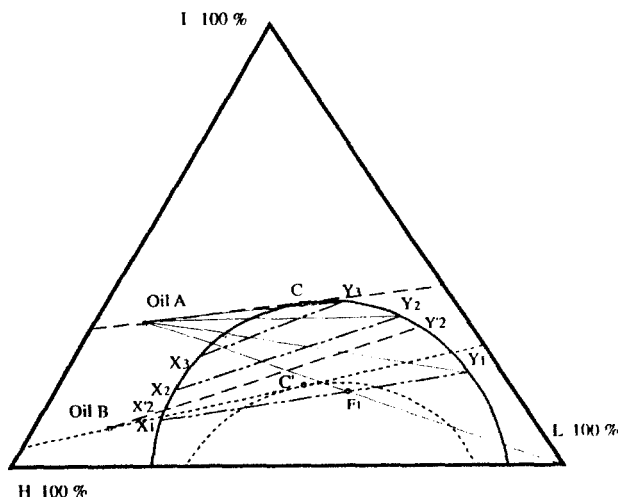


Figure 7.3. Schematic phase diagram of vaporising gas drive at minimum miscibility pressure.

In the vaporising gas drive, the miscibility is achieved at the front of the advancing gas. The gas composition varies gradually from that of the injected gas till reaching the critical composition. Then it miscibility displaces the original reservoir oil in a piston-type manner. No phase boundary exists within the transition zone.

The gas composition appears to have no effect on achieving the miscibility state in the vaporising gas drive as it is fully controlled by the oil phase, as demonstrated in Figure 7.3. A rich gas, not forming first contact miscibility with an oil, can, however, achieve multiple contact miscibility through condensing its intermediate fractions to the oil as shown



### Miscibility in Real Reservoir Fluids

The ternary phase diagram of a multicomponent reservoir fluid is often expressed by representing the fluid with three pseudo components. It is common to group  $C_1$  and  $N_2$  as the light (L),  $CO_2$ ,  $H_2S$  and  $C_2-C_6$  as the intermediate (I), and  $C_{7+}$  as the heavy (H) fraction. Pseudo-ternary diagrams have been misused, however, in describing the behaviour of real reservoir fluids in gas injection processes, particularly in estimating the optimum operating conditions such as MMP and MME.

The conceptual discussion on multiple contact miscible processes, using the ternary diagram, is not strictly valid for real reservoir fluids, and the diagram should not be used generally in the design of real processes. The basic idea of multiple contact miscibility through mass exchange between the phases, and the requirement of attaining the critical composition, are all valid for real systems. However, the existence of a large number of components in a real reservoir fluid provides additional possibilities for compositional variations, and achieving miscibility. In the following discussion, the miscible condition is referred to the condition where miscibility can just be achieved, that is, at MMP. At higher pressures, the miscibility will obviously be achievable.

The multiple contact miscibility, can be achieved only when the compositional path goes through the critical state. As the critical composition, hence the critical tie line, for a ternary system at a given set of temperature and pressure is unique, the miscibility is determined only by the two limiting tie lines. When the critical tie line coincides with the limiting tie line going through the original oil composition, the miscibility is achieved by the vaporising process. When the critical tie line coincides with the limiting tie line going through the injection gas composition, the miscibility is achieved by the condensing process.

In a real system, it is possible that neither of the limiting tie lines goes through the critical point, but miscibility still is achieved. This will occur if the fluid attains a critical state not at the leading or the trailing edges, but somewhere within the transition zone. Such a possibility exists for mixtures with more than three components. Indeed the prevailing mechanism for achieving miscibility in rich gas injection is often, if not always, the above mentioned case and not the condensing mechanism described for a ternary system.

The injected rich gas does not generally contain heavy fractions which are present in the oil. Hence, whilst the injection gas enriches the oil in light intermediate range, it strips the heavier fractions. The reservoir oil in contact with the fresh gas initially becomes lighter, but as it contacts more gas and loses only some of its lighter heavies, overall it tends to get enriched in very heavy fractions and thus becomes less similar to the injection gas. Figure 7.5 shows the variation of measured component groups in the oil phase at the injection point for a North Sea oil. As the oil is contacted with additional rich gas, the concentration of  $C_{7+}$  is decreased, apparently lightening the oil in its path towards achieving the condensing miscibility. An examination of the heavy end, e.g.  $C_{20+}$ , however, shows that this fraction has increased markedly due to vaporisation of the lighter heavies. This oil cannot become miscible with the fresh injection gas. The phase envelope, as determined by measuring the compositions of equilibrated phases at the injection point and also at the gas front in a laboratory test, is shown in Figure 7.6. Note that the bubble point and the dew point curves initially converge, demonstrated by shortening tie line lengths, and then diverge.

As the forward moving gas becomes richer in heavy fractions, it vaporises less of these compounds whilst losing intermediates to the oil. It is conceivable that at favourable conditions the combined vaporisation/condensation process results in a state within the transition zone where the compositional path goes through the critical point, achieving miscibility. This can be envisaged as a combination of the condensing process at the front, and the vaporising process

at the tail. This process, called the *condensing/vaporising gas drive*, was reported by Zick [1] in 1986, and detailed by Stalkup in 1987 [2].

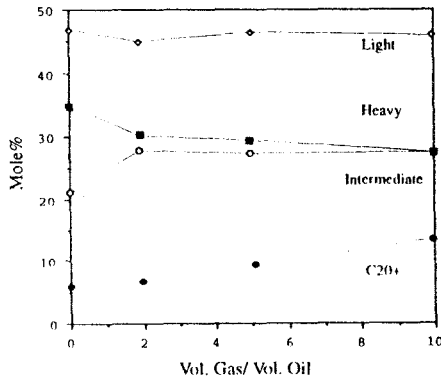


Figure 7.5. Variation of component groups in contacted oil at injection point with the ratio of injected gas volume to contacted oil volume.

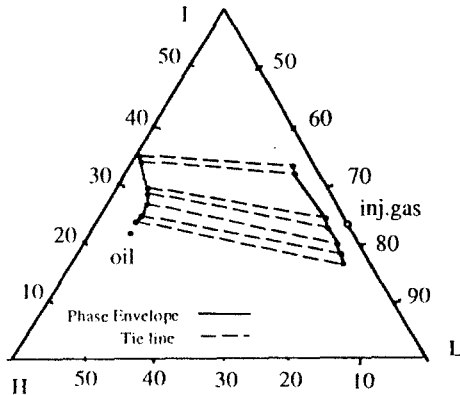


Figure 7.6. Phase diagram of a North Sea oil and rich injection gas determined experimentally during contact experiment.

The multiple contact miscibility in multicomponent systems is achieved in a dynamic process, hence, it can be affected by other factors additional to the fluid phase behaviour. The compositional path depends on other mechanisms such as multiphase fluid convection and dispersion in porous media. The two limiting critical tie lines, that is, those with extensions going through the original oil and the injection gas, depend only on the original fluids. Hence, the miscibility conditions can be determined by phase behaviour considerations only, if the miscibility is achieved by either vaporising or condensing gas drive mechanisms. Otherwise, the critical tie line, hence miscibility, depends on the local fluid mixture composition influenced

by flow factors. Therefore, a proper investigation of the multiple contact miscibility should involve the simulation of fluid phase and flow behaviour as closely as possible to that in the reservoir.

There are ample publications on mathematical simulation of multiple contact miscibility as developed in a one dimensional flow. The reports by Orr and co-workers [3-7], utilising an analytical method to solve the governing phase and flow behaviour equations with no dispersion, for a four component system provide valuable insight into the mechanisms of multiple contact miscibility. The authors demonstrate that the displacement in a multicomponent system, can be expressed by a series of pseudo-ternary diagrams, where the compositional path progressively moves from each diagram to the next. When the two phases of vapour and liquid at equilibrium are present, the transfer from one ternary diagram to the next must occur at a common tie line between the two diagrams, called the cross over tie line. The number of the pseudo-ternary diagrams increases with the number of components, with the number of cross over tie lines equal to the number of components minus three. For example, whilst the compositional path in a four component system can be depicted by two ternary diagrams, with a common cross over tie line, there are two cross over tie lines connecting three pseudo-ternary diagrams in a five component systems. Depending on the fluid composition, pressure and temperature, any of the cross over tie lines or the limiting tie lines can become the critical tie line. The miscibility is then achieved at that point.

Considering the above, the estimation of miscibility conditions based on the limiting tie lines is not generally adequate for real systems. When the process is known definitely to be vaporising, such as methane displacing an oil composed only of hydrocarbons, the oil tie line can be used to determine the miscibility condition. The estimation of miscibility in rich gas drive, using the injection gas tie line, is expected to be unreliable in most cases, if not in all. When the key tie line which controls the miscibility is one of the cross over tie lines, the estimation of miscibility conditions is not as straight forward. Even if the key tie line can be determined for a dispersion free, one dimensional flow, as suggested by Johns et al. [6], it may not represent the real process. It has been demonstrated that dispersion, viscous fingering and gravity segregation can impair the achievement of miscibility, causing two phase flow in reservoirs in which they would be miscible otherwise [8,9].

## 7.2 EXPERIMENTAL STUDIES

Gas injection experiments are conducted with several objectives. Most tests have been designed to directly measure the minimum miscibility pressure or enrichment. Tests are also conducted to generate volumetric and compositional data for specific studies, such as oil vaporisation by gas injection, or evaluation and tuning of phase behaviour models for numerical simulation of the reservoir performance.

Displacement of oil by gas through a porous medium, simulates the gas injection process more closely than other tests, and it is considered as the definitive test. The displacement is conducted either in a core, extracted from the reservoir, or more often in a long and narrow sand pack, known as the slim tube. Static tests, where the injection gas and the reservoir oil are equilibrated in a cell, are also conducted to determine the mixture phase behaviour. Although these tests do not closely simulate the dynamic reservoir conditions, they do provide accurate and well controlled data which are quite valuable, particularly for tuning the equation of state used in modelling the process.

### Slim Tube

Slim tube, a one dimensional model reservoir, is a narrow tube packed with sand, or glass beads, with a length between 5 and 40 m. A schematic diagram of the tube and the auxiliary equipment to allow displacement tests, is shown in Figure 7.7.

The tube is initially saturated with the oil at reservoir temperature above the bubble point pressure. The oil is then displaced by injecting gas into the tube at a constant inlet, or more often outlet, pressure controlled by a back pressure regulator. The pressure drop across the slim tube is generally small, therefore, the entire displacement process is considered to be at a single constant pressure. The slim tube effluent is flashed at the atmospheric conditions, and the rate of recovery, density and composition of produced fluids are measured. The gas break through is detected by continuously monitoring the effluent gas composition, and/or the producing gas to oil ratio.

The miscibility conditions are determined by conducting the displacement at various pressures, or injection gas enrichment levels, and monitoring the oil recovery. This can also be aided by visual observation of the flow through a sight glass placed at the tube outlet. The achievement of miscibility is expected to accompany a gradual change of colour of the flowing fluid from that of the oil to clear gas. Whereas, observing two phase flow is indicative of an immiscible displacement.

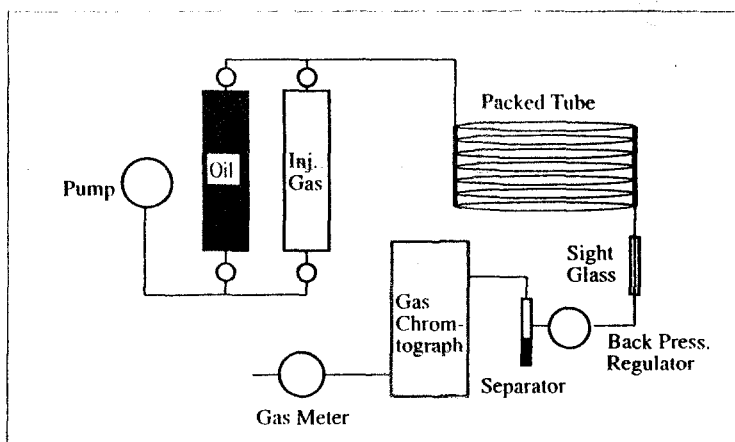


Figure 7.7. Schematic diagram of slim tube apparatus.

Slim tubes of different sizes and orientations have been used at various displacement conditions. The effect of tube geometry and flow parameters on fluid recovery has been systematically investigated [10]. An ideal tube should provide a one dimensional dispersion free displacement of oil by gas. This is not to suggest that such a displacement simulates the process in a real reservoir. It is merely a well controlled experiment, with valuable results for phase behaviour studies including miscibility evaluation. The actual displacement in a reservoir is influenced by various mechanisms, such as viscous fingering, gravity override and dispersion. Reservoir heterogeneity, at different scales, strongly divert the flow and affect the recovery. As it is impossible to simulate all these inter-related mechanisms in a slim tube, or even in a core, it is logical to avoid them all in phase behaviour tests. These factors, all important to the success of a gas injection scheme, could then be studied in other experiments and using compositional simulators.

Probably the simplest test using a slim tube, is determination of the miscibility conditions. Almost any slim tube, regardless of the design, can be used to estimate the effect of pressure

and gas enrichment on miscibility. Operating conditions, however, should be selected based on the tube design, and the prevailing mechanism which results in miscibility.

A tube length of 12 metres is adequate in most cases, and allows miscibility measurement within a reasonable test period and fluid consumption. The length is to provide sufficient contact between the phases to achieve miscibility, if attainable. Theoretically, miscibility is achieved almost at the tube entrance when no dispersion exists [4,11]. In practice, tubes as long as 36 meters have been recommended for displacement with nitrogen [12,13]. The improvement in oil recovery, by increasing pressure or gas enrichment, is often monitored to determine the miscibility conditions. Hence a long tube, which highlights changes in the oil recovery, provides a more definitive means for the judgement of miscibility conditions.

The tube diameter should be selected small enough to suppress viscous fingering by transverse dispersion along the tube, that is, the shorter the tube, the smaller the diameter. A 6.3 mm (0.25 in.) diameter tube is often used, and is considered adequate, in tubes of at least 10 m long, for justifying the assumption of one-dimensional flow in the slim tube. To minimise wall effects, the maximum grain diameter of the packing material should be less than 1/10 of the internal tube diameter [14]. Sand, or glass beads, of 100-200 mesh size are often used in packing the tube.

As a long tube cannot be placed in a straight line, it is to be coiled preferably cylindrical than flat, with gas injected from the top to promote gravity stable displacement.

A low gas injection rate can improve the contact between the phases in a short slim tube. It however, improves the recovery efficiency, particularly at immiscible conditions, hence reduces the recovery gain when achieving miscibility. This can reduce the accuracy in determining the miscibility conditions as measured by changes in the oil recovery. A gas injection rate with an advancement velocity of about 1.5-2.5 m/hr, generally should provide reliable recovery data within a reasonable experimental time.

The displacement is often terminated after injecting 1.2 pore volume (PV) gas. The recovery at that point is referred to as the ultimate recovery. The test may also be terminated at a pre-selected high producing gas to oil ratio, around 8000 vol/vol (40,000-50,000 SCF/STB), with the ultimate recovery determined at those conditions.

The volume of produced stabilised oil in the separator is generally converted to that at reservoir conditions, using the volume ratio measured on the original oil. At high pressure conditions, particularly in rich gas injection, a significant amount of the liquid collected in the separator can be due to condensate drop-out from the produced gas. The volume factor for such a liquid is different from that of the original oil. Furthermore, the liquid recovery at such conditions is not totally by displacement.

Figure 7.8 shows typical oil recovery plots at two pressures. At 24.15 MPa the gas breaks through at 38% pore volume (PV) gas injected, with an ultimate oil recovery of about 50% PV. The volume of recovered oil prior to the gas break through is almost equal to the injected gas volume. It is generally slightly less than the injected volume due to the shrinkage of the total gas-oil volume in contact. The oil recovery after break through drops sharply and can be quite small, particularly in efficient displacements. The gas to oil ratio (GOR) increases sharply after the breakthrough, as shown in Figure 7.9.

The low recovery at 24.15 MPa is indicative of an immiscible displacement. At the higher pressure of 28.25 MPa the gas break through occurs quite late. Note that the recovery, both the break through and the ultimate, has improved markedly at the higher pressure, indicating an approach towards miscibility. Although at miscibility conditions the displacement is quite efficient, a 100% oil recovery is not generally expected, unless the condensate recovery in rich gas injection is included, where the complete liquid recovery over 1 PV can be achieved.



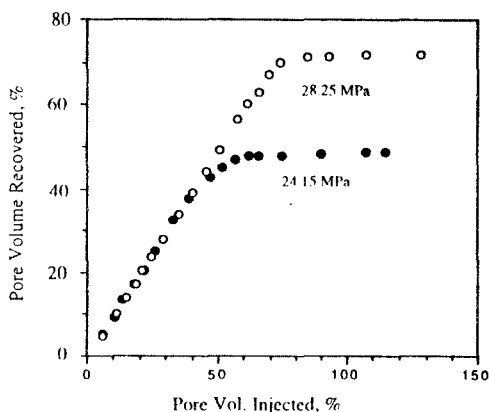


Figure 7.8. Oil recovery by gas injection at two different pressures.

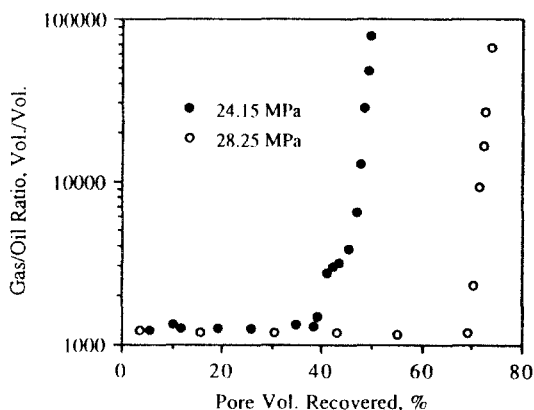


Figure 7.9. Producing gas to oil ratio in gas displacement at two different pressures.

Different recovery levels, such as 80% at the gas break through [15], or 90%-95% ultimate recovery [16,17], have been suggested as the criteria for miscible displacement. The oil recovery, however, depends on the tube design and operating conditions. A slim tube may only deliver 80% oil recovery at miscible conditions. The evaluation of recovery changes with displacement pressure, or gas enrichment, is more appropriate to determine miscibility conditions than searching for a high recovery. The most acceptable definition is the pressure, or enrichment level, at the break-over point of the ultimate oil recovery as shown in Figure 7.10. The recovery is expected to increase by increasing the displacement pressure, but the additional recovery above MMP is generally minimal.

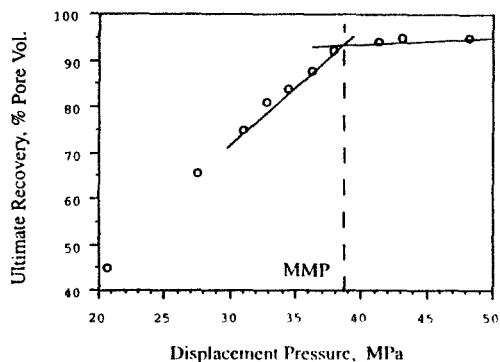


Figure 7.10. Determination of MMP by plotting ultimate recovery versus pressure.

The dispersion and compositional variations, particularly in rich gas injection, create concentration, and saturation banks along the tube, which can conveniently be detected by fluctuating producing GOR, as shown in Figure 7.11. The banks rich in intermediate and heavy fractions contribute more to the oil recovery. The relative location of the banks are determined by the composition of the injected and reservoir fluids and displacement conditions. The recovery of a rich bank may be delayed by enriching the injection gas, hence, it may be mistaken as a reduction in oil recovery [18]. If the displacement is terminated before major liquid producing banks appear, the change in liquid recovery may not properly reflect the impact of the varied pressure or gas enrichment.

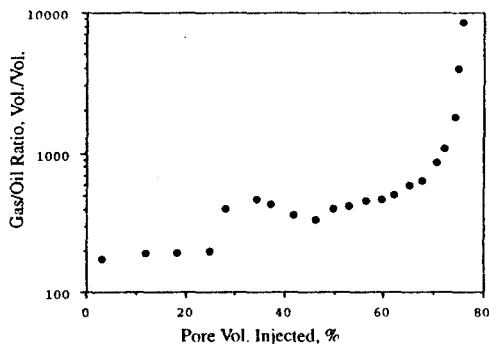


Figure 7.11. Variations of producing gas to oil ratio with injected rich gas volume.

The compositional variation of produced gas in an immiscible displacement of an oil by nitrogen is shown in Figure 7.12. At the gas break through, the methane concentration exceeds that in the original oil. This is due to the high volatility of methane which results in its vaporisation into the advancing nitrogen. An absence of methane bank [19], and a smooth profile of concentration of intermediates [10], have also been suggested as measures of miscible displacement. A combination of the above criteria, including sight glass observation, often is used to identify miscibility conditions.

When miscibility is achieved by the vaporising gas drive, flow factors, should not, at least theoretically, affect miscibility conditions as explained in Section 7.1. When miscibility is achieved within the transition zone, the critical state is expected to depend on flow and dispersion factors. The use of reservoir cores, is considered to include some of these factors. An arrangement composed of a slim tube ahead of a core, where the slim tube provides enough contacting length between the phases, to introduce miscible fluids into the core, is often considered. The advantages of such refinements, however, are open to question.

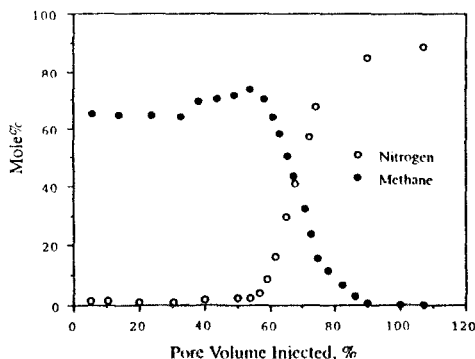


Figure 7.12. Concentration of methane and nitrogen in the produced gas.

The slim tube can provide very useful phase behaviour information, additional to MMP or MME, for evaluating phase behaviour models when applied in gas injection processes. This application will be described in Section 9.3, where tuning of equations of state will be addressed.

The MMP determined by slim tube displacement does not necessarily correspond to the thermodynamic miscibility, that is, the achievement of the critical state. Adverse effects such, as dispersion can prevent or delay thermodynamic miscibility [9, 20], but the prevailing low interfacial tension between the two phases still provides a highly efficient displacement.

### Rising Bubble Apparatus

The observation of a gas bubble behaviour, rising in a visual high pressure cell filled with the reservoir oil, has been suggested [21] as a quick method of measuring MMP. The apparatus is shown in Figure 7.13, where a small gas bubble is introduced into the bottom of oil column through a water phase, acting as a buffer between gas and oil containers. The gas bubble continually contacts the oil through its upward journey which results either in reaching equilibrium with the original oil, or achieving miscibility depending on the test pressure. A series of tests are conducted at different pressures, and the bubble shape is monitored as it rises up.

At pressures, far below MMP, the bubble retains its almost spherical shape, but its size is reduced as the gas is partially dissolved in the oil. At or slightly above MMP, the bubble develops wavy tail with the gas-oil interface vanishing from the bottom of the bubble. At pressures higher than MMP, the bubble disperses very rapidly and disappears into the oil. A

gas bubble not achieving miscibility, will also disappear into an undersaturated oil, but will not disperse.

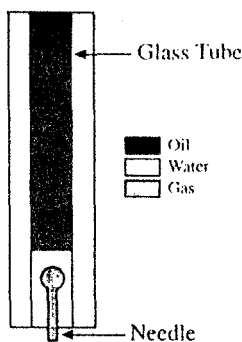


Figure 7.13. Schematic diagram of rising bubble apparatus, showing fluid phases at start of experiment [21].

The method is suitable only for the vaporising gas drive process, where the enrichment of advancing gas creates the miscible fluid. The measured MMP by the above method has been shown to agree reasonably with that by displacement using a slim tube [21].

### Contact Experiments

**Slim tube tests** do not generate all the volumetric and compositional data required for evaluation and calibration of phase behaviour models. Therefore, gas injection processes are often simulated in batch type tests, known as multiple contact experiments in PVT cells. In this method, finite volumes of reservoir oil and injection gas are repeatedly contacted, and shrinkage or swelling of the oil, and the density and composition of equilibrated oil and gas are measured.

Batch-type gas injection experiments are designed to generate phase behaviour data, particularly for calibration (tuning) of equation of state models used in simulation. The most common experiment is the *swelling test*, or *single contact gas injection*. A known amount of oil is loaded into an equilibrium cell and the injection gas is progressively added to the oil stepwise. After each addition of the gas, the mixture saturation pressure and volume are measured. A constant composition expansion test can then be conducted on the mixture, prior to the next gas addition, to generate additional information.

Figure 7.14 shows, the variation of mixture saturation pressure with added methane for a light oil. The bubble point pressure increases with addition of gas. The incremental increase of methane content of the fluid results in a critical state, point C, where the mixture behaves gas like with further injection of methane. The dew point initially increases, and then decreases, with increasing methane. The lines showing constant liquid volume fractions within the two phase envelope converge at the critical point.

Although the single contact experiment, does not simulate the continuous contact between the phases, as occurs in gas-oil displacement, it provides valuable data for tuning of EOS. It covers a wide range of fluid composition, with little experimental effort. Although the composition of the mixture does not follow the compositional path in a gas injection process,

the equilibrated phases below the saturation pressure provide information on fluids with various degrees of proximity to the critical point, albeit at different pressures.

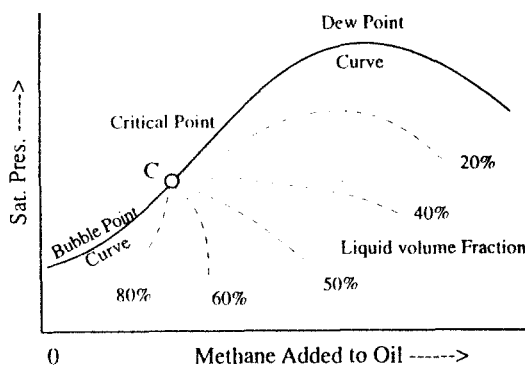


Figure 7.14. Variations of mixture saturation pressure with added methane to a light oil.

The static equilibrium tests which closely simulate continuous contact of injection gas and reservoir oil are multiple contact experiments. The *forward multiple contact* test, simulates conditions at the injection front, in which oil and gas are contacted at the reservoir pressure and temperature. The equilibrated gas in each contact is used in the next contact with the original reservoir oil, simulating gas advancement in reservoir (Figure 7.15). The volume, density and composition of the equilibrated phases are measured in each contact. The above procedure is continued until the injection gas either becomes miscible with the original oil, or attains equilibrium with it (limiting tie line).

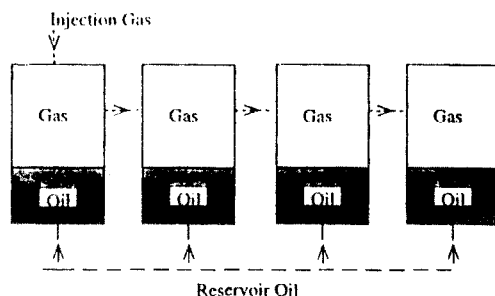


Figure 7.15. Flow diagram in multiple forward contact experiment.

Table 7.1 shows the composition of equilibrated gas and oil in a forward multiple contact test of a volatile oil and methane at 373 K and 35.26 MPa, where the gas has become progressively richer by contacting oil. The composition of equilibrated oil in the last contact is almost the same as that of the original oil, indicating an approach to the limiting tie line with no miscibility achieved.

Figure 7.16 shows the variation of equilibrium ratios of the mixture components due to compositional changes in different contacts. Each component has been identified by a physical property group as described in Section 3.2. A straight line can be drawn through the equilibrium ratios in each contact. Note that the slope of the line decreases progressively with each contact. For achieving miscibility, the line should have become horizontal with K-values equal to 1 for all the components. Figure 7.16 is also a revealing example of the effect of fluid composition on the equilibrium ratios, as the temperature and pressure are constant.

The *backward multiple contact* test, simulates the injection zone tail, that is, what takes place at the injection point. It is similar to forward contact test, but the equilibrated oil in each contact is used in the next contact with the fresh injection gas (Figure 7.17).

Table 7.1.

Composition (mole%) of equilibrated oil and gas in a four stage forward multiple contact test.

Contact No.	0	1		2		3		4	
Component	Orig. Oil	Oil	Gas	Oil	Gas	Oil	Gas	Oil	Gas
C <sub>1</sub>	57.53	57.87	78.24	57.03	74.46	57.10	72.25	56.73	71.47
C <sub>2</sub>	10.16	7.87	7.57	9.00	8.91	9.71	9.72	10.01	10.00
C <sub>3</sub>	5.83	4.89	4.04	5.40	4.69	5.69	5.06	5.80	5.22
i-C <sub>4</sub>	1.22	1.06	0.79	1.15	0.92	1.19	0.99	1.21	1.02
nC <sub>4</sub>	2.06	1.85	1.28	1.98	1.49	2.03	1.60	2.06	1.65
i-C <sub>5</sub>	1.01	0.95	0.59	0.99	0.69	1.01	0.74	1.02	0.76
nC <sub>5</sub>	1.70	1.62	0.97	1.68	1.12	1.70	1.20	1.72	1.24
C <sub>6</sub>	1.40	1.41	0.75	1.41	0.85	1.41	0.92	1.42	0.95
C <sub>7</sub>	2.16	2.26	1.04	2.32	1.23	2.27	1.33	2.27	1.36
C <sub>8</sub>	2.55	2.76	1.12	2.65	1.26	2.55	1.36	2.58	1.42
C <sub>9</sub>	2.00	2.23	0.82	2.19	0.98	2.11	1.05	2.11	1.08
C <sub>10</sub>	1.55	1.69	0.58	1.66	0.69	1.52	0.77	1.47	0.74
C <sub>11</sub>	1.10	1.36	0.36	1.30	0.41	1.16	0.51	1.18	0.54
C <sub>12</sub>	1.00	1.14	0.33	1.07	0.41	1.09	0.39	1.08	0.41
C <sub>13</sub>	0.99	1.19	0.29	1.10	0.36	1.05	0.47	1.03	0.40
C <sub>14</sub>	0.78	0.96	0.23	0.87	0.27	0.81	0.22	0.82	0.31
C <sub>15</sub>	0.85	1.05	0.23	0.97	0.28	0.92	0.31	0.90	0.32
C <sub>16</sub>	0.72	0.86	0.18	0.74	0.21	0.76	0.24	0.75	0.25
C <sub>17</sub>	0.49	0.66	0.11	0.63	0.15	0.54	0.16	0.54	0.16
C <sub>18</sub>	0.60	0.76	0.13	0.67	0.16	0.65	0.18	0.64	0.19
C <sub>19</sub>	0.51	0.65	0.10	0.61	0.13	0.56	0.15	0.55	0.15
C <sub>20+</sub>	3.81	4.92	0.26	4.57	0.33	4.17	0.38	4.13	0.39

Figure 3.8 shows the variation of equilibrium ratio for the same system as shown in Figure 7.16, but in backward contact test at the same temperature and pressure. The slope of the line increases with each contact, indicating that the properties of the two phases diverge progressively. Even, with rich gases the multiple backward contact test cannot generally provide miscible fluids in real cases as discussed in Section 7.1. The experiment, however, provides valuable information on the vaporisation effect of the injection gas. The test is particularly valuable to simulate gas recycling of partially depleted gas condensate or volatile oil reservoirs.

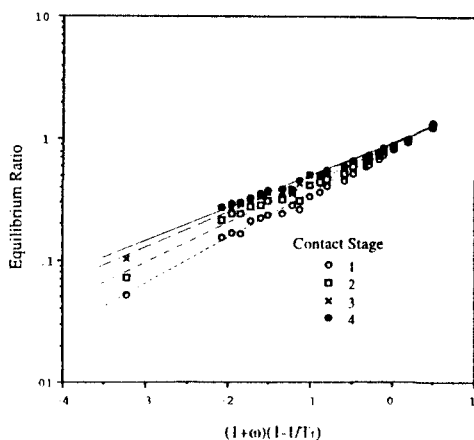


Figure 7.16. Variations of equilibrium ratio of fluid components in multiple forward contact test.

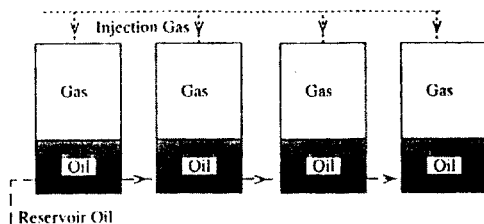


Figure 7.17. Flow diagram in multiple backward contact experiment.

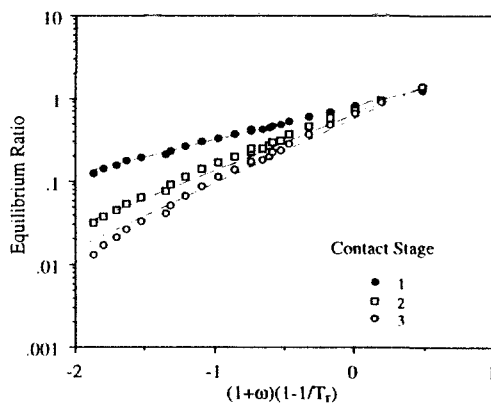


Figure 3.8. Variation of equilibrium ratios of fluid components in multiple backward contact test.

### 7.3 PREDICTION OF MISCIBILITY CONDITIONS

The values of MMP or MME may be estimated using empirical correlations, or a compositional phase behaviour model. Empirical correlations, mostly developed using slim tube displacement data, provide rough estimates of the minimum miscibility pressure or enrichment. They may be used for preliminary screening or feasibility studies, but should not be relied upon. Phase behaviour models, which provide information on thermodynamic miscibility, can be used with confidence, after being tuned to relevant experimental data (Section 9.3), to predict the miscibility conditions. Even when the miscibility conditions for a specific fluid system are experimentally known, tuned phase behaviour models are often required for compositional reservoir simulation of gas injection processes.

#### First Contact Miscibility

The injection gas and the reservoir oil should form a single phase fluid when mixed at any ratio in this process. This can happen either with very rich injection gases, or at very high pressures. The injection of such a highly rich gas to displace oil is not normally economical. It is also often beneficial to deplete a high pressure under saturated oil reservoir, and displace oil miscibly by vaporising gas drive at lower pressures than by first contact miscible displacement at high pressures, because high pressure gas injection is also usually a very expensive operation.

The single contact (swelling) test provides the first contact MMP data; it is the maximum pressure on the phase envelope boundary as shown Figure 7.14. Hence, it can be estimated by simulating the above test using a phase behaviour model.

Intermediate hydrocarbons, such as propane, butane and liquefied petroleum gases (LPG), known as solvents, are usually first-contact miscible with oil at typical reservoir conditions. As the solvents are expensive, they are generally injected as a slug, driven by a lean gas such as methane or nitrogen. The lean gas and the solvent slug should also be miscible for an efficient displacement.

Figure D.1 in Appendix D shows the locus of critical points of various binary mixtures. At any temperature, the associated critical pressure is MMP for the selected gas-solvent. Figure 7.18 may also be used to estimate the minimum pressure required to achieve first contact miscibility between propane, or butane, and several other injection gases [22]. Note that all the curves for different gases converge at the solvent critical point. At temperatures above its critical point, the solvent can never form two phases when mixed with the gas regardless of the pressure. It may, however, form two phases with the reservoir oil.

Figure 7.19 shows conceptually the miscibility behaviour of a single component injection gas, a single component solvent and oil system. The gas and the solvent are shown by their vapour pressure curves, whereas the reservoir oil is identified by its critical point. The loci of the critical points of mixtures formed by mixing gas and solvent or solvent and oil at various ratios are shown by the dotted curves. Any point above the curves is considered to be a single phase fluid. Hence, when the reservoir temperature,  $T_d$ , is above the critical point of the solvent, the achievement of miscible displacement is controlled by the solvent-oil behaviour. At such conditions, MMP can be estimated by simulating the single contact test between oil and solvent using a phase behaviour model. At a temperature below the critical temperature of solvent,  $T_c$ , the gas-solvent behaviour controls MMP, which can be estimated from Figure 7.19.

#### Vaporising Gas Drive

Methane (lean gas), or nitrogen can displace oil very efficiently by developing a miscible bank through vaporising the oil intermediates. The minimum miscibility pressure for methane or



nitrogen has been studied by several investigators [13, 23-26]. Firoozabadi and Aziz [23] used experimental slim tube data, and proposed a correlation to estimate MMP for VGD processes, though it was considered more reliable for methane than nitrogen injection.

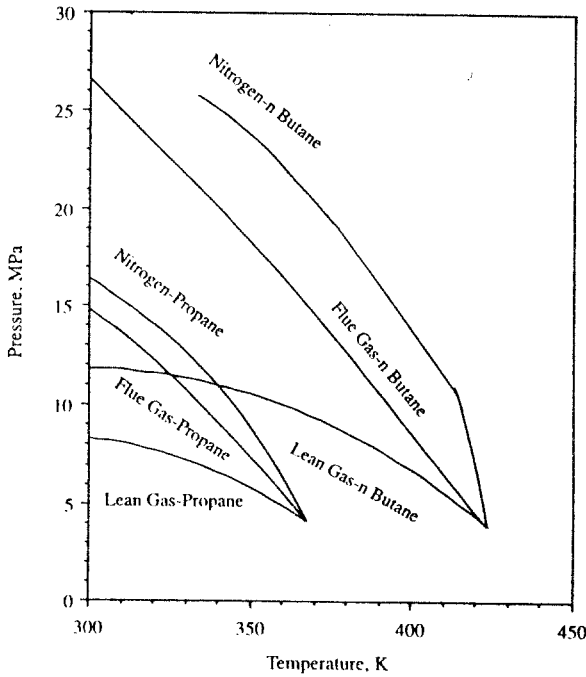


Figure 7.18. First contact minimum miscibility pressure for gas-solvent. SPE Copyright. Reproduced from [22] with permission.

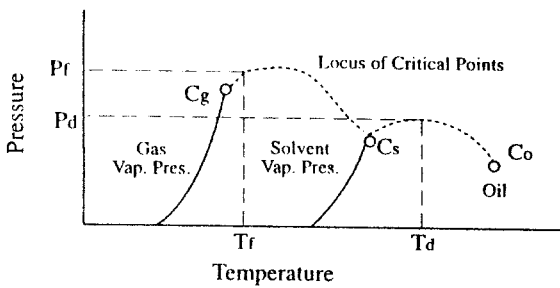


Figure 7.19. Conceptual phase behaviour diagram of first contact minimum miscibility pressure for gas-solvent-oil system.

$$P_m = 65.04 - 1.296 \times 10^5 x_{C_2-C_5} / (M_{C_7+} (1.8T - 460)^{0.25}) + 1430 \times 10^5 \left[ x_{C_2-C_5} / (M_{C_7+} (1.8T - 460)^{0.25}) \right]^2 \quad (7.1)$$

where,

$P_m$  = MMP, MPa

$x_{C_2-C_5}$  = mole fraction of intermediates in oil, ethane to pentane inclusive

$M_{C_7+}$  = molecular weight of heptane plus

$T$  = Temperature, K

Eq.(7.1) was found as the most reliable MMP correlation for lean gas and nitrogen injection, with a standard deviation of 11.5% and 25.3% respectively, in a comparative study of MMP correlations [27].

The above correlation which provides the same value of MMP, regardless of the injection gas composition, relies on the vaporising gas derive concept, where miscibility is controlled by the original oil composition only. The view that MMP for nitrogen and methane is the same, is also strengthened by the fact, that injected nitrogen vaporises the highly volatile methane to such an extent that the advancing gas front is very much dominated by methane instead of nitrogen. Koch and Hutchinson [24] showed, however, that MMP declined when a lean gas was added to nitrogen. The MMP for nitrogen is generally higher than that for methane, but the difference decreases for oil samples with high bubble point pressures, that is, fluids with a high methane content.

Hudgins et al. [13] concluded that the oil methane content is an important parameter for achieving miscibility in nitrogen injection and proposed the following correlation to estimate MMP for nitrogen.

$$P_m = 38.39 e^{-\lambda_1} + 25.10 e^{-\lambda_2} \quad (7.2)$$

where,

$$\lambda_1 = 792.06 x_{C_2-C_5} / (M_{C_7+} (1.8T - 460)^{0.25})^2 \quad (7.3)$$

$$\lambda_2 = 2.158 \times 10^6 x_{C_1}^{5.632} / (M_{C_7+} (1.8T - 460)^{0.25}) \quad (7.4)$$

The symbols are as defined in Eq.(7.1). The accuracy of the above correlation in predicting MMP for nitrogen was found [27] to be comparable to that of Eq.(7.1).

Dindoruk et al. [7] reviewed the literature on miscible displacement with nitrogen, and suggested some explanations on the apparently conflicting views presented by various investigators on the effect of injection gas and oil compositions on MMP. The authors studied the problem by analytically solving the governing equations for displacing a four component mixture with nitrogen-methane in a dispersion free one dimensional porous medium. They concluded that the oil tie line becomes the critical tie line for low nitrogen to methane ratio, hence, MMP is independent of gas composition. For gases with a high concentration of nitrogen, a cross over tie line becomes critical, hence, MMP is affected by the gas composition. For pure nitrogen injection, the oil tie line controls the miscibility, similar to low nitrogen gases.

The above conclusions, though generated on a four component mixture, are quite informative in explaining the apparent diverse views expressed by various investigators, and also helpful to select realistic methods of estimating MMP.

When miscibility is achieved by the vaporising process only, such as displacing a hydrocarbon mixture with methane or pure nitrogen, MMP can be calculated quite simply by a phase behaviour model. In this process, the critical tie line extension goes through the oil composition, which is independent of the injection gas composition.

Most methods that advocate using a phase behaviour model to predict the miscibility pressure, propose conducting the forward multiple contact test. The test is to be simulated by successively raising the pressure and monitoring the approach to the critical state.

A simple, yet quite rigorous, method is that of Jensen and Michelsen [28], which is based on the idea of negative flash calculation described in Section 5.1. As shown conceptually for a three component mixture in Figure 7.3, the limiting tie line and the final operating line are the same for Oil B. Hence, for example, when the gas  $Y'_2$  is incrementally added to the undersaturated Oil B, the mixture composition enriches in the light fraction by moving towards the composition  $X'_2$ , on the tie line, which is the same as the operating line. The mixture attains the composition  $X'_2$  at the bubble point condition. Further addition of the gas will take the mixture into the two-phase region, where the equilibrated gas and oil are shown by  $X'_2$  and  $Y'_2$  respectively.

The above analysis indicates that any mixture on the tie line extension, when flashed at the prevailing pressure and temperature, will produce equilibrated phases with compositions as those at the two ends of the tie line, but with a negative vapour volume. As the pressure increases and the miscibility is approached, the limiting tie line length decreases approaching zero at the critical point.

Invoking the component material balance in flash calculations, Eqs.(5.1-2) we get,

$$z_i = x_i(1 - n^V) + y_i n^V \quad i=1,2, \dots, N \quad (7.5)$$

where  $z_i$ ,  $x_i$  and  $y_i$  are the mole fractions of component  $i$ , in the initial oil, equilibrated oil and equilibrated gas respectively.  $n^V$  is the vaporised fraction of the feed (original oil) which will be negative in this case. As the tie line length decreases and miscibility is approached, the value of  $n^V$  decreases approaching minus infinity. Hence, MMP can be determined by flashing the oil at the reservoir temperature and successively increasing the pressure above the bubble point. The calculated vapour fraction is monitored, searching for a large negative number. As a practical rule values less than -10 indicate proximity to MMP[28].

### Condensing-Vaporising Gas Drive

The condensing-vaporising miscibility is achieved generally at lower pressures than those of the vaporising gas drive. As pointed out in Section 7.1, the achievement of miscibility by condensing gas drive alone is not generally expected for real reservoir fluids.

Benham et al. [29] assumed that the critical tie line is parallel to the L-H axis in the pseudo-ternary diagram to develop MMP correlations for rich gas injection. The results were presented by a set of curves correlating MMP with the concentration and molecular weight of the intermediate fractions of the injection gas, the molecular weight of the reservoir oil  $C_{5+}$ , and the temperature. Glaso [25] fitted curves to the results of Benham et al., as follows:

$$P_m = 43.74 - 0.1752M - (32.23 - 0.127M)y_1 + \left(0.777 \times 10^{-14} M^{5.258} e^{31980y_1} M^{-1.703}\right) (1.8T - 460) \quad (7.6)$$

For  $M_{C_{2-C_6}} = 34$

$$P_m = 38.04 - 0.1326M - (55.79 - 0.188M)y_1 + \left(1.172 \times 10^{-11} M^{3.730} e^{1356.7y_1 M^{-1.058}}\right) (1.8T - 460) \quad (7.7)$$

For  $M_{C_2-C_6} = 44$

$$P_m = 51.38 - 0.1772M - (50.69 - 0.147M)y_1 + \left(3.392 \times 10^{-16} M^{5.520} e^{2170.6y_1 M^{-1.109}}\right) (1.8T - 460) \quad (7.8)$$

For  $M_{C_2-C_6} = 54$

where  $P_m$  is MMP in MPa,  $y_1$  is the mole fraction of methane in the injection gas,  $T$  is the temperature in K, and  $M_{C_2-C_6}$  is the molecular weight of the  $C_2$  to  $C_6$  fraction in the injection gas.

As it is known that non-paraffin oils achieve miscibility at lower pressures, Glaso included the effect of oil type on MMP by calculating the molecular weight of the stock tank oil  $C_{7+}$ ,  $M$ , as,

$$M = 572.7 / (S_{C_7+})^{-5.573} \quad (7.9)$$

where  $S_{C_7+}$  is the specific gravity of  $C_{7+}$  fraction.

Kuo [30] simulated the backward multiple experiment, using the Peng-Robinson EOS, to predict the miscibility conditions for a number of oil and rich gas systems. The results were correlated as,

$$P_m = 18.46 \frac{y_1^C M_{C_{2-4}}^{E+FM_{C_{2-4}}}}{(1.8T - 460)^{(A+BT)} M_{C_{5+}}^D} \quad (7.10)$$

where  $y_1$  is the mole fraction of methane,  $M_{C_{2-4}}$  is the molecular weight of  $C_2$  to  $C_4$  fraction in the injected gas, and  $M_{C_{5+}}$  is the molecular of  $C_{5+}$  in the oil. The minimum miscibility pressure,  $P_m$  is in MPa, and  $T$  is in K. The values of the constants in the above equation are:

A= 0.7807248	B=-0.0017204
C= 1.7138599	D=-1.0695591
E= -0.9909715	F=-0.0010102

The above correlation was demonstrated to be superior to those of Benham et al. and Glaso in a comparative study [27], with a standard deviation of 13.3%.

The validity of the above methods, which are based on the criterion of critical injection gas tie line, for real reservoir fluids is in doubt.

Pedrood [31] simulated the displacement of oil by rich gases using a one dimensional compositional model. An extensive sensitivity analysis of the parameters affecting the miscibility resulted in the following correlation:

$$P_m = 49.15 - 0.6863\theta + 2.482 \times 10^{-4} \theta^2 - 0.2054\psi^2 \quad (7.11)$$

where  $\theta$  and  $\psi$  represent properties of the injected gas and reservoir oil, respectively, as follows,

$$\theta = 100(y_{C_4} + 0.8y_{C_3} + 0.5y_{C_2+CO_2})$$

and

$$\Psi = (10^6 y_{C_2-C_5}) / [M_{C_5+} (1.8T - 460)]$$

where  $y$  is the mole fraction, and  $P_m$  and  $T$  are in MPa and K, respectively.

The predicted MMP by the above correlation was compared with slim tube data on 11 oil reservoirs. The predicted values, ranging from 10 to 40 MPa, showed an average absolute deviation of 5%. The Benham correlation generally over predicted the results with an average absolute deviation of 37% [31].

At reservoir conditions,  $CO_2$  is often a super-critical compound and behaves as a strong solvent extracting components as heavy as  $C_{30}$  even at moderate pressures. Hence, MMP for  $CO_2$  is generally quite low. The solvency of  $CO_2$  increases with its density. Therefore, higher pressures are required at higher temperatures, to increase the  $CO_2$  density for achieving miscibility. In low temperature reservoirs, the  $CO_2$ -oil mixture may form two liquid phases, or three phases of vapour,  $CO_2$  rich liquid and hydrocarbon rich liquid.

Miscibility by carbon dioxide injection has been studied extensively, and various correlations to estimate MMP have been proposed. Enick et al. [32] reviewed 17 correlations proposed by different investigators.

Alston et al. [33] developed a correlation based on a large number of MMP data for pure  $CO_2$ ,

$$P_m = 6.05 \times 10^{-6} (1.8T - 460)^{1.06} M_{C_5+}^{1.78} (x_v / x_l)^{0.136} \quad (7.12)$$

where  $x_v$ , and  $x_l$  are the mole fraction of volatile ( $C_1$ ,  $N_2$ ), and intermediate components ( $C_2$ ,  $C_4$ ,  $CO_2$ ,  $H_2S$ ) in the oil, respectively. For oils with bubble point pressures less than 0.35 MPa, the value of  $(x_v/x_l)^{0.136}$  is taken as unity.

Contamination of  $CO_2$  with gases of higher volatility, i.e.  $N_2$  and  $C_1$ , increases MMP, whilst addition of less volatile components such as  $H_2S$ ,  $C_2$ , and  $C_3$  lowers MMP. The estimated MMP for  $CO_2$  can be corrected for the effect of impurities by empirical correlations. Alston et al. [33] proposed the following correction factor,  $\phi_p$ , to be multiplied to the estimated MMP of pure  $CO_2$ ,

$$\ln \phi_p = 1.935 \left( \frac{87.8}{1.8_p T_c - 460} \right) \ln \left( \frac{87.8}{1.8_p T_c - 460} \right) \quad (7.13)$$

where  $_p T_c$ , in K, is the pseudo-critical temperature of the impure  $CO_2$  gas, calculated by the weight average mixing rule,

$$_p T_c = \sum_i w_i T_{ci} \quad (7.14)$$

where  $w_i$  is the weight fraction of component,  $i$ , in gas mixture, and  $T_{ci}$  is the critical temperature of component  $i$ . The authors suggested to use a value of 325 K for the critical temperatures of  $H_2S$  and ethane, instead of their actual values to improve the results.

Other correlations, using the molar average mixing rule for calculating the pseudo-critical temperature have also been proposed [34].

Phase behaviour models can be used to estimate miscibility conditions in rich gas and CO<sub>2</sub> injection. As the miscibility is determined by a cross over tie line, the proper simulation of the compositional path is essential. The simulation of simple batch type experiments, such as the backward multiple contact test, cannot generally produce the miscible bank.

The most common method is the use of one-dimensional flow compositional models simulating displacement in a slim tube. MMP can be found by monitoring the compositional variations along the tube, or plotting the predicted liquid recovery similar to using slim tube experimental data.

Any reliable EOS may be used to predict the phase behaviour of injection gas and reservoir oil. The model also requires correlations for calculating the relative permeability, viscosity and interfacial tension. The selected mathematical parameters to solve the governing equations, such as the number of cells describing the tube and the time step, also affect the results by introducing numerical dispersion [14]. Further details on using a one-dimensional compositional simulator are given in Section 9.3.

#### Example 7.1.

Estimate MMP of the following reservoir oil and the injected rich gas at 367 K.

Component	C1	C2	C3	iC4	nC4	iC5	nC5	C6	C7+	CO2
Oil, mole %	54.50	8.09	5.82	0.78	2.17	0.94	1.65	2.39	23.66	
Gas, mole%	84.63	8.81	4.11	1.40						1.05

C7+ Properties: M=209 S=0.8323

#### Solution:

Glaso (Benham et al.) Method:

The adjusted molecular weight of the C<sub>7+</sub> fraction by Eq.(7.9), using its specific gravity, is calculated as 205.9. The molecular weight of the C<sub>2</sub>-C<sub>6</sub> is determined as,

$$M_{C_2-C_6} = \left( \sum_2^6 x_{C_i} M_{C_i} \right) / \sum_2^6 x_{C_i} = 36.84$$

The calculated MMP for M<sub>C<sub>2</sub>-C<sub>6</sub></sub> of 34, 44 and 54 at 367 K, using Eq.(7.6), Eq.(7.7), and Eq.(7.8), respectively, are as follows:

$$P_{m,34} = 53.32 \text{ MPa}$$

$$P_{m,44} = 56.27 \text{ MPa}$$

$$P_{m,54} = 56.62 \text{ MPa}$$

Interpolating between the above values for M<sub>C<sub>2</sub>-C<sub>6</sub></sub>=36.84, we obtain,

$$\text{MMP} = 54.16 \text{ MPa}$$

Kuo Method:

The calculated MMP by the Kuo correlation, Eq.(7.10), with M<sub>C<sub>5</sub></sub>=186.19, and M<sub>C<sub>2</sub>-C<sub>4</sub></sub>=37.33, is,

$$\text{MMP} = 40.54 \text{ MPa}$$

Pedrood Method:

The two parameters representing gas and oil in Eq.(7.11) are calculated as,

$$\theta=1124$$

$$\psi=52215$$

resulting in,

$$\text{MMP}=35.87 \text{ MPa}$$

The measured value using slim tube data is 39.99 MPa. The predicted value assuming miscibility by vaporising gas drive is expected to be higher than those by the condensing process. However, the Firoozabadi-Aziz correlation, Eq.(7.1), predicts  $\text{MMP}=36.51 \text{ MPa}$ , which is only slightly higher than the answer by Pedrood method, and much lower than the answers by Glaso and Kuo methods.

## 7.4 REFERENCES

1. Zick, A.A: "A Combined Condensing/Vaporising Mechanism in the Displacement of Oil by Enriched Gases", SPE 15493, Proc. of 61st Ann. Conf. (Oct., 1986).
2. Stalkup, F.I: "Displacement Behaviour of the Condensing/Vaporising Gas Drive Process", SPE 16715, Proc. of 62nd Ann. Conf. (Sept., 1987).
3. Monroe, W.W., Silva, M.K., Larse, L.L. and Orr Jr, F.M: "Composition Paths in Four-Component Systems, Effect of Dissolved Methane on 1D  $\text{CO}_2$  Flood Performance", SPE Res.Eng., 423-432 (Aug., 1990).
4. Orr Jr, F.M., Johns, R.T. and Dindoruk, B: "Development of Miscibility in Four-Component Gas Drives", SPE 22637, Proc. of 66th Ann. Conf. (Oct., 1991)
5. Johns, R.T., Dindoruk, B. and Orr Jr, F.M: "An Analytical Theory of Combined Condensing/Vaporising Gas Drives", SPE Advanced Technology Series, 1(2), 7-16 (1993).
6. Johns, R.T. and Orr Jr, F.M: "Miscible Gas Displacement of Multicomponent Oils", SPE 30798, Proc. of 70th Ann. Conf., 985-998 (Oct., 1995).
7. Dindoruk, B., Orr Jr, F.M. and Johns, R.T: "Theory of Multicomponent Miscible Displacement with Nitrogen", SPE 30771, Proc. of 70th Ann. Conf., Res. Eng., 725-738, (Oct., 1995).
8. Pande, K.K. and Orr Jr, F.M: "Interaction of Phase Behaviour, Reservoir Hetrogeneity and Cross Flow in  $\text{CO}_2$  Floods", SPE 19668, Proc. of 64th Ann. Conf. (Oct., 1989).
9. Johns, R.T., Fayers, F.J. and Orr Jr, F.M: "Effect of Gas Enrichment and Dispersion on Nearly Miscible Displacements in Condensing Vaporising Drives", SPE Advanced Technology Series, 2(2), 26-34 (1993).
10. Flock, D.L. and Nouar, A: "Parametric Analysis of the Determination of the Minimum Miscibility Pressure in Slim Tube Displacements", JCPT, 80-88 (Sept.-Oct., 1984).
11. Dumore, J.M., Hagoort, J. and Risseuw, A.S: "An Analytical Model for One-Dimensional, Three Component Condensing and Vaporizing Gas Drives", SPE J., 24, 169-179 (April, 1984).
12. Glaso, O: "Miscible Displacement, Recovery Tests with Nitrogen", SPE Res.Eng., 61-68 (Feb., 1990).
13. Hudgins, F.M., Llave, F.M. and Chung, F.T: "Nitrogen Miscible Displacement of Light Crude Oil, A Laboratory Study", SPE Res. Eng., 100-106, (Feb., 1990).

14. Dullien, F.A.L.: "Porous Media, Fluid Transport and Pore Structure". Academic Press, London (1979).
15. Holm, L.W. and Josendal, V.A.: "Effect of Oil Composition on Miscible-Type Displacement by Carbon Dioxide", SPE J., 87-98 (Feb., 1982).
16. Jacobson, H.A.: "Acid Gases and Their Contribution to Miscibility", JCPT, 57-59 (April-May, 1972).
17. Graue, D.J. and Zana, E.T.: "Study of a Possible CO<sub>2</sub> Flood in Rangely Field", JPT, 1312-1318 (July, 1981).
18. Tajdar, R.N., Danesh, A. and Gozalpour, F.: "An Investigation of Oil Displacement by Enriched Gases Using a Compositional Model and Its Application to Karanj Reservoir", Proc. of 2nd International Conference on Chemistry in Industry, ACS, Bahrain (Oct., 1994).
19. Sibbald, L.R., Novosad, Z. and Costain, T.G.: "Methodology for the Specification of Solvent Blends for Miscible Enriched-Gas Drives", SPE Res. Eng., 373-378 (Aug., 1991).
20. Walsh, B.W. and Orr Jr, F.M.: "Prediction of Miscible Flood Performance, the Effect of Dispersion on Composition Paths in Ternary Systems", In Situ, 14(1), 19-47 (1990).
21. Christiansen, R.L. and Haines, H.K.: "Rapid Measurement of Minimum Miscibility Pressure with the Rising-Bubble Apparatus", SPE Res. Eng., 523-527 (Nov., 1987).
22. Stalkup, F.I.: "Miscible Displacement", SPE Monograph Vol. 8 (1983).
23. Firoozabadi, A. and Aziz, K.: "Analysis and Correlation of Nitrogen and Lean-Gas Miscibility Pressure", SPE Res. Eng., 575-582 (Nov., 1986).
24. Koch Jr., H.A. and Hutchinson Jr., C.A.: "Miscible Displacements of Reservoir Oil Using Flue Gas", Trans. AIME, 213, 7-10 (1958).
25. Glaso, O.: "Generalised Minimum Miscibility Pressure Correlation", 927-934 (Dec., 1985).
26. Boersma, D.M. and Hagoort, J.: "Displacement Characteristics of Nitrogen Flooding vs. Methane Flooding in Volatile Oil Reservoirs", SPE Res. Eng., 261-265 (Nov., 1994).
27. Yurkiw, F.J. and Flock, D.L.: "A Comparative Investigation of Minimum Miscibility Pressure Correlations for Enhanced Oil Recovery", JCPT, 33, No. 8, 35-41 (1994).
28. Jensen, F. and Michelsen, M.L.: "Calculation of First and Multiple Contact Minimum Miscibility Pressures", In Situ, 14(1), 1-17 (1990).
29. Benham, A.L., Dowden, W.E. and Kunzman, W.J.: "Miscible Fluid Displacement, Prediction of Miscibility", Trans. AIME, 219, 229-37 (1960).
30. Kuo, S.S.: "Prediction of Miscibility for Enriched Gas Drive Processes", SPE 14152, Proc. of 60th SPE Ann. Conf. (Sept., 1985).
31. Pedrood, P.: "Prediction of Minimum Miscibility Pressure in Rich Gas Injection", M.Sc. Thesis, Tehran University, Tehran (1995).



32. Enik, R.M., Holder, G. and Morsi, B: "A Thermodynamic Correlation for the Minimum Miscibility Pressure in  $\text{CO}_2$  Flooding of Petroleum Reservoirs", SPE Res. Eng., 81-92 (Feb., 1988).
33. Alston, R.B., Kokolis, G.P. and James, C.F: "CO<sub>2</sub> Minimum Miscibility Pressure, A Correlation for Impure CO<sub>2</sub> Streams and Live Oil Systems" SPE J., 268-274 (April, 1985).
34. Sebastian, H.M., Wenger, R.S. and Renner, T.A: "Correlation of Minimum Miscibility Pressure for Impure CO<sub>2</sub> Streams", JPT, 2076-2082 (Nov., 1985).

## 7.5 EXERCISES

7.1. Use a phase behaviour model to develop a ternary diagram for  $\text{C}_1$ - $\text{C}_3$ - $n\text{C}_{10}$  at 377.6 K and 28 MPa. What is the minimum required concentration of propane in a gas composed of  $\text{C}_1$ - $\text{C}_3$  to miscibly displace an oil composed of  $\text{C}_1$  (60 mol%) and  $n\text{C}_{10}$  (40 mol%) at the above conditions.

7.2. The composition of a reservoir oil is given in the following table. The reservoir pressure and temperature are equal to 82.75 MPa and 387 K, respectively. The oil is to be displaced by methane. What is your recommended pressure for gas injection.

Component	C1	C2	C3	iC4	nC4	iC5	nC5	C6+	N2	CO2
Oil, mole %	41.35	7.61	4.77	0.99	2.61	1.05	1.51	35.41	0.33	4.37
C6+ Properties:	M=171			S=0.8527						

7.3. Calculate MMP in the above exercise, using the negative flash method.

7.4. Normal butane is to be used as the solvent slug in a methane gas injection process. Assuming the reservoir oil behaves as normal decane, estimate the minimum miscibility pressure at 360 K. What is MMP at 410 K?

7.5. Estimate MMP of the reservoir oil, described in Exercise 7.2, and the injected rich gas described in the following table. Compare various correlations (measured value=32.75 MPa).

Component	C1	C2	C3	iC4	nC4	iC5	nC5	C6+	N2	CO2
Oil, mole %	74.60	9.90	3.91	0.57	1.12	0.26	0.27	0.17	0.30	8.90

7.6. The reservoir oil, described in Exercise 7.2, is to be miscibly displaced by a gas composed of 90 mol%  $\text{CO}_2$  and 10 mol%  $\text{N}_2$ . Estimate the minimum miscibility pressure.



## 8

# INTERFACIAL TENSION

Surface forces affect fluid phase equilibria. A tension always exists at the interface of fluid phases, due to unbalanced molecular attractive and repulsive forces. For a pure compound, the vapour pressure over a meniscus in a pore which is concave toward the vapour phase is smaller than that over a flat surface and decreases as the radius of curvature decreases. Capillary condensation, where an unsaturated vapour forms condensate in tight pores is a manifestation

of the above effect. It, however, becomes only significant in very tight spaces. It is generally neglected in reservoir engineering studies, because the rock in majority of gas condensate reservoirs is water wet, hence, the tight corners are filled with water and not open to the hydrocarbon. Surface forces, however, affect the onset of formation of new phases and also play a major role in multiphase flow in hydrocarbon reservoirs and in pipelines.

A quantitative index of the molecular tension at the interface is the interfacial tension (IFT),  $\sigma$ , defined as the force exerted at the interface per unit length ( $\text{mN/m} = \text{dyne/cm}$ ).

The capillary pressure is the concept which is often used in reservoir studies to consider the effect of surface forces on the fluid distribution within a reservoir. The capillary pressure is related to the interfacial tension and the pore characteristics [1]. It has been established also that the relative permeability, which describes the multiphase flow behaviour in the reservoir rock, may strongly depend on the interfacial tension [2]. The application of IFT dependent relative permeability in the dynamic evaluation of phase behaviour models will be described in Section 9.3.

The evaluation of gas-liquid interfacial tension is of a major interest in gas injection processes where the relative magnitudes of surface, gravitational and viscous forces affect the recovery. The gravity drainage, controlled by the balance of gravity and surface forces, is a drive mechanism which is well recognised in the oil recovery. It is a common assumption that the liquid drop out by retrograde condensation in reservoir pores is immobile, hence, non-recoverable unless re-vaporised. Recent studies [3] have indicated that the condensate recovery by gravity drainage can also be quite significant when the gas-condensate interfacial tension is small.

The variation of gas-oil interfacial tension with pressure for a number of reservoir fluids is shown in Figure 8.1, where the interfacial tension increases with decreasing pressure [22]. An equation describing the reported data is also shown. The interfacial tension is very small for near critical mixtures and approaches zero as the critical point is approached. Hence the effect of temperature on IFT depends on the relative position to the critical point. For a gas

condensate, IFT is expected to decrease by decreasing temperature, where the opposite is expected for an oil sample.

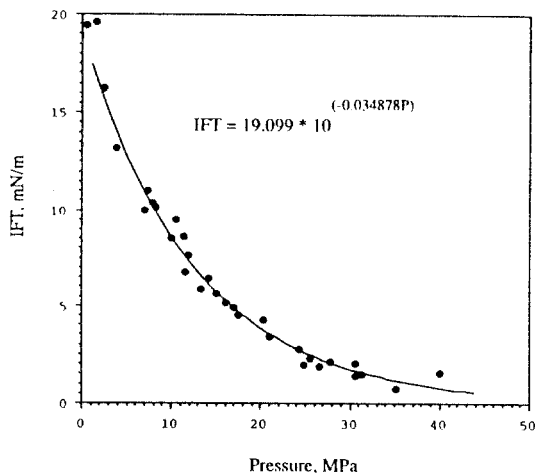
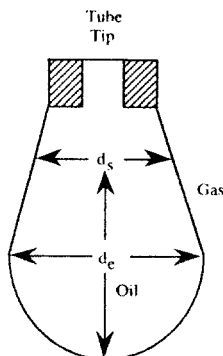


Figure 8.1. Variations of interfacial tension of gas-oil with pressure. SPE Copyright Reproduced from [22] with permission.

The interfacial tension between fluid phases at reservoir and surface conditions are measured by various techniques. Prediction methods, with an acceptable engineering accuracy, are also available. The most widely used and reliable methods are described in this chapter.

## 8.1 MEASUREMENT METHODS

The gas-liquid interfacial tension at high pressures is commonly measured by a pendant-drop apparatus. In this technique, a liquid droplet is allowed to hang from the tip of a capillary tube in a high pressure visual cell filled with its equilibrated vapour, as shown schematically in Figure 8.2. The shape of liquid droplet at static conditions, controlled by the balance of gravity and surface forces, is determined and related to the gas-liquid interfacial tension [4] by,



$$\sigma = \frac{gd_e^2}{f} (\rho^l - \rho^v) \quad (8.1)$$

Figure 8.2. IFT measurement by pendant drop method.

where,  $g$  is the acceleration due to gravity and  $\rho^L$  and  $\rho^V$  are the liquid and vapour phase (mass) densities, respectively.  $\ell$ , the drop shape factor, is a function of  $\mathcal{R} = d_e/d_s$ , where  $d_e$  is the equatorial diameter, or the maximum horizontal diameter of the drop and  $d_s$  is the diameter of the drop measured at the height  $d_e$  above the bottom of the drop, as shown in Figure 8.2. Tabulated values of  $\ell$ , determined by relating the pressure difference across the interface to the interface curvature, vs.  $\mathcal{R}$ , reported by several investigators [4,5], are given in Table 8.1.

The pendant drop method can also be applied to measure the interfacial tension of hydrocarbon-water systems.

Table 8.1.  
Values of the drop shape factor  $\ell$  [5].

$\mathcal{R}$	0	1	2	3	4	5	6	7	8	9
0.67	.90174	.89822	.89471	.89122	.88775	.88430	.88087	.87746	.87407	.87069
0.68	.86733	.86399	.86067	.85736	.85407	.85080	.84755	.84431	.84110	.83790
0.69	.83471	.83154	.82839	.82525	.82213	.81903	.81594	.81287	.80981	.80677
0.70	.80375	.80074	.79774	.79477	.79180	.78886	.78593	.78301	.78011	.77722
0.71	.77434	.77148	.76864	.76581	.76299	.76019	.75740	.75463	.75187	.74912
0.72	.74639	.74367	.74097	.73828	.73560	.73293	.73028	.72764	.72502	.72241
0.73	.71981	.71722	.71465	.71208	.70954	.70700	.70448	.70196	.69946	.69698
0.74	.69450	.69204	.68959	.68715	.68472	.68230	.67990	.67751	.67513	.67276
0.75	.67040	.66805	.66571	.66338	.66107	.65876	.65647	.65419	.65192	.64966
0.76	.64741	.64518	.64295	.64073	.63852	.63632	.63414	.63196	.62980	.62764
0.77	.62550	.62336	.62123	.61912	.61701	.61491	.61282	.61075	.60868	.60662
0.78	.60458	.60254	.60051	.59849	.59648	.59447	.59248	.59050	.58852	.58656
0.79	.58460	.58265	.58071	.57878	.57686	.57494	.57304	.57114	.56926	.56738
0.80	.56551	.56364	.56179	.55994	.55811	.55628	.55446	.55264	.55084	.54904
0.81	.54725	.54547	.54370	.54193	.54017	.53842	.53668	.53494	.53322	.53150
0.82	.52978	.52808	.52638	.52469	.52300	.52133	.51966	.51800	.51634	.51470
0.83	.51306	.51142	.50980	.50818	.50656	.50496	.50336	.50176	.50018	.49860
0.84	.49702	.49546	.49390	.49234	.49080	.48926	.48772	.48620	.48468	.48316
0.85	.48165	.48015	.47865	.47716	.47568	.47420	.47272	.47126	.46980	.46834
0.86	.46690	.46545	.46401	.46258	.46116	.45974	.45832	.45691	.45551	.45411
0.87	.45272	.45134	.44996	.44858	.44721	.44585	.44449	.44313	.44178	.44044
0.88	.43910	.43777	.43644	.43512	.43380	.43249	.43118	.42988	.42858	.42729
0.89	.42600	.42472	.42344	.42216	.42089	.41963	.41837	.41711	.41586	.41462
0.90	.41338	.41214	.41091	.40968	.40846	.40724	.40602	.40481	.40361	.40241
0.91	.40121	.40001	.39882	.39764	.39646	.39528	.39411	.39294	.39178	.39062
0.92	.38946	.38831	.38716	.38602	.38488	.38374	.38260	.38147	.38035	.37922
0.93	.37810	.37699	.37588	.37477	.37367	.37256	.37147	.37037	.36928	.36819
0.94	.36711	.36603	.36495	.36387	.36280	.36173	.36067	.35960	.35854	.35749
0.95	.35643	.35538	.35433	.35328	.35224	.35120	.35016	.34913	.34809	.34706
0.96	.34604	.34501	.34398	.34296	.34195	.34093	.33991	.33890	.33789	.33688
0.97	.33587	.33487	.33386	.33286	.33186	.33086	.32986	.32887	.32787	.32688
0.98	.32588	.32489	.32390	.32290	.32191	.32092	.31992	.31893	.31793	.31694
0.99	.31594	.31494	.31394	.31294	.31194	.31093	.30992	.30891	.30790	.30688
1.00	.30586	.30483	.30379							

#### Example 8.1.

The vapour-liquid interfacial tension of a methane-normal decane mixture is measured by the pendant drop method. The gas and liquid densities at the test conditions of 377.6 K and 23.59 MPa are equal to 143.5 and 544.7 kg/m<sup>3</sup>, respectively. Calculate the interfacial tension when the liquid droplet dimensions are  $d_e=0.600$  and  $d_s=0.472$  mm.

*Solution:*

For a calculated value of  $\mathcal{R}=0.472/0.600=0.787$ , a shape factor of  $\ell=0.5905$  is read from Table 8.1. Hence Eq.(8.1) results in,

$$\sigma=9.81 \times (0.0006)^2 \times (544.7-143.5)/0.5905=0.002399 \text{ N/m}$$

$$\sigma=2.4 \text{ mN/m}$$

At very low IFT values, the hanging liquid drop becomes very small, requiring a very narrow tube to remain stable. The use of a thin wire, under the tube, for the drop to hang from its tip, instead of the tube, is a more practical arrangement. At conditions close to the critical point, where the interfacial tension is close to zero, the pendant drop method may not be applicable. Laser light scattering techniques have been used [6,7] to measure the propagation of thermally excited capillary waves at the vapour-liquid interface, determining very low interfacial tension values (0.001 mN/m).

Low interfacial tension values have been determined successfully by measuring the gas-liquid interface curvature in an equilibrium cell [8]. The interface between the phases is curved due to surface forces, as depicted in Figure 8.3. This behaviour is indeed one of the sources of error in determining phase volumes in equilibrium cells by measuring fluid interfaces and assuming them flat. The interface curvature in a visual, or windowed, equilibrium cell, appears as a band with a finite thickness between the phases, due to light scattering. The thickness of the band increases with IFT as the curvature becomes more pronounced at lower pressures.

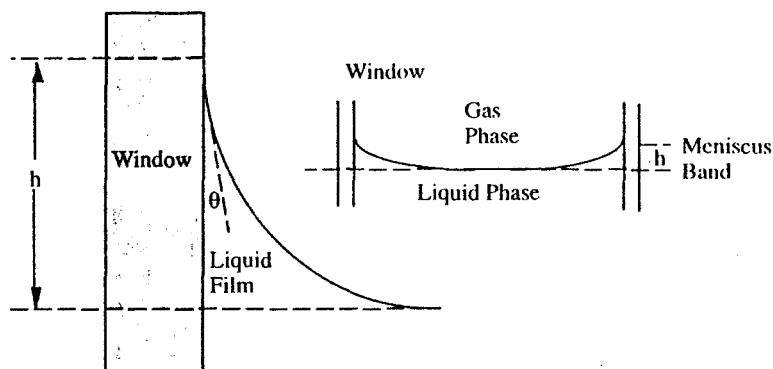


Figure 8.3. Gas-liquid interface curvature near the wall of a flat window.

At static conditions, the interface curvature can be related to the surface and gravity forces, resulting in differential equations which can be readily evaluated with the boundary conditions depending on the geometry of the equilibrium cell [8]. The rise of liquid on a flat window,  $h$ , is given by:

$$h = \left[ \frac{2\sigma(1 - \sin \theta)}{(\rho^L - \rho^V)g} \right]^{\frac{1}{2}} \quad (8.2)$$

where  $\theta$ , is the contact angle, Figure 8.3, and may be assumed zero at low interfacial tension as the liquid completely wets the window [9]. Hence,

$$\sigma = (\rho^L - \rho^V)gh^2 / 2 \quad (8.3)$$

The measurement of liquid rise on the equilibrium cell window provides accurate interfacial tension data with almost no extra effort during conventional PVT tests. It can be applied successfully to measure low IFT, down to values of the order of  $10^{-3}$  mN/m, where the interface between the vapour and liquid loses its definition.

## 8.2 PREDICTION OF INTERFACIAL TENSION

The interfacial tension between reservoir fluids can be predicted by several methods. Although the methods rely on some theoretical foundations, they require experimentally determined parameters.

The vapour-liquid interfacial tension of pure compounds has been related to various fluid properties, such as the density [10], compressibility [11] and latent heat of vaporisation [12], by various investigators. The relation between IFT and density has been extended to multicomponent systems successfully, resulting in a number of practical and widely used methods in the oil and gas industry.

An interesting approach is to consider the interface, as a third phase with properties varying between those at the bulk of the two phases. This approach, known as the gradient theory of inhomogeneous fluid, uses equilibrium thermodynamic concepts by employing an equation of state to calculate the required properties from volumetric data. The method has been successfully applied to binary systems [13]. It, however, requires experimentally determined parameters for all the components and their binaries. Because of its elaboration and lack of improved results relative to other methods, it has not received much attention in the industry. The two most widely used methods of predicting the interfacial tension in the petroleum industry are the parachor method, followed by the scaling law relying on the corresponding states principle.

### Parachor Method

It was first reported by Macleod [9], that the vapour-liquid interfacial tension of a pure compound is related to the density difference between the phases, as,

$$\sigma^L = P_\sigma (\rho_M^L - \rho_M^V) \quad (8.4)$$

where  $\rho_M^L$  and  $\rho_M^V$  are the molar density of the liquid and vapour phase, respectively, in gmol/cm<sup>3</sup> and  $\sigma$  is in mN/m.

The proportionality constant,  $P_\sigma$ , known as the *parachor*, has been extensively addressed by Sugden [14], as a parameter representing the molecular volume of a compound under conditions where the effect of temperature is neutralised. It is considered to have a unique value for each compound independent of pressure and temperature. The parachor values of various pure compounds have been determined from measured interfacial tension data, using Eq.(8.4) known as the Macleod-Sugden equation, reported by several investigators and reviewed by Ali [15].

Parachor values of homologous hydrocarbons show an almost linear relationship with the molecular weight [16-17]. A relation for the parachor of pure normal paraffins is as follows,

$$P_a = 21.99 + 2.892M \quad (8.5)$$

Parachor correlations in terms of critical properties have also been published [18].

$$P_a = 0.324 T_c^{\frac{1}{4}} v_c^{\frac{7}{8}} \quad (8.6)$$

where the critical temperature  $T_c$  is in K and the critical volume  $v_c$  is in  $\text{cm}^3/\text{gmol}$ .

Parachors of a number of pure compounds, to be used in Eq.(8.4), are given in Table 8.2 [19]. The values for compounds heavier than  $nC_8$  have been estimated from Eq.(8.5).

Table 8. 2.

Parachor and  $\zeta$  values of pure compounds.

Component	Parachor	$\zeta$ value
CO2	78.0	3.505
N2	41.0**	3.414
C1	77.0	3.409
C2	108.0	3.630
C3	150.3	3.681
iC4	181.5	3.597*
nC4	189.9	3.687
iC5	225.0	3.682*
nC5	231.5	3.695
nC6	271.0	3.726
nC7	312.5	3.748*
nC8	351.5	3.852
nC9	393.0	3.865
nC10	433.5	3.855
nC11	474.1	3.641
nC12	514.7	3.815
nC13	555.2	3.872
nC14	595.8	3.820
nC15	636.4	3.795
nC16	676.9	3.822

\*\* The given value is for nitrogen in hydrocarbon mixtures.

The value for pure nitrogen is 60.0.

\* Calculated values from Eq.(8.18).

The Macleod-Sugden equation, Eq.(8.4), has been extended to mixtures by incorporating various mixing rules. Weinaug and Katz [19] proposed simple molar averaging for the parachor,

$$\sigma^{\frac{1}{4}} = \rho_M^L \sum x_i P_{\sigma i} - \rho_M^V \sum y_i P_{\sigma i} = \sum P_{\sigma i} (x_i \rho_M^L - y_i \rho_M^V) \quad (8.7)$$

where  $x_i$  and  $y_i$  are the mole fractions of component  $i$  in the liquid and vapour phase, respectively.  $P_{\sigma i}$  is the parachor of component  $i$ .

Hugill and van Welsenes [20] proposed a quadratic mixing rule for estimation of the phase parachor,



$$P_{\sigma} = \sum_i \sum_j z_i z_j P_{\sigma ij} \quad (8.8)$$

where  $z_i$  is the mole fraction of component  $i$  in the liquid or vapour phase.  $P_{\sigma ij}$  is the average parachor of component  $i$  and  $j$ ,

$$P_{\sigma ij} = \frac{1}{2} (P_{\sigma i} + P_{\sigma j}) C_{ij} \quad (8.9)$$

where  $C_{ij}$  is a temperature dependent interaction parameter, determined experimentally using IFT data on binary mixtures.

The simple molar averaging as proposed by Weinaug and Katz, Eq.(8.8), is the method widely used in petroleum industry. The parachor value of a component in a mixture is the same as that when pure. The exception is that of nitrogen in reservoir fluids, as given in Table 8.2.

The relation between the parachor and the molecular weight of hydrocarbon groups, such as single carbon number groups, is considered to deviate significantly from linearity [21,22]. This trend should be expected as the parachor-molecular weight relation varies for various hydrocarbon homologues. The ratio of paraffins, aromatics and cyclic compounds in various SCN groups are not the same, resulting in a non-linear relation. Firoozabadi et al. [22] determined parachors for crude oil fractions of various molecular weights and proposed the following equation,

$$P_{\sigma} = -11.4 + 3.23M - 0.0022M^2 \quad (8.10)$$

It should be noted that generalised correlations are not expected to provide a reliable parachor value for the oil heavy end, which generally contains a high concentration of asphaltic and surface active materials. It is advisable to determine it experimentally.

The interfacial tension describes the nature of molecular forces at the interface, whereas the density or the molecular weight are bulk properties. In general all prediction methods which relate IFT to some bulk properties, such as the density, are not reliable for mixtures with component distribution at the interface different than that of the bulk.

### Example 8.2.

A reservoir oil has been modelled by a mixture of  $C_1$  and  $nC_{10}$  (60-40 mole%). The mixture bubble point pressure at 377.6 K is 23.59 MPa. The properties of the oil phase at the above conditions and its equilibrated gas, are as follows:

Phase	density, g/cm <sup>3</sup>	methane mole fraction
Oil	0.5447	0.6000
Gas	0.1435	0.9825

Estimate the gas-oil interfacial tension at the above conditions, using the parachor method. The measured value is 2.4 mN/m.

### Solution:

The molar density of both phases are calculated as  $\rho_m = p/M$ ,

$$M^l = \sum x_i M_i = 0.6 \times 16.043 + 0.4 \times 142.285 = 66.54 \text{ g/mol}$$

$$M^v = \sum y_i M_i = 0.9825 \times 16.043 + 0.0175 \times 142.285 = 18.25 \text{ g/mol}$$

$$\rho_M^L = 0.008186 \text{ gmol/cm}^3$$

$$\rho_M^V = 0.007862 \text{ gmol/cm}^3$$

The parachor values are read from Table 8.2 and used in Eq.(8.7) to calculate IFT.

$$\sigma^{0.25} = 77(0.6 \times 0.008186 - 0.9825 \times 0.007862) + 433.5(0.4 \times 0.008186 - 0.0175 \times 0.007862)$$

$$\sigma = 1.708 \text{ mN/m}$$

### Corresponding States Correlation (Scaling Law)

According to the corresponding states principle, Section 1.2, fluids behave similarly when scaled properly relative to their critical points. For a pure fluid, the vapour-liquid interfacial tension decreases with increasing temperature and becomes zero at the critical point. Hence the following scaling can be considered,

$$\sigma \approx (1 - T_r)^\theta \quad (8.11)$$

where  $T_r$  is the reduced temperature and the exponent  $\theta$  may be estimated experimentally or theoretically.

Brock and Bird [23] incorporated the dimensionless interfacial tension group of  $\sigma/(P_c^{2/3} T_c^{1/3})$  in the above scaling, adopted the empirical exponent value of  $\theta = 11/9$  reported by Guggenheim [24] and proposed,

$$\sigma = A_c (1 - T_r)^{11/9} \quad (8.12)$$

where,

$$A_c \equiv (0.132\beta_c - 0.279) (P_c^{2/3} T_c^{1/3}) \quad (8.13)$$

$\beta_c$  is the slope of the reduced vapour pressure curve, plotted vs. the reduced temperature, at the critical point and can be estimated from,

$$\beta_c = 0.9076 \left( \frac{1 + (T_b/T_c) \ln(P_c/P_a)}{(1 - T_b/T_c)} \right) \quad (8.14)$$

where  $T_b$  is the boiling point of the substance at the atmospheric pressure  $P_a$ .

Eq.(8.12), developed for pure fluids, cannot be used for mixtures as the composition of vapour and liquid changes with pressure and temperature.

Lee and Chien [25] replaced the temperature scale with the liquid-vapour density difference, as it also vanishes at the critical point,

$$(\rho^L - \rho^V) \approx (T_c - T)^\epsilon \quad (8.15)$$

They assumed  $\epsilon = 5/16$  as theoretically determined by Fisher [26] and proposed,

$$\sigma^{v/\theta} = (P_\sigma^L \rho_M^L - P_\sigma^V \rho_M^V) \quad (8.16)$$

where  $\rho_M^L$  and  $\rho_M^V$  are the molar densities of the liquid and vapour phases, respectively, and the exponent  $(\epsilon/\theta)$  is equal to  $(45/176)=(1/3.9111)$ .

The coefficient  $P_\sigma$  is equivalent to the parachor in Eq.(8.4) and is given by,

$$P_\sigma = A_c^{45/176} v_c / \zeta \quad (8.17)$$

where  $v_c$  is the molar critical volume and the value of  $\zeta$  is estimated from IFT data on pure compounds, as given in Table 8.2. It has been related also to the critical compressibility factor,  $Z_c$ , as [25],

$$\zeta = 1.854426 Z_c^{-0.52402} \quad (8.18)$$

although the correlation does not adequately match the reported values. For mixtures, molar averaging is used to calculate values  $\beta_c$ ,  $P_c$ ,  $T_c$ ,  $v_c$  and  $\zeta$ , for each phase to determine its parachor from Eq.(8.17). The interfacial tension is then calculated from Eq.(8.16).

### Comparison of Predictive Methods

An examination of the above two methods reveals that they are basically the same. Both use experimentally determined parachor coefficients, directly in the former and indirectly related to the critical property by  $\zeta$ , in the latter. Using a function relating the parachor to critical properties, such as Eq.(8.6), in the first method, will make the two even more similar. The first method, however, applies mixing rules directly to calculate the mixture parachor, whereas the pseudo mixture properties are initially calculated in the scaling law to determine the mixture parachor.

The main difference is the value of exponent in the IFT-density difference relation. This, however, does not limit any of the two methods to specific exponent values. Hough and Stegemeier [27] proposed an equation similar to Eq.(8.4), but with an exponent of 1/3.67, determined using IFT data of propane and butane in the critical region. It has been shown [6] that the Hough-Stegemeier equation is more accurate at low interfacial tension conditions ( $\sigma < 0.05$  mN/m).

The IFT density difference relation can be generalised as,

$$\sigma^{1/E} = (P_\sigma^L \rho_M^L - P_\sigma^V \rho_M^V) \quad (8.19)$$

where E has been assumed to be constant in the above methods.

Figure 8.4 shows IFT of a North Sea gas condensate measured during several tests, including the constant composition expansion, constant volume depletion and methane cycling at 383 K. All the measured points follow the same trend when plotted against the liquid-gas density difference. The relation is linear on the logarithmic plot, but the slope clearly changes around IFT=1 mN/m. The change of slope for other systems has been reported also by other investigators [28].

The deviation of predicted IFT by the Weinaug and Katz correlation from experimental data on seven hydrocarbon binary systems, including 213 data points, is shown in Figure 8.5 [29]. Note that the method generally under predicts at low IFT conditions, whilst it over predicts at high IFT conditions, with the most accurate results around IFT=1 mN/m. A similar trend was also observed for the Lee-Chien method [29].

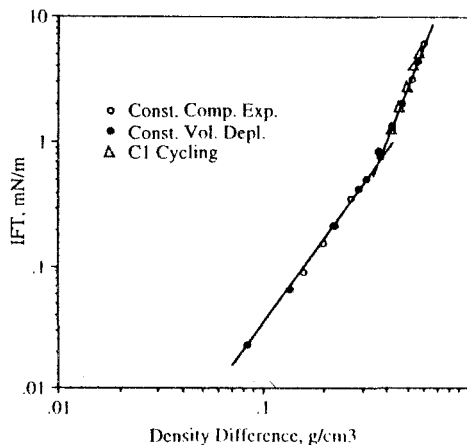


Figure 8.4. Measured gas-condensate IFT of a North Sea reservoir fluid at 383 K.

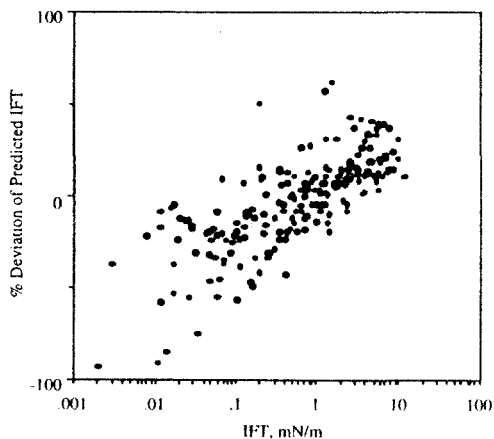


Figure 8.5. Deviations of predicted IFT by the Weinaug-Katz method for binary mixtures.

Both correlations can be improved by making the IFT exponent,  $1/E$ , a function of the liquid-vapour density difference [29]. The optimised value for the Weinaug-Katz correlation was determined by regressing  $E$  to minimise the deviations of the predicted binary results as,

$$E = 3.583 + 0.16(\rho_M^L - \rho_M^V) \quad (8.20)$$

where  $\rho_M$  is in  $\text{gmol}/\text{cm}^3$ . The contribution of the second term in the above correlation is negligible in most cases, resulting in a constant exponent in practice.

The above modification reduced the average absolute deviation from 23% to 14%, when tested against 65 data points on multicomponent model fluids. A similar improvement was also observed for real reservoir fluids including gas condensate and oil samples [30].

Schechter and Guo conducted a comprehensive survey [16] of reported IFT and density data and clearly demonstrated that the optimum value of  $E$ , particularly for hydrocarbon systems at low IFT conditions, is less than 4. Based on experimental data and molecular models, the authors concluded that a single constant value of  $E=3.88$  in Eq.(8.19) should suffice to predict IFT within a range where the critical point scaling is applicable, that is less than 1 mN/m.

$$\sigma^{L/R} = \sum P_m (x_i \rho_M^L - y_i \rho_M^V) \quad (8.21)$$

As changing the value of exponent results in change of the parachors, they calculated appropriate parachors for a large number of pure compounds, using experimental IFT data. Their calculated values are given in the physical property table, Table A.1, in Appendix A. The authors also developed linear correlations between the parachor and molecular weight for various hydrocarbon homologues. The correlation for alkanes is as follows,

$$P_s = 11.73 + 2.9871M \quad (8.22)$$

A linear relation between parachor values and molecular weight was also suggested for all types of hydrocarbons, with a deviation of 22%, as follows:

$$P_s = 3.72 + 2.9519M \quad (8.23)$$

The above correlation may be used to estimate parachor values for SCN groups.

### Example 8.3.

Predict the gas-liquid IFT of the mixture described in Example 8.2, using the Lee-Chien and Schechter-Guo methods.

*Solution:*

#### Lee-Chien Method

The component critical properties are read from Table A.1 in Appendix A. The values of  $\beta_c$  for each component is calculated using Eq.(8.14),

$$\beta_{c,C1} = 13.30947 \quad \beta_{c,C10} = 17.29700$$

Values of  $\zeta$  for methane and normal decane are read from Table 8.2, equal to 3.409 and 3.855, respectively.

The values of  $v_c$ ,  $T_c$ ,  $P_c$ ,  $\beta_c$  and  $\zeta$  of each phase are calculated by molar averaging and substituted in Eq.(8.13) and Eq.(8.17) to determine  $A_c$  and  $P_a$ , respectively.

Phase	$v_c$ , cm <sup>3</sup> /gmol	$T_c$ , K	$P_c$ , MPa	$\beta_c$	$\zeta$	$A_c$ , mN/m	$P_a$
Liquid	299.16	361.42	3.6034	14.9045	3.5874	28.2673	195.970
Vapour	107.37	198.04	4.5554	13.3793	3.4168	19.6633	64.104

Substituting the above values of  $P_a$  and molar densities, calculated in Example 8.2, in Eq.(8.16), we obtain,

$$\sigma^{(45/176)} = 195.970 \times 0.008186 - 64.104 \times 0.007862 = 1.10024$$

$$\sigma = 1.453 \text{ mN/m}$$

#### Schechter-Guo Method

The parachor values for methane and normal decane are read from Table A.1, equal to 74.05 and 440.69, respectively, and substituted in Eq.(8.7), but with the IFT exponent of (1/3.88),

$$\sigma^{(1/3.88)} = 74.05(0.6 \times 0.008186 - 0.9825 \times 0.007862) + 440.69(0.4 \times 0.008186 - 0.0175 \times 0.007862)$$

$$\sigma = 1.864 \text{ mN/m}$$

### 8.3 WATER-HYDROCARBON INTERFACIAL TENSION

The interfacial tension of pure hydrocarbon-water has been measured over wide ranges of temperature and pressure by various investigators [31-36]. The reported data often show substantial discrepancies as reviewed by Firoozabadi and Ramey [37]. The variation of methane-water IFT with pressure and temperature is shown in Figure 8.6. The interfacial tension decreases with increasing pressure and/or temperature over the tested region.

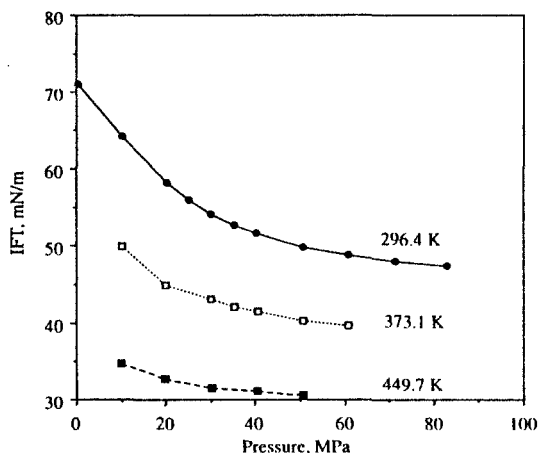


Figure 8.6. Methane-water interfacial tension. SPE Copyright. Reproduced from [35] with permission.

Figure 8.7 shows the variation of n-octane-water IFT, with pressure and temperature [36]. The interfacial tension decreases with increasing temperature. An increase in pressure, however, increases IFT, but the effect is small. There are reports showing slight reduction of IFT by increasing pressure [33], contrary to that in Figure 8.7. The effect of pressure on IFT of pure liquid hydrocarbon-water is generally small and can be neglected in most cases.

Comprehensive data on multicomponent hydrocarbons-water, particularly real reservoir fluids are scarce. For reservoir gases, the trend is very much similar to that of methane, Figure 8.6, with the presence of heavier compounds in the gas reducing IFT. The effect of pressure on oil-water IFT is minimal above the oil bubble point. The reduction of pressure below the oil bubble point generally reduces the oil-water IFT due to release of gas out of the liquid mixture. The oil-water interfacial tension is expected to decrease with increasing temperature, but results contrary to that at some conditions have also been reported [35].

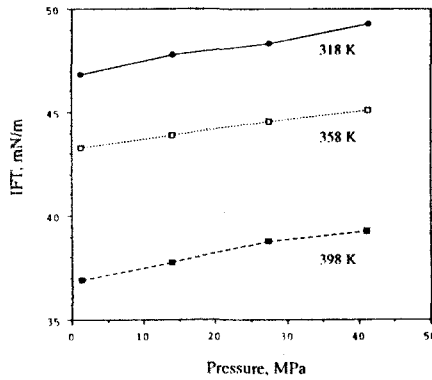


Figure 8.7. Water-n-octane interfacial. Petroleum Society of Canada Copyright. Reproduced from [36] with permission.

Although parachor values, about 52 [25, 38], have been reported for water, the use of vapour-liquid correlations, Eqs.(8.7) and (8.16), to estimate IFT of hydrocarbon-water is not recommend. These correlations can produce highly erroneous results, even for simple binary systems [37].

#### Example 8.4.

Estimate the interfacial tension between the gas in Example 8.2 and water.

#### Solution:

Considering that the gas is predominantly composed of methane, Figure 8.6 may be used to estimate gas-water IFT at 377.6 K and 23.59 MPa.

$$\sigma_{gw}=43 \text{ mN/m}$$

Firoozabadi and Ramey [37] demonstrated that IFT between water and pure hydrocarbons, over a wide range of temperature-pressure, can be described by a single plot shown in Figure 8.8. The IFT function is as follows:

$$\text{IFT Function} \equiv \left( \sigma_{hw}^{0.25} / (\rho^w - \rho^h) \right) (T/T_c^h)^{0.3125}$$

where,  $\sigma_{hw}$  is in mN/m,  $\rho^w$  and  $\rho^h$  are the water and hydrocarbon phase density in g/cm<sup>3</sup>, respectively, and  $T_c^h$  is the hydrocarbon phase critical temperature.

The reliability of correlation was demonstrated for various compounds ranging from methane to n-dodecane. The plot can be represented almost by the following equation,

$$\sigma_{hw} = 111(\rho^w - \rho^h)^{1.024}(T/T_c^h)^{-1.25} \quad (8.24)$$

which is also shown in Figure 8.8.

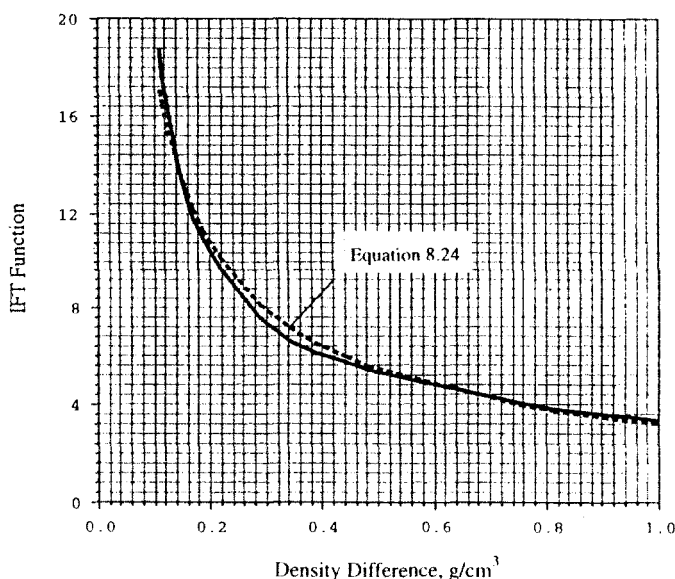


Figure 8.8. Generalised correlation for water-hydrocarbon interfacial tension Petroleum Society of Canada Copyright. Reproduced from [37] with permission.

The above correlation was evaluated for estimating the oil-water IFT, which indicated errors exceeding 30% [37]. The presence of surface active compounds in oil may prohibit the use of any generalised correlation which does not take such effects into account. When the IFT value at a single point, often at the atmospheric conditions, is known, a parallel curve to that in Figure 8.8 may be used to estimate IFT at other pressure-temperature values [37].

The presence of salts in water may alter its interfacial tension with oil slightly at typical reservoir conditions. The IFT may decrease [39], or increase [40] by increasing the salt concentration according to various reported data.

#### Example 8.5.

Estimate the oil-water and gas-water interfacial tension for fluids described in Example 8.2, using the generalised hydrocarbon water correlation.



*Solution:*

Neglecting the solubility of hydrocarbon in water, the water density at 377.6 K and 23.59 MPa can be estimated from Eq.(2.88), as in Example 2.15.

$$\Delta V_{wT} = -0.005781$$

$$\Delta V_{wT} = 0.046034$$

$$B_w = 1.03999$$

$$\rho^w = 1.040 \text{ g/cm}^3$$

Taking the molar average critical temperature of the hydrocarbon vapour and liquid phases as calculated in Example 4.3, neglecting the solubility of water in hydrocarbon phases and using Eq.(8.24), the interfacial tension is calculated.

Hydrocarbon	$\rho^w$ , g/cm <sup>3</sup>	$\rho^h$ , g/cm <sup>3</sup>	$\rho^w - \rho^h$ , g/cm <sup>3</sup>	$T_c$ , K	$T_r$	IFT, mN/m
vapour	1.04	0.1435	0.8965	198.04	1.9070	44
liquid	1.04	0.5447	0.4953	361.42	1.0448	51

The interfacial tension between the hydrocarbon liquid phase and water is expected to be lower than that of the vapour phase, contrary to the above calculated values. Using the original plot in Figure 8.8, instead of Eq.(8.24), results in a calculated vapour-water interfacial tension of 49 mN/m.

**8.4 REFERENCES**

1. Bardon, C. and Longeron, D.G: "Influence of Very Low Interfacial Tension on Relative Permeability", SPE J., 391-401 (Oct., 1980).
2. Danesh, A., Krinis, D., Henderson, G.D. and Peden, J.M: "Visual Investigation of Retrograde Phenomenon and Gas Condensate Flow in Porous Media", 5th European Symposium on Improved Oil Recovery, Budapest (1988).
3. Andreas, J.M., Hauser, E.A. and Tucker, W.B: "Boundary Tension by Pendant Drops", Presented at the 50th Colloid Symposium, Cambridge, Massachusetts (June, 1938).
4. Niederhauser, D.O. and Bartell, F.E: "A Corrected Table for Calculation of Boundary Tensions by Pendant Drop Method", Research on Occurrence and Recovery of Petroleum, A Contribution from API Research Project 27, 114-146 (Mar., 1947).
5. Haniff, M.S. and Pearce, A.J: "Measuring Interfacial Tension in a Methane - Propane Gas-Condensate System Using a Laser Light Scattering Technique", SPE Res.Eng. 589-594 (Nov., 1990).
6. Dorshow, R.B: "The Simultaneous Measurement of Interfacial Tension and Oil Viscosity at Reservoir Conditions for Prudhoe Bay Fluids by Surface Laser Light Scattering Spectroscopy", SPE 22633, Proc. of 66th Ann. Conf. (Oct., 1991).
7. Danesh, A., Todd, A.C., Somerville, J. and Dandekar, A: "Direct Measurement of Interfacial Tension, Density, Volume, and Compositions of Gas-Condensate System", Trans. IChemE, 68, Part A, 325-330 (July, 1990).
8. Cahn, J.W: "Critical Point Wetting", The J. Chem. Physics, 66, No. 8, 3667-3672, (April, 1977).
9. MacLeod, D.B: "On a Relation Between Surface Tension, Density", Trans. Faraday Soc., 19, 38-43 (1923).

10. Mayer, S.W: "A Molecular Parameter Relationship between Surface Tension and Liquid Compressibility", *J. Phys. Chem.*, 67, 2160-2164 (1963).
11. Sivaraman, A., Ziga, J. and Kobayashi, R: "Correlation for Prediction of Interfacial Tensions of Pure Alkane, Napthenic and Aromatic Compounds between their Freezing and Critical Points", *J. Fluid Phase Equilibria*, 18, 225-235 (1984).
12. Carey, B.S., Scriven, L.E. and Davis, H.T: "Semiempirical Theory of Surface Tension of Binary Systems", *AIChE*, 26, No. 5, 705-711 (Sept., 1980).
13. Carey, B.S., Scriven, L.E. and Davis, H.T: "Semiempirical Theory of Surface Tension of Binary Systems", *AIChE*, 26, No. 5, 705-711 (Sept., 1980).
14. Sugden, S: "The Parachors and Valency (Routledge, 1930); A List of Parachors", *Brit. Assoc. Report* (1932).
15. Ali, J.K: "Predictions of Parachors and Petroleum Cuts and Pseudocomponents", *J. Fluid Phase Equilibria*, 95, 383-398 (1994).
16. Schechter, D.S. and Guo, B: "Parachors Based on Modern Physics and Their uses in IFT Prediction of Reservoir Fluids", *SPE 30785 Proc. of Ann. Conf.*, Dallas, USA (Oct., 1995).
17. Baker, O. and Swerdloff, W: "Calculation of Surface Tensions, 3: Calculation of Surface Tension Parachor Values", *Oil and Gas Journal*, 53, 87 (1955).
18. Fanchi, J.R: "Calculation of Parachors for Compositional Simulation, An Update", *SPE RES.ENG.*, 433-436 (Aug., 1990).
19. Weinaug, C.F. and Katz, D.L: "Surface Tension of Methane - Propane Mixtures", *I & EC*, 239-246 (1943).
20. Hugill, J.A. and Welsenens, Van, A.J: "Surface Tension: A Simple Correlation for Natural Gas + Condensate Systems", *J. Fluid Phase Equilibria*, 29, 383-390 (1986).
21. Ahmed, T: "Hydrocarbon Phase Behaviour", Gulf Publishing Company (1989).
22. Firoozabadi, A., Katz, D.L., Soroosh, H. and Sajjadian, V.A: "Surface Tension of Reservoir Crude Oil/Gas Systems Recognising the Asphalt in the Heavy Fraction", *SPE Res. Eng.*, 265-272 (Feb., 1988).
23. Brock, J.R. and Bird, R.B: "Surface Tension and the Principle of Corresponding States", *AIChE*, 1, 174-177 (1955).
24. Guggenheim, E.A: "Thermodynamics", 3rd Ed., North-Holland Pub. Co., Amsterdam (1957).
25. Lee, S.T. and Chien, M.C.H: "A New Multicomponent Surface Tension Correlation Based on Scaling Theory", *SPE/DOE 12643, EOR Symposium*, Tulsa (1984).
26. Fisher, M.E. and Scesney, P.E: "Visibility of Critical Exponent Renormalization", *Physics Review A*, 2, 825-835 (1970).
27. Hough, E.W. and Stegemeier, G.L: "Correlation of Surface and Interfacial Tension of Light Hydrocarbons in the Critical Region", *SPE J.*, 259-263 (Dec., 1961).

28. Huygens, R.J.M., Ronde, H. and Hagoort, J: "Interfacial Tension of Nitrogen and Volatile Oil Systems", SPE 26643, Proc. of 68th Ann. Conf. (Oct., 1993).
29. Danesh, A., Dandekar, A., Todd, A.C. and Sarkar, R: "A Modified Scaling Law and Parachor Method Approach for Improved Prediction of Interfacial Tension of Gas-Condensate Systems", SPE 22710, Proc. of 66th Ann. Conf. (Oct., 1991).
30. Dandekar, A: "Interfacial Tension and Viscosity of Reservoir Fluids", PhD Thesis, Heriot-Watt University, Edinburgh, Scotland (1994).
31. Hough, E.W., Rzasa, M.S. and Wood, B.B: "Interfacial Tension at Reservoir Pressures and Temperatures, Apparatus and the Water-Methane System", Trans. AIME, 192, 57-60 (1951).
32. Michaelis, A.S. and Hauser, E.A: "Interfacial Tension at Elevated Pressure and Temperatures II", J. Phys. Chem., 55, 408-421 (1951).
33. Hassan, M.E., Nielson, R.F., Calhoun, J.C: "Effect of Pressure and Temperature on Oil-Water Interfacial Tensions for a series of Hydrocarbons", Trans. AIME, 198, 299-306 (1953).
34. Jennings Jr., H.Y: "The Effect of Temperature and Pressure on Interfacial Tension of Benzene-Water and Normal Decane-Water", J. Colloid & Interface Sci., 24, 323-329 (1967).
35. Jennings, H.Y. and Newman, G.H: "The Effect of Temperature and Pressure on the Interfacial Tension of Water Against Methane-Normal Decane Mixtures", SPE J., 171-175 (June, 1971).
36. McCaffery, F.G: "Measurement of Interfacial Tensions and Contact Angles at High Temperature and Pressure", JCPT, 26-32 (July-Sept., 1972).
37. Firoozabadi, A. and Ramey Jr., H.J: "Surface Tension of Water-Hydrocarbon Systems at Reservoir Conditions", JCPT, 27, 41-48 (May-June, 1988).
38. Hakim, D.I., Steinberg, D. and Stiel, L.I: "Generalised Relationship for the Surface Tension of Polar Fluids", Ind. Eng. Chem. Fund., 10, 174-175 (1971).
39. Bartell, F.E. and Niederhauser, D.O: "Film-Forming Constituents of Crude Petroleum Oils, Fundamental Research on Occurance and Recovery of Petroleum, 1946-1947", API, Maryland (1949).
40. Aveyard, R. and Haydon, D.A: "Thermodynamic Properties of Aliphatic hydrocarbon-Water Interfaces", Trans. Faraday Soc., 61, 2255-2261 (1965).

## 8.5 EXERCISES

8.1. The gas-liquid interfacial tension of methane-normal butane mixture at 311 K and 12.07 MPa is measured by the pendant drop method. Calculate the interfacial tension when the droplet dimensions are  $d_e=0.228$  and  $d_s=0.325$  mm.

8.2. The vapour-liquid equilibrium data of a five-component gas condensate mixture at 353.1 K in a constant composition expansion test are given in the following tables. Compare the measured IFT values with those predicted by the original Weinaug-Katz method and its modifications Eq.(8.21) by Schechter-Guo and Eq.(8.20), and the Lee-Chien method.

## Gas condensate composition.

Component	Methane	Propane	n-Pentane	n-Decane	n-Hexadecane
Mole Fraction	0.8205	0.0895	0.0500	0.0199	0.0201

## Liquid phase properties and gas-liquid interfacial tension.

Pressure MPa	Methane	Propane	n-Pentane	n-Decane	n-Hexadecane	Density g/cm <sup>3</sup>	IFT mN/m
Mole Fraction							
30.43	0.6880	0.1073	0.0772	0.0501	0.0774	0.480	0.118
29.06	0.6640	0.1115	0.0827	0.0564	0.0854	0.497	0.229
27.68	0.6414	0.1133	0.0886	0.0634	0.0933	0.513	0.390
26.30	0.6187	0.1186	0.0940	0.0689	0.0998	0.524	0.536
24.92	0.6003	0.1208	0.1001	0.0743	0.1045	0.535	0.738

## Vapour phase properties.

Pressure MPa	Methane	Propane	n-Pentane	n-Decane	n-Hexadecane	Density g/cm <sup>3</sup>
Mole Fraction						
30.42	0.8362	0.0869	0.0465	0.0167	0.0137	0.298
29.04	0.8448	0.0863	0.0445	0.0145	0.0099	0.278
27.66	0.8512	0.0857	0.0431	0.0127	0.0073	0.261
26.29	0.8580	0.0844	0.0414	0.0108	0.0054	0.246
24.91	0.8625	0.0841	0.0398	0.0095	0.0041	0.231

8.3. The interfacial tension, composition and density of gas and condensate phases were measured during a constant volume depletion tests. The results at two pressures are as follows:

Pressure, MPa	34.47		20.68	
Component, Mole%	Vapour	Liquid	Vapour	Liquid
N <sub>2</sub>	0.65	0.41	0.65	0.26
CO <sub>2</sub>	2.42	1.72	2.59	1.39
C <sub>1</sub>	78.06	49.82	78.88	35.36
C <sub>2</sub>	6.71	6.12	6.90	5.43
C <sub>3</sub>	2.99	3.30	3.04	3.36
iC <sub>4</sub>	0.60	0.74	0.59	0.82
nC <sub>4</sub>	1.25	1.68	1.25	1.94
iC <sub>5</sub>	0.48	0.75	0.48	0.95
nC <sub>5</sub>	0.59	0.95	0.58	1.23
C <sub>6</sub>	0.73	1.48	0.84	2.09
C <sub>7</sub>	1.10	2.25	1.02	3.38
C <sub>8</sub>	1.01	2.53	0.95	4.03
C <sub>9</sub>	0.68	1.96	0.65	3.29
C <sub>10</sub>	0.47	1.51	0.35	2.68
C <sub>11</sub>	0.33	1.22	0.32	2.26
C <sub>12</sub>	0.25	1.17	0.22	2.19
C <sub>13</sub>	0.22	1.11	0.14	2.09
C <sub>14</sub>	0.26	1.21	0.16	2.27
C <sub>15</sub>	0.19	1.16	0.13	2.11
C <sub>16</sub>	0.12	1.01	0.06	1.63
C <sub>17</sub>	0.11	0.77	0.04	1.51
C <sub>18</sub>	0.10	0.87	0.03	1.47
C <sub>19</sub>	0.09	0.84	0.02	1.35
C <sub>20+</sub>	0.57	15.42	0.11	16.91
Molecular Weight	28.05	97.44	25.32	120.62
density, g/cm <sup>3</sup>	0.242	0.593	0.143	0.628
Measured IFT, mN/m	0.372		1.389	

Compare the measured IFT values with those predicted by the Weinaug-Katz method as modified by Schechter-Guo, and the Lee-Chien method. It has been suggested to improve the prediction by adjusting the parachor value of the plus fraction to match the experimental data. Find the optimised parachor value of the plus fraction.

8.4. Estimate the interfacial tension between the gas in Exercise 8.2 and water, at the gas hydrocarbon dew point of 31.98 MPa and 353.1 K, using the generalised water-hydrocarbon correlation. Compare the results with the value obtained by assuming the gas as pure methane.



## 9 APPLICATION IN RESERVOIR SIMULATION

Phase behaviour models are used extensively in petroleum industry. A model can be used to evaluate the consistency of measured PVT data, or to generate such data as input in black oil reservoir simulation. The models are also used in pipeline and wellbore multi-phase flow calculations. In the design and operation of surface facilities, phase behaviour models are employed to determine the properties and the amount of equilibrated gas and oil. The main application of phase behaviour models, based on determining the fugacity of components in both phases by EOS, is however in compositional reservoir simulation.

In a simulator, the reservoir is commonly divided into a number of grid-blocks, or cells. The fluids within each cell are considered to be in equilibrium at the cell pressure and temperature. The change of reservoir conditions with time is investigated by determining average values in each cell during successive small time steps. The equilibrium condition over a time step is determined by flash calculations in each grid block. As reservoir calculations are generally iterative, more than one equilibrium flash calculation per each grid-block at any time step is required. For a large reservoir, the total number of equilibrium flashes may exceed many millions, consuming a large computational time and making the simulation very expensive. As the number of equations in conventional flash calculation increases with the number of components, see Section 5.1, the number of components characterising the fluid is commonly reduced by grouping to reduce the computational time.

An important consideration in applying a phase behaviour model to reservoir studies, is wide ranges of composition and pressure which are to be modelled by EOS. In the integrated modelling approach, where the phase behaviour model is to cover reservoir, wellbore, pipeline, separators, etc., in one simulation, the task becomes even more stringent and the model often fails to provide satisfactory results. The common approach is to calibrate, or tune the model, against experimental data. The selection of required data and parameters of EOS for adjustment in the tuning process and the use of relevant methods constitute a major task for reservoir engineer.

## 9.1 GROUPING

The concept of grouping has long been employed in fluid description, but this is done mostly due to limitations in the compositional analysis. The most conventional method is to describe the hydrocarbon mixture with discrete components to normal pentane and hexanes each as a single carbon group and lump all the heavy fractions as the heptanes plus ( $C_{7+}$ ). This is not an efficient method of describing a reservoir fluid, particularly in compositional simulation studies, where it is desirable to minimise the number of components while still retaining the reliability of predicted values by phase behaviour models.

It is **expected** that the fluid description requirement varies with the complexity of the process which is to be modelled. The phase behaviour of a reservoir fluid under pressure depletion may only be modelled by two components [1], whereas more than ten components may be required for miscibility studies.

The key points in component grouping are:

1. The number of groups required and the distribution of components within each group.
2. The estimation of group properties required in phase behaviour modelling.
3. The retrieval of fluid description in terms of the original components when needed.

### Group Selection

Many investigators [1-13] have given recommendations on selecting the number of pseudo components (groups). In general, 4-10 pseudo-components are considered adequate for simulation purposes.

A simple approach is to add nitrogen and carbon dioxide, at low concentrations, to methane and ethane, respectively, and to combine  $iC_4$  with  $nC_4$  and  $iC_5$  with  $nC_5$ . The  $C_{7+}$  fraction is also characterised by a number of pseudo-components and included.

Whitson [5] proposed representing the  $C_{7+}$  fraction of a mixture by  $N_p$  pseudo-components calculated as follows,

$$N_p = \text{Integer}[1 + 3.3 \log(N - 7)] \quad (9.1)$$

where  $N$  is the last carbon group number.

The boundary between the consecutive groups are based on the molecular weights  $M_k$ , given by:

$$M_k = M_7 \left\{ \exp \left[ \left( \frac{1}{N_p} \right) \ln \left( \frac{M_N}{M_7} \right) \right] \right\}^k \quad k = 1, 2, \dots, N_p \quad (9.2)$$

The components of the original fluid with molecular weights falling within  $M_{k-1}$  to  $M_k$  are included in group  $k$ .  $M_N$  is the molecular weight of last carbon group.



*Example 9.1.*

Describe the  $C_{7+}$  fraction of the oil in Example 6.3, identified to  $C_{45}$ , by a number of pseudo-components using the Whitson method.

*Solution:*

The last carbon number describing the  $C_{7+}$  is 45. Hence the number of pseudo-components for the  $C_{7+}$  fraction is calculated from Eq.(9.1), as

$$N_p = \text{Integer} [1 + 3.3 \log(45-7)] = 6$$

The components comprising each pseudo-component are identified by calculating the molecular weight boundaries of each pseudo-component. Using Eq.(9.2), with the generalised molecular weight of single carbon number groups, we obtain the upper molecular weight of first pseudo-component,

$$M_1 = 96 \{ \exp[(1/6) \ln(539/96)] \}^1 = 128$$

Hence,  $C_7$ ,  $C_8$  and  $C_9$ , with the last having a molecular weight of 121, are assigned to the first pseudo-component (group). Similarly, for other groups we obtain,

Group No, k	Upper M boundary, $M_k$	Components in Group
1	128	$C_7$ - $C_9$
2	171	$C_{10}$ - $C_{12}$
3	227	$C_{13}$ - $C_{16}$
4	303	$C_{17}$ - $C_{22}$
5	404	$C_{23}$ - $C_{31}$
6	539	$C_{32}$ - $C_{45}$

The application of continuous description to select 3-5 pseudo-components (multi carbon groups), at quadrature points, discussed in Section 6.3, is the recommended method of describing the heavy end. The selected pseudo-components will be as effective as choosing twice as many, selected randomly or at equal intervals [14].

Selecting 4 pseudo-components by the quadrature method to describe the  $C_{7+}$  fraction and following the simple approach of adding isomers to normal hydrocarbons, described above, will reduce the total number of components describing a fluid to around ten. The number of groups, however, can further be reduced particularly by grouping the light fractions.

Li et al. [11] proposed to group components on the basis of their volatility, using equilibrium ratios obtained by flashing the fluid at reservoir temperature and the average operating pressure. They presented different correlations for grouping of light and heavy components. Pedersen et al. [15] suggested to group the components based on mass, that is, each group containing approximately the same mass fraction. A number of fluids were described by 40, 20, 10, 6 and 3 pseudo-components and their saturation points were predicted using EOS. They concluded that a 6-component representation was sufficient for an accurate prediction of the saturation point. Cotterman and Prausnitz [14] used the criterion of equal mole fraction to select groups.

A representative fluid description is expected when the groups are formed by due consideration to the volatility and the concentration of components in the mixture. Newley and Merrill [12], suggested a method of grouping based on minimising the difference,  $\Delta$ , between the apparent

equilibrium ratio ( $K$ -value) of the pseudo-component and those of the original components comprising it,

$$\Delta = \sum_k \sum_{i(k)} \frac{(K_i - K_k^*)^2}{K_i^2} \quad (9.3)$$

where  $K_k^*$  is the apparent  $K$ -value of the pseudo-component  $k$ , defined as,

$$K_k^* = \frac{\sum_{i(k)} y_i}{\sum_{i(k)} x_i} \quad (9.4)$$

$y_i$  and  $x_i$  are the mole fractions of component  $i$  in the vapour and liquid phases at the saturation pressure, respectively, and  $i(k)$  denotes the components assigned to the pseudo-component  $k$ .

In the above proposed method, the mixture saturation pressure and the compositions of equilibrated phases at the saturation point are calculated by the phase behaviour model, using the full compositional description of the fluid. The components are then ordered according to their  $K$ -values and grouped initially by the equal mole criterion. The grouping is then adjusted by moving components within the adjacent groups to minimise the objective function  $\Delta$ .

The volatility of fluid components at high pressure conditions, depends on the mixture composition at a given temperature and pressure. Although the equilibrium ratio varies with the composition, the order of relative volatility of components remains the same. Hence, some component properties, such as the boiling point, critical temperature, molecular weight, or their combinations can be used to describe the relative volatility of components in a mixture. An example of such a trend was shown in Figure 3.8.

A grouping method based on the concentration and the molecular weight, representing the volatility, of components has been proposed [13]. The original components are arranged by the order of their normal boiling point temperatures and grouped together in an ascending order to form  $N_p$  groups so that the values of  $\sum z_i \ln M_i$  for all the groups become nearly equal. It can be expressed mathematically as,

$$\left[ \sum_{i(k)}^{\ell} z_i \ln M_i - (k/N_p) \sum_i^N z_i \ln M_i \right] \leq 0 \quad k=1,2,\dots,N_p \quad (9.5)$$

$$\left[ \sum_{i(k)}^{\ell+1} z_i \ln M_i - (k/N_p) \sum_i^N z_i \ln M_i \right] \geq 0 \quad k=1,2,\dots,N_p \quad (9.6)$$

where  $z_i$  and  $M_i$  are, respectively, the molar concentration and the molecular weight of component  $i$  in the mixture, fully described by  $N$  components. The last component in the group  $k$ , would be either,  $\ell$  or  $\ell+1$ , depending on which inequality, (9.5) or (9.6), is smaller, respectively. Methane, due to its high volatility in comparison with other hydrocarbons, should not be grouped with others except nitrogen at low concentrations.

A number of 25-component oil mixtures, Table 9.1, were subjected to single and multiple contact tests, simulating gas injection processes experimentally using different gases [13]. The fluids were described by various numbers of pseudo-components ranging from 2 to 25 groups

using different grouping schemes. Several EOS were used to simulate the test results. The average absolute deviations of predicted results by different methods are shown in Figures 9.1 and 9.2. Note that the reduction of the number of groups down to an optimum value did not impair the predicted results. Minor improvements by grouping observed at some conditions are due to the cancellation of errors. It appears that describing the oil by 4-6 groups is sufficient to model gas addition processes. Note that lowering the number of groups below the optimum value results in a drastic impairment of the results. The above conclusions were independent of the employed EOS and grouping method [13].

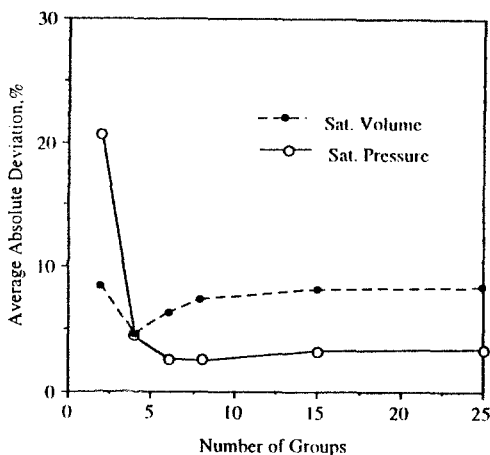


Figure 9.1. Effect of the number of groups describing fluid on predicted results by the Valderrama modification of Patel-Teja EOS, using grouping method of Eq.(9.5-6).

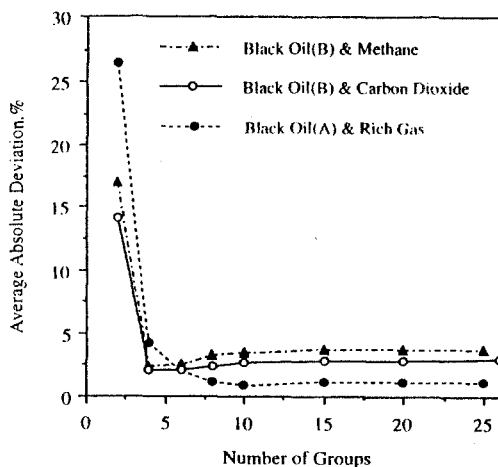


Figure 9.2. Effect of the number of groups describing fluid on predicted results by the Peng-Robinson EOS, using equal mole fraction grouping.

A comparative study [13] of various grouping methods, using 4 or 6 groups, indicated a preference for the method described by Eqs.(9.5-6) to that by equal mole fraction, with those of equal mass fraction and Li et al. [11] as the least reliable methods.

### Example 9.2

Describe the oil reported in Table 9.4 by three pseudo-components for a methane gas injection study at 373 K, using the methods of equal mass, equal mole, equal  $z_i \ln M_i$  and Newley-Merrill.

Table 9.1.  
Compositions and properties of model fluids at 373 K.

Component mole%	Black Oil(A)	Black Oil(B)	Volatile Oil(A)	Volatile Oil(B)	Rich Gas
C <sub>1</sub>	46.80	36.14	74.17	73.33	69.82
C <sub>2</sub>	8.77	12.17	5.32	5.35	13.09
C <sub>3</sub>	7.44	8.05	4.67	4.71	11.10
nC <sub>4</sub>	4.01	5.81	2.58	2.62	5.99
nC <sub>5</sub>	2.56	4.79	0.97	1.00	
nC <sub>6</sub>	1.77	3.81	0.69	0.71	
Met Cycl Pent	2.25	1.43	0.88	0.91	
Cycl Hex	2.20	1.45	0.86	0.89	
nC <sub>7</sub>	0.46	0.36	0.18	0.19	
Met Cycl Hex	2.36	2.49	0.94	0.98	
Toluene	0.72	0.76	0.28	0.30	
nC <sub>8</sub>	1.02	1.08	0.41	0.42	
o-Xylene	1.79	-	0.72	0.75	
nC <sub>9</sub>	1.66	3.16	0.66	0.70	
nC <sub>10</sub>	2.73	2.29	1.11	1.17	
nC <sub>11</sub>	2.37	1.91	0.96	1.02	
nC <sub>12</sub>	2.04	1.74	0.83	0.89	
nC <sub>13</sub>	1.77	1.47	0.73	0.78	
nC <sub>14</sub>	1.53	1.32	0.63	0.68	
nC <sub>15</sub>	1.34	1.22	0.56	0.60	
nC <sub>16</sub>	1.15	0.95	0.48	0.52	
nC <sub>17</sub>	0.99	0.85	0.42	0.45	
nC <sub>18</sub>	0.87	0.67	0.36	0.39	
nC <sub>19</sub>	0.75	0.57	0.32	0.34	
nC <sub>20</sub>	0.65	0.48	0.27	0.30	
nC <sub>24</sub>	-	5.03	-	-	
Sat. Pres., MPa	20.28	15.43	32.78	32.70	
Sat. Dens., g/cm <sup>3</sup>	0.541	0.583	0.389	0.398	
Pressure, MPa	Density, g/cm <sup>3</sup>				
20.79	0.542	0.593			0.192
24.23	0.550	0.601			0.217
27.68	0.557				0.237
31.13	0.564				0.255
34.58	0.569	0.613	0.390	0.399	0.271

### Solution:

Methane is selected as Group-I, particularly as the grouping is for a methane injection study and the rest is grouped into two pseudo-components.

Equal mole method:

The total mole% of Group-II and Group-III is equal to 52.802%, with an objective value for each  $=52.802/2=26.401$ . Adding components from  $C_2$  downwards, Group-I will consist of  $C_2-C_8$  with 23.091 mole% and the rest,  $C_4-nC_{20}$  with 29.711mole%, in Group-III.

Equal weight (mass) method:

The weight of each component is calculated as  $x_i M_i$ , with the total weight of  $C_2-nC_{20}$  for 100 kgmoles of oil  $\Sigma x_i M_i = 4692.2$  kg. The objective weight of each group is  $=4692.2/2=2346.1$ . Adding components from  $C_2$  downwards, Group-I will consist of  $C_2-nC_8$  with a weight of 2219.1 and the rest,  $nC_{10}-nC_{20}$  with a weight of 2473.1, in Group-III.

Equal  $x_i \ln M_i$  method:

The value for each component is calculated, with the total value for  $C_2-nC_{20}$ ,  $\Sigma x_i \ln M_i = 223.53$ . The objective value of each group  $=223.53/2=111.77$ . Adding components from  $C_2$  downwards, Group-I will consist of  $C_2-nC_4$  with  $\Sigma x_i \ln M_i = 111.66$  and the rest,  $nC_5-nC_{20}$  with a value of 111.87, in Group-III.

Newley-Merrill method:

The composition of vapour at the bubble point must be calculated using a tuned phase behaviour model, as suggested by the authors. In this example, the measured composition of the vapour, as reported in Table 9.4 is used instead.

The components of  $C_2-nC_{20}$  are initially grouped in two by equal mole and  $K^*$  and  $\Delta$  are calculated using Eqs.(9.4) and (9.3), respectively. The first component of Group-III is taken into Group-II and the corresponding value of  $\Delta$  is re-calculated for the new grouping, until the lowest value of  $\Delta$  is achieved. The calculation results for the first and the last few iterations are shown in the following Table.

Comp., mol %	$x_i$	$y_i$	$K_i$	G-II, $\Delta_i$	G-III, $\Delta_i$	G-II, $\Delta_i$	G-III, $\Delta_i$	G-II, $\Delta_i$	G-III, $\Delta_i$	G-II, $\Delta_i$	G-III, $\Delta_i$
$K^*$				1.89574	0.22018	0.74414	0.12960	0.73600	0.12357	0.72016	0.11514
$C_2$	11.618	11.767	1.01282	0.75992		0.07038		0.07471		0.08350	
$C_3$	11.473	9.041	0.78802	1.97594		0.00310		0.00436		0.00742	
$nC_4$	7.059	4.341	0.61496		0.41211	0.04412		0.03874		0.02927	
$nC_5$	1.295	0.634	0.48958		0.30278	0.27036		0.25335		0.22184	
$nC_6$	0.982	0.389	0.39613		0.19728	0.77178		0.73610		0.66912	
Met Cycl Pent	1.297	0.461	0.35544		0.14480	1.19593		1.14637		1.05297	
Cycl Hex	1.301	0.422	0.32437		0.10316	1.67476		1.61043		1.48893	
$nC_7$	0.279	0.090	0.32258		0.10076	1.70778		1.64246		1.51907	
Met Cycl Hex	1.463	0.423	0.28913		0.05687	2.47649		2.38868		2.22241	
Toluene	0.448	0.125	0.27902		0.04446	2.77883		2.68242		2.49976	
$nC_8$	0.648	0.174	0.26852		0.03240		0.26767	3.03090		2.82908	
o-Xylene	1.199	0.264	0.22018		0.00000		0.16927		0.19254	5.15626	
$nC_9$	1.112	0.247	0.22212		0.00008		0.17352		0.19686		0.23198
$nC_{10}$	1.923	0.353	0.18357		0.03979		0.08645		0.10683		0.13896
$nC_{11}$	1.733	0.261	0.15061		0.21343		0.01946		0.03223		0.05546
$nC_{12}$	1.545	0.192	0.12427		0.59566		0.00183		0.00003		0.00540
$nC_{13}$	1.382	0.144	0.10420		1.23910		0.05942		0.03457		0.01103
$nC_{14}$	1.219	0.119	0.09762		1.57626		0.10728		0.07065		0.03220
$nC_{15}$	1.089	0.082	0.07530		3.70233		0.51997		0.41096		0.27994
$nC_{16}$	0.956	0.061	0.06381		6.00615		1.06303		0.87721		0.64716
$nC_{17}$	0.833	0.045	0.05402		9.46080		1.95706		1.65741		1.27992
$nC_{18}$	0.735	0.034	0.04626		14.1364		3.24556		2.79316		2.21718
$nC_{19}$	0.646	0.025	0.03870		21.9918		5.51658		4.80937		3.90131
$nC_{20}$	0.567	0.019	0.03351		31.0331		8.22194		7.22300		5.93394
Total $\Delta$					94.12547		32.40257		32.01332		32.51408

The lowest value of  $\Delta$  is achieved when components  $C_7$ - $nC_8$  are included in Group-II, with Xylene- $nC_{20}$  in Group-III.

### Group Properties

Several methods have been proposed to calculate the properties of pseudo-components required in EOS[4,5,10,12,15].

The most common method is molar averaging,

$$\theta_k = \sum_{i(k)} x_i \theta_i / x_k \quad (9.7)$$

where  $x_k$  is the mole fraction of group  $k$  in the mixture,

$$x_k = \sum_{i(k)} x_i \quad (9.8)$$

$\theta$  represents the component property, such as the critical properties ( $T_c$ ,  $P_c$ ,  $v_c$ ,  $Z_c$ ), acentric factor, or the molecular weight.

Pedersen et al. [15] suggested using the mass fraction instead of the mole fraction in Eq.(9.7), whereas Wu and Batycky [10] proposed to calculate group properties by a combination of mass and mole concentrations.

The Lee-Kesler averaging method for critical properties [16,17] has also been used in the industry,

$$v_{ck} = \frac{1}{8} \sum_{i(k)} \sum_{j(k)} x_i x_j \left( v_{ci}^{\frac{1}{3}} + v_{cj}^{\frac{1}{3}} \right)^3 \quad (9.9)$$

$$T_{ck} = \frac{1}{8 v_{ck}} \sum_{i(k)} \sum_{j(k)} x_i x_j \left( T_{ci} T_{cj} \right)^{\frac{1}{2}} \left( v_{ci}^{\frac{1}{3}} + v_{cj}^{\frac{1}{3}} \right)^3 \quad (9.10)$$

$$Z_{ck} = 0.2905 - 0.085 \omega_k \quad (9.11)$$

$$P_{ck} = Z_{ck} R T_{ck} / v_{ck} \quad (9.12)$$

The molecular weight and the acentric factor are calculated by molar averaging in the above method.

The calculated properties of pseudo-components are not directly incorporated in most EOS, but are used to calculate the parameters of EOS. Hence, applying mixing rules directly to the parameters of original components to calculate the parameters of pseudo-components seems a reasonable approach [13],

$$a_k = \sum_{i(k)} \sum_{j(k)} x_i x_j \left( 1 - k_{ij} \right) \left( a_i a_j \right)^{\frac{1}{2}} / x_k^2 \quad (9.13)$$

$$b_k = \frac{1}{8} \sum_{i(k)} \sum_{j(k)} x_i x_j \left( b_i^{\frac{1}{3}} + b_j^{\frac{1}{3}} \right)^3 / x_k^2 \quad (9.14)$$

$$c_k = \frac{1}{8} \sum_{i(k)} \sum_{j(k)} x_i x_j \left( c_i^{\frac{1}{3}} + c_j^{\frac{1}{3}} \right)^3 / x_k^2 \quad (9.15)$$

where  $a_k$ ,  $b_k$  and  $c_k$ , are the parameters of EOS for the pseudo-component  $k$ .

The binary interaction parameters between the pseudo-components of  $k$  and  $q$ , are determined from,

$$k_{kq} = \sum_{i(k)} \sum_{j(q)} x_i x_j k_{ij} / x_k x_q \quad k \neq q \quad (9.16)$$

A comparison of the above methods did not indicate a clear preference for any of them [13]. The results depended on the selected EOS and the number of pseudo-components used to describe the fluid, probably due to the cancellation of errors, as improvements relative to those predicted using the full composition were also observed at some conditions.

Grouping is commonly conducted according to the concentration of components in the feed, often the original reservoir fluid. This approach is justified in predicting the single phase volumetric behaviour and to some extent the saturation pressure. It, however, deteriorates in flash calculations where the distribution of components in each pseudo-component will be different in the two phases. This can cause problems, particularly for gas condensate fluids where the retrograde condensate phase is over predicted, as the properties of the heavy pseudo components are those of the original gas and not the formed liquid.

Newley and Merrill [12] suggested to calculate the critical properties and the acentric factor of pseudo-components using a weighting factor, based on splitting of the original fluid at its saturation point,

$$\theta_k = \sum_{i(k)} \varphi_i \theta_i / \sum_{i(k)} \varphi_i \quad (9.17)$$

where the weighting factor,  $\varphi_i$ , is defined as,

$$\varphi_i = (x_i^s y_i^s)^{1/2} = z_i (K_i^s)^{-1/2} \quad (9.18)$$

where,  $x_i^s$ ,  $y_i^s$ , are the predicted mole fractions of component  $i$ , using the full description of the fluid, in the liquid and vapour at the saturation point, respectively, with the equilibrium ratio of  $K_i^s$  and  $z_i$  is the mole fraction of component  $i$  in the feed. The authors also suggested using the above weighting factor, instead of the mole fraction, in Eq.(9.16) to calculate the binary interaction parameters between the pseudo-components.

Newley and Merrill [12] compared their proposed grouping method with equal mole fraction, equal mass fraction and that of Whitson. They applied Eq.(9.17) to their own method and the molar averaging to others to estimate the properties of groups. The study for a lean gas condensate demonstrated the superiority of their method.

**Example 9.3**

Calculate the critical properties and acentric factor of Group-II in Example 9.2 comprised of C<sub>7</sub>, C<sub>8</sub> and nC<sub>4</sub>

*Solution:*

The component properties are read from Table A.1 in Appendix A and molar averaged, using Eq.(9.7), as shown in the following table.

Component	mole%	$x_i$	$M_i x_i$	$T_{ci} x_i$ , K	$P_{ci} x_i$ , MPa	$Z_{ci} x_i$	$w_i x_i$
C2	11.618	0.38534	11.587	117.65	18.53	0.108	0.0383
C3	11.473	0.38053	16.780	140.73	15.95	0.105	0.0580
nC4	7.059	0.23413	13.608	99.53	8.77	0.064	0.0469
Group-II	30.15	1.00000	41.975	357.92	43.25	0.277	0.1432

The method of Newley-Merrill is the same as the above, but with the weighting factors calculated from Eq.(9.18), instead of mole fractions, as follows.

Component	$K_i$	$(K_i)^{0.5} x_i$	$\phi_i$	$T_{ci} \phi_i$ , K	$P_{ci} \phi_i$ , MPa	$Z_{ci} \phi_i$	$w_i \phi_i$
C2	1.01282	0.38289	0.34491	105.31	16.58	0.096	0.0343
C3	0.78802	0.42867	0.38615	142.81	16.19	0.107	0.0588
nC4	0.61496	0.29856	0.26894	114.33	10.07	0.074	0.0538
Group-II		1.11012	1.00000	362.45	42.85	0.276	0.1470

**Composition Retrieval**

In some processes, such as gas-oil displacement and gas cycling, where the relative concentration of fluid components within each group varies significantly, the use of group properties generated from the original composition may be inadequate for an accurate prediction of the phase behaviour.

Table 9.2 shows the variation of concentration ratio of some components of a North Sea oil, when contacted with ten volumes of an injection gas in a backward multiple contact test. For example, consider a group formed by the three consecutive single carbon numbers of 7, 8 and 9. The properties of the group using the original compositions will be equally weighted for the properties of C<sub>7</sub> and C<sub>9</sub>. Clearly such properties will not be representative of that group, after contacting the gas, where the concentration of C<sub>7</sub> in the group is reduced to 42% of C<sub>9</sub>.

Table 9.2.

Molar concentration ratios of oil components before and after contacting gas.

Mole ratio	C <sub>7</sub> /C <sub>9</sub>	C <sub>10</sub> /C <sub>12</sub>	C <sub>13</sub> /C <sub>15</sub>
Original oil	1.00	1.76	1.49
After contact	0.42	1.36	1.06

The above problem can be alleviated by retrieving the fluid description in terms of the original components at some stages of cell to cell calculations in reservoir simulation and forming new groups accordingly.

Figure 3.7 shows the equilibrium ratios measured in a multiple backward contact gas injection test where Black Oil (B), Table 9.1, was vaporised repeatedly by methane at 34.58 MPa and 373 K. The variation of equilibrium ratio for each component is only due to changes in the mixture composition. Note that the log of equilibrium ratio can be expressed by a linear function as,



$$\ln K_i = c_0 + c_1(1 + \omega_i) \left( 1 - \frac{1}{T_{ri}} \right) \quad (9.19)$$

where  $K_i$ ,  $\omega$  and  $T_r$  are the equilibrium ratio, acentric factor and the reduced temperature respectively, and  $c_0$  and  $c_1$  are constants. The above function, is a modified form of the Wilson equation [18], Eq.(3.66).

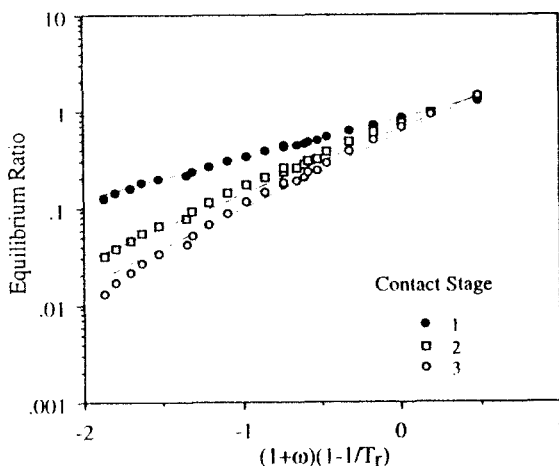


Figure 3.7. Equilibrium ratios in a test simulating oil vaporisation by methane at 34.58 MPa and 373K.

An inverse grouping method, to retrieve the fluid description using Eq.(9.19) has been developed [13]. In this procedure, equilibrium ratios of the groups, obtained by flash calculations, are used to determine the constants of the above equation by the least square method. The equation is then employed to calculate the equilibrium ratios of the original components and retrieving the full description of both phases by material balance calculations, Eqs.(5.4-5).

If further flash calculations are required, the mixture detailed compositional description can be used to form new groups. Clearly the above method would be practical only for rapid grouping methods, such as those described by Eq.(9.2) and Eqs.(9.5-6). Otherwise the retrieval and re-grouping can become excessively time consuming, beating the purpose of the exercise.

The simulated results of hydrocarbon recovery by gas cycling at two different pressures are shown in Figure 9.3. Note that the composition retrieval improves the results even for systems described by a large number of groups at the higher pressure where phase compositions changes markedly. The effect of compositional retrieval at the lower pressure becomes only significant when less than six groups are used to describe the fluid.

The computational (CPU) time for simulating the above process can be reduced by 75% due to grouping as shown in Figure 9.4. It also exhibits that the full composition retrieval and regrouping do not significantly increase the computational time.

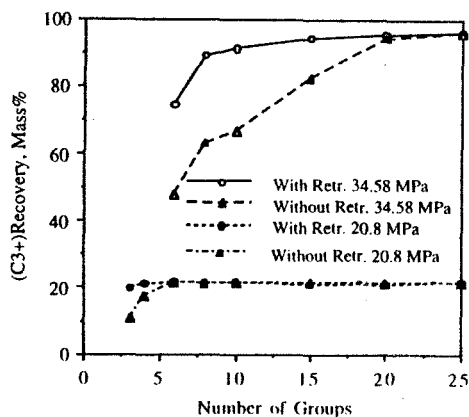


Figure 9.3. Effect of composition retrieval on predicted recovery of  $C_{3+}$  from Volatile Oil A by methane cycling at 373 K.

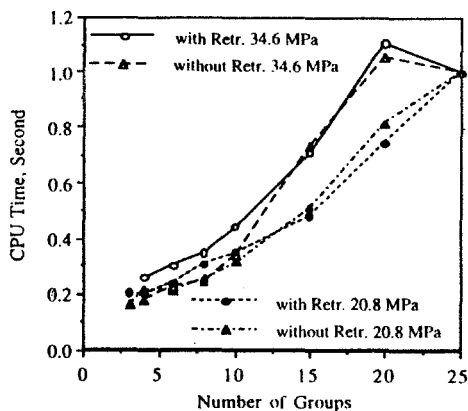


Figure 9.4. Computational time of simulating methane cycling.

#### Example 9.4.

The oil reported in Example 9.2 was flashed at the reservoir temperature of 373.0 K. The oil was described by methane and two component groups, using the equal  $\ln M$  method and molar averaged properties, as given in Example 9.3. The predicted results by a phase behaviour model, using the above fluid description, are given in the following table. Calculate the composition of equilibrated phases in terms of the original components.

Group	Feed Comp.	Oil Comp.	Gas Comp.	Equilibrium
	mole fraction			Ratio
I (methane)	0.47198	0.28419	0.71332	2.5100
II ( $C_2$ - $nC_4$ )	0.30150	0.32964	0.26533	0.8049
III ( $nC_5$ - $nC_{20}$ )	0.22652	0.38616	0.02135	0.0553

Liquid mole fraction=0.56239

*Solution:*

The critical temperature and acentric factor of the three groups are calculated by molar averaging and the coefficients of Eq.(9.19) are determined.

Group	$T_c$ , K	$T_r$	acentric factor	$(1+\omega)(1-1/T_r)$	$\ln k$
I (methane)	190.56	1.95739	0.0115	0.49474	0.920282
II ( $C_2$ - $nC_4$ )	357.92	1.04214	0.1432	0.04623	-0.218045
III ( $nC_5$ - $nC_{20}$ )	626.67	0.59521	0.4861	-1.01066	-2.894982

$$\ln K_i = -0.33416 + 2.5341 \left( 1 + \omega_i \right) \left( 1 - \frac{1}{T_r} \right)$$

Substituting the acentric factor and reduced temperature of each component in the above equation results in the equilibrium ratios of the original components.

The component balance for each component results in,

$$z_i / x_i = n^L + (1 - n^L) K_i$$

Substituting  $n^L = 0.56239$  in the above,

$$z_i / x_i = 0.56239 + 0.43761 K_i$$

the composition of equilibrated phases are calculated as shown in the following table.

Component, mole %	$(1+\omega)(1-1/T_r)$	$K_i$	$x_i$	$y_i$
$C_1$	0.49474	2.50819	0.28657	0.70604
$C_2$	0.19950	1.18696	0.10824	0.12620
$C_3$	0.00979	0.73393	0.13087	0.09435
$nC_4$	-0.16771	0.46807	0.09273	0.04264
$nC_5$	-0.32445	0.31463	0.01864	0.00576
$nC_6$	-0.46958	0.21781	0.01505	0.00322
Met Cycl Pent	-0.52701	0.18831	0.02027	0.00375
Cycl Hex	-0.58654	0.16194	0.02071	0.00329
$nC_7$	-0.60492	0.15457	0.00446	0.00068
Met Cycl Hex	-0.65952	0.13460	0.02373	0.00314
Toluene	-0.74148	0.10936	0.00740	0.00079
$nC_8$	-0.73432	0.11136	0.01069	0.00117
o-Xylene	-0.90576	0.07212	0.02035	0.00144
$nC_9$	-0.85759	0.08148	0.01874	0.00150
$nC_{10}$	-0.97900	0.05990	0.03293	0.00194
$nC_{11}$	-1.09131	0.04506	0.03001	0.00133
$nC_{12}$	-1.20449	0.03383	0.02698	0.00090
$nC_{13}$	-1.30953	0.02592	0.02428	0.00062
$nC_{14}$	-1.40954	0.02012	0.02151	0.00043
$nC_{15}$	-1.51451	0.01542	0.01929	0.00029
$nC_{16}$	-1.61150	0.01206	0.01697	0.00020
$nC_{17}$	-1.72225	0.00911	0.01482	0.00013
$nC_{18}$	-1.81626	0.00718	0.01310	0.00009
$nC_{19}$	-1.91179	0.00563	0.01153	0.00006
$nC_{20}$	-2.01937	0.00429	0.01013	0.00004

## 9.2 COMPARISON OF EOS

The capabilities of the equations presented in Section 4.2 and many other van der Waals type equations, have been evaluated by several investigators. The studies have resulted mainly in a general conclusion that none of them can be singled out as the most superior equation to best predict all properties at all conditions. A number of comparative studies [19-22] have, however, shown that certain equations exhibit a higher overall accuracy.

The accuracy of predicted results by any EOS depends not only on the reliability of that equation, but also on the mixing rules applied to its parameters, fluid characterisation, estimated critical properties of the fluid components, etc. Therefore, proper consideration of all pertinent factors when evaluating EOS is essential. For hydrocarbon fluids, the random mixing rules, described in Section 4.3, are considered adequate. These mixing rules have been used in almost all the comparative studies of EOS.

Any phase behaviour model is bound to carry errors introduced by inaccurate input data, particularly the properties of single and multiple carbon groups, into the predicted results. The problem can be alleviated, in comparative studies of EOS, by using data on model fluids, instead of real reservoir fluids. The use of many components with realistic concentrations, such as replacing each single carbon group with its pure equivalent in the model fluid, can produce reliable data with conclusions applicable to real fluids.

The performance of a number of leading EOS, namely the Zudkevitch-Joffe modification of Redlich-Kwong equation (ZJRK) [23], the Soave-Redlich-Kwong equation (SRK), [24] and its three-parameter form with the volume shift (SRK3) [25], the Peng-Robinson equation (PR) [26] and its three-parameter form with the volume shift (PR3) [27], the Schmidt-Wenzel equation (SW) [28], the Patel-Teja equation (PT) [29] and its modification by Valderrama (VPT) [30], are compared in this section. These equations were described in Section 4.2. The above equations have been selected either because they are widely used in the industry, or they have been shown to be reliable in reported comparative studies [19, 22].

Figures 9.5 and 9.6 compare deviations of predicted saturation pressure and saturation volume from experimental data, respectively, in a swelling experiment where Rich Gas was progressively added to Black Oil (A), both described in Table 9.1. The experimental data are given in Table 9.3. The results indicate that each EOS could be more successful depending on the compositional range. Hence, in a general comparative study, the evaluation should cover wide ranges of composition and temperature. The experimental data should be obtained preferably in tests simulating various pertinent reservoir process, such as multiple contacts and gas cycling for gas injection studies, in addition to conventional PVT tests.

Table 9.3.  
Experimental data on addition of Rich Gas to Black Oil (A) at 373 K.

Stage No.	1		2		3		4		5	
Phase State	Oil	Gas	Oil	Gas	Oil	Gas	Oil	Gas	Oil	Gas
$V_{add}, \text{cm}^3$	101.73	9.85	101.73	34.90	101.73	64.90	51.07	47.58	51.07	62.58
$P_h, \text{MPa}$	21.58		23.61		24.63		24.80		24.81	
$V_h, \text{cm}^3$	110.46		134.40		163.43		97.64		113.79	
$P_e, \text{MPa}$			20.57				24.58		24.69	
$V_e, \text{cm}^3$			109.96	36.36			83.72	14.61	85.93	28.29
$P_e, \text{MPa}$							24.34		24.04	
$V_e, \text{cm}^3$							77.34	21.61	67.81	48.36
$P_e, \text{MPa}$									23.00	
$V_e, \text{cm}^3$									61.52	57.14
Eq.Dens., $\text{g/cm}^3$									0.464	0.264

(1) Added oil and gas volumes,  $V_{add}$ , were measured at 20.79 and 31.13 MPa, respectively.

(2)  $P_h$  and  $V_h$  are the mixture bubble point pressure and volume, respectively.

(3) At some stages the pressure was lowered below the bubble point and the properties of the equilibrated phases (e) were measured.

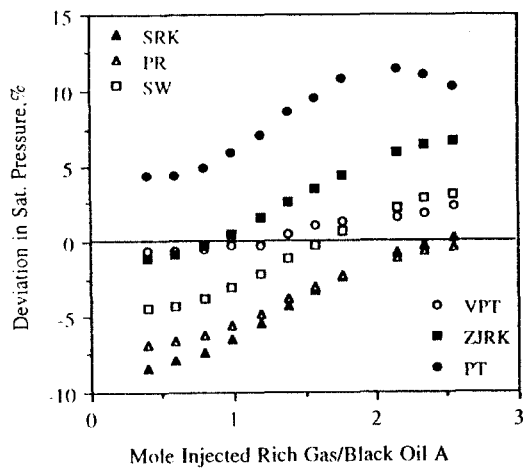


Figure 9.5. Comparison of errors in predicting saturation pressure at 373 K by various EOS.

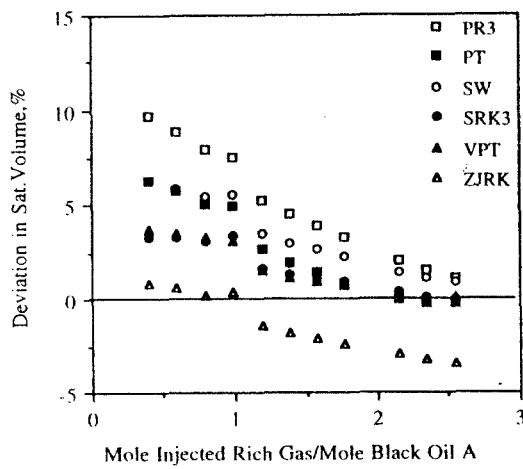


Figure 9.6. Comparison of errors in predicting saturation volume at 373 K by various EOS.

The evaluation of capabilities of van der Waals type EOS for reservoir studies is of a more interest in this section, than selecting a particular equation. The presented data are given as typical examples on the performance of these equations as reported in [19, 22, 31], where many hundreds of data points on various model and real reservoir fluids, generated at simulated

reservoir conditions, were used in the comparative studies. Other examples can be found in the literature [19-20].

### Phase Composition

The predicted composition of equilibrated phases is not only important in determining the phase behaviour in subsequent flash calculations, but also in predicting other properties such as the viscosity, interfacial tension and the density. All the above leading EOS, generally predict the composition satisfactorily. For example, the composition of equilibrated phases in the first contact of a test, where 120 cm<sup>3</sup> of Rich Gas was added to 60 cm<sup>3</sup> of Black Oil (A) at 20.79 MPa and 373 K, are given in Table 9.4. The equilibrium ratios at the above conditions predicted by various EOS are compared with the experimental data in Figure 9.7. Note that all the equations predict the equilibrium ratios similarly. Figure 9.8 highlights the relative errors of predicted equilibrium ratios in the same test, where each component has been identified by its reduced temperature. The concentration of heavy components in the vapour phase is relatively low resulting in a high relative error band experimentally. This can produce a large deviation between the measured and calculated values. Nevertheless, the percentage deviation of the predicted equilibrium ratio by all the equations, increases systematically, positive or negative depending on EOS, for heavier compounds. This trend should be expected for a number of reasons. The heavier a compound is, the further its behaviour deviates from that of a compound with simple spherical molecules, on which EOS models are based. Furthermore, the parameters of EOS, particularly the attractive term, have been correlated using vapour pressure data biased towards the light components as described in Section 4.2.3.

Table 9.4.  
Composition of equilibrated phases at 20.79 MPa and 373 K.

Component, mole %	Oil	Gas
C <sub>1</sub>	47.198	70.287
C <sub>2</sub>	11.618	11.767
C <sub>3</sub>	11.473	9.041
nC <sub>4</sub>	7.059	4.341
nC <sub>5</sub>	1.295	0.634
nC <sub>6</sub>	0.982	0.389
Met Cycl Pent	1.297	0.461
Cycl Hex	1.301	0.422
nC <sub>7</sub>	0.279	0.090
Met Cycl Hex	1.463	0.423
Toluene	0.448	0.125
nC <sub>8</sub>	0.648	0.174
o-Xylene	1.199	0.264
nC <sub>9</sub>	1.112	0.247
nC <sub>10</sub>	1.923	0.353
nC <sub>11</sub>	1.733	0.261
nC <sub>12</sub>	1.545	0.192
nC <sub>13</sub>	1.382	0.144
nC <sub>14</sub>	1.219	0.119
nC <sub>15</sub>	1.089	0.082
nC <sub>16</sub>	0.956	0.061
nC <sub>17</sub>	0.833	0.045
nC <sub>18</sub>	0.735	0.034
nC <sub>19</sub>	0.646	0.025
nC <sub>20</sub>	0.567	0.019
Equi. Vol., cm <sup>3</sup>	63.06	110.60
Equi. Dens., g/cm <sup>3</sup>	0.4939	0.2238

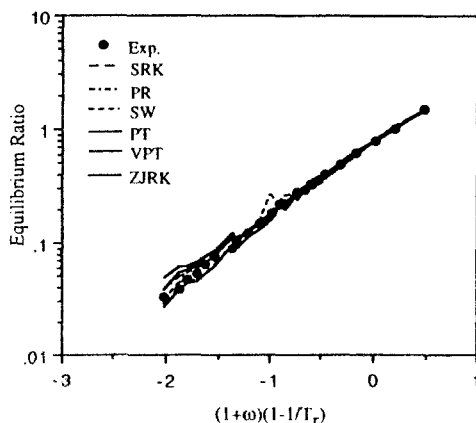


Figure 9.7. Comparison of predicted equilibrium ratios by various EOS with experimental data.

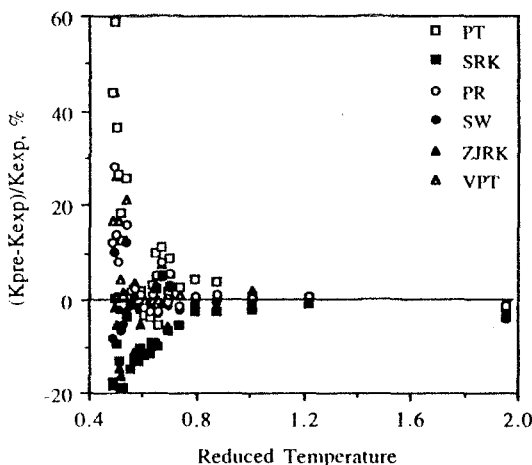


Figure 9.8. Comparison of errors in predicting equilibrium ratios by various EOS.

The average absolute deviation of predicted equilibrium ratio by EOS, for a large number of compositional data [22] are shown in Table 9.5. The comparison of average percentage deviation of predicted equilibrium ratios can be misleading, as they are strongly influenced by the large values of heavy components with low equilibrium ratios. A more useful comparison is that of the average error in predicted composition, as also shown in Table 9.5. The deviations of predicted compositions are quite acceptable and in most cases comparable with error bands of experimental data.

Ahmed [19] compared the performance of eight EOS for predicting the phase behaviour of ten real gas condensate systems after matching the dew point of each fluid by adjusting the interaction parameter between methane and the plus fraction. All the above leading EOS predicted the concentration of major components of the vapour phase in constant volume depletion tests within a deviation of 2%.

Table 9.5.  
Average absolute deviations of predicted equilibrium ratio and composition from experimental.

Equation	Equil. ratio	Oil	Gas
	%	mole fraction	
SRK	16.27	0.0021	0.0018
SRK3	16.45	0.0021	0.0017
PR	18.35	0.0019	0.0011
PR 3	18.56	0.0019	0.0011
SW	17.17	0.0020	0.0014
PT	22.70	0.0020	0.0012
VPT	21.72	0.0014	0.0011
ZJRK	14.61	0.0014	0.0012

Considering typical errors in measuring compositions in tests such as constant volume depletion, differential liberation and gas cycling, the predicted phase composition by EOS for properly characterised fluids could be as reliable as the experimental data. The errors associated with measured compositional data of equilibrated phases using poor practices were described in Chapter 2. In such cases it is probably more beneficial to direct the effort towards characterising the original fluid and generating reliable PVT data, and then use a tuned phase behaviour model to predict the produced fluid composition.

### Saturation Pressure

Table 9.6 lists the average deviation of predicted bubble point pressure for a variety of oil samples, including those with non-hydrocarbon gases added to them in swelling tests [22]. The equations are generally capable of predicting the bubble point pressure within 5% deviation for hydrocarbon systems over the whole range of phase envelope including near critical conditions. The deviations are generally higher for fluids with high concentrations of non-hydrocarbon gases. The VPT and ZJRK appear to be overall more accurate than others, with a deviation of about 2%. The deviation of predicted values by VPT for CO<sub>2</sub> rich systems is relatively high. It should be noted that no binary interaction parameter was used in VPT. All EOS generally require binary interaction parameters for hydrocarbon-CO<sub>2</sub>.

Table 9.6.  
Average absolute deviations of predicted saturation pressures.

Inj Gas	Hydrocarbon	N2	CO2	Overall
Equation	Average	Absolute	Deviation	%
SRK	4.77	12.05	11.02	6.16
SRK3	4.77	12.05	11.02	6.16
PR	4.22	12.29	4.80	4.35
PR3	4.22	12.29	4.80	4.35
SW	3.13	9.90	2.77	3.05
PT	6.52	3.62	23.87	10.38
VPT	1.04	1.91	8.20	2.63
ZJRK	2.57	1.39	2.36	2.52



Considering the reliability of EOS for prediction of equilibrium ratios of light components, the success of these equations in predicting the bubble point is expected, as the bubble point pressure is mainly controlled by the behaviour of light components. High deviations in predicted equilibrium ratios of heavy components should, however, lead to unreliable estimation of the dew point.

The deviations of predicted dew point pressure from experimental data, by the leading EOS, can exceed 20% [31], even for well defined synthetic model fluids. The deviation can be much higher for real fluids due to the presence of very large molecules, which strongly affect the dew point, even at low concentrations. The behaviour of these compounds are not only difficult to model by EOS, but their identification and characterisation are also quite demanding. Ahmed [19] evaluated the reliability of leading EOS to predict the dew point of a number of gas condensate mixtures in swelling tests. Although the dew points of original fluids were initially matched by tuning EOS, the deviation of predicted values after adding gas exceeded 30%.

### Density

Table 9.7 shows the average deviation of predicted saturation volume and liquid and gas densities in various gas injection tests [22]. A similar accuracy is expected for gas condensate systems. Note that in order to produce reliable density of equilibrated phases, EOS should predict both the phase composition and the molar volume of a fluid with known composition reliably.

All the 3-parameter equations, where the third parameter is included for improving density data, as discussed in Section 4.2.2, are more reliable than the 2-parameter equations. The exception is ZJRK. Although it is a two parameter equation, it uses density data to determine EOS parameters. Deviations, up to 25%, were noticed using SRK, but the inclusion of the volume translation, SRK3, enhanced its capability to one of the leading equations [22].

Table 9.7.  
Average absolute deviations of predicted liquid saturation volume,  
and gas and liquid densities at equilibrium.

Equation	Saturation Volume	Liquid Density	Gas Density
	Average Absolute Deviation %		
SRK	16.99	16.63	10.06
SRK3	3.34	4.55	6.78
PR	6.73	8.19	2.61
PR 3	4.83	5.94	2.31
SW	4.57	6.85	3.71
PT	3.44	3.53	2.44
VPT	2.45	2.80	3.33
ZJRK	2.39	2.81	2.18

The gas density is generally predicted more reliably than that of the liquid by two-parameter equations. The performance is equally well for both phases with three-parameter equations. This is mostly due to the use of saturated liquid density data in correlating the third parameter in these EOS. It is not unusual to find three-parameter EOS predicting the liquid density more reliably than that of its equilibrated gas, particularly for gas condensate systems [26].

As the third parameter has been generally correlated using saturated liquid volumes, EOS may predict erroneous density for highly under-saturated liquids. It is advisable to calculate the saturated liquid density by EOS and then adjust it for compression due to the excess pressure above the bubble point. The isothermal compressibility coefficient, described in Section 2.3, can be used to estimate the increase in liquid density by pressure. Alternatively, empirical

methods of estimating oil density, presented in Section 2.3, may be used to calculate the density of under-saturated liquids.

### Gas and Liquid Volumes

The errors involved in predicting phase composition and density are combined to make the calculated phase volume in flash calculations as the least reliable predicted information by almost all EOS. Table 9.8 demonstrates the average absolute deviation of predicted gas and liquid volumes for a large number of data generated in various simulated gas injection processes [22]. Note that the error in predicted phase volume ratio is the highest in all the cases. EOS generally predict the total volume more reliably than the volume of each phase at equilibrium. Hence, an over estimation of one phase is generally accompanied by under estimation of the other, resulting in a large deviation in predicted phase volume ratio.

Table 9.8.  
Average absolute deviations of predicted volumes at equilibrium.

Equation	Single Contact			Multiple Contact		
	Gas	Liquid	Gas/Liquid	Gas	Liquid	Gas/Liquid
Average Absolute Deviation %						
SRK	37.49	27.10	46.25	41.41	32.91	48.59
SRK3	16.47	30.24	41.05	31.56	35.11	46.77
PR	20.12	25.68	36.40	32.21	32.50	43.64
PR 3	14.18	24.70	30.75	31.84	33.29	44.64
SW	11.59	14.65	19.71	29.13	32.67	42.06
PT	9.68	24.27	44.77	11.53	10.71	15.53
VPT	11.51	11.19	27.77	14.84	17.81	19.94
ZJRK	4.54	10.31	14.02	21.95	25.96	32.38

The error in predicting phase volume increases sharply when the critical point is approached. The results of first contact between Volatile Oil(A), Table 9.1 and methane at 373 K and 34.58 MPa are shown in Table 9.9. Note the severe mass exchange between the phases where the oil/gas volume ratio of 4 prior to the contact changed to 0.2 at equilibrium, with almost no change in the total volume. The deviations of predicted equilibrium volumes by various leading EOS are shown in Table 9.10. Note that errors of over 100% are quite common. Such high errors near critical conditions should not be surprising as a small pressure reduction below the bubble point can vaporise almost half the liquid volume. Hence, for example a 100% error in predicted gas/liquid ratio could be equivalent to only an error of less than 0.1% in the predicted bubble point pressure. Whilst such an error in predicting the saturation pressure by EOS is highly encouraging, its effect on the volume ratio is totally unacceptable. The improvement in predicting phase ratio, by inclusion of the near critical density correction, Section 4.2.1, has been found to be negligible [32]. Whereas tuning of EOS to experimental data, generated in the critical region, can significantly improve the results.

In compositional reservoir simulation, where the reservoir is described by a number of equilibrium cells, the predicted results in each cell provide the input data for the neighbouring cells in the flow direction. This generally results in compounding errors. Figure 9.9 shows the deviation of predicted phase volume by various EOS at the front of a forward moving gas in a reservoir described by four cells. Although VPT was found to be reliable for the original oil, it resulted in a significant deviation of the predicted gas/oil volume ratio in the final stage.

Therefore, the overall error in a multiple contact simulation is expected to be significantly higher than that in flash calculations of the original fluid.

Table 9.9.

First contact data of methane-Volatile Oil (A)  
at 373 K and 34.58 MPa.

Component, Mole %	Oil	Gas
C <sub>1</sub>	72.266	80.887
C <sub>2</sub>	4.479	4.292
C <sub>3</sub>	4.075	3.720
nC <sub>4</sub>	2.398	2.007
nC <sub>5</sub>	0.958	0.742
nC <sub>6</sub>	0.712	0.515
Met Cycl Pent	0.944	0.650
Cycl Hex	0.948	0.627
nC <sub>7</sub>	0.199	0.135
Met Cycl Hex	1.060	0.676
Toluene	0.325	0.204
nC <sub>8</sub>	0.462	0.293
o-Xylene	0.876	0.501
nC <sub>9</sub>	0.790	0.471
nC <sub>10</sub>	1.374	0.767
nC <sub>11</sub>	1.242	0.651
nC <sub>12</sub>	1.117	0.548
nC <sub>13</sub>	1.014	0.470
nC <sub>14</sub>	0.918	0.402
nC <sub>15</sub>	0.830	0.348
nC <sub>16</sub>	0.744	0.295
nC <sub>17</sub>	0.661	0.249
nC <sub>18</sub>	0.594	0.213
nC <sub>19</sub>	0.533	0.181
nC <sub>20</sub>	0.480	0.154
V <sub>add</sub> , cm <sup>3</sup>	80.00	20.00
V <sub>c</sub> , cm <sup>3</sup>	17.02	81.90
Eq.Dens., g/cm <sup>3</sup>	0.4327	0.3310

Table 9.10.

Percentage error in predicting phase volume by various EOS.

EOS	ZRK	SRK	SRK3	PR	PR3	SW	PT	VPT
Oil Vol.	-118	-182	-152	-126	-126	-135	-53	-50
Gas Vol.	26	28	31	27	25	26	9	11

The capability of EOS in predicting the phase volume of gas condensate systems, particularly within the retrograde region, is generally inferior to that of gas-oil systems. Such a behaviour is expected as the accuracy in modelling the behaviour of heavy compounds, which dominate the liquid formation, is generally inferior. The volumetric behaviour of a gas condensate, with the composition given in Figure 4.6, as predicted by several EOS is shown in Figure 9.10. Note that the predictions of all EOS approach the experimental values quite closely within the vaporising region, where the system behaves oil-like.

The error in predicting the retrograde liquid volume below the dew point can be reduced markedly by tuning EOS to match the dew point.

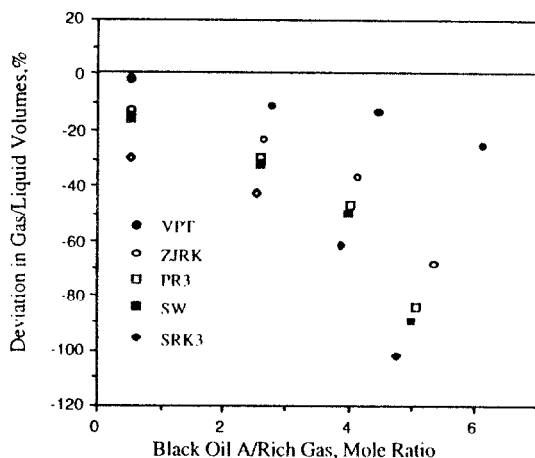


Figure 9.9. Error in predicting phase ratio by various EOS at front of Rich Gas advancing in Black Oil (A) at 373 K and 20.8 MPa.

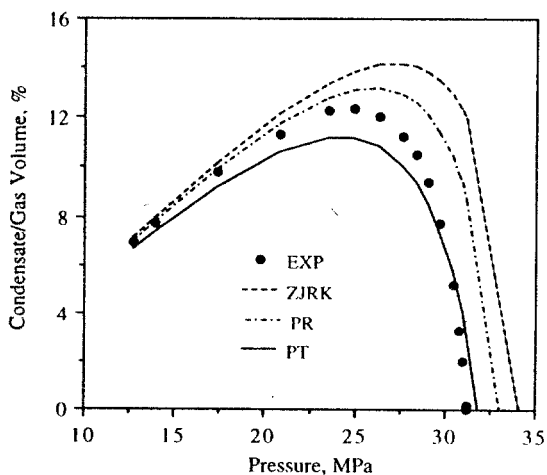


Figure 9.10. Comparison of predicted condensate/gas volumetric ratio in a constant composition expansion test at 383 K by various EOS.

### Robustness

The robustness of a phase behaviour model in converging to a solution is more dependent on factors such as the mathematical methods of solving the governing equations and initial guesses used in iterations, than EOS characteristics. The pertinent conditions of composition, temperature and pressure can also have profound effects on the convergence of EOS to a

solution. All cubic equations generally exhibit a similar convergence behaviour, they either cannot easily converge, or converge to the trivial solution of equal partitioning of components between the phases, at conditions close to the critical point. Convergence problems may be observed also at conditions near the maximum pressure and the maximum temperature of the phase boundary. EOS which locate the prevailing conditions away from the difficult conditions, such as the critical point, often converge, whilst others may fail. Hence, the converged equations are not necessarily more reliable, or applicable to that system.

### 9.3 TUNING OF EOS

The inherent deficiencies of EOS, particularly for multicomponent mixtures, were described in Chapter 4. Phase behaviour models based on these equations may predict highly erroneous results, particularly for near critical fluids, even for well characterised model fluids as shown in Section 9.2. Real reservoir fluids, composed of thousands of compounds, are described by a limited number of pure substances and carbon groups. The compositional analysis of these fluids are not always very reliable and the carbon groups are not fully defined. Generalised correlations, often with significantly diverging results amongst themselves, are used to estimate the critical properties of the carbon groups required for EOS calculations. All these factors further deteriorate predictions of EOS for real reservoir fluids.

The current approach in the industry to encounter the above deficiencies is to calibrate, or tune, an EOS model against experimental data generated at pertinent conditions for specific field studies. Although the industry has not adapted a single standard method for tuning, the various approaches are basically similar; some uncertain values of input data to the phase behaviour model are adjusted to minimise the difference between the predicted and measured values.

As the model is to predict the phase behaviour and various fluid properties within wide ranges in compositional reservoir simulation, a large number of experimental data are often used in tuning. The exercise is basically to minimise an objective function, defined as the sum of weighted squared deviations,

$$\Delta = \sum_{j=1}^{N_{\text{data}}} \left[ w_j \left( \frac{\Psi_j^{\text{pred}}(X_i) - \Psi_j^{\text{exp}}}{\Psi_j^{\text{exp}}} \right)^2 \right] \quad (9.20)$$

where each element of the objective function expresses the weighted difference between the predicted and experimental values,  $\Psi^{\text{pred}}$  and  $\Psi^{\text{exp}}$ , respectively;  $w$  is the weighting factor and  $N_{\text{data}}$  expresses the number of measured data points to be fitted;  $X_i$  designates the regression (tuned) variables.

The optimum values of variables are obtained by minimising the function  $\Delta$ . Although various methods [33-35] have been suggested for solving multi-variable regression problems, none can be guaranteed to solve the problem in all cases. A modification of the Levenberg-Marquardt method [35] is often used to minimise the value of  $\Delta$  in Eq.(9.20).

The importance of a property is emphasised by multiplying its deviation with a high weighting factor. The saturation pressure is perhaps the most important property of a reservoir fluid for phase behaviour studies. Furthermore, it needs a high weighting factor if it is to become effective, as generally the number of data points on the fluid saturation pressure is much fewer than those of other properties. High weighting factors could also be assigned to more reliable experimental data. Less reliable data, such as the composition of equilibrated phases, should receive low weighting factors, or preferably not used at all. Table 9.11 provides weighting factors as a rough guide [33].

Table 9.11.  
Weighting factors of properties in tuning of EOS.

Property	Bubble Point	Density	Volume	Composition
Weighting Factor	40	20	10	1

Although the dew point is an important parameter and its accurate prediction is desirable, assigning a high weighting factor to it may increase the deviation of predicted retrograde condensate volume. Many gas condensate samples show a liquid drop-out tail during depletion, as described in Section 2.2.4. Matching the dew point generally results in over prediction of the liquid volume during the early depletion stages for these fluids. As the measurement of dew point is quite subjective, tuning EOS with a higher emphasis on the liquid volume, instead of the dew point, is preferred.

The deviation between the predicted and experimental data is not only due to deficiencies of EOS, but mostly due to the input data, excluding the near critical conditions. Hence, the tuning process should primarily be conducted to evaluate and improve the input data, instead of modifying EOS parameters indiscriminately to match the experimental data. Generally a severe tuning could indicate overlooked problems. Furthermore, the tuning should not be regarded purely as a mathematical regression problem. The parameters to be regressed need to be selected based on physical concepts and varied within reasonable limits.

### Fluid Characterisation

A proper analysis and characterisation of the reservoir fluid is the most important step in successful application of a compositional model to determine the fluid behaviour and properties. Pedersen et al. [36] provide many examples, where a proper characterisation of real reservoir fluids has resulted in reliable predictions by phase behaviour models without any tuning.

Comparative studies, where the same fluid has been sent to different laboratories for compositional analysis, have revealed striking information on the disparity of results, particularly for gas condensate systems. The use of high pressure analysis techniques, to avoid loss of compounds in the flash (blow down) method, Section 2.2, is recommended. This is particularly valuable for gas condensate fluids, where the flash method results in an analysis often leaner than the real fluid due to the loss of collected condensate.

When compositional data generated by different methods, such as distillation, gas chromatography, high pressure analysis and mass spectrometry, are available, they all should be used to determine the most probable composition of the fluid. The capabilities of each method should be considered in driving the final analysis, rather than averaging the reported compositions. For example, the most reliable information on the relative concentration of light components is obtained by gas chromatography of the flashed gas, whereas distillation provides reliable data on heavy components, particularly the plus fraction. The high pressure compositional data on intermediates and lighter heavies are generally more reliable than those by other methods. The high pressure analysis also provides valuable information for evaluating the reliability of the vapour to liquid ratio used in deriving the overall composition by the flash method.

The concentration of components is almost always measured in mass (or volume) basis in distillation and also in gas chromatography. The results are generally reported in mole basis, either by using the measured, or the generalised single carbon group, molecular weights. It is always advantageous to work with the compositional analysis in mass fractions. The molecular weight of heavy fractions, particularly the plus fraction due to its low reliability, may be varied as a tuning parameter. Working in mass basis will retain the original compositional data, when questionable molecular weight data are adjusted.

The characterisation of single and multiple carbon groups has a major impact on the results predicted by EOS. Guidelines on the number and selection of groups and the estimation of group properties were given in Section 9.1. Occasionally, improper characterisation, such as describing the heavy fraction with too few pseudo components, may lead to lower deviations of predicted results than that of an appropriate method. This can be due to the cancellation of errors at some conditions and should not be adopted. It is more logical to use proper characterisation and then attempt to improve other shortcomings, than relying on uncontrollable cancellation of errors.

Tuning of EOS can be conducted with the fluid described by any number of components. In general describing the  $C_{7+}$  with 4 groups, using the quadrature method, and all the discrete compounds as reported, should be adequate in most compositional models. The components with their optimised properties could be grouped again to reduce their number, if required. An additional minor tuning of the new group properties, depending on the grouping method, may be necessary.

### Selection of EOS

Forcing EOS to match certain data by excessive adjustment of its parameters, may lead to highly unreliable information at other conditions where experimental data is lacking. In general any leading EOS which predicts phase behaviour data reasonably well without tuning, would be the most appropriate choice.

Tuning should not be conducted without consideration to capabilities of EOS. For example, tuning of a two-parameter EOS, known to be weak in predicting the liquid density, to match experimental density data, may lead to serious problems with prediction of other data, or even further deterioration of predicted density outside the range of available experimental data.

Although most of the van der Waals type EOS are basically very similar, certain equations may be preferable to others. As reliable volumetric data are also required in reservoir fluid studies, three-parameter EOS should be selected in preference to the two-parameter equations. Certain equations, such as the Valderrama modification of Patel-Teja EOS, which have consistently demonstrated their reliability, could be considered amongst the first choices.

### Experimental Data

All reliable experimental data should be used in tuning of EOS. The experimental data, however, seldom cover all prevailing conditions. Conventional PVT data may not be adequate generally for tuning of EOS, which is often used in simulation of reservoir processes other than simple pressure depletion. Experimental data should be generated at conditions closely simulating reservoir processes. For example, if gas injection is to be modelled by EOS, multiple contact test data are highly valuable for the tuning. The swelling test with a rich gas, particularly covering compositions around the critical point, provides useful information for miscible displacement processes.

The type of experimental data required for tuning has been addressed by several investigators [37,38]. In general, the data should cover the pertinent range of composition, pressure and temperature. Tests are generally conducted at the reservoir temperature to simulate reservoir processes and at the separator temperature to simulate surface conditions.

Compositional data on equilibrated phase are known to be generally unreliable, hence, seldom used in the tuning. When the estimation of produced fluid composition by gas cycling in a reservoir is the main target of the study, such a treatment of compositional data will be

unjustifiable. In such cases, reliable compositional data, by methods such as high pressure fluid analysis, should be generated, evaluated and improved prior to being used in tuning.

Material balance calculations are the most popular method of evaluating experimental data. It must be ensured, however, that such calculations have not been previously implemented to smooth or even generate data by the laboratory. The accuracy of reported phase composition can be evaluated by comparing the number of moles of each component in the feed with the sum of those in the produced streams. The total and component balance equations are essentially those used in flash calculations,

$$n^L + n^V = n^F \quad (5.1)$$

and

$$z_i n^F = x_i n^L + y_i n^V \quad i=1,2,\dots,N \quad (5.2)$$

The component balance equation, Eq.(5.2), can be presented graphically [39] as shown in Figure 9.11 for the data reported in Table 9.4. The deviation of any point from the straight line of ordinate+abscissa=1, identifies the error associated with the measured data of that component. Random deviations generally show errors in the compositional analysis, whereas systematic ones can be due to the error in measuring the amounts of phases. Certain plots, such as the Hoffmann plot [40] or the modified Wilson equation plot, described in Section 3.2, can also be used to evaluate the internal consistency of compositional data.

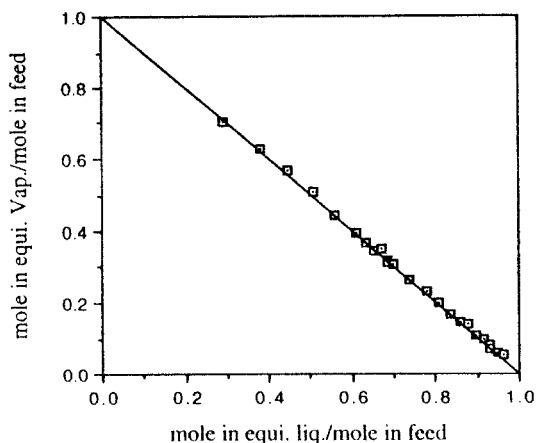


Figure 9.11. Material balance plot of the compositional data reported in Table 9.4.

Smoothing data may sometimes mask certain uncommon features of a particular fluid. An example was given in Section 1.3 where the liquid phase volume increased with decreasing pressure over a short pressure range below the oil bubble point. Clearly if such data had been smoothed by the laboratory, the correctly predicted behaviour by EOS could have been regarded as a flaw.



### Selection of Regression Variables

The parameters that are often used in tuning are binary interaction parameters, properties of pseudo-components, particularly the critical properties and parameters of EOS. An effective, but not necessarily the most appropriate, approach is to select and adjust those parameters upon which the predicted properties are most sensitive. The tuning is then achieved with minor changes in original parameters. The relative effectiveness of various parameters may depend on the fluid type.

In multi-variable regression, the mathematical routine may be designed to rely on adjusting the parameters which show high values of derivatives of the objective function relative to them. Agarwal et al. [41] proposed a method where the most effective parameters were selected dynamically from a large set of parameters during the regression process. Gani and Fredenslund [42] suggested a tuning procedure based on establishing the sensitivity of the predicted results, depending on the fluid and the prediction problem and selecting the most effective variables for regression. In a number of tested cases, the binary interaction parameter (BIP) was selected as one of the most effective parameters.

The most common approach is to adjust BIP between the lightest component, present at a significant concentration in the mixture, and the heavy end fraction [33]. The values of BIP between the lightest and the rest of components, or between all the components, may also be adjusted by regressing the parameters of a generalised correlation for BIP, such as Eq.(4.80).

The selection of BIP as a regression variable is mainly based on the view that BIP is more of a fitting parameter than a physical property. It is also very effective in changing the predicted results of EOS. This approach can, however, divert attention from adjusting other uncertain input parameters of EOS, such as properties of the pseudo components, which may actually require improvement.

The critical properties and the acentric factor of pseudo components are probably the least accurate input data, hence, may be used in tuning. The critical properties are often estimated from the specific gravity and the boiling point, or the molecular weight, of fractions using generalised correlations presented in Section 6.2. Deviations as high as  $\pm 6\%$  for the critical temperature and acentric factor and  $\pm 30\%$  for the critical pressure of hydrocarbons may result from these correlations. The adjustment of critical properties affect the predicted results through changing parameters of EOS, Section 4.2. A direct regression of EOS parameters, or their coefficients  $\Omega_a$  and  $\Omega_b$ , have also been suggested [33].

The sensitivity of predicted saturation pressure, equilibrated phase volumes and densities to the properties of pseudo components in various processes, such as swelling and multiple contact tests, was evaluated for a wide range of fluids [38]. The adjustable parameters of the pseudo components were varied in the range of  $-5\%$  to  $+5\%$  of their original values to study their effects on predicted phase behaviour and properties. For example, Figures 9.12-14 demonstrate the effect of adjusting the parameters on deviations of predicted properties in a multiple forward contact test of a black oil with methane. The experimental data are given in Table 9.12. The phase behaviour was predicted using PR with the oil heavy end fraction described by only one pseudo-component of  $C_{6+}$ . Note that changing the specific gravity of the pseudo component, resulting in adjustment of critical properties calculated by the Twu method, Section 6.2, had a profound effect on the results. The predicted properties, however, lost their sensitivity to the specific gravity, or the trend reversed when it was increased by more than 3%. A change in sensitivity can also be observed for the EOS co-volume parameter, 'b'. Contrary to the common view, the parameter 'b' can become more effective than the attractive term parameter 'a' in predicting phase behaviour of high pressure fluids. Amongst the evaluated properties of pseudo components, including the molecular weight, specific gravity, composition and parameters of EOS, the specific gravity was found generally to be the most effective parameter in tuning of EOS [38].

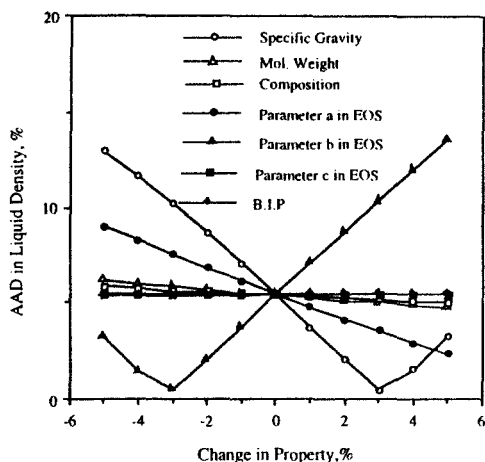


Figure 9.12. Effect of adjusting various heavy end properties on deviation of predicted liquid density.

Table 9.12 .  
Composition and properties of Black Oil (C).

Component	Mole%	M	S
C <sub>1</sub>	34.00		
C <sub>2</sub>	12.45		
C <sub>3</sub>	8.42		
i-C <sub>4</sub>	1.29		
nC <sub>4</sub>	4.56		
i-C <sub>5</sub>	1.60		
nC <sub>5</sub>	2.98		
C <sub>6</sub>	2.45	84	0.694
C <sub>7</sub>	3.66	94	0.730
C <sub>8</sub>	3.64	117	0.754
C <sub>9</sub>	2.97	126	0.769
C <sub>10</sub>	2.34	140	0.785
C <sub>11</sub>	1.96	153	0.799
C <sub>12</sub>	1.63	165	0.806
C <sub>13</sub>	1.59	180	0.820
C <sub>14</sub>	1.31	197	0.843
C <sub>15</sub>	1.36	209	0.844
C <sub>16+</sub>	11.80	374	0.909
Sat. Pres., MPa		17.91	
Sat. Dens., g/cm <sup>3</sup>		0.6553	
S (C <sub>6+</sub> )		0.838	
M (C <sub>6+</sub> )		194	
Pres., MPa	Density, g/cm <sup>3</sup>		
20.79	0.6599		
34.58	0.6784		

Table 9.12 (Con.)

Forward-contact experimental data at 373 K and 20.79 MPa.

Stage No.	1		2	
Phase	Oil	Gas	Oil	Gas
Added Vol., cm <sup>3</sup>	90.00	90.00	135.00	45.00
Equi. Vol., cm <sup>3</sup>	77.04	99.01	137.79	36.16
Equi. Dens., gram/cm <sup>3</sup>	0.6896	0.1621	0.6491	0.1939

The equilibrated gas from the first stage was contacted with the fresh oil in the second stage.

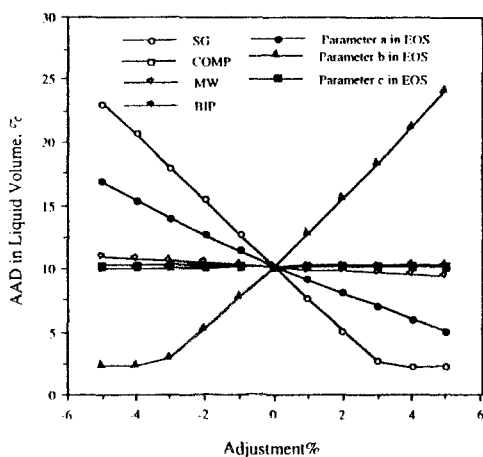


Figure 9.13. Effect of adjusting various heavy end properties on deviation of predicted liquid volume.

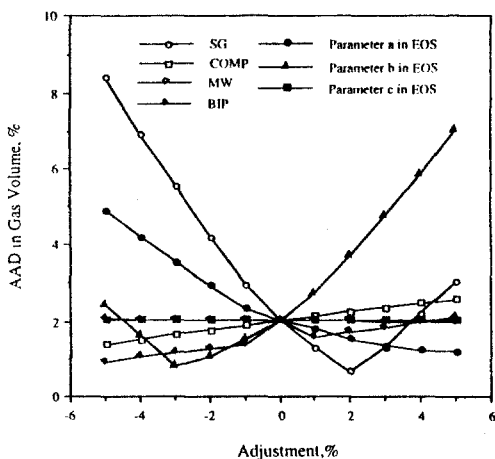


Figure 9.14. Effect of adjusting various heavy end properties on deviation of predicted gas volume.

Concentration of the plus fraction and its properties, are probably the least reliable input information, hence, their adjustment is quite justified. The plus fraction properties strongly affect predicted properties of condensing fluids. Sensitivity of the predicted results to adjusting input data generally increases when the critical point is approached.

### Limits of Tuned Parameters

It is reasonable to adjust measured parameters within their error bands in tuning. Wider limits for tuned parameters provide higher flexibility for matching experimental data. That could, however, lead to unrealistic values for the tuned parameters.

The accuracy of measured molecular weight is much less than that of the specific gravity. Typical error bands for measured molecular weight, boiling point and the specific gravity of pseudo components are about,  $\pm 1\%$ ,  $\pm 1\%$  and  $\pm 0.2\%$  respectively. The above bands, particularly for the average boiling point, are much wider for the plus fraction. The adjustment of the above properties within their error bands, however, may not be sufficient to achieve the required tuning. Pedersen [36] suggested adjusting the molecular weight by as high as 10%. As these experimental data are employed to calculate the critical properties of pseudo components, using generalised property correlations which introduce additional errors into EOS, wider adjustments are acceptable. The deviations of these correlations, reported previously, can be regarded as the limits for adjusting the properties.

### Methodology

It is advisable to reduce the number of variables in the regression to avoid numerical problems and improve the search for the global minimum of the objective function. Hence, for example, regressing the parameters of the BIP correlation, Eq.(4.80), and those of the volume shift correlation, Eq.(4.36), are preferable to adjusting a large number of BIP values and shift parameters.

Although simultaneous adjustment of regressed variables may lead to satisfactory results, the multistage tuning, where selected parameters are adjusted in turn can be more appropriate. For example, when using a two-parameter EOS such as PR and SRK, the density data can be initially left out of regression. Then the volume shift factors of pseudo components can be adjusted to match the density data, prior to going back to the other regressed parameters for fine tuning.

It is important to maintain the consistency of regressed parameters when more than a single variable is used to tune a phase behaviour model. The critical temperature, acentric factor and the boiling point temperature should generally increase with the molecular weight or carbon number of pseudo components, whereas the trend should be opposite for the critical pressure.

The above critical properties are calculated from generalised correlations based on the specific gravity and normal boiling point temperature of carbon groups. Specific gravity is one of the most effective parameter in adjusting the predicted results of EOS. It can be selected as the tuning parameter, with the boiling point related to it by maintaining the Watson characterisation factor,  $K_w$ , constant equal to its original value, as the variation of this factor is relatively small for carbon groups.

$$K_w = \left[ (1.8T_b)^{\frac{1}{3}} \right] / S \quad (6.2)$$

As all the critical properties and the acentric factor are calculated from the specific gravity and boiling point data, they will be adjusted consistently when the specific gravity is varied to tune EOS.

Although adjustment of BIP in tuning of EOS is quite common, a highly effective tuning can be achieved, without resorting to BIP, by just adjusting the properties of carbon groups. This will allow rapid flash calculations in compositional reservoir simulation as described in Section 5.1.

A comprehensive data set on a volatile oil, was used by several investigators in a comparative tuning exercise [39]. All the participants used the Peng Robinson EOS (PR), applying different in-house tuning methods. They all, however, used BIP as a tuning parameter. For example, the results of the tuned models for some properties are shown in Figures 9.15 and 9.16. The results of a tuning method using PR but with no BIP, are also shown in these Figures. In this method [43], the specific gravity of the plus fraction and also its measured concentration, as the least reliable compositional information, were used as the regression parameters. The shift parameters of carbon groups were also adjusted. The results clearly demonstrate that effective and probably more physically based tuning, can be achieved without using BIP. The suitability of the method for gas condensate systems has also been demonstrated [44].

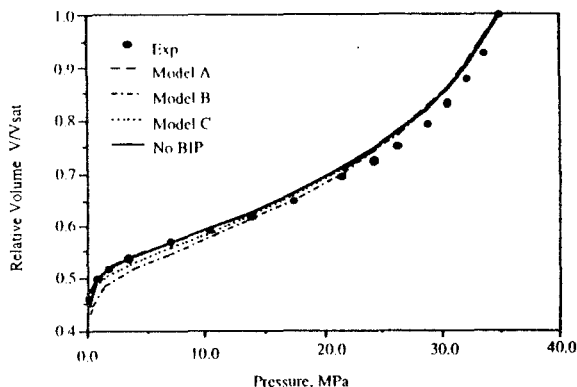


Figure 9.15. Comparison of relative volume in differential liberation experiment predicted by various tuned models.

The main drawback of using only the properties of pseudo components, particularly of the plus fraction, is that the gas phase properties, such as the density particularly at low pressures, are not very sensitive to them due to their low concentrations. A powerful tuning parameter is the temperature coefficient of the attractive term in EOS. This coefficient and its adjustment for super-critical components, were described in Section 4.4.3. It can be readily used as a tuning variable, along with heavy end properties.

A combination of reliable EOS and properly characterised fluid data should lead to predicted results close to experimental values, hence, very little need for tuning. A phase behaviour model with its input parameters adjusted widely would lead to unrealistic results at conditions other than those tested in the tuning. As experimental data set covering all possible conditions within a reservoir is not forthcoming in most cases, severe tuning should be avoided. Pedersen et al. [36] have reviewed the danger of tuning by considering various cases.

## 9.4 DYNAMIC VALIDATION OF MODEL

Typical laboratory measurements used in tuning include conventional PVT data, swelling and multiple contact vapour-liquid phase equilibrium data. In 1985, Kossack and Hagen [45]

studied the capability of EOS, tuned against static experimental data, in simulating the gas-oil phase behaviour in slim tube displacement tests. They concluded that an EOS tuned to the static PVT data was not adequate for simulating fluid displacement. A different set of EOS parameters was required to match both PVT and displacement data. A similar conclusion was reached also by Mansoori et al. [46].

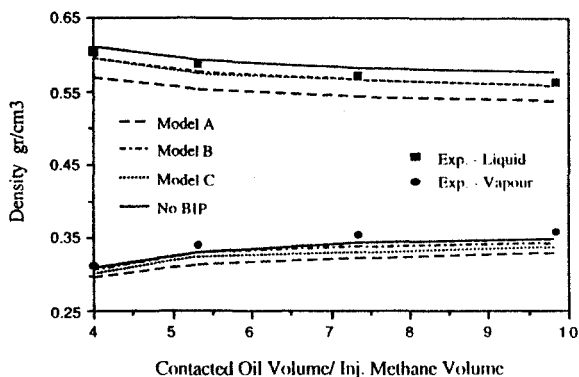


Figure 9.16. Comparison of gas and oil density in a forward contact experiment predicted by various tuned models.

The slim tube, described in Section 7.2, is the simplest apparatus that can be used to physically simulate compositional changes resulting from the continuous contact between the injection gas and the reservoir oil. The choice of an almost one-dimensional flow in a properly designed tube displacement is reasonable, as the effects of dispersion, viscous fingering, gravity override and heterogeneity, which are significant in a large three dimensional system, are minimised. It is, therefore, reasonable to expect that a reliable phase behaviour model, which is to be used in a reservoir simulator to study gas injection, should be able to predict the fluid conditions in such a simple displacement. Hence, the comparison of the displacement data with simulated results of a compositional model using the tuned EOS can be employed to evaluate and, if necessary, further tune the phase behaviour model.

The experimental data used in tuning of EOS should cover the compositional range occurring in the displacement process. Generation of such data for some processes, such as rich gas injection, where miscibility is not achieved at the two leading and trailing edges of the transition zone, is not practicable in static tests. Therefore, it is advisable to further evaluate the phase behaviour model, that is tuned to all the relevant static data, by checking its performance in predicting slim tube displacement data. The test could also indicate unexpected phase changes, such as asphaltene deposition, which may not be evident in static tests.

The flow parameters and numerical methods incorporated in the simulation model can strongly affect the prediction. Hence, these factors need to be carefully isolated and determined, if the phase behaviour model is to be evaluated against displacement data. It has been demonstrated [47] that, after proper implementation of the above factors in a numerical simulator, an accurate prediction of the displacement can be expected from a reliable phase behaviour model.

The flow of gas and oil in a slim tube is described by the Darcy's equation,

$$\bar{v}_g = \frac{k k_{rg} \Delta P}{\mu_g L} \quad (9.21)$$

and

$$\bar{v}_o = \frac{k k_{ro} \Delta P}{\mu_o L} \quad (9.22)$$

where,  $\bar{v}$  is the fluid velocity,  $\Delta P/L$  is the pressure gradient along the tube,  $\mu$  is the viscosity and  $k$  is the tube absolute permeability.  $k_r$  is the relative permeability which depends on the fluid saturation, the interfacial tension (IFT) and velocity at the displacement conditions.

Eqs.(9.21-22) clearly demonstrate that the ratio of the flowing phases, which determines the mixture composition, hence, the phase behaviour, depends on the relative permeability correlations employed in the simulation model and the viscosity of both phases. These parameters, therefore, should be determined reliably in advance.

### Relative Permeability Function

Khazam et al. [47], investigated the relative permeability of gas-oil in a slim tube using binary fluids. Two phase mixtures equilibrated at the test temperature and pressure were prepared. The slim tube was packed with the liquid and displaced with the equilibrated gas, at almost no mass transfer conditions. The test was conducted at different pressures over the interfacial tension range of 9.8 to 0.04 mN/m. The results are shown in Figure 9.17. It is evident that as IFT approaches zero, that is approaching miscibility, the residual oil saturation, the immobile oil left behind, decreases towards zero and the relative permeabilities increase. The investigators conducted displacement tests, using different fluids, including real reservoir samples and concluded that a single set of relative permeability-saturation curves is adequate in describing the flow behaviour of all fluid systems which have the same IFT value.

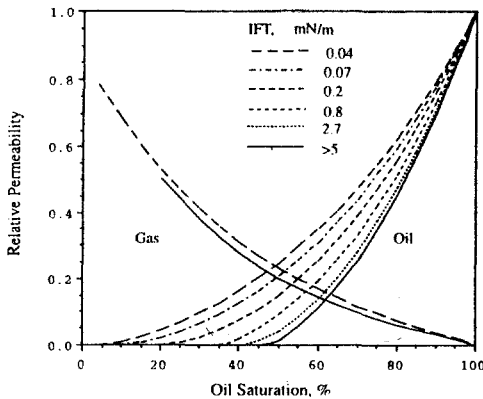


Figure 9.17. Variation of gas and oil relative permeability with interfacial tension (IFT).

As the measurement of relative permeability in a slim tube at various IFT values involves a major effort, relative permeability correlations may be used instead. It is, however, essential to

measure the relative permeabilities at a single high IFT condition (base curves) as the starting input data. Displacing a binary oil with its equilibrated gas, and measuring the production rate and the differential pressure across the tube, provide all the required data to determine the relative permeability using a graphical method [48]. There is no need, however, to measure the change of relative permeabilities with IFT extensively. One set of relative permeability curves at a low IFT value and the base curves are sufficient to define the parameters of a generalised relative permeability correlation.

A number of correlations [47, 49-51] have been developed to account for the effect of IFT on relative permeability. One of the earliest attempts to correlate gas-oil relative permeability with IFT is that of Coats [50]. The Coats correlation is based on the concept that as the interfacial tension between the two phases approaches zero near the critical point (miscible condition), the residual phase saturation values decrease towards zero and the relative permeability curves vs. saturation approach straight diagonal lines. He suggested to estimate the relative permeability at any IFT value, by interpolation between the base curve determined at high IFT and the straight diagonal line,

$$k_r = F_\sigma k_{rb} + (1 - F_\sigma) k_{rm} \quad (9.23)$$

where  $k_r$  is the relative permeability to gas or oil, and  $F_\sigma$  is the scaling factor between the base relative permeability  $k_{rb}$  and the miscible relative permeability  $k_{rm}$ .

$F_\sigma$  is a function of the interfacial tension,  $\sigma$ , as follows:

$$F_\sigma = (\sigma / \sigma_b)^{1/n} \quad (9.24)$$

where  $\sigma_b$  is the base IFT and  $n$  depends on the porous medium type with a default value of 7 [52].

The value of  $k_{rm}$  can be assumed equal to the phase saturation. Although this simple interpolation approach, Eq.(9.23), will result in zero residual oil at all IFT conditions, its effect on the evaluation of phase behaviour model, using slim tube displacement data, is insignificant.

### Viscosity Prediction

The viscosity of a single phase reservoir fluid increases with pressure, except at near critical conditions. The increase of temperature, decreases the liquid viscosity whilst it increases the gas viscosity at moderate and low pressures. At high pressures, the behaviour of gas viscosity is more liquid-like (Figure 2.23). Hence, those correlations developed either for gas or for liquid, Section 2.3, may not be suitable for reservoir conditions, particularly for gas injection processes. It is required to use a single method to predict the viscosity of both phases at such conditions, especially when miscibility is approached and the properties of vapour and liquid become similar. A number of methods are applied to both gas and liquid in reservoir studies, which can be classified into three groups:

First, the corresponding states methods, where the reduced viscosity, defined as the ratio of the fluid viscosity to that at the critical point, is related to two reduced state properties, such as the reduced pressure and reduced temperature, Pedersen et al. [53], or the reduced temperature and reduced density, Ely and Hanley [54]. As reservoir fluids cannot be modelled accurately by the simple two parameter corresponding states principle, some correction factors are included in these correlations. The correction factors adjust the deviation of the predicted result by comparing it with the viscosity of one reference fluid, methane [53-54], or two reference fluids, methane and decane [55]. Although the viscosity is not a thermodynamic state property, the above approach predicts acceptable data in most cases.



The second approach is based on the analogy between viscosity-temperature and specific volume-temperature behaviour. Cubic equations, similar to van der Waals type equations, but with volume replaced by viscosity, have been proposed [56, 57]. There is very little reasoning behind this approach, apart from the similarity of pressure-volume-temperature and pressure-viscosity-temperature plots.

The third approach uses the concept of residual viscosity, which is defined as the difference between viscosity at prevailing conditions and that at low pressure where the viscosity depends only on the thermal energy. The residual viscosity can be related to the fluid density, whereas the viscosity of gases at low pressure can be reliably determined by the kinetic theory of gases. This approach, as implemented by Lohrenz-Bray-Clark (LBC) [58], is used widely in the petroleum industry, particularly in reservoir simulation. The method is basically that of Jossi et al. [59] for pure compounds, extended to hydrocarbon reservoir fluids, as described below.

The kinetic theory of gases shows that the viscosity is inversely proportional to,

$$\lambda \equiv T_c^{\frac{1}{2}} M^{-\frac{1}{2}} P_c^{-\frac{2}{3}} \quad (9.25)$$

Jossi et al. [59] multiplied the residual viscosity by  $\lambda$  to make it dimensionless and correlated it with the reduced density,  $\rho_r = \rho/\rho_c$ , for pure compounds as,

$$\left[ (\mu - \mu^0) \times \lambda + 10^{-4} \right]^{\frac{1}{4}} = a_1 + a_2 \rho_r + a_3 \rho_r^2 + a_4 \rho_r^3 + a_5 \rho_r^4 \quad (9.26)$$

$$\begin{aligned} \text{where } a_1 &= 0.10230 \\ a_2 &= 0.023364 \\ a_3 &= 0.058533 \\ a_4 &= -0.040758 \\ a_5 &= 0.0093324 \end{aligned}$$

and  $\mu^0$  is the low pressure viscosity which can be determined as,

$$\mu^0 = 34 \times 10^{-5} T_r^{0.94} / \lambda \quad T_r \leq 1.5 \quad (9.27)$$

$$\mu^0 = 17.78 \times 10^{-5} (4.58 T_r - 1.67)^{\frac{1}{2}} / \lambda \quad T_r > 1.5$$

Note that the units of  $T_c$  and  $P_c$  in Eq.(9.25) should be K and atm (MPa/0.101325) in order to obtain the viscosity in mPa.s (cp).

Lohrenz et al. [58] extended the above to mixtures, by proposing the Herning-Zipperer mixing rule [60] for the low pressure viscosity and the molar mixing rule for other properties as follows,

$$\mu^0 = \left[ \sum_{i=1}^N x_i \mu_i^0 M_i^{\frac{1}{2}} \right] / \left[ \sum_{i=1}^N x_i M_i^{\frac{1}{2}} \right] \quad (9.28)$$

$$\lambda = \left( \sum_{i=1}^N x_i T_{ci} \right)^{\frac{1}{6}} \left( \sum_{i=1}^N x_i M_i \right)^{-\frac{1}{2}} \left( \sum_{i=1}^N x_i P_{ci} \right)^{-\frac{2}{3}} \quad (9.29)$$

$$\rho_{Mc} = (v_c)^{-1} = \left( \sum_{i=1}^N x_i v_{ci} \right)^{-1} \quad (9.30)$$

$$\rho_r = v_c / v$$

where  $\rho_{Mc}$  is the molar critical density and  $v_c$  is the critical molar volume. The authors used the viscosity data of a number of reservoir fluids to back calculate and correlate the critical molar volume of  $C_{7+}$  as,

$$(v_c)_{C_{7+}} = 1.3468 + 9.4404 \times 10^{-4} M_{C_{7+}} - 1.72651 S_{C_{7+}} + 4.4083 \times 10^{-3} M_{C_{7+}} S_{C_{7+}} \quad (9.31)$$

where  $M$  and  $S$  are the molecular weight and specific gravity, respectively and the estimated critical volume is in  $m^3/kgmol$ .

The method of Lohrenz et al. is quite sensitive to the fluid density, as apparent in Eq.(9.26). Hence it should be used only in combination with EOS which are known to predict gas and liquid density reliably.

Figure 9.18 shows the deviation of predicted viscosity by Eq.(9.26) for pure compounds. Clearly the correlation loses its reliability for heavy compounds. Hence, the method becomes unreliable for dense fluids with reduced densities over 2.5 [61]. It may predict oil viscosity with deviations exceeding 100%.

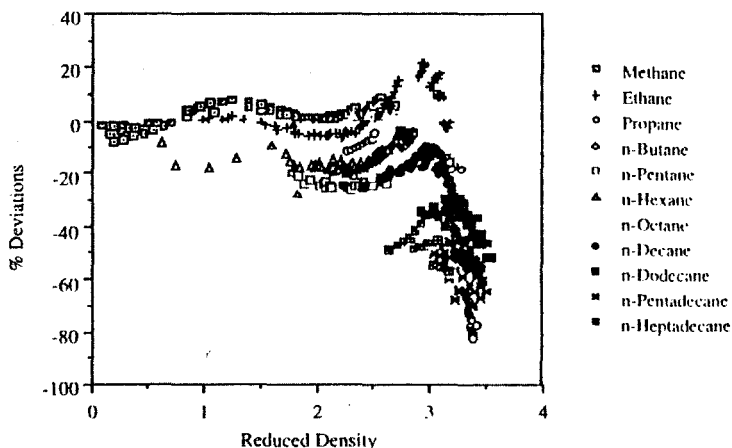


Figure 9.18. Deviation of predicted viscosity of pure hydrocarbons by the method of Jossi et al.

It is common to tune the model by adjusting the critical volume of the  $C_{7+}$  fraction to match the measured data. The above approach improves the predicted results markedly in processes where the heavy fraction remains almost intact. A successful example of such practice, where the measured and predicted viscosities have been matched only at the bubble point, is shown in Figure 9.19.

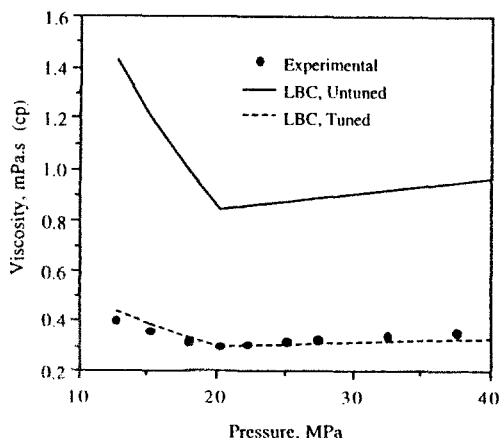


Figure 9.19. Comparison of predicted viscosity by LBC method with experimental data of a North Sea oil at 371 K.

#### Example 9.5.

Estimate the viscosity of a liquid mixture composed of  $C_1=59.30$ ,  $C_3=37.46$  and  $nC_8=3.24$  mole% at 311 K and 20.68 MPa. The liquid density at the above conditions is  $0.368 \text{ g/cm}^3$ . The measured viscosity is  $0.0510 \text{ mPa.s}$  ( $0.0510 \text{ cp}$ ).

#### Solution:

The properties of pure components are read from Table A.1 in Appendix A, with the critical pressure converted to atm (divided by 0.101325) and their viscosity is calculated from Eq.(9.27), as follows.

Comp.	x	M, g/gmol	$T_c$ , K	$P_c$ , atm	$v_c$ , $\text{cm}^3/\text{mol}$	$T_i$	$\lambda$	$\mu^0$ , mPa.s
C1	0.593	16.043	190.56	45.4	98.6	1.63203	0.04706	0.01134
C3	0.3746	44.096	369.83	41.9	200	0.84092	0.03343	0.00864
nC8	0.0324	114.231	568.7	24.6	486	0.54686	0.03186	0.00605

The mixture properties are then calculated using the mixing rules given in Eqs.(9.28-30).

Component	$x\mu^0 M^{0.5}$	$xM^{0.5}$	$xT_c$	$xM$	$xP_c$	$xv_c$
C1	0.02693	2.37519	113.00	9.513	26.915	58.47
C3	0.02150	2.48752	138.54	16.518	15.705	74.92
nC8	0.00210	0.34629	18.43	3.701	0.796	15.75
Total	0.05052	5.20900	269.97	29.733	43.417	149.14

The value of  $\mu^0$  for mixture is calculated from Eq.(9.28) to be  $0.0096992 \text{ mPa.s}$ . The value of  $\lambda$  for mixture is calculated from Eq.(9.29) to be  $0.0377423$ . The mixture reduced density is calculated from Eq.(9.30), as,

$$\rho_r = (0.368/29.733) \times 149.14 = 1.84583$$

Substituting the above values in Eq.(9.26) results in,  $\mu - \mu^0 = 0.037145$  mPa.s. Hence,

$$\mu = 0.04684 \text{ mPa.s}$$

The predicted value deviates by 8% from the measured viscosity.

### Implementation

Most reservoir simulators available today obtain solutions to fluid flow equations (non-linear partial differential equations) by replacing the derivatives with finite-difference approximations. The use of these approximations introduces truncation errors and numerical dispersion. The simulation results are, therefore, sensitive to the number of grid-blocks and time-step size used to model the slim tube displacement. These parameters should be selected so that the numerical dispersion becomes close to that of the physical dispersion in the tube.

The degree of slim tube packing homogeneity and the associated physical dispersion, can be identified by conducting miscible liquid-liquid displacement [47]. For any number of grid-blocks, the optimum time step, which yields the best match between the predicted and the experimental effluent profile, can be identified as shown in Figure 9.20. For the optimised grid size-time step, the numerical dispersion can be considered equivalent to the physical dispersion.

In the slim tube displacement the physical dispersion is generally small and can be assumed zero in most cases for homogeneous sand packs. The method proposed by Lantz [62] can be used to determine the optimum time step-grid block with zero dispersion, instead of conducting liquid-liquid displacement. For a typical slim tube, 100 grid blocks are generally needed to achieve a stable numerical solution. At conditions approaching miscibility, indicated by low IFT regions, more grid blocks are required due to sharp changes of fluid properties.

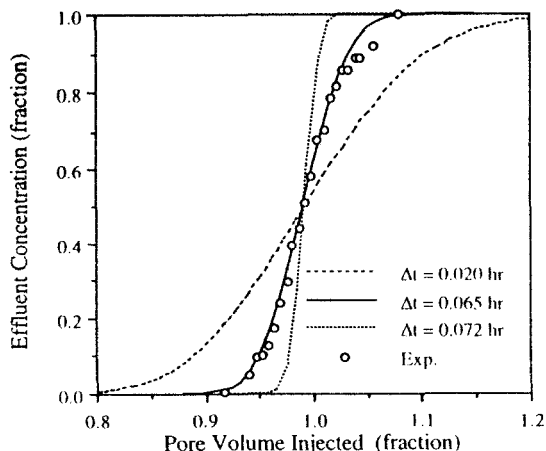


Figure 9.20. Variation of simulated effluent concentration profile with time step size in a slim tube modelled by 100 grid blocks.

The above approach was applied by Khazam et al.[47] to a liquid mixture of C1/C3/nC10 displaced by methane in a slim tube at two pressures of 13.79 and 20.68 MPa and temperature

of 311 K. The Peng-Robinson EOS was tuned to the vapour-liquid equilibrium experimental data of Sage and Berry [63] on the above ternary system and multiple forward contact test data [64], at the test temperature and pressure. The multiple contact test at 20.68 MPa indicated the achievement of miscibility. The tuned model matched the volumes of vapour and liquid phases in equilibrium tests with an average absolute deviation of about 3%, with the composition and density reliably predicted.

The tuned phase behaviour model was incorporated in a one-dimensional numerical model, along with measured relative permeability curves and the optimum grid-time step sizing, to predict the above. The simulated displacement results at 13.79 MPa are shown in Figure 9.21. The model tuned to the static data clearly is capable of predicting the dynamic experimental results. The results at 20.68 MPa were also quite reliable, demonstrating miscible displacement [64]. To indicate the sensitivity of displacement results to the phase behaviour model, the authors deliberately mistuned the model against the static data, which resulted in a significant deviation between the predicted and measured displacement data, particularly the gas break through and producing gas to oil ratio values.

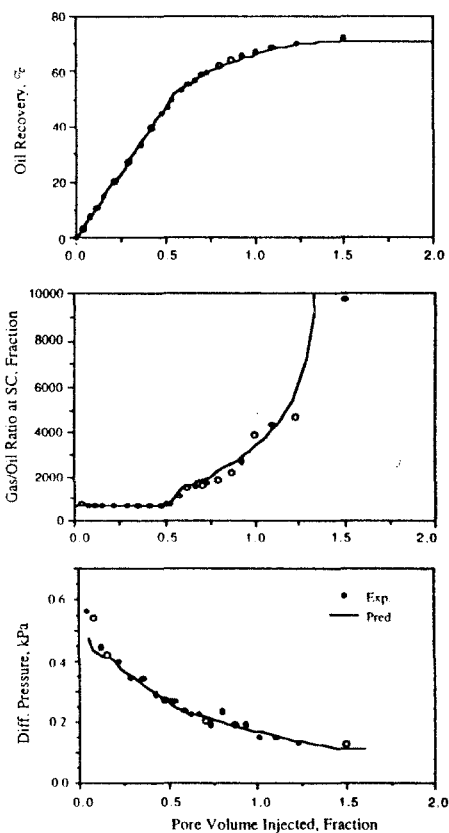


Figure 9.21. Measured and predicted displacement data.

The slim tube displacement data are certainly valuable for evaluating a tuned phase behaviour model which is to be used in reservoir simulation of gas injection. In immiscible displacement processes, however, tuning of the phase behaviour model to relevant static equilibrium data should generally suffice and there is very little need for relatively time consuming displacement tests. The swelling test, covering both sides of the critical point, will be highly useful to generate static data for miscible processes [12].

## 9.5 EVALUATION OF RESERVOIR FLUID SAMPLES

The collection of a sample that reliably represents the reservoir fluid is essential in any phase behaviour studies. After all, a model tuned to experimental data of a sample, with properties significantly different to those of the reservoir fluid, will be of little value in studying that reservoir. Challenges in obtaining representative samples from gas condensate and volatile oil reservoirs have been well acknowledged by those involved. Some of the key issues and pitfalls in fluid sampling were described in Section 2.1.

Any fluid produced from a reservoir should, in principle, provide valuable information on the reservoir fluid. However, it may not have the same composition and properties as the original reservoir fluid. The collected sample may have gone through certain unwanted processes, resulting in changes of its properties. If these processes can be reasonably identified, it may be possible to trace back the original fluid from the collected sample. Phase behaviour models can play an important role in helping the above task.

Evaluation and improvement of a collected sample generally benefit from a combined experimental and numerical modelling effort. Some processes, such as a single equilibrium flash, can be physically simulated by simple experiments. Phase behaviour models are required to simulate more demanding equilibrium tests. Processes occurring within the reservoir generally need to be modelled by a reservoir simulator.

The main source of error in sampling is the phase transition and collection of co-exiting fluids at an improper ratio. Reffstrup and Olsen [65] studied fluid compositional changes during surface sampling under non-ideal sampling conditions. They used a modified black oil simulator to produce from a low permeability lean gas condensate reservoir and an EOS model to simulate the recombination of separator samples. The authors showed that the dew point pressure of a wellstream (recombined sample) was lower than the initial dew point of reservoir, but higher than the bottom hole pressure. They recommended a method to back calculate the initial reservoir fluid composition by matching the initial reservoir dew point pressure. Fevang and Whitson [66] extended the Reffstrup and Olsen's method to cover other types of reservoirs. The authors conducted an extensive investigation of sampling from depleted reservoirs to determine the original reservoir fluid using compositional simulation. They proposed experimental methods to obtain the original fluid from collected samples, based on their simulation results. A key recommendation to obtain the original reservoir fluid in saturated reservoirs was to equilibrate the samples collected from the gas cap and the oil zone at the original reservoir gas-oil contact, pressure and temperature. The equilibrated oil and gas phases, then, represent the original reservoir fluid in oil and gas condensate reservoirs, respectively.

A main concern in surface sampling is the recombining proportion of the collected liquid and gas from the test separator. Any uncertainty in the measured gas to liquid ratio in the field directly affects the composition of recombined sample and its properties. Imperfect separation of the phases also causes either some liquid to be carried over with the gas from an upstream separator to the next (carryover) or some gas to be produced with the liquid (carry through), disturbing the produced gas to liquid ratio.

In a saturated reservoir, the saturation point of coexisting gas and oil phases should be equal to the reservoir temperature-pressure at the gas-oil contact. Hence, neglecting the compositional grading in space, it is expected that the measured bubble point of the oil sample, or the dew point of the gas sample, be close the above value. In practice, however, the compositional variations with depth and area are rarely negligible.

The bubble point pressure of oil is a monotonic function of the gas to liquid recombination proportion, i.e., the bubble point pressure increases with increasing gas to liquid ratio (GLR). Hence, it is a reasonable practice to ignore the measured GLR during oil sampling and take oil and gas samples from the separator and recombine them to achieve the target bubble point. The dew point pressure, however, may increase, decrease, or remain almost unchanged by increasing GLR, Figure 2.2. As the GLR-dew point pressure curve is dome-like shape in gas condensate mixtures, it is possible to obtain the same dew point pressure with two different GLR's.

The behaviour of a typical North Sea gas condensate, with a dew point of 31.94 MPa at 383 K, was simulated by flashing it at various pressures. The equilibrated gas and condensate phases were then recombined at different ratios at each pressure. Figure 9.22 shows the predicted dew point of the different recombined fluids. The results clearly show that the higher the separator pressure, the higher is the difference between the two recombination ratios which result in the same dew point. Therefore, it is less likely to select the wrong recombination ratio at high pressures when aiming to match the dew point.

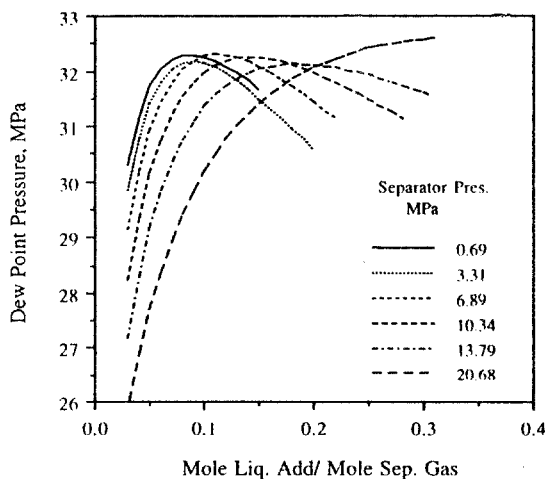


Figure 9.22. Predicted dew point pressure of recombined separator gas and liquid samples.

The plot also demonstrates that the dew point becomes less sensitive to the recombination ratio as the separator pressure increases. As the target dew point has a certain error band, the lack of sensitivity affects the recombination ratio markedly at high pressures. However, as the two phases at high pressures are more similar than at lower pressures, the effect of deviated gas to liquid ratio in recombination on the total fluid composition and its behaviour is less significant at higher pressures. If the separator pressure is equal to the saturation pressure, no condensate will form. Theoretically, if the condensate formed at the dew point is added to the saturated

gas, regardless of the phase ratio, the gas composition remains unchanged at the dew point pressure.

The predicted liquid drop out of the mixtures in the above exercise recombined at the atmospheric pressure, with a false GLR selected, is shown in Figure 9.23. The mixture clearly lacks the true behaviour of the reservoir fluid. The predicted results with -3% error in the target dew point pressure are also shown. Note that although the -3% error in dew point corresponds to a much higher deviation in the recombination ratio at the higher pressure (Figure 9.22), the results are more acceptable than those at the lower pressure.

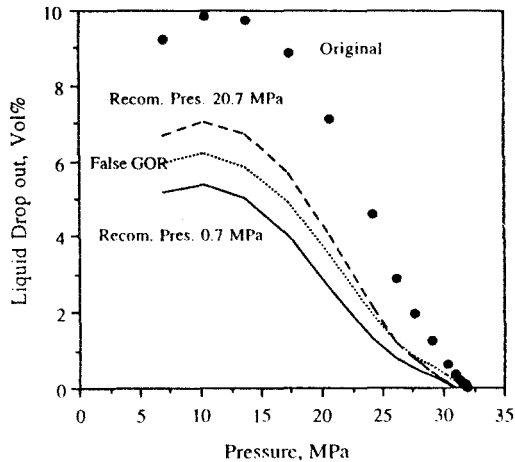


Figure 9.23. Predicted liquid drop out in constant composition test at 383 K for various recombined fluids.

The main impeding factor in collecting a representative fluid sample is the phase transition due to pressure reduction and the variable mobility of the phases within the reservoir. Some recommendations to alleviate the above problem were given in Section 2.1. A long flow period to stabilise the well and its drainage zone is often advocated. It was noted, however, that for a gas condensate reservoir a representative sample may be obtained during normal operation if a quasi-steady state zone around the producer can be achieved.

The condensate initially is formed around the wellbore, when the pressure falls below the dew point and the two phase region, referred to as the condensate ring, grows into the reservoir bulk by continual production, Figure 9.24. The condensate saturation at any location increases due to the local reduction of pressure and the inflow of rich gas towards the producer. The increase in condensate saturation increases the condensate relative permeability and decreases the relative permeability of the gas, Figure 9.17. This results in an increase of condensate to gas fractional flow out of that region as described by Eqs.(9.21-22). Hence, the condensate saturation increases only to the value which maintains the associated fractional flow. As the condensate accumulation diminishes, an approximate quasi steady state may be established in that region, with the overall composition of the outflow being the same as that flowing into the region. However, if the above argument was strictly valid throughout the two phase region, the region should not grow at all which is not the case. Nevertheless, it is a reasonable assumption for practical purposes.



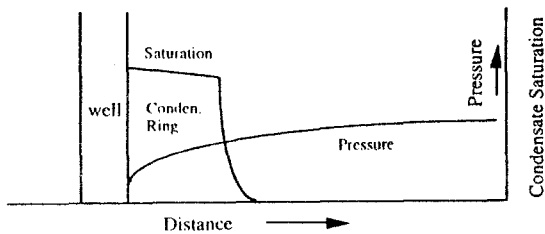


Figure 9.24. Gas-condensate distribution around a producer.

Figure 9.25 shows the growth of the two phase region by depletion as simulated numerically for a typical North Sea producer. The overall composition of the produced fluid with time is shown in Table 9.13. Note that the composition changes very little with time and it is almost the same as that of the original reservoir fluid, in spite of the significantly extended condensate ring. Hence collecting the produced fluid can provide a reasonable representative sample of the original single phase gas. If the rate is decreased to reduce the draw down, similar to the method used in oil sampling, the resulting pressure build-up not only vaporises the condensate into the gas phase, but also dumps some condensate into the well, as a lower condensate saturation is required to maintain the reduced condensate fractional flow. Both actions may lead to a sample much richer than the original reservoir fluid.

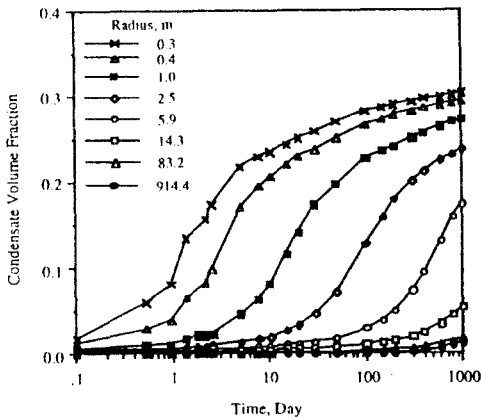


Figure 9.25. Growth of condensate ring with time for a typical North Sea producer.

The collected sample can be improved further when the reservoir gas dew point is known, using the conclusion obtained in the recombination exercise described in Figure 9.22, as follows. The two phase samples collected at the surface are recombined at the measured GLR to obtain the wellhead stream. The mixture is then brought to equilibrium at the average reservoir flowing pressure (or the bottom hole pressure) and temperature and the remaining liquid phase is removed. An adequate volume of the removed liquid is added back to the gas to match its dew point pressure to the initial reservoir value.

Table 9.13.  
Variations of produced fluid composition with time.

Comp., mole %	Original	1 day	10 days	100 days	1000 days
N2	1.024	1.026	1.026	1.026	1.029
CO2	2.088	2.089	2.089	2.089	2.090
C1	75.543	75.646	75.652	75.655	75.767
C2	7.375	7.373	7.373	7.373	7.372
C3	3.764	3.760	3.759	3.759	3.754
IC4	0.534	0.533	0.533	0.533	0.532
NC4	1.366	1.363	1.362	1.362	1.359
IC5	0.441	0.440	0.440	0.439	0.438
NC5	0.613	0.611	0.611	0.611	0.608
C6	0.832	0.828	0.828	0.828	0.823
C7	1.405	1.396	1.396	1.395	1.385
C8	1.400	1.389	1.389	1.388	1.377
C9	0.854	0.846	0.846	0.846	0.837
C10	0.541	0.535	0.535	0.535	0.528
C11	0.384	0.379	0.379	0.379	0.373
C12	0.296	0.292	0.292	0.292	0.287
C13	0.246	0.242	0.242	0.242	0.237
C14	0.306	0.300	0.300	0.300	0.293
C15	0.221	0.216	0.216	0.216	0.211
C16	0.160	0.156	0.156	0.156	0.152
C17	0.108	0.105	0.105	0.105	0.102
C18	0.095	0.092	0.092	0.092	0.089
C19	0.078	0.075	0.075	0.075	0.072
C20+	0.326	0.307	0.306	0.306	0.286

Figure 9.26 shows the predicted liquid drop-out from fluids prepared by recombining the collected separator gas and condensate after producing the reservoir for 1000 days in the above example. The wellhead fluid refers to the recombination based on the measured producing GLR. As expected it provides a leaner fluid compared with the original one, Table 9.13, due to loss of condensate within the reservoir. Applying the contact method, described above, provides very reliable results, when the dew point is accurately known. Ignoring the measured GLR during sampling and recombining the two phases at the low separator pressure conditions to match the dew point, results in a sample which is inferior to the wellstream sample. An error of 2% in dew point impairs the results for both adjusted fluids, with the contact method affected less severely.

Although matching the bubble point by adjusting the phase ratio during the recombination process is adequate to improve the oil sample in most cases, the contact method is the preferred option, particularly for volatile oils. In the contact method for oil all the remaining equilibrium gas is removed at constant pressure, then adequate volume of it is added back to the liquid to match the bubble point pressure.

It should be mentioned that if the recombined sample remained single phase at the contact pressure, most probably due to improper collected phase ratio at the surface, the contact pressure could be reduced to form two phases. Then the removed phase is added to a portion of the remaining phase to match the saturation pressure.

In this section the application of phase behaviour models in alleviating a number of impeding factors in fluid sampling was described. One can easily identify other problems associated

with fluid sampling, such as fluid contamination [67], which can be evaluated and rectified by applying phase behaviour models.

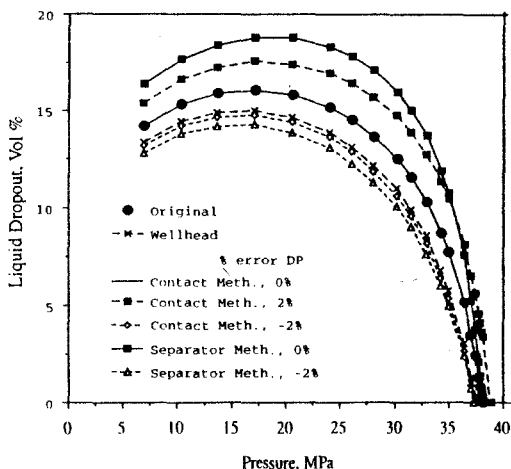


Figure 26. Predicted liquid drop-out of various samples in constant composition expansion test at 383 K.

## 9.6 REFERENCES

1. Coats, K.H: "Simulation of Gas Condensate Reservoir Performance", JPT, 1870-1886 (Oct., 1988).
2. Jacoby, R.H., Koeller, R.C. and Berry, U.J: "Effect of Composition and Temperature on Phase Behaviour and Depletion Performance of Rich Gas-Condensate Systems", Trans. AIME, 216, 406-411 (1959).
3. Lee, S.T., et al: "Experimental and Theoretical Studies on the Fluid Properties Required for Simulation of Thermal Processes", SPE J., 535-50, (Oct., 1981).
4. Hong, K.C: "Lumped-Component Characterisation of Crude Oils for Compositional Simulation", SPE/DOE 10691, presented at the 3rd Joint Symposium on EOR, Tulsa (1982).
5. Whitson, C.H: "Characterising Hydrocarbon Plus Fractions", SPE J., 683-694 (Aug., 1983).
6. Schlijper, A.G: "Simulation of Compositional Processes, the Use of Pseudocomponents in Equation of State Calculations", SPE/DOE 12633, presented at the SPE/DOE 4th Symposium on EOR, Tulsa (April, 1984).
7. Montel, F. and Gouel, P: "A New Lumping Scheme of Analytical Data for Composition Studies", SPE 13119, Proc. of 59th Ann. Conf. (Sept., 1984).
8. Behrens, R.A. and Sandler, S.I: "The Use of Semicontinuous Description to Model the  $C_7$  Fraction in Equation of State Calculations", SPE/DOE 14925, presented at the 5th Symposium on EOR, Tulsa (April., 1986).

9. Gonzalez, E., Colonomos, P. and Rusinek, I: "A New Approach for Characterising Oil Fractions and For Selecting Pseudocomponents of Hydrocarbons", JCPT, 78-84 (March-April, 1986).
10. Wu, R.S. and Batycky, J.P: "Pseudo-Component Characterisation for Hydrocarbon Miscible Displacement", SPE 15404, Proc. of 61st Ann. Conf. (Oct., 1986).
11. Li, Y-K., Nghiem, L.X. and Siu, A: "Phase Behaviour Computations for Reservoir Fluids: Effect of Pseudo-Components on Phase Diagrams and Simulation Results", JCPT, 29-36 (Nov.-Dec., 1988).
12. Newly, T.M.J. and Merrill Jr, R.C: "Pseudocomponent Selection for Compositional Simulation", SPE 19638, Proc. of 64th Ann. Conf. (Oct., 1989).
13. Danesh, A., Xu, D. and Todd, A.C: "A Grouping Method to Optimise Oil Description for Compositional Simulation of Gas Injection Processes", SPE Res.Eng., 343-348, (1992).
14. Cotterman, R.L. and Prausnitz, J.M: "Flash Calculations for Continuous or Semicontinuous Mixtures Using an Equation of State", I & EC Proc. Des. Dev., 24, 434-443 (1985).
15. Pedersen, K.S., Thomassen, P., Fredenslund, A.A: "Thermodynamics of Petroleum Mixtures Containing Heavy Hydrocarbons. 1. Phase Envelope Calculations by Use of the Soave-Redlich-Kwong Equation of State", Ind. Eng. Chem. Proc. Des. Dev., 23, 163 (1984).
16. Kesler, M.G. and Lee, B.I: "Improve Predictions of Enthalpy of Fractions", Hydro. Proc., 153-158 (March, 1976).
17. Lee, B.I. and Kesler, M.G: "Improve Vapour Pressure Prediction", Hydro. Proc., 163-167 (July, 1980).
18. Wilson, G: "A Modified Redlich-Kwong Equation of State, Application to General Physical Data Calculations", Paper 150, AIChE National Meeting, (May, 1968).
19. Ahmed, Y., Sugie, H. and Lu, B.C.Y: "Comparative Study of Eight Equations of State for Predicting Hydrocarbon Volumetric Phase Behaviour", SPE Res.Eng., 337-348, (Feb., 1988).
20. Firoozabadi, A: "Reservoir-Fluid Phase Behaviour and Volumetric Prediction with Equations of State", JPT, 40(4), 397-406 (1988).
21. Martin, J.J: "Cubic Equations of State - Which?", Ind. Eng. Chem. Fundam., 18(2), 81-97 (1979).
22. Danesh, A., Xu, D. and Todd, A.C: "Comparative Study of Cubic Equations of State for Predicting Phase Behaviour and Volumetric Properties of Injection Gas-Reservoir Oil Systems", J. Fluid Phase Equilibria, 63, 259-278 (1991).
23. Zudkevitch, D. and Joffe, E: "Correlation and Prediction of Vapour-Liquid Equilibria with the Redlich-Kwong Equation of State", AIChE, 16(1), 112 (1970).
24. Graboski, M.S. and Daubert, T.E: "A Modified Soave Equation of State For Phase Equilibrium Calculations. 1. Hydrocarbon Systems", Ind. Eng. Chem. Process Des. Dev., 17(4), 443-448 (1978).

25. Peneloux, A. and Rauzy, E: "A Consistent Correction for Redlich-Kwong-Soave Volumes", *J. Fluid Phase Equilibria*, 8, 7-23 (1982).
26. Robinson, D.B. and Peng, D.Y: "The Characterisation of the Heptanes and Heavier Fractions for the GPA Peng-Robinson Programs", GPA Research Report 28, Tulsa (1978).
27. Jhaveri, B.S. and Youngren, G.K: "Three-Parameter Modification of the Peng-Robinson Equation of State to Improve Volumetric Predictions", *SPE* 13118 (1984).
28. Schmidt, G. and Wenzel, H: "A Modified Van der Waals Type Equation of State", *Chem. Eng. Sci.*, 135, 1503-1512 (1980).
29. Patel, N.C. and Teja, A.S: "A New Cubic Equation of State for Fluids and Fluids Mixtures", *Chem. Eng. Sci.*, 77(3), 463-473 (1982).
30. Valderrama, J.O: "A Generalised Patel-Teja Equation of State for Polar and Non-Polar fluids and Their Mixtures", *J. Chem. Eng. Japan*, 23(1), 87-91 (1990).
31. "Condensate PVT Studies, 1989-1990, Final Report", Report No: PVT/91/1, Dept. of Pet. Engng., Heriot-Watt University (Jan., 1991).
32. Danesh, A., Xu, D. and Todd, A.C: "An Evaluation of Cubic Equations of State for Phase Behaviour Calculations Near Miscibility Conditions", *Proc. of the SPE/DOE 7th Symposium on EOR*, 915-924 (April, 1990).
33. Coats, K.H. and Smart, G.T: "Application of a Regression-Based EOS PVT Program to Laboratory Data", *SPE Res. Eng.*, 575-582 (Nov., 1986).
34. Watson, S.T. and Lee, W.J: "A New Algorithm for Automatic History Matching Production Data", *SPE* 15228 presented at the 1986 SPE Unconven. Gas Technology Symposium, (May, 1986).
35. Marquardt, D.W: "An Algorithm for Least Square Estimation of Non-linear Parameters", *J. Soc. Ind. Appl. Math.*, 11(2), 431-441 (1963).
36. Pedersen, K.S., Thomassen, P. and Fredenslund, A: "On the Dangers of "Tuning" Equation of State Parameters", *Chem. Eng. Sci.*, 43(2), 269-278 (1988).
37. Merrill, R.C. and Newly, T.M.J: "A Systematic Investigation into the Most Suitable Data for the Development of Equations of State for Petroleum Reservoir Fluids", *J. Fluid Phase Equilibria*, 82, 101-110 (1993).
38. "Reservoir Fluid Studies, 1990-1993 Final Report", Vol. 1, Report No: PVT/93/2, Dept. of Pet. Engng., Heriot-Watt University (July, 1993).
39. Merrill, R.C., Hartman, K.J. and Creek, J.L: "A Comparison of Equation of State Tuning Methods", *SPE* 28589, *Proc. of 69th Ann. Conf.* (Sept., 1994).
40. Hoffmann, A.E., Crump, J.S. and Hocott, C.R: "Equilibrium Constants for a Gas-Condensate System", *Trans. AIME*, 198, 1-10 (1953).
41. Agarwal, R.K., Li, Y.-K. and Nghiem, L: "A Regression Technique With Dynamic Parameter Selection for Phase-Behaviour Matching", *SPE Res.Eng.*, 115-119 (Feb., 1990).

42. Gani, R. and Fredenslund, A: "Thermodynamics of Petroleum Mixtures Containing Heavy Hydrocarbons: An Expert Tuning System", *Ind. Eng. Chem. Res.*, 26(7), 1304-1312 (1987).
43. Danesh A., Gozalpour, F., Todd, A.C. and Tehrani, D.H: "Reliable Tuning of Equation of State with No Binary Interaction Parameter", *Proceedings of the IEA Conference, Australia* (1996).
44. Danesh, A., Tehrani, D.H., Todd, A.C., Tohidi, B., Gozalpour, F., Malcolm, K., Reid, A., Bell, K., Elghayed, K. and Burgass, R: "Phase Behaviour And Properties Of Reservoir Fluids", *Proceedings of the UK DTI EOR Seminar, London, England, June 19-20* (1996).
45. Kossack, C.A. and Hagen, S: "The Simulation of Phase Behaviour and Slim Tube Displacements with Equation-of-State", paper SPE 14151 presented at the 60th SPE Annual Technical Conference and Exhibition, Las Vegas, NV, September 22-25 (1985).
46. Mansoori, J., Haag, G.L. and Bergman, D.F: "An Experimental and Modelling Study of the Miscibility Relationship and Displacement Behaviour for a Rich-Gas/Crude-Oil System", paper SPE 20521 presented at 65th Annual Technical Conference and Exhibition of the SPE, New Orleans, LA, September 23-26 (1990).
47. Khazam, M., Danesh, A., Tehrani, D.H. and Todd, A.C: "Dynamic Validation of Phase Behaviour Models for Reservoir Studies of Gas Injection Schemes", *Proceedings of the Society of Petroleum Engineers 69h Annual Conference, New Orleans, (Sep. 1994)*.
48. Bardon, C. and Longeron, D.G: "Influence of Very Low Interfacial Tension on Relative Permeability", *SPE J.*, 391-401, (Oct. 1980).
49. Nghiem, L.X., Fong, D.K. and Aziz, K: "Compositional Modelling with an Equation of State", *SPE J.*, 688-698, (Dec. 1981).
50. Coats, K.H: "An Equation of State Compositional Model", *SPE J.*, 363-376, (Oct. 1980).
51. Amaefule, J.O. and Handy, L.L: "The Effect of Interfacial Tensions on Relative Oil/Water Permeabilities of Consolidated Porous Media", *SPE J.*, 371-381, (June 1982).
52. Bette, S., Hartman, K.J. and Heinemann, R.F: "Compositional Modelling of Interfacial Tension Effects in Miscible Displacement Processes", *J. Pet. Sci. Eng.*, 6, 1-14, (1991).
53. Pedersen, K.S. and Fredenslund, A: "An Improved Corresponding States Model for Prediction of Oil and Gas Viscosities and Thermal Conductivities", *Chem. Eng. Sci.*, 42, 182-186, (1987).
54. Ely, J.F. and Hanley, H.J.M: "Prediction of Transport Properties. 1. Viscosity of Fluids and Mixtures", *I&EC Fund.*, 20, 323-332 (1981).
55. Aasberg-Petersen, K., Knudsen, K. and Fredenslund, A: "Prediction of Viscosities of Hydrocarbon Mixtures", *J. Fluid Phase Equilibria*, Vol. 70, 293-308, (1991).
56. Little, J.E. and Kennedy, H.T: "A Correlation of the Viscosity of Hydrocarbon Systems with Pressures, Temperature and Composition", *SPE J.*, 157-162, (Jun. 1968).

57. Wang, L. and Guo, T: "A Unified Viscosity Model for Hydrocarbon Gases and Liquids Based on Transposed Patel-Teja Equation of State", *Huagong Xuebao / Journal of Chemical Industry and Engineering (China)*, English Edition, Vol. 6, No. 1, 38-49 (1991).
58. Lohrenz, J., Bary, B.G. and Clark, C.R: "Calculating Viscosities of Reservoir fluids from Their Compositions", *JPT*, 1171-1176, (Oct. 1964).
59. Jossi, J.A., Stiel, L.I. and Thodos, G: "The Viscosity of Pure Substances in the Dense Gaseous and Liquid Phases", *AIChE J.*, 8, 59-63, (1962).
60. Herning, F. and Zipperer, L: "Calculation of the Viscosity of Technical Gas Mixtures from the Viscosity of Individual Gases", *Gas U. Wasserfach*, No. 49, (1936).
61. Dandekar, A., Danesh, A., Tehrani, D.H. and Todd, A.C: "A Modified Residual Viscosity Method for Improved Prediction of Dense Phase Viscosities", Presented at the 7th European Improved Oil Recovery (IOR) Symposium in Moscow, Russia, October 27-29, (1993).
62. Lantz, R.B: "Quantitative Evaluation of Numerical Diffusion (Truncation Error)," *SPE J.*, 315-20 (Sept. 1971).
63. Sage, B.H. and Berry, V.M: "Phase Equilibria in Hydrocarbon Systems", API Publication, (1971).
64. Khazam, M: "Application of Phase Behaviour and Flow Models to Gas Injection and Gas Condensate Recovery Processes", PhD Thesis, Heriot-Watt University, Edinburgh (1994).
65. Reffstrup, J. and Olsen, H: "Evaluation of PVT Data from Low Permeability Gas Condensate Reservoirs", *North Sea Oil and Gas Reservoirs - III*, 289-296, Kluwer Academic Press (1994).
66. Fevang, Ø. and Whitson, C.H: "Accurate Insitu Compositions in Petroleum Reservoirs", SPE 28829, Presented at the European Petroleum Conference, London, 25-27 October (1994).
67. MacMillan, D.J., Ginley, G.M. and Dembicki, Jr., H: "How to Obtain Reservoir Fluid Properties from an Oil Sample Contaminated with Synthetic Drilling Mud", SPE 38852, Presented at the 1997 SPE Annual Technical Conference and Exhibition, San Antonio, 5-8 October (1997).

## 9.7 EXERCISES

9.1. The reported composition of a reservoir oil is as follows:

Component	C1	C2	C3	iC4	nC4	iC5	nC5	C6	C7+
Oil, mole %	54.50	8.09	5.82	0.78	2.17	0.94	1.65	2.39	23.66
C7+ Properties: M=209 S=0.8323									

Describe the oil by three pseudo components for application in simulation of a lean gas injection process.

9.2. Estimate the viscosity of a gas mixture composed of 90 mol% C<sub>1</sub> and 10 mol% nC<sub>10</sub> at 377.5 K and 34.47 MPa. The measured viscosity is 0.052 mPa.s (cp).

9.3. Estimate the viscosity of the reservoir oil sample described in Exercise 2.1 at its bubble point using the LBC method.

9.4. The reservoir oil in Exercise 9.5 was flashed at the reservoir temperature of 373.0 K and pressure of 20.79 MPa. The oil was described by methane and two component groups, using the equal  $z_{lnM}$  method and molar averaged properties, as given in Example 9.3. The predicted results by a phase behaviour model, using the above fluid description, are given in the following table. Calculate the composition of equilibrated phases in terms of the original components.

Group/mole frac.	Oil	Gas
I (methane)	0.44611	0.79450
II	0.28748	0.20083
III	0.26641	0.00467

Liquid mole fraction=0.62975

9.5. The following set of experimental data is available on a volatile oil. Tune a phase behaviour model to the measured data, and compare the predictions of tuned and untuned models with the experimental results.

#### Compositional analysis of volatile oil.

Component	Mole%	Molecular Weight	Specific Gravity
C1	57.53		
C2	10.16		
C3	5.83		
i-C4	1.22		
nC4	2.06		
i-C5	1.01		
nC5	1.70		
C6	1.40	85	0.671
C7	2.16	96	0.726
C8	2.55	104	0.756
C9	2.00	116	0.776
C10	1.55	131	0.781
C11	1.10	148	0.791
C12	1.00	162	0.798
C13	0.99	175	0.813
C14	0.78	187	0.832
C15	0.85	201	0.831
C16	0.72	218	0.837
C17	0.49	229	0.828
C18	0.60	243	0.839
C19	0.51	260	0.847
C20+	3.81	419	0.903

#### Constant composition expansion tests at 373.1 K.

Pressure MPa	Relative Vol. ( $V/V_{sat}$ )	Liquid Vol. Frac. %
35.96	0.9954	
35.82	0.9958	
35.61	0.9970	
35.34	0.9978	
34.92	1.0000	100.00*
31.13	1.0394	83.66
27.68	1.0872	75.00
24.24	1.1508	68.14
20.79	1.2470	60.10
17.34	1.3948	52.54



13.89	1.6424	42.56
10.45	2.0934	31.57
7.00	2.9968	17.31

\* Saturated liquid with a density of 561 kg/m<sup>3</sup>.

Differential liberation test at 373.1 K.

Pressure MPa	R <sub>sd</sub> , Solution Gas/Oil Ratio	B <sub>od</sub> , Relative Oil Volume	B <sub>td</sub> , Relative Total Volume	Z, Liberated Gas Compressibility Factor	B <sub>g</sub> , Gas Formation Volume Factor
34.92	405	2.342	2.342		
33.54	356	2.168	2.368	1.040	0.00406
32.16	321	2.051	2.395	1.007	0.00410
30.44	286	1.940	2.429	0.956	0.00411
28.72	258	1.854	2.487	0.948	0.00433
26.30	230	1.759	2.554	0.916	0.00456
24.24	203	1.689	2.661	0.890	0.00481
21.48	177	1.622	2.787	0.838	0.00511
17.34	138	1.513	3.220	0.836	0.00639
13.89	111	1.441	3.767	0.839	0.00791
10.45	86	1.377	4.823	0.862	0.01082
7.00	64	1.329	7.112	0.907	0.01699
3.55	38	1.252	13.777	0.927	0.03422
1.83	25	1.212	27.571	0.969	0.06956
0.79	14	1.168	63.435	0.963	0.15944
0.1	0	1.076		1.000	

3.0352 grams of condensate was collected from the liberated gas at 288 K and 0.1 MPa of mercury pressure.

Separator test at 293.6 K.

Pressure MPa	Gas / Oil Ratio (1)	Formation Volume Factor (2)	Separator Volume Factor (3)
5.27	225		1.132
0.79	44		1.039
0.10	17		1.004
Total	286	1.764	

Density of the stock tank oil at 288 K = 810 kg/m<sup>3</sup>

- (1) Separator flashed gas volume (sc) per volume of stock tank oil.
- (2) Volume of saturated oil at 34.92 MPa and 373.1 K per volume of stock tank oil.
- (3) Volume of oil at separator pressure and temperature per volume of stock tank oil.

Forward contact experimental data with methane at 373.1 K and 35.26 MPa.

Stage No.	1		2		3		4	
Phase	Oil	Gas	Oil	Gas	Oil	Gas	Oil	Gas
Component	Mole%							
C <sub>1</sub>	57.87	78.24	57.03	74.46	57.10	72.25	56.73	71.47
C <sub>2</sub>	7.87	7.57	9.00	8.91	9.71	9.72	10.01	10.00
C <sub>3</sub>	4.89	4.04	5.40	4.69	5.69	5.06	5.80	5.22
i-C <sub>4</sub>	1.06	0.79	1.15	0.92	1.19	0.99	1.21	1.02
nC <sub>4</sub>	1.85	1.28	1.98	1.49	2.03	1.60	2.06	1.65

i-C <sub>5</sub>	0.95	0.59	0.99	0.69	1.01	0.74	1.02	0.76
nC <sub>5</sub>	1.62	0.97	1.68	1.12	1.70	1.20	1.72	1.24
C <sub>6</sub>	1.41	0.75	1.41	0.85	1.41	0.92	1.42	0.95
C <sub>7</sub>	2.26	1.04	2.32	1.23	2.27	1.33	2.27	1.36
C <sub>8</sub>	2.76	1.12	2.65	1.26	2.55	1.36	2.58	1.42
C <sub>9</sub>	2.23	0.82	2.19	0.98	2.11	1.05	2.11	1.08
C <sub>10</sub>	1.69	0.58	1.66	0.69	1.52	0.77	1.47	0.74
C <sub>11</sub>	1.36	0.36	1.30	0.41	1.16	0.51	1.18	0.54
C <sub>12</sub>	1.14	0.33	1.07	0.41	1.09	0.39	1.08	0.41
C <sub>13</sub>	1.19	0.29	1.10	0.36	1.05	0.47	1.03	0.40
C <sub>14</sub>	0.96	0.23	0.87	0.27	0.81	0.22	0.82	0.31
C <sub>15</sub>	1.05	0.23	0.97	0.28	0.92	0.31	0.90	0.32
C <sub>16</sub>	0.86	0.18	0.74	0.21	0.76	0.24	0.75	0.25
C <sub>17</sub>	0.66	0.11	0.63	0.15	0.54	0.16	0.54	0.16
C <sub>18</sub>	0.76	0.13	0.67	0.16	0.65	0.18	0.64	0.19
C <sub>19</sub>	0.65	0.10	0.61	0.13	0.56	0.15	0.55	0.15
C <sub>20+</sub>	4.92	0.26	4.57	0.33	4.17	0.38	4.13	0.39
V <sub>add</sub> , cm <sup>3</sup>	90.00*	22.50**	40.52*	90.00	22.50*	25.00	50.00*	20.00
V <sub>equi</sub> , cm <sup>3</sup>	67.98	43.71	34.39	67.98	43.71	27.77	48.96	20.92
ρ <sub>e</sub> , kg/m <sup>3</sup>	604.3	312.0	580.9	604.3	312.0	350.5	564.8	358.5

\* Volume of fresh oil contacted with a density of 563 kg/m<sup>3</sup>.

\*\* Volume of methane contacted at 35.26 MPa.

## APPENDICES

<b>Appendix A: Tables</b>	<b>Page Number</b>
A.1 Properties of Pure Compounds	354
A.2 Properties of Single Carbon Number Groups	356
A.3 Universal Gas Constant	357
A.4 Binary Interaction Parameters	358
A.5 Conversion Factors	363
 <b>Appendix B: Critical Property Correlations in Field Units</b>	 364
 <b>Appendix C: Equation of State Expressions</b>	 368
 <b>Appendix D: Equilibrium Ratios</b>	 372

Equilibrium Ratio Charts at 5000 psia (34.47 MPa) Convergence Pressure  
GPA Copyright. Reproduced with permission from: "SI Engineering Data Book" (1980).

Table A.1.  
Properties of pure compounds.

Name	MW kg/kgmol	T <sub>b</sub> K	T <sub>c</sub> K	P <sub>c</sub> MPa	v <sub>c</sub> m <sup>3</sup> /kgmol	Z <sub>c</sub>	acentric factor	Rackett Z <sub>RA</sub>	parachor **	Sp.Gr.
Methane	16.043	111.66	190.56	4.599	0.0986	0.2862	0.0115	0.28941	74.05	0.3000
Ethane	30.070	184.55	305.32	4.872	0.1455	0.2793	0.0995	0.28128	112.91	0.3562
Propane	44.096	231.11	369.83	4.248	0.2000	0.2763	0.1523	0.27664	154.03	0.5070
i-Butane	58.123	261.43	408.14	3.648	0.2627	0.2824	0.1770	0.27569	185.32	0.5629
n-Butane	58.123	272.65	425.12	3.796	0.2550	0.2739	0.2002	0.27331	193.90	0.5840
i-Pentane	72.150	300.99	460.43	3.381	0.3058	0.2701	0.2275	0.2706*	229.37	0.6247
Neopentane	72.150	282.65	433.78	3.199	0.3036	0.2693	0.1964	0.27570	236.00	0.5974
n-Pentane	72.150	309.22	469.7	3.370	0.3130	0.2701	0.2515	0.26853	236.00	0.6311
2-Methylpentane	86.177	333.41	497.5	3.010	0.3664	0.2666	0.2781	0.2662*	269.15	0.6578
n-Hexane	86.177	341.88	507.6	3.025	0.371	0.2659	0.3013	0.26355	276.71	0.6638
n-Heptane	100.204	371.58	540.2	2.740	0.428	0.2611	0.3495	0.26074	318.44	0.6882
n-Octane	114.231	398.83	568.7	2.490	0.486	0.2559	0.3996	0.25678	359.33	0.7070
n-Nonane	128.258	423.97	594.6	2.290	0.544	0.2520	0.4435	0.25456	399.57	0.7219
n-Decane	142.285	447.3	617.7	2.110	0.600	0.2465	0.4923	0.25074	440.69	0.7342
n-Undecane	156.312	469.08	639	1.949	0.659	0.2419	0.5303	0.24990	482.00	0.7445
n-Dodecane	170.338	489.47	658	1.820	0.716	0.2382	0.5764	0.24692	522.26	0.7527
n-Tridecane	184.365	508.62	675	1.680	0.775	0.2320	0.6174	0.24698	563.77	0.7617
n-Tetradecane	198.392	526.73	693	1.570	0.830	0.2262	0.6430	0.24322	606.05	0.7633
n-Pentadecane	212.419	543.83	708	1.480	0.889	0.2235	0.6863	0.2303*	647.43	0.7722
n-Hexadecane	226.446	560.01	723	1.400	0.944	0.2199	0.7174	0.2276*	688.50	0.7772
n-Heptadecane	240.473	575.3	736	1.340	1.000	0.2190	0.7697	0.23431	730.05	0.7797
n-Octadecane	254.500	589.86	747	1.270	1.060	0.2168	0.8114	0.22917	771.95	0.7820
n-Nonadecane	268.527	603.05	758	1.210	1.120	0.2150	0.8522	0.2158*	813.85	0.7869
n-Eicosane	282.553	616.93	768	1.160	1.170	0.2126	0.9069	0.22811	853.67	0.7924
n-Heneicosane	296.580	629.7	781.7	1.147	1.198	0.2114	0.9220	0.2097*	897.64	0.7954
n-Docosane	310.610	641.8	791.8	1.101	1.253	0.2095	0.9550	0.2068*	939.55	0.7981
n-Tricosane	324.630	653.4	801.3	1.059	1.307	0.2078	0.9890	0.2038*	981.43	0.8004
n-Tetracosane	338.680	664.4	810.4	1.019	1.362	0.2061	1.0190	0.2011*	1023.40	0.8025

\* Z<sub>RA</sub> from [1.15] except those identified by \* which are calculated from the Yamada-Gunn correlation, Eq.(1.13).

\*\* Parachor values are to be used only in Eq.(8.21).

Table A.1 (Cont.).  
Properties of pure compounds.

Name	MW kg/kgmol	T <sub>b</sub> K	T <sub>i</sub> K	P <sub>c</sub> MPa	v <sub>c</sub> m <sup>3</sup> /kgmol	Z <sub>c</sub>	acentric factor	Rackett parachor Z <sub>RA</sub>	parachor **	Sp.Gr.
Ethylene	28.054	169.47	282.36	5.032	0.1291	0.2767	0.0852	0.28054	101.53	0.5000
Propylene	42.081	225.43	364.76	4.612	0.1810	0.2753	0.1424	0.27821	143.02	0.5210
1-Butene	56.107	266.9	419.59	4.020	0.2399	0.2765	0.1867	0.27351		0.6005
cis-2-Butene	56.107	276.87	435.58	4.206	0.2340	0.2717	0.2030	0.27044		0.6286
trans-2-Butene	56.107	274.03	428.63	4.103	0.2382	0.2742	0.2182	0.27212		0.6112
Propadiene	40.065	238.65	393.15	5.470	0.1620	0.2711	0.1596	0.27283		0.5997
1,2-Butadiene	54.092	284	444	4.500	0.2190	0.2670	0.2509	0.2685*		0.6576
1,3-Butadiene	54.092	268.74	425.37	4.330	0.2208	0.2704	0.1932	0.27130		0.6273
1-Pentene	70.134	303.11	464.78	3.529	0.2960	0.2703	0.2329	0.27035		0.6458
cis-2-Pentene	70.134	310.08	475.93	3.654	0.3021	0.2790	0.2406	0.2694*		0.6598
trans-2-Pentene	70.134	309.49	475.37	3.654	0.3021	0.2793	0.2373	0.2697*		0.6524
2-Methyl-1-Butene	70.134	304.3	465	3.400	0.2920	0.2568	0.2287	0.2705*		0.6563
3-Methyl-1-Butene	70.134	293.21	450.37	3.516	0.3021	0.2837	0.2286	0.2705*		0.6322
2-Methyl-2-Butene	70.134	311.71	471	3.400	0.2920	0.2535	0.2767	0.2663*		0.6683
1-Hexene	84.161	336.63	504.03	3.140	0.3540	0.2653	0.2800	0.2660*		0.6769
1-Heptene	98.188	366.79	537.29	2.830	0.4130	0.2616	0.3310	0.2615*		0.7015
Cyclopentane	70.134	322.4	511.76	4.502	0.2583	0.2733	0.1943	0.26824	210.05	0.7603
Methylcyclopentane	84.161	344.96	532.79	3.784	0.3189	0.2725	0.2302	0.2704*		0.7540
Cyclohexane	84.161	353.87	553.54	4.075	0.3079	0.2726	0.2118	0.27286	247.89	0.7835
Methylcyclohexane	98.188	374.08	572.19	3.471	0.3680	0.2685	0.2350	0.26986	289.00	0.7748
Ethylcyclopentane	98.188	376.62	569.52	3.397	0.3745	0.2687	0.2715	0.2667*		0.7712
Ethylcyclohexane	112.215	404.95	609.15	3.040	0.4500	0.2701	0.2455	0.2690*	328.74	0.7921
Benzene	78.114	353.24	562.16	4.898	0.2589	0.2714	0.2108	0.26967	210.96	0.8829
Toluene	92.141	383.78	591.79	4.109	0.3158	0.2637	0.2641	0.2639*	252.33	0.8743
Ethylbenzene	106.167	409.35	617.17	3.609	0.3738	0.2629	0.3036	0.26186	292.27	0.8744
o-Xylene	106.167	417.58	630.37	3.734	0.3692	0.2630	0.3127	0.2620*		0.8849
m-Xylene	106.167	412.27	617.05	3.541	0.3758	0.2594	0.3260	0.2620*		0.8694
p-Xylene	106.167	411.51	616.26	3.511	0.3791	0.2598	0.3259	0.2870*		0.8666
Nitrogen	28.014	77.35	126.1	3.394	0.0901	0.2917	0.0403	0.28971	61.12	0.8094
Oxygen	31.999	90.17	154.58	5.043	0.0734	0.2880	0.0218	0.28962		1.1421
Carbon Monoxide	28.010	81.7	132.92	3.499	0.0931	0.2948	0.0663	0.28966		
Carbon Dioxide	44.010	194.67	304.19	7.382	0.0940	0.2744	0.2276	0.27275	82.00	0.8180
Hydrogen Sulphide	34.082	212.8	373.53	8.963	0.0985	0.2843	0.0827	0.28476	85.50	0.8014
Sulphur Dioxide	64.065	263.13	430.75	7.884	0.1220	0.2686	0.2451	0.26729		1.3946
Hydrogen	2.016	20.39	33.18	1.313	0.0642	0.3053	-0.2150	0.31997		
Water	18.015	373.15	647.13	22.055	0.0560	0.2294	0.3449			1.0000

\* Z<sub>RA</sub> from [1.15] except those identified by \* which are calculated from the Yamada-Gunn correlation, Eq.(1.13).

\*\* Parachor values are to be used only in Eq.(8.21).

Table A.2.  
Generalised single carbon number group properties.

SCN	MW	T <sub>b</sub> K	Sp.Gr.	T <sub>c</sub> K	P <sub>c</sub> MPa	v <sub>c</sub> m <sup>3</sup> /kgmol	Z <sub>c</sub>	Acent. Fact.	Rackett Z <sub>RA</sub>
C6	84	337	0.690	510	3.271	0.348	0.268	0.251	0.269
C7	96	366	0.727	547	3.071	0.392	0.265	0.280	0.266
C8	107	390	0.749	574	2.877	0.433	0.261	0.312	0.263
C9	121	416	0.768	603	2.665	0.484	0.257	0.352	0.260
C10	134	439	0.782	627	2.481	0.532	0.253	0.389	0.256
C11	147	461	0.793	649	2.310	0.584	0.250	0.429	0.253
C12	161	482	0.804	670	2.165	0.635	0.247	0.467	0.250
C13	175	501	0.815	689	2.054	0.681	0.244	0.501	0.247
C14	190	520	0.826	708	1.953	0.727	0.241	0.536	0.244
C15	206	539	0.836	727	1.853	0.777	0.238	0.571	0.240
C16	222	557	0.843	743	1.752	0.830	0.235	0.610	0.237
C17	237	573	0.851	758	1.679	0.874	0.233	0.643	0.234
C18	251	586	0.856	770	1.614	0.915	0.231	0.672	0.232
C19	263	598	0.861	781	1.559	0.951	0.229	0.698	0.229
C20	275	612	0.866	793	1.495	0.997	0.226	0.732	0.226
C21	291	624	0.871	804	1.446	1.034	0.224	0.759	0.224
C22	300	637	0.876	815	1.393	1.077	0.221	0.789	0.221
C23	312	648	0.881	825	1.356	1.110	0.220	0.815	0.219
C24	324	659	0.885	834	1.314	1.147	0.217	0.841	0.217
C25	337	671	0.888	844	1.263	1.193	0.215	0.874	0.214
C26	349	681	0.892	853	1.230	1.226	0.213	0.897	0.212
C27	360	691	0.896	862	1.200	1.259	0.211	0.944	0.200
C28	372	701	0.899	870	1.164	1.296	0.209	0.968	0.198
C29	382	709	0.902	877	1.140	1.323	0.207	0.985	0.196
C30	394	719	0.905	885	1.107	1.361	0.205	1.008	0.194
C31	404	728	0.909	893	1.085	1.389	0.203	1.026	0.193
C32	415	737	0.912	901	1.060	1.421	0.201	1.046	0.191
C33	426	745	0.915	907	1.039	1.448	0.199	1.063	0.189
C34	437	753	0.917	914	1.013	1.480	0.197	1.082	0.188
C35	445	760	0.920	920	0.998	1.502	0.196	1.095	0.187
C36	456	768	0.922	926	0.974	1.534	0.194	1.114	0.185
C37	464	774	0.925	932	0.964	1.550	0.193	1.124	0.184
C38	475	782	0.927	938	0.941	1.583	0.191	1.142	0.182
C39	484	788	0.929	943	0.927	1.604	0.190	1.154	0.181
C40	495	796	0.931	950	0.905	1.636	0.188	1.172	0.180
C41	502	801	0.933	954	0.896	1.652	0.187	1.181	0.179
C42	512	807	0.934	959	0.877	1.680	0.185	1.195	0.178
C43	521	813	0.936	964	0.864	1.701	0.184	1.207	0.177
C44	531	821	0.938	970	0.844	1.733	0.181	1.224	0.175
C45	539	826	0.940	974	0.835	1.749	0.180	1.232	0.174

T<sub>c</sub>, P<sub>c</sub>, and v<sub>c</sub>: Calculated from Two correlations, Eqs.(6.23-25).

Z<sub>c</sub>: Calculated from  $P_c v_c = Z_c R T_c$ .

Acentric factor: Calculated from the Lee-Kesler correlation, Eqs.(6.9-10).

Z<sub>RA</sub>: Calculated from the Yamada-Gunn correlation, Eq.(1.13).

Table A.2 (Cont.).

Generalised single carbon number group properties.

Ahmed's Correlation\*:

$$\theta = A_1 + A_2(C_n) + A_3(C_n)^2 + A_4(C_n)^3 + A_5/(C_n)$$

where,

 $\theta$  : Any physical property $C_n$  : Carbon group number

with constants as follows:

$\theta$	$A_1$	$A_2$	$A_3$	$A_4$	$A_5$
M	-131.11375	24.96156	-0.34079022	2.4941184 E-3	468.32575
$T_b$ , °R	434.38878	50.125279	-0.9027283	7.0280657 E-3	-601.85651
S	0.86714949	3.4143408 E-3	-2.839627 E-5	2.4943308 E-8	-1.1627984
$\omega$	-0.50862704	8.700211 E-2	-1.8484814 E-5	1.4663890 E-5	1.8518106
$T_c$ , °R	915.53747	41.421337	-0.7586859	5.8675351 E-3	-1.3028779 E3
$P_c$ , psia	275.56275	-12.522269	0.29926384	-2.8452129 E-3	1.7117226 E3
$v_c$ , ft <sup>3</sup> /lb	5.223458 E-2	7.8709139 E-4	-1.9324432 E-5	1.7547264 E-7	4.4017952 E-2

The correlation gives the calculated critical properties by Whitson using the Riazi-Daubert correlation, Eq.(6.14), and not those given in Table A.2.

\* Ahmed, T: "Hydrocarbon Phase Behaviour", Gulf Publishing Company, Houston (1989).

Table A.3.

Universal gas constant values.

P, Pressure	T, Temperature	$v$ , Mol. Vol.	R
atm	K	cm <sup>3</sup> /gmol	82.0567
bar	K	lit/gmol	0.083144
MPa	K	m <sup>3</sup> /kgmol	0.0083144
psia	°R	ft <sup>3</sup> /lbmol	10.732

Table A.4.1.

Binary interaction parameters for Zudkevitch-Joffe-Redlich-Kwong equation of state.

No.	Component	1	2	3	4	5	6	7	8	9	10-24
1	N <sub>2</sub>	.0000									
2	CO <sub>2</sub>	.0600	.0000								
3	C <sub>1</sub>	.0280	.0760	.0000							
4	Ethylene	.1000	.1000	.0000	.0000						
5	C <sub>2</sub>	.0610	.1090	-.0030	.0000	.0000					
6	Propylene	.1000	.1300	.0060	.0000	.0020	.0000				
7	C <sub>3</sub>	.1240	.1370	.0050	.0000	.0010	.0000	.0000			
8	iC <sub>4</sub>	.1200	.1300	.0190	.0000	.0040	.0005	.0000	.0000		
9	nC <sub>4</sub>	.1690	.1300	.0230	.0000	.0090	.0006	.0100	.0000	.0000	
10	iC <sub>5</sub>	.1600	.1000	.0230	.0100	.0380	.0010	.0060	.0000	.0000	.0000
11	Neopentane	.1600	.1000	.0190	.0100	.0350	.0010	.0004	.0000	.0000	.0000
12	nC <sub>5</sub>	.1870	.1000	.0190	.0100	.0185	.0000	.0000	.0000	.0000	.0000
13	nC <sub>6</sub>	.1900	.1000	.0300	.0100	.0380	.0000	.0000	.0000	.0300	.0000
14	Met Cyc Pent	.1900	.1000	.0130	.0100	.0100	.0000	.0000	.0000	.0000	.0000
15	Cyc Hex	.1900	.1000	.0130	.0100	.0100	.0000	.0000	.0000	.0000	.0000
16	nC <sub>7</sub>	.1900	.1000	.0130	.0100	.0100	.0000	.0000	.0000	.0000	.0000
17	Met Cyc Hex	.1900	.1000	.0200	.0100	.0100	.0000	.0000	.0000	.0000	.0000
18	Toluene	.1900	.1000	.0200	.0100	.0100	.0000	.0000	.0000	.0000	.0000
19	o-Xylene	.1900	.1000	.0270	.0100	.0200	.0400	.0400	.0350	.0300	.0000
20	nC <sub>8</sub>	.1900	.1000	.0150	.0100	.0100	.0000	.0000	.0000	.0000	.0000
21	nC <sub>9</sub>	.1900	.1000	.0150	.0100	.0100	.0000	.0000	.0000	.0220	.0000
22	nC <sub>10</sub> -nC <sub>14</sub>	.1900	.1000	.0100	.0060	.0080	.0000	.0000	.0000	.0000	.0000
23	nC <sub>15</sub> -nC <sub>19</sub>	.1900	.1000	.0100	.0080	.0000	.0000	.0000	.0000	.0000	.0000
24	nC <sub>20</sub> -nC <sub>24</sub>	.1900	.1000	.0000	.0000	.0000	.0000	.0000	.0000	.0000	.0000

From: Yarborough, L. : "Applications of a Generalized Equation of State to Petroleum Reservoir Fluids", Equations of State in Engineering, Advances in Chemistry Series, Edited by K. C. Chao and Robinson, R. L., American Chemical Society, Washington, DC, 182, page 385-435(1979).



Table A.4.2.  
Binary interaction parameters for Soave-Redlich-Kwong equation of state.

No.	Component	1	2	3	4	5	6	7	8	9	10-24
1	N <sub>2</sub>	.0000									
2	CO <sub>2</sub>	.0000	.0000								
3	C <sub>1</sub>	.0278	.1107	.0000							
4	Ethylene	.0300	.1000	.0189	.0000						
5	C <sub>2</sub>	.0407	.1363	-.0078	.0026	.0000					
6	Propylene	.0800	.1000	.0289	.0000	.0200	.0000				
7	C <sub>3</sub>	.0763	.1000	.0080	.0080	-.0220	.0033	.0000			
8	iC <sub>4</sub>	.0944	.1000	.0241	.0900	-.0010	-.0144	-.010	.0000		
9	nC <sub>4</sub>	.0700	.1000	.0056	.1000	.0067	.0000	.0000	.0000	.0000	
10	iC <sub>5</sub>	.0867	.1000	-.0078	.0120	.0050	.0000	.0078	.0000	.0000	.0000
11	Neopentane	.0870	.1000	-.0078	.0120	.0050	.0000	.0078	.0000	.0000	.0000
12	nC <sub>5</sub>	.0878	.1000	.0019	.0120	.0056	.0050	.0230	-.0300	.0204	.0000
13	nC <sub>6</sub>	.1400	.1000	.0374	.0140	-.0156	.0050	-.0022	.0000	-.0111	.0000
14	Met Cyc Pent	.1400	.1000	.0400	.0140	.0330	.0050	.0030	.0000	.0000	.0000
15	Cyc Hex	.1400	.1000	.0333	.0150	.0230	.0050	.0030	.0005	.0000	.0000
16	nC <sub>7</sub>	.1422	.1000	.0307	.0144	.0411	.0100	.0044	.0005	.0000	.0000
17	Met Cyc Hex	.1450	.1000	.0500	.0150	.0230	.0100	.0050	.0005	.0000	.0000
18	Toluene	.1500	.1000	.0978	.0300	.0900	.0300	.0300	.0200	.0100	.0000
19	o-Xylene	.1500	.1000	.1000	.0250	.0500	.0300	.0300	.0200	.0100	.0000
20	nC <sub>8</sub>	.1500	.1000	.0448	.0200	.0170	.0100	.0040	.0015	.0000	.0000
21	nC <sub>9</sub>	.1500	.1000	.0448	.0200	.0170	.0100	.0040	.0015	.0000	.0000
22	nC <sub>10</sub> -nC <sub>14</sub>	.1500	.1000	.0550	.0300	.0200	.0150	.0040	.0020	.0010	.0000
23	nC <sub>15</sub> -nC <sub>19</sub>	.1500	.1000	.0600	.0400	.0350	.0250	.0005	.0025	.0010	.0000
24	nC <sub>20</sub> -nC <sub>24</sub>	.1500	.1000	.0650	.0450	.0400	.0300	.0010	.0050	.0015	.0000

From: Knapp, H. and Doring, R.: "Vapour-Liquid Equilibria for Mixtures of Low Boiling Substances",  
Berhens, D. and Eckerman R., Eds(Dechema Chemistry Data Ser.), Part I- Binary System (1986).

Table A.4.3.  
Binary interaction parameters for Peng-Robinson equation of state.

No.	Component	1	2	3	4	5	6	7	8	9	10-24
1	N <sub>2</sub>	.0000									
2	CO <sub>2</sub>	.0000	.0000								
3	C <sub>1</sub>	.0311	.1070	.0000							
4	Ethylene	.0500	.1200	.0215	.0000						
5	C <sub>2</sub>	.0515	.1322	.0026	.0089	.0000					
6	Propylene	.0600	.1300	.0330	.0000	.0089	.0000				
7	C <sub>3</sub>	.0852	.1241	.0140	.0100	.0011	.0100	.0000			
8	iC <sub>4</sub>	.1000	.1400	.0256	.0200	-.0067	.0080	-.0078	.000		
9	nC <sub>4</sub>	.0711	.1333	.0133	.0200	.0096	.0080	.0033	.0000	.0000	
10	iC <sub>5</sub>	.1000	.1400	-.0056	.0250	.0080	.0080	.0111	-.004	.0170	.0000
11	Neopentane	.1000	.1400	-.0056	.0250	.0080	.0080	.0111	-.0040	.0170	.0000
12	nC <sub>5</sub>	.1000	.1400	.0236	.0250	.0078	.0100	.0120	.0020	.0170	.0000
13	nC <sub>6</sub>	.1496	.1450	.0422	.0300	.0140	.0110	.0267	.0240	.0174	.0000
14	Met Cyc Pent	.1500	.1450	.0450	.0310	.0141	.0120	.0270	.0242	.0180	.0000
15	Cyc Hex	.1500	.1450	.0450	.0310	.0141	.0120	.0270	.0242	.0180	.0000
16	nC <sub>7</sub>	.1441	.1450	.0352	.0300	.0150	.0140	.0560	.0250	.0190	.0000
17	Met Cyc Hex	.1500	.1450	.0450	.0300	.0160	.0150	.0580	.0250	.0200	.0000
18	Toluene	.1700	.1800	.0600	.0400	.0200	.0210	.0600	.0300	.0110	.0000
19	o-Xylene	.1500	.1400	.0470	.0300	.0160	.0150	.0590	.0260	.0120	.0000
20	nC <sub>8</sub>	.1500	.1400	.0470	.0300	.0160	.0150	.0590	.0260	.0120	.0000
21	nC <sub>9</sub>	.1550	.0145	.0474	.0400	.0190	.0200	.0070	.0060	.0100	.0000
22	nC <sub>10</sub> -nC <sub>14</sub>	.1550	.0145	.0500	.0450	.0300	.0250	.0200	.0100	.0010	.0000
23	nC <sub>15</sub> -nC <sub>19</sub>	.1550	.0145	.0600	.0500	.0400	.0300	.0250	.0150	.0010	.0000
24	nC <sub>20</sub> -nC <sub>24</sub>	.1550	.0145	.0700	.0600	.0500	.0350	.0300	.0200	.0015	.0000

From: Knapp, H. and Doring, R.: "Vapor-Liquid Equilibria for Mixtures of Low Boiling Substances",  
Berhens, D. and Eckerman R., Eds(Dechema Chemistry Data Ser.), Part I- Binary System (1986).

Table A.4.4.  
Binary interaction parameters for Patel-Teja equation of state.

No.	Component	1	2	3	4	5	6	7	8	9	10-24
1	N <sub>2</sub>	.0000									
2	CO <sub>2</sub>	.0600	.0000								
3	C <sub>1</sub>	.0320	.0930	.0000							
4	Ethylene	.0400	.1100	.0080	.0000						
5	C <sub>2</sub>	.0600	.1280	.0050	.0010	.0000					
6	Propylene	.0800	.1300	.0090	.0200	.0050	.0000				
7	C <sub>3</sub>	.0740	.1280	.0040	.0300	.0002	.0000	.0000			
8	iC <sub>4</sub>	.0540	.1270	.0020	.0300	.0010	.0005	.0000	.000		
9	nC <sub>4</sub>	.0310	.1150	.0020	.0300	.0010	.0006	.0100	.0000	.0000	
10	iC <sub>5</sub>	.0110	.1250	.0100	.0300	.0010	.0010	.0060	.0000	.0000	.0000
11	Ncopentane	.0110	.1000	.0100	.0400	.0010	.0010	.0004	.0000	.0000	.0000
12	nC <sub>5</sub>	.0000	.1350	.0100	.0400	.0000	.0000	.0000	.0000	.0000	.0000
13	nC <sub>6</sub>	.0100	.1400	.0360	.0400	.0000	.0000	.0000	.0000	.0000	.0000
14	Met Cyc Pent	.0120	.1400	.0370	.0400	.0000	.0000	.0000	.0000	.0000	.0000
15	Cyc Hex	.0140	.1400	.0370	.0400	.0000	.0000	.0000	.0000	.0000	.0000
16	nC <sub>7</sub>	.0160	.1400	.0370	.0400	.0000	.0000	.0000	.0000	.0000	.0000
17	Met Cyc Hex	.0180	.1400	.0380	.0400	.0000	.0000	.0000	.0000	.0000	.0000
18	Toluene	.0300	.1500	.0620	.0400	.0000	.0000	.0000	.0000	.0000	.0000
19	o-Xylene	.0600	.1600	.0620	.0500	.0450	.0400	.0400	.0350	.0300	.0000
20	nC <sub>8</sub>	.0400	.1400	.0600	.0400	.0000	.0000	.0000	.0000	.0000	.0000
21	nC <sub>9</sub>	.0450	.1400	.0400	.0400	.0000	.0000	.0000	.0000	.0000	.0000
22	nC <sub>10</sub> -nC <sub>14</sub>	.0500	.1500	.0430	.0600	.0000	.0000	.0000	.0000	.0000	.0000
23	nC <sub>15</sub> -nC <sub>19</sub>	.0550	.1800	.0800	.0800	.0000	.0000	.0000	.0000	.0000	.0000
24	nC <sub>20</sub> -nC <sub>24</sub>	.0600	.2000	.1280	.1000	.0000	.0000	.0000	.0000	.0000	.0000

From: Willman, B. T. and Teja, A. S.: "Continuous Thermodynamics of Phase Equilibria Using a Multivariate Distribution Function and an Equation of State", AIChE J, 32(12), 2067-2078 (1986).

Table A.4.5.

Interaction parameters of CO<sub>2</sub>, N<sub>2</sub> and H<sub>2</sub>S binaries for Valderrama-Patel-Teja equation of state.

Component (1)	Carbon Dioxide	Nitrogen	Hydr. Sulfide
Methane	0.092	0.035	0.080
Ethane	0.134	0.038	0.095
Propane	0.128	0.070	0.088
i-Butane	0.126	0.134	0.050
n-Butane	0.138	0.114	0.050
n-Pentane	0.141	0.088	0.047
n-Hexane	0.118	0.150	0.047
n-Heptane	0.110	0.142	0.047
Carbon Dioxide	-	-0.036	0.088
Nitrogen	-	-	0.176

All hydrocarbon-hydrocarbon BIP=0

Table A.4.6.

Interaction parameters and coefficients of methanol and water binaries for Valderrama-Patel-Teja equation of state with non-random mixing rule, Eqs.(4.86-89).

Component (1)	$k_{ii}$	Methanol		$k$	Water	
		$I_{pi}^0$	$I_{pi}^0$ E-4		$I_{pi}^0$	$I_{pi}^0$ E-4
Methane	0.2538	0.7319	6.88	0.5028	1.8180	49.00
Ethane	0.0137	0.0519	21.70	0.4974	1.4870	45.40
Propane	*	0.0779	0.00	0.5465	1.6070	39.30
i-Butane	0.1233	0.3209	17.60	0.5863	1.7863	37.40
n-Butane	0.1465	0.2917	0.00	0.5800	1.6885	33.57
n-Pentane	0.2528	0.7908	58.28	0.5525	1.6188	23.72
n-Hexane	0.2245	0.5607	17.54	0.4577	1.5730	31.41
n-Heptane	0.1461	0.4592	27.17	0.4165	1.5201	35.21
n-Octane	0.1403	0.5331	36.91	0.3901	1.5200	35.31
Carbon dioxide	0.0510	0.0700	11.56	0.1965	0.7232	23.74
Nitrogen	0.2484	1.0440	7.22	0.4792	2.6575	64.46
Hydrogen sulfide	0.0694	0.1133	0.00	0.1382	0.3809	13.24
Methanol	0.0000	0.0000	0.00	**	0.0000	0.00
Water	**	0.0000	0.00	0.0000	0.0000	0.00

\*  $k_{ij}$  of propane-methanol temperature dependent:  $k_{pm}=0.0278+0.000911(T-273)$ .

\*\*  $k_{ij}$  of water-methanol is temperature dependent:  $k_{mw}=-0.100+0.000185(T-273)$

Table A.5.

SI metric conversion factors.

API		$141.5/(131.5 + ^\circ\text{API})$		= g/cm <sup>3</sup>
atm(std)	×	1.013 250*	E + 05	= Pa
bar	×	1.0*	E + 05	= Pa
bbl (US)	×	1.589 873	E - 01	= m <sup>3</sup>
bbl/D	×	1.589 873	E - 01	= m <sup>3</sup> /s
Btu	×	1.055 056	E + 00	= kJ
°C		°C + 273.15		= K
cp (centi poise)	×	1.0*	E + 00	= mPa.s
cSt (centi Stoke)	×	1.0*	E + 00	= mm <sup>2</sup> /s
d (darcy)	×	9.869 233	E - 13	= m <sup>2</sup>
dyne	×	1.0*	E - 02	= mN
dync/cm	×	1.0*	E + 00	= mN/m
ft	×	3.048*	E - 01	= m
ft <sup>2</sup>	×	9.290 304*	E - 02	= m <sup>2</sup>
ft <sup>2</sup> /s	×	9.290 304*	E + 04	= mm <sup>2</sup> /s
ft <sup>3</sup>	×	2.831 685	E - 02	= m <sup>3</sup>
ft <sup>3</sup> /bbl	×	1.781 076	E - 01	= m <sup>3</sup> /m <sup>3</sup>
ft <sup>3</sup> /lbm	×	6.242 796	E - 02	= m <sup>3</sup> /kg
°F		(°F - 32)/1.8		= °C
°F		(°F + 459.67)/1.8		= K
gal (US)	×	3.785 412	E - 03	= m <sup>3</sup>
in.	×	2.54*	E - 02	= m
in. <sup>2</sup>	×	6.451 6*	E - 04	= m <sup>2</sup>
in. <sup>3</sup>	×	1.638 706	E - 05	= m <sup>3</sup>
lbf	×	4.448 222	E + 00	= N
lbf.s/m <sup>2</sup>	×	6.894 757	E + 03	= Pa.s
lbm	×	4.535 924	E - 01	= kg
lbm/ft <sup>3</sup>	×	1.601 846	E + 01	= kg/m <sup>3</sup>
mL	×	1.0*	E - 06	= m <sup>3</sup>
mmHg=torr	×	1.333 224	E - 02	= MPa
psi	×	6.894 757	E - 03	= MPa
°R	×	1/1.8*		= K
St (stoke)	×	1.0*	E - 04	= m <sup>2</sup> /s

SI Unit Prefixes: m(milli)=E - 03 k(kilo)=E + 03 M(mega)=E + 06

\* Conversion factor is exact

## CORRELATIONS FOR ESTIMATING CRITICAL PROPERTIES IN FIELD UNITS

The units of temperature, pressure and volume are Rankine, psia, and ft<sup>3</sup>/lbmol, respectively, in all the following equations. The specific gravity, *S*, is defined relative to water at 60 °F. The correlations in SI unit are given in Section 6.2.

### Lee-Kesler Correlations

$$T_c = 341.7 + 811S + (0.4244 + 0.1174S)T_b + (0.4669 - 3.2623S) \times 10^{-5} / T_b$$

$$\ln P_c = 8.3634 - 0.0566/S - (0.24244 + 2.2898/S + 0.11857/S^2) \times 10^{-1} T_b \\ + (1.4685 + 3.648/S + 0.47227/S^2) \times 10^{-7} T_b^2 - (0.42019 + 1.6977/S^2) \times 10^{-10} T_b^3$$

$$\omega = (\ln P_{br} - 5.92714 + 6.09648/T_{br} + 1.28862 \ln T_{br} - 0.169347T_{br}^6) / \\ (15.2518 - 15.6875/T_{br} - 13.4721 \ln T_{br} + 0.4357T_{br}^6) \quad \text{for } T_{br} \leq 0.8$$

$$\omega = -7.904 + 0.1352K_w - 0.007465K_w^2 + 8.359T_{br} \\ + (1.408 - 0.01063K_w)/T_{br} \quad \text{for } T_{br} > 0.8$$

where  $P_{br}=P_b/P_c$ ,  $T_{br}=T_b/T_c$ ;  $P_b$  is the pressure at which  $T_b$  is measured, e.g., the normal boiling point at 14.69 psia, and  $K_w$  is the Watson characterisation factor, Eq.(6.2).

### Cavett Correlations

$$T_c = 768.071 + 1.7134 (T_b - 459.67) - 0.10834 \times 10^{-2} (T_b - 459.67)^2 + 0.3889 \times 10^{-6} (T_b - 459.67)^3 \\ - 0.89213 \times 10^{-2} (T_b - 459.67)API + 0.53095 \times 10^{-5} (T_b - 459.67)^2 API + 0.32712 \times 10^{-7} (T_b - 459.67)^2 API^2$$

$$\log P_c = 2.829 + 0.9412 \times 10^{-3} (T_b - 459.67) - 0.30475 \times 10^{-5} (T_b - 459.67)^2 \\ + 0.15184 \times 10^{-8} (T_b - 459.67)^3 - 0.20876 \times 10^{-4} (T_b - 459.67)API + 0.11048 \times 10^{-7} (T_b - 459.67)^2 API \\ - 0.4827 \times 10^{-7} (T_b - 459.67)API^2 + 0.1395 \times 10^{-9} (T_b - 459.67)^2 API^2$$

where  $API = (141.5/S) - 131.5$ .

**Riazi-Daubert Correlations**

$$\theta = a \left[ \exp(b\theta_1 + c\theta_2 + d\theta_1\theta_2) \right] \theta_1^e \theta_2^f$$

where, a to f, are constants for each property as follows:

$\theta$	$\theta_1$	$\theta_2$	a	b	c	d	e	f
$T_c$	$T_b$	S	10.6443	$-5.1747 \times 10^{-4}$	-0.54444	$3.5995 \times 10^{-4}$	0.81067	0.53691
$T_c$	M	S	554.4	$-1.3478 \times 10^{-4}$	-0.61641	0.0	0.2998	1.0555
$P_c$	$T_b$	S	$6.162 \times 10^6$	$-4.725 \times 10^{-3}$	-4.8014	$3.1939 \times 10^{-3}$	-0.4844	4.0846
$P_c$	M	S	$4.5203 \times 10^4$	$-1.8078 \times 10^{-3}$	-0.3084	0.0	-0.8063	1.6015
$(v_c/M)$	$T_b$	S	$6.233 \times 10^{-4}$	$-1.4679 \times 10^{-3}$	-0.26404	$1.095 \times 10^{-3}$	0.7506	-1.2028
$(v_c/M)$	M	S	$1.206 \times 10^{-2}$	$-2.657 \times 10^{-3}$	0.5287	$2.6012 \times 10^{-3}$	0.20378	-1.3036
M	$T_b$	S	581.96	$5.43076 \times 10^{-4}$	-9.53384	$1.11056 \times 10^{-3}$	0.97476	6.51274
$T_b$	M	S	6.77857	$3.77409 \times 10^{-3}$	2.984036	$-4.25288 \times 10^{-3}$	0.401673	-1.58262
$(70 < M < 300) \quad 540 < T_b < 1110^\circ \text{R}$								

**Two Correlations**

The method initially correlates the properties of normal paraffins as the reference. The calculated values are then adjusted for petroleum fractions using the difference between the specific gravity of the hydrocarbon fraction and that of the normal paraffin with the same boiling point as the correlating parameter.

*Normal Paraffins:*

The properties of normal paraffins are correlated with the normal boiling point temperature,

$$T_{cp} = T_b \left[ 0.533272 + 0.191017 \times 10^{-3} T_b + 0.779681 \times 10^{-7} T_b^2 \right.$$

$$\left. - 0.284376 \times 10^{-10} T_b^3 + 0.959468 \times 10^2 / (T_b / 100)^{13} \right]^{-1}$$

$$P_{cp} = (3.83354 + 1.19629\psi + 34.8888\psi + 36.1952\psi^2 + 104.193\psi^4)^2$$

$$v_{cp} = \left[ 1 - (0.419869 - 0.505839\psi - 1.56436\psi^3 - 9481.70\psi^{14}) \right]^8$$

$$S_p = 0.843593 - 0.128624\psi - 3.36159\psi^3 - 13749.5\psi^{12}$$

where the subscript p refers to properties of normal paraffins and,

$$\psi = 1 - T_b / T_{cp}$$

The molecular weight of paraffins is given by the following implicit relation,

$$T_b = \exp \left[ (5.71419 + 2.71579 \ln M_p - 0.286590 (\ln M_p)^2 - 39.8544 / (\ln M_p) - 0.122488 / (\ln M_p)^2) \right. \\ \left. - 24.7522 \ln M_p + 35.3155 (\ln M_p)^2 \right]$$

which can be solved iteratively using the following initial guess,

$$M_p = T_b / (10.44 - 0.0052 T_b)$$

### *Petroleum Fractions:*

The properties of any petroleum fraction are estimated by adjusting the calculated properties of the normal paraffin with the same boiling point as,

Critical Temperature:

$$T_c = T_{cp} \left[ (1 + 2f_T) / (1 - 2f_T) \right]^2$$

$$f_T = \Delta S_T \left[ -0.362456 / T_b^{1/2} + \left( 0.0398285 - 0.948125 / T_b^{1/2} \right) \Delta S_T \right]$$

$$\Delta S_T = \exp [ 5 (S_p - S) ] - 1$$

Critical Volume:

$$v_c = v_{cp} \left[ (1 + 2f_v) / (1 - 2f_v) \right]^2$$

$$f_v = \Delta S_v \left[ 0.466590 / T_b^{1/2} + \left( -0.182421 + 3.01721 / T_b^{1/2} \right) \Delta S_v \right]$$

$$\Delta S_v = \exp [ 4 (S_p^2 - S^2) ] - 1$$

Critical Pressure:

$$P_c = P_{cp} (T_c / T_{cp}) (v_{cp} / v_c) \left[ (1 + 2f_p) / (1 - 2f_p) \right]^2$$



$$f_p = \Delta S_p \left[ \left( 2.53262 - 46.1955/T_b^{\frac{1}{2}} - 0.00127885T_b \right) + \left( -11.4277 + 252.140/T_b^{\frac{1}{2}} + 0.00230535T_b \right) \Delta S_p \right]$$

$$\Delta S_p = \exp [0.5 (S_p - S)] - 1$$

Molecular Weight:

$$\ln M = (\ln M_p) \{ (1 + 2f_M) / (1 - 2f_M) \}^2$$

$$f_M = \Delta S_M \left[ |\Psi| + \left( -0.0175691 + 0.193168/T_b^{\frac{1}{2}} \right) \Delta S_M \right]$$

$$\Psi = 0.0123420 - 0.328086/T_b^{\frac{1}{2}}$$

$$\Delta S_M = \exp [5 (S_p - S)] - 1$$

## EQUATION OF STATE EXPRESSIONS

The general cubic equation of state, Eq.(4.12),

$$P = \frac{RT}{v-b} - \frac{a}{v^2 + uv - w^2}$$

takes the following dimensionless form:

$$Z^3 - (1+B-U)Z^2 + (A-BU-U-W^2)Z - (AB-BW^2-W^2) = 0$$

where

$$A \equiv \frac{aP}{(RT)^2}, \quad B \equiv \frac{bP}{RT}, \quad U \equiv \frac{uP}{RT}, \quad W \equiv \frac{wP}{RT}, \quad \text{and} \quad Z \equiv \frac{vP}{RT}$$

The above equation results in the following expression for the *fugacity coefficient of a pure compound*:

$$\ln \phi = (Z-1) - \ln(Z-B) - \frac{A}{\sqrt{U^2+4W^2}} \ln \frac{2Z+U+\sqrt{U^2+4W^2}}{2Z+U-\sqrt{U^2+4W^2}}$$

The expression for *fugacity of a component in a mixture* is:

$$\ln \phi_i = -\ln(Z-B) + \frac{B_i B}{Z-B} + \frac{A}{\sqrt{U^2+4W^2}} \left[ A_i - \frac{U_i U^2 + 4W_i W^2}{U^2 + 4W^2} \right] \ln \left[ \frac{2Z+U-\sqrt{U^2+4W^2}}{2Z+U+\sqrt{U^2+4W^2}} \right] -$$

$$A \left[ \frac{2(2Z+U)W_i W^2 + (UZ-2W^2)U_i U}{(Z^2 + UZ - W^2)(U^2 + 4W^2)} \right]$$

where, the dimensionless derivatives of EOS parameters are defined as,

$$A_i \equiv \frac{1}{an} \left[ \frac{\partial(n^2 a)}{\partial n_i} \right]_{n_{j \neq i}, T}, \quad B_i \equiv \frac{1}{b} \left[ \frac{\partial(nb)}{\partial n_i} \right]_{n_{j \neq i}, T}, \quad U_i \equiv \frac{1}{u} \left[ \frac{\partial(nu)}{\partial n_i} \right]_{n_{j \neq i}, T}, \quad \text{and} \quad W_i \equiv \frac{1}{w} \left[ \frac{\partial(nw)}{\partial n_i} \right]_{n_{j \neq i}, T}$$

with the total number of moles,  $n$ , defined as,

$$n \equiv \sum_i n_i$$

Implementing the random mixing rules for the mixture EOS parameters (Section 4.3.1),

$$a = \sum_i \sum_j x_i x_j a_{ij}, \quad b = \sum_i x_i b_i, \quad u = \sum_i x_i u_i, \quad \text{and} \quad w = \sum_i x_i w_i$$

we obtain,

$$\ln \phi_i = -\ln(Z - B) + \frac{B(b_i/b)}{Z - B} + \frac{A}{\sqrt{U^2 + 4W^2}} \left[ 2 \sum_i x_i a_{ij}/a - \frac{(u_i/u)U^2 + 4(w_i/w)W^2}{U^2 + 4W^2} \right] \times \\ \ln \left[ \frac{2Z + U - \sqrt{U^2 + 4W^2}}{2Z + U + \sqrt{U^2 + 4W^2}} \right] - A \left[ \frac{2(2Z + U)(w_i/w)W^2 + (UZ - 2W^2)(u_i/u)U}{(Z^2 + UZ - W^2)(U^2 + 4W^2)} \right]$$

### Solution of Cubic Equation

$$Z^3 + a_1 Z^2 + a_2 Z + a_3 = 0$$

Let,

$$Q = (3a_2 - a_1^2)/9 \quad J = (9a_1 a_2 - 27a_3 - 2a_1^3)/54 \quad D = Q^3 + J^2$$

If  $D > 0$ , the equation has only one real root:

$$Z_1 = (J + \sqrt{D})^{1/3} + (J - \sqrt{D})^{1/3} - a_1/3$$

If  $D < 0$ , the equation has three real roots:

$$Z_1 = 2\sqrt{-Q} \cos(\theta/3) - a_1/3$$

$$Z_2 = 2\sqrt{-Q} \cos(\theta/3 + 120^\circ) - a_1/3$$

$$Z_3 = 2\sqrt{-Q} \cos(\theta/3 + 240^\circ) - a_1/3$$

where,

$$\theta = \cos^{-1} \left( J / \sqrt{-Q^3} \right)$$

If  $D = 0$ , the equation has three real roots, at least two of them are equal:

$$Z_1 = 2J^{1/3} - a_1/3$$

$$Z_2 = Z_3 = -J^{1/3} - a_1/3$$

## THERMODYNAMIC PROPERTIES USING PENG-ROBINSON EOS (PR)

$$P = RT/(v - b) - a_c \alpha / [v(v + b) + b(v - b)] \quad (4.27)$$

$$\alpha = [1 + m(1 - T_r^{0.5})]^2 \quad (4.23)$$

$$v^{cor} = v - c \quad (4.31)$$

**Molar Enthalpy**

The total **enthalpy** is calculated from the following thermodynamic relation,

$$H = \int_v \left[ P - T \left( \frac{\partial P}{\partial T} \right)_{v,n} \right] dv + PV + \sum_i^n n_i \bar{u}_{i,0}$$

where the last term is the total internal energy at low pressure and prevailing temperature, and it is determined by summing the internal energy of individual pure components.

Applying the Peng-Robinson equation of state to calculate  $\left( \frac{\partial P}{\partial T} \right)_{v,n}$ , using the random mixing rules, Eqs.(4.74) and (4.78), and dividing the obtained expression by the total number of moles,  $n$ , result in,

$$\bar{h} = \frac{a'}{2\sqrt{2}b} \ln \left( \frac{v - (\sqrt{2} - 1)b}{v + (\sqrt{2} + 1)b} \right) + Pv + \sum_i^n x_i \bar{u}_{i,0}$$

where,

$$a' = \sum_i^n \sum_j^n x_i x_j (1 - k_{ij}) a_i^{1/2} a_j^{1/2} \left[ m_i T_n^{1/2} + \alpha_j^{1/2} \right]$$

When using the volume shift concept to correct the predicted molar volume by PR, Eq.(4.31), the corrected molar enthalpy is given by,

$$\bar{h}^{cor} = \bar{h} - cP$$

**Partial Molar Enthalpy**

$$h_i = \left( \frac{\partial H}{\partial n_i} \right)_{T,P,n_{j \neq i}}$$

Multiplying the molar enthalpy,  $\bar{h}$ , derived above, by  $n$  and differentiating the obtained expression of the total enthalpy, we obtain,

$$h_i = \frac{a'}{2\sqrt{2}b} \left[ \left( \frac{a'_i}{a'} - \frac{b_i}{b} \right) \ln \left( \frac{v - (\sqrt{2} - 1)b}{v + (\sqrt{2} + 1)b} \right) + \frac{v_i - (\sqrt{2} - 1)b_i}{v - (\sqrt{2} - 1)b} - \frac{v_i + (\sqrt{2} + 1)b_i}{v + (\sqrt{2} + 1)b} \right] + Pv_i + \bar{u}_{i,0}$$

where  $v_i$  is the partial molar volume.

When using the volume shift, the corrected partial molar enthalpy is given by,

$$h_i^{\text{cor}} = h_i - c_i P$$

### Partial Molar Volume

$$v_i = \left( \frac{\partial V}{\partial n_i} \right)_{T, P, n_{j \neq i}}$$

Converting the molar volume in PR to total volume, by multiplying it with  $n$ , and differentiating it, we obtain,

$$v_i = \frac{(RT + b_i P)(v^2 + 2bv - b^2) + \left( 2b_i RT - 2 \sum_j^N x_j a_{ij} - 2b_i P(v - b) \right)(v - b) + b_i a}{P(v^2 + 2bv - b^2) + 2P(v - b)(v + b) - 2RT(v + b) + a}$$

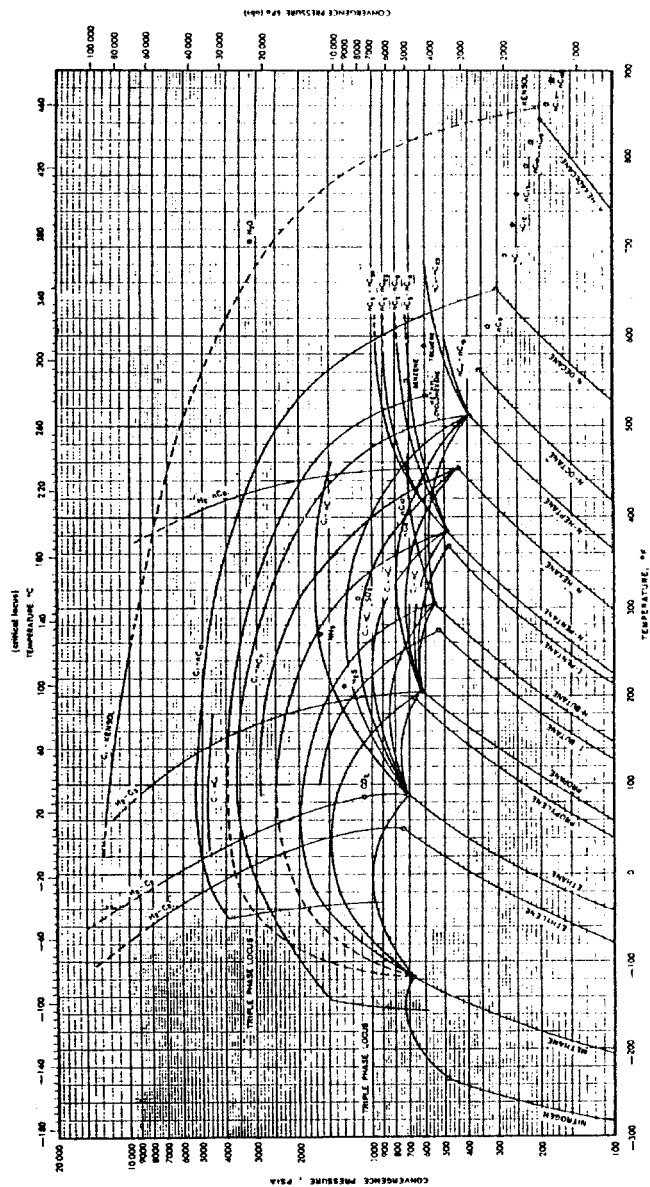


Figure D1. Convergence pressure of hydrocarbon mixtures for use with GPA equilibrium ratio charts.

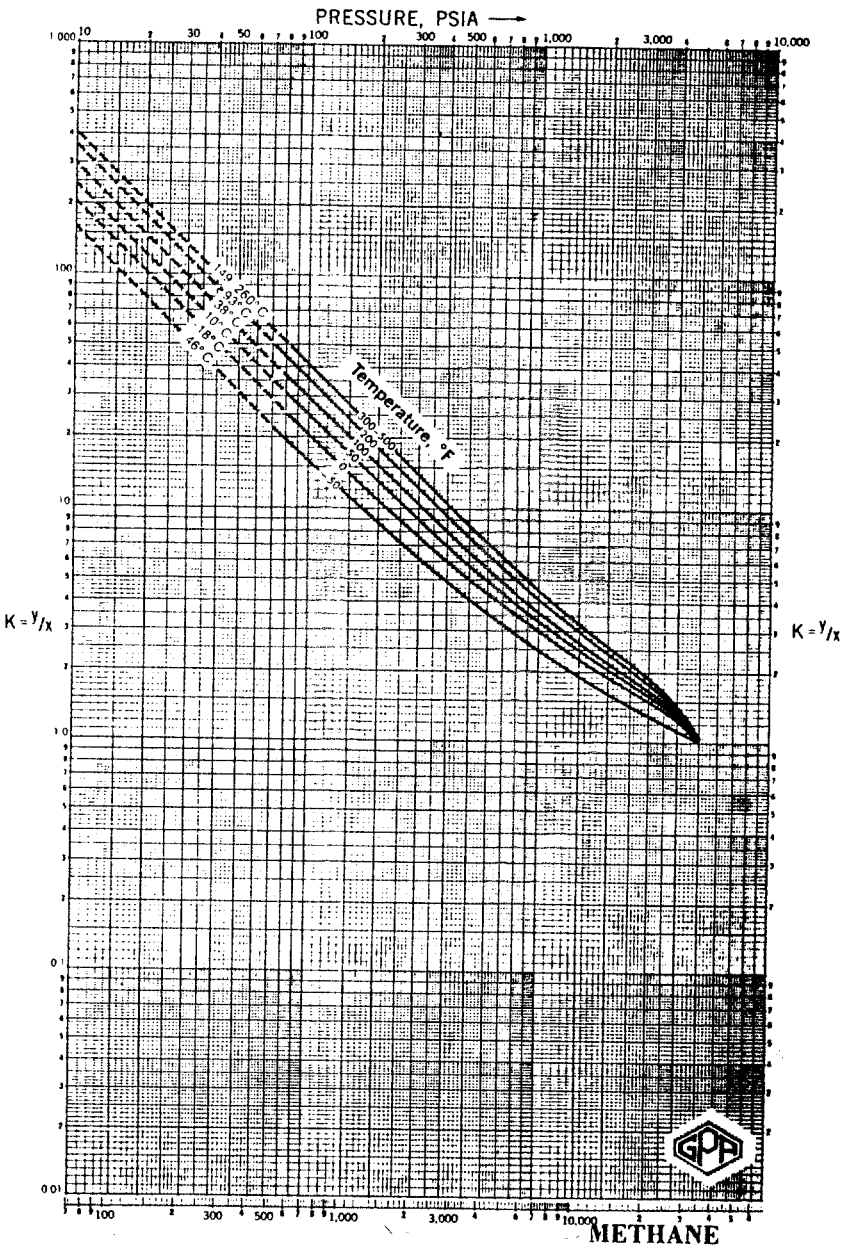


Figure D.2. Equilibrium ratio at 34.47 MPa (5000 psia) convergence pressure.

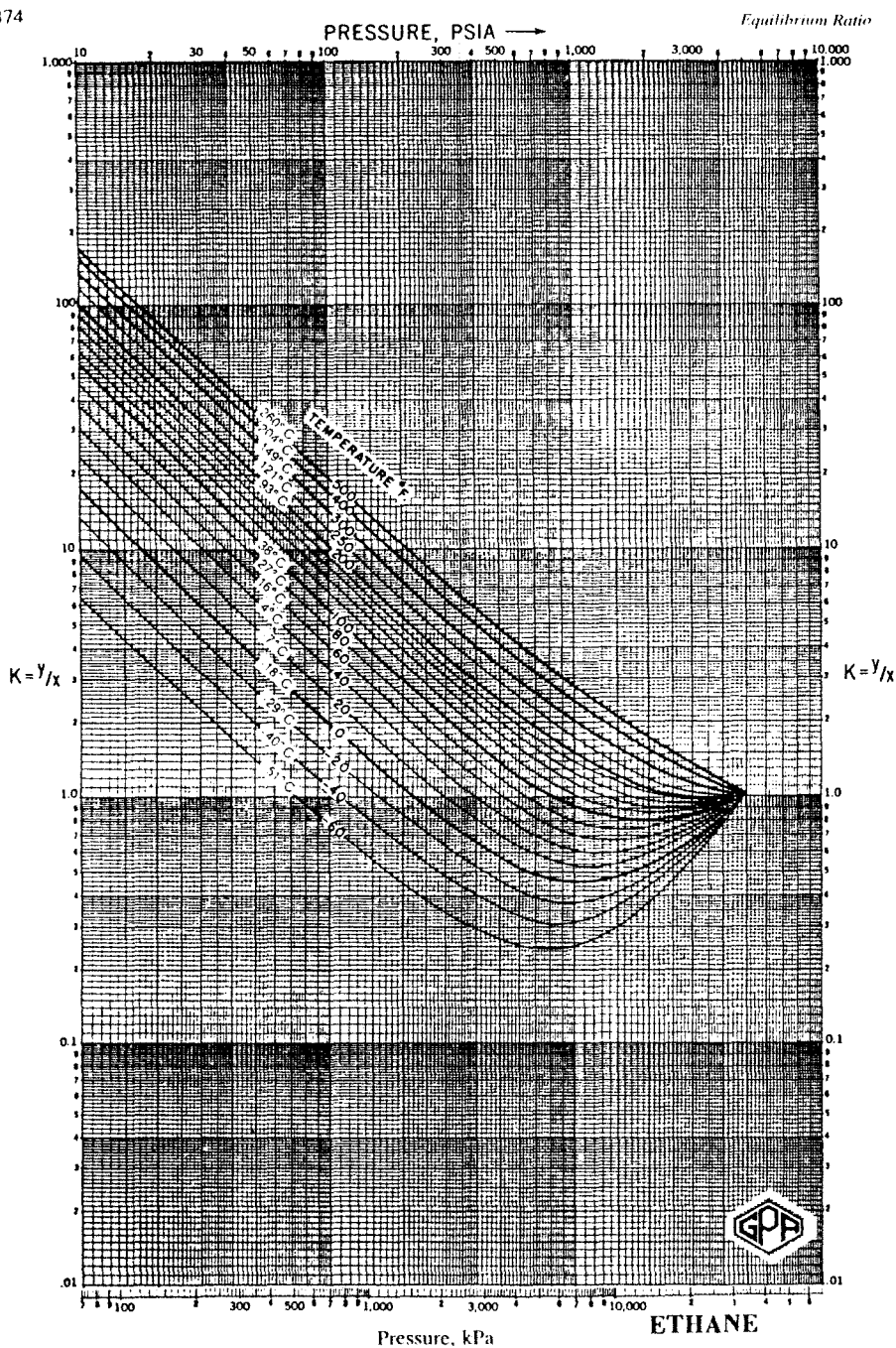


Figure D.3. Equilibrium ratio at 34.47 MPa (5000 psia) convergence pressure.



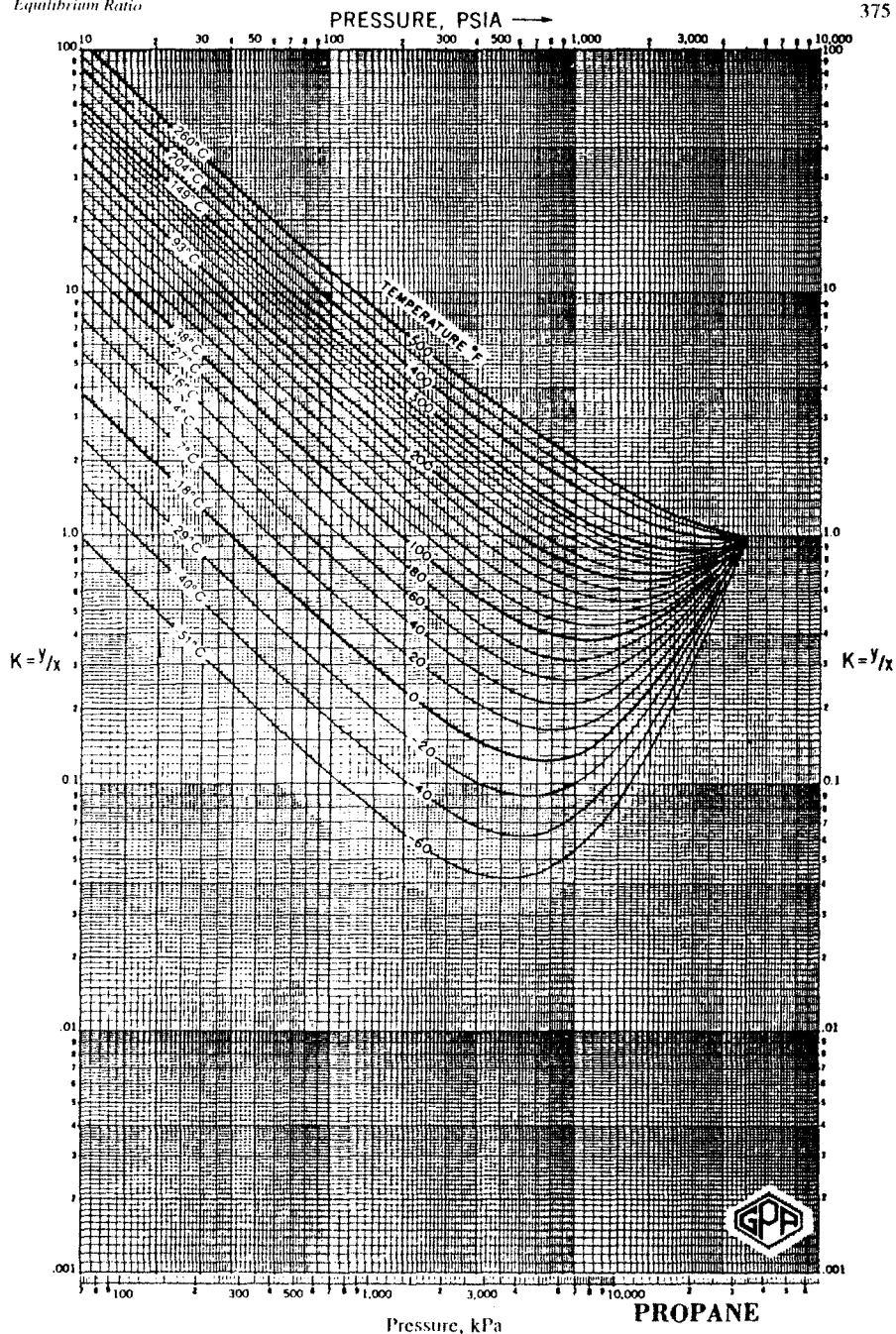


Figure D.4. Equilibrium ratio at 34.47 MPa (5000 psia) convergence pressure.

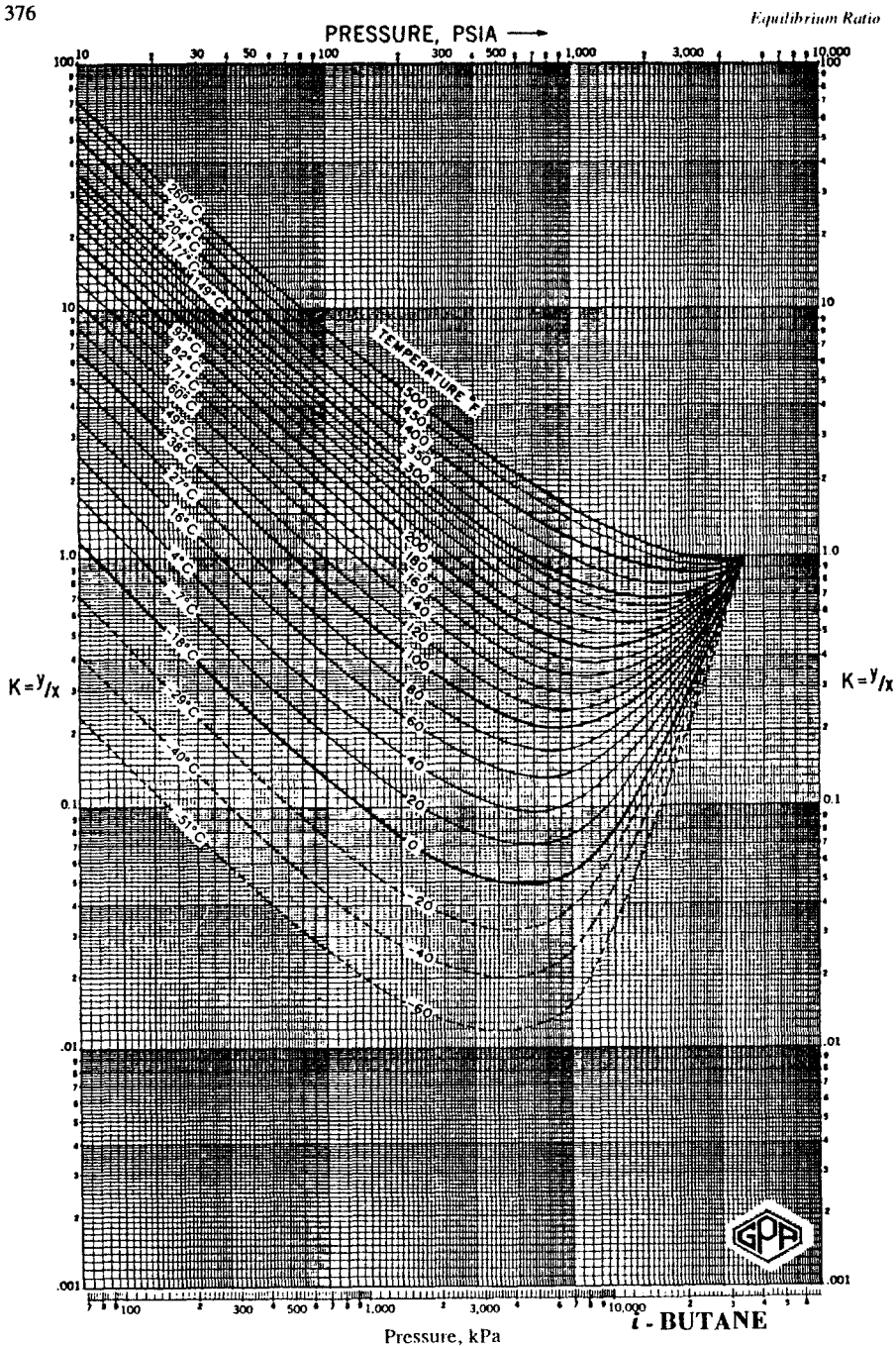


Figure D.5. Equilibrium ratio at 34.47 MPa (5000 psia) convergence pressure.

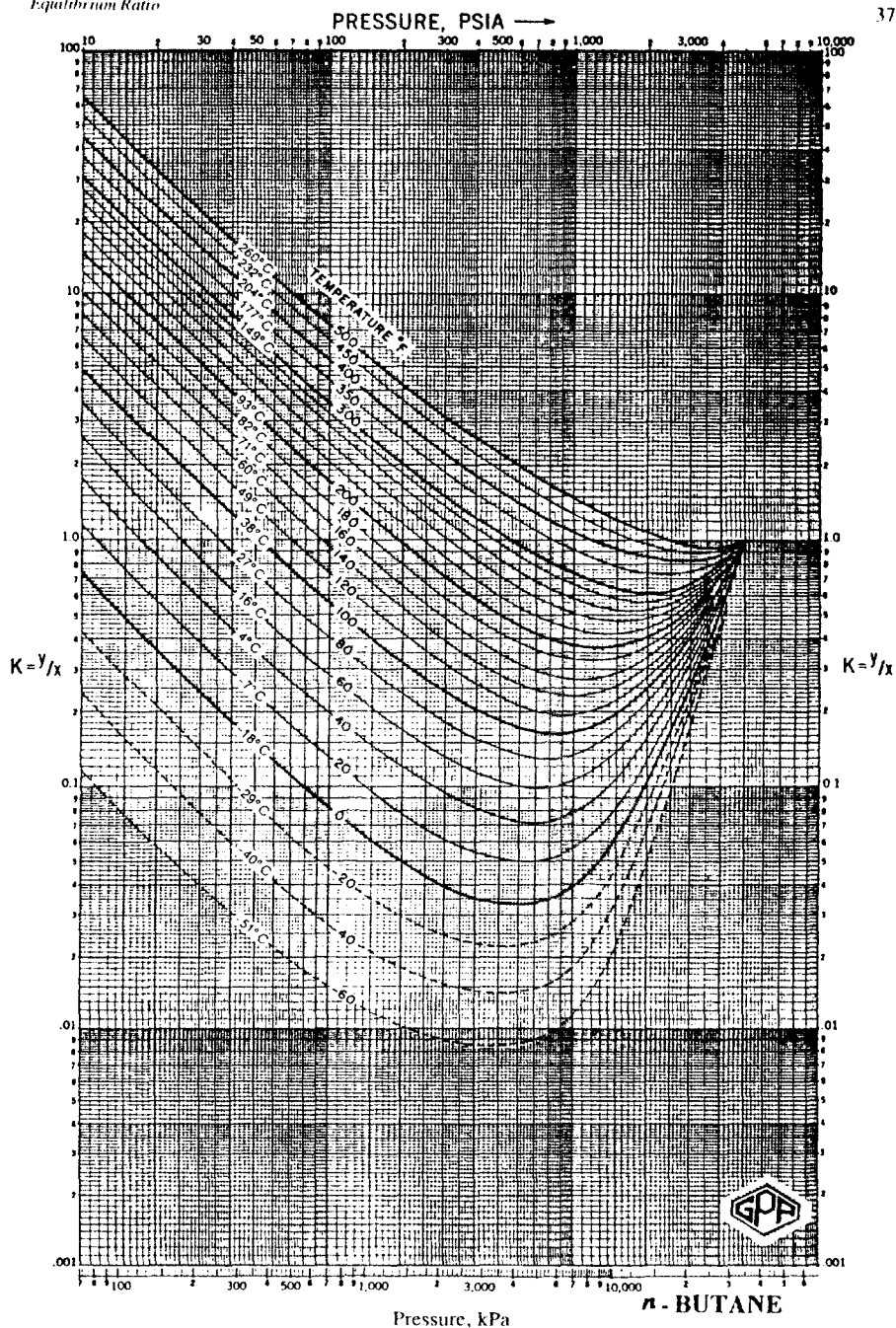


Figure D.6. Equilibrium ratio at 34.47 MPa (5000 psia) convergence pressure.

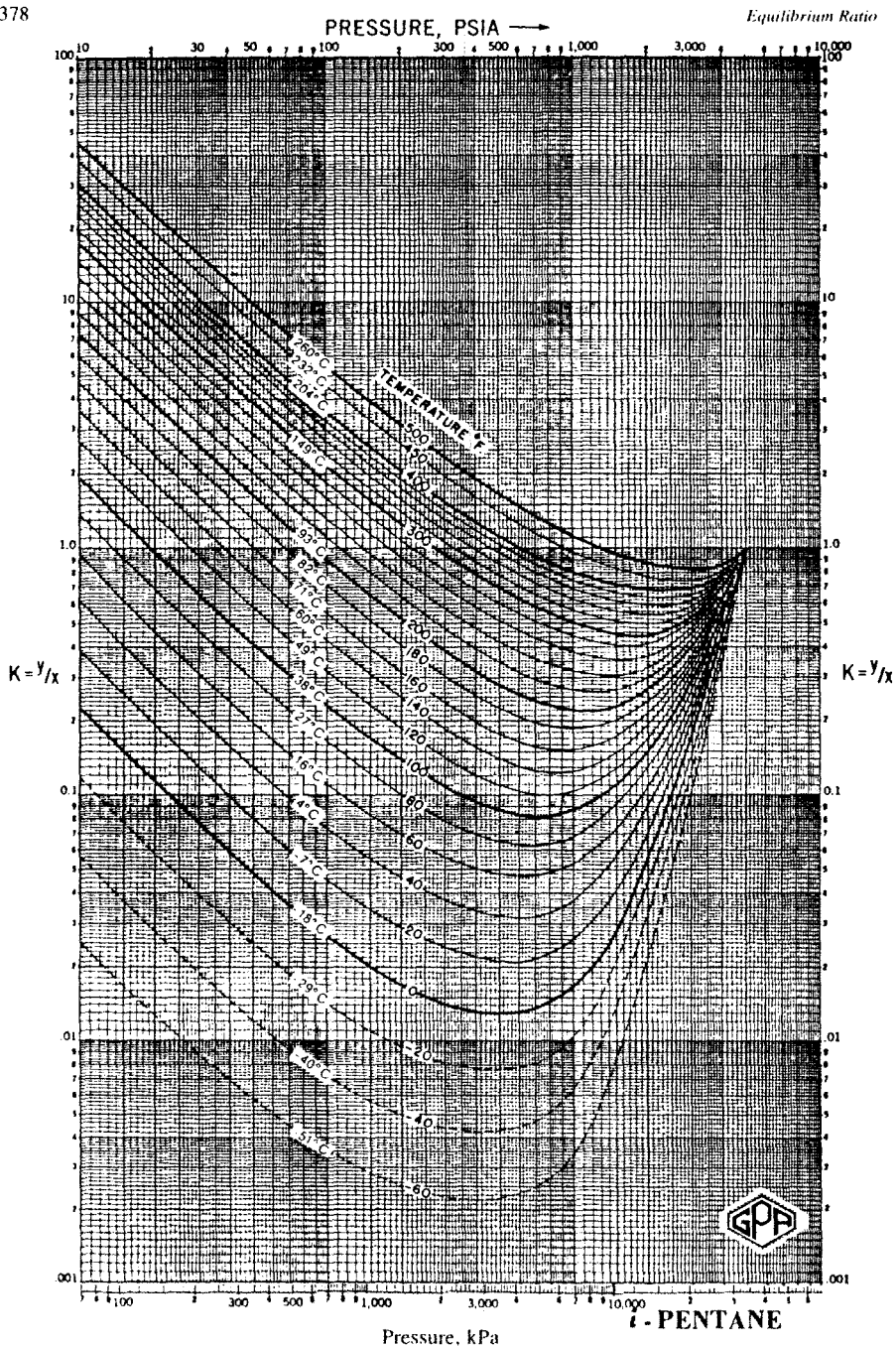
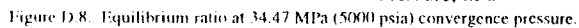


Figure D 7. Equilibrium ratio at 34.47 MPa (5000 psia) convergence pressure.



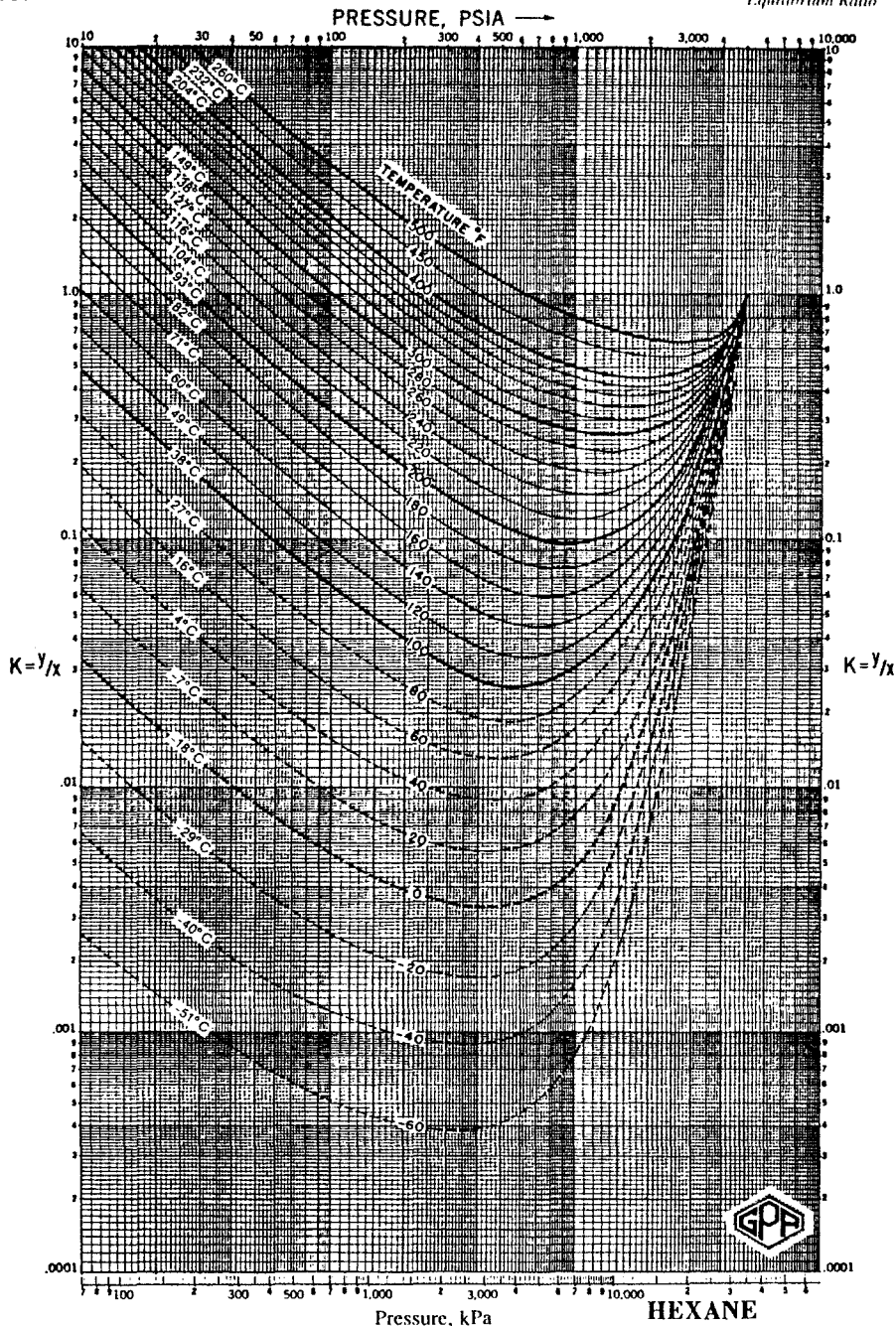


Figure D.9. Equilibrium ratio at 34.47 MPa (5000 psia) convergence pressure.



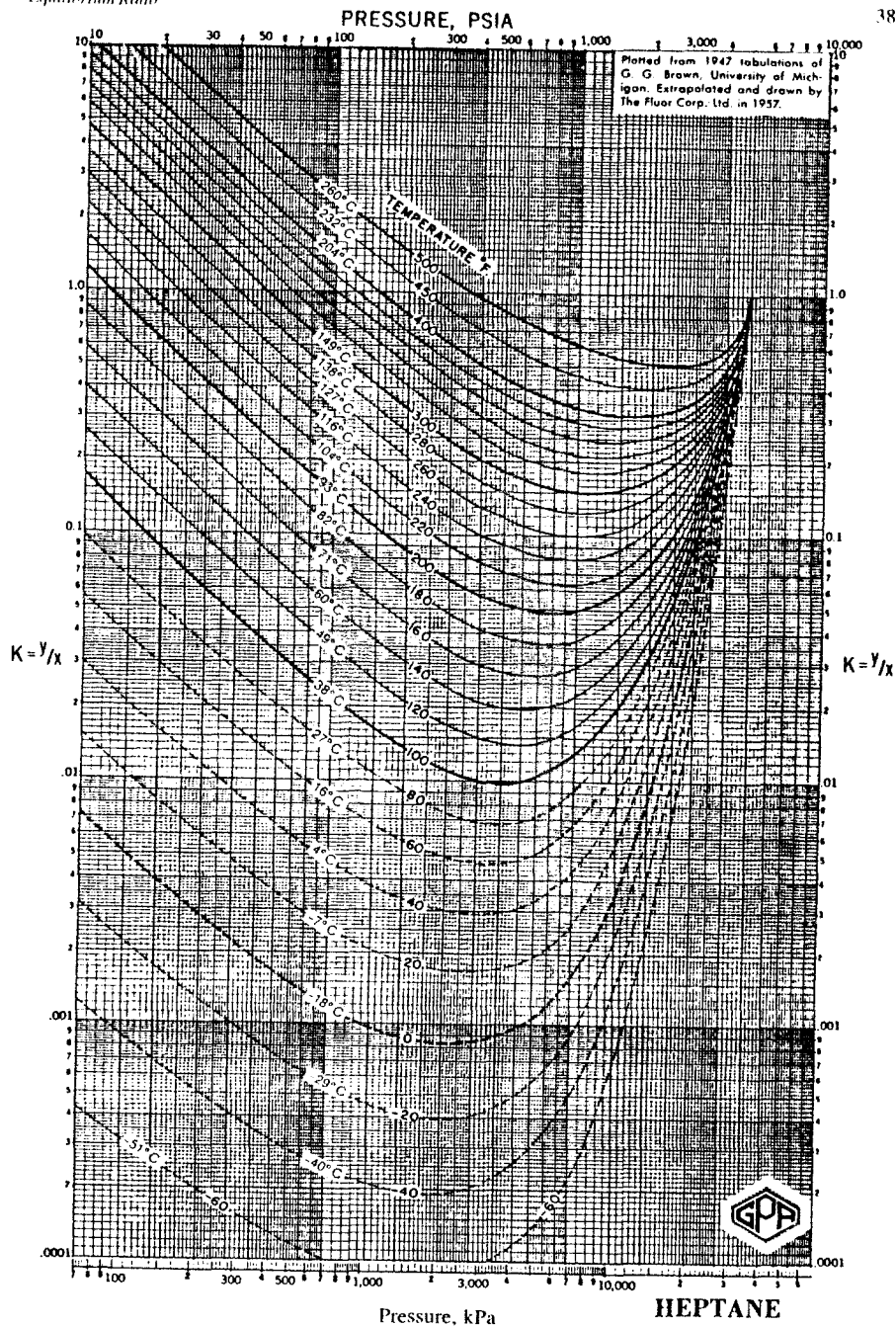


Figure D.10. Equilibrium ratio at 34.47 MPa (5000 psia) convergence pressure.

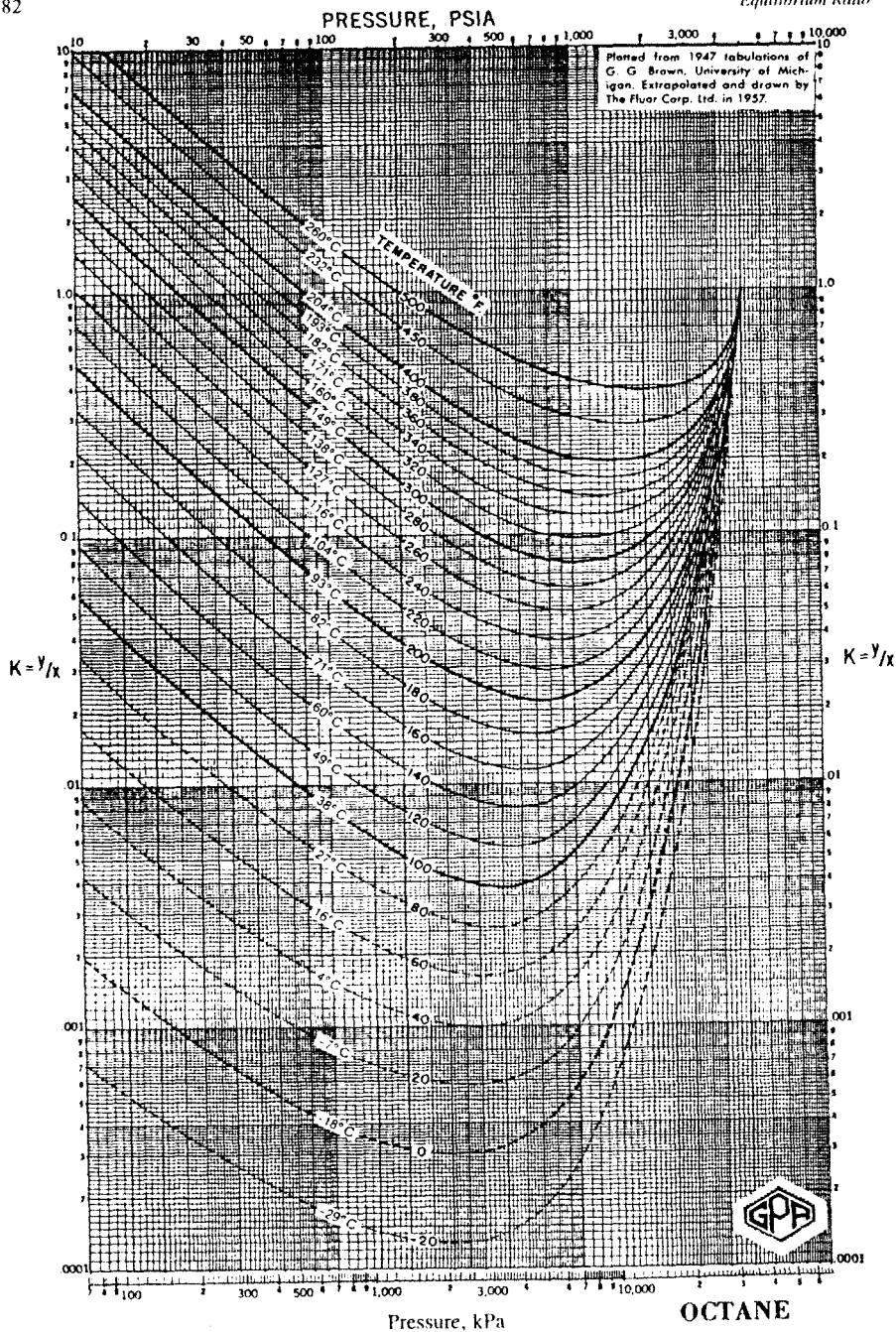


Figure D 11. Equilibrium ratio at 34.47 MPa (5000 psia) convergence pressure.



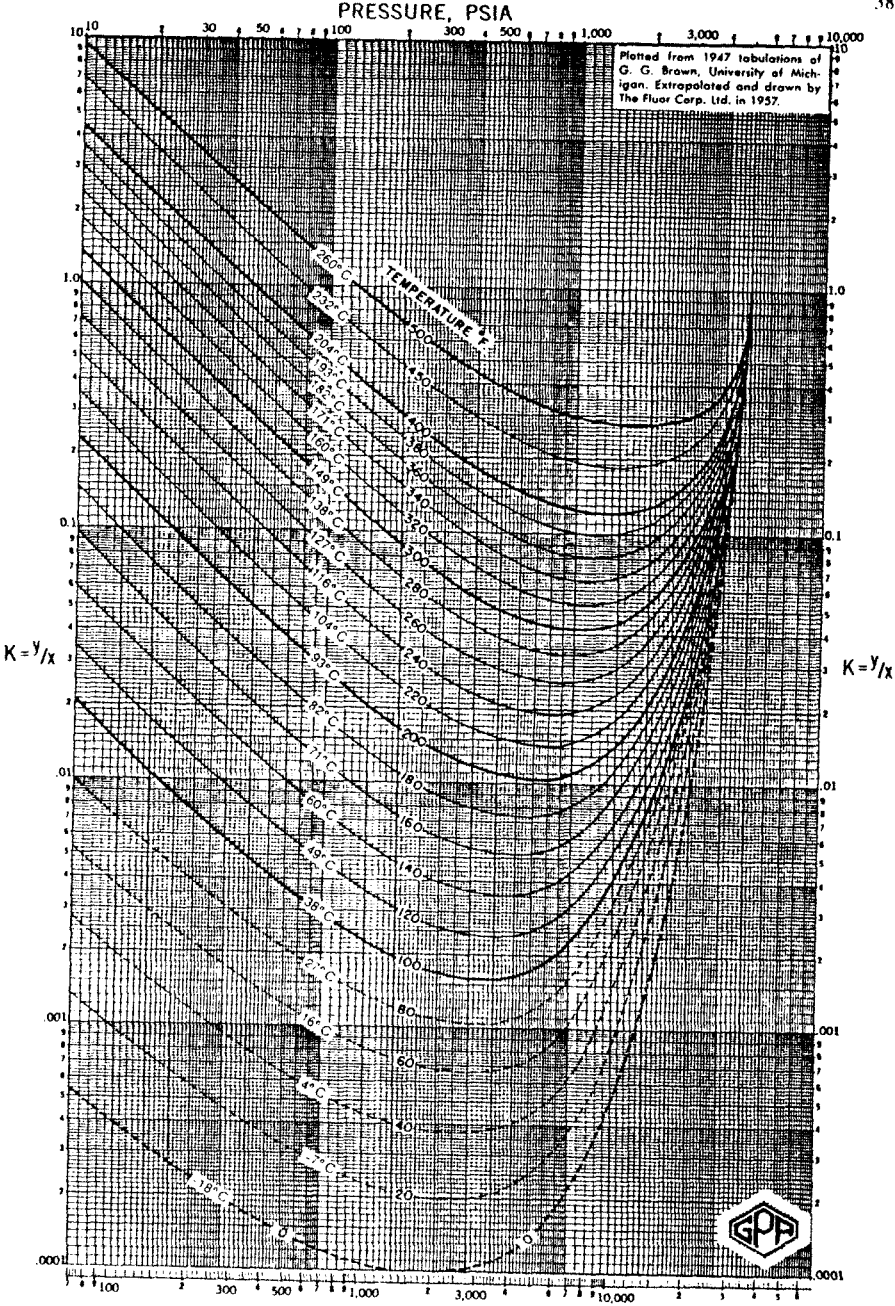
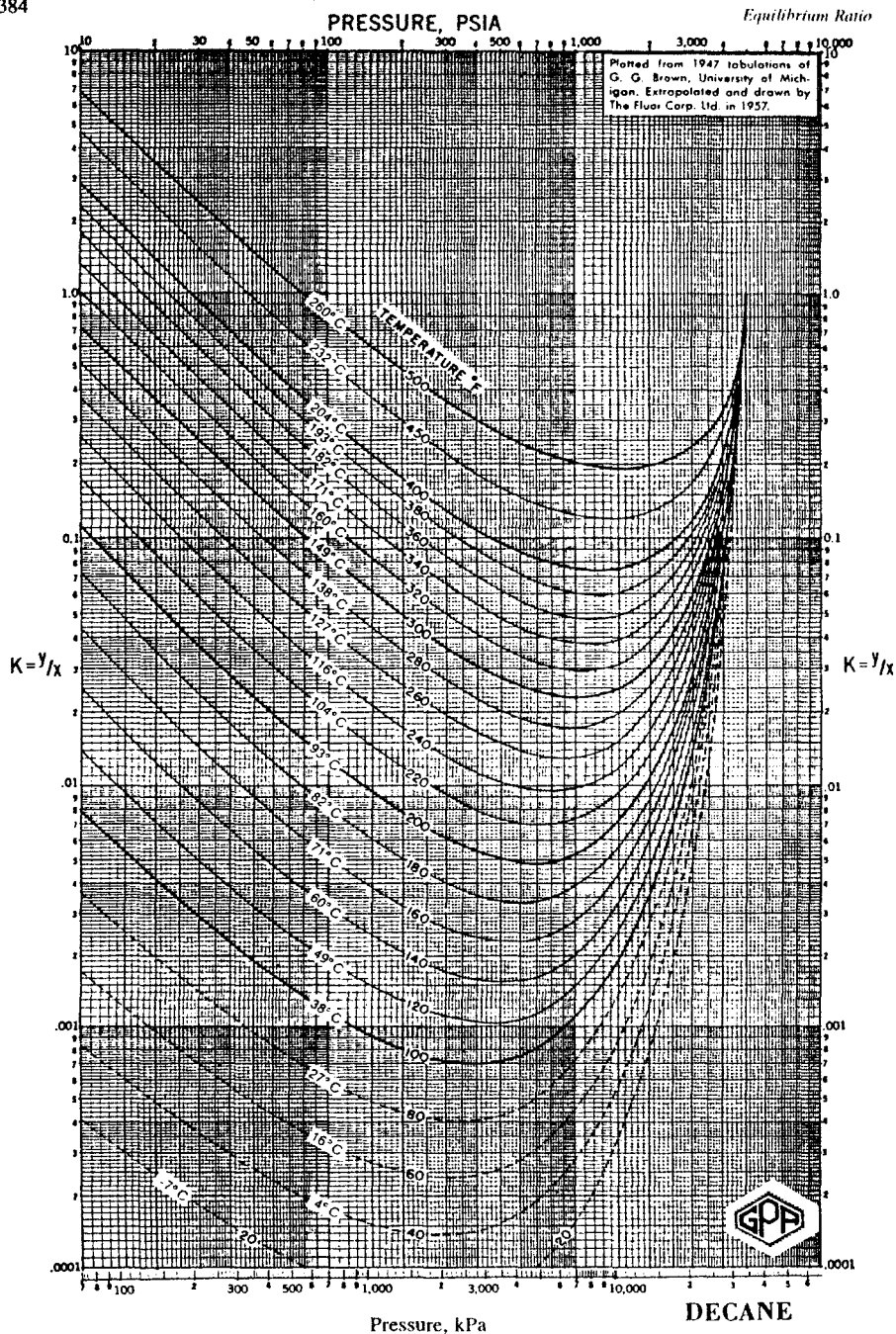


Figure D 12 Equilibrium ratio at 34.47 MPa (5000 psia) convergence pressure



## INDEX

- acentric factor, 13, 221, 222, 352-357
- activity coefficient, 111
- Alani and Kennedy equation, 75, see also density alkanes, 2
- API gravity, 23
- apparent oil density, 73
- apparent liquid density of natural gas, 73
- aromatics, 2, 213, 214
- asphaltenes, 2
  - adsorbed material on rock, 37
- attractive term, 132, 149, 154, see also equation of state
- backward multiple contact, 268, 276, see also gas injection tests
- boiling point,
  - normal, 4
  - true, 210
- Benedict-Webb-Rubin EOS, 131
  - Starling modification, 131
- binary interaction parameter, 152, 155, 180, 327, 331, see also mixing rules
- black oil, 28-29
  - correlations, 67-79
  - tests, 42-52, see also oil tests
- bubble point pressure, 64, 86
  - calculation, 169, 173
  - correlations, 68
- C7+ characterisation, See also continuous description
  - critical property correlations, 119
  - critical molar volume, 336
- capillary condensation, 38
- carbenes, 2
- carboids, 2
- carbon group
  - critical properties, 221-227, 356-357
    - Cavett correlation, 222
    - Edmister correlation, 222
    - Lee-Kesler critical correlations, 221
    - perturbation expansion correlations, 223
    - Riazi-Daubert Correlations, 222
  - properties by mixing, 308-309
  - single carbon number group, 211
    - molecular weight, 213
    - molecular weight boundaries, 239
    - normal boiling point, 213
    - specific gravity, 213
- Cavett correlation, 222, see also carbon group characterisation factor, see Watson characterisation factor
- chemical potential, 107-108, 183, 197
  - gradient, 200
- classification of reservoir fluids, 22-29
- compositional grading, 2, 38, 195-203
  - aromatic effect, 202
  - heat of transport, 199, 200-201
  - non equilibrium, 198-201
  - Onsager relations, 199
  - significance, 201
  - thermal gradient, 201
- compositional analysis, 38
  - blow-down, 39
  - data evaluation, 326
  - full stream (direct) sampling, 39
- composition retrieval, see inverse grouping
- compressibility factor, see gas compressibility factor
- continuous description 234-246, see also carbon group
  - exponential distribution, 237
  - gamma probability distribution, 236, 241, 243
- critical properties
  - binaries, 18, see also critical point
  - pure compounds, 353-354
  - single carbon groups, 355-356,
- condensing gas drive, 257-258, see also gas injection, minimum miscibility pressure
- condensing/vaporising gas drive, 259, see also gas injection, minimum miscibility pressure
- convergence pressure, 117, see also equilibrium ratio
- corresponding states, 10
- Cox chart, 4, see also vapour pressure
- cricondentherm, 15, see also gas condensate
- critical compressibility factor, 11, see also critical properties
- critical point, 5, 134, 143
  - calculation, 192-195
    - Kreglewski and Kay method, 194
    - Li's mixing rule, 193
    - volume, 194
- critical tie line, 256-260, 272-273, see also minimum miscibility pressure
- cross over tie lines, 260, see also minimum miscibility pressure
- Darcy's equation, 332
- degrees of freedom, See Gibbs phase rule
- density
  - prediction
    - Alani and Kennedy equation, 75
    - EOS, 319
    - saturated pure compounds, 8
    - Standing and Katz method, 73-74

dew point, 10, 19, 37, 56, 64, 341, 343, see also  
     gas condensate  
     calculation, 169

distillation, 210-215

dry gas, 24

Edmister correlation, 222, see also carbon group

enthalpy  
     constant flash, 175  
     definition, 106

equation of state  
     comparison, 314-323  
     general van der Waals type, 135  
     Patel-Teja, 147, 305, 314, 325, 347, 348  
     Peng-Robinson EOS, 141, 156, 172, 178, 314, 339  
     prediction reliability  
         phase composition, 316  
         volumes, 320  
         saturation pressure, 318  
     Redlich-Kwong, 138, 314, 346  
     robustness, 182, 322  
     Schmidt and Wenzel EOS, 146, 155, 314  
     selection, 325  
     sensitivity, 327  
     Soave-Redlich-Kwong, 140, 152, 156, 314, 346, Graboski and Daubert modification, 141  
     Starling-Benedict-Webb-Rubin, 131  
     tuning, see tuning  
     Valderrama-Patel-Teja EOS, 148, 160  
     van der Waals EOS, 132,  
     virial, 130-131  
     volume shift, 141  
         Jhaveri and Youngren, 143  
         near critical point, 143, 149  
         Peneloux et al, 142  
     Zudkevitch-Joffe EOS, 138, 314

equilibrium ratio, 111-125, 171, 310  
     estimation 116-125  
         EOS, 317  
         GPA K-value, 118  
         intermediate pressures, 121  
         Møllerup equation, 123  
         Wilson equation, 122  
     internal consistency, 59, 124  
     split method, 112

equilibrium flash calculations 168-183  
     computational time, 179-182  
     negative flash, 175, 189  
     robustness, 182  
     root selection, 175  
     trivial solution, 171

first contact miscibility, 255

flash calculations, see equilibrium flash calculations

formation water, 86-94

forward multiple contact, 267-268, 273, 329, see  
     also gas injection tests

fugacity, 108-110  
     Lewis rule, 109

fugacity coefficient, 109, 129, 157, 174  
     pure substance, 136

gamma probability distribution, 236, 241, 243, see  
     also continuous description

gas  
     density, see gas compressibility factor  
     formation volume factor, 40  
     ideal gas volume, 11  
     molecular weight, 79  
     specific gravity, 68  
     viscosity, see viscosity

gas chromatography, 215-221  
     capillary columns, 217  
     comparison with distillation, 215  
     non-eluted fraction, 217  
     packed columns, 215

gas compressibility factor, 45  
     chart, 80  
     Dranchuk and Abou-Kassem correlation, 80  
     H<sub>2</sub>S and CO<sub>2</sub> effect, 82

gas condensate, 25-27

gas condensate tests, 52-65  
     constant composition expansion, 53  
     constant volume depletion, 53  
     colour change, 54  
     dew point, 56, see also dew point  
     gas cycling, 263, see also gas injection  
     material balance, 59-61  
     pressure build-up test, 63

gas formation volume factor, 46,

gas hydrates, 86

gas injection tests  
     backward multiple contact, 268, 276,  
     gas cycling, 263  
     forward multiple contact, 267-268, 273, 329,  
     rising bubble apparatus, 265  
     swelling, 266  
     single contact, see swelling  
     slim tube, 260-265, 332, 338

gas in solution, 50-51

gas recycling, see gas injection tests

gas solubility in water  
     Krichevsky-Kasarnovsky equation, 116  
     Henry's law, 114, 116,

gas to oil ratio, 23, 340

gas viscosity, see viscosity

generalised single carbon group, see carbon group

Gibbs energy  
     change, 176  
     definition, 106  
     minimisation, 183  
     stability, 184, 185

- Gibbs phase rule, 4
- Grouping, 302-314
  - Danesh et al., 304
  - equal mole fraction, 306
  - equal weight (mass), 307
  - Gaussian quadrature, 243
  - inverse grouping, 310-311
  - Newley and Merrill, 303, 306, 307, 309, 310
  - optimum number, 305
  - selection, 302-307
  - Whitson, 302
- Lee-Kesler critical property correlations, 221, see also carbon group
- Helmholtz energy, 106, 191, 193
- Henry's law, 114, 116, see also gas solubility
- Hoffmann plot, 124, 326, see also equilibrium ratio
- hydrates, 86
- interfacial tension
  - measurement, 282-285
    - interface curvature, 283-284
    - pendant drop, 282-283
  - relation with density difference, 289
- prediction method for hydrocarbons
  - Lee and Chien, 288
  - Macleod-Sugden, 285
  - scaling law, 288
  - Schechter and Guo, 291
  - Weinaug and Katz, 286
- water-hydrocarbon
  - methane-water, 292
  - prediction method, 292, 293
  - salts in water, 294
  - water-normal octane, 293
- intrinsic stability, 190, see also stability
- invariance condition, 159, 161, see also mixing rules
- Kay's mixing rule, 17
- Lee-Kesler vapour pressure correlation, 13, see also vapour pressure
- Lee-Kesler critical property correlations, 221, see also carbon group
- Lewis rule, 109, see also fugacity
- limiting tie line, 256-258, 260, 267-268, 273, see also miscibility
- liquid-liquid displacement, 338, see also tuning
- Lohrenz-Bray-Clark correlation, 335, see also viscosity
- melting point, 5
- miscibility
  - concepts, 254-260
  - experimental studies, 260-269, see also gas injection
  - real reservoir fluids, 258-260
- mixing rules, 142-161
  - invariance condition, 159, 161
  - local composition, 159
  - non-random, 159-161
  - polar-polar interaction coefficients, 160
  - random mixing rules, 159
  - minimum miscibility enrichment, 257
  - minimum miscibility pressure, 256-257
  - prediction methods
    - Benham et al., 273
    - carbon dioxide, 275
    - Firoozabadi and Aziz, 271, 277
    - first contact miscibility, 270
    - Glaser, 274, 276
    - Hudgins et al., 272
    - Jensen and Michelsen, 273
    - Kuo, 274, 276
    - Pedrood, 274, 276
- molecular weight
  - condensate, 79
  - measurement, 212
  - mixtures, 245
  - rich gas, 42
- multiple contact tests, 304, 314, 321, see also gas injection tests
- naphthene, 2, 213-214
- oil compressibility, 43
- oil density, 71, 73
- oil correlation
  - bubble point, 69
  - formation volume factor, 70
  - isothermal compressibility coefficient, 70
  - total formation volume factor, 71-72
  - viscosity, see viscosity
- oil tests
  - combination of data, 49-52
  - differential liberation, 45
  - differential vaporisation, 45
  - separator, 46-49
- oil specific gravity, 23
- olefins. *See* alkenes
- paraffins, 2, 212, 214, 223
- Patel-Teja EOS, 147, 305, 314, 325, 347, 348, see also equation of state
- Peng-Robinson EOS, 141, 151, 156, 172, 178, 314, 339, see also equation of state
- perturbation expansion critical property correlations, 223, see also carbon group
- phase diagram
  - ethane-heptane, 15
  - gas condensate, 26
  - multicomponent mixture, 19
  - pure substance, 9-10
- PNA, 220
- pseudo critical conditions, 176
- pseudo critical values, 17
- pseudo reduced properties, 17, 192-194

- quadrature points, 243-244, see also continuous description
- Rackett compressibility factor, 14, 142
- Rackett equation, 14
- Raoult's law, 112
- Redlich-Kwong EOS, 138, 314, 346, see also equation of state
- reduced properties, 11
- relative permeability, 333
  - miscible, 334
  - relation with IFT, 334
- relative volume, 43-46, see also black oil correlations
- repulsive term, 154, see also equation of state
- residual oil, 45, see also oil tests
- residual viscosity, 335, see also viscosity resins, 2
- retrograde condensation, 19, 321, see also gas condensate
- retrograde vaporisation, 19
- Riazi-Daubert correlations, 222, see also carbon group
- sampling
  - condensate ring, 342
  - evaluation of reservoir fluid samples, 340-345
  - gas condensate, 340
  - iso-kinetic sampling, 36
  - minimum gas well flow, 35
  - recombination, 36, 341
  - sample collection, 36-38
  - surface sampling, 340
  - well preparation, 34
- Schmidt and Wenzel EOS, 146, 155, 314, see also equation of state
- Soave-Redlich-Kwong, 140, 156, 314, 346, see also equation of state
- solution gas to oil ratio, 46, 47
  - vented at stock tank, 68
- stability analysis, 183-192
  - limit, 189-190
  - Michelsen method, 187
- Standing oil correlations, 67, 68, 69, see also black oil correlations
- stock tank oil, 47
- sublimation curve, 5
- swelling test, 266, see also gas injection tests
- temperature dependency parameter, 136
  - Mathias and Copeman correlation, 150
  - super critical hydrocarbon components, 153
  - Twu et al. correlation, 151
- ternary diagram, 254
- tie line, 254
- triple point, 5
- tuning, 323-331
  - consistency of regressed parameters, 330
  - dynamic, 331-340
  - experimental data, 325
  - fluid characterisation, 324
  - grid-time step sizing, 339
  - limits of parameters
  - regression variables, 327
  - weighting factors, 324
- Valderrama-Patel-Teja EOS, 148, 160, see also equation of state
- van der Waals EOS, 132, see also equation of state
- vaporising gas drive, 255-256, see also gas injection, minimum miscibility pressure
- vapour pressure
  - Cox chart, 4
  - Lee-Kesler correlation, 13
  - water, 87
- Vasquez-Beggs correlations, 67, 69, see also black oil correlations
- virial EOS, see also equation of state
  - Benedict-Webb-Rubin EOS, 131
  - Starling modification, 131
  - virial coefficients, 130, 154
- viscosity
  - prediction
    - corresponding states, 334
    - Ely and Hanley, 334
    - gas, 83
    - Herning-Zipperer, 335
    - Lohrenz-Bray-Clark, 335
    - low pressure viscosity, 335
    - oil, 77-78
    - water, 93
    - tuning, 336
- volatile oil, 65, 27, see also oil
- volume factor, see relative volume
- volume shift, 141, 314, 330, see also equation of state
- water
  - compressibility, 92
  - content of hydrocarbon phase, 87, 89
  - content of liquid hydrocarbons, 88
  - density, 93
  - formation volume factor, 92
  - hydrocarbon solubility in water, 90-91, see also gas solubility in water
  - vapour pressure, 87
  - viscosity, 93
- Watson characterisation factor, 212-214, 330
- wet gas, 25
- Wilson equation, 122, see also equilibrium ratio
- Y function, 43, see also oil testing
- Yamada-Gunn correlation, 14, 354-356, see also critical compressibility factor
- Zudkevitch-Joffe EOS, 138, 314, see also equation of state

